Mutual Design Considerations for Overhead AC Transmission Lines and Gas Transmission Pipelines Volume 1: Engineering Analysis

EL-904
Research Project 742-1
PRC/A.G.A. Contract No. PR132-80

Final Report, September 1978

Volume 1: Engineering Analysis
Volume 2: Prediction and Mitigation Procedures

Prepared by

IIT RESEARCH INSTITUTE
10 West 35th Street
Chicago, Illinois 60615

Principal Authors
J. Dabkowski, Ph.D.
A. Taflove, Ph.D.

Prepared for

Electric Power Research Institute
3412 Hillview Avenue
Palo Alto, California 94304

EPRI Project Manager
Richard E. Kennon
Electrical Systems Division

A.G.A. Catalog No. L51278
Price $20.00
4C9.78-652
Printed in U.S.A.

ABSTRACT

As a result of a program jointly funded by the Electric Power Research Institute (EPRI) and the Pipeline Research Committee (PRC) of the American Gas Association (A.G.A.), known data has been consolidated and a systematic investigation has been made into the mutual effects of ac electric power transmission lines (power lines) and natural gas transmission pipelines (pipelines) jointly sharing rights-of-way. The results presented are of use to both the electric power and natural gas transmission industries for addressing problems arising from a mutual coexistence. Program objectives were:

1. to consolidate known data concerning mutual effects arising from power lines and pipelines sharing a common right-of-way;
2. to develop a unified and systematic method for predicting electromagnetically induced voltages and currents on pipelines; and
3. to investigate mitigation techniques to minimize interference effects upon pipeline and component reliability and personnel safety.

In the fulfillment of these objectives, new techniques for coupling prediction and pipeline mitigation have been developed and other available data has been collected and summarized.

The overall objective of the program was to develop a reference book which concisely presented the coupling prediction and mitigation information derived in a manner useful to both power and pipeline industry users in the design, construction and operation of their respective systems.

EPRI PERSPECTIVE

PROJECT DESCRIPTION

This project was a joint effort by the Pipeline Research Committee of the A.G.A. and EPRI to develop analytical techniques for determining the induced potential on pipelines that parallel electric transmission lines. This is an area of interest to both electrical system and pipeline operators.

The purpose of this project was to develop analytical methods for prediction and mitigation of voltages induced on pipelines by nearby ac transmission lines. Verification by actual tests was necessary. Further, analyses of ac corrosion effects, personnel safety and pipeline component reliability were sought.

PROJECT OBJECTIVES

The contractor was asked to first assess commonly used methods to compute induced voltages and to determine their accuracy and applicability. This was necessary since considerable literature plainly states that calculations of pipeline voltages are often different by a factor of 10 from measured voltages. The next step was to develop valid analytical techniques that could be verified by both theory and field tests. In a follow-on effort IITRI engineers were asked to develop simplified methods of computing induced voltages that could be executed on a programmable hand calculator. Then mitigation techniques were to be developed.

CONCLUSIONS AND RECOMMENDATIONS

The contractor did develop the required analytical techniques, which are reasonable and supported by field test results. New mitigation methods were then developed and old ones evaluated for their effectiveness. All of the mathematical analyses were to be compared with several sets of data from field tests. The accounts of these tests are well documented in this report.

The theoretical considerations are discussed in Volume 1 of this report. Included are discussions on prediction, mitigation, personnel safety and pipeline susceptibility. In Volume 2 techniques for performing the necessary calculations are

presented without proof or discussion. It is anticipated that Volume 2 will be useful as a workbook.

It was especially gratifying for those participating in the project to work in the atmosphere of cooperation that existed between the two sponsors.

Richard E. Kennon, Program Manager
Electrical Systems Division
EPRI

FOREWORD

This two volume reference book is a result of a program jointly funded by the Electric Power Research Institute (EPRI) and the Pipeline Research Committee (PRC) of the American Gas Association (A.G.A.). This program has consolidated known data and has made a systematic investigation into the mutual effects of ac electric power transmission lines (power lines) and natural gas transmission pipelines (pipelines) jointly sharing rights-of-way. The results presented here are of use to both the electric power and natural gas transmission industries for addressing problems arising from a mutual coexistence. Program objectives were:

1. to consolidate known data concerning mutual effects arising from power lines and pipelines sharing a common right-of-way.

2. to develop a unified and systematic method for predicting electromagnetically induced voltages and currents on pipelines; and

3. to investigate mitigation techniques to minimize interference effects upon pipeline and component reliability and personnel safety.

In the fulfillment of these objectives, new techniques for interference prediction and mitigation have been developed and other available data has been collected and summarized. The work performed during the program is presented in detail in Volume 1 of this book.

The overall objective of the program was to develop a reference book to present the information and the methodologies derived in a manner useful to both power and pipeline industry users in the design, construction and operation of their respective systems.

In compiling this book, advantage was taken of the knowledge available and applicable information has been categorized and summarized for inclusion into this book. However, in certain areas, existing gaps in knowledge became apparent, and original research was conducted to advance the state-of-the-art. From this work, several significant accomplishments have resulted which have been verified by field tests.

- A method for the prediction of electromagnetically coupled pipeline voltages and currents has been developed.
- Instrumentation has been developed for direct measurement of the longitudinal electric field from a power line.
- Techniques for the mitigation of induced interference on pipeline systems have been investigated and design procedures for the optimum implementation of these techniques have been developed.

The book consists of two volumes. Volume 1 contains detailed engineering analyses encompassing the areas of:

- Interference Level Prediction
- Susceptibility Evaluation
- Mitigation Techniques
- Measurement Procedures

A complete summary of Volume 1 is presented in Volume 1.

Volume 2 is a much synopsized version of Volume 1. The intent of the second volume is to provide the user with a procedures manual which will allow him to determine interference levels and estimate mitigation design requirements in the field. Hence, the material presented in this volume is restricted to coverage of objective 2 and a part of objective 3. More specifically, the following areas are covered:

1. Procedures for calculation of electrostatically and electromagnetically induced voltages and currents are presented in a concise manner. Even though similar material exists in Volume 1, the presentation here allows for more rapid access.
2. Discussion of mitigation procedures has been restricted to basically the use of grounding techniques. The reason for this approach is that the user in the field is generally faced with an "after the fact" situation. Other mitigation techniques such as pipeline and power line design modification are normally instituted during the planning stages of a project.

Liberal use of hand calculator programs, developed specifically for this book, is suggested to ease computational complexity. Since the underlying theory is not presented in this volume, it would be expected that the user have some familiarity with the contents of Volume 1 in order to answer questions of procedures applicability to the more difficult systems interaction situations.

AUTHORS

Principal authors are Dr. J. Dabkowski and Dr. A. Taflove. Dr. Dabkowski primarily acted in the capacity of project engineer and directed the field verification pipeline mitigation activities. Dr. Taflove was primarily responsible for development of the electromagnetic coupling equations, the pipeline equivalent circuit concept, and the hand calculator programs.

Dr. Dabkowski's specific technical contributions are the case histories of Section 3, the material in Section 7, and Appendices B, C, D and E. Dr. Taflove is responsible for the material in Section 2, the coupling analyses in Sections 3 and 4, and the calculator programs in Appendix A. Both authors contributed to Sections 8 and 9.

Other contributors to this manual are Mr. M. Genge, who authored Appendices F and G; Mr. V. Formanek, who contributed to Section 7; Dr. W. Wells, who wrote Section 5; and Dr. E. R. Whitehead, who authored Section 6.

ACKNOWLEDGEMENTS

The authors wish to thank Dr. A. R. Valentino, Manager of the IITRI EM Effects Section, for guidance and assistance; and Messrs. M. Genge, W. Lancaster and S. Tumarkin who contributed measurably to the success of the experimental portion of the program. Appreciation is extended to Ms. L. Wyatt for her timely and efficient secretarial support.

The authors also wish to thank the chairman of the EPRI/A.G.A. Steering Committee, Mr. R. E. Hodge, Natural Gas Pipeline Company of America; vice chairman, Mr. R. E. Kennon, EPRI; and other committee members, for their invaluable guidance throughout the program.

STEERING COMMITTEE MEMBERS

EPRI

R. E. Kennon, Vice Chairman
Electric Power Research Institute

E. H. Boesenberg
Commonwealth Edison Company

R. D. West
Duquesne Light Company

W. J. Fern (alternate)
Commonwealth Edison Company

A.G.A.

R. E. Hodge
Natural Gas Pipeline Co. of America

D. C. Anderson
Southern California Gas Company

F. E. Bower
El Paso Natural Gas Company

A. W. Hamlin (alternate)
Consumers Power Company

J. M. Holden, Secretary
American Gas Association

CONTENTS

ILLUSTRATIONS

ILLUSTRATIONS (Cont.)

ILLUSTRATIONS (Cont.)

ILLUSTRATIONS (Cont.)

ILLUSTRATIONS (Cont.)

TABLES

TABLES (Cont.)

SUMMARY

INTRODUCTION

This reference book, in two volumes, is a result of a program jointly funded by the Electric Power Research Institute (EPRI) and the Pipeline Research Committee (PRC) of the American Gas Association (A.G.A.). This program has consolidated known data and has made a systematic investigation into the mutual effects of ac electric power transmission lines (power lines) and natural gas transmission pipelines (pipelines) jointly sharing rights-of-way. The results of the program are of use to both the electric power and natural gas transmission industries for addressing problems arising from a mutual coexistence.

Program objectives were:

1. to consolidate known data concerning mutual effects arising from power lines and pipelines sharing a common corridor;

2. to develop a unified and systematic method for predicting electromagnetically induced voltages and currents on pipelines; and

3. to investigate mitigation techniques to minimize interference effects upon pipeline and component reliability and personnel safety.

The overall objective of the program was to develop a reference book to present the information and the methodologies derived in a manner useful to both power and pipeline industry users in the design, construction and operation of their respective systems. In the fulfillment of these objectives, new techniques for interference prediction and mitigation have been developed and other available data has been collected and summarized. Complete reporting of the work performed during the program is presented in Volume 1.

Advantage was taken of the knowledge available and applicable information has been ordered and summarized for inclusion into this book. However, in certain areas, existing gaps in knowledge became apparent, and original research was conducted so as to advance the state-of-the-art. From this work, several significant

original accomplishments have resulted which have been verified by field tests, namely,

- A method for the prediction of electromagnetically coupled pipeline voltages and currents has been developed.
- Instrumentation has been developed for direct measurement of the power line longitudinal electric field.
- Techniques for the mitigation of induced interference on pipeline systems have been investigated and design procedures for the optimum implementation of these techniques have been developed.

The book consists of two volumes. Volume 1 contains detailed engineering analyses encompassing the areas of:

- Interference Level Prediction
- Susceptibility Evaluation
- Mitigation Techniques
- Measurement Procedures

Listings for a set of hand calculator (Texas Instruments TI-59) programs developed specifically for this project are also presented. These programs are designed for use in predicting electromagnetic coupling levels and implementing subsequent mitigation procedures.

Volume 2 is a much synopsized version of Volume 1. The intent of this volume is to provide the user with a procedures manual which will allow him to predict interference levels and estimate mitigation design requirements in the field. Hence, the material presented in Volume 2 is restricted to coverage of objective 2 and a part of objective 3. More specifically, the following areas are covered:

1. Procedures for calculation of electrostatically and electromagnetically induced voltages and currents are presented in a concise manner. Even though similar material exists in Volume 1, the presentation here allows for more rapid access; and
2. Discussion of mitigation procedures has been restricted to basically the use of grounding techniques. The reason for this approach is that the user in the field is generally faced with an "after the fact" situation and other mitigation techniques such as pipeline network design or power line phasing are best instituted during the planning stages of a project.

TASK REVIEW

One of the initial tasks in assembling information for incorporation into this book was a literature search and review. Based on the results of this task, deficiencies in theory and practices were identified. Thus, the initial thrust was provided for the effort required to develop original information to complement this book. Highlights of the innovative work appearing in this book are as follows.

Interference Level Prediction

Electromagnetic Interference. Voltages and currents may be coupled into pipelines by several mechanisms, i.e., capacitive (electrostatic) inductive (electromagnetic) and resistive (conductive). Previously available techniques for the prediction of electromagnetically coupled voltages have been largely inaccurate. The research presented provides a unified and systematic solution to this prediction problem. One of the important breakthroughs in developing the prediction theory was to take advantage of the analogous electrical equivalence between a buried pipeline and a classical transmission line. This permitted representation of the pipeline by a Thevenin equivalent (electrical) circuit which, in turn, allowed prediction of pipeline behavior in a given coupling environment.

The method developed allows the prediction of the location and magnitude of coupled peak voltages all along a pipeline even for a complex interaction geometry.

Electrostatic Coupling. In reviewing the literature, it was found that available techniques for predicting electrostatic (above-ground pipeline) coupling levels were quite adequate. Hence, the material assembled in this book is essentially a compendium of existing information.

The two available analytical methods for predicting the voltages and shock currents electrostatically induced by electric power transmission lines on nearby above-ground pipelines are summarized. The first approach, the network solution method, translates the coupling problem to a circuit problem and solves the latter by inverting a potential coefficient matrix. This method involves considerable complexity for power lines with either multiple circuits or several shield wires. The second approach, the voltage gradient method, develops approximations for the peak voltage gradient and also the variation of the electrostatic field with distance from the power line and uses these approximations to obtain the pipeline induction effects.

Transient Coupling. It has been found that little analysis has been attempted for the case of transient coupling to buried pipelines. All previous attempts to estimate the inductive effects of power line faults have considered only 60 Hz coupling to an above-ground conductor and adequate methods do not appear to be available in the literature which are useful for calculating inductive coupling to buried pipelines due to either 60 Hz or high frequency power line transients.

For the case of the above-ground conductor, electrostatic or capacitive coupling determines the voltage induced when a switching or lightning induced transient appears on a power line phase conductor, and analytical methods for solution of this problem are available.

A very important transient effect is caused by the ground currents associated with a phase-to-ground fault. The ground current produces large potentials relative to remote earth on the power line structures. Formulas are available for the potential of the faulted structure and the soil potential in its vicinity. These results are used to estimate step and touch potentials and to find an upper limit on the voltage across pipeline coatings.

Lightning Exposure Parameters. Probabilities for the pipeline lightning exposure rate have been determined. An analytical/empirical expression for the relative number of lightning strokes in the vicinity of the pipeline when on the same right-of-way as a power line was developed.

It was found that the presence of a power line along the same right-of-way reduced the number of direct lightning strokes to buried natural gas transmission pipelines.

Susceptibility Evaluation

The effect of coupled voltages and currents on pipeline component reliability, pipe steel corrosion and related personnel hazards was reviewed. The results are summarized below.

Pipeline Component Reliability. A review of the literature to assess the effects of induced ac voltages on the reliability of pipeline components has yielded very little definitive data as to observed component susceptibility threshold levels.

Measured values of various voltages and currents on pipelines as obtained from a search of the open literature were gathered to determine the range of the induced levels and, thus, indicate the possible damage mechanisms that could occur. It was found that the high voltages and currents produced during a fault condition of a nearby power line can produce many types of damage to a pipeline and its components. The pipeline components which are mainly damaged during a fault, as reported in the literature, are pipeline coatings, the pipes themselves, insulating joints, and cathodic protection facilities.

Corrosion Effects. Corrosion data for various ac current levels are available from a number of sources. In general, inspection of the data from various investigators shows that test conditions were vastly different so that comparison of various data sets could not be easily made. The available data, however, were quantified according to the following variables: material, frequency, current density, electrolyte characteristics, and length of test. The results show that for ferrous materials at a frequency of 60 Hz, and for a wide variety of experimental test conditions and electrolyte characteristics, the ac corrosion effect on a long-term basis is approximately 0.01 to 0.1 percent of that of an equal magnitude dc current. It also appears that the application of cathodic protection will mitigate ac induced corrosion effects.

Electric Shock Effects on Humans. The work reported summarizes the effects of electric shock on humans, and includes data on dc, 60 Hz, and impulse shocks. Effects were evaluated by studying the available literature and presenting the data obtained in a unified form. Major areas investigated were perception, let-go, ventricular fibrillation, respiratory inhibition, and impulse current shocks. While no conclusions have been made regarding safety thresholds, a procedure to estimate potential effects is presented.

Mitigation Techniques

A review of previously available and a presentation of new design techniques for pipeline mitigation are presented. Much of the new material in this book, e.g., pipeline network design and use of horizontal grounding electrodes has been verified experimentally and represents a body of original work. New results have been obtained regarding design techniques for differently configured horizontal ground mitigation electrodes, the use of voltage cancellation techniques and requirements for pipeline mitigation over large distances.

Mitigation Techniques for Above-Ground Pipelines. During the construction of a pipeline, it is possible that long sections of pipe may rest above the ground surface. If the pipe is located near a high voltage ac power line, it can assume a large voltage-to-ground. The voltage is due to the capacitances between the power line conductors and the pipe, and between the pipe and ground, which form a capacitive voltage divider. Hazards caused by this voltage can be mitigated in three ways: (1) grounding of pipe sections; (2) bonding to the power system ground; and (3) construction of ground mats. The important elements of each mitigation approach are reviewed.

Mitigation Techniques for Buried Pipelines. Possibly the simplest technique is that of providing adequate spacing between the respective transmission systems. In the same vein, design of the pipeline network to minimize physical discontinuities is an extremely effective measure. Likewise, effective mitigation may be obtained by grounding of the pipeline near voltage maxima if the grounding impedance is significantly less than the pipeline characteristic impedance. Other mitigation techniques also investigated have been optimum power line phase sequencing and the use of an auxiliary screening conductor.

Measurements

AC measurement techniques and the effects of ac induced interference on dc measurements are reviewed. Knowledge of the magnitude and phase characteristics of the longitudinal electric field due to a power transmission line is required in order to predict electromagnetic coupling levels. Heretofore, instrumentation for the direct measurement has not been available and such instrumentation has been developed and field evaluated during the program.

A brief discussion of present practices with regard to ac field measurements is also given. It is shown that care must be taken in making ac measurements, since the accuracy of some measurements may be more affected than others. Two examples are given: (1) measurement of ac pipe-to-soil potential which is essentially unaffected by the presence of ac electric fields; and (2) measurement of ac pipeline current by the voltage drop technique which can present difficulties under certain conditions.

CONCLUSIONS

As a result of this program, available knowledge concerning mutual effects arising from power lines and pipelines sharing a common utility corridor has been collected, categorized, and summarized. In addition, new techniques for interference prediction, pipeline interference mitigation, and longitudinal electric field measurements have been developed.

This information is presented in this reference book as an aid to both power and pipeline industry users in the design, construction and operation of their respective systems.

Section 1

INTRODUCTION

OBJECTIVES

This reference book is a result of a program jointly funded and supervised by the Electric Power Research Institute (EPRI) and the Pipeline Research Committee (PRC) of the American Gas Association (A.G.A.). Program objectives were:

1. to consolidate known data concerning mutual effects arising from electric power transmission lines (power lines) and natural gas transmission pipelines (pipelines) sharing a common right-of-way (ROW) or utility corridor;

2. to develop a unified and systematic method for predicting electromagnetically induced voltages and currents on pipelines; and

3. to investigate mitigation techniques to minimize interference effects upon pipeline and component reliability and personnel safety.

In the fulfillment of these objectives, new techniques for interference prediction and mitigation have been developed and other available data has been collected and summarized. It is expected that the information presented will be useful to both power and pipeline industry users in the design, construction and operation of their respective systems in a state of coexistence.

PROLOGUE

The material presented herein is a combination of information obtained from available sources and new techniques investigated and developed especially for this book. Broadly, it may be characterized as follows:

- Interference Level Prediction
- Susceptibility Evaluation
- Mitigation Techniques
- Measurement Procedures

One of the initial tasks in assembling information for incorporation into this book was a literature search and review. Based on the results of this task, deficiencies in theory and practices were identified. Thusly, the initial thrust was provided for the direction of the effort required to develop original information to complement this book. Highlights of the innovative work appearing in this book are as follows.

Interference Level Prediction

Electromagnetic Interference. Voltages and currents may be coupled into pipelines by several mechanisms, i.e., capacitive (electrostatic) inductive (electromagnetic) and resistive (conductive). Section 3 considers the electromagnetic coupling process in considerable detail and represents a large portion of the original work done for this book. Previously available techniques for the prediction of electromagnetically coupled voltages have been largely inaccurate, and the developments presented here provide a unified and systematic solution to the prediction problem. One of the important breakthroughs in developing the prediction theory was to expand upon the concept that an analogous electrical equivalence exists between a buried pipeline and a classical transmission line.* This permitted representation of the pipeline by a Thevenin equivalent (electrical) circuit which, in turn, simplified the prediction of pipeline behavior in a given interference environment.

The essence of the approach is to model the pipeline as a classical transmission line assuming a distributed source voltage which is proportional to the parallel electric field existing at the pipeline.

The method developed allows prediction for coupled peak voltages all along a long length pipeline given the interaction geometry. Cases which can be handled by the method are:

---

*In this book, the words "classical transmission line" will always be used in the generic sense defined below:

> A system of two conductors separated by a dielectric material, or a single conductor with an earth return. The current flow in the system is affected by a distributed series inductance and resistance; the voltage between the conductors acts across a distributed shunt capacitance and conductance.

- Parallel configuration of a pipeline and a power line
- Nonparallel or intersecting configurations
- Combinations of parallel and nonparallel configurations
- Discontinuities such as
  - --power line transpositions
  - --power line terminations at a substation
  - --above/below ground junctions (pipelines)
  - --various pipeline terminations (insulators, etc.)
  - --variations in soil resistivity
- Combinations of multiple power lines and pipelines.

The basic theory can be easily extended to the calculation of the induced voltage distribution on a long pipeline which is composed of many buried and/or above ground sections having differing orientations with respect to the electric power line. The analysis is based upon the decomposition of the pipeline run into sections of uniform spatial properties, the replacement of pipeline sections by their Thevenin equivalent circuits, and the recombination of adjacent sections. The location of points along the pipeline of peak induced voltage can be found along with their magnitudes. The derivation of the required electrical pipeline parameters for constructing an equivalent circuit is covered in Section 2.

Section 3 concludes with five examples of "case histories" showing practical application and use of the developed theory.

Electrostatic Coupling. This coupling mechanism is reviewed in Section 4. In reviewing the literature, it was found that available techniques for predicting electrostatic (above-ground pipeline) coupling levels were quite adequate. Hence, the material assembled in this section is essentially a compendium of existing information.

The two available analytical methods for predicting the voltages and shock currents electrostatically induced by electric power transmission lines on nearby above-ground pipelines are summarized. The first approach, the network solution method, translates the coupling problem to a circuit problem and solves the latter by inverting a potential coefficient matrix. This method involves considerable

complexity for power lines with either multiple circuits and/or several shield wires. The second approach, the voltage gradient method, develops approximations for the peak voltage gradient and also the variation of the electrostatic field with distance from the power line and uses these approximations to obtain the pipeline induction effects. This approach is useful for many different power line configurations and is suitable for use with hand calculators.

Transient Coupling. Section 5 considers transients coupled to pipelines. It has been found that very little analysis has been done for the case of transient coupling to buried pipelines. All previous attempts to estimate the inductive effects of power line faults have considered only 60 Hz coupling to an above-ground conductor and adequate methods have not been discovered in the literature which were useful for calculating inductive coupling to buried pipelines due to either 60 Hz or high frequency power line transients.

For the case of the above-ground conductor, electrostatic or capacitive coupling determines the voltage induced when a switching or lightning induced transient appears on a power line phase conductor. An equivalent circuit analysis is used for solution. The transient becomes a double exponential time domain voltage source. The coupling is modeled using phase wire-to-pipeline and pipeline-to-ground capacitances. The latter is shunted by the internal impedance of a pipeline worker and/or by the impedance of a grounding electrode. The resulting pipeline voltage transient is also expressed as an energy equivalent which can be used to determine if a shock hazard exists.

A phase-to-ground fault is assumed as causing the principal transient problem in the methods described for studying the effects of electromagnetic and ground current coupling to pipelines. Transient electromagnetic or inductive coupling is similar to steady state inductive coupling except that one phase conductor has a much larger current than the others. Thus, the transient analysis may be based on the analytical techniques described for steady state electromagnetic coupling. The accuracy of this approach is dependent upon the bulk of the transient energy being in the 60 Hz portion of the spectrum.

A very important transient effect is caused by the ground currents associated with a phase-to-ground fault. The ground current produces large potentials relative to remote earth on the ac power line structures. Formulas are given for the potential of the faulted structure and the soil potential in its vicinity. These

results are used to estimate step and touch potentials and to find an upper limit on the voltage across pipeline coatings.

Lightning Exposure Parameters. Probabilities for pipeline lightning exposure rate are determined in Section 6. An analytical/empirical expression was developed for the relative number of lightning strokes in the vicinity of the pipeline when in proximity to the electric transmission system. For typical power line parameters, the results show an approximate doubling of the lightning stroke frequency due to the effective "gathering area" of the electrical transmission system. However, it appears that the pipeline will in the net suffer less overall voltage stress because of the following factors:

1. Even though the near stroke frequency rate is higher, the presence of the power line shield wires will cause the more severe strokes to be captured, thus providing a "protective umbrella" for the pipeline.

2. Additionally, ground ionization effects will mitigate against the occurrence of severe pipeline stress due to lightning strokes if the distance between the pipeline and the ground electrode, i.e., the power line structure, is about 20 meters or more.

In essence then, it was found that the presence of a power line along the same right-of-way actually reduced the number of direct lightning strokes to buried pipelines.

Susceptibility Evaluation

The effects of coupled voltages and currents on pipeline component reliability, pipe steel corrosion and related personnel hazards are covered in Section 7.

Pipeline Component Reliability. A review of the literature to assess the effects of induced ac voltages on the reliability of pipeline components has yielded very little definitive data as to observed component susceptibility threshold levels.

Measured values of various voltages and currents on pipelines as obtained from a search of the open literature were initially gathered to determine the range of the induced levels, and thusly, indicate the possible damage mechanisms that could occur. It was found that abnormal conditions occurring on a power line can cause much larger voltages and currents to be induced on nearby pipelines. One such dominant condition is a fault whereby one phase of the power line becomes grounded.

For this type of fault, very large current surges flow into the earth in the area at which the fault occured, which are then coupled into a nearby pipeline.

The high voltages and currents produced during a fault condition of a nearby power line can produce many types of damage (mostly due to arcing and heating) to a pipeline and its components. The pipeline components which are mainly damaged during a fault, as reported in the literature, are pipeline coatings, the pipes themselves, and insulating joints such as flanges used along the pipeline.

Corrosion Effects. Corrosion data for various ac current levels are available from a number of sources. In general, inspection of the data from various investigators shows that in many cases there was not only lack of consistency between the data from any one investigator, but also that test conditions were vastly different so that direct comparison of various data sets could not be easily made. The available data were quantified according to the following variables; material, frequency, current density, electrolyte characteristics, and length of test. The results obtained showed that for ferrous materials at a frequency of 60 Hz, and for a wide variety of experimental test conditions and electrolyte characteristics, the ac corrosion effect on a long-term basis is approximately 0.1 percent of that of an equal magnitude dc current. It also appears that the application of an adequate cathodic protection level will tend to mitigate ac induced corrosion effects.

Electric Shock Effects on Humans. The work reported summarizes the effects of electric shock on humans, and includes data on dc, 60 Hz and impulse shocks. Effects were evaluated by studying the available literature and presenting the data obtained in a unified form. Major areas investigated were perception, let-go, ventricular fibrillation, respiratory inhibition, and impulse current shocks. While no conclusions have been made regarding safety thresholds, a procedure to estimate potential effects is presented.

For example, to determine if personnel susceptibility exists in a given situation, it is necessary to determine the voltage and current levels that can be coupled from the system and compare these levels to the reported thresholds found in the literature. The problem that exists when attempting this is that voltages are the quantities usually measured or calculated for most systems, so these voltages must be converted into body currents. The problem in converting these voltages to currents is that the equivalent circuit used has resistances which are highly

variable both from a physiological and an operational viewpoint. That is, not only is the body resistance of a human highly variable, but there exists a wide range of possible scenarios that could change these conditions. To take care of such variability, worst case assumptions have been made so as to yield results on the "safe" conservative side when using the equivalent circuit to estimate coupling levels.

Mitigation Techniques

A review of previously available and a presentation of new design techniques for pipeline mitigation are presented in Section 8. Much of the new material in this section, e.g., pipeline network design and use of horizontal grounding electrodes has been verified experimentally and represents a body of recent work completed for this book. New results have been obtained regarding design techniques for differently configured horizontal ground mitigation electrodes, the use of voltage cancellation techniques and requirements for pipeline mitigation over large distances.

Other new techniques investigated and evaluated in Section 8 have been pipeline network design for mitigation and electric transmission line design to reduce electromagnetic coupling levels.

Mitigation Techniques for Above-Ground Pipelines. During the construction of a pipeline, it is possible that long sections of pipe may rest on or above the ground surface. If the pipe is located near a high voltage ac power line, it can assume a large voltage-to-ground. The voltage is due to capacitances between the power line conductors and the pipe, and between the pipe and ground, which form a capacitive voltage divider. This voltage can be mitigated in three ways: namely, (1) grounding of long pipe sections; (2) bonding to the power system ground; and (3) construction of ground mats. The important elements of each mitigation approach are reviewed in the book.

Mitigation Techniques for Buried Pipelines. Possibly the simplest technique is that of providing adequate spacing between the respective transmission systems. In the same vein, design of the pipeline network to minimize physical discontinuities is an extremely effective measure. Likewise, effective mitigation may be obtained by grounding of the pipeline near voltage maxima if the ac grounding impedance is significantly less than the pipeline characteristic impedance.

Typical pipeline grounding systems discussed in the text are vertical anodes, and horizontal conductors. Other mitigation techniques have also been investigated such as optimum power line phase sequencing and inductive interference mitigation by hanging an additional ground wire between adjacent structures below the phase conductors. By varying the height of the structure wire, an optimum interference reduction can be obtained for any phase configuration. However, practical limitations limit the usefulness of this technique.

Measurements

AC measurement techniques and the effects of ac induced interference on standard dc measurements are discussed in Section 9. Knowledge of the magnitude and phase characteristics of the longitudinal electric field due to a power line is required in order to predict electromagnetic coupling levels. Heretofore, instrumentation for the direct measurement has not been available. Such instrumentation has recently been developed and field evaluated, and is described in the text.

The material covers the use of probe wire techniques to determine: (1) longitudinal electric fields which provide the basic voltage coupling mechanism on pipelines; (2) the effect of the very high transverse electric fields present in the vicinity of the power line upon the accuracy of the probe wire measurements; and (3) the use of multi-point electrodes for obtaining grounding impedances.

A brief discussion of present practices with regard to ac field measurements is also given. It is shown here that care must be taken in making ac measurements, since the accuracy of some measurements may be more affected than others. Two examples are given: (1) measurement of ac pipe-to-soil potential which is essentially unaffected by the presence of ac electric fields; and (2) measurement of ac pipeline current by the voltage drop technique which can present difficulties under certain conditions.

Use of This Book

This volume contains the engineering analyses appropriate to the work performed. With discrimination, it may be used in the manner of a text. However, it should be expected that because of diverse engineering backgrounds, not all sections will be assimilable with equal facility. In this subsection, a brief description of each section and appendix is proffered, but perhaps what is more important for the guidance of the reader, is that the interrelationships between the various sections are given.

Coupling. Interference coupling mechanisms are discussed in Sections 3 through 6. Sections 4 through 6, i.e., electrostatic coupling, transient coupling and lightning exposure parameters are essentially self-contained and may be studied individually as the need arises.

Section 3 considers the prediction technique for steady state electromagnetic coupling. Use of this prediction technique requires knowledge of the pipeline equivalent circuit derivation, thus necessitating study of Section 2 as preparation. Appendices B and C can be considered supplemental to Section 3. Appendix B discusses longitudinal electric field measurements made under a 345 kV power line. It provides the reader with insight as to the temporal and spatial variations occurring in the electric field in the vicinity of a power line. Appendix C uses the method of symmetrical components to quantify the spatial variation in a more elegant manner. It also introduces a probability model which explains the time variations observed in electric field and pipeline voltages due to electric power line current unbalances.

Section 3 concludes with five "case history" examples wherein the prediction theory is applied in practical situations. Strict application of the theory requires the use of complex algebra and in order to spare the engineer the manual effort, required procedures have been programmed for the Texas Instruments TI-59 programmable desk hand calculator. Program descriptions and listings are presented in Appendix A.

When applying the prediction formulas to the situation where more than one conductor carrying an induced current is present on the ROW, mutual coupling between conductors must be considered. This effect is accounted for when using the hand calculator program CURRENTS if the length of parallelism between conductors is very large. For shorter parallel runs the currents computed by the program will be in error and too large. Appendix D provides a mathematical derivation which leads to a relatively simple remedy requiring only a modification in the inputting of the impedance matrix terms to the program.

Susceptibility. This material is presented in Section 7 and is essentially self-contained and independent of the other sections. It may be perused as the need arises in order to identify potential hazards to pipeline components and personnel.

Mitigation. Section 8 is a self-complete discourse on mitigation for electrostatic (above-ground), electromagnetic (below-ground) and transient coupling to pipelines. Known mitigation techniques are reviewed and discussion and examples of mitigation techniques recently investigated by IITRI such as pipeline network design, horizontal grounding electrodes, power line phase sequencing, and the use of grounded structure wires are given. The latter three techniques are discussed more comprehensively in Appendices E, F and G, respectively. Appendix E describes the Mojave Desert mitigation tests and the associated data reduction, while the latter appendices are primarily analytical studies of the proposed techniques.

Measurements. AC measurements and possible ac interference to dc measurements are discussed in Section 9 which is self-contained. Section 9 also discusses the electric field measurement instrumentation developed during the program. This instrumentation was used to obtain the electric field mapping discussed in Appendix B.

This volume contains all the technical material generated throughout the program. A synopsized and more direct presentation of the material pertaining to the prediction of electromagnetic and electrostatic coupling and mitigation is bound separately as Volume II.

Section 2

PIPELINE ELECTRICAL PARAMETERS

INTRODUCTION

The voltage/current prediction techniques discussed in the following sections, especially for the steady-state induction on a buried pipeline, are based upon the treatment of the pipeline as a lossy transmission line. Hence, its terminal behavior can be characterized from knowledge of its characteristic impedance, Z_o, and propagation constant, γ.

In this section, computer generated graphs are presented from which nominal values of these parameters may readily be obtained for most pipelines of interest. For situations where more accuracy is desired, the hand calculator program, PIPE, (c.f. Appendix A) is available.

Analysis of a Classical Transmission Line with a Distributed Source

In the analysis of the coupling of electromagnetic fields to a transmission line, the source of the voltage that drives the line is distributed along its length. The transmission line with a distributed source voltage is, by definition, one that has an increment of source voltage in each increment of line length. An element, dx in length, of such a transmission line is illustrated in Figure 2-1. Except for the source labeled E_x in the figure, this transmission line is identical to classical transmission lines, and the techniques for determining the impedance per unit length $Z = R + j\omega L$ and the admittance per unit length $Y = G + j\omega C$ are the same as for classical transmission lines. The source term E_x has the dimensions of electric field strength (V/m).

The differential equations for the voltage and current along the transmission line of Figure 2-1, for harmonically varying signals ($e^{j\omega t}$), are

$$\frac{dV}{dx} = E_x - IZ \qquad (2\text{-}1a)$$

$$\frac{dI}{dx} = - VY. \qquad (2\text{-}1b)$$

By differentiating one and substituting the other, the second-order differential equation can be obtained:

$$\frac{d^2V}{dx^2} - \gamma^2 V = \frac{dE_x}{dx} \tag{2-2a}$$

$$\frac{d^2I}{dx^2} - \gamma^2 I = - YE_x \tag{2-2b}$$

where

γ = transmission line propagation constant

= $\sqrt{ZY}$ meters^{-1}.

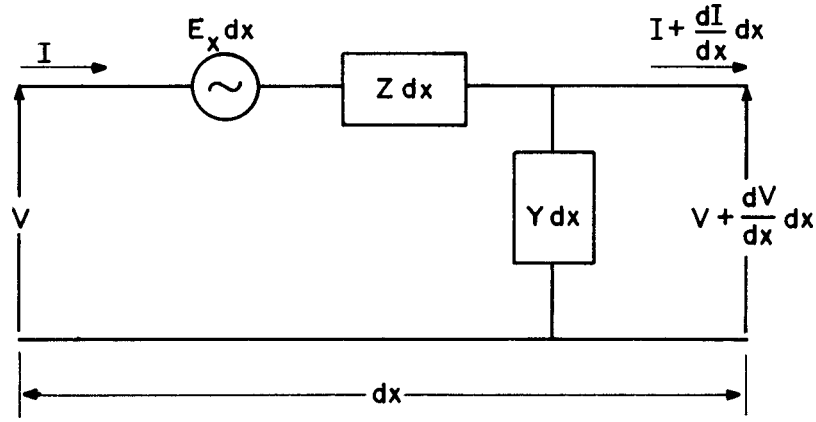

Figure 2-1. Equivalent Transmission Line Circuit

Except for the terms containing E_x, Equations 2-1 and 2-2 are identical to the equations for the classical transmission line. Assuming the terminating impedances Z_1 at $x = x_1$ and Z_2 at $x = x_2$ (for $x_2 > x_1$), the solutions to Equations 2-2a and 2-2b are

$$I(x) = \left[K_1 + P(x)\right]e^{-\gamma x} + \left[K_2 + Q(x)\right]e^{\gamma x} \text{ amperes} \tag{2-3a}$$

$$V(x) = Z_o\left\{\left[K_1 + P(x)\right]e^{-\gamma x} - \left[K_2 + Q(x)\right]e^{\gamma x}\right\} \text{ volts} \tag{2-3b}$$

where

Z_o = transmission line characteristic impedance

= $\sqrt{Z/Y}$ ohms

$$P(x) = \frac{1}{2Z_o}\int_{x_1}^{x} e^{\gamma s} E_x(s)\, ds \qquad (2\text{-}4a)$$

$$Q(x) = \frac{1}{2Z_o}\int_{x}^{x_1} e^{-\gamma s} E_x(s)\, ds \qquad (2\text{-}4b)$$

$E_x(s)$ = "undisturbed" electric field, i.e., the electric field that would exist along and parallel to the original path of a transmission line if the line were removed.

$$K_1 = \rho_1 e^{\gamma x_1} \frac{\rho_2 P(x_2) e^{-\gamma x_2} - Q(x_1) e^{\gamma x_2}}{e^{\gamma(x_2-x_1)} - \rho_1\rho_2 e^{-\gamma(x_2-x_1)}} \qquad (2\text{-}5a)$$

$$K_2 = \rho_2 e^{-\gamma x_2} \frac{\rho_1 Q(x_1) e^{\gamma x_1} - P(x_2) e^{-\gamma x_1}}{e^{\gamma(x_2-x_1)} - \rho_1\rho_2 e^{-\gamma(x_2-x_1)}} \qquad (2\text{-}5b)$$

ρ_1, ρ_2 are reflection coefficients given by:

$$\rho_1 = \frac{Z_1 - Z_o}{Z_1 + Z_o}; \qquad \rho_2 = \frac{Z_2 - Z_o}{Z_2 + Z_o} \qquad (2\text{-}6)$$

Using Equations 2-3 to 2-6, this analysis permits a unified treatment of inductive coupling to arbitrary above-ground and buried cables, conduits, and pipelines. With this approach, the transmission line characteristics of the conductor are accounted for by γ and Z_o. Therefore, the application of this analysis to a particular above-ground or buried pipeline is made simply by determining γ and Z_o of the pipeline, computing $E_x(s)$ and inserting these data into the appropriate coupling formula.

DETERMINATION OF THE TRANSMISSION LINE PARAMETERS OF A PIPELINE

The pipeline parameters, Z_o (characteristic impedance), and γ (propagation constant) are required for use in the coupling formulas and equivalent circuits developed in following sections of this book. Methods for determining these parameters are now discussed.

Above-Ground Pipeline

Propagation Constant. A simplified expression for the propagation constant, γ, of a pipeline of diameter, d, and height, h, above the ground may be derived (1).

$$\gamma = \frac{-\omega/c}{2\ln\left(\frac{4h}{d}\right)} \cdot \tan^{-1}\left(\frac{-1}{1+\sqrt{2\omega\tau_h}}\right) + j\frac{\omega}{c}\left[1 + \frac{1}{2\ln\left(\frac{4h}{d}\right)} \cdot \ln\sqrt{1 + \sqrt{\frac{2}{\omega\tau_h}} + \frac{1}{\omega\tau_h}}\right] m^{-1}$$

$$\simeq \frac{-\omega/c}{2\ln\left(\frac{4h}{d}\right)} \cdot \left(-\frac{\pi}{4}\right) + j\frac{\omega}{c}\left[1 + \frac{\ln\frac{2}{\sqrt{\omega\tau_h}}}{2\ln\left(\frac{4h}{d}\right)}\right] m^{-1}$$

$$\simeq \frac{4.93 \times 10^{-7}}{\ln\left(\frac{4h}{d}\right)} + j\,1.26 \times 10^{-6}\left[1 + \frac{\ln\frac{45.9}{h\sqrt{\sigma}}}{2\ln\frac{4h}{d}}\right] m^{-1} \qquad (2\text{-}7)$$

where

$\omega = 2\pi \cdot 60$ Hz

$\mu_o = 4\pi \cdot 10^{-7}$ H/m

$c = 3 \times 10^8$ m/s

σ = soil conductivity in mhos/m ($10^{-4} < \sigma < 10^{-1}$ is assumed. This is equivalent to a soil resistivity in the range of 10^3 to 10^6 ohm-cm.)

$\tau_h = \mu_o \sigma h^2$

$\gamma \equiv \alpha + j\beta\ m^{-1}$

Example 2-1: The propagation constant of a 0.508 m (20 inch) diameter pipeline located at a height of 1 m above $2 \cdot 10^4$ ohm-cm soil is to be determined.

Solution: The soil conductivity is simply $\sigma = 1/(2 \cdot 10^4$ ohm-cm) = 0.005 mho/m.

From Eq. 2-7,

$$\gamma \simeq \frac{4.93\cdot10^{-7}}{\ln\left(\frac{4\cdot1.0}{0.508}\right)} + j\ 1.26\cdot10^{-6}\left[1 + \frac{\ln\left(\frac{45.9}{1.0\sqrt{0.005}}\right)}{2\ln\left(\frac{4\cdot1.0}{0.508}\right)}\right]$$

$$\simeq 2.39\cdot10^{-7} + j\ 3.24\cdot10^{-6}\ m^{-1}$$

$$\simeq 2.39\cdot10^{-4} + j\ 3.24\cdot10^{-3}\ km^{-1}$$

Characteristic Impedance. In a similar manner, a simplified expression for the characteristic impedance, Z_o, of an above-ground pipeline may be derived.

$$Z_o = 60\ \ln\left(\frac{4h}{d}\right) + 30\ \ln\sqrt{1 + \sqrt{\frac{2}{\omega\tau_h}} + \frac{1}{\omega\tau_h}}$$

$$+ j\ 30\ \tan^{-1}\left(\frac{-1}{1 + \sqrt{2\omega\tau_h}}\right)\ \text{ohms}$$

$$\simeq 60\ \ln\left(\frac{4h}{d}\right) + 30\ \ln\left(\frac{1}{\sqrt{\omega\tau_h}}\right) + j\ 30\cdot\left(\frac{-\pi}{4}\right)\ \text{ohms}$$

$$\simeq 60\ \ln\left(\frac{4h}{d}\right) + 30\ \ln\left(\frac{45.9}{h\sqrt{\sigma}}\right) - j\ 23.6\ \text{ohms} \qquad (2\text{-}8)$$

Example 2-2: The characteristic impedance of the above-ground pipeline of Example 2-1 is to be determined.

Solution: From Eq. 2-8,

$$Z_o \simeq 60\ \ln\left(\frac{4\cdot1}{0.508}\right) + 30\ \ln\left(\frac{45.9}{1.0\sqrt{0.005}}\right) - j\ 23.6\ \text{ohms}$$

$$\simeq 123.8 + 194.3 - j\ 23.6\ \text{ohms}$$

$$\simeq 318.1 - j\ 23.6\ \text{ohms}.$$

Buried Pipeline

Buried Pipeline Propagation Constant, γ. From (2), the following transcendental equation for the propagation constant, γ, of a pipeline of radius, a, and burial depth, $\bar{h}$, is obtained:

$$\gamma^2\left[\frac{1}{Y_i} + \frac{\ln\left(\frac{1.12}{\gamma a'}\right)}{\pi(\sigma + \omega\varepsilon)}\right] = Z_i + \frac{j\omega\mu_o}{2\pi}\cdot\ln\left[\frac{1.85}{a'\sqrt{\gamma^2 + j\omega\mu_o(\sigma + j\omega\varepsilon)}}\right] \qquad (2\text{-}9)$$

where

$\omega = 2\pi \cdot 60$ Hz

$\mu_o = 4\pi \cdot 10^{-7}$ H/m

σ = soil conductivity in mhos/m

ε = soil permittivity in F/m

Y_i = admittance (mhos) per meter of pipeline coating

Z_i = pipeline internal impedance in ohms/m

$a' = \sqrt{a^2 + 4h^2}$ m

γ = Real(γ) + j Im(γ) $\equiv \alpha + j\beta$.

Hand calculator Program PIPE (c.f., Appendix A) solves Eq. 2-9 exactly using Newton's method for specific pipeline cases. However, to allow the user to obtain approximate data at a glance for a pipeline having nominal parameters, this section now presents graphical results for γ and Z_o. The following assumptions were made in developing these data:

1. The soil permittivity, ε, is equal to $3\varepsilon_o$, where ε_o is the permittivity of free space.

2. The steel used for the pipeline has an average resistivity, ρ_s, equal to $1.7 \cdot 10^{-7}$ ohm-m, and an average permeability, μ_s, equal to 300 μ_o, where μ_o is the permeability of free space. The usual pipe steel, depending upon chemical composition, may have a resistivity of from 15 to 20 $\mu\Omega$-cm, and depending upon magnetizing force a relative permeability of several hundred to a thousand or more. The nominal values used here are sufficiently accurate for present purposes, i.e., prediction of pipeline induced voltage levels.

3. The pipeline wall thickness, t, varies with the pipeline diameter, D, as

$$t = 0.132\ D^{0.421}$$

where t and D are in inches.

4. The pipeline internal impedance, $Z_i = R_i + jX_i$, is given as a function of ρ_s, μ_s, t, and D by the following expression derived from (3),

$$R_i = \frac{R_s}{(2\pi)(0.0127D)} \cdot \left[\frac{\sinh(t_n) + \sin(t_n)}{\cosh(t_n) - \cos(t_n)}\right]$$

$$X_i = \frac{R_s}{(2\pi)(0.0127D)} \cdot \left[\frac{\sinh(t_n) - \sin(t_n)}{\cosh(t_n) - \cos(t_n)}\right]$$

where

$$R_s = \sqrt{\pi \cdot 60\ \text{Hz} \cdot \mu_s \cdot \rho_s}$$

and

$$t_n = 0.0508 \cdot \frac{t \cdot R_s}{\rho_s}$$

5. $\bar{h} = 1$ meter .

The first assumption is completely non-critical because $\omega\varepsilon < 0.0001\ \sigma$ at 60 Hz for all values of σ considered and for all possible values of ε. The second, third, and fourth assumptions apply to the pipe steel skin depth and its effect upon Z_i. Assumption 2 assigns average values of resistivity and permeability to the pipe steel. Assumption 3 assigns pipe wall thicknesses based upon an exponential curve fit to available data for standard pipe. Assumption 4 takes Z_i to be the unit length impedance of a thin walled tubular conductor where the wall thickness is comparable to the electromagnetic skin depth. For practical purposes, the results are relatively insensitive to the exact values chosen for wall thickness and burial depth.

Real and Imaginary Parts of γ. Figures 2-2 and 2-9 graph the results obtained in the computer solution of Eq. 2-9 for the following soil resistivities: 1 kΩ-cm; 2 kΩ-cm; 4 kΩ-cm; 10 kΩ-cm; 20 kΩ-cm; 40 kΩ-cm; 100 kΩ-cm; and 200 kΩ-cm. Each figure plots Real(γ) and Im(γ) as a function of pipe diameter from 2 inches to 48 inches for pipe coating resistivities of zero (bare pipe), 1 kΩ-ft^2, 10 kΩ-ft^2, 100 kΩ-ft^2, and 1 MΩ-ft^2.

The figures indicate that the principal effect of the pipe coating is to decrease both Real(γ) and Im(γ) from the bare pipe values at any particular pipe diameter. As expected, well coated pipes having coating

resistivities exceeding 100 kΩ-ft^2 have values of Real(γ) and Im(γ) virtually unaffected by the resistivity of the surrounding soil. On the other hand, bare or poorly coated pipes have values of γ that can vary by as much as ten to one, depending upon the soil resistivity.

Example 2-3: The propagation constant of 0.508 m (20 inch) diameter pipeline having a coating resistance of $5 \cdot 10^4$ ohms-ft^2 and buried in $2 \cdot 10^4$ ohm-cm soil, is to be estimated.

Solution: The soil conductivity is simply $\sigma = 1/(2 \cdot 10^4 \text{ ohm-cm}) = 0.005$ mho/m. Figure 2-6 is seen to give graphs of the real and imaginary parts of the propagation constant for this soil conductivity. In Figure 2-6, the curves for a coating resistance of 50 kΩ-ft^2 are interpolated. At a pipe diameter of 20 inches, the following propagation constant value is read off from the curves

$$\gamma \simeq 0.27 + j\,0.24 \text{ km}^{-1}$$
$$\equiv \alpha + j\beta \quad .$$

This propagation constant value can be directly compared to that for the same pipeline located 1 m above the earth's surface, obtained in Example 2-1. α for the buried pipeline is seen to be 1000 times larger than α for the above-ground pipeline; β is seen to be 75 times larger than that for the above-ground case.

Buried Pipeline Characteristic Impedance, Z_0. From (2), the following equation relating the characteristic impedance, Z_0, of a pipeline of radius, a, and burial depth, $\bar{h}$, to its propagation constant, γ, is obtained:

$$Z_0 = \gamma \cdot \left[\frac{1}{Y_i} + \frac{\ln\left(\frac{1.12}{\gamma a'}\right)}{\pi(\sigma + j\omega\varepsilon)} \right] \tag{2-10}$$

where γ is obtained by solving Eq. 2-9, and Y_i, a', σ, and ε are defined as before.

The solution of Eq. 2-10 has been programmed on a computer to obtain easily used graphical results for Z_0. Figures 2-10 to 2-17 graph these results for the same set of soil resistivities and pipe coating resistivities used in the previous graphs for the propagation constant.

The figures indicate that the principal effect of the pipe coating is to increase both Real$|Z_0|$ and Im(Z_0) from the bare pipe values at any particular pipe diameter.

Well coated pipes having coating resistivities exceeding 100 kΩ-ft^2 have values of Z_o virtually unaffected by the resistivity of the surrounding soil. On the other hand, poorly coated pipes have values of Z_o that can vary by as much as ten to one, depending upon the soil resistivity.

Example 2-4: The characteristic impedance of the buried pipeline of Example 2-3 is to be estimated.

Solution: Figure 2-14 gives the graphs of the real and imaginary parts of the characteristic impedance for the 0.005 mhos/m soil conductivity. By interpolation, the curves for a coating resistance of 50 kΩ-ft^2 are located. Values read from the curves yield

$$Z_o = 1.1 + j\ 0.9 \text{ ohms.}$$

FIELD ESTIMATION OF Z_o

Knowledge of both the propagation constant γ, and the characteristic impedance Z_o, is necessary in order to determine the induced voltage profile on a pipeline. As seen from the preceding graphs, determination of both quantities requires the pipe coating resistivity to be known, which in many situations can only be estimated.

This problem of establishing the pipeline electrical parameters may be solved in a practical manner for a pipeline wherein access to a reasonably good grounding system, such as a road casing, is possible. At the location where the ground system exists (this site must also be far enough away from any points of pipeline discontinuity so that the characteristic impedance level is established), the pipeline is shorted to ground and the drop in the pipeline induced voltage level is measured along with the impedance of the ground to remote earth. Insertion of these measured values into the pipeline Thevenin equivalent circuit (c.f. Section 3) will allow calculation of Z_o. Entering the preceding characteristic impedance curves with this value of Z_o, allows an estimate for the coating resistivity to be made. With this information, an estimate of the propagation constant can also then be made using the preceding γ curves.

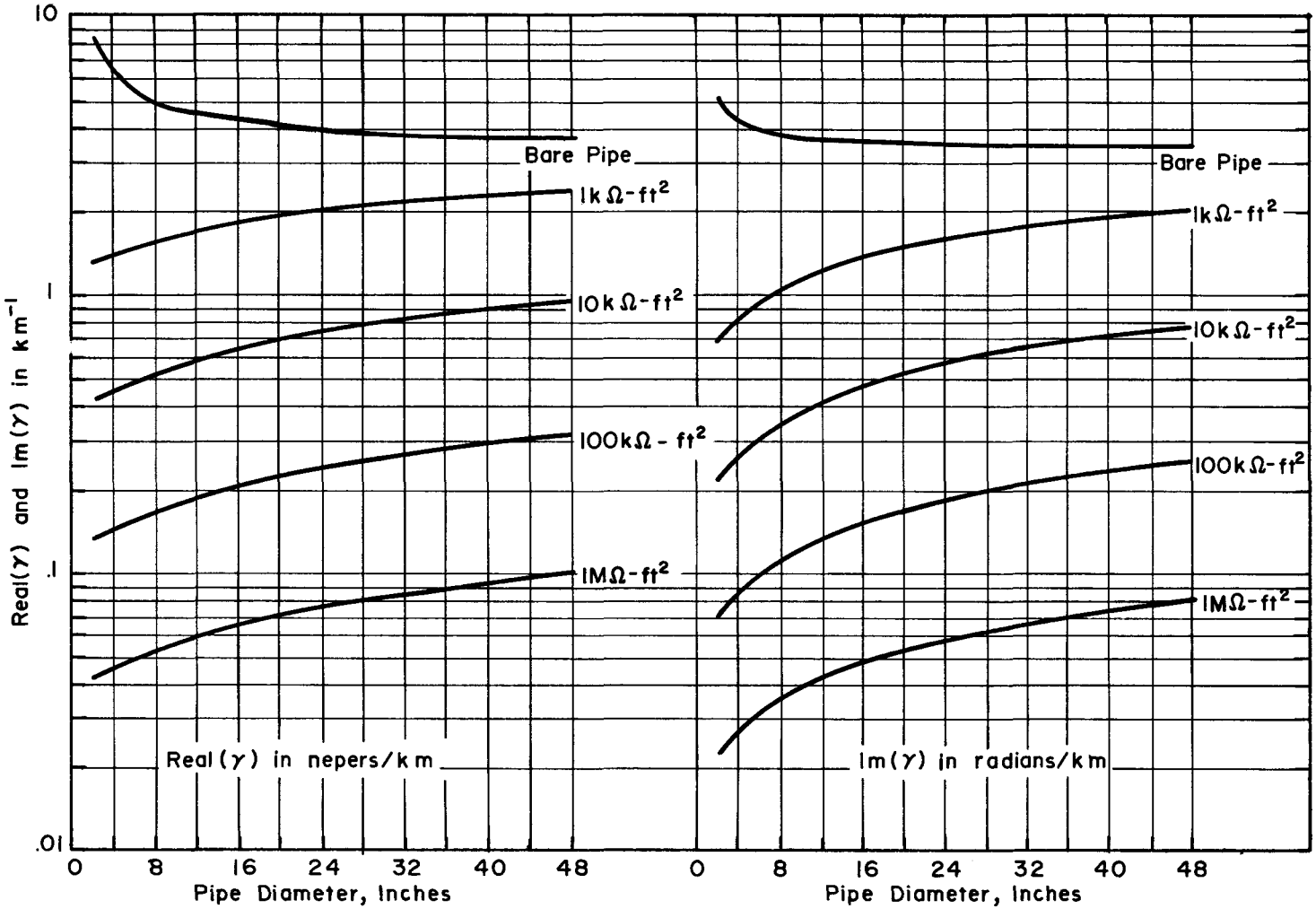

Fig. 2-2 BURIED PIPELINE PROPAGATION CONSTANT, γ, FOR $\rho = 1k\Omega\text{-cm}$ ($\sigma = 0.1$ mho/m) SOIL

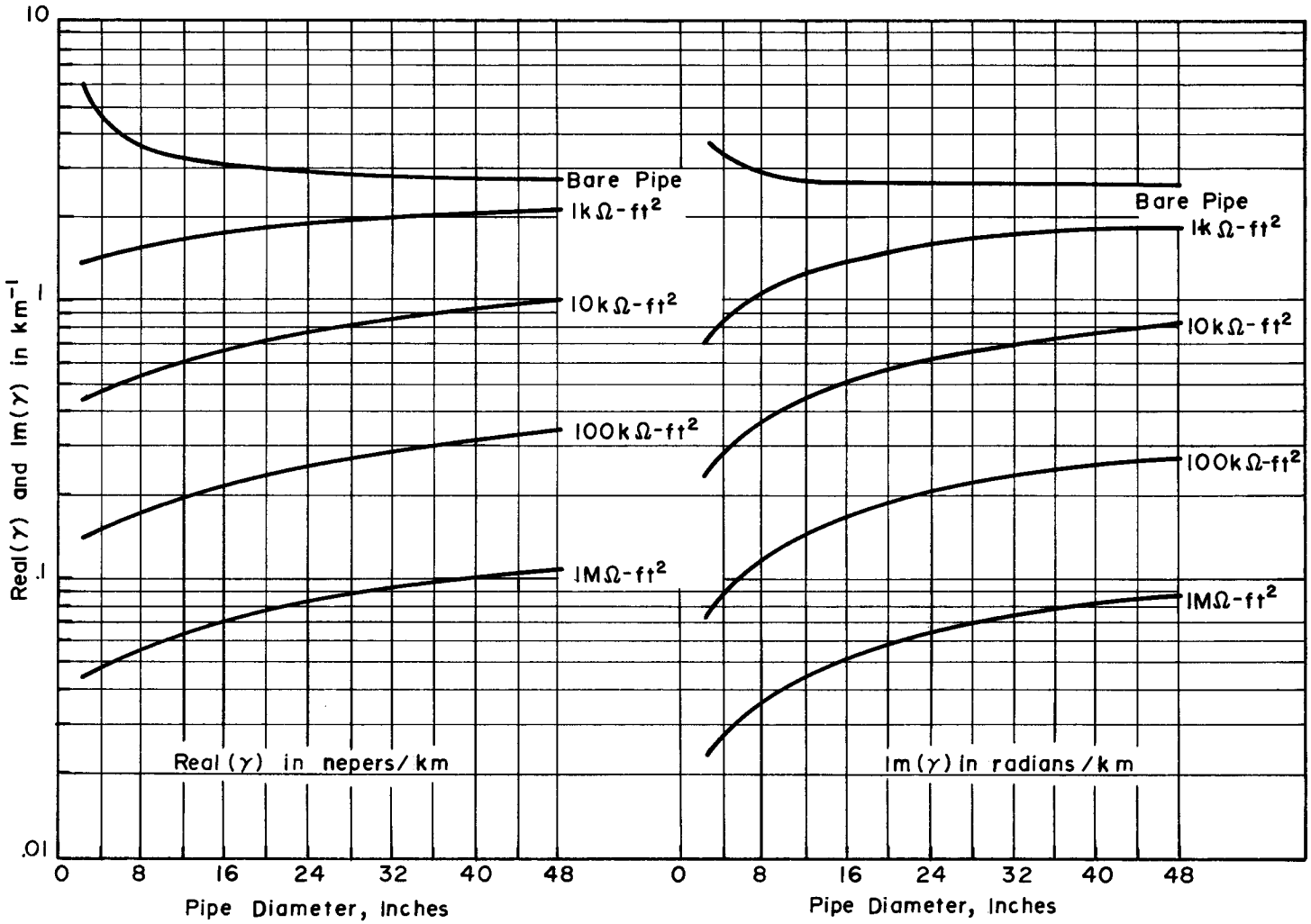

Fig.2-3 BURIED PIPELINE PROPAGATION CONSTANT, γ, FOR $\rho = 2\,k\Omega$-cm ($\sigma = 0.05$ mho/m) SOIL

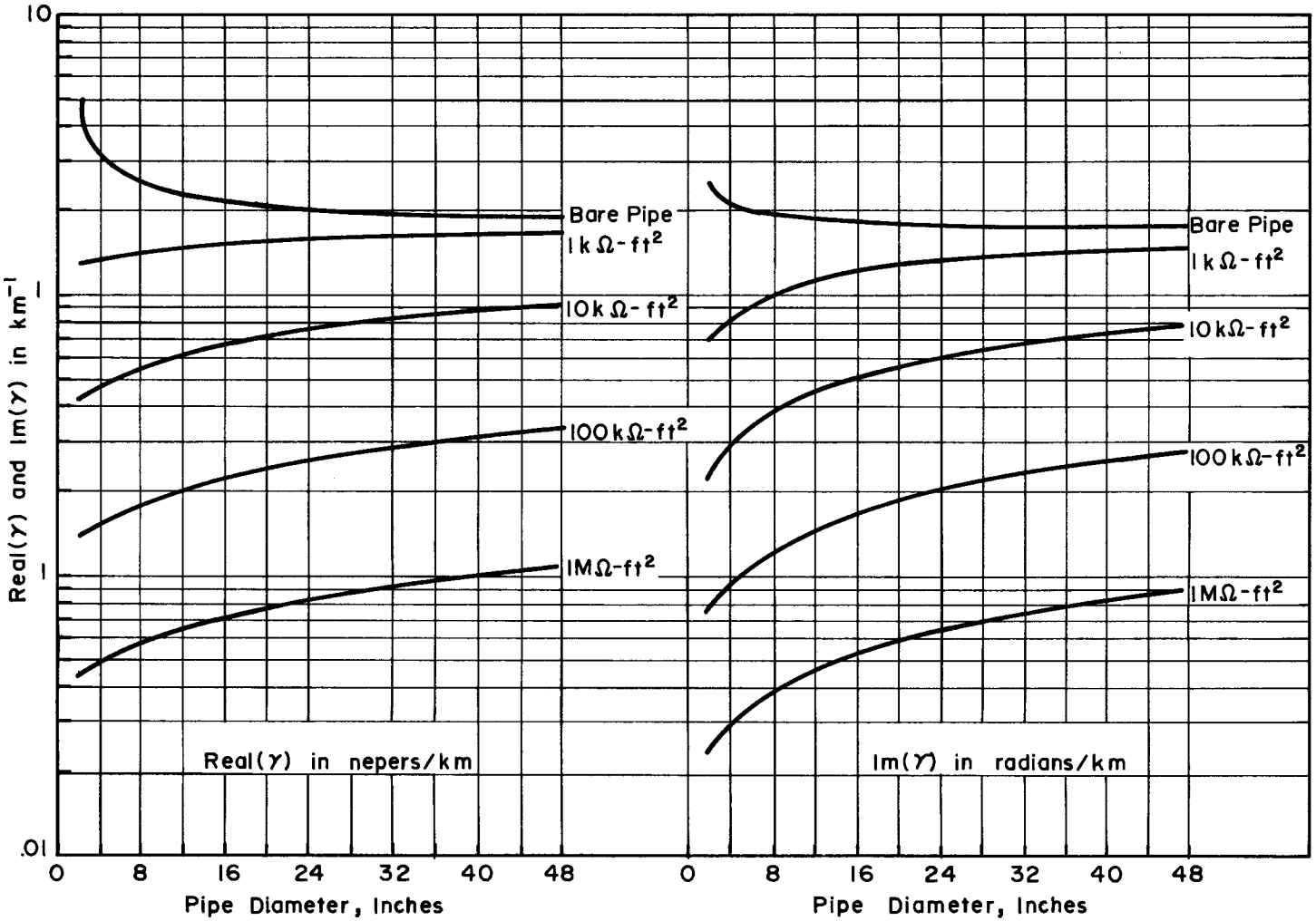

Fig. 2-4 BURIED PIPELINE PROPAGATION CONSTANT, γ, FOR $\rho = 4\,k\Omega\text{-cm}$ ($\sigma = 0.025$ mho/m) SOIL

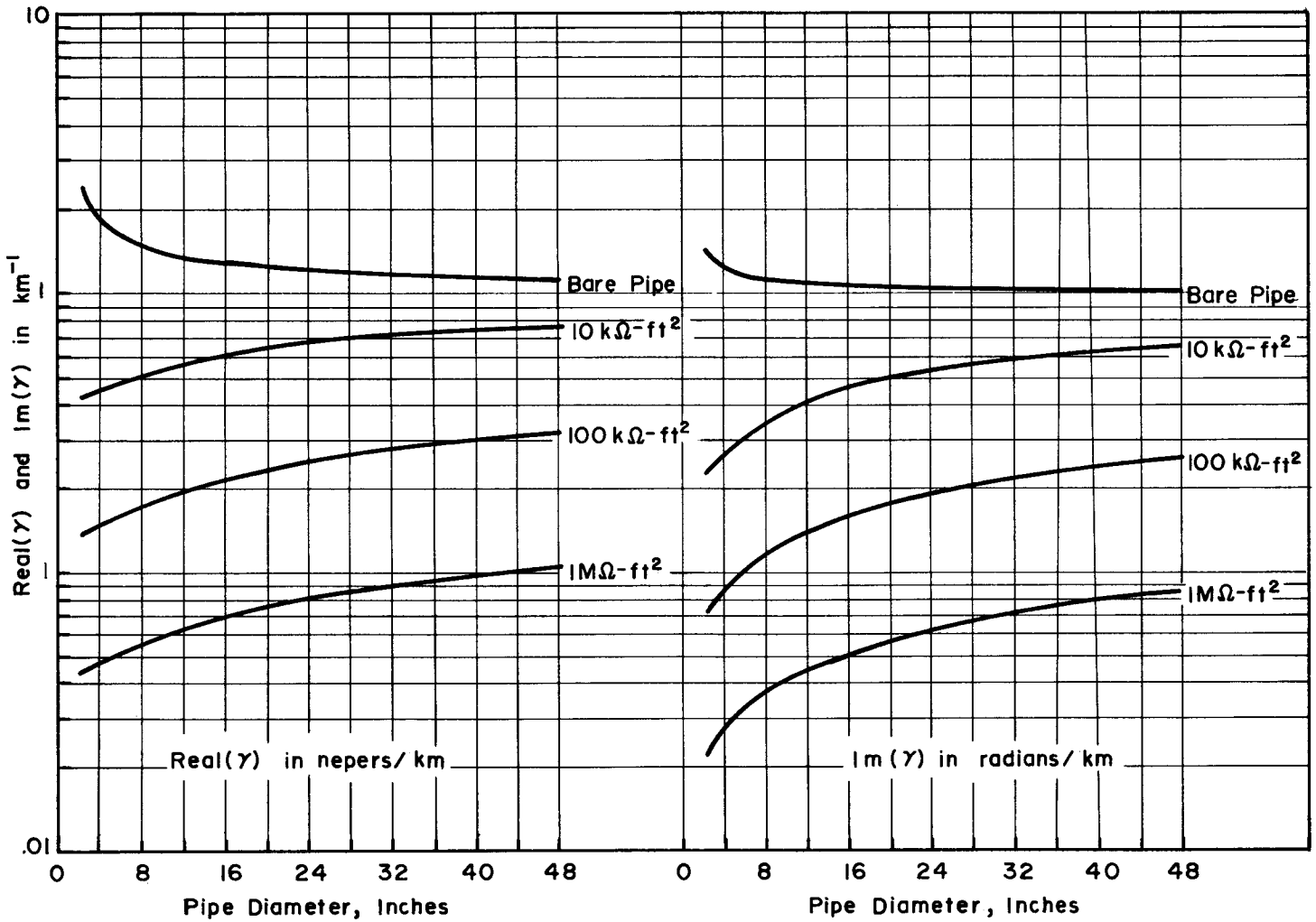

Fig. 2-5 BURIED PIPELINE PROPAGATION CONSTANT, γ, FOR $\rho = 10\,k\Omega\text{-cm}$ ($\sigma = 0.01$ mho/m) SOIL

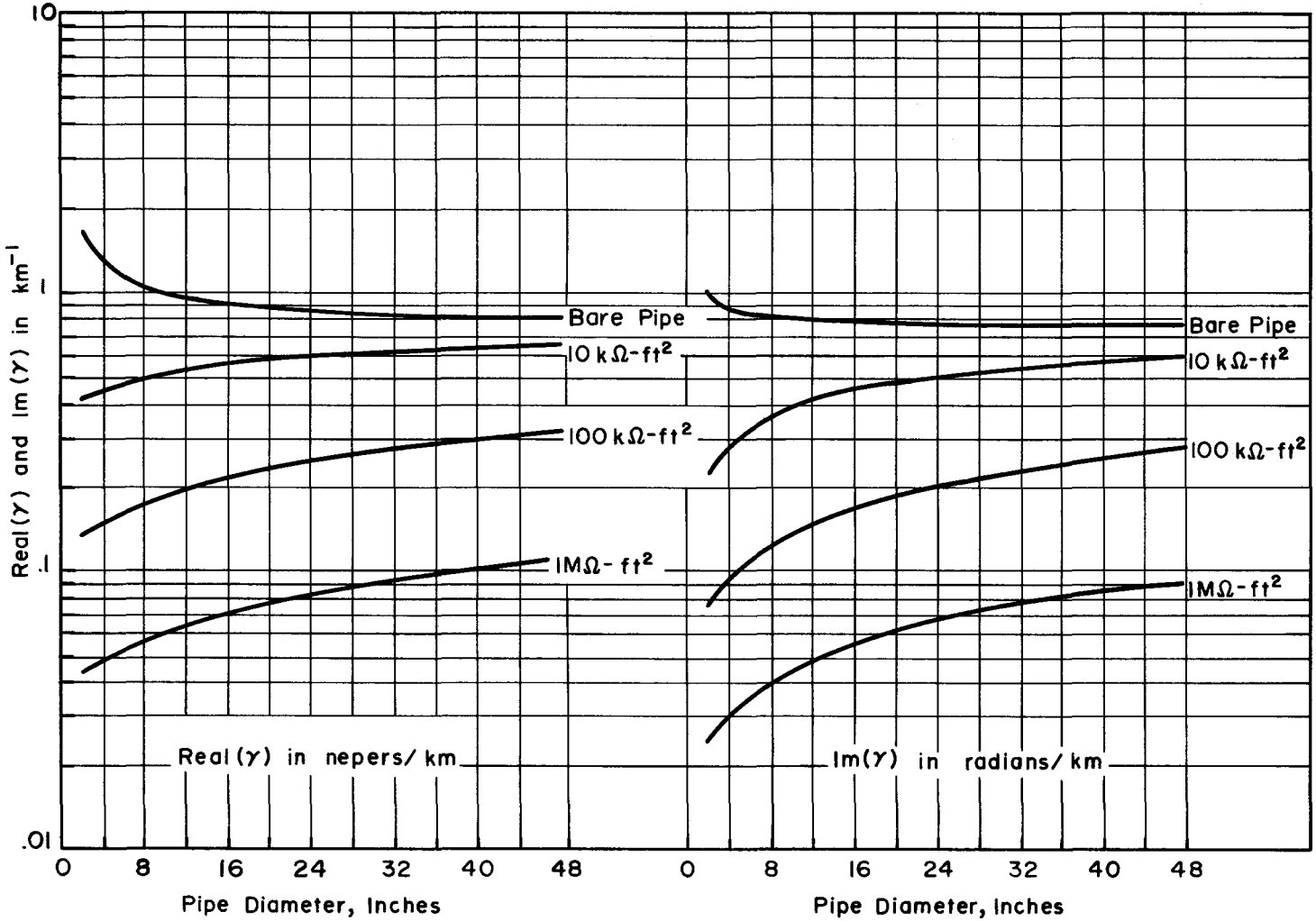

Fig. 2-6 BURIED PIPELINE PROPAGATION CONSTANT, γ, FOR $\rho = 20\,k\Omega\text{-cm}$ ($\sigma = 0.005$ mho/m) SOIL

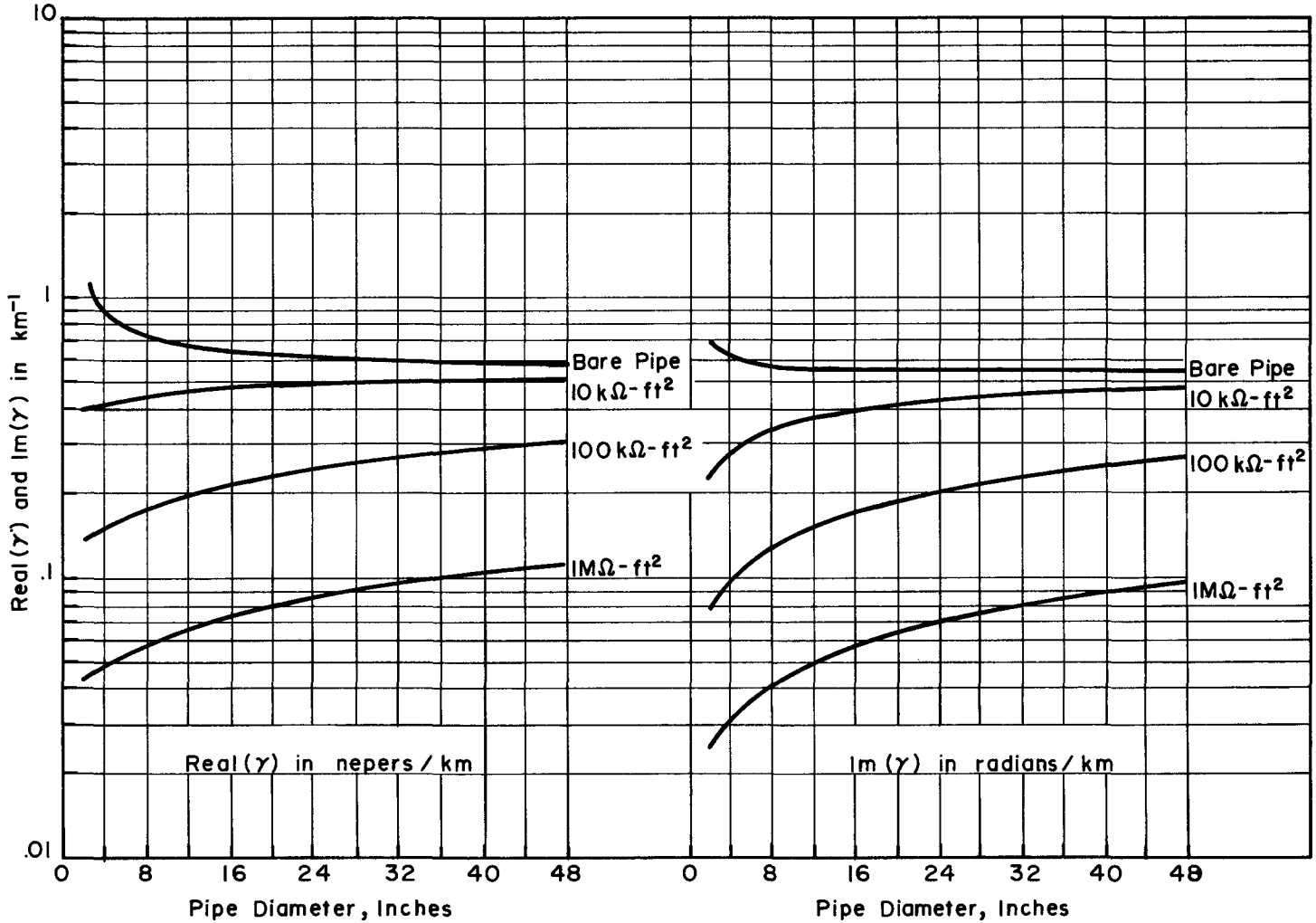

Fig.2-7 BURIED PIPELINE PROPAGATION CONSTANT, γ, FOR $\rho = 40\ k\Omega\text{-cm}$ ($\sigma = 0.0025$ mho/m) SOIL

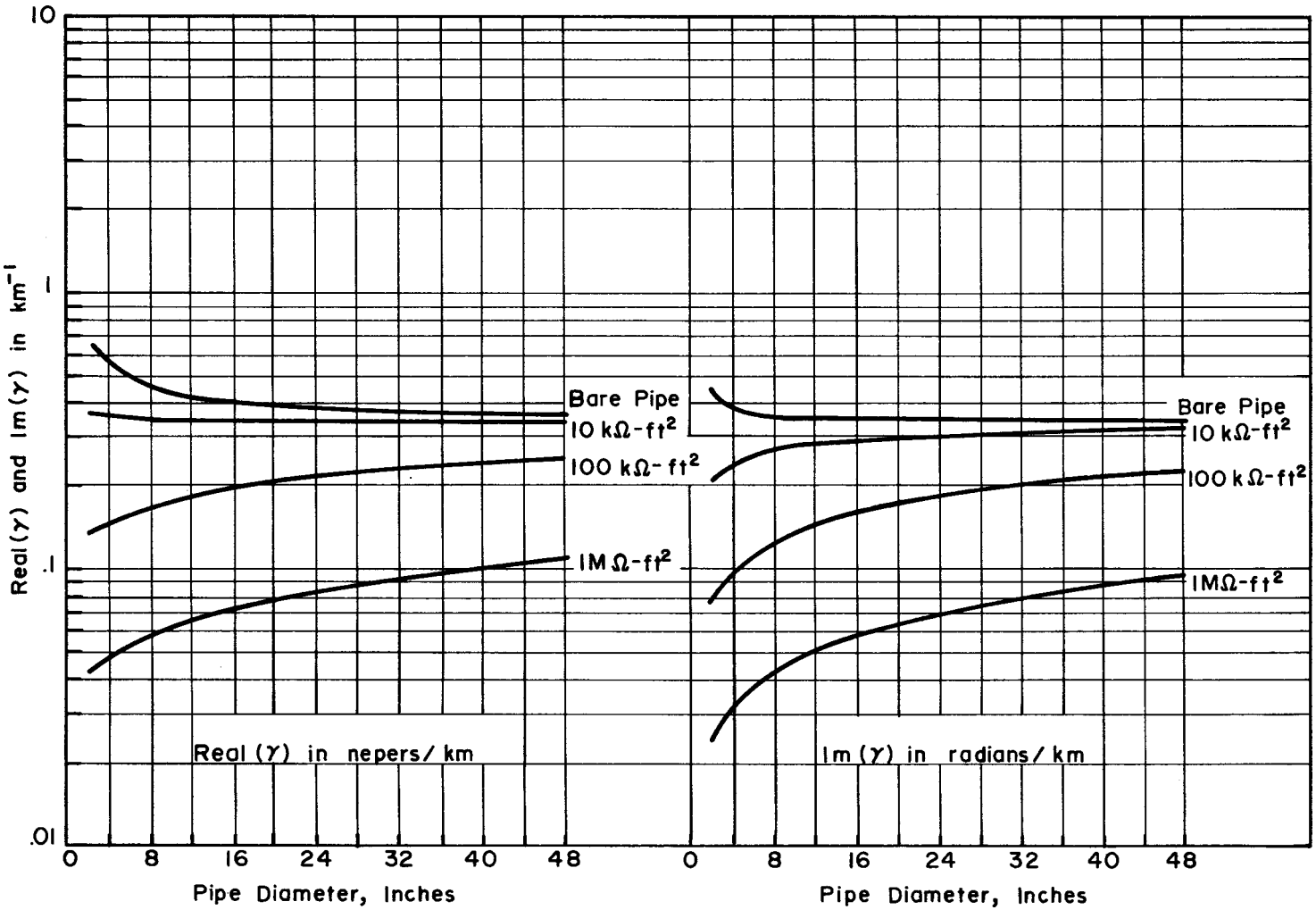

Fig. 2-8 BURIED PIPELINE PROPAGATION CONSTANT, γ, FOR $\rho = 100\,k\Omega\text{-cm}$ ($\sigma = 0.001$ mho/m) SOIL

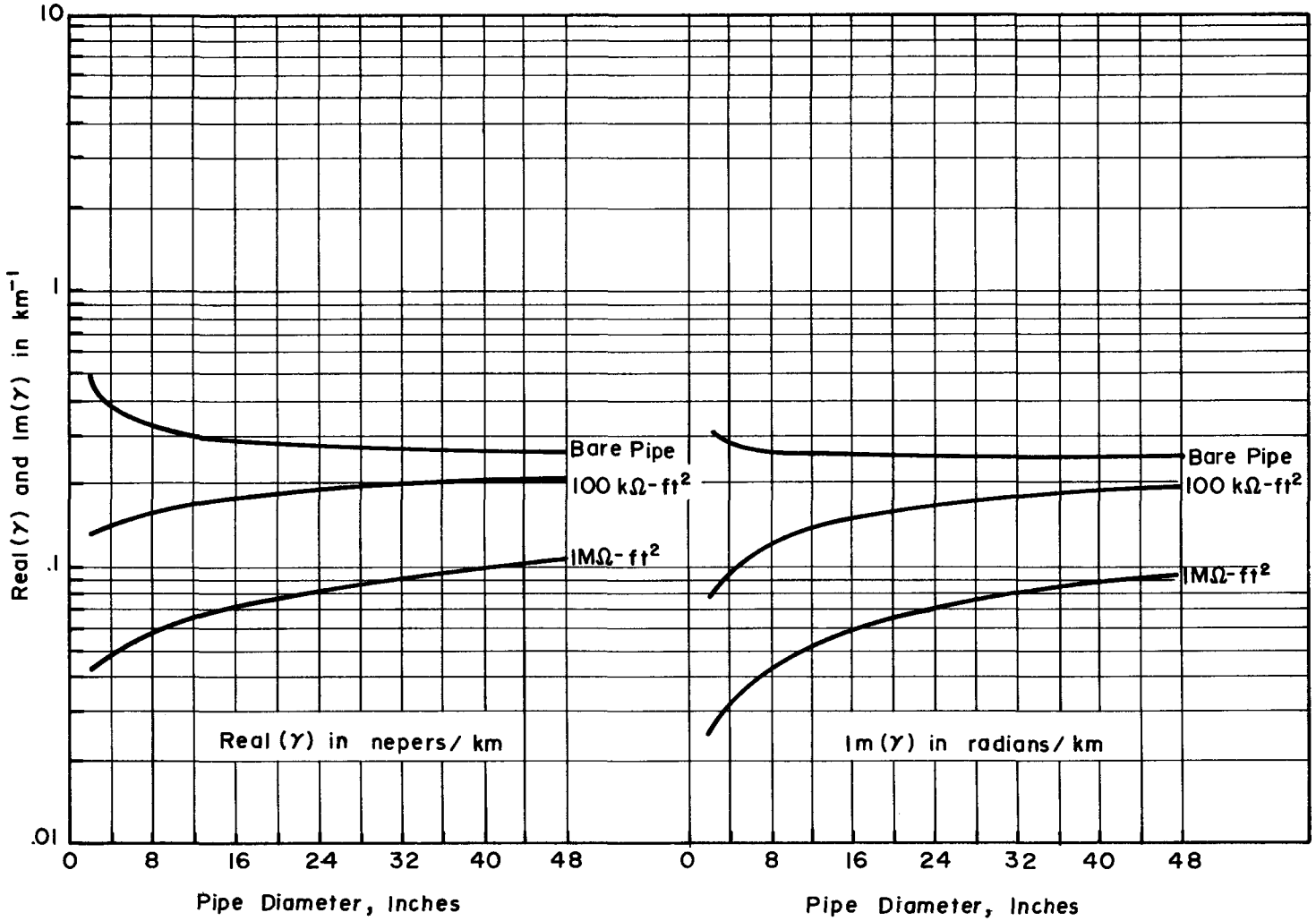

Fig. 2-9 BURIED PIPELINE PROPAGATION CONSTANT, γ, FOR ρ=200 kΩ-cm (σ=0.0005mho/m) SOIL

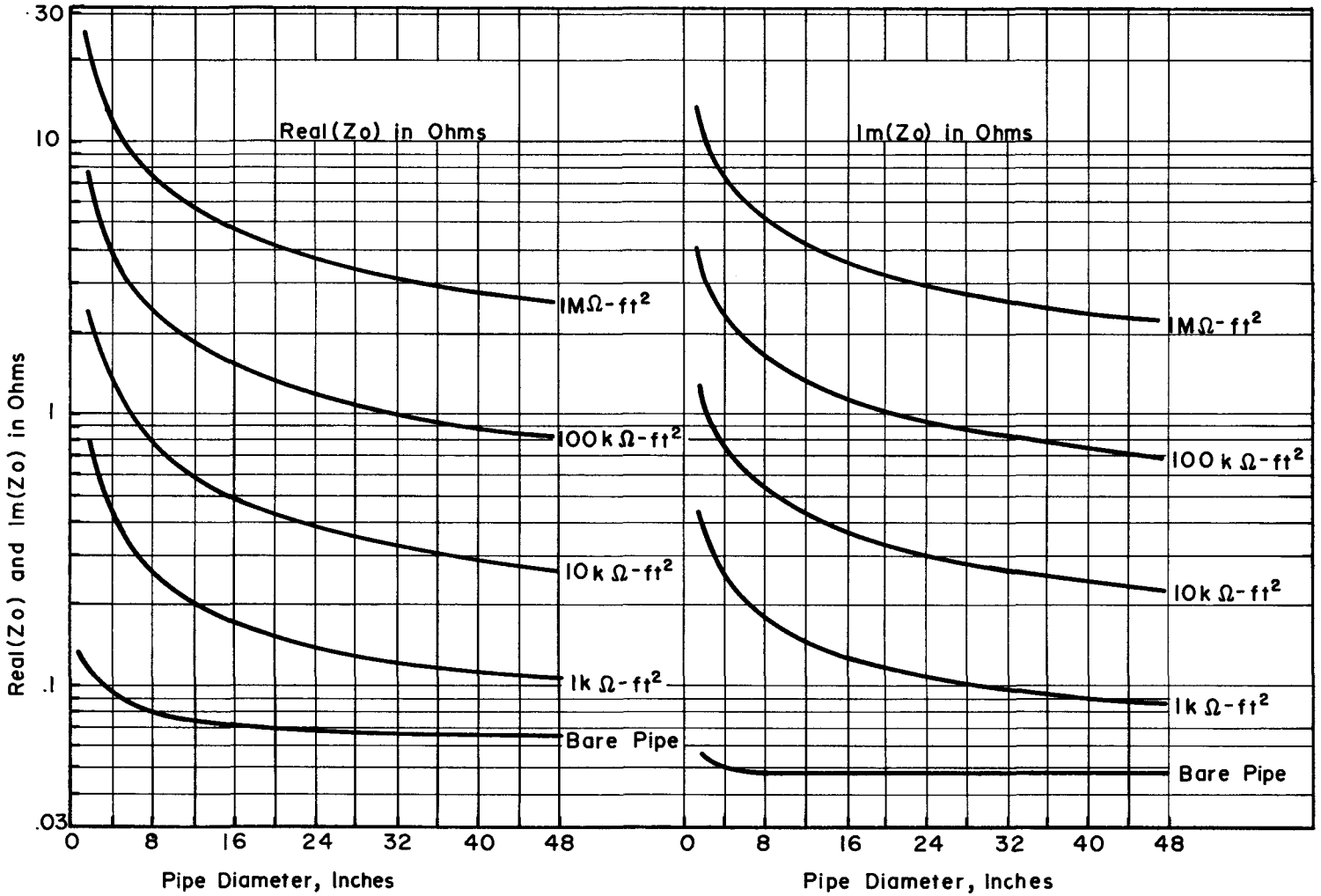

Fig. 2-10 BURIED PIPELINE CHARACTERISTIC IMPEDANCE, Z_o, FOR ρ = 1 kΩ-cm (σ = 0.1 mho/m) SOIL

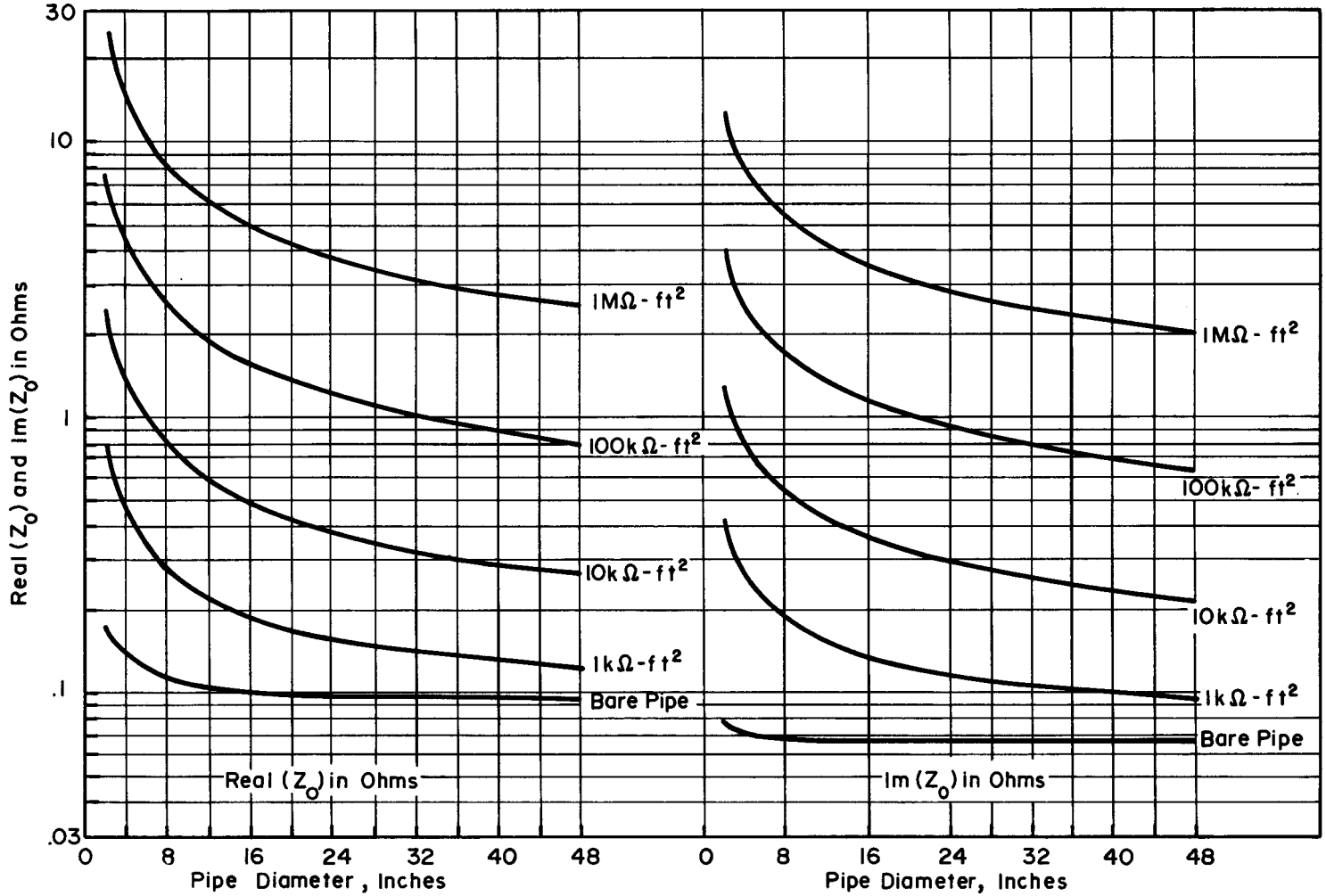

Fig. 2- 11 BURIED PIPELINE CHARACTERISTIC IMPEDANCE, Z_0, FOR $\rho = 2\,k\Omega\text{-cm}$ ($\sigma = 0.05$ mho/m) SOIL

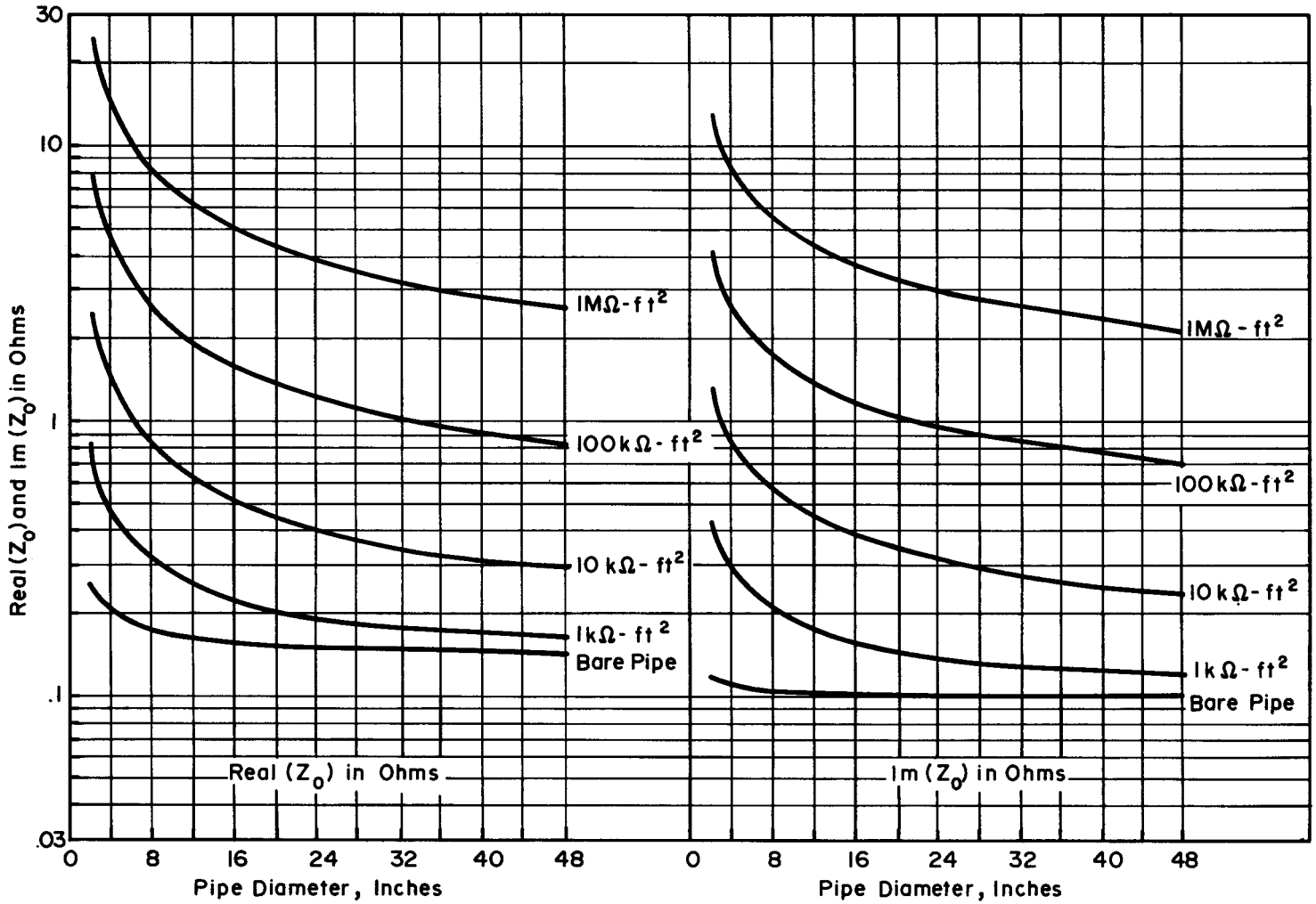

Fig. 2- 12 BURIED PIPELINE CHARACTERISTIC IMPEDANCE, Z_0, FOR $\rho = 4\,k\,\Omega$-cm (σ=0.025 mho/m) SOIL

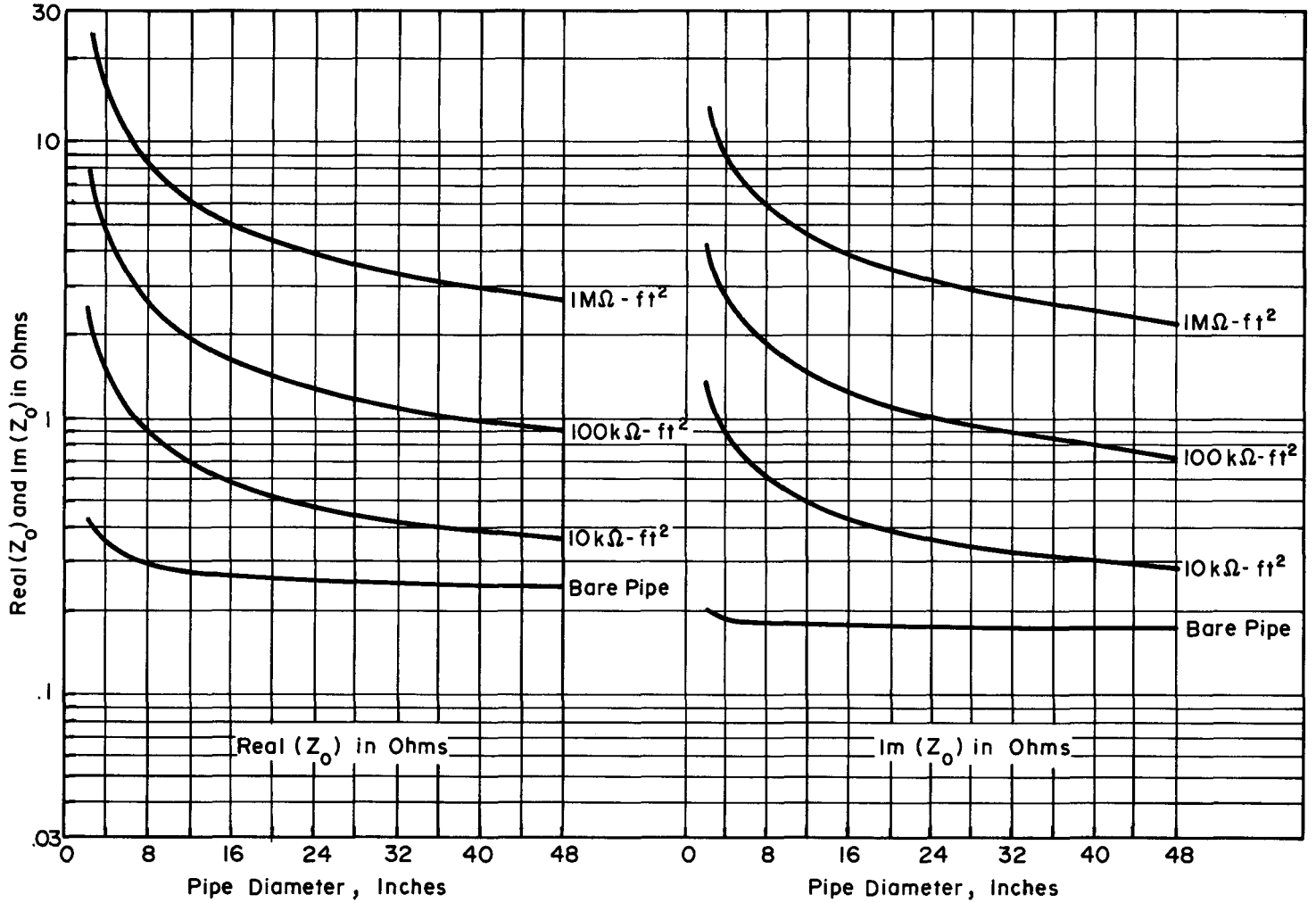

Fig.2-13 BURIED PIPELINE CHARACTERISTIC IMPEDANCE, Z_0, FOR ρ = 10 kΩ-cm (σ = 0.01 mho/m) SOIL

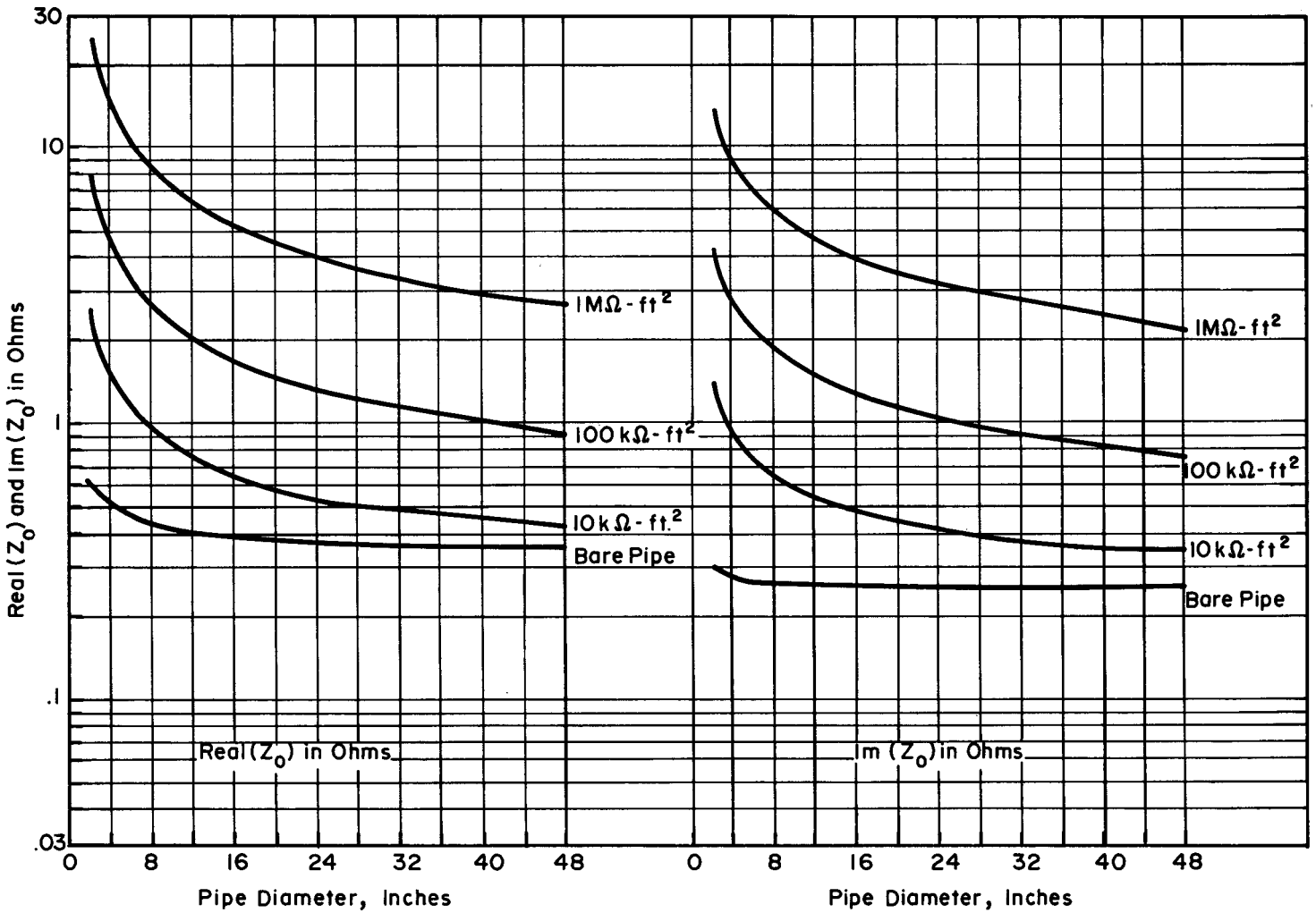

Fig. 2-14 BURIED PIPELINE CHARACTERISTIC IMPEDANCE, Z_0, FOR $\rho = 20\ k\Omega$-cm ($\sigma = 0.005$ mho/m) SOIL

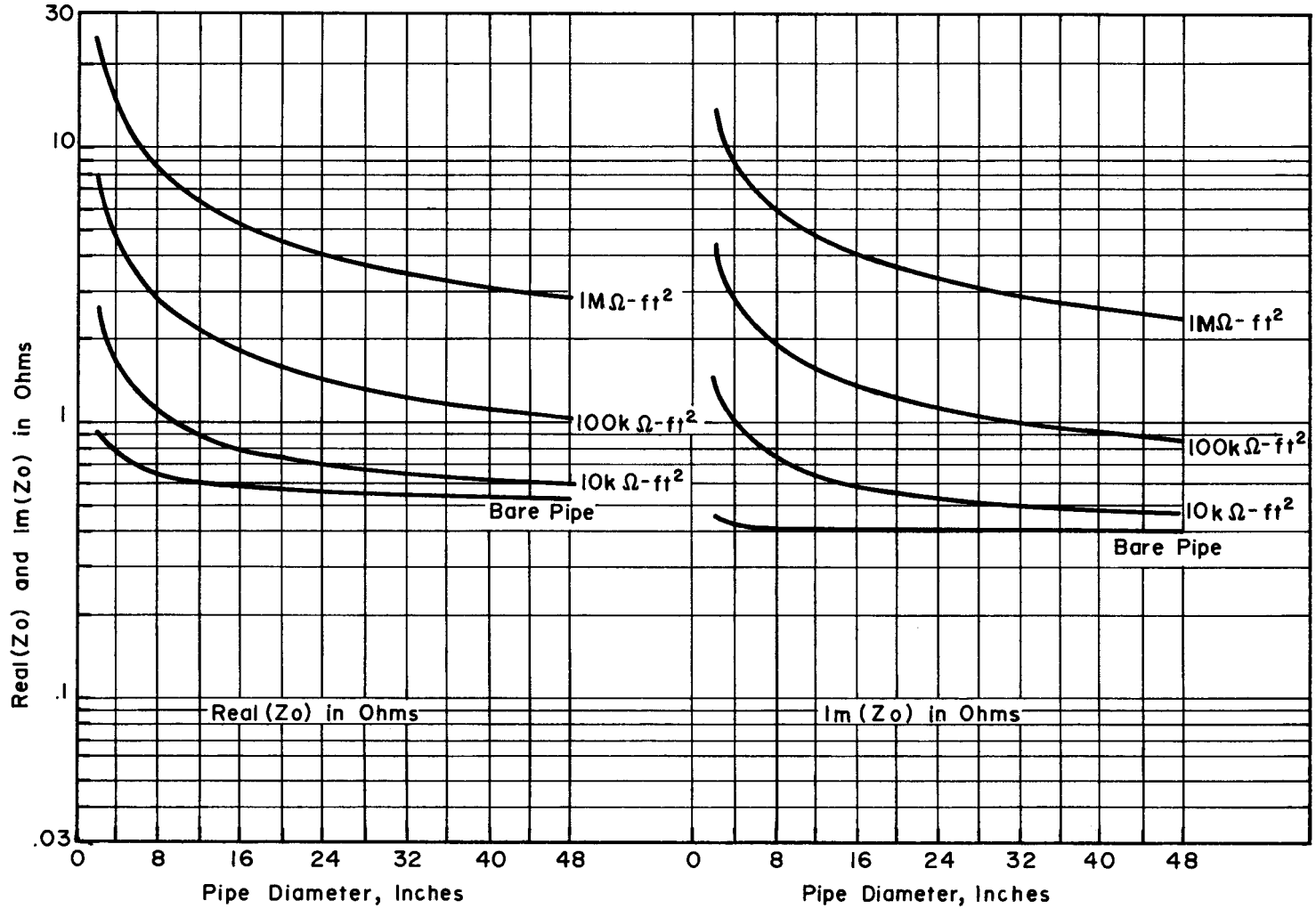

Fig.2-15 BURIED PIPELINE CHARACTERISTIC IMPEDANCE, Z_o, FOR $\rho = 40k\,\Omega$-cm ($\sigma = 0.0025$ mho/m) SOIL

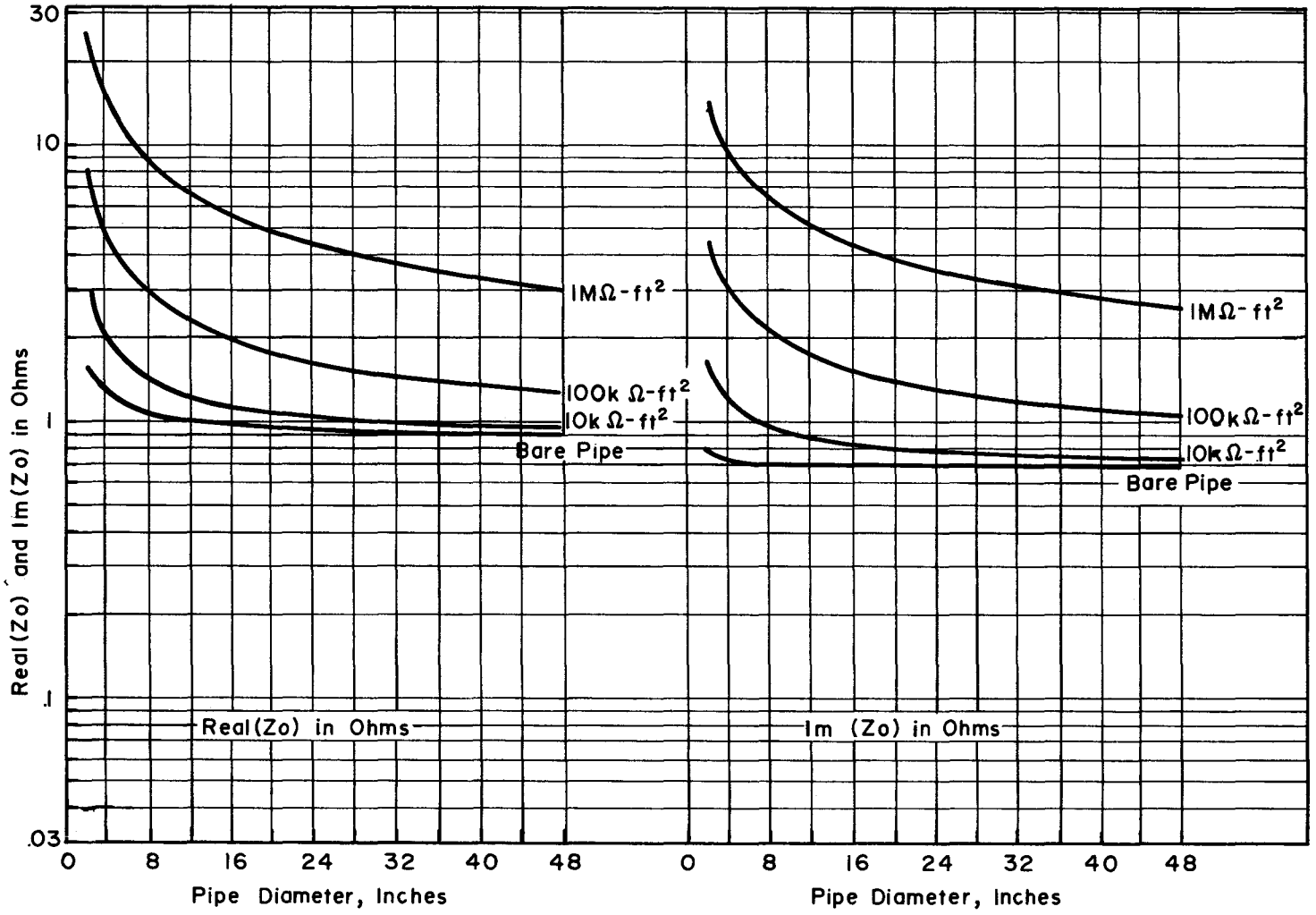

Fig. 2-16 BURIED PIPELINE CHARACTERISTIC IMPEDANCE, Z_0, FOR ρ=100kΩ-cm (σ=0.001mho/m) SOIL

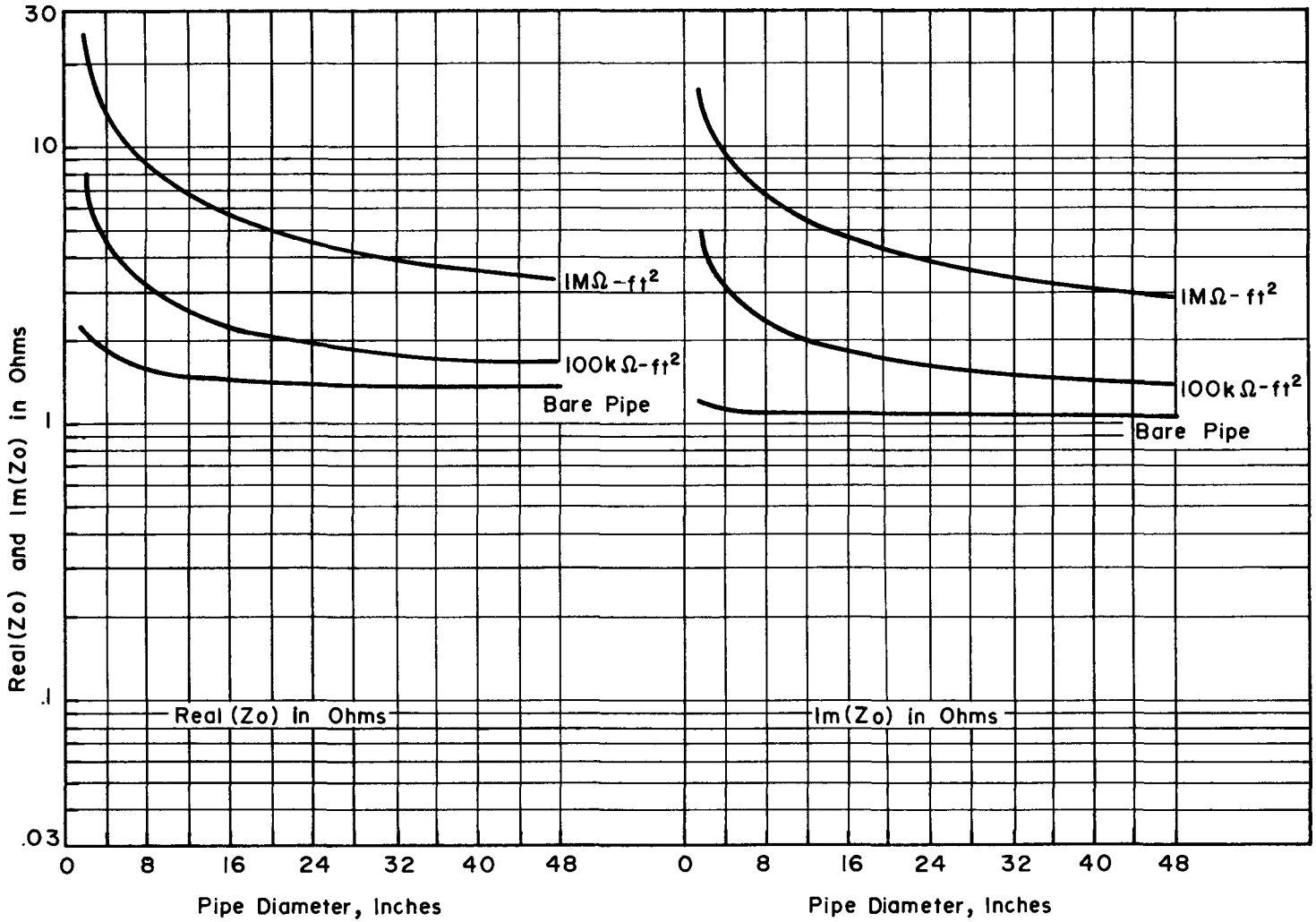

Fig. 2-17 BURIED PIPELINE CHARACTERISTIC IMPEDANCE, Z_o, FOR ρ=200kΩ-cm (σ=0.0005 mho/m) SOIL

REFERENCES

1. E. F. Vance, DNA Handbook Revision, Chapter 11, Coupling to Cables (for Dept. of the Army, Contract DAAG39-74-C-0086). Stanford Research Institute Menlo Park, California, December 1974.

2. E. D. Sunde, Earth Conduction Effects in Transmission Systems. New York: Dover Publications, 1968.

3. S. Ramo, J. R. Whinnery, and T. Van Duzer, Fields and Waves in Communication Electronics. New York: John Wiley & Sons, pp. 301-303, 1967.

Section 3

TECHNIQUES FOR PREDICTING STEADY STATE PIPELINE VOLTAGES AND CURRENTS DUE TO ELECTROMAGNETIC INDUCTION

INTRODUCTION

This section presents a unified, analytical method for predicting the voltages and currents induced by 60 Hz electromagnetic fields on buried and above-ground pipelines. The approach allows the location and quantization of pipeline voltage maxima using only a hand calculator. Complex ac power line features, such as multiple circuits, shield wires, and phase transpositions can be modeled in a systematic way. This approach promises to be more accurate than heretofore existing methods, and is easily applied to realistic pipeline cases. The prediction method developed has been validated by field testing, as exemplified by the documented case histories presented later in the section.

This section first reviews and evaluates available analytical methods for prediction of electromagnetic coupling to pipelines. Next, the basic elements of the new approach are presented. Simplified equations and equivalent circuits are derived to estimate the electromagnetic coupling for the following cases of pipeline interaction geometry with an ac power line.

1. parallel configurations;
2. non-parallel or intersecting configurations;
3. combinations of parallel and non-parallel configurations and power line discontinuities such as transpositions;
4. multiple power circuits and multiple pipelines.

REVIEW OF AVAILABLE ANALYTICAL TECHNIQUES

Methods Inappropriate To the Buried Pipeline Case

For many years, concern was directed to interference between overhead HVAC power lines and adjacent above-ground communication circuits. Equations presented originally by Westinghouse (1) have been used to predict the induced voltage per mile on an above-ground conductor due to single-phase and three-phase power lines.

An equivalent approach (2) used Carson's series (3) to compute the mutual impedances between the power line conductors and the affected communications line. The International Telegraph and Telephone Consultative Committee (CCITT) has summarized available prediction and mitigation methods for induced voltages on above ground conductors (4).

In one body of literature, these above-ground coupling equations have been applied directly to the case of the buried pipeline (5-10). All of these papers determined the induced pipeline voltage in the following general way:

$$V_{max} = f(I,d) \cdot L \qquad (3\text{-}1)$$

where V_{max} is the maximum expected voltage; f is some function of power line current, I, and distance, D, from the pipeline; and L is the length of the pipeline. Uniformly, for long length pipelines, the values of pipeline voltage calculated using this method are too high. Peabody and Verhiel acknowledge that with their formula,

> "....the actual field measurements are normally not more than 10 to 15 percent of the calculated values..." (5)

Aerospace Corporation concurs, saying that

> "....it must be remembered that actual field measurements rarely exceed 10 percent of these calculated figures..." (10)

In order to apply this method to the buried pipeline case and still obtain useful results, investigators have been successful in applying empirical methods based upon years of extensive experience in the industry.

Methods Valid for the Buried Pipeline Case

The CCITT methods fail for the buried pipeline case simply because a buried pipeline differs electrically from an overhead conductor. A buried pipeline, either bare or wrapped in an electrically insulating coating, has a finite resistance to earth distributed over its entire length, whereas an overhead line, at most, has point grounds at large intervals. To describe the distributed interaction between a buried pipeline and its surrounding earth, factors such as pipeline diameter, coating resistivity, earth resistivity, depth of burial, and pipe longitudinal resistance and inductance must be taken into account.

A second body of literature has attempted to construct such a realistic model of inductive coupling to a buried pipeline (11-14). The analytical approach used in these references considers a buried pipeline as a lossy transmission line with a distributed voltage source function due to electromagnetic coupling.

None of these papers, however, presents enough details of the analysis to permit extension of the results to several important cases of pipeline construction. Further, none of these papers derives simplified methods suitable for the prediction of electromagnetic coupling in a realistic multi-use corridor using only a slide rule or hand calculator.

THE DISTRIBUTED SOURCE ANALYTICAL APPROACH

Summary

The analytical approach discussed here allows the prediction of inductive coupling to both above-ground and buried pipelines using a single theory, the distributed source analysis (15). Here, a pipeline and its nearby or surrounding earth form a lossy transmission line characterized by the propagation constant, γ, and the characteristic impedance, Z_o. The inductive coupling effect of a nearby power line is included by defining a distributed voltage source function, $E_x(s)ds$, along the pipeline, where $E_x(s)$ is the longitudinal driving electric field along and parallel to the path of the pipeline.

As shown in Figure 3-1, specific pipeline coupling problems can be treated as special cases of the general distributed source theory. The general theory is first specialized with respect to the orientation of the pipeline section relative to the adjacent power line:

1. Parallel case (pipeline section parallel to the power line);
2. Non-parallel case (pipeline section at an angle to, or intersecting the power line).

The theory is further specialized by grouping pipeline sections according to electrical length, which allows simplifications of the analysis.

1a, 2a. Electrically short case

$$L < \frac{0.1}{|\gamma|} \approx \begin{cases} 10^4 \text{ m, above-ground pipeline case} \\ 300 \text{ m, buried pipeline case} \end{cases}$$

where L is the length of the pipeline section;

1b, 2b. Electrically long/lossy case

$$L > \frac{2}{\text{Real}(\gamma)} \simeq \begin{cases} 10^7 \text{ m, above-ground pipeline case} \\ 10^4 \text{ m, buried pipeline case} \end{cases}$$

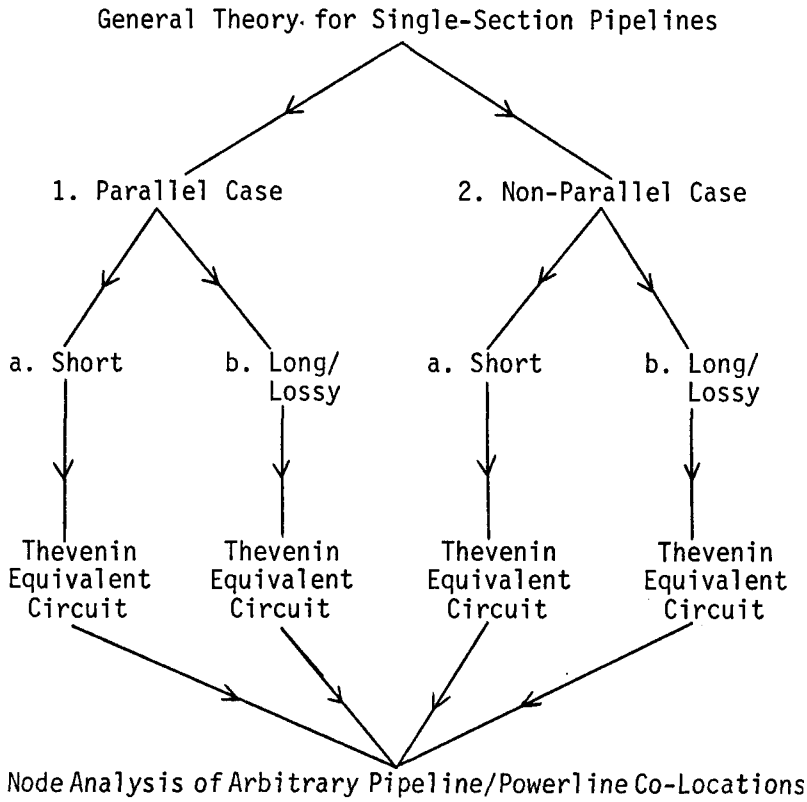

Figure 3-1. Application of the Distributed Source Analysis

The grouping of pipeline sections according to their electrical length is almost the same as a grouping according to their buried or above-ground nature. This is because almost all above-ground pipelines are found to be electrically short, while almost all buried pipelines are found to be electrically long/lossy.

The terminal behavior of pipeline sections of classes 1a, 1b, 2a, and 2b can be described by simple Thevenin equivalent circuits. These circuits can be combined to allow prediction of the inductive coupling to the arbitrary pipeline composed of several connected, dissimilar sections.

The following information about a pipeline-power line system is required to obtain numerical results using the distributed source analysis.

A. Magnitude and phase of the longitudinal driving electric field, $E_x(s)$, due to the power line at the location of the pipeline, requiring either

   1. direct measurement of the field, or

   2. estimation of the electric field, requiring knowledge of:

      a. the separation of the pipeline from the power line at each milepost of the pipeline;

      b. the phasing of each circuit of the power line;

      c. the positioning of each phase conductor and shield wire (the latter is not required if each shield wire is either insulated or grounded only at one point);

      d. the location of each power line discontinuity, such as phase transpositions and substations.

B. Pipeline propagation constant, γ, and characteristic impedance, Z_o, requiring measurement or estimation of:

   1. the pipeline diameter;

   2. the conductivity of the pipeline coating;

   3. the soil conductivity.

C. Pipeline network specifications:

   1. position of pipeline insulators, ground beds, and junctions;

   2. magnitude and phase of the pipeline impedance terminations (ground beds and insulators).

The conclusions of this analysis are that induced voltage peaks are expected at the following points in a pipeline run:

1. Impedance termination (insulator or ground bed) of a long/lossy section;

2. Junction between a long/lossy parallel section and a long/lossy non-parallel section;

3. Junction between two long/lossy parallel sections having different separations from the power line;

4. Adjacent to a power line phase transposition or a substation where phasing is altered in some way;

5. Junction between two long/lossy sections of differing electrical characteristics (for example, at a high resistivity soil - low resistivity soil transition).

The magnitude of the voltage peak at any of these points is computed simply by determining Thevenin equivalent circuits for the pipeline sections on either side of the discontinuity.

Analytical Determinations of the Longitudinal Electric Field Parallel to the Pipeline

The longitudinal driving electric field, $E_x(s)$, is required for use in the coupling formulas and equivalent circuits developed in this section. Methods for analytically determining E_x will now be discussed (16,17).

E_x is generated by the linear superposition of the electric fields due to all nearby current-carrying conductors. These conductors are classified into two groups:

1. Active conductors (those designed to carry current) such as the power line phase conductors; and
2. Passive conductors (those carrying current due to inductive coupling) such as multiple-grounded power line shield wires, long fence wires, telephone wires, railroad tracks, or other pipelines.

The passive conductors must be included in the analysis because they have been shown to be significant contributors to electromagnetic coupling by power lines (17). Since the currents in the passive conductors are initially unknown and influence each other through mutual coupling, the solution for these currents must be obtained by solving a set of complex-valued simultaneous equations describing the interactions, discussed below.

Approximation of the Currents in Long, Grounded Passive Conductors. Using Eq. 2-3a, it may be shown that the induced current in a long, multiple-grounded passive conductor is almost constant with position along the conductor, and is given by

$$-I_{C_{m_o}} Z_{C_{m_o} C_{m_o}} \simeq E(C_{m_o}) \qquad (3\text{-}2)$$

where

$I_{C_{m_o}}$ and $Z_{C_{m_o} C_{m_o}}$ are, respectively the induced current and series self-impedance per meter of the m_oth passive conductor, and $E(C_{m_o})$ is the driving electric field at the m_oth passive conductor.

$I_{C_{m_o}}$ can be approximated using the Carson coupling approach (18). With this approach, $E(C_{m_o})$ is taken as the summation of the electric field contributions of all of the adjacent current-carrying conductors, including power line phase wires 1, 2, ..., N carrying currents I_{ϕ_n}, and passive conductors 1, 2, ..., m_o-1, m_o+1, ..., M carrying currents I_{C_m}.

$E(C_{m_o})$ is therefore given by

$$E(C_{m_o}) = \sum_{n=1}^{N} I_{\phi_n} Z_{C_{m_o}\phi_n} + \sum_{\substack{m=1 \\ m\neq m_o}}^{M} I_{C_m} Z_{C_{m_o} C_m} \qquad (3\text{-}3)$$

where $Z_{C_{m_o}\phi_n}$ is the Carson mutual impedance between the m_oth passive conductor and the nth phase conductor, and $Z_{C_{m_o} C_m}$ is the Carson mutual impedance between the m_oth passive conductor and the mth passive conductor (for $m\neq m_o$). The set of unknown currents in the passive conductors can be found by writing Eqs. 3-2 and 3-3 for each of the M conductors, and then solving the resulting system of simultaneous equations (show below).

$$\begin{aligned}
Z_{C_1C_1}I_{C_1} + Z_{C_1C_2}I_{C_2} + \ldots + Z_{C_1C_M}I_{C_M} &= -\left[Z_{C_1\phi_1}I_{\phi_1} + Z_{C_1\phi_2}I_{\phi_2} + \ldots + Z_{C_1\phi_N}I_{\phi_N}\right] \\
Z_{C_2C_1}I_{C_1} + Z_{C_2C_2}I_{C_2} + \ldots + Z_{C_2C_M}I_{C_M} &= -\left[Z_{C_2\phi_1}I_{\phi_1} + Z_{C_2\phi_2}I_{\phi_2} + \ldots + Z_{C_2\phi_N}I_{\phi_N}\right] \\
&\;\;\vdots \\
Z_{C_MC_1}I_{C_1} + Z_{C_MC_2}I_{C_2} + \ldots + Z_{C_MC_M}I_{C_M} &= -\left[Z_{C_M\phi_1}I_{\phi_1} + Z_{C_M\phi_2}I_{\phi_2} + \ldots + Z_{C_M\phi_N}I_{\phi_N}\right]
\end{aligned} \qquad (3\text{-}4)$$

M unknown currents, I_{C_m} — N known phase currents, I_{ϕ_n}

A program for the TI-59 hand claculator which permits solution of the system of Eq. 3-4 has been developed. This program, called CURRENTS, uses the Gauss-Seidel iterative method to process as many as five unknown passive conductors adjacent to 25 power line phase conductors, yielding both the magnitude and phase of each unknown current. The listing for Program CURRENTS, as well as detailed usage instructions, is included in Appendix A. For joint-use corridors having more than five unknown passive conductors, it has been found sufficiently accurate to use Program CURRENTS to solve simultaneous equations for five-element sub-sets of closely spaced passive conductors, and assume negligible coupling between the sub-sets. A discussion of the usage of this program with actual case histories is given later in the section.

Computation of Carson Mutual Impedances. As seen from the previous discussion, knowledge of the Carson mutual impedances $Z_{C_{m_o}\phi_n}$ and $Z_{C_{m_o}C_m}$ is essential for setting up the system of equations for the set of unknown currents. A program for the TI-59 calculator has also been developed that computes the Carson mutual impedance between two adjacent, parallel, earth-return conductors using Carson's infinite series. This program, called CARSON, computes and sums as many terms of the Carson series as is required to achieve 0.1% accuracy. The program listing and usage instructions are contained in Appendix A.

The Driving Electric Field. By Eq. 3-2, the longitudinal driving electric field for a pipeline or other passive conductor is equal to the negative of the product of the current, I_{C_m}, obtained via Program CURRENTS times the conductor self impedance, $Z_{C_mC_m}$. For a power line shield wire, the self impedance can be computed using the expression

$$Z_{C_mC_m} = (R_{C_m} + 5.92\cdot10^{-5}) + j\left\{1.88\cdot10^{-5} + 3.77\cdot10^{-5}\left[2\ln\frac{.79\delta}{r_{C_m}} + 1\right]\right\} \text{ ohm/m} \qquad (3\text{-}5a)$$

where R_{C_m} is the dc resistance per meter of the shield wire, r_{C_m} is the radius of the shield wire, and δ is the earth electrical skin depth at 60 Hz given by

$$\delta = \frac{64.9}{\sqrt{\sigma}} \text{ m} \quad (\sigma = \text{soil conductivity}) \qquad (3\text{-}5b)$$

For computational ease, the program SHIELD (c.f., Appendix A) has been written to compute $Z_{C_m C_m}$.

For a buried pipeline, the self impedance is equal to

$$Z_{C_m C_m} = \gamma Z_o \tag{3-5c}$$

where γ is the pipeline propagation constant and Z_o is its characteristic impedance. These parameters may be found from the graphs in Section 2 or by means of the Program PIPE.

Example 3-1: Set up and solve the system of simultaneous equations for the approximate shield wire currents in a single-circuit, 3-phase power line with two grounded shield wires. Assume no other conductors in the utility corridor.

Solution: Set up the system of Eq. 3-4 for the shield wires. At the first shield wire:

$$Z_{C_1C_1} I_{C_1} + Z_{C_1C_2} I_{C_2} = -\left[Z_{C_1\phi_1} I_{\phi_1} + Z_{C_1\phi_2} I_{\phi_2} + Z_{C_1\phi_3} I_{\phi_3}\right] \equiv V_1$$

At the second shield wire:

$$Z_{C_2C_1} I_{C_1} + Z_{C_2C_2} I_{C_2} = -\left[Z_{C_2\phi_2} I_{\phi_1} + Z_{C_2\phi_2} I_{\phi_2} + Z_{C_2\phi_3} I_{\phi_3}\right] \equiv V_2$$

Hence

$$I_{C_1} = \frac{V_1 Z_{C_2C_2} + V_2 Z_{C_1C_2}}{Z_{C_1C_1} Z_{C_2C_2} - \left[Z_{C_1C_2}\right]^2}$$

and

$$I_{C_2} = \frac{V_2 Z_{C_1C_1} + V_1 Z_{C_1C_2}}{Z_{C_1C_1} Z_{C_2C_2} - \left[Z_{C_1C_2}\right]^2}$$

where it has been assumed that $Z_{C_1C_2} = Z_{C_2C_1}$. The solution for the currents I_{C_1} and I_{C_2}, done here by hand, is made automatically by the program CURRENTS.

The numerical values of Carson mutual impedances can be obtained by means of Program CARSON. For distances less than about 300 meters (for 60 Hz induction) the first term of the Carson series yields a reasonable approximation to the mutual impedance value. Hence,

$$Z_{C_{m_o} C_m} \simeq 5.92 \cdot 10^{-5} + j\ 3.77 \cdot 10^{-5} \left[2 \ln\left(\frac{0.79\delta}{d_{C_{m_o} C_m}} \right) + 1 \right] \qquad (3\text{-}6)$$

where δ is defined by Eq. 3-5b and $d_{C_{m_o} C_m}$ is the radial separation (in meters) between conductors, C_{m_o} and C_m. For short distances, Eq. 3-6 provides a useful check on the programming of Program CARSON.

Example 3-2: Compute the shield wire currents for the following power line geometry:

Single-circuit, flat configuration with two symmetrically positioned grounded shield wires;

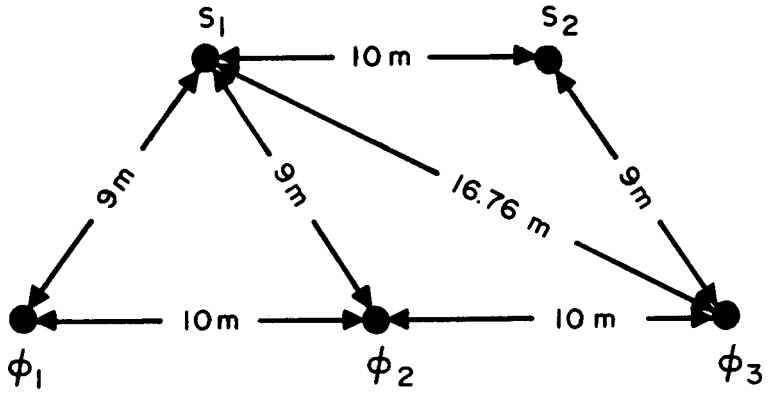

S_1, S_2 are 5/8" diameter conductors with 1 ohm per mile dc resistance.

$I_{\phi_1} = I_o e^{j0^o} = I_o$ amps

$I_{\phi_2} = I_o e^{j120^o} = I_o(-0.5 + j\,0.866)$ amps

$I_{\phi_3} = I_o e^{-j120^o} = I_o(-0.5 - j\,0.866)$ amps

Soil resistivity = $2 \cdot 10^4$ ohm-cm.

Figure 3-2 Power Line Geometry for Example 3-2

Solution: First, compute the series impedance per meter of each shield wire, using Eqs. 3-5a and 3-5b, or alternatively by means of Program SHIELD.

$$\sigma = 1/(2\cdot 10^{4} \text{ ohm-cm}) = 0.005 \text{ mho/m}$$

$$\delta = \frac{64.9}{\sqrt{0.005}} = 917.8 \text{ m}$$

$$R_{C_1} = R_{C_2} = 1 \text{ ohm/mi} = 1 \text{ ohm/1609 m} = 6.215\cdot 10^{-4} \text{ ohm/m}$$

$$r_{C_1} = r_{C_2} = 5/16 \text{ in.} = 5/16 \cdot 0.0254 \text{ m} = 7.938\cdot 10^{-3} \text{ m}$$

$$Z_{C_1} = Z_{C_2} = (6.214\cdot 10^{-4} + 5.92\cdot 10^{-5}) + j \left\{1.88\cdot 10^{-5} + 3.77\cdot 10^{-5} \left[2 \ln\left(\frac{0.79\cdot 917.8}{7.938\cdot 10^{-3}}\right) + 1\right]\right\} = (6.806 + j\ 9.177)\cdot 10^{-4} \text{ ohm/m.}$$

Next, compute the various Carson mutual impedances using Eq. 3-7, or Program CARSON.

$$Z_{C_1C_2} = 5.92\cdot 10^{-5} + j\ 3.77\cdot 10^{-5} \left[2 \ln\left(\frac{0.79\cdot 917.8}{10.0}\right) + 1\right]$$
$$= (0.592 + j\ 3.607)\cdot 10^{-4} \text{ ohm/m}$$

$$Z_{\phi_1C_1} = Z_{\phi_2C_1} = Z_{\phi_2C_2} = Z_{\phi_3C_2} = 5.92\cdot 10^{-5} + j\ 3.77\cdot 10^{-5} \left[2 \ln\left(\frac{0.79\cdot 917.8}{9.0}\right) + 1\right] = (0.592 + j\ 3.686)\cdot 10^{-4} \text{ ohm/m}$$

$$Z_{\phi_3C_1} = Z_{\phi_1C_2} = 5.92\cdot 10^{-5} + j\ 3.77\cdot 10^{-5} \left[2 \ln\left(\frac{0.79\cdot 917.8}{16.76}\right) + 1\right] = (0.592 + j\ 3.218)\cdot 10^{-4} \text{ ohm/m}$$

Note that the formulas for I_{C_1} and I_{C_2} developed in Example 3-1 apply to the power line geometry of this example. To apply these formulas, we must next compute the quantities V_1 and V_2 defined in Example 3-1, using the values for mutual impedance just calculated.

$$V_1 = 10^{-4} I_o \begin{bmatrix} (0.592 + j\ 3.686) + \\ (0.592 + j\ 3.686)(-0.5 + j\ 0.866) + \\ (0.592 + j\ 3.218)(-0.5 - j\ 0.866) \end{bmatrix}$$

$$= 10^{-4} I_o \ (-0.405 + j\ 0.234) \text{ volts/m}$$

$$V_2 = 10^{-4} I_o \begin{bmatrix} (0.592 + j\ 3.218) + \\ (0.592 + j\ 3.686)(-0.5 + j\ 0.866) + \\ (0.592 + j\ 3.686)(-0.5 - j\ 0.866) \end{bmatrix}$$

$$= 10^{-4} I_o \ (0 - j\ 0.468) \text{ volts/m}$$

Finally, we can compute I_{C_1} and I_{C_2} using the formulas developed in Example 3-1.

$$-I_{C_1} = \frac{10^{-8} I_o \begin{bmatrix} (-0.405 + j\ 0.234)(6.806 + j\ 9.177) + \\ (0 - j\ 0.468)(0.592 + j\ 3.607) \end{bmatrix}}{10^{-8} \left[(6.806 + j\ 9.177)^2 - (0.592 + j\ 3.607)^2 \right]}$$

$$= (-0.0137 + j\ 0.0295) I_o = 0.0325\ e^{j115^o} I_o$$

$$-I_{C_2} = \frac{10^{-8} I_o \begin{bmatrix} (0 - j\ 0.468)(6.806 + j\ 9.177) + \\ (-0.45 + j\ 0.234)(0.592 + j\ 3.607) \end{bmatrix}}{10^{-8} \left[(6.806 + j\ 9.177)^2 - (0.592 + j\ 3.607)^2 \right]}$$

$$= (-0.0411 - j\ 0.0180) I_o = 0.0449\ e^{j204^o} I_o$$

The solution for these currents could also have been obtained by means of the Program CURRENTS.

The shield wire currents are seen to be of the order of 3 percent to 5 percent of the power line current. These currents are comparable in magnitude to the expected zero sequence current of the power line. Thus, the overall electromagnetic coupling of the power line can be strongly influenced by the presence of grounded shield wires.

Typical Longitudinal Electric Field Variation

Figure 3-3 depicts the typical variation of E_x with separation from a one-ampere, single-phase power line (at three earth conductivities, for separations up to 1000 m) (18). Normalized in this manner, the graphs of this figure are also equivalent to graphs of the Carson mutual impedance versus separation. At large separations, the real part of the mutual impedance begins to decrease from the value given in Eq. 3-5c. However, the imaginary part decreases even faster so that the Carson mutual impedance approaches a pure real number at spacings in excess of several kilometers. The transition from a reactive to a resistive mutual impedance indicates that the phase of the longitudinal electric field can change by as much as 90^{o} over the length of a pipeline approaching or intersecting a power line. This phase behavior must be taken into account to allow the accurate prediction of induced pipeline voltages.

The longitudinal electric field variation with separation as shown in Figure 3-3 is representative of only the simplest case, i.e., a single-phase power line. Generally, the power line currents contributing to the distributed pipeline source electric field will be components from up to several three-phase electric power transmission circuits with shield wires. Hence, the electric field variation with separation is more complex. Because of time-varying line current values and associated electric load unbalances, the resultant electric field may exhibit large fluctuations, both in time and with separation distance. At best, these can only be characterized in a probabilistic manner. Likewise, these fluctuations will impose a time variation upon the induced pipeline voltage and current.

The properties of these fluctuations and their probabilistic characterization are discussed in Appendices B and C, respectively.

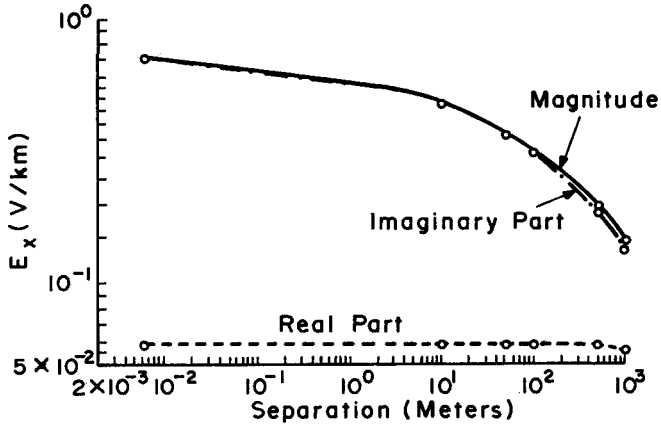

(a) Earth Conductivity $\sigma = 2 \cdot 10^{-4}$ mhos/m

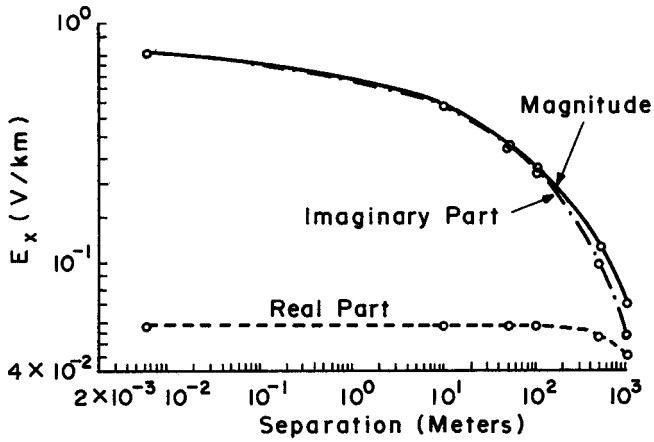

(b) $\sigma = 2 \cdot 10^{-3}$ mhos/m

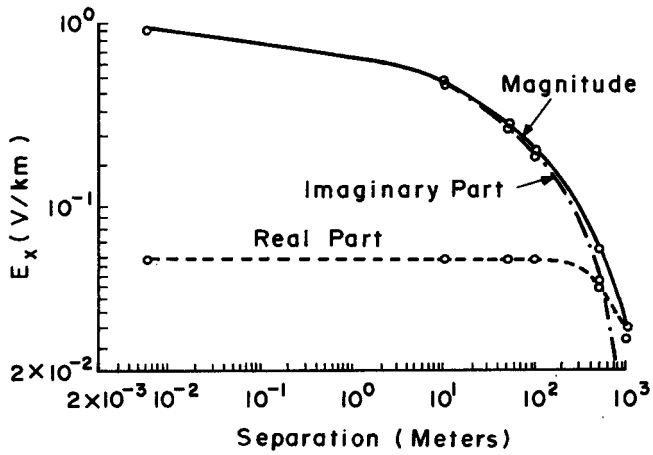

(c) $\sigma = 1 \cdot 10^{-2}$ mhos/m

Fig. 3-3 TYPICAL VARIATION OF E_x COMPONENTS WITH SEPARATION FROM A ONE AMPERE SINGLE-PHASE POWER LINE AT THREE EARTH CONDUCTIVITIES

Summary of Calculator Method for
Determining Electric Field at the Pipeline

The previous subsections outline the analytical methodology for calculating the driving electric field at the pipeline. In order to simplify the calculations, use of the programs written for the TI-59 calculator is advisable. Briefly, the procedure for determining the driving electric field using the programs is as follows:

- Single Pipeline, Ungrounded Shield Wires
  - Use the program CARSON to determine the appropriate mutual impedances
  - Calculate the electric field directly by means of the program, FIELD
- One or More Pipelines, and/or Grounded Shield Wires
  - Use the program CARSON to determine the appropriate mutual impedances
  - Use the program PIPE to determine the self-impedances of the pipelines. Note: The self impedance is equal to γ times Z_o
  - Calculate shield wire self impedance by means of the program, SHIELD
  - *Calculate the induced conductor currents using the program, CURRENTS
  - The driving electric field for a pipeline or other conductor is equal to the product of the current obtained above times the wire self impedance obtained from the program PIPE.

Application of the Distributed Source Analysis to
the Parallel Pipeline with Arbitrary Terminations

In the following analysis, the driving field, $E_x(s)$, of Eq. 2-4 is assumed to equal E_o, a constant. This assumption is valid for above-ground and buried pipelines parallel to long power lines which continue significantly beyond the region

---

*If a conductor's length is short compared to $|\gamma|^{-1}$, its self impedance and the mutual impedances to other conductors must be appropriately modified before running the program CURRENTS, c.f., Appendix D.

The program CURRENTS can only accommodate up to five unknown current-carrying conductors. The Texas Gas Transmission Corporation, Memphis, Tennessee, case history illustrates a procedure for increasing the number of unknowns that can be handled.

of parallelism. The pipeline is assumed to extend from x = 0 to x = L meters, as shown in Figure 3-4. At the end points, the pipeline is assumed to be connected to remote earth through the grounding impedances Z_1 and Z_2. These terminations may be realized by grounding systems (i.e., a ground rod array, grounding cell, etc.), by connected non-parallel pipeline sections, or by insulating joints. The analysis is sufficiently general to cover all possible grounding impedances and pipeline lengths for single-section buried and above-ground parallel pipelines. Non-parallel and multi-section pipelines will be discussed below.

General Solution for the Pipeline Potential. The analysis is begun by substituting $E_x(s) = E_o$ into Equations 2-4a and 2-4b to obtain

$$P(x) = \frac{1}{2Z_o}\int_o^x e^{\gamma s} E_o ds = \frac{E_o}{2\gamma Z_o}(e^{\gamma x}-1) \tag{3-7a}$$

$$Q(x) = \frac{1}{2Z_o}\int_x^L e^{-\gamma s} E_o ds = \frac{E_o}{2\gamma Z_o}(e^{-\gamma x}-e^{-\gamma L}). \tag{3-7b}$$

Next, the results of Equation 3-7 may be used to derive K_1 and K_2 of Equation 2-5.

$$K_1 = \frac{\rho_1 E_o}{2\gamma Z_o}\left[\frac{\rho_2(1-e^{-\gamma L}) + 1-e^{\gamma L}}{e^{\gamma L}-\rho_1\rho_2\, e^{-\gamma L}}\right] \tag{3-8a}$$

$$K_2 = \frac{\rho_2 E_o e^{-\gamma L}}{2\gamma Z_o}\left[\frac{\rho_1(1-e^{-\gamma L}) + 1-e^{\gamma L}}{e^{\gamma L}-\rho_1\rho_2\, e^{-\gamma L}}\right] \tag{3-8b}$$

Substituting K_1, K_2, P(x), and Q(x) into Equation 2-3b, the general solution for V(x) is obtained:

$$V(x) = \frac{E_o\{[(1+\rho_2)\rho_1-(1+\rho_1)e^{\gamma L}]e^{-\gamma x} - [(1+\rho_1)\rho_2-(1+\rho_2)e^{\gamma L}]e^{\gamma(x-L)}\}}{2\gamma(e^{\gamma L} - \rho_1\rho_2\, e^{-\gamma L})} \tag{3-9a}$$

In terms of the terminating impedances Z_1 and Z_2, V(x) is given by

$$V(x) = \frac{E_o\{[Z_2(Z_1-Z_o)-Z_1(Z_2+Z_o)e^{\gamma L}]e^{-\gamma x}-[Z_1(Z_2-Z_o)-Z_2(Z_1+Z_o)e^{\gamma L}]e^{\gamma(x-L)}\}}{\gamma[(Z_1+Z_o)(Z_2+Z_o)e^{\gamma L}-(Z_1-Z_o)(Z_2-Z_o)e^{-\gamma L}]} \tag{3-9b}$$

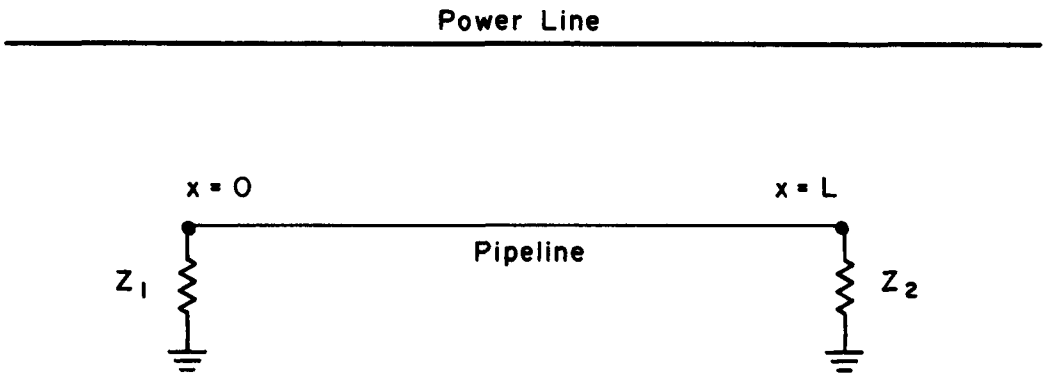

Fig. 3-4 GEOMETRY OF A SINGLE - SECTION, BURIED OR ABOVE-GROUND PIPELINE PARALLEL TO A POWER LINE

At $x = 0$ or at $x = L$, it can be shown that the dependence of $V(0)$ and $V(L)$ upon the terminating impedances, Z_1 and Z_2, respectively, can be modeled by Thevenin equivalent circuits. For example, at $x = 0$,

$$V(0) = V_\theta \cdot \frac{Z_1}{Z_1+Z_\theta} \tag{3-10a}$$

where V_θ is the Thevenin equivalent voltage source given by

$$V_\theta = V(0)\Big|_{Z_1 = \infty}$$

$$= \frac{E_o}{\gamma} \cdot \frac{2Z_2-(Z_2+Z_o)e^{\gamma L}-(Z_2-Z_o)e^{-\gamma L}}{(Z_2+Z_o)e^{\gamma L}-(Z_2-Z_o)e^{-\gamma L}} \tag{3-10b}$$

and Z_θ is the Thevenin source impedance* given by

$$Z_\theta = Z_o \cdot \left[\frac{(Z_2+Z_o)e^{\gamma L}+(Z_2-Z_o)e^{-\gamma L}}{(Z_2+Z_o)e^{\gamma L}-(Z_2-Z_o)e^{-\gamma L}}\right] \tag{3-10c}$$

Recognition of the ability to employ Thevenin decomposition procedures is of prime importance since, in this way, the effect of the load impedance can be separated from that of the distributed voltage sources along the pipe. Thus, the analysis of a multi-section pipeline or a pipeline subject to sharp variations in the induced field because of geometrical or electrical discontinuities can be treated by applying Thevenin procedures at the junctions or field discontinuities, as discussed later in this section.

Equations 3-9 and 3-10 will now be simplified for the two most important pipeline cases: the electrically short pipeline; and the electrically long/lossy pipeline.

*Note that Z_θ is exactly the input impedance of a transmission line of characteristic impedance, Z_o, propagation constant, γ, and length, L, terminated by Z_2.

The Electrically Short Pipeline. For this analysis, the length, L, of an electrically short pipeline satisfies the inequality

$$L < \frac{0.1}{|\gamma|} \simeq 300 \text{ m} \tag{3-11}$$

The limit of L for electrical shortness can be obtained by computing representative values of $|\gamma|$ using the calculator programs described later.

Subject to the inequality of Eq. 3-11, the first-order-correct approximations

$$e^{\pm\Delta} \simeq 1 \pm \Delta \text{ for } \Delta = \left\{ \begin{matrix} \gamma L \\ \gamma x \\ \gamma(x-L) \end{matrix} \right\} \tag{3-12}$$

can be used with the assurance that the error introduced is of the order of only 10 percent. Substituting the approximations of Eq. 3-12 into the general solution of Eq. 3-9 results in the following expression for the induced potential on a parallel, electrically short pipeline:

$$V(x) \simeq E_o \left(x - \frac{L Z_1}{Z_1+Z_2} \right) \tag{3-13}$$

The potential is seen to vary linearly with distance from termination Z_1, as shown in Figure 3-5a. The terminal values of V(x) are given by

$$V(0) \simeq -E_o L \cdot \frac{Z_1}{Z_1+Z_2} \tag{3-14a}$$

$$V(L) \simeq E_o L \cdot \frac{Z_2}{Z_1+Z_2} \tag{3-14b}$$

The dependence of V(0) and V(L) upon the values of Z_1 and Z_2 is modeled by the Thevenin equivalent circuit of Figure 3-5b. In the figure, the Thevenin source impedance, Z_θ, is shown equal to Z_r, the terminating impedance remote from the observation point. The magnitude of the Thevenin voltage source, V_θ, is proportional to the length of the pipeline section. V_θ assumes the "-" sign if $\vec{E}_o$ points toward the remote termination, and the "+" sign if $\vec{E}_o$ points toward the Thevenin observation point.

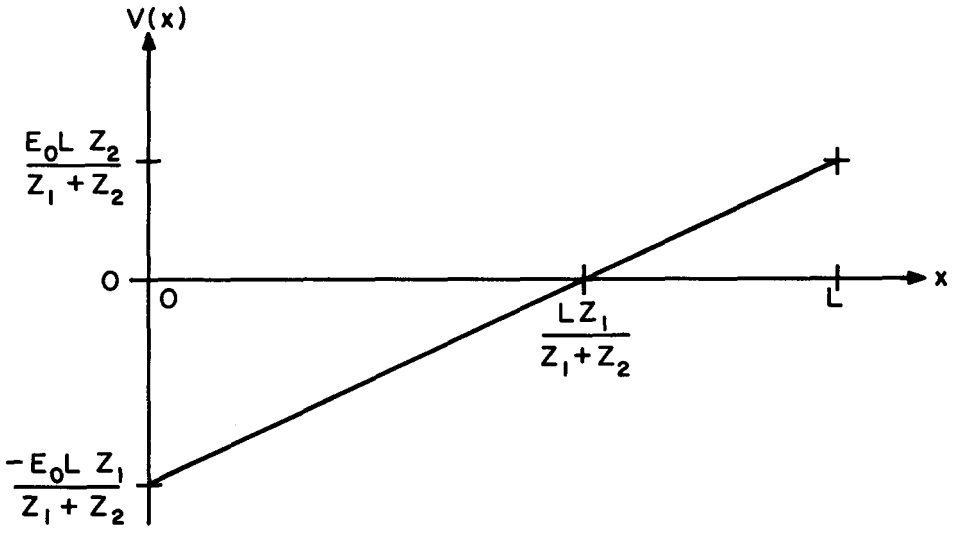

(a) Potential Distribution For Z_1, Z_2 Assumed To Be Purely Resistive

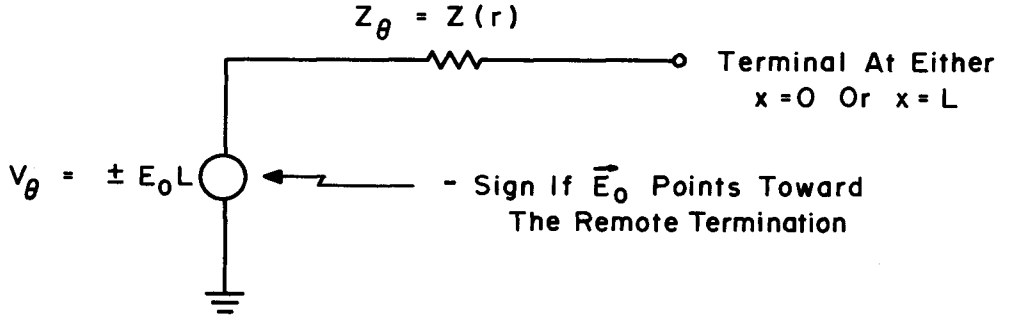

(b) Thevenin Equivalent Circuit For The Terminal Behavior Of The Pipeline

Fig. 3-5 ELECTROMAGNETIC COUPLING TO AN ELECTRICALLY SHORT PARALLEL PIPELINE

The Electrically Long/Lossy Pipeline. The criterion for an electrically long/lossy pipeline is defined as

$$L > 2/\text{Real}(\gamma) \simeq 10 \text{ km.} \tag{3-15}$$

Subject to this condition, it can be stated that

$$|e^{-\gamma L}| \simeq 0.1 << 1. \tag{3-16}$$

The limit of L for large electrical length/loss is obtainable by computing representative values of $\text{Re}(\gamma)$ using the calculator programs discussed later.

Using the inequality of Eq. 3-16, the general solution of Eq. 3-9 can be reduced to obtain the following simple result for the induced potential on a parallel, electrically long/lossy pipeline:

$$V(x) \simeq \frac{E_o}{\gamma}\left[-\frac{Z_1}{Z_1+Z_o} \cdot e^{-\gamma x} + \frac{Z_2}{Z_2+Z_o} \cdot e^{\gamma(x-L)}\right] \tag{3-17}$$

The potential is seen to vary exponentially with distance from each termination, as shown in Figure 3-6a. The terminal values of V(x) are given by

$$V(0) \simeq \frac{E_o}{\gamma} \cdot \frac{Z_1}{Z_1+Z_o} = V_\theta \frac{Z_1}{Z_1+Z_o} \tag{3-18a}$$

$$V(L) \simeq \frac{E_o}{\gamma} \cdot \frac{Z_2}{Z_2+Z_o} = V_\theta \frac{Z_2}{Z_2+Z_o} \tag{3-18b}$$

where $V_\theta \equiv \pm \frac{E_o}{\gamma}$ is the Thevenin voltage source with polarity as discussed below.

From Figure 3-6a, V(0) and V(L) are seen to be the maximum induced pipeline voltages. These voltages are independent of pipeline length, assuming that the long/lossy criterion is met. Further, the magnitude of each terminal voltage is fixed by the local terminating impedance and is independent of the nature of the remote terminating impedance.

The dependence of V(0) and V(L) upon the values of Z_1 and Z_2 is modeled by the Thevenin equivalent circuit of Figure 3-6b. In the figure, the Thevenin source impedance, Z_θ, is shown to equal Z_o, the characteristic impedance of the pipeline. The magnitude of the Thevenin voltage source, V_θ, is independent of pipeline length. V_θ assumes the "-" sign if $\vec{E}_o$ points toward the remote termination.

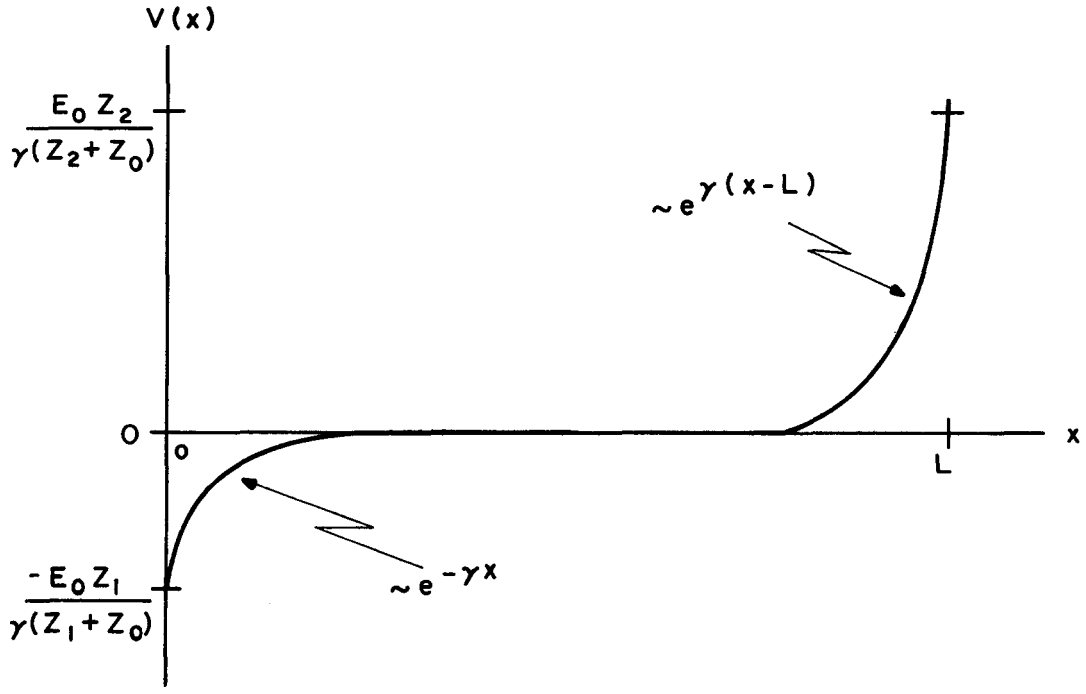

(a) Potential Distribution For Z_1, Z_2 Assumed To Be Purely Resistive

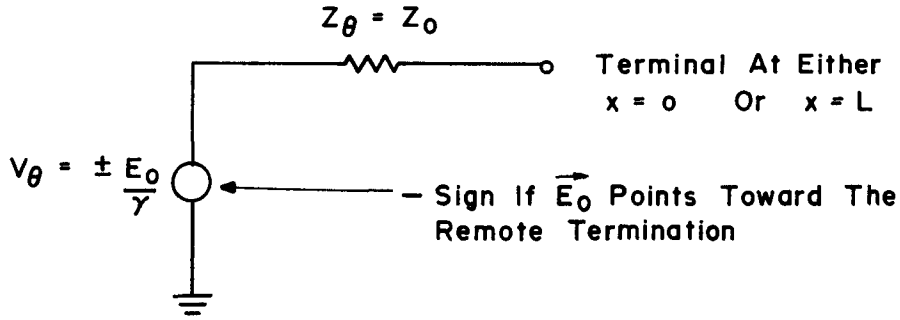

(b) Thevenin Equivalent Circuit For The Terminal Behavior Of The Pipeline

Fig. 3-6 ELECTROMAGNETIC COUPLING TO A LONG / LOSSY PARALLEL PIPELINE

Effect of a Non-Constant Driving Electric Field

The driving electric field, $E_x(s)$, can depend upon position along a pipeline which does not parallel a power line or is adjacent to a power line electrical discontinuity. Two situations commonly occur as diagrammed in Figure 3-7, namely

1. where a relatively short section of pipeline intersects the power line by crossing the right-of-way, and

2. where a pipeline approaches or recedes from a power line without actually crossing under the line.

Consider this latter case first.

The Long/Lossy Pipeline Approach Section. Upon entering or leaving a right-of-way jointly shared with a power line, a pipeline is subject to a driving electric field which is virtually zero at its remote termination and maximum at the joint corridor. This behavior of the driving field permits simplification of Eq. 2-3 to 2-6, resulting in a convenient integral expression for the terminal characteristics of a long/lossy pipeline approach section at its entry to the corridor.

For a long/lossy pipeline approach section of length, L, terminated by an arbitrary Z_1 at x = 0 far from the joint corridor, the effective remote termination sensed at x = L (the entry to the corridor) is simply the pipeline characteristic impedance, Z_o. This is because the driving field falls to zero somewhere between x = 0 and x = L along the pipeline, allowing the portion of the pipeline subjected to zero field to act as a characteristic impedance load for the portion being driven. Thus, ρ_1 of Eq. 2-6, and K_1 of Eq. 2-5a are equal to zero.

Now, the Thevenin equivalent voltage source for the pipeline approach section, as observed at x = L, the corridor entry point, is simply the open circuit pipe voltage at L:

$$V_\theta = V(L)\Big|_{Z_2 = \infty} \tag{3-19a}$$

With $Z_2 = \infty$, ρ_2 of Eq. 2-6 is equal to 1. After computing K_2, P(L), and Q(L) for this case, V_θ is found to be

$$V_\theta = e^{-\gamma L} \int_0^L E_x(s)\, e^{\gamma s}\, ds \tag{3-19b}$$

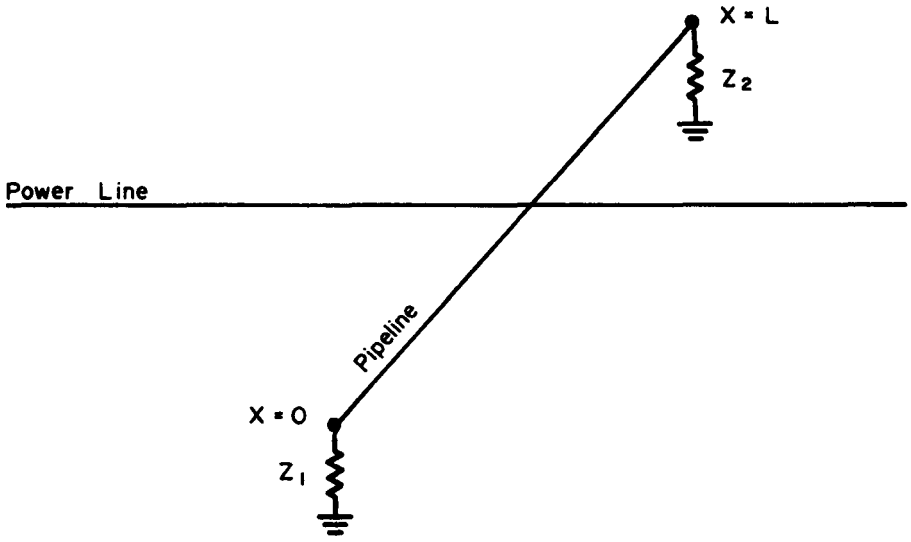

(a) Intersecting Case

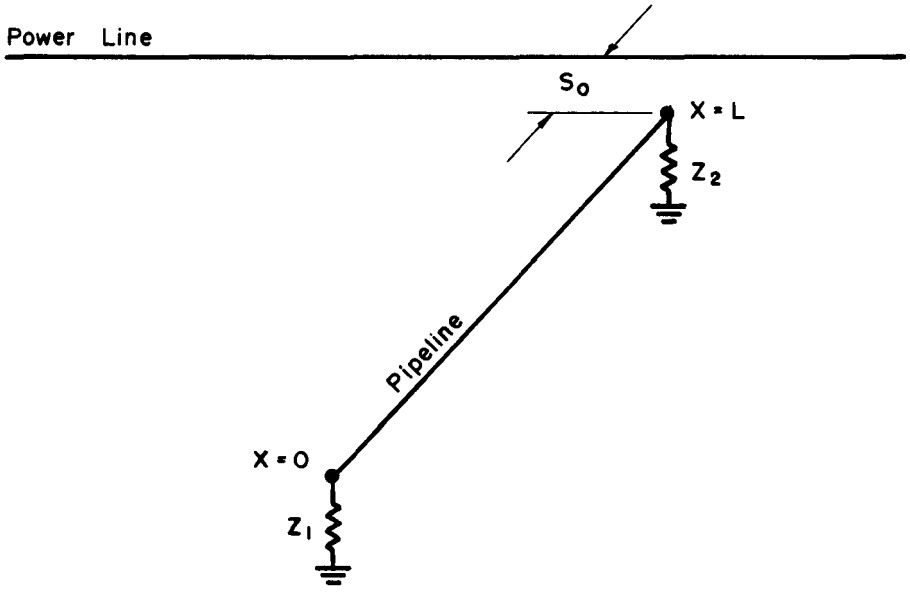

(b) Non - Intersecting Case

Fig. 3-7 GEOMETRY OF A SINGLE-SECTION, BURIED OR ABOVE-GROUND PIPELINE AT AN ANGLE TO A POWER LINE

This expression for V_θ is directly useful in its integral form for practical problems, as is explicitly shown in the Mojave Desert case history reviewed later in this section. It is understood that Z_θ is equal to Z_o, the pipe characteristic impedance, because of the long/lossy nature assumed for the approach section.

A convenient approximation to the integral of Eq. 3-19b may be found as follows: $E_x(s)$ will have its largest value at the point of closest approach of the angular pipeline section to the power line. Call this distance, S_o. A convenient approximation for the variation of the field is to assume that the magnitude of the field varies inversely with the separation distance from the powerline, from S_o out to a distance d_o. At d_o, it is assumed that the field is negligible in value. With these assumptions, an approximate evaluation of Eq. 3-19b is

$$V_\theta \simeq \frac{E_x(S_o)(d_o-S_o)}{4 \tan \theta} \qquad (3\text{-}20)$$

where

S_o is the point of closest approach of the pipeline to the power line,

θ is the acute angle of the approach, and

d_o is a variable dependent upon the power line tower geometry. For practical situations, a reasonable value for d_o has been found to be 300 meters.

For situations where $S_o \geq 300$ meters, a good approximation to Eq. 3-19b is $V_\theta \simeq 0$.

The Intersecting Pipeline. This situation, as diagrammed in Figure 3-7a, can best be handled by the node analysis considered in the following subsection. That is, for any point along the pipeline section, a Thevenin equivalent circuit (c.f., Eq. 3-19 or 3-20) must be derived for each direction to either side of the point in question and these equivalent circuits then combined by a node voltage analysis.

NODE ANALYSIS OF ARBITRARY PIPELINE/POWER LINE COLLOCATIONS

This section presents a computation method for the peak induced voltages on a buried pipeline having multiple sections with differing orientations with respect to an adjacent power line, or subject to pronounced variations of the driving field due to power line discontinuities. The method is based upon Thevenin decomposition procedures, leading to a node voltage analysis at pipeline or inducing field discontinuities.

Figure 3-8a illustrates the connection of several arbitrary pipeline sections adjacent to a power line with an electrical discontinuity (phase transposition). The peak induced voltages are computed by introducing a Thevenin observation plane at each junction, M, between dissimilar pipeline sections or at discontinuities of the driving field, as illustrated in Figure 3-8b. This placement of the Thevenin plane is based upon the previous analyses which showed the generation of exponential pipeline voltage peaks at all non-zero impedance terminations of a long/lossy pipe section.

In Figure 3-8b, $V_{\theta_{left}}$ and $Z_{\theta_{left}}$ denotes the Thevenin source voltage and impedance, respectively, for the pipeline seen to the left of the observation point. Similarly,

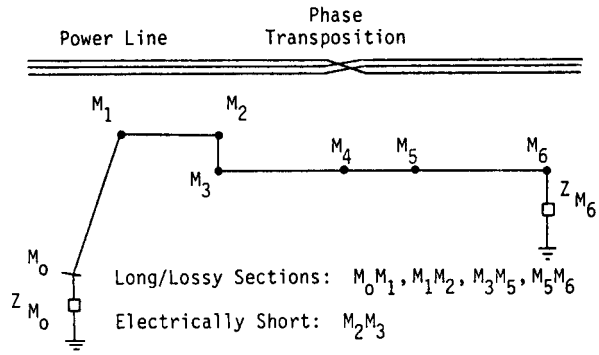

(a) Locations of Thevenin Observation Planes

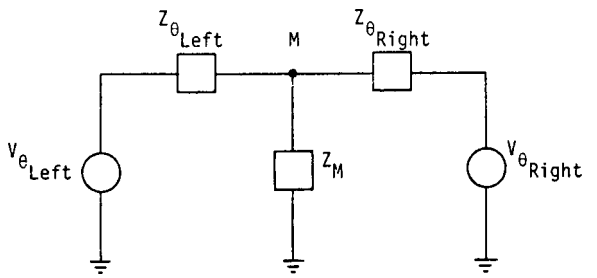

(b) Connected Thevenin Circuits for the Induced Voltage Peak at Observation Plane M

Figure 3-8. Peak-Voltage Analysis of a General Multi-Section Pipeline

$V_{\theta_{right}}$ and $Z_{\theta_{right}}$ denote the Thevenin equivalent circuit of the pipeline to the right of the observation point. Z_M denotes the mitigating grounding impedance (if any) at M. The voltage peak, V(M), is given by

$$V(M) = \frac{\dfrac{V_{\theta_{left}}}{Z_{\theta_{left}}} + \dfrac{V_{\theta_{right}}}{Z_{\theta_{right}}}}{\dfrac{1}{Z_{\theta_{left}}} + \dfrac{1}{Z_M} + \dfrac{1}{Z_{\theta_{right}}}} \qquad (3\text{-}21)$$

where V_θ and Z_θ can be obtained from the Thevenin equivalent circuits discussed previously.

From Eq. 3-21, $|V(M)|$ can equal zero if either

1. $Z_M = 0$, or (3-22a)

2. $V_{\theta_{left}} Z_{\theta_{right}} = -V_{\theta_{right}} Z_{\theta_{left}}$. (3-22b)

For arbitrarily arranged sections of buried pipeline, Eq. 3-22b is virtually the same as specifying an assembled pipeline with constant physical and electrical characteristics, spatial orientation, and driving field distribution. In other words, an induced voltage peak is expected on a buried pipeline where one of these properties changes abruptly, including the following points:

1. Junction between a long/lossy parallel section and a long/lossy non-parallel section (point M_1);
2. Junction between two long/lossy parallel sections having different separations from the power line (points M_2 and M_3);
3. Adjacent to a power line phase transposition or a substation where phasing is altered in some way (point M_4);
4. Junction between two long/lossy sections of differing electrical characteristics, for example, at a high resistivity soil - low resistivity soil transposition (point M_5);
5. Impedance termination (insulator or ground bed) of a long/lossy section (point M_6).

Points M_1, M_2, M_3, and M_6 are illustrative of pipeline orientation or termination discontinuities; point M_4 is illustrative of a discontinuity of the driving field; and point M_5 is illustrative of a discontinuity of the pipeline electrical characteristics. The magnitude of the voltage peak at any of these points is computed simply by applying Eq. 3-21 at the discontinuity to the Thevenin equivalent circuits for the pipeline sections on either side. In this way, the use of a single node equation, along with a collection of Thevenin equivalent pipeline circuits, is sufficient to estimate the voltage peaks on an arbitrary multi-section, buried pipeline.

Example: Application to Coupling at a Phase Transposition

Buried pipelines passing near phase transposition points of a power line have been observed to develop high induced voltages at the points of closest approach to the transpositions (8,19). No satisfactory theory for this phenomenon has been found in references reviewed to date. The phase transposition problem will be used as an example of the application of the unified coupling theory presented in this book.

The phase transposition is assumed to be as shown in Figure 3-9a. The following phase conductor currents are assumed:

$$I_1 = I_o$$

$$I_2 = I_o\, e^{j120^o} = I_o(-0.5 + j\ 0.866)$$

$$I_3 = I_o\, e^{-j120^o} = I_o(-0.5 - j\ 0.866)$$

To the left of the phase transposition, the undisturbed electric field at the nearby buried pipeline is given by Eq. 3-6b (for the case of no power line shield wires present) and by Eq. 3-5c (for the Carson mutual impedances between the phase conductors and the pipeline) as

$$E_{o_{left}} = \left\{ I_o \left\{ 5.92\cdot10^{-5} + j\ 3.77\cdot10^{-5}\left[2\ln\left(\frac{0.79\delta}{d_R}\right) + 1\right]\right\} + \right.$$

$$\left. I_o \left\{ 5.92\cdot10^{-5} + j\ 3.77\cdot10^{-5}\left[2\ln\left(\frac{0.79\delta}{d_S}\right) + 1\right]\right\} \cdot (-0.5 + j\ 0.866) + \right.$$

$$\left. I_o \left\{ 5.92\cdot10^{-5} + j\ 3.77\cdot10^{-5}\left[2\ln\left(\frac{0.79\delta}{d_T}\right) + 1\right]\right\} \cdot (-0.5 - j\ 0.866) \right.$$

$$= 3.77\cdot10^{-5}\, I_o \cdot \left[1.732\, \ln\left(\frac{d_S}{d_T}\right) + j\, \ln\left(\frac{d_S\, d_T}{d_R^{\,2}}\right)\right] \qquad (3\text{-}23a)$$

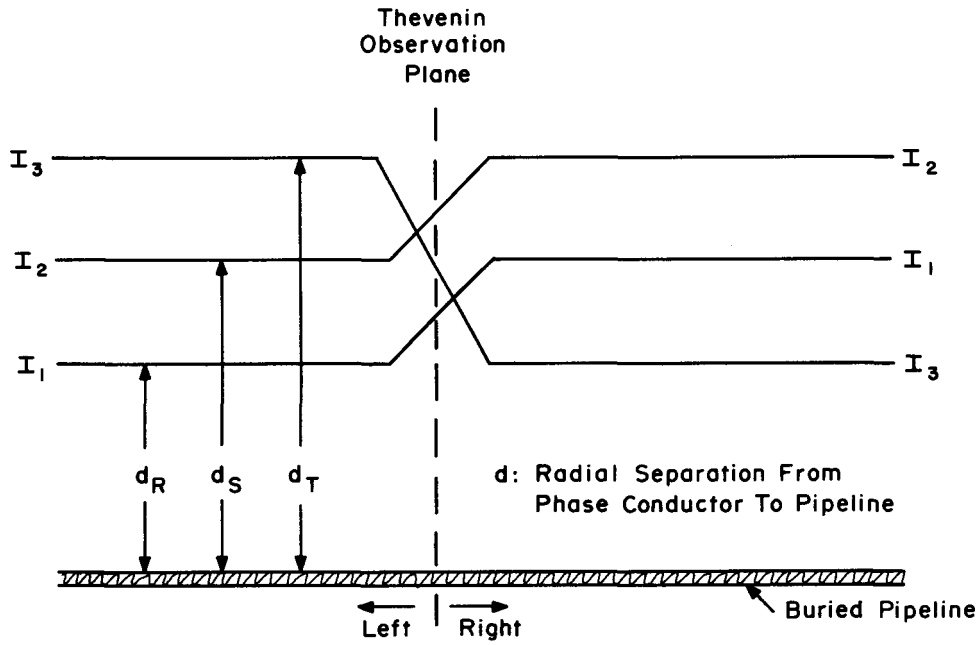

a) Phase Transposition Configuration

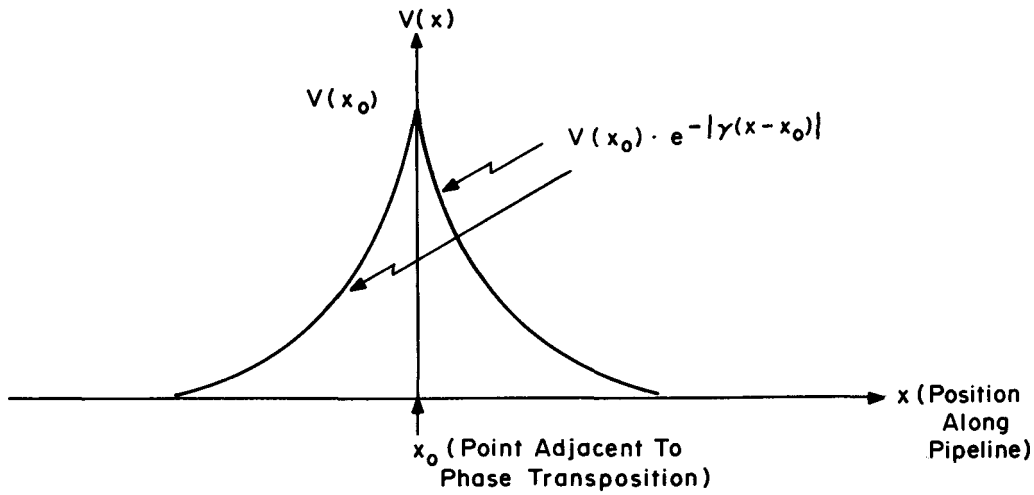

b) Induced Pipeline Potential

Fig. 3-9 PHASE TRANSPOSITION COUPLING EXAMPLE

To the right of the phase transposition, the undisturbed electric field at the buried pipeline is given by Eqs. 3-6b and 3-5c, as

$$E_{o_{right}} = \begin{cases} I_o \left\{5.92\cdot10^{-5} + j\ 3.77\cdot10^{-5}\left[2\ln\left(\frac{0.79\delta}{d_R}\right) + 1\right]\right\} \cdot (-0.5 - j\ 0.866) + \\ I_o \left\{5.92\cdot10^{-5} + j\ 3.77\cdot10^{-5}\left[2\ln\left(\frac{0.79\delta}{d_S}\right) + 1\right]\right\} + \\ I_o \left\{5.92\cdot10^{-5} + j\ 3.77\cdot10^{-5}\left[2\ln\left(\frac{0.79\delta}{d_T}\right) + 1\right]\right\} \cdot (-0.5 + j\ 0.866) \end{cases}$$

$$= 3.77\cdot10^{-5}\ I_o \cdot \left[1.732\ \ln\left(\frac{d_T}{d_R}\right) + j\ \ln\left(\frac{d_T\, d_R}{d_S^{\,2}}\right)\right] \qquad (3\text{-}23b)$$

In general, $E_{o_{right}} \neq E_{o_{left}}$. From the coupling theory developed, the discontinuity in the electric field must generate an induced pipeline voltage peak at the point of discontinuity (here, adjacent to the phase transposition). Introducing an observation plane at this point, the Thevenin equivalent circuits for the buried pipeline are given in Figure 3-6b as:

Looking to the left:

$$V_{\theta_{left}} = + \frac{E_{o_{left}}}{\gamma}\ ; \qquad Z_{\theta_{left}} = Z_o. \qquad (3\text{-}24a)$$

Looking to the right:

$$V_{\theta_{right}} = - \frac{E_{o_{right}}}{\gamma}\ ; \qquad Z_{\theta_{right}} = Z_o. \qquad (3\text{-}24b)$$

From Eq. 3-21, we have

$$|V(x_o)| = \left| \frac{\frac{E_{o_{left}}/\gamma}{Z_o} + - \frac{E_{o_{right}}/\gamma}{Z_o}}{\frac{1}{Z_o} + \frac{1}{Z_M} + \frac{1}{Z_o}} \right|$$

$$= \left| \left(\frac{E_{o_{left}} - E_{o_{right}}}{\gamma} \right) \cdot \left(\frac{Z_M}{Z_o + 2Z_M} \right) \right| \qquad (3\text{-}25a)$$

where Z_M is the mitigation grounding impedance at x_o. Substituting the results of Eq. 3-23 into Eq. 3-25a gives

$$|V(x_o)| = \left|\frac{3.77\cdot10^{-5}\ I_o\ Z_M}{\gamma(Z_o+2Z_M)}\right| \cdot \sqrt{3\left[\ln\left(\frac{d_R\,d_S}{d_T^{\,2}}\right)\right]^2 + 9\left[\ln\left(\frac{d_S}{d_R}\right)\right]^2} \qquad (3\text{-}25b)$$

where

d_R = 100 m, d_S = 110 m, d_T = 120 m;

I_o = 200 amperes;

$|\gamma|$ = 2 x 10^{-4} m^{-1}; and

Z_M = ∞.

Eq. 3-25b yields

$|V(x_o)|$ = 105 volts

as the value of the induced pipeline voltage at the point nearest the transposition.

For $Z_M = Z_o$, $|V(x_o)|$ drops only slightly to 70 volts, thus showing the ineffectiveness of even a relatively good grounding bed at x_o. The pipeline potential distribution decays exponentially from $|V(x_o)|$ with increasing distance from x_o, as shown in Figure 3-9b.

Alternative Method of Calculating Induced Pipeline Voltage

The transposition example presented again exemplifies the purely analytical approach to the solution of the voltage prediction problem. An alternative and computationally simpler approach is the use of the TI-59 hand calculator programs. Briefly, the following procedure is applicable to finding the induced voltage at any location along the pipeline.

1. Using the program PIPE, define the pipeline parameters.
2. Using the programs CARSON and CURRENTS for multiple pipelines or CARSON and FIELD for single pipeline situations, derive the driving electric source fields for the Thevenin equivalent circuits to either side of the point.
3. Define the node voltages and impedances for the equivalent circuits using the program THEVENIN.
4. Solve for the induced voltage at the point using the calculator program NODE.

The utilization of these programs is illustrated in the next section, where several "case histories" of induced pipeline voltage predictions are reviewed.

CASE HISTORIES OF PIPELINE INDUCED VOLTAGE PREDICTIONS

Five "case histories" of voltage prediction are presented here. The situations analyzed are varied and thus provide a diverse set of illustrative examples. In studying the examples, particular attention should be taken as to the approach to the problem, the use of the hand calculator programs and, in particular, the use of the Thevenin equivalent circuit concept.

A listing of the examples in the order they are presented and the principal points of theory or prediction methodology they demonstrate is as follows:

- Southern California Gas Company Line 235, Mojave Desert, Needles, California. This case history vividly shows the appearance of voltage peaks at the locations predicted, i.e., points of physical or electrical discontinuity. It also illustrates the simplicity of the prediction methodology when successive points of discontinuity are sufficiently separated so as to provide electrical isolation. For such a situation, simple calculations are sufficient and use of the hand calculator programs is not required.

- Northern Illinois Gas Company, Aurora, Illinois. The treatment for this pipeline is essentially non-mathematical. The ROW is relatively complex and the desire here was to illustrate the methodology to be used for identifying the critical points of voltage induction by inspection.

- Consumers Power Company Line 1800, Kalamazoo, Michigan. The mathematical/hand calculator oriented approach is used here to derive the pipeline voltage profile. The ROW configuration is relatively simple, thus providing a good first introduction to obtaining mathematical solutions. This case illustrates how to take into account end terminations of the pipeline and evaluate their effects.

- Texas Gas Transmission Corporation, Memphis, Tennessee. This case history of voltage prediction is possibly the most complicated of the set presented in that four gas pipelines are collocated with several power circuits. The analysis becomes difficult because of electrical interties between the pipelines at several locations. The solution illustrates repeated use of the Thevenin equivalent circuit concept to produce successive simplifications of the problem.

- Consumers Power Company Karn-Weadock Line, Bay City, Michigan. The solution of the induced voltage prediction problem for this crude oil pipeline is obtained by an approach utilizing field measured data as much as possible in contrast to the purely analytical solutions presented for the previous case histories.

Voltage Prediction
Southern California Gas Company Line 235, Needles, California

This case history vividly shows the appearance of voltage peaks at the locations predicted, i.e., points of physical or electrical discontinuity. It also illustrates the simplicity of the prediction methodology when successive points of discontinuity are sufficiently separated so as to provide electrical isolation. For such a situation, simple hand calculations are sufficient and use of the hand calculator programs is not required.

Corridor Description. The Southern California Edison 500 kV electric power transmission line meets the Southern California Gas Company 34-inch diameter gas pipeline at pipeline milepost 47 (47 miles west of Needles, California) and leaves it at milepost 101.7, as shown in Figure 3-10. The power line has a horizontal configuration with a full clockwise (phase-sense) transposition at milepost 68 and single-point-grounded lightning shield wires. During the test period, an average loading of 700 amperes was reported for each phase conductor. No other power lines, pipelines, or long conductors share the right-of-way.

Measurements performed during the tests indicated an average earth resistivity of 400 ohm-meter. Based upon furnished data, a value of 700 $k\Omega\text{-}ft^2$ was assumed as the average pipeline coating resistivity. Using these values as data input for the pipeline parameter graphs of Section 2, the pipeline propagation constant, γ, was obtained as $(0.115 + j\ 0.096)\ km^{-1} = 0.15\underline{/40^o}\ km^{-1}$; and the pipeline characteristic impedance, Z_o, was obtained as $(2.9 + j\ 2.4)$ ohms $= 3.4\underline{/40^o}$ ohms. Alternatively, the program PIPE may be used to find these parameters more accurately.

Voltage Peak Locations and Magnitudes. The node analysis discussed earlier in the section predicts the appearance of separably calculable pipeline voltage peaks at all discontinuities of a pipeline-power line geometry spaced by more than $2/\text{Real}(\gamma)$ meters along the pipeline. Using the value of γ obtained for the pipeline, all geometry discontinuities spaced by more than $(2/0.115)$ km $= 17.4$ km $\simeq 10$ miles can be assumed to be locations of separable induced voltage peaks. These discontinuities include:

1. Milepost 101.7 (near end of pipeline approach section);
2. Milepost 89 (separation change);
3. Milepost 78 (separation change);

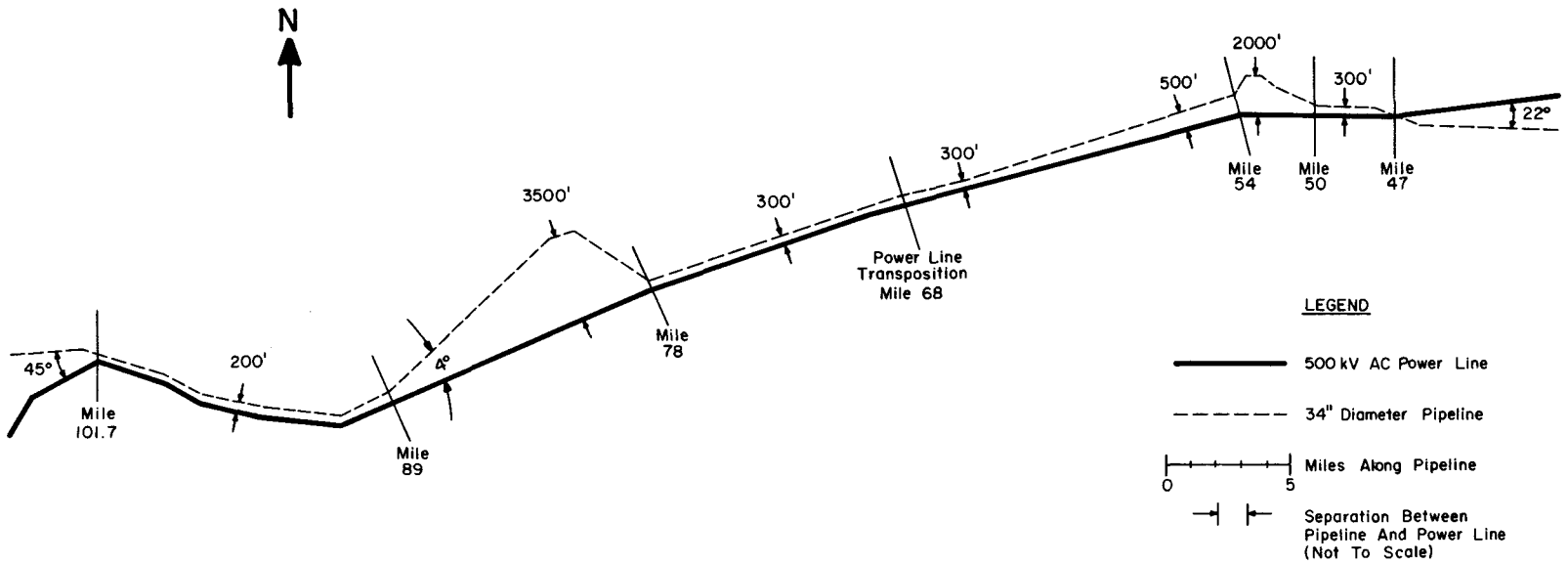

Fig. 3-10 MOJAVE DESERT PIPELINE–POWER LINE GEOMETRY

4. Milepost 68 (power line phase transposition);

5. Milepost 54 (separation change); and

6. Milepost 47 (near end of pipeline departure section).

The voltages at these points of electrical discontinuity were predicted by application of Eq. 3-21 to the Thevenin equivalent pipeline circuits derived for either direction from each of the points. The pipeline characteristics, γ and Z_o, were assumed constant with position along the pipeline, causing each Thevenin source impedance to be fixed at Z_o (due to the long/lossy nature of the adjacent pipe sections). Further, Z_M was assumed to equal infinity at each Thevenin plane because no ac mitigating grounds were connected at the time to the pipeline, thus simplifying the equation to

$$V(M) = \frac{V_{\theta_{left}} + V_{\theta_{right}}}{2} \qquad (3\text{-}26)$$

To illustrate this approach, the predicted voltage peaks are calculated using Eq. 3-26. Tables 3-1 and 3-2 list the results. The predicted electric fields were based on the following power line geometry:

1. The geometric mean height of the phase conductor equal to 60 feet;

2. Distance between phase wires equal to 32 feet; and

3. Horizontal circuit configuration.

At a given distance measured from the center phase wire, insertion of the appropriate distances into the program CARSON yielded the mutual impedances between each phase conductor and the pipeline (burial depth equal to three feet). The following phase currents were then assumed:

1. Phase wire closest to pipeline: $I = 700\underline{/+120^o}$ amperes

2. Center phase wire: $I = 700\underline{/-120^o}$ amperes

3. Farthest phase wire: $I = 700\underline{/0^o}$ amperes

Program FIELD was then used to calculate the electric field using the above currents and the mutual impedances found by Program CARSON.

Table 3-1

LONGITUDINAL ELECTRIC FIELD MAGNITUDE*

Distance from Center Phase (feet)	Predicted Field (volts/km)	Measured Field (volts/km)
0	10.2	10.4
20	18.3	14.3
40	27.3	24.5
60	29.0	27.0
80	27.2	22.2
100	24.2	22.2
200	14.0	14.0
300	9.5	8.5
600	4.8	4.0
1000	2.9	1.6
5000	0.4	-
10,000	0.1	-

Table 3-2

ELECTRIC FIELD PHASE**

	West of Transposition	East of Transposition
North of power line	-120^{o}	0^{o}
South of power line	$+ 60^{o}$	180^{o}

*For the balance current case, $|E_x|$ was found to be the same for equal distances both north and south of the power line and also on both sides of the power line transposition.

**Table 3-2 lists the predicted phase of E_x at distances between 60 feet and 2000 feet from the power line. The phase tended to remain relatively constant at the tabulated values except for rapid variations directly under the power line. The current in the southernmost phase wire, I_A, serves as the phase reference ($\phi=0^{o}$).

It was not possible to measure the absolute values of the electric field phase relative to the reference phase current, I_A. However, phase measurements relative to two ground locations were possible, and hence differences of the absolute values listed in Table 2 were measurable. For example, confirmation of the phase reversal occurring on opposite sides of the power line was readily obtained.

Milepost 101.7. A voltage peak occurs here because of a corridor geometric discontinuity, namely, the convergence of the pipeline and power line at an angle of 45° to a separation of 200 feet (0.06 km). Based upon a predicted longitudinal electric field of $14.0\angle -120^{\circ}$ V/km at this separation, apply Eqs. 3-20 and 3-18 to compute the two Thevenin voltage sources.

Looking to the west:

$$V_{\theta_{west}} \simeq \frac{14\angle -120^{\circ} \times (0.3 - 0.06)}{4 \times \tan 45^{\circ}} = 0.8\angle -120^{\circ} \text{ volts}$$

Looking to the east:

$$V_{\theta_{east}} = \frac{-14\angle -120^{\circ}}{0.15\angle 40^{\circ}} = 93.3\angle 20^{\circ} \text{ volts}$$

Combining the Thevenin equivalent circuits by using Eq. 3-26

$$|V(101.7)| = 0.5 \times |(0.8\angle -120^{\circ} + 93.3\angle 20^{\circ})| = 46.3 \text{ volts}$$

The actual measured pipeline voltage at this point was 46 volts.

Milepost 89. A voltage peak occurs here because of a corridor geometric discontinuity, namely, the divergence of the pipeline and power line at an angle of about 4° from a separation of 150 feet (0.046 km) to a separation of 3500 feet (1.07 km). Based upon a predicted electric field of $18.0\angle -120^{\circ}$ V/km at the 150-foot separation, Eqs. 3-18 and 3-20 are similarly applied to compute the Thevenin voltage sources.

Looking to the west:

$$V_{\theta_{west}} = \frac{18\angle -120^{\circ}}{0.15\angle 40^{\circ}} = 120.0\angle -160^{\circ} \text{ volts}$$

Looking to the east:

$$V_{\theta_{east}} \simeq \frac{-18\angle -120^{\circ} \times (0.3 - 0.046)}{4 \times \tan 4^{\circ}} = 16.3\angle 60^{\circ} \text{ volts}$$

Combining the Thevenin equivalent circuits:

$$|V(89)| = 0.5 \times |(120\angle -160^{\circ} + 16.3\angle 60^{\circ})| = 54.0 \text{ volts}$$

The actual measured pipeline voltage at this point was 53 volts.

Milepost 78. A voltage peak occurs here because of a corridor geometric discontinuity, namely, the convergence of the pipeline and power line at an angle of about 19^{o} from a separation of 3500 feet (1.07 km) to a separation of 300 feet (0.092 km). Based upon a predicted electric field of $9.5\angle -120^{o}$ V/km at the 300-foot separation, Eqs. 3-18 and 3-20 are again used to compute the Thevenin voltage sources.

Looking to the west:

$$V_{\theta_{west}} \simeq \frac{9.5\angle -120^{o} \times (0.3 - 0.092)}{4 \times \tan 19^{o}} = 1.4\angle -120^{o} \text{ volts}$$

Looking to the east:

$$V_{\theta_{east}} = \frac{-9.5\angle -120^{o}}{0.15\angle 40^{o}} = 63.3\angle 20^{o} \text{ volts}$$

Combining the Thevenin equivalent circuits:

$$|V(78)| = 0.5 \times |(1.4\angle -120^{o} + 63.3\angle 20^{o})| = 31.1 \text{ volts}$$

The actual measured pipeline voltage at this point was 34 volts.

Milepost 68. A voltage peak occurs here because of a corridor electrical discontinuity, namely, the power line transposition at a constant separation of 300 feet (0.092 km). Based upon a predicted electric field of $9.5\angle -120^{o}$ V/km at the 300-foot separation to the west of the transposition, and a predicted field of $9.5\angle 0^{o}$ V/km at the 300-foot separation to the east of the transposition, application of Eq. 3-18 yields the Thevenin voltage sources.

Looking to the west:

$$V_{\theta_{west}} = \frac{9.5\angle -120^{o}}{0.15\angle 40^{o}} = 63.3\angle -160^{o} \text{ volts}$$

Looking to the east:

$$V_{\theta_{east}} = \frac{-9.5\angle 0^{o}}{0.15\angle 40^{o}} = 63.3\angle 140^{o} \text{ volts}$$

Combining the Thevenin equivalent circuits:

$$|V(68)| = 0.5 \times |(63.3\angle -160^{o} + 63.3\angle 140^{o})| = 54.8 \text{ volts}$$

The actual measured pipeline voltage at this point was 54 volts.

Milepost 54. A voltage peak occurs here because of a corridor geometric discontinuity, namely, the divergence of the pipeline and power line from a separation of 500 feet (0.15 km) to an average separation of about 1200 feet (0.37 km). Based upon a predicted electric field of $5.8\underline{/0^o}$ V/km at the 500-foot separation, and a predicted field of $2.4\underline{/0^o}$ V/km at the 1200-foot separation, again applying Eq. 3-18, yields:

Looking to the west:

$$V_{\theta_{west}} = \frac{5.8\underline{/0^o}}{0.15\underline{/40^o}} = 38.7\underline{/-40^o} \text{ volts}$$

Looking to the east:

$$V_{\theta_{east}} = \frac{-2.4\underline{/0^o}}{0.15\underline{/40^o}} = 16.0\underline{/140^o} \text{ volts}$$

Combining the Thevenin equivalent circuits:

$$|V(54)| = 0.5 \times |(38.7\underline{/-40^o} + 16.0\underline{/140^o})| = 11.4 \text{ volts}$$

The actual measured pipeline voltage at this point was 11 volts.

Milepost 47. A voltage peak occurs here because of a corridor geometric discontinuity, namely, the divergence of the pipeline and power line at an angle of 22^o from a separation of 300 feet (0.092 km). Based upon a predicted electric field of $9.5\underline{/0^o}$ V/km at this separation, Eqs. 3-18 and 3-20 give:

Looking to the west:

$$V_{\theta_{west}} = \frac{9.5\underline{/0^o}}{0.15\underline{/40^o}} = 63.3\underline{/-40^o} \text{ volts}$$

Looking to the east:

$$V_{\theta_{east}} = \frac{-9.5\underline{/0^o} \times (0.3 - 0.092)}{4 \times \tan 22^o} = 1.2\underline{/180^o} \text{ volts}$$

Combining the Thevenin equivalent circuits:

$$|V(47)| = 0.5 \times |(63.3\underline{/-40^o} + 1.2\underline{/180^o})| = 31.2 \text{ volts}$$

The actual measured pipeline voltage at this point was 25 volts.

Figure 3-11 plots both the measured ac voltage profile of the Mojave pipeline and the predicted voltage peaks. The solid curve represents voltages measured during the field test; the dashed curve is a set of data (normalized to 700 amperes power line current) obtained by a Southern California Gas Company survey. From this figure, it is apparent that the prediction method succeeded in locating and quantizing each of the pipeline voltage peaks with an error of less than ± 20%. In a dense urban environment, the prediction calculations would become more complex, as shown in the following case histories, but would still be within the scope of the distributed source theory and the programmable calculator programs.

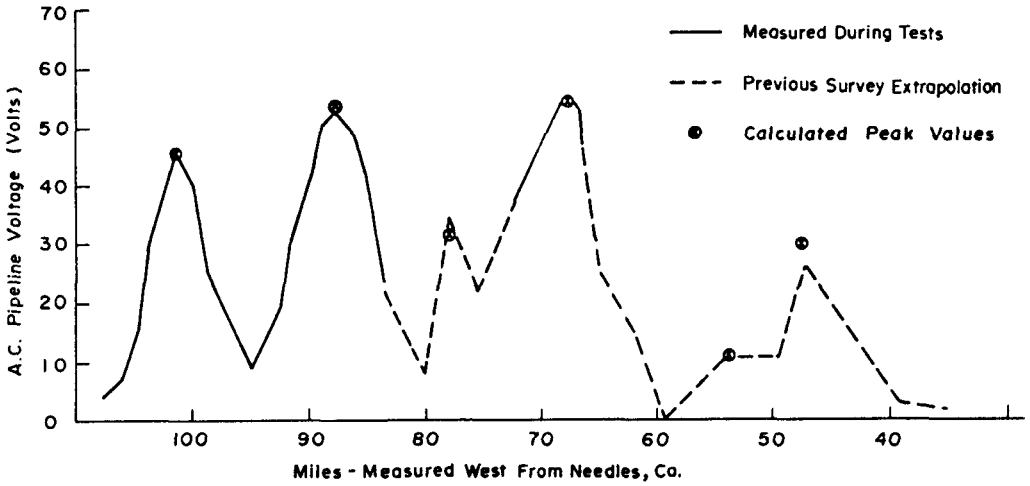

Figure 3-11. Mojave Desert Pipeline Voltage Profile

Induced Voltage Prediction
Northern Illinois Gas 36-Inch Aux Sable Pipeline, Aurora, Illinois

Introduction. The treatment for this pipeline is essentially non-mathematical. The ROW is relatively complex and the desire here was to illustrate the methodology to be used for identifying the critical points of voltage induction by inspection. Induced voltage predictions for the 36-inch Aux Sable line have been made and the resulting voltage profile presented in Figure 3-14. The voltage predictions have been made on the basis of longitudinal electric field measurements along the pipeline route in combination with an analytical model to obtain worst case estimates. The following discusses field measurements and subsequent electric field calculations, both of which are plotted in Figure 3-13. Rationale for derivation of the voltage profile is also presented.

The pipeline section under consideration extends in a north-south direction for a distance of approximately thirty miles. It leaves a synthetic gas plant (electrically terminated in an insulator) at Station #00+00 and proceeds northward to a valve site at Station #1661+00 where it likewise is terminated in an insulator. The principal characteristics of the ROW profile are diagrammed in Figure 3-12.

It enters the Commonwealth Edison ROW at Station #62+100, where it encounters four 345 kV vertical circuits and one 138 kV horizontal circuit as shown. In the region from Station #167+70 to Station #740+54, a ten-inch diameter hydrocarbon pipeline joins the ROW moving from one side of the ROW to the other and back again, as shown. At Station #740+54, the two east towers and the ten-inch hydrocarbon pipeline leave the ROW, and the Aux Sable pipeline crosses the ROW to within thirty feet of the remaining westernmost tower. At Station #903+65, two vertical 138 kV circuits enter the ROW. At Station #1046+50, the pipeline crosses to between the two towers and a 34-inch Lakehead pipeline is encountered, which leaves the ROW at approximately Station #1540+85.

Inspection of Figure 3-12 shows several electrical/physical discontinuities, thus leading to the prediction of a like number of voltage peaks on the pipeline.

Measured Longitudinal Electric Field. Measurement of the magnitude of the longitudinal electric field existing along the pipeline route was made at the following stations: 73+00, 114+20, 178+50, 335+00, 506+30, 640+00, 761+00, 836+50, 845+00, 960+00, 1118+48, 1123+00, 1302+00, 1488+00, 1606+60. The data are plotted in Figure 3-13.

Data were obtained with a HP3581A electronically tuned voltmeter which measured the voltage drop in a 15-meter horizontal probe wire laid along the ROW and grounded at both ends to a depth of approximately 18 inches. Electric field strength was calculated by dividing the measured voltage by the length of the probe wire.

Inspection of Figure 3-13 shows the field extant at approximately Station 62+00, where the pipeline enters the Edison ROW. The field strength rises sharply at approximately Station 500+00. This rise is primarily due to the reduction in separation between the pipeline and the overhead transmission lines at this point. The electric field drops to a much lower value at Station 640+00 because of the

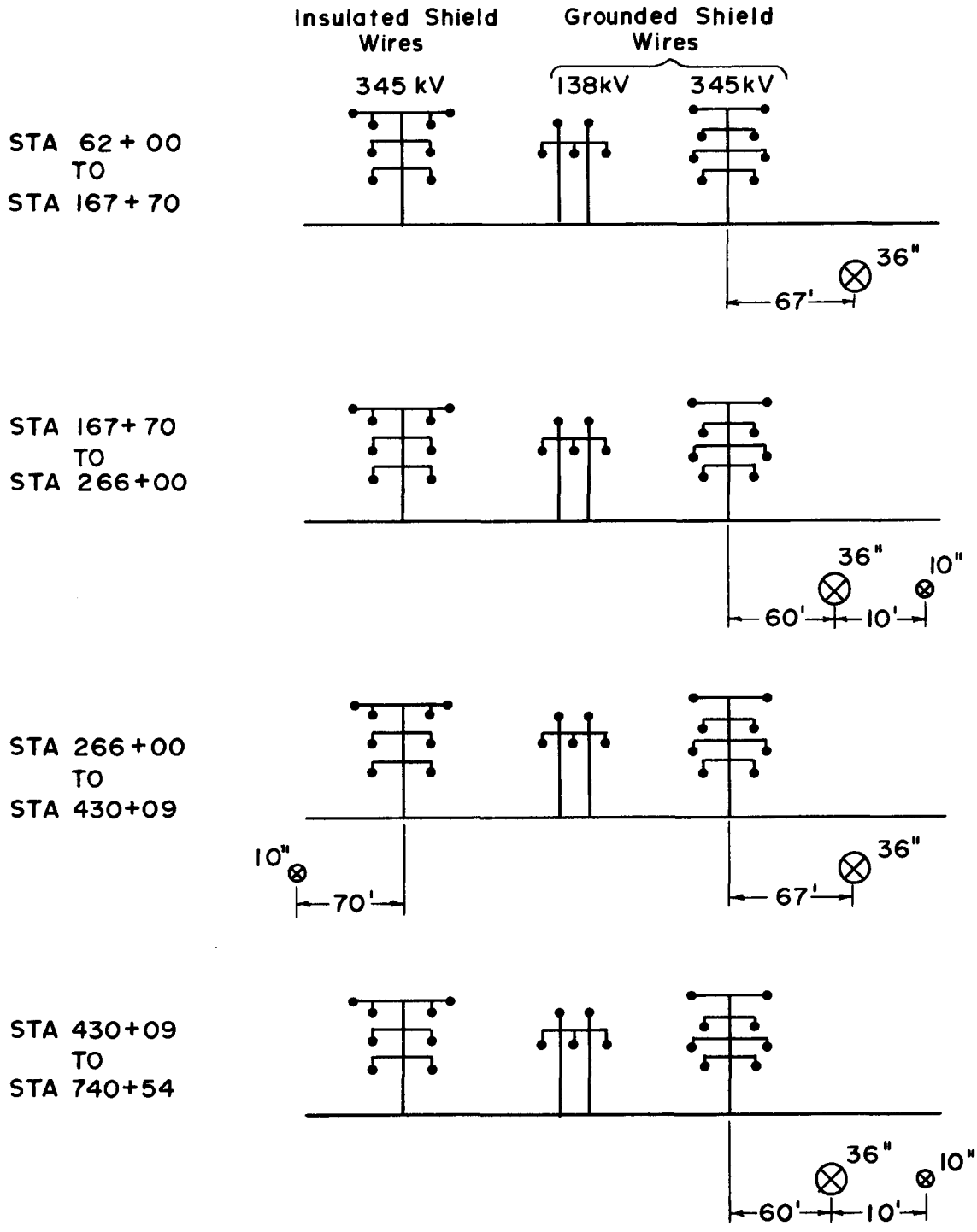

Fig. 3-12 PROFILE LOOKING NORTH

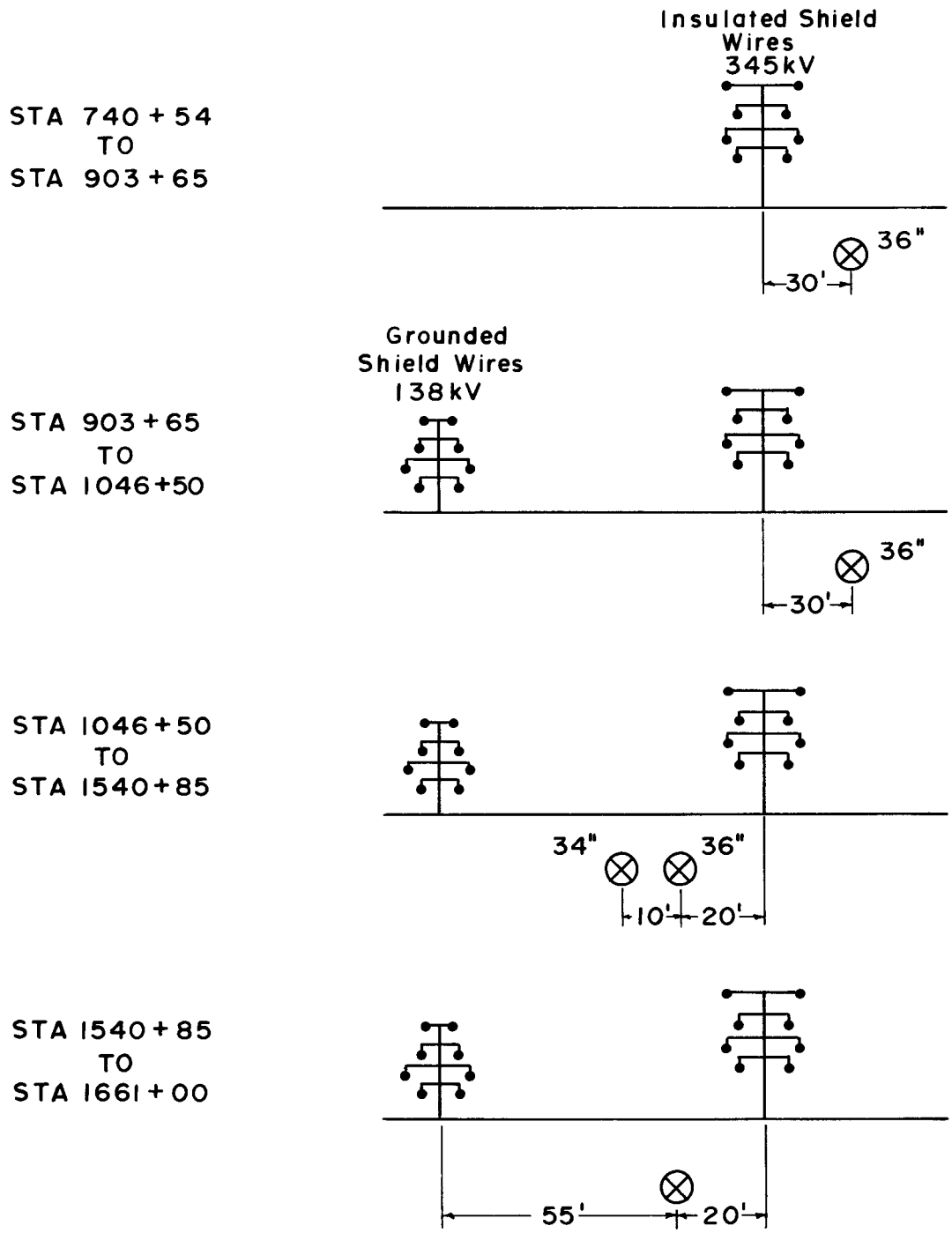

Fig. 3-12 (cont.) PROFILE LOOKING NORTH

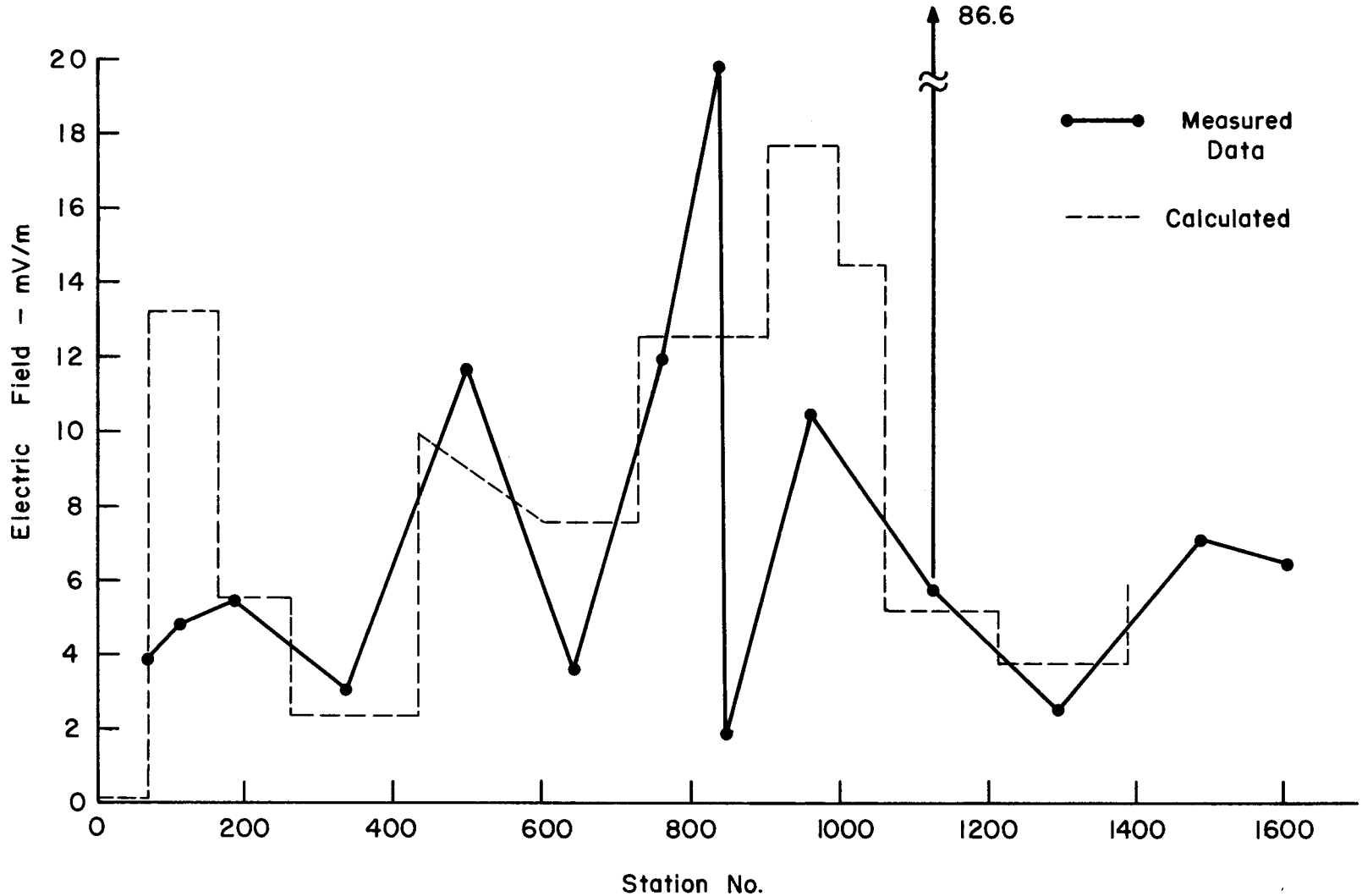

Fig. 3-13 36" AUX SABLE HORIZONTAL ELECTRIC FIELD PROFILE

ten-inch hydrocarbon pipeline which leaves the ROW at Station 740+00. (A similar drop at Station 334+00 is attributable to the particular power line current unbalances at the time of the measurement.)

Measurements made at Stations 836+50 and 845+00 show a ten-to-one variation in less than 1000 feet which can be attributable only to localized interference. These measurements were made in proximity to the village of Plainfield pumping station and possibly suffer interference from stray underground pipe currents. Although these electric fields were in existence at the time of measurement, because of their localized nature, their effect upon the resulting pipeline voltage would be small.

An extremely high electric field, again of a localized nature, was noted at Station 1118+48. This field appears to be introduced by electric currents leaking off of a grounded pipeline casing at this location. Apparently, the 34-inch Lakehead pipeline sharing the Edison ROW is capacitively connected to the road crossing casing at this point. To determine the effects of this current leakage induced electric field in detail would have required a more extensive set of measurements in this area. However, it appears that because of the localized nature of this electric field discontinuity, its effects upon the overall pipeline voltage profile will be superseded by higher magnitude effects arising from the electric field discontinuity appearing at Station 1050+00. Hence, additional measurements in this location would not be considered cost effective.

The electric field experiences a strength reduction in the vicinity of Station 1302+00 because of a phase transposition on a 138-kV circuit in this area. The electric field from this location to the insulator at Station 1618 is difficult to measure with certainty because of the junction of many electrical transmission circuits at Station 1606+00.

Computed Electric Field. In the interest of economy, magnitude only electric field data were measured. In order not to predict unduly pessimistic induced voltage levels on the pipeline, a knowledge of the phase of the electric field is necessary. Hence, computations of the electric field expected along the ROW were made using values for the electric transmission line phase currents existing at the time measurements were made. These currents were monitored and recorded by Commonwealth Edison on an hourly basis.

The calculations were made by the use of Carson's mutual impedance formulas and the electric field contributions from the individual power line circuits were vectorially added for the specific locations at which measurements were made along the ROW. A plot of the calculated magnitude for the electric field is also made in Figure 3-13 for comparison with the measured data. Except for a few points which will be individually discussed, the calculated and measured values generally agree. The shapes of the curves, however, are different. The measured data points were arbitrarily connected by straight lines. However, calculated data points were joined by step functions. The reason for this is that along the ROW if the pipeline-power line physical geometry or electrical coupling remains constant, then the electric field also is constant. However, locations of electrical or physical discontinuity cause a relatively sudden change in the electric field, as shown by the step function variations in Figure 3-13. The approximate locations of the significant discontinuities are:

Station No.	Discontinuity
62+00	36-inch Aux Sable pipeline enters Edison ROW
167+00	10-inch Hydrocarbon pipeline enters ROW
270+00	10-inch Hydrocarbon line crosses to far end of ROW
430+00	10-inch Hydrocarbon line crosses ROW, separation of 36-inch pipe from Edison tower reduced to 30 feet
740+00	Three electrical circuits leave the ROW
900+00	Two 138-kV circuits enter the ROW
990+00	Transposition of phases on 138-kV circuit
1060+00	34-inch Lakehead pipeline enters ROW: Aux Sable pipeline crosses to center of ROW
1220+00	138-kV circuit phase transposition
1390+00	138-kV circuit phase transposition
1618+00	Pipeline insulator.

The first and largest deviation in calculated electric field magnitude relative to the measured value occurs between stations 62+00 and 167+00. The reason for this deviation is that the calculation of the electric field is critically dependent upon knowing the exact value of the electric circuit currents. Because of

the vectorial nature of the electric field, calculation of its magnitude at times involves the subtraction of two nearly equal large numbers and, hence, a small error in one number can result in a much larger variation in the result. Recognition of this fact and knowledge of the physical processes involved allows compensation to be made, thus minimizing errors in subsequent voltage computations. In general, heretofore, this effect has not been appreciated, thus leading to apparent inconsistencies in the functional relationships between the sources of the induced field, that is, the electric circuit's phase currents and the resulting pipeline voltages. This effect does not negate the theory, but yields an explanation for observed variations. Progressing along the ROW, the one exception to the step function discontinuity rule is found in the Station 430+00-600+00 region. Here, the electric field strength diminishes in roughly linear fashion to a low in the Station 600+00-730+00 region. This gradual reduction is a result of induced current in the ten-inch hydrocarbon pipeline lying along the ROW. It shows that multiple pipelines on the same ROW will, in general, cause a weakening of the electric field at the other pipelines and, thus, effect a reduction in the induced pipeline voltage. The plot for the calculated field shows that the extreme variations experienced between Stations 836+00 and 845+00 cannot be accounted for on the basis of purely inductive effects. Hence, it is believed that these variations are local effects due to the Plainfield Village pumping station and, as such, do not impact the voltage calculations to a significant extent. The difference between the calculated and measured electric field values in the region Stations 900+00-990+00 can be accounted for again by small variations in one or more of the power line currents, and this deviation does not significantly impact the induced voltage predictions.

Since differences in the computed and measured electric field magnitudes can be accounted for, it is believed that calculated electric field phase information is reasonably correct. Hence, the voltage profile discussed in the following subsection was based on the joint use of measured magnitude data and calculated phase information.

Voltage Profile from Measured Data. A pipeline voltage profile determined from the measured magnitude data and calculated phase is plotted as the dashed curve in Figure 3-14. Inspection of the plot shows that peaks of induced voltage appear at locations corresponding to power line-pipeline discontinuities with an exponential decay betweek peaks. If the discontinuities are reasonably separated, the voltage peak is approximately equal to

NOTE: Profiles Are Drawn For A Pipe
Coating Resistance Of 100,000 ohms-ft^2
For 200,000 ohms-ft^2 Coating Resistance
Multiply Voltages By 1.5 .

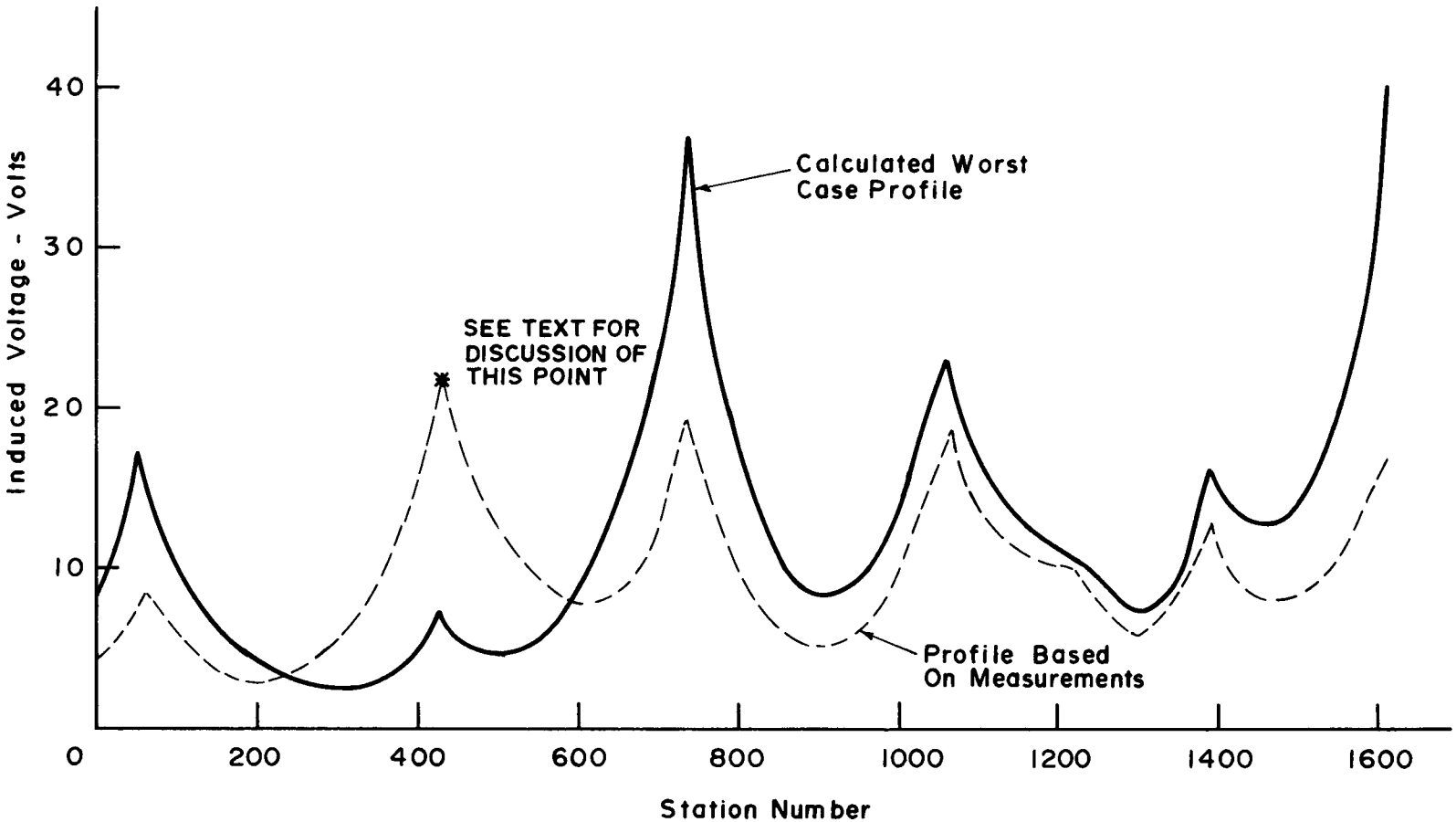

Fig. 3-14 36" AUX SABLE LINE VOLTAGE PROFILE

$$V_{peak} = \frac{E_1 - E_2}{2\gamma} \qquad (3\text{-}27)$$

where E_1 and E_2 are, respectively, the vector electric fields on either side of the discontinuity, and γ is the pipeline propagation constant which is a function of pipe steel parameters, pipe diameter, ground resistivity and especially of pipe coating conductivity. Since E_1 and E_2 are vectors, their difference angle is of extreme importance. For example, if it approaches zero, the resultant field will be the difference of the two, thus resulting in a relatively low voltage at the discontinuity. This point is exemplified at Station 900 since even though it is a location of a discontinuity, the resultant voltage is low. However, when the fields differ in angle by 180 degrees, then their effects are additive, thus causing high induced voltages such as at Station 740.

Insulators appearing at the ends of the pipeline act as <u>severe</u> electrical discontinuities and the voltage peak at an insulator may be approximated by

$$V_{ins} \simeq \frac{E}{\gamma} \qquad (3\text{-}28)$$

where E is the electric field in the vicinity of the insulating junction.

The predicted voltage plot of Figure 3-14 covers the ROW from Station 00 to Station 1618+00, which represents the region of highest induced voltages for the pipeline.

<u>Pipeline Propagation Constant</u>. The previous calculations show that the induced voltage peaks are an inverse function of the pipeline propagation constant, the value of which is extremely sensitive to pipeline coating resistance. The curve of Figure 3-14 is based on a value of $|\gamma| = 0.37\ km^{-1}$, which conforms to a pipeline coating resistance of 100,000 ohms-ft^2 for the pipe diameter and average soil conditions. Although higher resistances are desirable when considering cathodic protection requirements, they cause an increase in the induced pipeline voltage. For example, a coating resistance of 200,000 ohm-ft^2 would result in a value of $|\gamma| = 0.25$, and thusly increase predicted voltage levels in Figure 3-14 by 48%; 300,000 ohms-ft^2 would result in a value of $|\gamma| = 0.21\ km^{-1}$, causing an increase in predicted voltage levels of 76%.

The coating resistivity after construction is completed is difficult to predict. For example, it has been reported that a coating with an average measured

resistivity after burial of 200,000 ohms-ft^2 in moderately conductive soil was found to exhibit a high value of as much as 1,135,000 ohms-ft^2 and a low value of 10,000 ohms-ft^2 over a short section.

"Worst Case" Voltage Profile. A pipeline situated on a ROW with electrical circuits is in a constantly changing electromagnetic environment. Hence, depending upon the loading of the power lines, the degree of load unbalance, etc., the pipeline voltage at a given location will vary in time, and significant changes can occur in a time frame of hours or less. The profile determined from the measured data nearly approximates the pipeline voltage which would have existed at the time of electric field measurement. Some differences will exist because logistics force measurements to be made over a period of time greater than the period of "electrical stationarity" of the power line phase currents. An instantaneous "snapshot" of the electric field over the complete line length would provide the necessary information for an exact profile determination. However, compensation of data obtained in time sequence is possible.

It must be recognized that a dynamic situation exists on the ROW as regards electromagnetic induction. Measurements made in a relatively short time frame constitute only a single sampling of a time varying process; i.e., the voltage profile can vary in time. Hence, to account for these variations, a "worst case" profile has been computed for the condition of average load currents on the electrical circuits carried on the ROW, but where peak unbalances in phase load currents for a given circuit of up to $\pm$ 5% may be expected. (Such unbalanced conditions generally are the principal cause of pipeline voltage fluctuations.)

Applying a probability model for the induction phenomena to this situation results in the solid curve profile plotted in Figure 3-14. Since this curve more nearly represents worst case conditions, it can be expected to always lie above the dashed curve representing conditions at the time of measurement. One exception to this rule is found at Station 430+00 and vicinity. Here, the "worst case" computed curve lies below the voltage peak calculated from measured data. Detailed analytical investigation of the electrical characteristics of the discontinuity at this location has shown that the peak calculated from the measured data is incorrect and appears because of a relatively significant change in power line current between the times the electric field was measured at locations south and north of Station 430+00, respectively.

Voltage Profile
Consumer Power Company, Kalamazoo Line 1800 Pipeline

Introduction. The mathematical/hand calculator oriented approach is used here to derive the pipeline voltage profile. The ROW configuration is relatively simple, thus providing a good first introduction to obtaining mathematical solutions. This case illustrates how to take into account end terminations of the pipeline and evaluate their effects. Line 1800 is a 20-inch-diameter gas transmission pipeline located north of Kalamazoo, Michigan. It runs approximately south to north for a distance of 31.1 km, starting at the Plainwell valve site and terminating at the 30th Street valve site at the north end. It parallels two 345 kV, three-phase circuits for a distance of 27.1 km, starting at a distance of 3.0 km north of the Plainwell valve site and ending at approximately 1 km south of the 30th Street valve site. For the region of parallelism, the average ROW profile is shown in Figure 3-15.

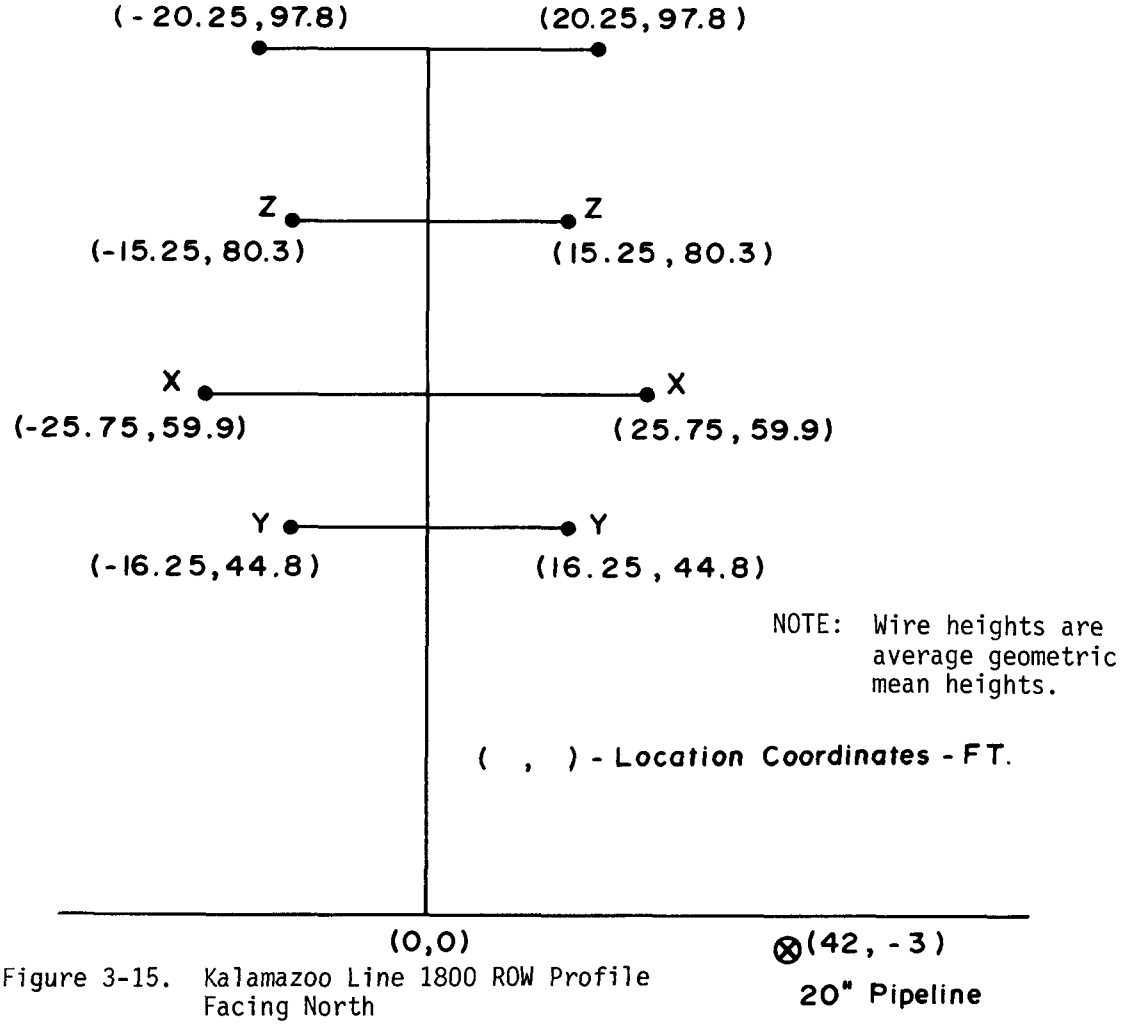

Figure 3-15. Kalamazoo Line 1800 ROW Profile Facing North

An ac pipeline voltage survey was made along this ROW at a time when the currents in the electric circuits were being monitored. Based upon the developed prediction theory, a voltage profile was calculated. The calculated and measured profiles are plotted in Figure 3-16 and, as shown, good agreement between both plots exists.

The pipeline is terminated at both ends in insulators with grounding cells across the insulators. At the time of the survey, it appeared that the grounding cell at the 30th Street valve site was partially shorted since bonding across the insulator did not cause a significant redistribution in pipe voltage and current. Hence, the pipeline at this location was electrically connected to a 24-inch pipeline (which, in turn, was electrically bonded to another 16-inch pipeline).

At the Plainwell valve site, a relatively good grounding system exists to the south of the pipeline insulator which is formed by the electrical connection of a 12-inch pipeline, several ground rods at the valve site, and a tie-in to the electrical power system neutral at this point. With the grounding cell connected across the insulator, which is normal operation, the pipeline is well grounded at the south end, and hence, mitigates ac induction at this end. The grounding cell at this end was fairly well dried out, and hence, the pipeline experiences relatively high voltage levels at the valve site if this bond is removed.

Inspection of Figure 3-16 shows the voltage reduction experienced by bonding across the insulator and achieving pipeline grounding at this point. Experimental and calculated profiles agree excellently. At several points along the pipeline, magnesium anodes have been installed, but were disconnected while measurements were being made. To test the effect of such anodes on the reduction of induced ac voltages, measurements were also taken with a mag anode connected at 112th Street ($\simeq$ 5 km north of Plainwell valve). A single anode will provide an ac voltage reduction only at or near the point of connection, and the resulting calculated and measured voltage levels are plotted as the diamond-shaped points in the figure. In general, if voltage mitigation by means of mag anodes was desired over a large distance, placement of successive anodes at distances much less than γ^{-1}, the pipeline propagation constant, would be necessary. This procedure would effect the equivalent of a pipe coating of lower resistivity and, hence, uniformly reduce the voltage along the complete length of the pipeline.

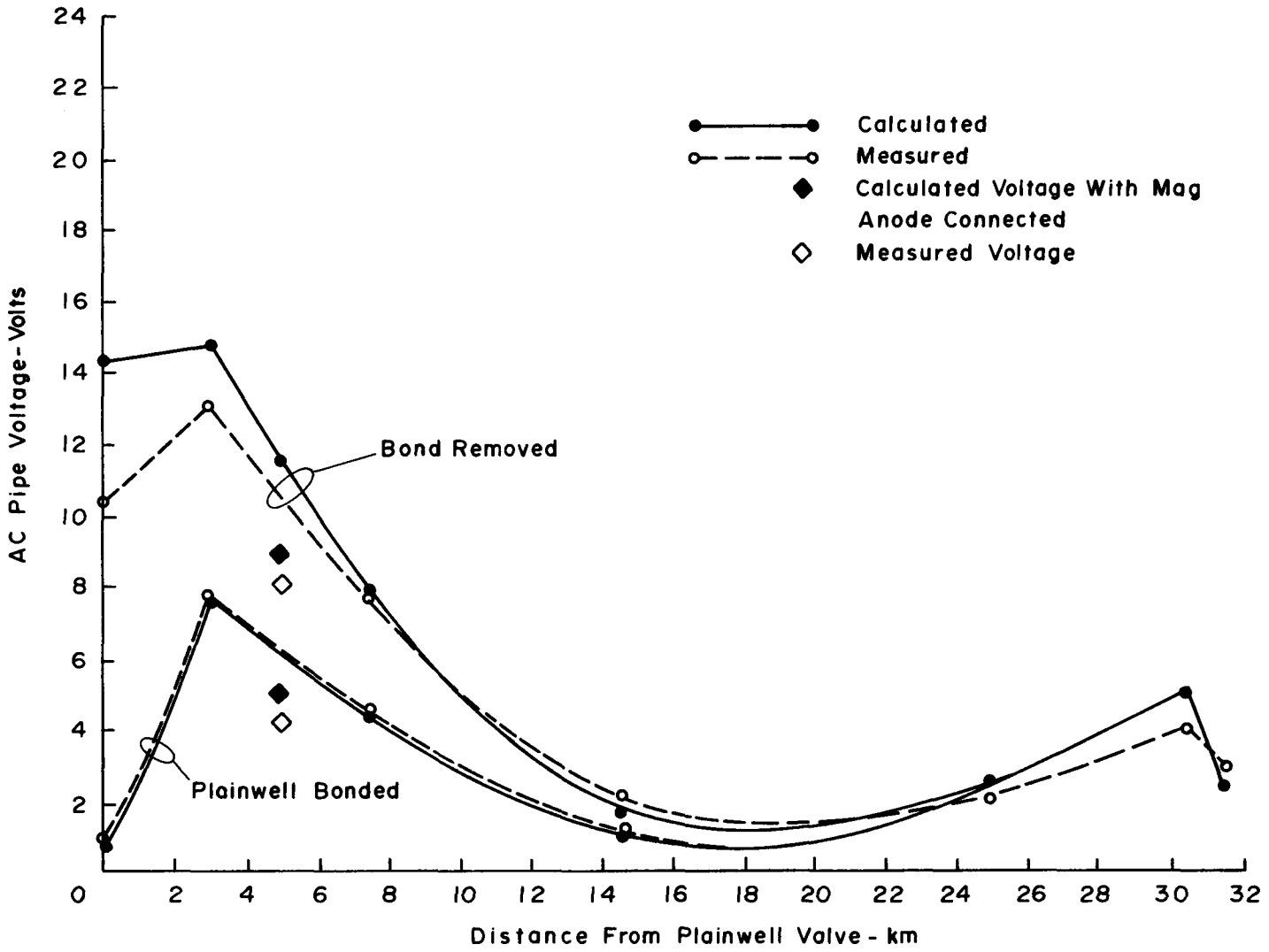

Fig. 3-16 LINE 1800 VOLTAGE PROFILE

With the bond removed at Plainwell, the induced voltage levels at the north end are not affected due to the attenuation of the pipeline. They rise, however, at the south end due to the severe discontinuity the insulator presents to the pipe. Inspection of the plots shows a deviation between measured and calculated values at or near the Plainwell valve site. The discrepancy can be accounted for, however, by the fact that for the calculations a perfect insulator was assumed (infinite resistance), but obviously some leakage did occur across the existing ground cell which resulted in measured voltages being somewhat smaller than the calculated values.

The results plotted in Figure 3-16 verify the developed prediction technique. Details of the calculations are described in the following sections.

Electric Field Calculation. The first step in predicting the voltage developed on the pipeline is to determine the longitudinal electric field driving the pipeline. The procedure is as follows:

1. From Figure 3-15, determine the distances (using geometric mean height of the conductors) from each of the six phase line conductors to the shield wires and the pipeline. Also determine the distance between each shield wire and the pipeline.

2. Using the mutual impedance program CARSON developed for the TI-59 programmable calculator, determine the mutual impedances between the phase conductors, the shield wires and the pipeline. (An average ground resistivity of 400 ohms-meter is assumed.)

3. From available programs, calculate the self impedances of the shield wires (c.f., program SHIELD) and the pipeline (c.f., program PIPE) calculated self impedances are: shield wire, $Z = 2.05\underline{/29.2^{o}}$ ohms/km; pipeline, $Z = 0.596\underline{/77.6^{o}}$ ohms/km. (The shield wire dc resistance was assumed to be $\underline{1.727}$ x 10^{-3} ohms/m. The radius of the shield wire is 4.978 x 10^{-3} m. The pipeline self impedance is obtained by multiplying γ and Z_o together. These latter parameters were obtained by means of program PIPE, with the following input parameters: (1) pipe burial depth - 36 inches, (2) pipe thickness - 0.32 inch, (3) ground resistivity - 400 ohm-m, (4) pipe steel relative permeability - 300, (5) pipe steel resistivity - 0.17 $\mu\Omega$-m, (6) pipe diameter - 20 inches, (7) coating resistivity - 300,000 ohms-ft^2. With these input parameters, calculated pipeline parameters were: $\gamma = 0.1397 + j\ 0.1129\ km^{-1}$ and $Z_o = 2.593 + j\ 2.075$ ohms.)

4. Input the mutual and self impedances into the TI-59 program CURRENTS and for an assumed set of power line currents determine the pipeline current. Multiplication of the pipeline current and self impedance yields the driving electric field at the pipeline. Calculations were made assuming 50 amperes load in each phase conductor (phasing sequence X, Y, Z: CCW). The hand calculator program CURRENTS yields

a pipe current of $6.43/\underline{128.9^{o}}$ amperes, and hence, a source field of $E_{o} = 3.83/\underline{26.5^{o}}$ volts/km.* This value is obtained by multiplying the negative of the pipe current times the pipe self impedance.

Pipeline Load Impedances

Plainwell Valve Site. Due to the fact that a complex grounding system exists at the valve site, e.g., ground rods, pipelines, and a tie-in to the electrical distribution system neutral, the grounding impedance was measured rather than calculated. With a bond across the insulator, a value of 0.15 ohm was measured. This measurement was made with a voltmeter and ammeter and, hence, the grounding impedance phase was not directly measurable. It was estimated to be in the vicinity of zero degrees, i.e., primarily resistive, and subsequent calculations made using this assumption yielded calculated voltage profiles commensurate with measured values. The estimate was based on prior field experience which has indicated that the impedance of short ground rods, lossy conductors and so forth, tends to be primarily resistive. The ground bed at this valve site is a composite of such grounds. With the bond removed, an infinite load impedance was assumed, which the plots of Figure 3-16 show as being slightly in error; i.e., some leakage existed through the nominally dry grounding cell.

Thirtieth Street Valve Site. The valve at this site is physically connected to a 24-inch pipeline having a poorer coating ($\simeq$ 100,000 ohms-ft^{2}) and this pipeline, in turn, is electrically bonded to a 16-inch pipeline with a coating resistivity of about the same magnitude. Hence, the load impedance seen by the pipeline with a shorted insulator at the valve site will be one-half of the parallel combination of the 16-inch and 24-inch pipeline characteristic impedances. This value was calculated to be $0.506/\underline{38.4^{o}}$ ohms, and was found by the following procedure. When

*Loading on these circuits varied considerably during the course of the measurements due to changes in current levels, line unbalances, and even in change of direction of power flow for one of the circuits relative to the other. For the variations observed within a 24-hour period, the pipe induced voltage could change by factors of three to four higher or lower than the calculations presented here.

an electrical bond is made to a pipeline extending for a significant distance to either side of the bond, the input impedance into the bond is equal to one-half of the pipeline characteristic impedances. By bonding to two pipelines, the impedances looking into each of the pipe bonds are in parallel. Hence, the effective impedance as seen by the 20-inch pipeline is the product of each external pipeline bond impedance divided by their sum.

Equivalent Circuit Derivation. At each location along the pipeline for which a voltage prediction is desired, Thevenin equivalent electric network circuits must be derived looking in both directions along the pipeline from that location. These equivalent circuits may then be combined as discussed in the following section, to determine the voltage at that point.

To elucidate the procedure, a sample calculation for a point approximately 7.2 km north of the Plainwell valve site (115th Street) will be made. (It will be assumed that the bond across the Plainwell insulator is removed.)

Equivalent circuit derivation is accomplished through repeated use of program THEVENIN, as follows.

To the North. The 30th Street valve site is approximately 23.9 km away from the location. However, the pipeline follows the electric transmission for the first 22.9 km. Hence:

1. Find the input impedance to the pipeline at a point 1 km south of the 30th Street valve. With the load impedance of $0.506/38.4^{o}$ at the valve site, the input impedance is calculated as $3.32/38.7^{o}$ ohms.

2. This calculated impedance is then used as the load impedance for the 22.9 km pipeline length. As previously determined, the driving electric field is $3.83/26.5^{o}$ volts/km, and using these parameters in the THEVENIN program yields an equivalent circuit consisting of a voltage generator of $22.1/-191.2$ volts in series with an impedance of $3.32/38.7$ ohms.

To the South. The infinite impedance at the Plainwell valve site transforms through the use of Program THEVENIN to an impedance of $6.23/5.14^{o}$ at a point 3.0 km north of Plainwell (location where the pipeline first contacts the power line). This impedance is then used as the load impedance for the 4.4 km of pipeline extending from the point of first contact

to 115th Street. Using the previously calculated field of $E_0 = 3.83/\underline{26.5} + 180^o$ results in an equivalent circuit generator of $11.5/\underline{19.9^o}$ volts in series with $3.23/\underline{24.6^o}$ ohms using the THEVENIN program.

Pipeline Voltage Calculation. The pipeline voltage at this location is calculated by combining the two equivalent circuits and calculating the resulting voltage at the point of connection. To effect this solution easily, the hand calculator program NODE is used. Inputting the equivalent circuit parameters into the program yields a pipe voltage of $8.0/\underline{130.4^o}$ volts and a pipe current of $5.0/\underline{147.6^o}$ amperes.

The Program NODE also has the added capability of solving for the resulting voltage with either a mitigation (ground) wire or anode connected to the pipeline at the location. (When a ground or mitigation wire is not used, the impedance $|Z_2|$ must be set to a high value for the program to yield a correct result. A value of 10,000 or higher should be sufficient.)

Voltage Prediction
Texas Gas Transmission Corporation, Memphis, Tennessee

Introduction. This case history of voltage prediction is possibly the most complicated of the set presented, in that four gas pipelines are collocated with several power circuits. The analysis becomes difficult because of electrical interties between the pipelines at several locations. The solution illustrates repeated use of the Thevenin equivalent circuit concept to produce successive simplifications of the problem. Near the city of Memphis, Tennessee, the Texas Gas Transmission Corporation and the Memphis Gas, Light and Water Company share a common right-of-way for a distance of approximately 1.9 km. Four pipelines and the two existing power lines (three circuits) share the right-of-way. An additional power line with two vertical circuits is planned for the near future on the west side of the right-of-way, as shown in Figure 3-17. In this section, the right-of-way lies in an almost north-south direction, from Highway 72 on the north end (Station #254+1377) to Messick Road on the South (Station #253+984).

A study of the impact the new circuits will make on the induced pipeline voltage distributions for both the steady state and transient conditions has been made.

Predicted Voltage Levels. Tabulated results of the steady state analyses and the transient analyses made in the following subsections are summarized here.

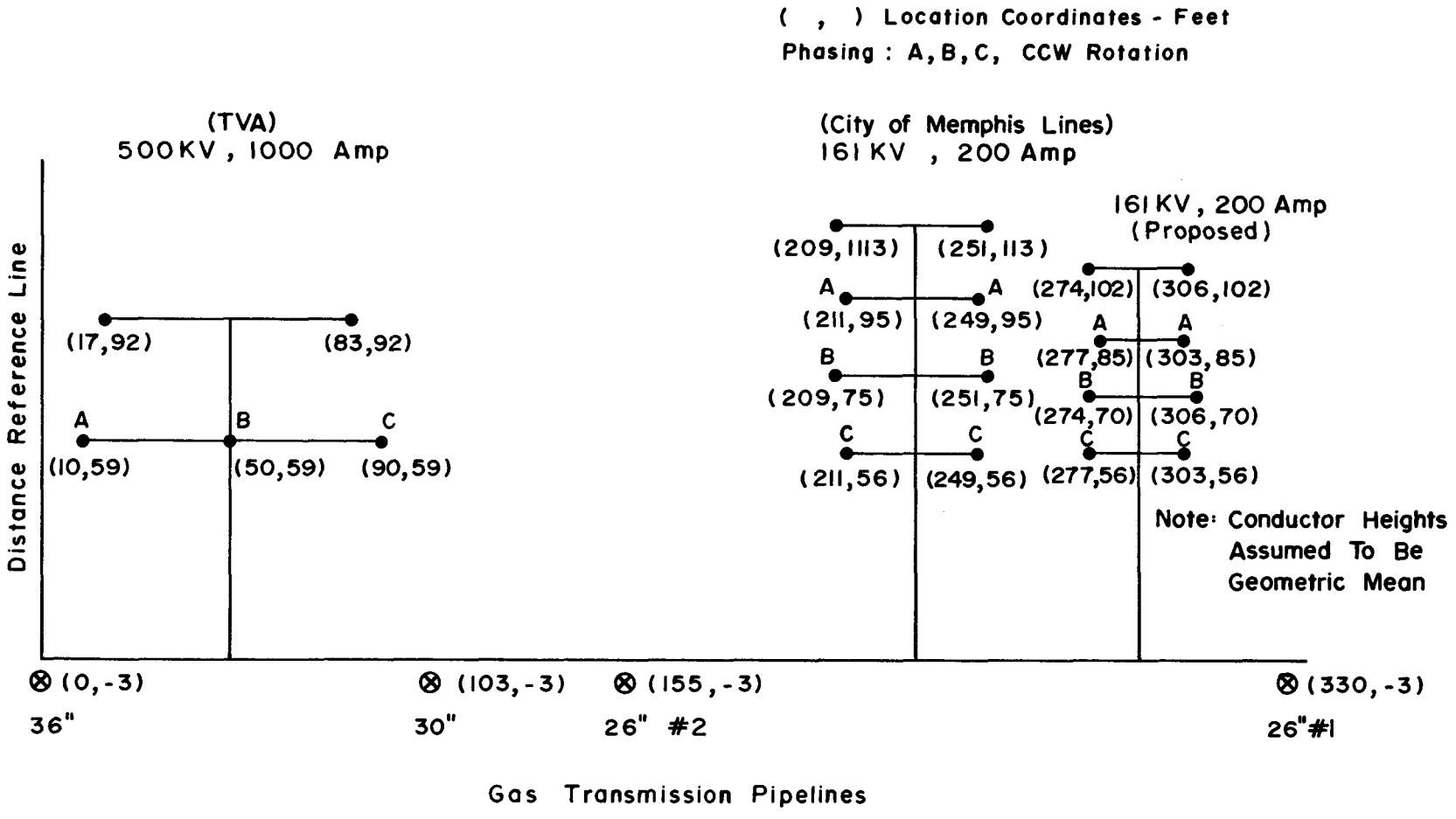

Fig. 3-17 AVERAGE RIGHT OF WAY PROFILE

Steady State. Calculations for the peak voltages which occur at the north and south ends of the parallel exposure were made for the following conditions:

1. for the existing circuits (fully loaded, i.e., 1000 amperes for the 500 kV circuit and 200 amperes each for the 161 kV circuits) with the cathodic protection (C.P.) bond wire connecting all four pipelines at Poplar Pike - both connected and disconnected, and

2. for the fully loaded existing circuits plus the proposed circuits loaded to 200 amperes each (Tables 3-3 and 3-4).

Transient Voltage Levels. For a single phase line to ground fault, the worst case voltage stress across the pipeline coating is estimated at 6748 volts. Simultaneously, the pipe steel will rise to a level of 109 volts for the duration of the fault.

A station fault will cause an induced voltage to occur on all conductors along the right-of-way, i.e., phase wires, shield wires and pipelines. Due to the large number of conductors, an exact solution for the induced voltage level on any one conductor is not possible with the presently available hand calculator program. A worst case analysis, for example, gives 665 volts on the 26-inch - #1 pipeline, but in practice it would be expected that the actual voltage level would be a small fraction of this value.

Summary of Results. A comparison of Tables 3-3 and 3-4 shows that the addition of the proposed two circuits on the right-of-way primarily affects the voltage levels on the 26-inch - #1 pipeline. The voltage levels are increased from 19 to 27 volts at the south end of the exposure, Messick Road, and from 15 to 20 volts at the north end at Highway 72 (CP bond connected). It should be noted, however, that these are not the highest voltage levels that can be experienced on the right-of-way. Even with the existing circuits only in operation, a 1000 ampere loading on the 500 kV TVA line could induce higher levels on the 30-inch and 36-inch lines (c.f., Messick Road).

The worst situation transient problem occurs with a single phase tower fault in which a voltage stress of approximately 6700 volts is induced across the pipe coating.

Table 3-3

VOLTAGE LEVELS - EXISTING CIRCUITS

Pipeline	Messick Road		Highway 72	
	CP Bond In	Bond Out	CP Bond In	Bond Out
26" - #1	19 V	20 V	15 V	20 V
26" - #2	36	33	19	36
30"	29	29	19	27
36"	38	29	6	27

Table 3-4

VOLTAGE LEVELS WITH PROPOSED CIRCUITS

Pipeline	Messick Road		Highway 72	
	CP Bond In	Bond Out	CP Bond In	Bond Out
26" - #1	27 V	26 V	20 V	26 V
26" - #2	39	36	25	36
30"	29	29	20	27
36"	38	29	5	27

Steady State Voltage Prediction. The analytical approach to the problem is generally dictated by the number of pipelines, the electrical bonds between them, and the number of electrical circuits and associated unknown shield wire currents. Referring to Figure 3-17, the right-of-way consists of (after installation of the proposed tower) 15 phase current carrying conductors, 6 shield wires, and 4 pipelines carrying unknown currents. In addition, as shown in Figure 3-18, the following electrical bonds exist between the pipelines:

- 26-inch - #1 and 26-inch - #2 are electrically tied together at approximately 2.15 km south of Messick Road (south end of parallel exposure).
- All four pipelines are tied together at a distance of 8.3 km south of Messick Road.

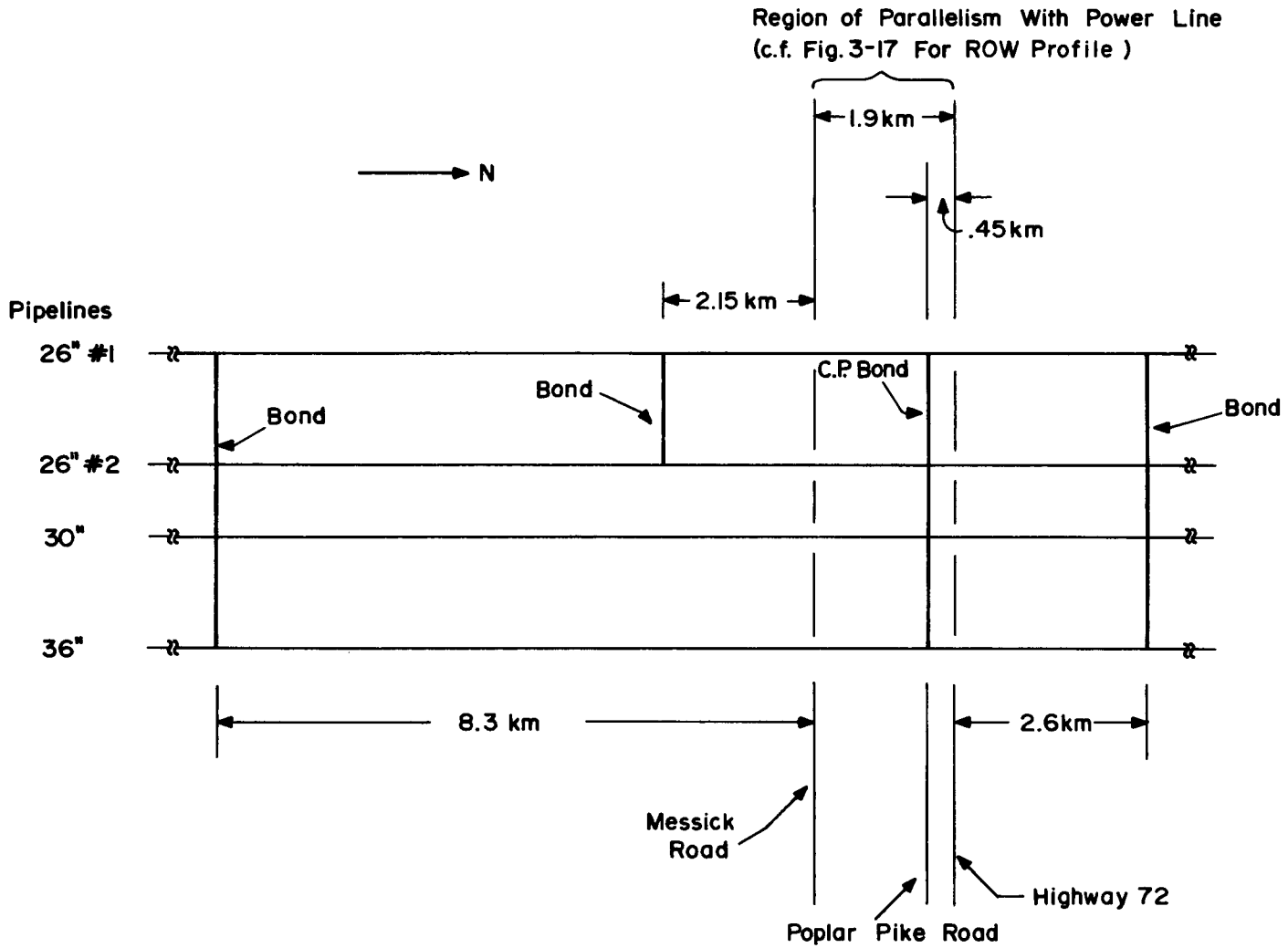

Fig. 3-18 ELECTRICAL BONDS BETWEEN PIPELINES

- All four pipelines are tied together at a distance 2.6 km north of Highway 72 (north end of parallel exposure).
- A (removable) cathodic protection bond is made to all the pipelines at Poplar Pike, a distance 0.45 km south of Highway 72.

A rigorous solution to the voltage prediction problem for this right-of-way requires the simultaneous solution of equations for the ten unknown currents; this is complicated by the fact that not only does inductive coupling occur between the pipelines, but also direct coupling, as exemplified by the existing cross ties and bond wires. Cost effectiveness requires simplification of the problem, but in a proper manner so as not to compromise the solution. The approach used may be outlined as follows. Program CURRENTS can solve for unknown currents in up to five conductors in the presence of up to 25 known current-carrying conductors. In order not to exceed the program's capability, the following sub-set problems were solved:

1. The shield wire currents (4) for the 161 kV circuits were obtained by solving simultaneous equations, taking into account only the 12-phase wires on the two towers. The rationale behind this approximation is that these shield wires are primarily driven by their own phase wires, and hence, neglecting the other conductors (including the pipelines) will not materially affect the solution.

2. Assuming that the 500 kV phase wires were the prime driving sources for the shield wires mounted on the same tower, a solution for these shield wire currents was then obtained.

The solutions thusly obtained for the six shield wire currents reduce the number of unknowns to four (the pipeline currents), thus allowing the use of program CURRENTS directly for their solution. (Since the parallel exposure length is quite small, it would be necessary to input a modified set of mutual and self impedances into the program, which is discussed in Appendix D.)

However, an alternative approach was used, namely considering each pipeline individually, calculating the electric field, and hence, the voltage at each pipeline ignoring mutual coupling effects between the pipes themselves. The reason for this approach was that the pipeline(s) response to an individual electric circuit was desired and proved simpler than successively re-inputting the calculator program parameters. Generally, neglect of the mutual impedances between pipelines would lead to relatively large errors in the predicted voltage level. In the present situation this is allowable because (1) the short exposure length limits the individual pipe currents so that the electric fields produced by them are

relatively small, and (2) because of like phasing for the electrical circuits, the electric field from the power lines is relatively large, thus tending to mask the pipeline current contributions.

With the cathodic protection bond wires opened at Poplar Pike, calculation of the voltage profiles on each of the pipelines is relatively simple. Picking a point of observation (generally, the north or south end exposure points since peak voltages occur at these points), the equivalent circuit approach was used with numerical calculations made by means of the THEVENIN program. The principal point to keep in mind is that since the pipelines are tied together both north and south of the parallel exposure, they are not terminated in their characteristic impedances, and the effective end loadings must be determined.

For the case where the cathodic protection bonds are connected at Poplar Pike, the equivalent circuit voltage calculations become more difficult because this is a location along the parallel exposure. The procedure here is to find the Thevenin circuit for each pipeline to the north and south of Poplar Pike and parallel-connect all eight circuits. A Thevenin equivalent generator may then be derived, i.e., the connected bond(s) voltage at Poplar Pike. The peak voltages for each of the pipelines may then be calculated, e.g., from the south end of the exposure looking north or the north end looking south, with the transmission line(s) terminated in the Poplar Pike Thevenin equivalent generator.

The intermediate calculations are discussed in the following subsections.

Pipe Parameter Calculations. Averaged pipe parameters were obtained assuming a ground resistivity of 5000 ohm-cm and coating resistivities for all pipes of 100,000 ohms-ft^2. The propagation constant and characteristic impedance for each pipe was determined as,

$$\gamma = .26 + j.20 = .328/\underline{37.6^{o}}\ km^{-1}$$

$$Z_o = 1.2 + j\ 1 = 1.56/\underline{39.8}\ ohms$$

Even though the pipes varied in diameter, the same parameters were assumed for all the pipes, since possibly unknown variations in the above resistivities could supercede variations caused by the differences in the diameters.

Shield Wire Current Calculations. Using the approximate method outlined previously, the shield wire currents were calculated on the basis of 1000-ampere phase currents in the 500 kV circuit and 200 ampere currents in the four remaining 161 kV circuits (all circuits delivering power south). The Carson mutual impedance was calculated between each phase wire and shield wire using the program CARSON. Solution of the simultaneous equations for the unknown currents was made by the program CURRENTS. Results are:

500 kV Circuit*

East Shield Wire: $I = 27.7/214.4^{o}$ amperes

West Shield Wire: $I = 29.1/48.26^{o}$ amperes

East (existing) 161 kV Tower**

East Shield Wire: $I = 13.4/190.8^{o}$ amperes

West Shield Wire: $I = 18.0/194.9^{o}$ amperes

West (proposed) 161 kV Tower***

East Shield Wire: $I = 9.6/207.2^{o}$ amperes

West Shield Wire: $I = 6.8/202.7^{o}$ amperes

Electric Field Calculations. The voltage appearing on any of the pipelines is proportional to the driving electric field impinging upon the pipeline. For calculating the electric field, the program CARSON was used to find the mutual impedance between each pipe and all of the phase and shield wires. Because of the short exposure length of the pipelines to the power lines, mutual coupling effects between the pipelines themselves were ignored.

Calculated shield wire self impedance;

* $2.11/25.6^{o}$ ohms/km (wire resistance = 1.85×10^{-3} ohms/m; wire radius = $.44 \times 10^{-2}$ m)

** $1.373/40.6^{o}$ ohms/km (wire resistance = 0.984×10^{-3} ohms/m; wire radius = $.55 \times 10^{-2}$ m)

*** $2.38/22.4^{o}$ ohms/km (wire resistnace = 2.14×10^{-3} ohms/m; wire radius = $.44 \times 10^{-2}$ m).

26-inch - #1 Pipeline. The electric field calculations for the phase current loading given in Figure 3-17 yield the following:

Partial electric field due to existing 161 kV circuit = $10.7/\underline{254.9^{o}}$ V/km.

Partial electric field due to proposed 161 kV circuit = $10.8/\underline{245.5^{o}}$ V/km.

Partial electric field due to existing 500 kV circuit = $18.4/\underline{231.7^{o}}$ V/km.

Total electric field at pipeline = $39/\underline{243^{o}}$.

Hence, addition of the proposed 161 kV circuits to the ROW will increase the steady state voltage at the pipeline by approximately one-third when the other circuits are fully loaded.

26-inch - #2 Pipeline.

Partial field due to existing 161 kV circuit = $12.5/\underline{252.5^{o}}$ V/km.

Partial field due to proposed 161 kV circuit = $4.54/\underline{274.4^{o}}$ V/km.

Partial field due to existing 500 kV circuit = $37.7/\underline{234.1^{o}}$ V/km.

Total field at pipeline = $53.5/\underline{241.5^{o}}$ V/km.

30-inch Pipeline.

Electric field due to 500 kV circuit = $38/\underline{240.7^{o}}$ V/km.

Electric field from other lines small.

36-inch Pipeline

Electric field due to 500 kV circuit = $35.7/\underline{56.9^{o}}$ V/km

Electric field from other lines small.

Voltage Calculations (Cathodic Protection Bond at Piplar Pike Disconnected)

30-Inch/36-Inch Pipelines (Messick Road). The voltage calculations for either pipeline are almost identical and will be made for one of the pipelines only (30"). Due to all the pipelines being tied together at 2.6 km north of Highway 72, the load impedance for the pipeline seen at this point is $Z_o/7$. Using program THEVENIN, this load impedance transforms into an impedance of $1.29/\underline{59^{o}}$ ohms at Highway 72. In turn, for 1.9 km of pipe, this impedance is changed to a value of $1.614/\underline{47.9^{o}}$ ohms at Messick Road. The Thevenin open circuit voltage at this point is found to be $58.8/\underline{48.2^{o}}$ volts.

The program THEVENIN is used many times in this book and was used in deriving the above equivalent circuit parameters. In order to keep the case histories from becoming unduly lengthy, details of each calculation are generally not given. However, as an illustrative example for aiding reader comprehension, the steps leading to the above equivalent circuit are presented here.

Two iterations of the program THEVENIN are required to arrive at the result:

1. Find input impedance at Highway 72 looking to the north.

   THEVENIN program inputs:

   $\text{Real}(\gamma) = 0.26$

   $\text{Im}(\gamma) = 0.20$

   $\text{Real}(Z_o) = 1.20$

   $I_m(Z_o) = 1.0$

   $|V_L| = 0$ (power lines not parallel to pipeline at 2.6 km north of Highway 72)

   $\angle V_L = 0$

   $|Z_L| = 1.56 \div 7 = .223$ (with four pipelines tied together the input impedance looking to the north at 2.6 km north of Highway 72 is $Z_o/7$, i.e., seven pipe characteristic impedances in parallel)

   $\angle Z_L = 39.8^o$

   $|E_o| = 0$

   $\angle E_o = 0$

   $L = 2.6$ km

Exercise of program THEVENIN yields a Thevenin voltage generator of $0/\underline{0^o}$ and a Thevenin impedance of $1.29/\underline{59^o}$ ohms. These quantities become V_L and Z_L for the next iteration.

2. Find the Thevenin equivalent circuit looking to the north at Messick Road. THEVENIN program inputs

$\text{Real}(\gamma) = 0.26$

$I_m(\gamma) = 0.20$

$\text{Real}(Z_o) = 1.20$

$\text{Im}(Z_o) = 1.0$

$|V_L| = 0$

$\underline{/V_L} = 0$

$|Z_L| = 1.29$

$\underline{/Z_L} = 59^o$

$|E_o| = 38$ (electric field at 30" pipeline)

$\underline{/E_o} = 240.7^o$

$L = 1.9$ km

Exercise of program THEVENIN yields the Thevenin voltage of $58.8\underline{/48.2^o}$ volts and the Thevenin impedance of $1.614\underline{/47.9^o}$ ohms given previously.

The actual pipeline voltage at Messick Road is the open circuit Thevenin voltage corrected for the voltage division occurring between the pipe impedance ($1.614\underline{/47.9^o}$) seen looking to the north of Messick Road and the impedance looking to the south ($1.59\underline{/39.6^o}$). The latter impedance is obtained by calculating the input impedance of the pipe with a load of $Z_o/7$ at a distance of 8.3 km. The resulting calculated voltage is $29.3\underline{/44^o}$ volts.

At the north end of the exposure, Highway 72, the voltage division impedances are different, i.e., $1.29\underline{/59^o}$ to the north and $1.59\underline{/39.6^o}$ to the south, yielding a computed voltage of approximately 26.7 volts.

26-Inch - #2 Pipeline. This pipeline is tied to 26-inch - #1 at approximately 2.15 km south of Messick Road and to the other three lines at 2.6 km north of Highway 72. Such interconnection will tend to equalize the peak voltages appearing at both ends of the parallel exposure.

To compute the voltage at Messick Road, i.e., south end of the exposure, the following procedure is used:

Assume a load resistance of $Z_0/3$ at the tie-in point south of Messick Road. The THEVENIN program transforms this impedance to $1.26/\underline{54.1^o}$ at Messick Road. In like manner, as for the 30 and 36-inch pipelines, the pipeline input impedance is calculated at $1.614/\underline{47.9^o}$ ohms, with an open circuit voltage generator $82.9/\underline{49^o}$ volts. Calculating the voltage division due to the two impedances yields $36.4/\underline{52.5^o}$ volts. The voltage at the north end of the exposure will be approximately the same.

26-Inch - #1 Pipeline. Because of the identical cross ties, the impedance transformations are the same as for the 26-inch - #2 pipeline. The electric field is less at this pipeline, resulting in a peak voltage at both ends of approximately (39/53.5)36.4 - 26.5 volts.

Voltages (Cathodic Protection Bond Connected). The cathodic protection bond, when connected, electrically ties all four pipelines together at Poplar Pike, and thus causes a voltage and current redistribution among the pipelines. In order to calculate the peak voltages on the individual pipelines, the following procedure must be used:

1. Calculate a Thevenin equivalent circuit for each pipeline looking to the north and to the south of Poplar Pike, eight total, and connect them in parallel using the program THEVENIN.

2. Recalculate a new Thevenin equivalent circuit for the above. This circuit then acts as the load for each of the pipelines using program THEVENIN.

3. Using the modified input parameters and the THEVENIN program, calculate the voltage at the north or south terminal exposure points.

A rigorous calculation for the above is rather elaborate. However, the procedure may be simplified as follows:

1. Assume that all lengths of pipeline have an input impedance equal to their characteristic impedance. This yields a Thevenin equivalent circuit impedance of $Z_0/8$.

2. With equal impedance in each leg, the voltage at Poplar Pike may be found by weighted averaging of the electric fields at the pipelines. Hence,

$$V = \frac{1}{8} \sum_{i=1}^{4} E_{o_i} \left(1.2\underline{/-7.8^{o}} + .425\underline{/177.5^{o}}\right) \qquad (3\text{-}29)$$

where

$1.2\underline{/-7.8^{o}}$ is the Thevenin equivalent generator voltage produced in a pipeline length of 1.45 km (distance to Messick Road from Poplar Pike) for a driving electric field at the pipeline of $1\underline{/0^{o}}$ volt/km; $0.425\underline{/179.5^{o}}$ is the open circuit voltage generator for a pipeline length of 0.45 km (distance to Highway 72) for a driving electric field of $1\underline{/0^{o}}$ volt/km; and E_{o_i} is the electric field at the ith pipeline.

Solution of the previous equation yields a bond wire voltage of $9.2\underline{/233.2^{o}}$ volts for the case where the proposed circuits are in operation. For the circuits existing presently on the right-of-way, the bond voltage level is $7.7\underline{/232.8^{o}}$ when all circuits are fully loaded.

Using the THEVENIN program, the voltage levels at both ends of the exposure were calculated for each pipeline for the electrical circuits existing at present and also for the future case where the additional tower is placed on the right-of-way. The program yielded the Thevenin resistance and the open circuit voltages for each of the pipes and terminal points. The pipeline voltage was then computed assuming voltage division through the following terminating impedances:

26" - #1 26" - #2	$1.26\underline{/54.1^{o}}$ ohms at south end
30" 36"	$1.59\underline{/39.6^{o}}$ ohms at south end
26" - #1 26" - #2 30" 36"	$1.29\underline{/59^{o}}$ ohms at north end.

These computed results have been tabulated in Tables 3-3 and 3-4.

Transient Voltages. Due to right-of-way restrictions, the distance between the power line structure footings and 26-inch - #1 pipeline become small at several locations with a minimum separation of 16 feet. The magnitudes of the transient voltages induced by conductive and inductive coupling are considered in this section.

Conductive Coupling. A phase-to-ground fault at a tower in close proximity to the pipeline will cause a voltage gradient in the ground which will stress the pipeline coating.

Data provided by Memphis Light, Gas and Water indicate a tower to ground resistance of 3 ohms and a single phase-to-ground fault current of 10,988 amperes. Because of the grounded shield wires, the fault current will be divided between the tower and the shield wires. The impedance to earth as seen from the faulted tower is

$$Z_e \simeq .5\sqrt{R_T\ Z_S}$$

$$= .5\sqrt{3 \times 0.4}$$

$$= .55\ \Omega \qquad (3\text{-}30)$$

where

R_T is the tower to ground resistance, (3Ω), and

Z_S is the series impedance of the shield wires to the next tower - estimated at .4 Ω.

Because of the current division, the actual current flowing through the tower ground is

$$I_T = \frac{Z_e}{R_T} \cdot I_F = \frac{.55}{3} \cdot 10988 = 2014 \text{ amperes.} \qquad (3\text{-}31)$$

Using a dc approximation for the current distribution in the earth, the voltage appearing at the pipeline coating is

$$V_C = \frac{I_T \rho}{8\pi} \sum_{i=1}^{4} \frac{1}{d_i} \qquad (3\text{-}32)$$

where

ρ is the ground resistivity, and

d_i is the distance of each of the tower legs to the pipeline.

A worst case ground resistivity of 17,500 Ω-cm will be assumed. (This value was measured near Poplar Pike at a depth of 2'7".) The calculated voltage at the pipe coating is,

$$V_C = \frac{2014}{8\pi} (175)(.489) = 6857 \text{ volts.}$$

Due to conductive current leakage onto the pipe, the local potential of the pipe steel will also rise, and may be calculated by the following formula:

$$V_S = \frac{\gamma_\rho I_T}{8\pi} \sum_{i=1}^{4} [\gamma d_i - \ln \gamma d_i + 0.116] \qquad (3\text{-}33)$$

where

γ = $(.26 + j\ .20)\ 10^{-3}\ m^{-1}$, the pipeline propagation constant.

Assuming the worst case ground resistivity then yields

$$V_S = (.328) \frac{(10^{-3})(175)(2014)}{8\pi} [23.8]*$$

= 109 volts.

The calculated voltage stress across the pipeline coating is 6857 - 109 = 6748 volts.

Inductive Coupling of Transients. A single phase fault at a substation represents the worst case. Data supplied give 2635 amperes as the worst case current in one phase wire along the right-of-way. The worst case condition of induced voltage on the pipeline would occur if only the faulted phase conductor (the one closest to the pipeline) and a single pipeline were present on the right-of-way. For this situation, a worst case transient voltage of 665 volts could occur at the 26-inch - #1 pipeline (assuming coupling of all high frequency components to be the same as the 60 Hz component). However, due to the multiplicity of other conductors, i.e., phase wires, shield wires, pipelines on the right-of-way, induced current division between conductors will cause the actual induced voltage at any one conductor to be a small fraction of the calculated worst case voltage.

---

*d_1 = 4.88 m, d_2 = 12.13 m, d_3 = 7.81 m, d_4 = 13.6 m.

Voltage Prediction
Consumers Power Company Karn-Weadock Line, Bay City, Michigan

Introduction. The solution of the induced voltage prediction problem for this crude oil pipeline is obtained by an approach utilizing field measured data as much as possible in contrast to the purely analytical solutions presented for the previous case histories. This 16" pipeline runs north and south approximately 10.6 km from the Karn-Weadock power plants on the north end to a tap site and tank farm on the south end. It is terminated in an insulator and high resistance grounding cell on the north end ($Z_0 \rightarrow \infty$) and an insulator and a low impedance grounding cell at the south end. The principal right-of-way (ROW) characteristics are diagrammed in Figure 3-19.

The pipeline shares the ROW with six 3ϕ circuits. Starting from the west there are two 138 kV horizontal circuits, each on an H-frame. Next, there are two vertical circuits carried on a single tower with the west circuit at 46 kV and the east circuit at 138 kV. The easternmost tower on the ROW carries two vertical 138 kV circuits. The pipeline ROW may be conveniently divided into five regions on the basis of the principal interaction characteristics with the electric power lines. These are as follows:

Region 1: In this region, the pipeline lies on the west end of the ROW. The distance to the nearest structure varies, however, and is equal to 70 feet in 1a; 190 feet in 1b, and approximately 380 feet in 1c. The extent of each region with distances measured from the north terminus are as shown in Figure 3-19.

2: The pipeline crosses over to the east side of the ROW and hence is subject to a completely different excitation field.

3: The pipeline remains in the same position, but the 46 kV circuit (second tower from right) leaves the ROW. The excitation to the pipeline is only slightly changed because of "shielding" of the pipeline by the circuits on the east tower.

4: The pipeline moves to the center of the ROW, i.e., between the horizontal and vertical circuits. It experiences a relatively large change in source driving field at this point.

5: The pipeline remains in the same position, but the easternmost tower leaves the ROW. The excitation to the pipeline is modified, but not significantly, due to "shielding" by the single circuit remaining on the tower to the east. (This condition prevails because the two circuits on the east tower

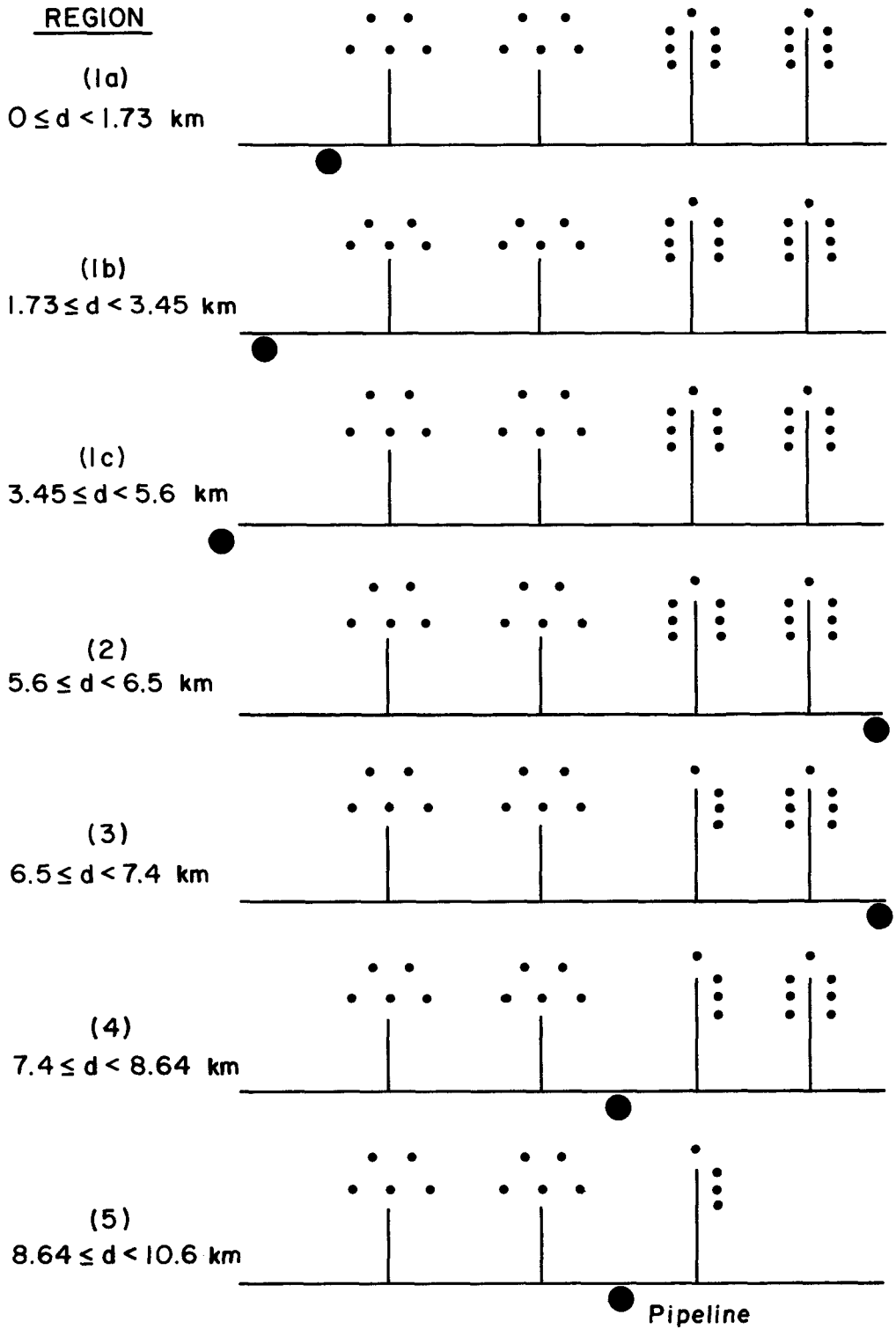

Fig.3-19 BAY CITY ROW PROFILE LOOKING NORTH

in Region 4 are phased in partial opposition and, hence their contribution to the total electric field at the pipeline is small compared to that produced by the single circuit on the adjoining tower.)

Pipeline Voltage Prediction Approach. A purely analytical approach to the prediction of the pipeline voltage profile is primarily a two step process: (1) calculate the driving source electric field at the pipeline; and (2) using Thevenin equivalent circuits derived from the program THEVENIN, compute the voltage profile on a point-by-point basis. This procedure was followed, for example, in the Texas Gas Transmission Corporation (Memphis, Tennessee) and the Consumer Power Company (Kalamazoo, Michigan) case histories. For the situation where an existing ROW does not have all the electric power circuits installed, for example, and the effect of future circuits needs to be determined, then this purely analytical approach is necessary. However, in the present situation, where the power lines are already installed on the ROW, a measurement approach to obtaining the free field (Step 1) is possible and, especially in this case, desirable. The reason for this is that the ROW illustrated in Figure 3-19 is quite complicated. For example, up to 18 phase lines and six shield wires may exist on the ROW. In addition, although not shown in the figure, there is another 16-inch pipeline sharing the ROW. Hence, there are eight unknown current-carrying conductors on the ROW which require a simultaneous solution for the unknown currents. This exceeds the capacity of the existing program CURRENTS; but as discussed in the Texas Gas Transmission Corporation case history, this limitation may be eliminated by solving for the shield wire currents on an individual piece-meal basis. However, as shown in Figure 3-19, seven regions are distinguishable, thus requiring as many sets of calculations; and in addition, the phase line currents must be reasonably well known for all conductors in order to proceed with the calculations. Hence, the necessary calculations to typify this ROW are many and, at best, tedious.

An alternate and very viable approach to determine the driving electric field for the pipeline is by direct measurement, using the electric field magnitude and phase instrumentation developed during the program. An attractive feature of this approach is that knowledge of the phase line current values is not necessary. In using this approach, however, the following considerations apply:

1. The voltage profile calculated using this approach may not be as accurate as when using the calculative procedure. The reason for this is that it may take a better part of a day to make all of the measurements; and because line currents are dynamically varying, the measurements may not be completely consistent with each other. However, it appears in general that the resulting errors are at acceptable levels (c.f., Figure 3-20).

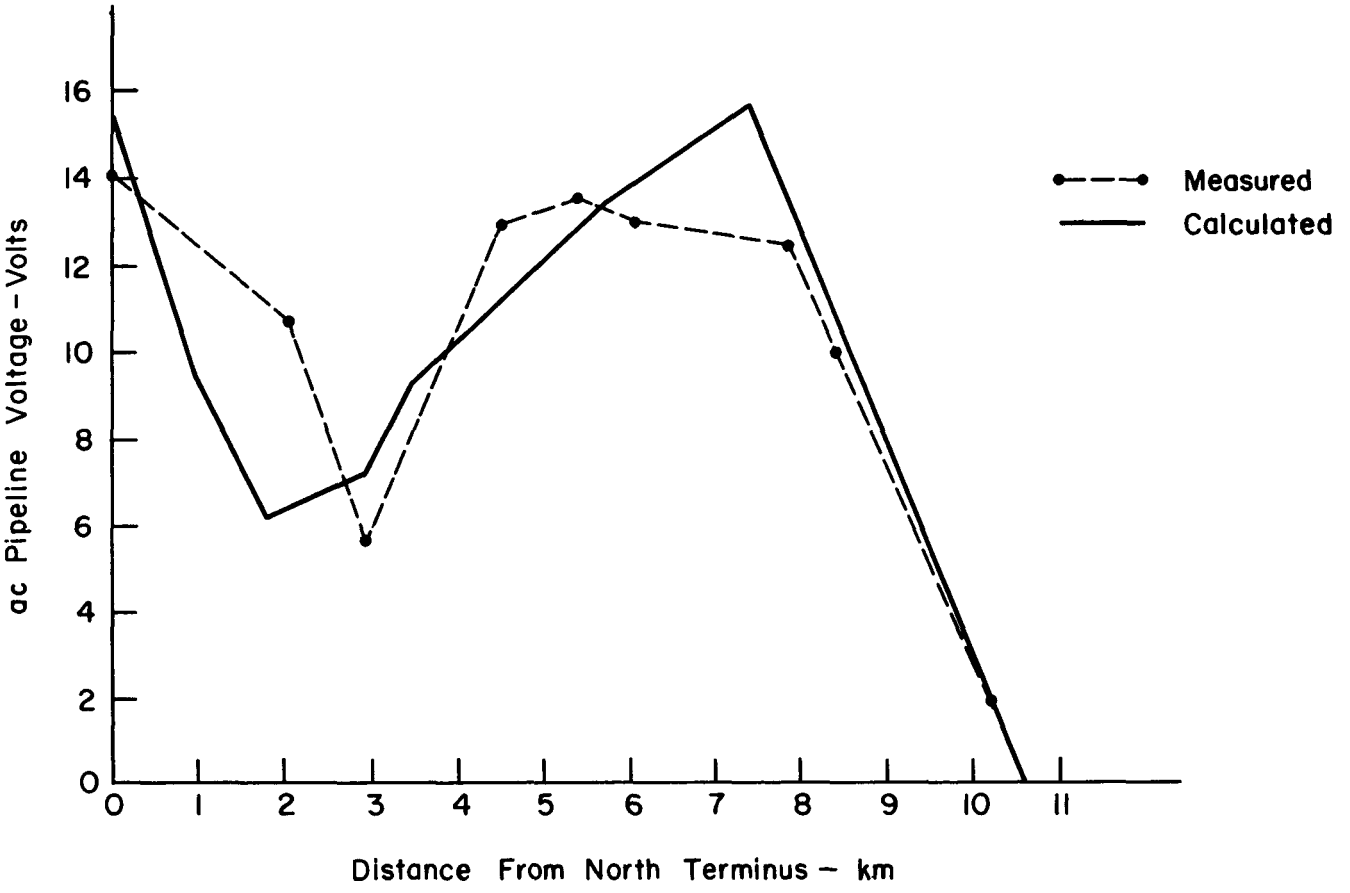

Fig. 3-20 PIPELINE VOLTAGE PROFILE

2. It is necessary to measure the pipeline driving electric field for each location of the pipeline relative to the power lines. However, the measurements cannot be made in the vicinity of the pipeline itself since the pipeline current will perturb the measurements. Hence, the following procedure or a conceptually similar one may be used. For example, to obtain an approximation to the pipeline driving electric field in regions 1a, 1b and 1c, measure the electric field at the same distances from the power lines in region 2, since the pipeline has crossed over to the opposite side of the ROW. Likewise, the driving electric field for the pipeline in region 2 can be approximated by measurements at the same location relative to the power lines in any of the sub-regions of region 1. Similar considerations hold for the other regions.

3. A common phase reference must be established between all the electric field measurements made in the different regions. This is best accomplished by locating the equipment reference probe at the same location relative to the power lines in each of the regions that measurements are made. Two requirements must be made in choosing the reference probe location: (1) the electric field at the reference probe must be approximately the same, i.e., at least the closest power line circuits must be the same for all regions, and (2) the pipeline cannot be buried at this location in any of the regions. Reference to Figure 3-19 shows that a location between the two westernmost structures will satisfy these requirements. In making the electric field measurements, the phase of each measured field is known relative to the reference probe and, hence, relative to any other measured electric field anywhere on the ROW. Arbitrarily, any one of the measured fields (or the field at the reference probe) may be assigned as the zero phase reference and all other electric field phases adjusted in a corresponding manner.

4. This measurement procedure is reasonably accurate (as in the situation here) if the presence of the subject pipeline on the ROW does not significantly alter the currents in other conductors situated on the ROW.

Measured Electric Source Fields. After adjusting the measured phase of the electric fields so as to be commensurable with a single phase reference common to all regions, the values shown in Table 3-5 were obtained. (Note: The measured field magnitudes are not modified in any way.)

Pipeline Parameters. Knowledge of the pipeline parameters, γ, the propagation constant and Z_0, the characteristic impedance, are necessary in order to calculate the voltage profile. This, in turn, requires knowledge of the coating resistivity which, at best, can only be estimated. An additional complication exists for this line in that during construction, 17-pound magnesium anodes were installed every one-quarter mile and are inaccessible for measurement. (With such a close separation, the magnesium anodes in the aggregate act as a continuous holiday and, hence, basically lower the average resistivity of the pipe coating.)

Table 3-5

ELECTRIC FIELD MEASUREMENTS

Region		Electric Field (volts/km)
1a	$0 \leq d < 1.73$ km	$7.0/\underline{10^{o}}$
1b	$1.73 \leq d < 3.45$ km	$4.0/\underline{0^{o}}$
1c	$3.45 \leq d < 5.6$ km	$1.2/\underline{-10^{o}}$
2	$5.6 \leq d < 6.5$ km	$2.3/\underline{65^{o}}$
3	$6.5 \leq d < 7.7$ km	$\simeq 2.3/\underline{65^{o}}$
4	$7.4 \leq d < 8.64$ km	$7.0/\underline{178^{o}}$
5	$8.64 \leq d < 10.6$ km	$\simeq 7.0/\underline{178^{o}}$

This problem of establishing the pipeline parameters was solved practically in the following manner. At a point (far enough from either end so as to establish the characteristic impedance level) on the pipeline where a casing existed, the pipeline was shorted to the casing and the drop in the induced voltage level measured along with the resistance of the casing to remote earth. For example, it was found that for a casing of 1.3 ohms resistance, the pipeline voltage was reduced to one-half. This established the pipeline characteristic impedance as being approximately 2.6 ohms.

Using the hand calculator program PIPE, several trial runs were made with different assumed values of coating resistivity. It was found that a coating resistivity of about 200,000 ohms-ft^2 yielded a reasonably close approximation to the measured pipeline impedance. Substituting this value back into the program resulted in the following estimates for the pipeline parameters:

$$\gamma = 0.1473 + j\ 0.1084 = 0.183/\underline{36.3^{o}}\ \text{km}^{-1}$$

$$Z_0 = 2.151 + j\ 1.586 = 2.67/\underline{36.3^{o}}\ \text{ohms}.$$

Voltage Calculations. Using the established pipeline parameters and the measured value of the source electric field, the induced voltage was calculated on a point-by-point basis, and the results are plotted in Figure 3-20. A sample point calculation is given below for a distance of 5.6 km south of the north terminus.

Sample Voltage Calculation. As a first step, it is necessary to determine the Thevenin equivalent circuits to either side of the location. Considering first the equivalent circuit looking to the north, the following procedure is used.

1. Assume $Z_L = \infty$, because of the insulator at the north end of the pipeline. Using the program THEVENIN, find the equivalent circuit (to the north) at a distance of 1.73 km. Using the electric field appropriate to region 1a yields a solution for the open circuit voltage and Thevenin impedance as, $V_{OC} = 6.04/\underline{189.5^o}$ volts and $Z_{TH} = 8.53/\underline{1.79^o}$ ohms, respectively.

2. Using the quantities V_{OC} and Z_{TH} above for the load, program THEVENIN is used to find the equivalent circuit into the pipeline at the distance of 3.45 km. Using the driving source field appropriate to region 1b yields, $V_{OC} = 8.09/\underline{181.7^o}$ volts, and $Z_{TH} = 4.44/\underline{6.81^o}$ ohms.

3. Using the values of V_{OC} and Z_{TH} calculated in (2) as the load termination, calculate the input equivalent circuit at a distance of 5.6 km. Using the driving source field appropriate to region 1c yields the (north) Thevenin equivalent circuit of $V_{OC} = 6.84/\underline{173.3^o}$ volts and $Z_{TH} = 3.04/\underline{15.8^o}$ ohms.

To complete the prediction, the Thevenin equivalent circuit looking to the south at the point 5.6 km must now be calculated. The procedure is as follows:

1. Assume a very low terminating impedance at the south end, i.e., $Z_L \simeq 0$. Calculate the input impedance to the pipeline (to the south) at a distance of 3.2 km from the south end (or 7.4 km from the north end). Using the driving source field common to both regions 4 and 5 yields, $V_{OC} = 21.5/\underline{172.1^o}$ volts, and $Z_{TH} = 1.50/\underline{66.8^o}$ ohms.

2. Using these computed values as the new load termination, the (south) input equivalent circuit for the pipeline is calculated at 5.6 km. The driving source field appropriate to regions 2 and 3 is used, yielding values of $V_{OC} = 19.0/\underline{148.8^o}$ volts and $Z_{TH} = 2.17/\underline{59.5^o}$ ohms.

3. Using the north and south equivalent circuits just derived, the program NODE results in a predicted voltage of 13.4 volts.

Similar equivalent circuit calculations for other distances were made and the predicted voltage profile for the pipeline is plotted in Figure 3-20.

Critique. Comparison of the measured and predicted values of the pipeline voltage shows a very good agreement, in general. The largest discrepancy lies in the region of from 1.5 to 2.5 km, and is presumed to occur because of a possible error in the electric field phase differential between one or more regions. Such a result is not surprising since it took the better part of the day to make the electric field measurements; and because of the time-varying power line currents, all the measurements were not necessarily commensurable.

A second deviation between the calculated and measured curves occurs at 7.4 km. Here, theory indicates the occurrence of a peak, but unfortunately, a measurement was not made close enough to the vicinity of the predicted peak to enable verification of its value. However, immediate data points on either side of the indicated peak exhibit excellent agreement with predicted values.

In summary, this case history, as presented, illustrates a field measurement oriented approach to the prediction of pipeline voltages. It is particularly useful, as in this case, where the interaction geometry between multiple power line circuits and the subject pipeline is varying, thus requiring many sets of calculations to be made if a purely analytical approach were used. Its principal benefits are that power line currents do not have to be known, and the interaction of other conductors such as other buried pipelines is automatically taken into account. The basic disadvantage to the method is that prediction errors can creep in because of changing power line currents while measurements are being made. However, as the results of this case history indicate, the prediction accuracy obtained is still at an acceptable level.

REFERENCES

1. Electrical Transmission and Distribution Reference Book, Fourth Edition. Westinghouse Electric Corp., 1964.

2. "Electromagnetic Effects of Overhead Transmission Lines - Practical Problems, Safeguards, and Methods of Calculation," by IEEE Working Group on E/M and E/S Effects of Transmission Lines, IEEE Trans. Power App. Systems, Vol. PAS-94, pp. 892-899, May/June 1974.

3. H. W. Dommel et al, Discussion, IEEE Trans. Power App. Systems, Vol. PAS-92, pp. 900-904.

4. Directives Concerning the Protection of Telecommunication Lines Against Harmful Effects from Electricity Lines. International Telegraph and Telephone Consultative Committee (CCITT), International Telecommunications Union, 1962 (supplemented 1965).

5. A. W. Peabody and A. L. Verhiel, "The Effects of High Voltage Alternating Current (HVAC) Transmission Lines on Buried Pipe Lines," Paper No. PCI-70-32 presented at IEEE/IGA Petroleum and Chemical Industry Conference, Tulsa, Oklahoma, September 15, 1970.

6. C. G. Siegfried, "AC Induced Interference on Pipelines," presented at Interpipe 73 Conference, Houston, Texas, October 31, 1973.

7. C. A. Royce, "Alternating Current Problems of Pipelines," presented at A.G.A. Operating Section Transmission Conference, Houston, Texas, May 18, 1971.

8. E. C. Paver, Sr., "The Effects of Induced Current on a Pipeline," Paper No. 54 presented at NACE 26th Annual Conference, Philadelphia, Pa., March 2-6, 1970.

9. M. A. Puschel, "Power Lines and Pipelines in Close Proximity During Construction and Operation," Materials Performance, Vol. 12, pp. 28-32, December 1973.

10. Technical Compatibility Factors for Joint-Use Rights-of-Way (for Bureau of Land Management, Contract 08550-CT5-5). Aerospace Corp., February 1, 1975.

11. J. Pohl, "Influence of High-Voltage Overhead Lines on Covered Pipelines," Paper No. 326 presented at CIGRE, Paris, France, June 1966.

12. B. Favez and J. C. Gougeuil, "Contribution to Studies on Problems Resulting From the Proximity of Overhead Lines with Underground Metal Pipe Lines," Paper No. 336 presented at CIGRE, Paris, France, June 1966.

13. D. N. Gideon et al., Final Report on Project Sanguine. Parametric Study of Costs for Interference Mitigation in Pipelines (to IIT Research Institute). Battelle Columbus Laboratories, Columbus, Ohio, September 30, 1971.

14. J. R. Sherbundy, The Effects of High Voltage Overhead Transmission Lines on Underground Pipelines. M.S. Thesis, Dept. of Electrical Engineering, Ohio State University, 1975.

15. E. F. Vance, DNA Handbook Revision, Chapter 11, Coupling to Cables (for Dept. of the Army, Contract DAAG39-74-C-0086). Stanford Research Institute, Menlo Park, California, December 1974.

16. E. D. Sunde, Earth Conduction Effects in Transmission Systems. New York: Dover Publications, 1968.

17. A.H.E. Manders et al., "Inductive Interference of the Signal and Protection System of the Netherlands Railways by High Voltage Overhead Lines Running Parallel with the Railways," Paper 36-02 presented at CIGRE, Paris, France, August 1974.

18. Inductive Interference Engineering Guide (preliminary issue). Bell Laboratories Electromagnetic Interference Department, Loop Transmission Division, March 1974.

19. A. W. Peabody, Consulting Report: Recommendations for Mitigation of Induced AC on the 34-Inch Diameter, Newberry to Needles Pipeline No. 235 (for Southern California Gas Company). Ebasco Services, Houston, Texas, June 27, 1975.

Section 4

SUMMARY OF ANALYTICAL METHODS FOR PREDICTING ELECTROSTATIC COUPLING TO PIPELINES

INTRODUCTION

Two available analytical methods for predicting the voltages and shock currents electrostatically induced by ac power lines on nearby above-ground pipelines are summarized. The first approach, the network solution method, translates the coupling problem to a circuit problem and solves the latter by inverting a potential coefficient matrix. This method involves considerable complexity for power lines with either multiple circuits or several shield wires. The second approach, the voltage gradient method, develops approximations for the variation of the electrostatic field with distance from the power line, and uses these approximations to obtain the pipeline induction effects. This approach is useful for many different power line configurations and is suitable for hand calculation.

NETWORK SOLUTION METHOD

It is often useful to interpret the electrostatic coupling problem in circuit form, i.e., to reduce what is really a problem in electrostatic field theory to one of network solution (1-3).

Figure 4-1 illustrates this interpretation for a pipeline parallel to an arbitrary configuration of N power line phase conductors and shield wires. In this figure, C'_{mn} is the capacitance/meter between the mth and nth conductors in the presence of the other N-1 conductors. The current flow from the nth conductor to the pipeline, the (N+1)th conductor, is simply

$$I_{n,N+1} = (V_n - V_{N+1})\, j\omega C'_{n,N+1}\, \ell \text{ amps} \qquad (4\text{-}1)$$

where $\omega = 2\pi 60$ sec^{-1} and ℓ = pipeline length in meters. The total current flow to the pipeline is thus

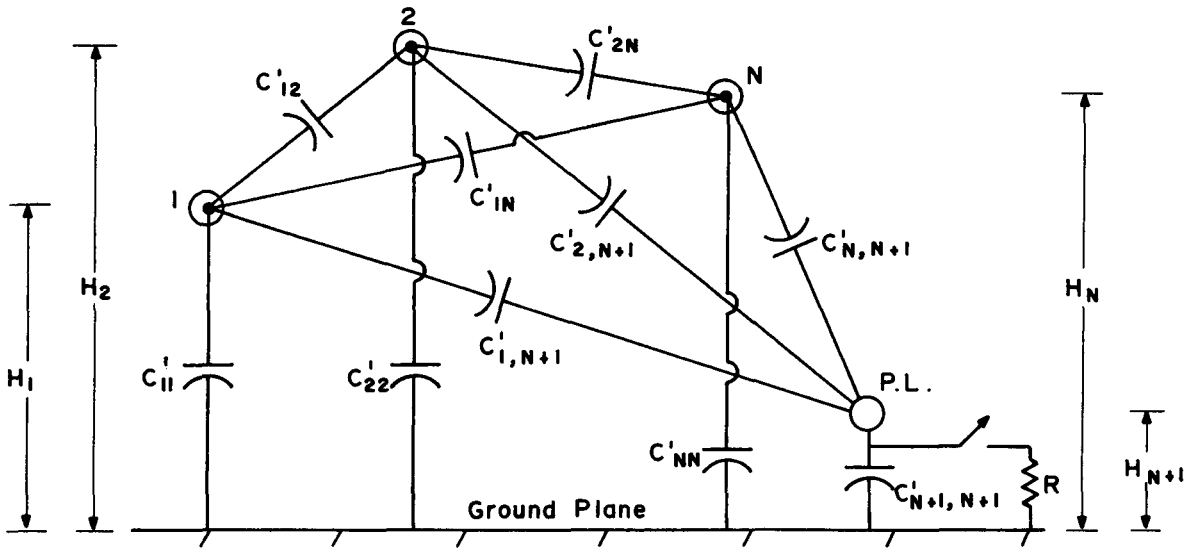

Fig 4-1 EQUIVALENT CIRCUIT FOR THE STUDY OF ELECTROSTATIC INDUCTION ON A PARALLEL PIPELINE BY N PHASE CONDUCTORS AND GROUND WIRES

$$I_{N+1} = j\omega\ell \sum_{n=1}^{N} C'_{n,N+1} (V_n - V_{N+1}) \text{ amps.} \quad (4\text{-}2)$$

Because the pipeline is much closer to the ground than to any of the other conductors,

$$C'_{N+1,N+1} >> C'_{n,N+1} \quad n = 1, 2, \ldots, N. \quad (4\text{-}3a)$$

Therefore, the capacitive reactance of the pipeline to ground is much less than the capacitive reactances of any of the other conductors to the pipeline. Using simple voltage divider arguments, we find that

$$|V_{N+1}| << |V_n|, \; n\varepsilon \{n_p\} = \text{subscripts of the phase conductors} \quad (4\text{-}3b)$$

and approximate the current flow to the pipeline and the pipeline potential as

$$I_{N+1} \simeq j\omega\ell \sum_{\{n_p\}} C'_{n,N+1} \cdot V_n \text{ amps} \quad (4\text{-}4a)$$

$$V_{N+1} = \frac{I_{N+1}}{j\omega C'_{N+1,N+1}\ell} \simeq \frac{1}{C'_{N+1,N+1}} \sum_{\{n_p\}} C'_{n,N+1} \cdot V_n \text{ volts} \quad (4\text{-}4b)$$

Now, let us assume that the pipeline is suddenly grounded through R, the body resistance of a pipeline worker. This grounding results in two electric shock hazards for the worker. First, the energy stored in the pipeline capacitance-to-ground is discharged through his body in a pulse having a maximum energy of

$$W_{max} = \ell C'_{N+1,N+1} |V_{N+1}|^2 \simeq \frac{\ell}{C'_{N+1,N+1}} \left| \sum_{\{n_p\}} C'_{n,N+1} \cdot V_n \right|^2 \text{ joules} \quad (4\text{-}5a)$$

Second, a steady-state current having a maximum magnitude of

$$I_{max} = |I_{N+1}| \simeq \omega\ell \left| \sum_{\{n_p\}} C'_{n,N+1} \cdot V_n \right| \text{ amps} \quad (4\text{-}5b)$$

flows through his body, assuming that contact with the pipeline is maintained.

From Eq. 4-5, we see that knowledge of the set $\{C'_{n,N+1}\}$ is essential for the determination of pipeline shock effects using this method. This set can be derived in the following way. First, we define the Maxwell potential coefficient matrix, [P], for the system of Figure 4-1 using the equation

$$\begin{bmatrix} V_1 \\ V_2 \\ \cdot \\ \cdot \\ \cdot \\ V_{N+1} \end{bmatrix} = \begin{bmatrix} P_{11} & P_{12} & \cdots & P_{1,N+1} \\ P_{21} & P_{22} & \cdots & P_{2,N+1} \\ \cdot & \cdot & \cdot & \\ \cdot & \cdot & \cdot & \\ \cdot & \cdot & \cdot & \\ P_{N+1,1} & P_{N+1,2} & \cdots & P_{N+1,N+1} \end{bmatrix} \begin{bmatrix} Q_1 \\ Q_2 \\ \cdot \\ \cdot \\ \cdot \\ Q_3 \end{bmatrix} \qquad (4\text{-}6a)$$

where $V_1, \ldots, V_{N+1}$ are the phasor potentials of the conductors, $Q_1, \ldots, Q_{N+1}$ are the phasor charges on the conductors and the elements of are given by

$$P_{nn} = \frac{1}{2\pi\varepsilon_o} \cdot \ln\left(\frac{4H_n}{d_n}\right)$$

$$P_{mn} = \frac{1}{2\pi\varepsilon_o} \cdot \ln\left(\frac{D'_{mn}}{D_{mn}}\right) \qquad (4\text{-}6b)$$

where

H_n = height of the nth conductor, in meters, above ground;

D_{mn} = distance between the mth and nth conductors, in meters;

D'_{mn} = distance between the mth conductor and the image of the nth conductor, in meters;

ε_o = free space permittivity = 8.85×10^{-12} F/m

d_n = diameter of the nth conductor, in meters, or the equivalent diameter, d_{eq}, of a bundle conductor, given by

$$d_{eq} = d_{bundle} \left(\frac{k d_{subcon.}}{d_{bundle}} \right)^{1/k} \quad m, \tag{4-6c}$$

where d_{bundle} is the bundle circular diameter; $d_{subcon.}$ is the subconductor diameter; and k is the number of bundle subconductors.

Now the required capacitance matrix, [C'] is derived from Eq. 4-6a by left-multiplying both sides by $[P]^{-1}$ to get

$$\begin{bmatrix} P_{11} & P_{12} & \cdots & P_{1,N+1} \\ P_{21} & P_{22} & \cdots & P_{2'N+1} \\ \cdot & \cdot & \cdot & \\ \cdot & \cdot & \cdot & \\ \cdot & \cdot & \cdot & \\ P_{N+1,1} & P_{N+1,1} & \cdots & P_{N+1,N+1} \end{bmatrix}^{-1} \begin{bmatrix} V_1 \\ V_2 \\ \cdot \\ \cdot \\ \cdot \\ V_{N+1} \end{bmatrix} = \begin{bmatrix} Q_1 \\ Q_2 \\ \cdot \\ \cdot \\ \cdot \\ Q_{N+1} \end{bmatrix} \tag{4-7a}$$

and using the general capacitance relation for a network,

$$[C'] \; [V] = [Q] \tag{4-7b}$$

to obtain the identity

$$[C'] = [P]^{-1} \; . \tag{4-7c}$$

To determine specific elements of [C'], namely $\{C'_{n,N+1}\}$ we compute

$$C'_{n,N+1} = \frac{(-1)^n \text{ cofactor of } P_{n,N+1}}{\text{determinant of } [P]} \; , \quad n = 1, 2, \ldots, N+1 \tag{4-7d}$$

VOLTAGE GRADIENT METHOD

This method is used to avoid the matrix inversion calculations of Eq. 4-7. Referring to Figure 4-1 and to the previous discussions the key simplifying assumptions are (3-10)

$$V_{N+1} \simeq E_{N+1}\, H_{N+1} \text{ volts};\quad C'_{N+1,N+1} \simeq C_{N+1,N+1} \tag{4-8}$$

where E_{N+1} is the ground-level transverse voltage gradient (in volts/meter) at the pipeline location without the pipeline present, and $C_{N+1,N+1}$ is the pipeline capacitance to ground in the absence of the other conductors. Subject to these assumptions, Eq. 4-5 becomes

$$W_{max} = \ell C'_{N+1,N+1} \left|V_{N+1}\right|^2 \simeq \ell C_{N+1,N+1} \left|E_{N+1}\, H_{N+1}\right|^2 \text{ joules} \tag{4-9a}$$

$$I_{max} = \omega \ell C'_{N+1,N+1} \left|V_{N+1}\right|^2 \simeq \omega \ell C_{N+1,N+1} \left|E_{N+1}\, H_{N+1}\right| \text{ amps} \tag{4-9b}$$

where

$$C_{N+1,N+1} = \frac{2\pi\varepsilon_o}{\ln\left(4H_{N+1}/d_{N+1}\right)} \text{ farads/m} \quad . \tag{4-9c}$$

The problem of estimating the maximum shock energy and current is thus reduced to one of estimating the unperturbed transverse voltage gradient at the pipeline.

NOTE: The unperturbed transverse voltage gradient, discussed in this section, is not the same as the longitudinal driving electric field discussed in Section 3 for electromagnetic coupling. The transverse voltage gradient results from the potential of the power line conductors with respect to ground; the longitudinal electric field results from the current flow through the power line conductors.

Exact Computation of the Voltage Gradient

For the power line example of Figure 4-1, the voltage gradient at the adjacent pipeline is given by (8):

$$E_{N+1} = \frac{1}{\pi\varepsilon_o} \sum_{n=1}^{N} \frac{Q_n H_n}{D^2_{n,N+1}} \text{ volts/m} \tag{4-10}$$

where Q_n, H_n, $D_{n,N+1}$ and ε_o are as defined for Eq. 4-6. Because $[P]^{-1}$ must be calculated to determine $[Q]$ (as shown in Eq. 4-7a), this computation is virtually identical to that of Eq. 4-7d and, therefore, is not easily performed by hand.

For the voltage gradient method to be useful, methods for the approximation of E_{N+1} are essential. These are now discussed.

Estimate of the Peak Voltage Gradient

A graphical method for the computation of E_{pk}, the peak value of E_{N+1} within the power line right-of-way has been developed (8). This method is applicable to single and double circuits with either flat, delta, or vertical configurations of the phase conductors. The required data include the line-to-line voltage, the circular diameter of a conductor bundle, the phase conductor height and spacing, and the phase sequence for the case of double circuits. The required graphical aids for several single-circuit cases are depicted in Figure 4-2.

To illustrate this approach, we consider the computation of E_{pk} for a power line with the following characteristics:

1. Single circuit, flat configuration
2. Line-to-line voltage: V_{LL} = 500 kV
3. Bundle data: d_{bundle} = 0.46 m
   $d_{subcon.}$ = 0.043m
   k = 2
4. Phase-to-phase spacing: S = 10.67 m
5. Height of phase conductors: H = 10.67 m

Using Eq. 4-6c, we first calculate the equivalent bundle diameter, d_{eq}, as

$$d_{eq} \simeq 0.46\left(\frac{2 \times 0.043}{0.46}\right)^{1/2} = 0.199 \qquad (4\text{-}11a)$$

We also calculate two parameters:

$$\frac{H}{d_{eq}} = \frac{10.67}{0.199} = 53.6$$

$$\frac{S}{H} = \frac{10.67}{10.67} = 1.0 \qquad (4\text{-}11b)$$

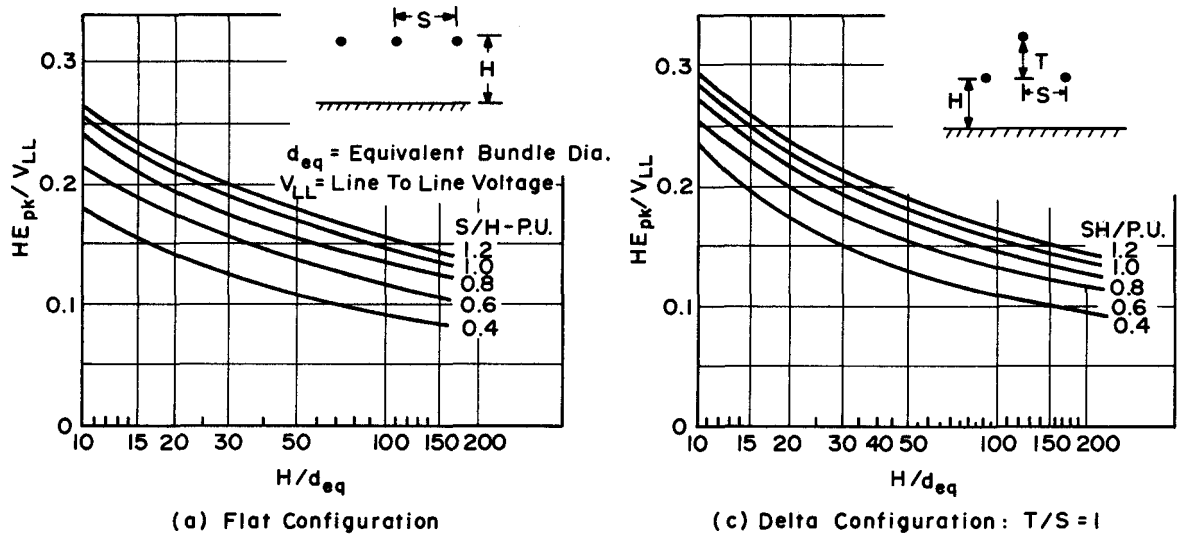

(a) Flat Configuration

(c) Delta Configuration: T/S = 1

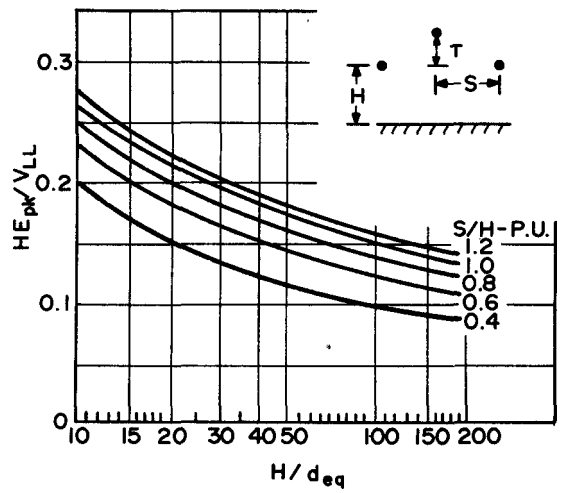

(b) Delta Configuration: T/S = 0.5

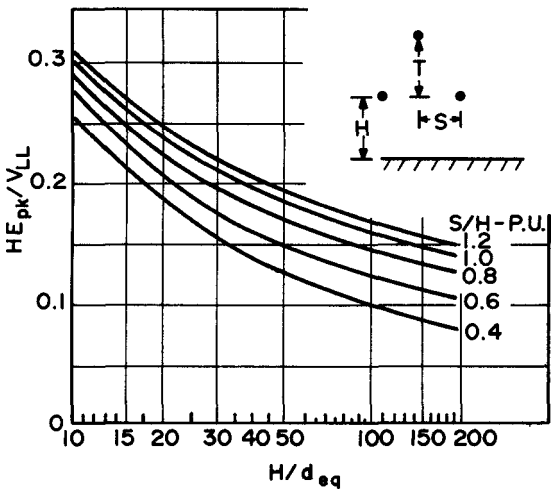

(d) Delta Configuration: T/S = 1.5

Fig.4-2 GRAPHICAL AIDS FOR THE COMPUTATION OF E_{pk} (13)

Next, we use Figure 4-2a for the single circuit, flat configuration case. Entering the graph at the abscissa value $H/d_{eq} = 53.6$, we intersect the curve having the parameter $S/H = 1.0$ at the ordinate value of $H \cdot E_{pk}/V_{LL} \simeq 0.17$. Thus,

$$E_{pk} \simeq \frac{0.17\ V_{LL}}{H} = \frac{0.17 \times 500}{10.67} = 8.0 \text{ kV/m} \qquad (4\text{-}11c)$$

The peak voltage gradient usually appears almost directly beneath the outer phase conductor for a flat configuration. This method yields information only about this worst-case pipeline position. The method does not describe the variation of E_{N+1} with distance from the power line.

Estimate of the Variation of the Voltage Gradient with Distance

Straight-Line Approximation (Zone Diagram Method). A simple method to estimate the variation of E_{N+1} with distance from the power line has been developed (3). This method uses straight lines to approximate the exactly computed curves of E_{N+1} vs. distance for single circuit, flat configuration power lines. The formulae for the straight lines are simple enough to be hand calculable, and yet accurate enough to be highly useful. The required data include the line-to-line voltage and the height and spacing of the phase conductors.

To illustrate this approach, Figure 4-3 depicts the straight-line approximation, or zone diagram, for the variation of E_{N+1} near the 500 kV power line used in the previous example. The exactly computed values of E_{N+1} are bounded by the zone perimeter, which is defined in the general case by:

$$E_{pk} = K_1\ V_{LL}\ V_{pu}\ \sqrt{S}\ H^{-K_2} \text{ kV/m} \qquad (4\text{-}12a)$$

$$E_{co} = K_3\ V_{pu} \text{ kV/m} \qquad (4\text{-}12b)$$

$$D_{co} = K_4\ S + K_5 \text{ m} \qquad (4\text{-}12c)$$

$$\beta = K_6\ H^{-2} \text{ kV/m}^2 \qquad (4\text{-}12d)$$

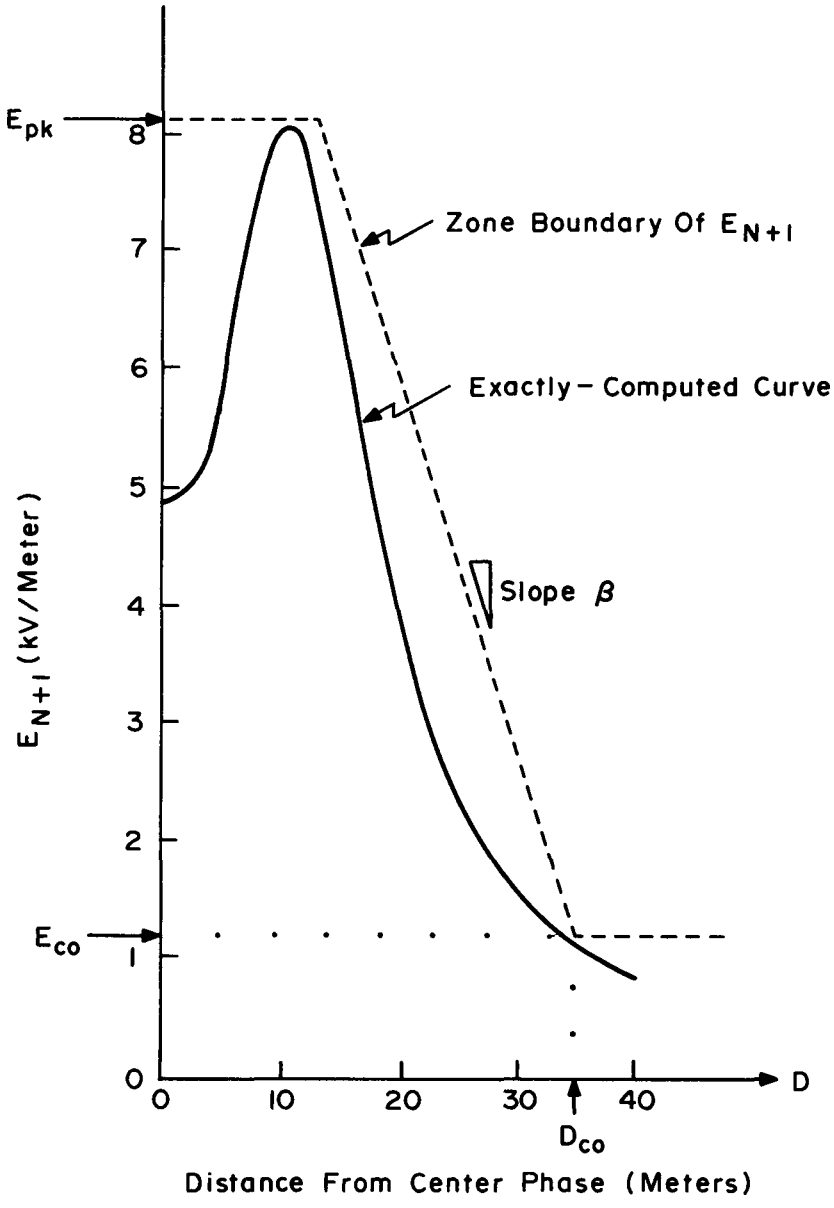

Fig. 4-3 ZONE DIAGRAM FOR A 500 kV, SINGLE-CIRCUIT, FLAT-CONFIGURATION POWER LINE (15)

where

E_{pk} = peak voltage gradient

E_{co} = cut-off voltage gradient

D_{co} = cut-off distance

β = zone slope

V_{LL} = line-to-line voltage (kV)

V_{pu} = per unit operating voltage of line (kV/kV)

S = phase-to-phase spacing (m)

H = phase conductor height (m)

K_1-K_6 = multiplying factors having the following dependence on V_{LL}

V_{LL}	K_1	K_2	K_3	K_4	K_5	K_6
345	0.255	1.692	0.89	2.055	12.21	23.34
500	0.307	1.742	1.18	1.604	17.89	37.04
765	0.308	1.682	2.00	1.491	20.20	72.98
1100	0.253	1.588	3.35	1.640	17.01	115.57

For the specific case of Figure 4-3, Eq. 4-12 yields

$$E_{pk} = (0.307)(500)(1.0)(\sqrt{10.67})(10.67)^{-1.742} = 8.11 \text{ kV/m}$$

$$E_{co} = (1.18)(1.0) = 1.18 \text{ kV/m}$$

$$D_{co} = (1.604)(10.67) + 17.89 = 35.00 \text{ m}$$

$$\beta = (37.04)/(10.67)^2 = 0.32 \text{ kV/m}^2$$

The value of E_{pk} calculated here differs from that obtained using the graphical method (8) by only about 2 percent. However, in addition to E_{pk}, we now have a useful estimate of the drop-off of E_{N+1} from E_{pk} as the distance to the power line increases up to D_{co}. Beyond D_{co}, the zone diagram method (3) upper bound for E_{N+1} is simply E_{co}, which is independent of phase spacing and conductor height.

Cut-Off Zone Gradient Approximation. The zone defined by $D \geq D_{co}$, $E_{N+1} \leq E_{co}$, yields an upper bound for E_{N+1} that has no dependence on distance (3). However, as seen in Figure 4-3, the exactly computed curve for E_{N+1} continues to decrease in amplitude as D increases beyond D_{co}. A more useful bound for this case is

$$E_{N+1} \leq E_{co} \left(\frac{D_{co}}{D}\right)^2 , \quad D \geq D_{co} \tag{4-13}$$

which represents the drop-off of the gradient for a single phase conductor above ground, as seen from Eq. 4-10.

Extension to Different Single and Double Circuit Conductor Configurations. An extension of the zone approach to delta, inverted delta, single circuit vertical configurations, and to center line symmetrical and center point symmetrical double circuit configurations, shown in Figure 4-4 has been proposed (6). The recommended procedure is as follows:

1. Determine V_{LL}, V_{pu}, S, and H for the power line configuration of interest, with S and H defined for the configuration as in Figure 4-4.
2. Determine E_{pk}, E_{co}, D_{co} and β, using Eq. 4-12 and the parameters of Step 1 above.
3. For the configuration desired, multiply the values determined in Step 2 by the following factors:

Phase Conductor Configuration	Multiplying Factors for E_{pk}	E_{co}	D_{co}	β
(a) Single circuit, flat	1.0	1.0	1.0	1.0
(b) Single circuit, delta	0.9	0.8	0.8	0.93
(c) Single circuit, inverted delta	0.9	0.78	0.5	1.15
(d) Single circuit, vertical	1.0	0.4	0.6	1.03
(e) Double circuit, center line symmetrical	1.3	0.5	0.8	1.3
(f) Double circuit, center point symmetrical	0.84	0.5	0.75	1.0

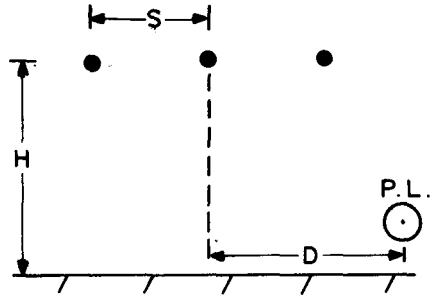

a) Single - Circuit, Flat

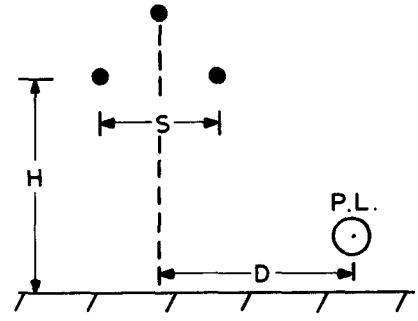

b) Single - Circuit, Delta

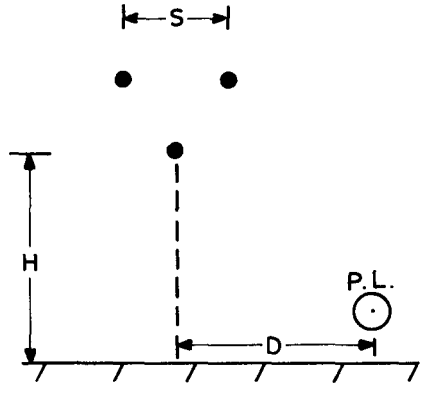

c) Single Circuit, Inverted Delta

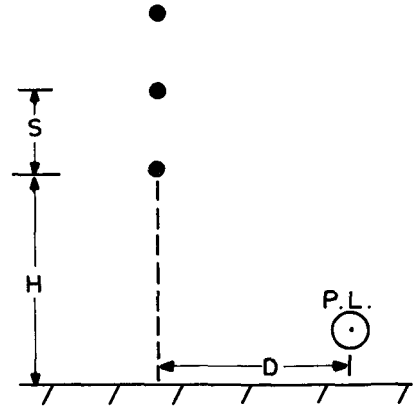

d) Single Circuit, Vertical

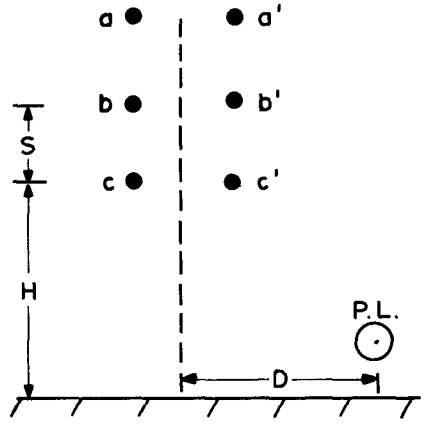

e) Double Circuit, Center - Line Symmetrical

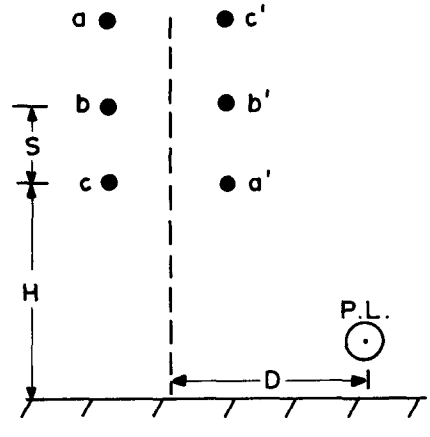

f) Double Circuit, Center - Point Symmetrical

Fig. 4-4 LINE CONFIGURATIONS FOR THE EXTENDED ZONE METHOD (10)

In this manner, the significantly different voltage gradient profiles of six power line configurations can be estimated by a single, hand calculable method.

Extension of the Non-Parallel Pipeline Case. If the pipeline is built in different sections or if it is not parallel to the power line, computations should be made for each section, accounting also for the phase of the ground voltage gradient (8). This phase accounting requirement greatly complicates the computation procedure because no zone diagrams for the phase of the gradient are available at this time. Therefore, the profile of gradient phase along the pipeline must be obtained by using Eq. 4-10, the exact formula. The recommended computation procedure is as follows.

1. Compute D_{co} for the power line.

2. Divide the pipeline run that is located less than D_{co} from the power line into sections having $\Delta D = S$, where ΔD is the change of distance of the pipeline segment from the power line, and S is the phase conductor spacing. Divide the pipeline run that is located more than D_{co} from the power line into sections having $\Delta D = S\ (D/D_{co})^2$.

3. Approximate $Q_1, Q_2, \ldots Q_N$ by

$$\begin{bmatrix} Q_1 \\ Q_2 \\ . \\ . \\ . \\ Q_n \end{bmatrix} \simeq \begin{bmatrix} P_{11} & P_{12} & \cdots & P_{1,N} \\ P_{21} & P_{22} & \cdots & P_{2,N} \\ . & . & . & . \\ . & . & . & . \\ . & . & . & . \\ P_{N,1} & P_{N,2} & \cdots & P_{N,N} \end{bmatrix}^{-1} \begin{bmatrix} V_1 \\ V_2 \\ . \\ . \\ . \\ V_N \end{bmatrix} \qquad (4\text{-}14)$$

4. Compute the voltage gradient at the midpoint of each pipeline section by

$$E_{N+1,i} = \frac{1}{\pi\varepsilon_o} \sum_{n=1}^{N} \frac{Q_n H_n}{D^2_{n,(N+1,i)}} \text{ volts/m} \qquad (4\text{-}15)$$

where $\{Q_n\}$ has been determined in Step 3 above, and the subscript N+1,i denotes the ith section of the pipeline (the (N+1)th conductor).

5. Compute the current flow to each pipeline section by using the equation

$$I_{N+1,i} = j\omega C_i \cdot E_{N+1,i} \cdot H_{N+1,i} \text{ amps,} \tag{4-16}$$

where $\{E_{N+1,i}\}$ has been determined in Step 4, and C_i is the capacitance-to-ground of the ith pipeline section given by

$$C_i = \frac{2\pi\varepsilon_o \ell_i}{\ln (4 H_{N+1,i}/d_{N+1,i})} \text{ farads.} \tag{4-17}$$

6. Compute the total current flow to the pipeline

$$I_{N+1} = \sum_i I_{N+1,i} \text{ amps,} \tag{4-18a}$$

and the total pipeline capacitance

$$C_{N+1,N+1} = \sum_i C_i \text{ farads.} \tag{4-18b}$$

7. Compute the magnitude of the open circuit pipeline voltage, given by

$$V_{oc} = \frac{|I_{N+1}|}{\omega C_{N+1,N+1}} \text{ volts.} \tag{4-19}$$

8. Compute the maximum electric shock hazards:

$$W_{max} = \ell C_{N+1,N+1} \cdot V_{oc}^2 \text{ joules;} \tag{4-20a}$$

$$I_{max} = |I_{N+1}| \text{ amperes.} \tag{4-20b}$$

SUMMARY

The available analytical methods for predicting the voltage and shock currents electrostatically induced by power lines on nearby above-ground pipelines has been summarized. Specifically, this section first reviewed the network solution method, in which the electrostatic field problem posed by the power line-pipeline geometry is reduced to a network analysis problem. Here, the interactions between power line phase conductors, power line shield wires, and the adjacent pipeline are modeled by computing equivalent capacitances between the respective conductors, and solving the resulting capacitive network for the pipeline voltage and current. Because computation of the capacitances requires the inversion of a fairly large matrix, hand calculation can be difficult and time consuming with this approach.

The voltage gradient method allows an accurate approximation of electrostatically induced pipeline voltage and current levels. This is accomplished by first determining the transverse voltage gradient at the pipeline location and then using Eqs. 4-8 and 4-9b, to determine the voltage and current levels, respectively.

Methods for direct measurement of the transverse gradient are described elsewhere (8-12).

REFERENCES

1. IEEE Working Group. "Electrostatic Effects of Overhead Transmission Lines. Part II - Methods of Calculation." IEEE Trans. Power App. Systems, Vol. PAS-91, March/April 1972, pp. 426-430.

2. E. T. Gross and M. H. Hesse. "Electrostatically Induced Voltages About High Voltage Lines." J. Franklin Inst., Vol. 295, No. 2, February 1973, pp. 89-101.

3. T. M. McCauley. "EHV and UHV Electrostatic Effects: Simplified Design Calculations and Preventative Measures." IEEE Trans. Power App. Systems, Vol. PAS-94, November/December 1975, pp. 2057-2065.

4. D. W. Deno. "Calculating Electrostatic Effects of Overhead Transmission Lines." IEEE Trans. Power App. Systems, Vol. PAS-93, September/October 1974, pp. 1458-1466.

5. J. C. Procario and S. A. Sebo. "Electric Field Strength at Ground Due to High Voltage Overhead Transmission Lines: Its Cause and Effects; Methods of Reduction." Proc. 1974 Midwest Power Symposium, Rolla, Missouri October 1974.

6. A. S. Timascheff. "Fast Calculation of Gradients of a Three Phase Bundle Conductor Line With Any Number of Subconductors -- Part II." IEEE Trans. Power App. Systems, Vol. PAS-94, January/February 1975, pp. 104-107.

7. R. F. Lehman and D. F. Shankle. "Transmission Line Electrostatic Induction Effects." Proc. American Power Conference, Vol. 37, 1975, pp. 1186-1193.

8. Electric Power Research Institute. Transmission Line Reference Book, 345 kV and Above. Chapters 3 and 8. New York: Fred Weidner & Son, Inc., 1975.

9. D. W. Deno. "Electrostatic Effect Induction Formulae." IEEE Trans. Power App. Systems, Vol. PAS-94, September/October 1975, pp. 1524-1532.

10. T. D. Bracken. "Field Measurements and Calculations of Electrostatic Effects of Overhead Transmission Lines." IEEE Trans. Power App. Systems, Vol. PAS-95, March/April 1976, pp. 494-502.

11. J. C. Procario and S. A. Sebo. Discussion, IEEE Trans. Power App. Systems, Vol. PAS-94, November/December 1975, pp. 2066-2070.

12. Electrostatic and Electromagnetic Effects of Ultrahigh-Voltage Transmission Lines. Palo Alto, California: Electric Power Research Institute, June 1978. EL-802.

Section 5

COUPLING OF POWER LINE TRANSIENTS TO PIPELINES

INTRODUCTION

The purpose of this section is to summarize available methods for predicting the worst case voltages which could be induced on pipelines by power line transients. These transients, which are a consequence of power line faults and line switching, produce both 60 Hz and high frequency effects in the pipeline via three coupling modes -- conductive, inductive and capacitive. Although large power line transients are relatively rare events, the resulting voltages coupled to an adjacent pipeline are much larger than the voltages induced under normal operating conditions. The higher voltages are a potential danger to pipeline workers and can damage the pipeline insulation, the cathodic protection system, and even the pipe itself.

A summary of the situations reviewed here with commentary is as follows.

Capacitive Coupling to Above Ground Pipelines

- Exact formulas for calculating the complete transient waveform are available.

Inductive Coupling to Buried Pipelines

- The 60 Hz component of the induced transient can be computed by the method used for steady state analysis.
- Development of computational methods for determining the higher frequency components will require additional significant effort. At the present, it is not known if the energy levels in these components are of sufficient intensity to cause a hazard.

Conductive Coupling to Buried Pipelines

- Formulas for step and touch potentials and the total pipeline system induced voltage level are presented.

Power Line Transients

There are two characteristics of power line transients that cause large signals to be coupled to a pipeline. These are the abnormal amplitude of the voltage and/or current in a phase conductor and the non-symmetrical excitation of the power line phase and shield wire conductors. For example, the voltage on a phase conductor during line switching is up to twice the normal operating level. When a phase to ground fault occurs, the current in the faulted phase conductor is typically five to fifty thousand amperes. This is at least ten times greater than normal. Large fault currents return to the source through the ground and the shield wires. Under the right circumstances, the shield wire fault current is larger than that normally in any phase conductor.

The duration of a power line fault is determined by the reaction time of the overcurrent protection on the power line; this is typically 0.1 to 0.5 seconds or 6 to 30 cycles of the 60 Hz power. All types of transients have high frequency components whose duration is usually less than 0.01 second. This is less than one cycle of the 60 Hz power and not more than a small multiple of the time required for a signal to propagate down the length of the power line. Thus, the amplitude of a transient voltage coupled to a pipeline must be larger than the amplitude of the steady state voltage for each to cause the same physiological effects.

For a specific electric power line, values for the fault current, fault duration, and the frequency of occurrence should be obtained from the designer or operator of the power line. Similar data for line switching transients should also be sought from the same sources.

Coupling Modes

As mentioned previously, there are three coupling modes to be considered. Inductive or electromagnetic coupling and capacitive or electrostatic coupling are two of the ways by which a power line transient interacts with a pipeline. Each of these has been discussed in detail as a normal steady state coupling problem. In this section, the discussion of these modes is restricted to describing how to apply the steady state methods to the transient case. Recall that inductive coupling is especially important for buried pipelines, although this mode can also affect above ground pipelines. Capacitive coupling is the predominant mode for the above ground pipeline.

The new mode is called conductive or ground current (resistive) coupling. A line fault to ground results in a large, short circuit current which returns to the source through the earth and the shield wires. When it enters the earth, the fault current raises the potential of local ground relative to remote earth. The first part of the conductive coupling discussion considers this potential difference and the part which appears across the pipeline coating. At some distance from the location of the fault, there is no longer a voltage gradient across the pipe's (imperfect) insulation, but there is a large fault current flowing on the pipe. The magnitude of this current is also discussed.

Review of Available Methods for the Analysis of Transient Coupling

Very little analysis has been done for the case of transient coupling to pipelines. However, there is considerable material concerning the effects of power line transients on telecommunications cables and on workers near high voltage lines. For example, the problem of the potential rise near an earth electrode due to a fault current has been studied by several authors, each with different objectives. Endrenyi (1) is concerned about the touch and step potential in the vicinity of a tower and the hazards this presents to workers. His analysis considers both infinite and finite electrical transmission lines, with shield wires, between the fault and the line terminals. Pesonen, et al. (2), are interested in the effects on telecommunications lines. Using formulas for infinite lines with and without shield wires, the potential as a function of distance from the faulted tower is derived. The potentials transferred to a communications system earth electrode and to an uninsulated buried cable are given. A scale model experiment is discussed by Cherney (3) which shows the effect an uncoated pipeline has on the earth potential rise. Cherney also presents some measurements, made during actual fault tests, of the conductively coupled current on pipelines and shows that the pipelines carry most of the ground current.

All previous attempts to estimate the inductive effects of power line faults have considered only 60 Hz coupling to an above ground conductor. In particular, Jaczewski and Pilatowicz (4) and Dubanton and Grand (5) have suggested revisions to the C.C.I.T.T. Directives (6) to include the effects of shield wires on the inductive coupling to telecommunications lines. Cherney (3) has estimated the inductive coupling to an above ground pipeline using a very simple approach, based on Carson's method, that ignores the small shield wire contribution. Fortunately, the methods developed for the analysis of steady state inductive coupling can be

applied directly to the 60 Hz transient case if the power line conductor currents are known. This method can treat both above ground and buried pipelines and includes the effects of shield wires, multiple circuits, phase transpositions and pipeline insulators and grounds. No adequate methods are known for estimating the high frequency inductive coupling to pipelines.

The capacitive coupling problem for a 60 Hz transient is also a simple extension of the steady state case with proper choice of conductor potentials. The effects of a fast rise time transient capacitively coupled to a vehicle are the subject of a paper by Cosma and Yu (7). The method they used is similar to the steady state calculation for an above ground pipeline.

TRANSIENT CAPACITIVE COUPLING

This subsection examines the capacitive or electrostatic coupling to an above ground pipeline which is parallel to an ac power line which experiences a large voltage transient on one of its phase conductors. An equivalent circuit is developed and used to find the voltage across and the current through the impedance (this may be a person) which grounds the pipeline.

The methods used here are similar to those used by Cosma and Yu (7) who were concerned with transient electrostatic effects on large vehicles.

Transient Voltage Source

Line Switching Transients. Line switching operations generally cause a high voltage impulse to appear on the phase conductors of the power line. The peak amplitude of the impulse is less than the insulation level and the over-voltage protection level of the power line. One of these is usually set at about twice the normal operating voltage. The switching impulse can rise to near its peak amplitude in a time as short as one microsecond. Usually the impulse decays rather slowly, dropping to 37 percent of its peak in about one millisecond. An analytical expression which describes such an impulse is

$$V_s(t) = V_o(e^{-t/T_1} - e^{-t/T_2}) \qquad (5\text{-}1)$$

where $T_1 = 10^{-6}$ seconds and $T_2 = 10^{-3}$ seconds are the time constants that describe

the rise and fall of the pulse, respectively, and V_o is the peak amplitude of the pulse.

In addition to the impulse described previously, line switching could result in a non-symmetrical excitation of the power line. If only one phase conductor were energized, then it could electrostatically induce a larger 60 Hz voltage on a pipeline than would be induced by a symmetrically excited line. Since such coupling can be treated using the steady state coupling analysis in Section 4, this problem is not developed here.

Lightning Transients. A lightning stroke can also cause a high voltage impulse to appear on a phase conductor. Because of the shorter duration of this transient, the peak amplitude can be higher. The limitations are the corona level and the impulse insulation level. The analytic expression of Eq. 5-1 can be used to describe lightning impulses with typical values for the time constants being $T_1 = 1.5 \times 10^{-6}$ seconds and $T_2 = 4.5 \times 10^{-5}$ seconds.

Equivalent Circuit Analysis

Values for Circuit Elements. The basic circuit which is used to model the phase wire, the pipeline and the impedance to ground is shown in Figure 5-1a. The resistance R can be the internal impedance of a pipeline worker who is in contact with the pipeline and the ground, the impedance of a grounding rod or a parallel combination of these two. The value of R for a worker can be estimated at approximately 1500 ohms.

The capacitances C_1 and C_2, using Eq. 4-7 of Section 4, are

$$C_1 = C'_{12} = -P_{12}/K \tag{5-2}$$

$$C_2 = C'_{22} = P_{11}/K \tag{5-3}$$

where $K = P_{11}P_{12} - P_{12}^2$. The Maxwell potential coefficients are

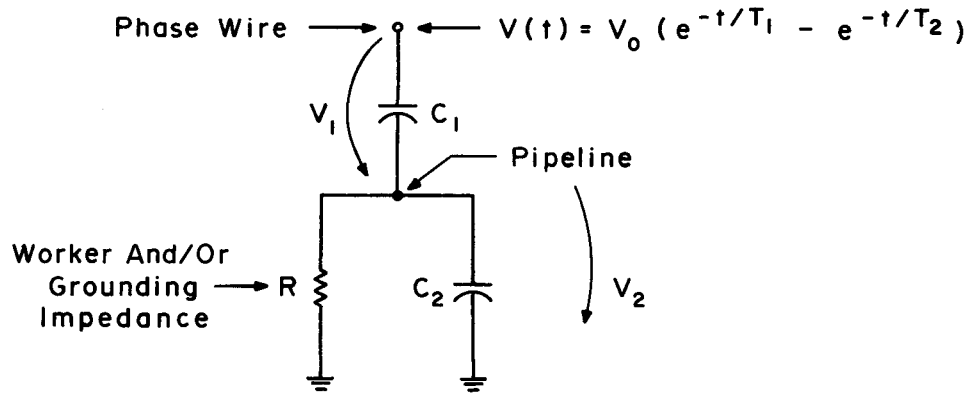

(a) Equivalent Circuit

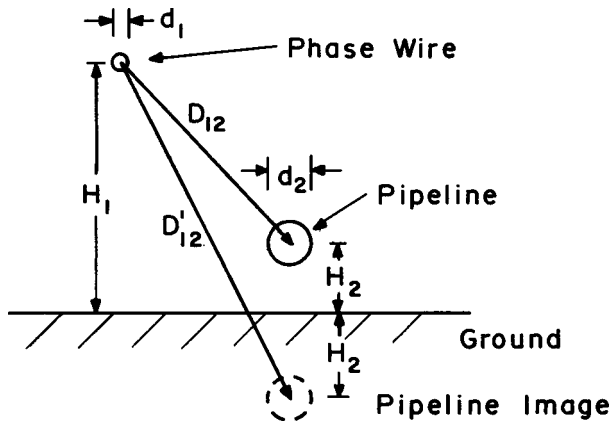

(b) Model

Fig. 5-1 EQUIVALENT CIRCUIT AND MODEL FOR ANALYSIS OF TRANSIENT ELECTROSTATIC COUPLING

$$P_{11} = \frac{1}{2\pi\varepsilon_o} \ln \left(\frac{4H_1}{d_1} \right) ,$$

$$P_{12} = P_{21} = \frac{1}{2\pi\varepsilon_o} \ln \left(\frac{D_{12}}{D'_{12}} \right) , \qquad (5\text{-}4)$$

$$P_{22} = \frac{1}{2\pi\varepsilon_o} \ln \left(\frac{4H_2}{d_2} \right) .$$

The appropriate dimensions are shown in Figure 5-1b. Usually it can be stated that $P_{11}P_{12} >> P_{12}^2$, so that

$$C_2 = C'_{22} \simeq \frac{1}{P_{22}} = C_{22} , \qquad (5\text{-}5)$$

or simply that the pipeline capacitance to ground is not affected by the presence of the other conductor.

The Circuit Equation. The analysis of the equivalent circuit is based on the application of the Kirchoff current law. Recall that the current through a capacitor is C·dV/dt and that through a resistor is V/R. The basic equation states that the current from the phase wire through C_1 onto the pipeline is equal to the current leaving the pipeline through C_2 and R to ground; namely

$$C_1 \frac{dV_1}{dt} = C_2 \frac{dV_2}{dt} + \frac{V_2}{R} . \qquad (5\text{-}6)$$

But the voltage V_1 across C_1 is equal to V, the source voltage in Eq. 5-1 less the voltage V_2 across C_2. Thus, Eq. 5-6 becomes

$$C_1 \frac{dV}{dt} = (C_1 + C_2) \frac{dV_2}{dt} + \frac{V_2}{R} \qquad (5\text{-}7)$$

which can be solved for V_2.

When V is given by Eq. 5-1 the solution to this differential equation is

$$V_2(t) = \frac{C_1 V_o}{C_1 + C_2} \left[\frac{1}{1/T_1 - 1/T} \left(\frac{1}{T_1} e^{-t/T_1} - \frac{1}{T} e^{-t/T} \right) - \frac{1}{1/T_2 - 1/T} \left(\frac{1}{T_2} e^{-t/T_2} - \frac{1}{T} e^{-t/T} \right) \right] \tag{5-8}$$

where $T = R(C_1 + C_2)$. Substitution of Eqs. 5-1 and 5-8 into Eq. 5-7 shows that this is a valid solution. This equation is easily evaluated using a (programmable) calculator.

Calculation of Energy. The criterion for hazardous transient electrical shocks is generally based on an energy threshold. The energy deposited in a worker is

$$W_b = \frac{1}{R_b} \int_o^\infty \left[V_2(t) \right]^2 dt \tag{5-9}$$

where R_b is the body resistance. This integration can be done numerically on a programmable calculator or the long analytic expression in Reference 8 can be evaluated.

TRANSIENT INDUCTIVE COUPLING

This section considers the inductive or electromagnetic coupling of power line transients to pipelines. The method of analysis is quite similar to steady state coupling except for the determination of the currents on the power line conductors and the shield wires. It is shown that the worst case, and thus the primary concern, is the phase-to-ground fault which is characterized by a large 60 Hz current in the faulted phase wire and with a return through the ground which includes the pipeline. After the discussion of the coupling produced by the 60 Hz portion of the transient, some comments are made concerning the coupling due to the high frequency components of power line transients.

General Method for 60 Hz Transient Inductive Coupling

The analytical method presented in this section is suitable for the prediction of inductive coupling to both above ground and buried pipelines. It is based on

formulas for the induced voltages and currents on a transmission line, due to a distributed interference source. This method was developed originally by Vance and is applied to the pipeline case in Section 3 of this report. With this approach, worst case estimates can be made for the induced transient voltages and currents on typical or actual pipelines. The important elements of this method are summarized here, although details which are common to the steady state case are not to be repeated. This method can be applied directly to the case where the dominant source of interference is the large 60 Hz current in a phase wire due to a ground fault.

Transmission Line Analysis with a Distributed Source. As established in the analysis of steady state inductive coupling, transmission line methods are needed to study the coupling onto pipelines from power lines. There are several reasons why these methods are appropriate. The first is that the coupled ac source is a continuous or distributed source. It is not a discrete source that can be handled with standard circuit theory. The second point to be made is that both above ground and buried pipelines do form two conductor electrical transmission lines with the pipe as one conductor and the earth as the return. And finally, there are general and simplified methods for determining the voltages and currents present on a transmission line due to a distributed source (see Section 2).

Pipeline Parameters. To perform a classical transmission line analysis on a pipeline, it is necessary that the transmission line parameters be known. These parameters are the characteristic impedance (Z_0) and the propagation constant (γ). Formulas for Z_0 and γ are given in Section 2 for both above-ground pipelines and buried pipelines.

The Parallel Driving Electric Field. The formulas that predict inductive or electromagnetic coupling require a knowledge of the parallel driving electric field, $E_x(s)$. The calculation for $E_x(s)$ is accomplished by a linear superposition of the electric fields due to all nearby current-carrying conductors. For transient cases, as it was for steady state coupling, the currents in both the phase conductors and the shield wires must be considered. In this section, only the phase-to-ground fault is considered since this transient results in the largest values of $E_x(s)$.

Current on a Faulted Phase Conductor. The phase-to-ground fault is selected as the worst case for transient 60 Hz inductive coupling because it results in the largest and least symmetrical currents in the power line conductors. The current in the faulted phase wire may be on the order of 10,000 amperes. The presence of the pipeline is expected to increase the magnitude of the fault current since it can decrease the impedance from the fault to remote earth. For some proposed power lines the maximum fault current may be close to 100,000 amperes. In any case, the fault current is much larger than the normal current. Although some of the current in the faulted phase wire is coupled to other phase wires which are also carrying normal phase currents, for the purposes of a worst case estimate, the fault currents in the nonfaulted conductors can be neglected. The duration of a phase-to-ground fault is typically 0.1 to 0.5 seconds. The length of this interval is determined by the design of the overcurrent protection devices used on the power line.

The location of the fault with respect to the terminals of the power line and with respect to the natural gas pipeline cannot be specified. This is one more factor that makes it difficult to state what the magnitude and duration of phase-to-ground fault are. There will be a current in the faulted phase wire between the fault and both ends of the transmission line unless one end has no source of current available to it.

The single phase-to-ground fault is generally the most common type of fault. The other types do not result in much greater inductive coupling. Phase-to-phase faults result in significantly lower phase wire currents. Multiple phase-to-ground faults have similar phase wire currents and similar symmetry for a two phase fault and less effective symmetry for a three phase fault. As a consequence of line switching operations there may also be short intervals during which all three phases are not energized. Although this results in a nonsymmetrical excitation of the power line, the phase wire currents and usually the durations, too, are less than the typical values given above for the case of a phase-to-ground fault.

Currents in Other Conductors. A complete solution of the inductive coupling problem requires that the contributions by all current carrying conductors be taken into account. The simplest case and the one that results in the

greatest inductive coupling is when the pipeline section being studied is far from the fault and far from the power line substation. In this case, the currents on the shield wires and the non-faulted phase wires are small compared to that on the faulted phase conductor. At such a location the fault current is returning through the ground, including the pipeline. A simple and reasonable approximation is to determine the parallel electric field at the pipeline for this case using only the current in the faulted phase. Note that a self-consistent matrix method would be needed to determine the current on the pipeline including the effects of currents induced on the shield wires and other phase wires.

Whenever the pipeline section is taken to be near the fault or near a substation, the shield wire currents are significant and should be included in the calculation of the parallel electric field at the pipeline. The use of a self-consistent matrix method would be the best way to determine current on the pipeline.

In the immediate vicinity of the fault, a major portion of the fault current may flow on the shield wires. In the case of a fault fed from both sides, the shield wire current is only slightly less than the phase wire current, and this current significantly reduces the electromagnetic coupling. However, for a fault fed from one side only there is a shield wire current on both sides of the fault and on each side its magnitude is almost half of the fault current. In this case, there is shield wire current and no faulted phase wire current on the unfed side of the fault. This situation produces strong electromagnetic coupling, but not as great as the first case discussed. For any given situation, a division of the fault current between the tower footings and the shield wires will occur and will depend (1) upon where the shield wires are grounded, and (2) upon the relative resistances of the parallel return current paths provided by the shield wires and through the structure grounds.

The situation near a substation that is feeding the fault is similar to the conditions near the fault. Namely, there may be almost as much current on the shield wires as on the faulted phase conductor. If the pipeline is connected to the substation ground, then there will be significant current on the pipeline. In any event, the electromagnetic coupling is not greater for a pipeline section near the substation than it is for a section lying between the fault and substation.

Superposition of Parallel Electric Fields. Generally, the parallel electric field, $E_x(s)$, is found by summing the field due to each nearby current carrying conductor. The field produced by the nth conductor is given by the product of the conductor current, I_n, and the Carson mutual impedance, Z_{nx}, between the nth conductor and the pipeline. For the worst case calculation being considered here, the only significant current is that in the faulted phase. The value of Z_{nx} is about the same for all phase wires, so it makes little difference which phase wire is assumed to carry the fault current.

Application of the General Method

In Section 3, two general applications of this method are discussed. The first case applies when there is a constant parallel electric field, and the second applies to the case where this field, as a function of position along the pipeline, is approximated by a linear decrementation out to approximately 300 meters. The constant electric field approach can be used when there is little variation in the magnitude of the interfering current, the power line conductor - pipeline mutual impedance and the pipeline - earth transmission line parameters. These conditions can be satisfied by a pipeline section which is parallel to the power line. The ends of the pipeline section may be connected to remote earth by the arbitrary impedances Z_1 and Z_2. These impedances may be realized by a grounding system, a connected non-parallel pipeline section, or an insulating joint. As shown in Section 3, the expressions for the constant field case are simplified for the case of short pipeline sections and the case of long/lossy sections. A Thevenin equivalent circuit is developed for both of these simplified cases. Similarly, for cases such as non-parallel or an intersecting pipeline section, simplified solutions may be obtained. Also, as shown in Section 3, the Thevenin equivalent circuits of adjacent pipeline segments may be combined to give the junction voltage.

The analysis of the voltages induced on a particular pipeline segment by a phase-to-ground fault should use a value of the parallel electric field caused by a fault which is far from the pipeline segment. The other parameters required are similar to those needed for the steady state case. A realistic worst case value for the pipeline voltage will be obtained using this method for all pipeline sections except those near substations. While this procedure may overestimate the inductive coupling near substations, the additional complications of including shield wire currents discourages this more accurate approach.

Comments on Inductive Coupling Due to High Frequency Transients

A detailed examination of fault current or line switching transient waveforms reveals that a wide range of higher frequencies are present in addition to the 60 Hz frequency of the ac generator. The power line transient caused by electromagnetic coupling from a nearby lightning stroke also has its energy distributed over a wide range of high frequencies. There are two ways to solve a coupling problem when the excitation is due to a multi-frequency transient. In the first approach, the coupling calculations are made in the frequency domain at many frequencies. These results are then Fourier transformed into the time domain. The other approach is to formulate the coupling problem in the time domain using as an excitation some simple transient waveform such as a step function or a decaying exponential.

In principle, the method used for steady state 60 Hz coupling can be used as the basis for the frequency domain analysis of inductive coupling caused by a transient. However, almost every parameter used in the calculations will have a new value at each of the new frequencies. Since the results must be Fourier transformed, too, this type of calculation must be done on a large digital computer.

Time domain solutions have been developed for the coupling of an electromagnetic plane wave transient to both above ground and buried conductors. These solutions are used to predict the currents induced on cables by the electromagnetic pulse (EMP) that is produced by detonating a nuclear weapon. If these methods are applied to the problem of transient inductive coupling to pipelines, the power line transients must be converted into equivalent plane wave transient waveforms. A method for performing this conversion would have to be developed. This approach has promise for being a simple way to make transient calculations. One qualification is that only simple excitations, such as step functions and decaying exponentials, can be used to describe the incident transient waveform.

One of these methods should be used to determine whether high frequency inductive coupling is as hazardous as the coupling due to the 60 Hz component of the phase-to-ground fault. An analysis of this kind is beyond the scope of this book at this point in time.

GROUND CURRENT COUPLING

During a phase-to-ground fault, large currents may enter the ground near the fault location (c.f. Figure 5-2), and flow through the ground to the power line substations. Eventually, if not immediately, a portion of this current flows along a pipeline which is adjacent to the power line. This section shows that these ground currents produce significant voltages on the towers and in the surrounding earth. Some or all of these potentials are transferred to nearby conductors which are in contact with the ground, including pipelines. The effects discussed here are step and touch potentials, which are a possible hazard to workers, and the voltage across the pipe and its coating, which is important because high voltages can puncture either the coating or the pipe or both. Although the greatest hazard is expected to occur near a faulted tower, lesser hazards can occur near the substation and at any location where the pipeline enters or departs the vicincity of the power line. Since any tower can be the faulted one, these other locations for hazards can never be the worst case.

Structure (Tower) Potentials

For ground fault conditions, large currents flow through the structures of the power line. This current then goes into the earth through the tower ground impedances. As shown in Figure 5-2, portions of the fault current, I_f, also flow through the shield wires to adjacent towers before entering the ground. However, the largest current usually flows through the tower where the fault occurs. This current through the tower grounding impedance, called Z_t in Figure 5-3, causes the tower to assume a voltage, V_t, with respect to remote earth. This voltage is determined by the magnitude of the current, I_f, and the effective impedance of the network of shield wire impedances and grounding impedances. It is assumed that the magnitude of the current resulting from a phase-to-ground fault is known. This discussion regarding the flow of current along shield wires and to towers implicitly assumes grounding of the shield wires at each tower. Where this is not the case, the apportionment of current between shield wires and adjacent tower footings will be different, and must be calculated for each situation separately.

The effective impedance offered to a fault current can be computed using simple circuit theory. Assume that all shield wire resistances per span, and tower grounding resistances are equal, as shown in Figure 5-3, and let the number of towers be very large. The input impedance to an infinite ladder network of Z_s's and Z_t's, such as that to the right or left of the faulted tower, is

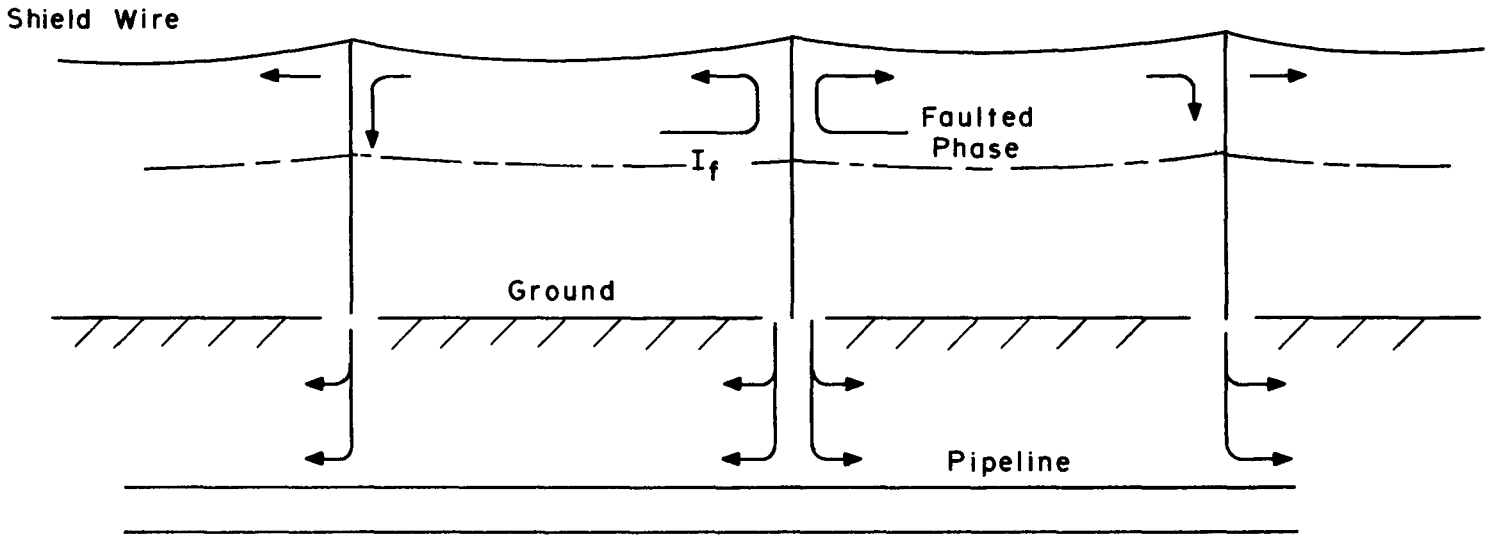

I_f ~ 30 KA (60 Hz)

Duration ~ 0.3 Sec.

Fig. 5-2 PRINCIPLE OF CONDUCTIVE COUPLING

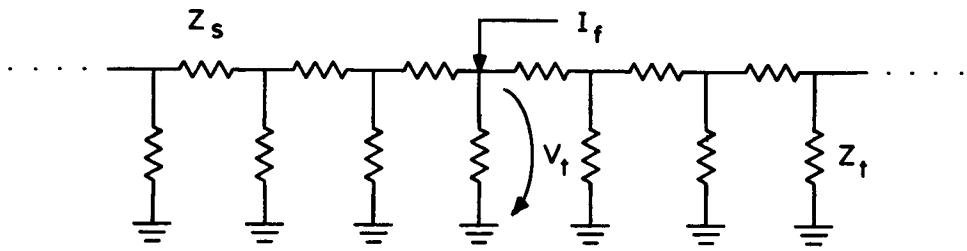

Which Simplifies To

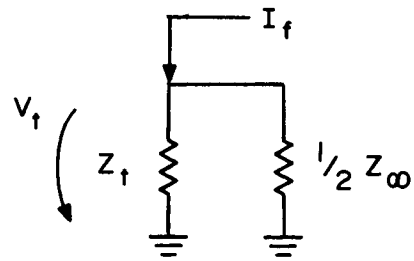

Where $Z_\infty = \frac{1}{2} Z_s + \sqrt{Z_s Z_t + \frac{1}{4} Z_s^2}$

Fig. 5-3 EQUIVALENT CIRCUIT FOR CONDUCTIVE CASE

$$Z_\infty = \tfrac{1}{2} Z_s + \sqrt{Z_s Z_t + \tfrac{1}{4} Z_s^2} \qquad (5\text{-}10)$$

In general, Z_s is much smaller than Z_t so that Z_∞ is much smaller than Z_t. That is, the shield wires have significantly reduced the tower potentials. Results for finite ladder networks and for lines with continuous counterpoises are given in Reference 1.

Now the equivalent circuit can be simplified (see Figure 5-3) with the effective impedance being one Z_t in parallel with two Z_∞'s. Thus, the tower potential is given by

$$V_t = I_f (1/Z_t + 2/Z_\infty)^{-1} \qquad (5\text{-}11)$$

For any tower other than the faulted one, the structure potential is smaller than the value given by Eq. 5-11. Often a finite line is terminated in a substation grounding impedance which is less than Z_∞. If so, then the value given by Eq. 5-11 is somewhat larger than would be obtained using a more detailed method.

The full tower potential would, in general, not be present as a threat to either workers or to the pipeline. However, if spark gaps or polarization cells were used to connect the pipeline to the power line ground, then the full tower potential could appear across the spark gap or across the polarization cell. Such connections can be expected to reduce the tower grounding impedance. Consequently, this analysis should take any such connections into account if they exist. This is accomplished by using in Eqs. 5-10 and 5-11 a tower grounding impedance which is one half of the characteristic impedance of the buried pipeline.

Step and Touch Potentials

A fraction of the tower potential can appear between the feet (a step potential) or between a hand and a foot (a touch potential) of a worker. Both of these potentials can be easily evaluated if some simplifying assumptions are made.

First, the tower ground is approximated by a hemispherical electrode with an effective radius, r_e. Then the tower grounding impedance is given by

$$Z_t = (2\pi r_e \sigma)^{-1} \qquad (5\text{-}12)$$

where σ is the soil conductivity. For a hemispherical electrode the soil potential with respect to remote earth is V_t (the potential of a faulted tower) for a radius less than r_e, and for r larger than r_e

$$V_r = V_t r_e / r \quad . \tag{5-13}$$

This functional form, shown in Figure 5-4, is a good approximation to the soil potential for a tower without a linear counterpoise. Whether this functional form holds near a tower depends upon how the shape of the actual grounding electrode compares to the assumed hemisphere. Frequently, the soil potential near the tower is determined experimentally using a scale model of the actual grounding electrode which is submerged in a water bath with the soil conductivity simulated by adding an electrolyte. This approximation also breaks down very far from a tower, where the potential due to other towers is significant.

The step potential at a distance, r, from a tower is

$$V_{step} = \frac{r_e}{r(r-1)} V_t \tag{5-14}$$

when both feet are at a local soil potential. This result is obtained by subtracting the soil potential at r from the soil potential at a distance one meter closer to the tower. If one foot is on a ground mat or other conducting surface, the step potential is larger. Let the conducting surface have an effective radius of r_c. It assumes the soil potential at its center. Then the step potential between a location r meters away from the tower and the ground mat at a distance $r + r_c + 1$ m is

$$V_{step} = \frac{r_e (r_c + 1)}{r(r + r_c + 1)} V_t \quad . \tag{5-15}$$

Equation 5-15 assumes that the ground mat does not disturb the potentials nearby and it does not apply to a ground mat which is connected to a pipeline or some other long conductor which is grounded at several locations. It is not easy to predict the potential of the pipeline--it may be anywhere between zero and the highest soil potential in the absence of the grounding electrodes. As a worst case then, the step potential should be taken as the highest soil potential

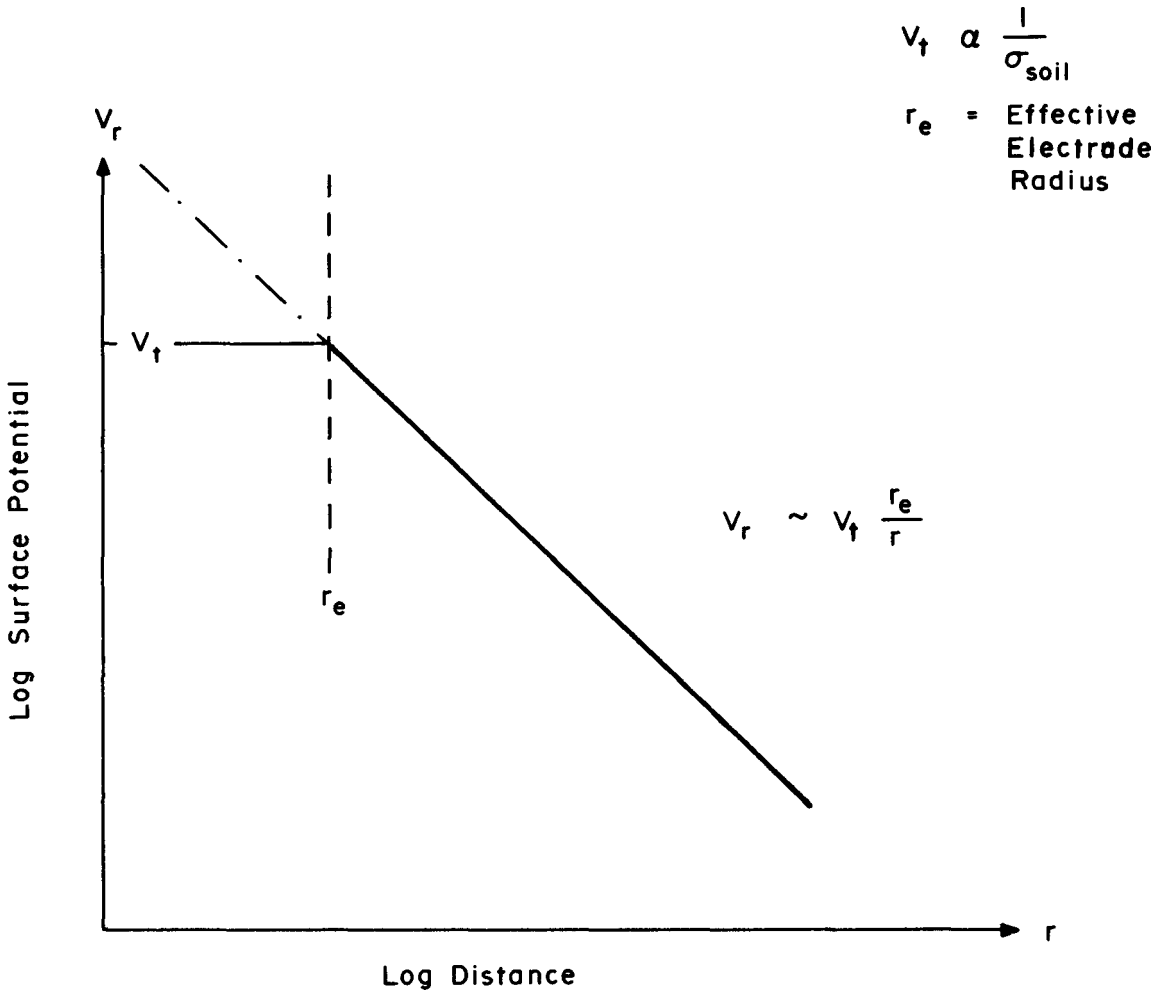

Fig. 5-4 SURFACE POTENTIALS NEAR FAULTED TOWER

computed using Eq. 5-13. This worst case is realized if the worker is a distance r from the tower and the pipe is grounded much farther away, or if the pipe is grounded at r_{min} and the worker is much farther away.

There is no touch potential when the worker is standing on a ground mat which is connected to the object. Similarly, a well grounded object, having a grounding electrode with a large horizontal area, has little or no touch potential. However, there is a significant touch potential when there is no ground mat or large area grounding electrode. Assuming that the grounding of an object does not disturb the nearby soil potentials, touch potentials can be calculated using Eqs. 5-13 and 5-15. When the object being touched is small and is grounded r meters from the tower so that it is at local soil potential, then Eq. 5-14 is the proper choice. If the object being touched is large and is grounded at a distance r_c + 1 m from the worker's location, then Eq. 5-15 is appropriate. And finally, an upper limit for touch potential to a pipeline or other long conductor which is grounded at one or more locations is found by using the minimum pipeline - tower distance in Eq. 5-13.

Potentials Across Pipeline Coatings

Because it is a good electrical conductor, a buried pipe with an insulating coating cannot have as large a potential gradient as the soil near a faulted tower. This means that there must be places where there is a large voltage across the pipeline coating. Consider first the case of a long pipeline passing near a faulted tower and which has no grounding electrodes near the towers. Then, it is reasonable to assume that the pipeline potential is everywhere near that of remote earth so that the voltage across the coating is approximately the same as the surface potential given by Eq. 5-13. The maximum voltage across the coating is, therefore

$$V_{c,max} = V(r_{min}) = V_t \frac{r_e}{r_{min}} \qquad (5\text{-}16)$$

where r_{min} is the minimum distance between the pipeline and the faulted tower. It is this maximum potential which should be used to determine whether the pipeline coating would be punctured by the ground current transient.

Next, assume that a long pipeline has a grounding electrode at a distance r_g from the faulted tower. The surface potential at the location of the grounding electrode

determines the open circuit voltage that can be coupled to the pipeline via this electrode. The actual potential at the connection between the pipe and the grounding electrode is smaller, namely

$$V_g(r_g) = V_t \left(\frac{r_e}{r_g}\right) \left(\frac{\frac{1}{2}Z_o}{Z_g + \frac{1}{2}Z_o}\right) \quad . \tag{5-17}$$

The last term is the ratio of the load impedance (one half of the characteristic impedance of a long buried pipeline as given in Eq. 5-13) to the total impedance, which is the sum of the load impedance and the source impedance. The source impedance is the impedance to remote earth of the grounding electrode, Z_g. The voltage across the pipeline coating is now

$$V_c = V(r) - V_g(r_g) \quad . \tag{5-18}$$

The maximum voltage is somewhat less. The maximum reduction is 50 percent which is achieved only when $V_g(r_g)$ is equal to $\frac{1}{2}V(r_{min})$.

Another interesting case involves a pipeline which has the same potential as the tower. This is possible if a solid connection is made between the two or if a spark gap, polarization cell or ionization of the soil causes a low impedance path to be formed between them. Since the pipeline becomes a part of the tower ground, the tower potential is reduced. However, the pipeline potential is reduced only when there already is strong ground current coupling. For this case, the maximum voltage across the pipeline coating is close to the tower potential with respect to remote earth.

The calculation of the pipeline potential gets quite complicated if there are many grounding electrodes near towers or if the pipe has a shield wire buried with it. Some calculations of such potentials have been done by Personen, et al (2). In any event, it appears that $V(r_{min})$ is a useful approximation to the maximum voltage across the pipeline coating.

Current on a Long Pipeline

Between the fault location and the power line substation, but relatively far from both, there is a large current flowing in the earth. This current density in the soil, i_s, causes a surface electric field, e_s, given by

$$e_s = i_s/\sigma_s \tag{5-19}$$

where σ_s is the soil conductivity. Similarly, for a buried pipeline there is an electric field along the pipe given by

$$e_p = i_p/\sigma_p \tag{5-20}$$

where i_p is the current density in the pipe and σ_p is the conductivity of the pipe. Equilibrium is achieved when e_s is equal to e_p and, therefore

$$i_p = i_s \sigma_p/\sigma_s \tag{5-21}$$

A typical value for σ_p at 60 Hz is 3×10^5 mho/m which, although it is less than the dc conductivity of the pipe, is many orders of magnitude larger than typical soil conductivities. (A relatively large value of σ_s is 10^{-2} mho/m.) Because of the large conductivity ratio, a large fraction of the ground current is concentrated on the pipe. Using measurements made during staged fault tests, it has been shown experimentally that essentially all of the ground current is on the pipeline (3).

When e_s and e_p are in equilibrium there are no hazards to workers or to the pipeline coating. The hazards occur when equilibrium does not exist, such as near the fault, near the substation or near locations where the pipeline enters or leaves the vicinity of the power line. These other locations are not expected to be more hazardous than the situations already discussed near a faulted tower.

SUMMARY AND CONCLUSIONS

The three coupling modes associated with induced transients on pipelines have been considered. Computational methods for calculating transient voltage or current levels for each case have been reviewed.

In the case of capacitive coupling to an above ground pipeline, exact methods are available for calculating the voltage transient induced on the pipeline for the cases of line switching and lightning induced transients.

The most severe inductive coupling to buried pipeline systems is caused by power line phase conductor to ground faults. The induced transient on the pipeline can easily be handled by techniques developed previously for the steady state coupling calculations when considering the 60 Hz component of the transient. The higher frequency components of the induced transient present a much more formidable problem and, in general, a simple method for determing their coupling factors is not presently available. However, in concept, a solution can be found. The necessity for having available such techniques has not been determined as yet. The question to be answered is if sufficient higher frequency energy and/or voltage components are coupled into the pipeline system to present a hazard to personnel safety or component reliability.

During a phase-to-ground fault large currents may enter the ground near the fault location. These ground currents produce significant potentials on the power line structures and in the surrounding earth. Formulas for the touch and step potentials and the (worst case) voltage developed across the pipeline and/or its coating are developed.

REFERENCES

1. J. Endrenyi. "Analysis of Transmission Tower Potentials During Ground Faults." IEEE Trans. on Power Apparatus and Systems, Vol. PAS-86, No. 10 pp. 1274-1283. October 1967.

2. A. Pesonen and J. Kattelus. "Earth Potential Rise and Telecommunication Lines." Int'l Conf. on Large Electric Systems at High Tension (CIGRE) Proceedings, 23rd Session, Aug./Sept. 1970.

3. E. A. Cherney. "Pipeline Voltage Hazards on High Voltage AC Transmission Lines." Materials Performance, March 1975, pp. 29-33.

4. M. Jaczewski and A. Pilatowics. "Interference Between Power and Telecommunication Lines Field and Model Tests." Int'l Conf. on Large Electric Systems at High Tension (CIGRE) Proceedings, 23rd Session, Aug./Sept. 1970.

5. C. Dubanton and G. Grand. "Influence on the Location of the Fault on the Screening Effect of Earth Wires." Int'l Conf. on Large High Voltage Electric Systems (CIGRE) Proceedings, 25th Session, Aug. 21-29, 1974, Vol. II.

6. Directives Concerning the Protection of Telecommunication Lines Against Harmful Effects from Electricity Lines. International Telegraph and Telephone Consultative Committee (CCITT), International Telecommunications Union, 1962 (supplemented 1965).

7. R.P. Cosma and L.Y.M. Yu. "Transient Electrostatic Induction by EHV Transmission Lines." IEEE Trans. on Power Apparatus and Systems, Vol. PAS-88, No. 12, pp. 1783-1787, December 1969.

Section 6

LIGHTNING EXPOSURE PARAMETERS AND PROBABILITIES

INTRODUCTION

There are two main classes of lightning effects which are involved when underground pipelines are located on common right-of-way (ROW) with overhead power lines:

1. Transient currents and voltages caused by direct strokes to the shield wires or towers of the power line or to earth near the pipeline. The time domain of these effects is measured in microseconds (μs).

2. Transient ground fault currents arising from lightning flashover of the power line insulator strings. Fault durations are commonly measured in milliseconds (ms).

In each of these classes, the mechanisms affecting the pipeline may be due to either electromagnetic or conductive coupling, the latter representing a formidable hazard to the protective coating of the pipeline. Coupling to the pipeline is treated elsewhere in this book.

The primary purpose of this section is to provide data on the rate at which the pipeline experiences these two lightning effects. Direct strokes to the shield wires or structures are given by the factor, N_s, expressed as the number of strokes per 100 km-years. Calculation of the number of ground faults is a much more difficult problem and has not been attempted here. However, if the power line quality (performance order) is known, data is given from which it is possible to estimate the specific tripout rate for the line. For typical power line parameters, results show that the lightning stroke frequency is increased in the vicinity of the pipeline. However, because of certain mitigative effects, it has been found that the presence of a power line actually reduces the frequency of direct lightning strokes to buried pipelines.

Frequency of Occurrence

The frequency of occurrence of both classes of events is an important consideration in the design of both electric power lines (1,2) and pipelines. In some cases mean values are commonly used, while in others frequency distribution curves or cumulative probability curves are required.

Direct Strokes

The correct technical term here should be "flashes" but the more familiar term "direct strokes" will be used until discrimination is required. The basic data required are:

- TD the number of thunderdays per year
- N_g the ground stroke density in strokes (km^{-2} yr^{-1}) per sq km per year
- N_s the linear density of strokes to the towers and shield wires in strokes 10^{-2} (km^{-1} yr^{-1}) per km per year.

Figure 6-1 illustrates these concepts and shows simplified formulas in current use which relate the basic data.

$$N_g \simeq 0.04\ (TD)^{1.35} \tag{6-1}$$

for the continental United States. The value of N_s depends on the value of N_g and the collection area for 100 kilometers of line determined by the relation

$$\text{Collection area per 100 km} = \overline{W}\ 10^{-1}\ km^{-2} \tag{6-2}$$

where $\overline{W}$ is the effective collection "width" in meters and

$$\overline{W} = D + 4\overline{H}^{1.09} \tag{6-3}$$

for a single circuit transmission line. As in Figure 6-1, $\overline{H}$ is the height of the shield wires above ground and D is the separation between the two shield wires. Thus, the linear stroke density is given by

$$N_s = N_g \overline{W}\ 10^{-1} \text{ strokes/100 km-yr.} \tag{6-4}$$

Frequency Distribution of Lightning Current Amplitudes

Since different designs of electric power lines have differing critical or threshold current amplitudes at and above which insulator flashover can occur, no single threshold value can be assigned. Thus, a cumulative probability curve is required so that the flashover rate can be determined for the design threshold

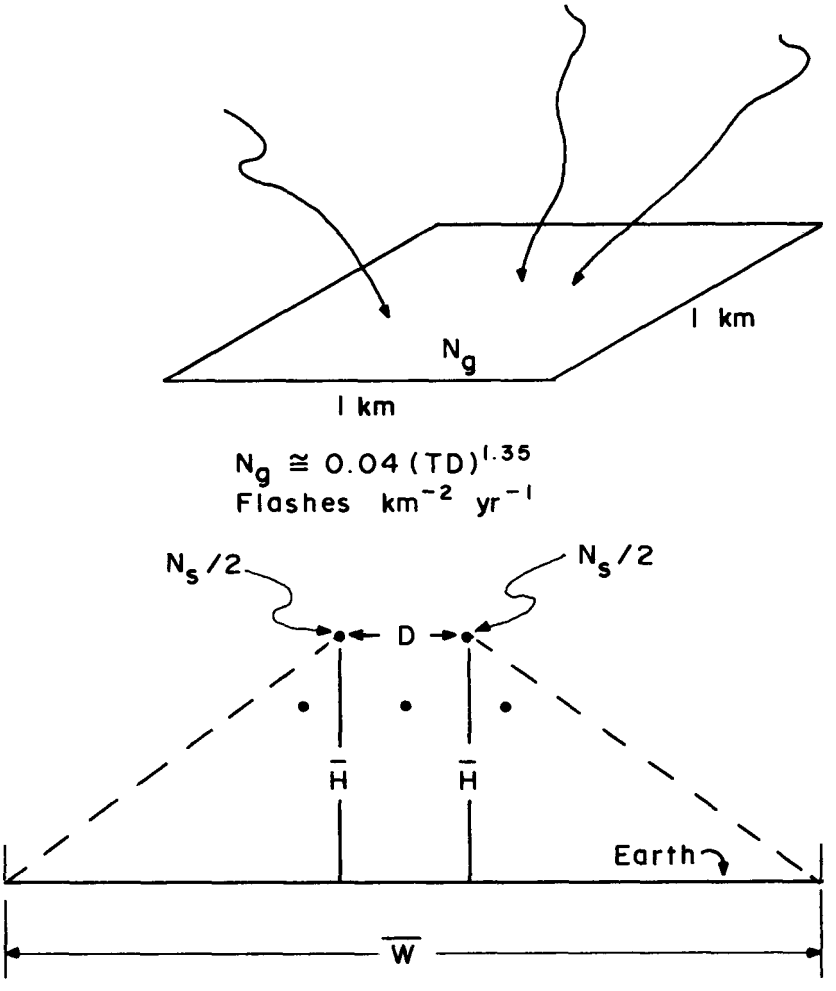

Fig 6-1 LIGHTNING EXPOSURE PARAMETERS

current of a specific power line. Figure 6-2 shows such a curve in generalized form. Use of this chart requires a prior assignment of the median current amplitude I(50%) and a value of σ_{ln}, given by

$$\sigma_{ln} = \ln [I(16\%)/I(50\%)] \qquad (6\text{-}5)$$

for the particular distribution used. A currently-used common value of σ_{ln} is 0.9. The value of the median current amplitude for bare earth is 13.0 kA and that for the strikes to the shield wires of a power line depends on their height. An empirical relation for this is

$$I(50\%) = 13.0 + 0.07\ \overline{H}^{1.25}\ \text{kA} \qquad (6\text{-}6)$$

Tables 6-1 and 6-2 give typical collection widths $\overline{W}$ and linear flash density, N_s, for high-voltage (HV), extra-high-voltage (EHV) and ultra-high-voltage (UHV) lines for various mean heights, $\overline{H}$, and thunderday levels, TD. The collection widths are useful for comparison with widths of ROW, and the N_s values are useful to determine the number of strokes attracted to the ROW, but at a known location.

Table 6-1

MEAN TRANSVERSE EXPOSURE
$\overline{W}$ FOR SHIELD WIRE HEIGHT $\overline{H}$

H	HV Lines D = 5m	EHV Lines D = 15m	UHV Lines D = 25m
10m	53m	63m	73m
20	107	117	127
30	163	173	183
40	220	230	240
50	279	289	299
60	338	348	358
70	398	408	418
80	459	469	479
90	521	531	541
100	583	593	603

For other than the average conditions tabulated, use the relation $\overline{W} = D + 4\ \overline{H}^{1.09}$.

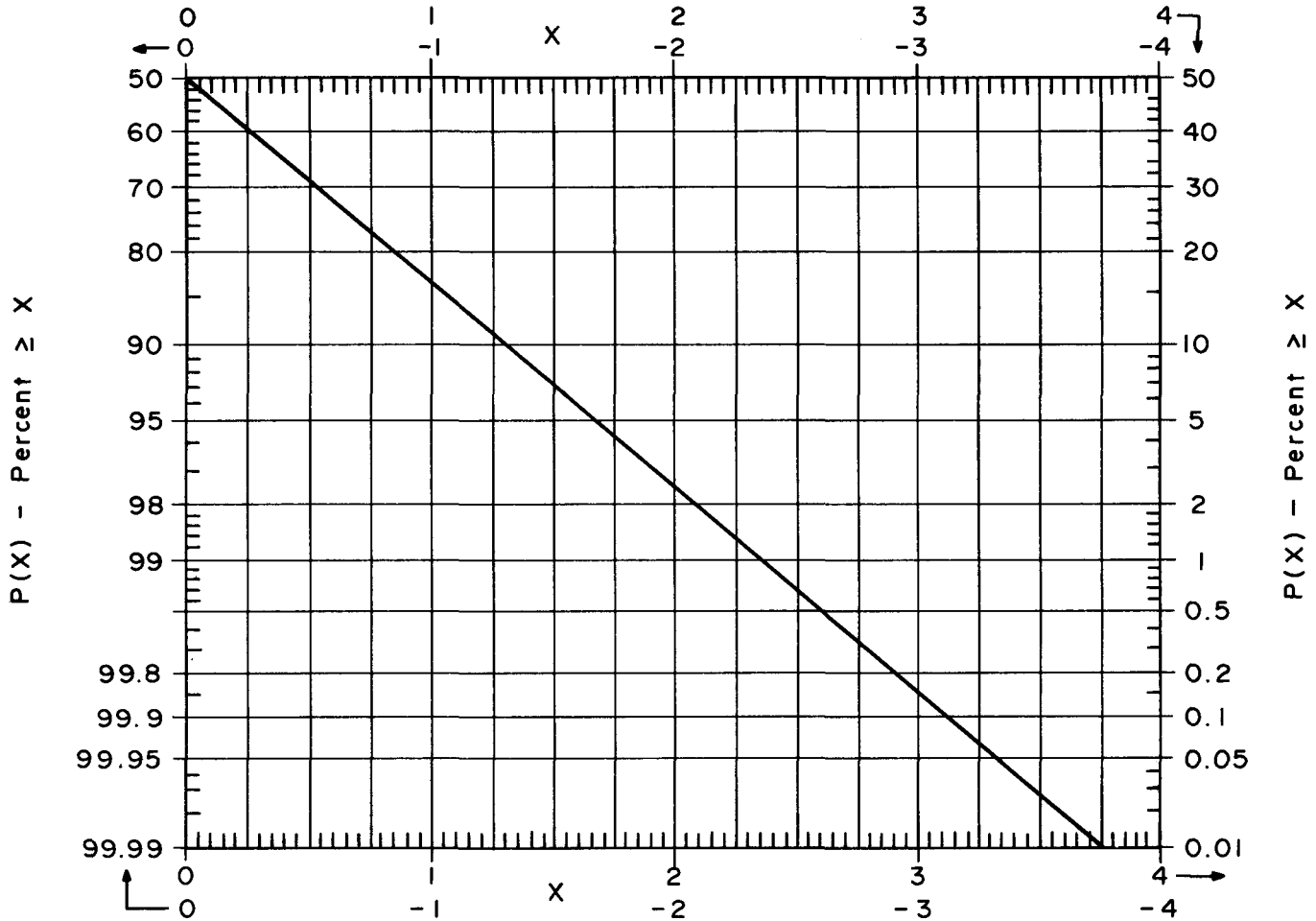

$$X = \frac{\ln(i/I_{50\%})}{\ln(I_{16\%}/I_{50\%})}$$

Fig. 6-2 NORMALIZED CURRENT AMPLITUDE DISTRIBUTION, P(X)

Table 6-2

LINEAR FLASH DENSITY TO SHIELD WIRES, N_s - FLASHES 10^{-2} km^{-1} yr^{-1}
AS A FUNCTION OF MEAN SHIELD WIRE HEIGHT $\overline{H}$ AND ANNUAL THUNDERDAYS, TD

		Mean Height of Shield Wires -$\overline{H}$ in Meters									
TD	Line	10	20	30	40	50	60	70	80	90	100
10	HV	4.8	9.6	14.6	19.8	25.0	30.4	35.8	41.2	46.4	52.4
	EHV	5.7	10.5	15.5	20.7	26.0	31.3	36.7	42.2	47.8	53.4
	UHV	6.6	11.4	16.4	21.6	26.9	32.2	37.6	43.0	48.6	54.2
20	HV	12.2	24.5	37.4	50.6	64.0	77.7	91.6	105.6	119.8	134.1
	EHV	14.5	26.8	39.7	52.9	66.3	80.0	93.9	107.9	122.1	136.4
	UHV	16.8	29.1	47.7	55.2	68.6	82.3	96.2	110.2	124.4	138.7
30	HV	20.7	41.6	63.4	85.8	108.6	131.8	155.3	179.1	203.2	227.4
	EHV	24.6	45.5	67.3	89.7	112.5	135.7	158.2	183.0	207.0	231.3
	UHV	28.5	49.4	71.2	93.6	116.4	139.6	163.1	186.9	211.0	235.2
40	HV	30.8	61.9	94.2	127.5	161.5	196.0	231.0	266.4	302.2	338.2
	EHV	36.6	67.7	100.0	133.3	167.3	201.8	236.8	272.2	308.0	344.0
	UHV	42.4	73.5	105.8	139.1	173.1	207.6	242.6	278.0	131.8	349.8
50	HV	41.8	83.9	127.7	172.8	218.9	265.7	313.1	361.0	409.5	458.4
	EHV	49.7	91.8	135.6	180.8	226.8	273.6	321.0	368.9	417.4	466.3
	UHV	57.6	99.7	143.5	188.5	234.7	281.5	328.9	376.8	425.3	474.2

NOTE: The average shield wire spacing, $\overline{D}$, is taken as $\overline{D}$(HV) = 5m, $\overline{D}$(EHV) = 15m and $\overline{D}$(UHV) = 25m.

Table 6-2 (Cont.)

TD	Line	Mean Height of Shield Wires -$\overline{H}$ in Meters									
		10	20	30	40	50	60	70	80	90	100
60	HV	53.1	106.7	162.5	219.9	278.5	338.0	398.3	459.3	521.0	583.2
	EHV	63.1	116.7	172.5	229.9	288.5	238.0	408.3	469.3	531.0	593.2
	UHV	73.1	126.7	182.5	239.9	298.5	358.0	418.3	479.3	541.0	603.2
70	HV	65.8	132.3	201.5	272.7	345.3	419.1	493.9	569.5	646.0	723.2
	EHV	78.2	144.7	213.9	285.1	357.7	431.5	506.3	581.9	658.4	735.6
	UHV	90.6	157.1	226.3	297.5	370.1	443.9	518.7	594.3	670.8	748.0
80	HV	78.6	159.9	240.5	325.4	412.2	500.2	589.5	679.8	771.1	863.1
	EHV	94.1	172.7	255.3	340.2	427.0	515.0	604.3	694.6	785.9	877.9
	UHV	108.2	187.5	270.1	355.0	441.8	529.8	619.1	708.4	800.7	892.7
90	HV	92.4	185.7	282.7	382.6	484.6	588.1	693.0	799.2	906.5	1014.8
	EHV	109.8	203.1	300.1	400.0	502.0	605.5	710.4	816.6	923.9	1032.2
	UHV	127.2	220.5	317.5	417.4	519.4	622.9	727.8	834.0	941.3	1049.6
100	HV	106.2	213.4	325.0	439.8	557.0	676.0	796.6	918.5	1042.0	1166.0
	EHV	126.2	233.4	325.0	459.8	577.0	696.0	816.6	938.5	1062.0	1186.0
	UHV	146.2	253.4	365.0	479.8	597.0	716.0	836.6	958.5	1082.0	1206.0

NOTE: The average shield wire spacing, $\overline{D}$, is taken as $\overline{D}$(HV) = 5m, $\overline{D}$(EHV) = 15m and $\overline{D}$(UHV) = 25m.

Lightning Ground Faults

In the case of ground faults caused by lightning, it is clear that the power line introduces a new type of exposure. The analysis is complicated because of the complexity introduced by the shield wires and the multiple tower grounding which distribute the total fault current. These matters are considered elsewhere in this book. Further, the estimation of the frequency of occurrence of lightning faults is an extremely complex process for a particular line and is beyond the scope of this investigation. Fortunately, however, a good overview of actual line performance of EHV lines can be obtained from Table 6-3, taken from Reference 1. For this table, the symbols S.T.R. (40) mean the "Specific Tripout Rate at 40 thunderdays per year." The "Performance Order" M is defined by the equation:

$$\text{S.T.R. (40)} = 2^{M} \qquad (6\text{-}7)$$

Table 6-3

VALUES OF THE BINARY ORDER PERFORMANCE INDEX M WITH QUALITATIVE COMMENTS

Performance Order M	S.T.R. (40) $10^{-2}km^{-1}yr^{-1}$	Qualitative Comments
-4	0.00-0.0625	"Lightning proof"
-3	0.125	Superior grounding and shielding
-2*	0.250*	Excellent grounding* and shielding
-1	0.500	Good grounding and shielding
0	1.00	Good or fair grounding Fair or good shielding
1	2.00	Good grounding, fair shielding
2	4.00	Fair grounding, poor shielding
3	8.00	Poor grounding and/or poor shielding
4-5	16-32	Poor grounding, poor shielding low insulation level or unshielded lines

*The median value of S.T.R. (40) for effectively-shielded lines of 15 countries participating in the CIGRE Survey (1) was 0.26.

Approaches to Mitigation

The basic requirement for protection of the pipeline or its coating from puncture is the reduction of the current density in the soil to acceptable levels. Assuming that there is some threshold level, two fundamental approaches are possible:

1. Increasing depth of the pipeline
2. Diversion of external current away from the pipeline.

The first approach may be neither feasible nor economic. The second can sometimes be accomplished by shielding. Buried shield wire systems have been employed for large pre-stressed concrete water lines in soil of high resistivity. In such cases, however, external current has sometimes been led periodically into the longitudinal rebars in the region of lightning current ingress and out of the rebars at remote regions. The following discussion indicates that the presence of an ac power line can provide a form of shielding, provided that line stroke collection width, $\overline{W}$, available ROW and pipeline location are properly coordinated.

As the height of the shield wires increases, the collection width $\overline{W}$ increases and is much larger than the ROW. The ROW, however, may be sufficiently small so that the pipeline is well protected from direct high-current strokes to earth and simultaneously sufficiently large to permit locating the pipeline well away from the tower grounding system so as to minimize the probability of sparking in the soil from the tower ground to the pipeline. As an example of the possible application of the foregoing relations, consider the following conditions (with TD = 40 yr^{-1})

Line	ROW	N_g	N_s(no line)	$\overline{H}$	$\overline{W}$	N_s(to line)
HV EHV	50m	5.8	29.0	30m	168m	97.4
UHV	100m	5.8	58.0	50m	299m	173.4

In the case of no power line, but the same ROW, the whole range of lightning currents can strike the earth near the pipeline with virtually certain puncture of the protective coating. With the power line present, and proper location of the pipeline, only the weakest strokes can penetrate the shielding afforded by the shield wires and towers of the electric power line.

For this reasoning to be valid, something must be known of the soil ionization characteristics. Table 6-4 has been prepared to give a preliminary illustration of

the soil ionization radius and resulting tower footing resistance at crest current. For this table, the soil breakdown gradient has been taken as 1 megavolt per meter as a representative value. This results in the following relations

Resistivity Ohm Meters	Ionization Radius $\bar{r}$	Resistance at Crest Current I kA
100	$0.126\ I^{0.5}$	$R = 126\ I^{-0.5}$
1,000	$0.400\ I^{0.5}$	$R = 398\ I^{-0.5}$
10,000	$1.260\ I^{0.5}$	$R = 1264\ I^{-0.5}$

Since the ionization radius is a mean value that could be exceeded by localized streamers and because of the field intensification caused by the proximity of the pipeline, it is prudent to provide a large margin in the separation between the outermost grounding element and the pipeline. A separation of perhaps 20 meters would probably prove adequate for all but the highest earth resistivities and lightning currents.

Table 6-4

THEORETICAL IONIZATION RADIUS ($\bar{r}$) AND GROUNDING IMPEDANCE (R) AT CREST CURRENT FOR A HEMISPHERICAL GROUND ELECTRODE IN HOMOGENEOUS SOIL HAVING A SOIL BREAKDOWN GRADIENT OF ONE MEGAVOLT PER METER

Crest Current kA	P(i) (1)	100 ohm meters		1000 ohm meters		10000 ohm meters	
		$\bar{r}$ m	R ohms	$\bar{r}$ m	R ohms	$\bar{r}$ m	R ohms
0(2)	100	0.64	25.0	2.01	79.1	6.37	150.0
50	16	0.89	17.9	2.83	56.3	8.91	179.0
100	3.7	1.26	12.6	4.00	39.8	12.60	127.0
150	1.4	1.54	10.3	4.90	32.5	15.43	103.0
200	0.6	1.78	8.9	5.66	28.1	17.82	89.0
250	0.3	1.99	8.0	6.32	25.2	19.92	80.0
300	0.15	2.18	7.3	6.93	23.0	21.82	73.0

NOTE (1): Percent of strokes having current equal to or greater than value given. For mean shield wire height of 40 meters, or I(50%) equal to 20 kA.

NOTE (2): Metallic electrode without ionization.

As an example of the use of these tables, consider the 250 kA current level. For a resistivity of 1000 ohm meters, one would estimate that a soil striking radius of 6.32 meters would be exceeded approximately 0.3% of the time. From Table 6-2 one can select, say, an EHV line of 40 m height in an area of 40 TD to obtain 133.3 strokes to the line per 100 kilometer years. Thus the radius given would be exceeded 0.003 x 133.3 or 0.4 times per 100 km-years; in other terms, once in 250 kilometers per year. A separation of 20 meters would provide a high degree of safety from the type of direct contact considered here, but further analysis and probably tests would be highly desirable to determine the current density which the protective coating can accept without puncture.

The coordinated approach suggested above appears most promising, but requires more detailed analysis after all aspects of transient and steady state exposures have been placed in perspective.

SUMMARY AND CONCLUSIONS

It has been shown that for typical power line parameters, the frequency of direct strokes in the vicinity of the pipeline may be increased by a factor on the order of two to three. The number of power line ground faults caused by lightning strokes is much more difficult to ascertain and is dependent upon the line quality, exemplified by its "performance order" number. Data is given which allows the Specific Tripout Rate to be calculated for a power line of known quality.

It was found, however, that the presence of a power line along the same right-of-way, actually caused a reduction in effects caused by direct lightning strokes. This is due to the fact that although the near stroke frequency rate is higher, the presence of the power line shield wires causes the more severe strokes to be captured by them, thus providing a "protective umbrella" for the pipeline.

In addition, ground ionization effects mitigate against the occurrence of severe pipeline stress because of lightning strokes. Tabular data is given which allows calculation of the ground ionization radius beyond which the effects are minimized. In general, however, for most situations it may be assumed that if the pipeline is situated 20 meters or more distant from a ground electrode, i.e., a structure footing, the stress effects upon the pipeline are effectively eliminated.

REFERENCES

1. E. R. Whitehead, "The CIGRE Survey of the Lightning Performance of EHV Transmission Lines," ELECTRA, No. 33, pp. 63-89, March 1974.

2. D. W. Gilman and E. R. Whitehead, "The Mechanism of Lightning Flashover on High-Voltage and Extra-High-Voltage Transmission Lines," ELECTRA, No. 27, pp. 65-96, March 1973. (This is an official report, approved by the Edison Electric Institute, on the EEI Research Project RP 50, conducted by IIT Research Institute with E. R. Whitehead as principal investigator.)

Section 7

PIPELINE SYSTEM SUSCEPTIBILITY

INTRODUCTION

General guidelines are presented in this section to assist the pipeline engineer in properly evaluating the significance of the induced voltage levels. These guidelines are developed through the presentation of actual field measurements and experiences as reported in the literature. It is thought to be entirely unrealistic to define specific interference thresholds and limit all pipe-to-soil potentials to these levels. Each situation encountered by the pipeline field engineer will be different and, therefore, will demand different judgements as to whether further action is warranted to assure the reliable and safe operation of a given facility.

Specific topics reviewed are (1) ac corrosion effects, (2) damage thresholds of pipelines and components, especially to transient voltages, and (3) safety hazards to personnel.

AC CORROSION EFFECTS

To date, many investigators (1-8) have attempted to determine the corrosive effects of induced ac voltages upon various metals. In general, the interpretation of experimental results has been difficult, due to the fact that even a slight change in the experimental conditions, unknown to the observer, could lead to inconclusive or ambiguous results. For the most part, the experiments performed by the various investigators involved the passage of an ac current through a set of metal electrodes immersed in an electrolyte, thus comprising a galvanic cell. For all but a few of the experiments reported in the literature, metal electrodes were not cathodically protected.

Considering the case of most interest here, namely that of steel corroded by 60 Hz ac, the results of many experimenters may be summarized as: "the corrosiveness of an induced ac current is equal to approximately 0.1 percent of an equivalent value dc current". The actual percentage value equivalency is a

function of several factors such as electrolyte resistivity, the ac current density level, etc. This equivalency statement effectively summarizes the present state-of-the-art as regards the corrosive effects of induced ac voltages and currents. A survey of available experimental data has been made and review of this data indicates that further consideration of the factors defining the corrosion level would be desirable: (1) although the figure of 0.1 percent equivalency is available, the user of this number can justly feel uncomfortable with regard to its applicability to all situations. Sparse experimental data which is not substantiated by analysis can be subject to misinterpretation, and (2) in practice, pipelines are generally cathodically protected, and the question arises as to the interrelationships between dc corrosion, ac caused corrosion and mitigation effectiveness due to the applied cathodic protection.

The analytical work presented in this subsection allows the interpretation of available experimental results to situations where ac is present with cathodic protection also applied. In addition, the analytical results corroborate the percent ac current equivalency figure obtained experimentally.

Attempts to model the corrosion process have always been fraught with difficulties due to the complex geometry and electrochemistry of the cell. Therefore, a general analysis to evaluate the dc corrosion, for example, of a pipeline is not available. To date corrosion estimates have been based on experimental results. The intent of the study presented here is to provide a means of estimating the corrosive effects of the induced ac. The results are limited because of the simplified analysis employed which only considers the additional corrosion due to induced ac for a given original (dc) corrosion level.

The analysis made to determine the corrosion due to induced ac is detailed in the following subsection. The galvanic cell polarization diagram is used as a basis for interpretation of the physical situation and formulation of the solution.

In summary, the analysis derives an equation for the additional corrosion caused by induced ac voltages for various levels of partial cathodic protection. Extension of this analysis for the zero applied cathodic protection case leads to an approximate corroboration of the 0.1 percent ac current equivalency for iron established experimentally. Due to necessary approximations, this analysis is

limited to consideration of applied ac potentials and cathodic protection levels (pipe-to-soil potential shifts) of approximately 150 mV or less. At this level, the applied cathodic protection is only partial and large increases in the corrosion level are shown for small increases in the induced ac voltage. This result is not borne out in practice because of the higher levels of cathodic protection which are normally applied. Cathodic protection levels normally used tend to negate the effects of ac on corrosion.

Review of Experimental Corrosion Data

In general, inspection of the data from various investigators (1-8) shows that in many cases there was not only a lack of consistency between the data from any one investigator, but also that test conditions were vastly different so that comparison of various data sets could not be easily made. In attempting to comparatively quantify the available data, the following variables were initially considered.

1. Material - Although data are available on electrode material other than ferrous, the effort here was restricted only to the effects of ac current on ferrous materials.

2. Frequency - Not all experimenters considered the whole range of possible frequencies of interest, but in many cases data were available at frequencies other than 60 Hz. In general, the higher the frequency of applied current, the lower the corrosive effects. For the present purpose, the analysis is restricted to the 60 Hz data.

3. Current Density - It was found that almost without exception the current density was considered as an independent variable within an experiment. The general range of current densities at which most experiments were performed ranged between 10 and 100 ma/cm^2. Densities of this range will generally be experienced at holidays in coated pipelines.

4. Electrolyte Characteristics - Among the various experimenters, electrolytes ranging from real soil to various types of simulated soils were used. The characteristics of the soils initially considered important in assessing the data were:

   --resistivity

   --pH

   --movement of electrolyte

   --temperature of electrolyte

   --diffusion characteristics

   --oxygen content of electrolyte

The measured corrosion rate was a function of all of these characteristics. However, attempts at trying to categorize the trends in the corrosion rate with these variables were not fruitful with inconsistencies readily apparent. Hence, the data has been categorized only in the grossest sense, that is, the spread of the data is herein reported without regard to experimental variables other than the current density. Rather than plotting the data in terms of actual corrosion rate, it was found convenient with regard to establishing a pattern to normalize all of the data to the percentage of the equivalent dc current producing the same amount of corrosion. Using the applied current density as an independent variable, an equivalence plot of the ac corrosive effect for the data available is given in Figure 7-1.

Most of the data were obtained by the coupon weight loss technique. The loss in weight of a specimen is proportional to the corrosive effect of the current and the percentage equivalence was calculated by dividing the observed weight loss by the expected weight loss which would have occurred if the current were dc rather than ac.

Weight loss for a dc current level may be calculated from the standard electrochemical formula. For iron, the equivalence is that 1 mA/cm^2 of applied dc current will cause a removal of 9.13 $grams/cm^2$ of active anode area per year. Assuming uniform corrosion over the surface, this is also equivalent to a uniform penetration of 456 mils per year (mpy).

The only exception to the coupon weight loss method for determining corrosion was that of some of the data taken by Battelle Memorial Institute (3). The corrosion rate of these data was obtained by a linear polarization technique which resulted in a measure of the short term or near instantaneous corrosion rate which tends to be higher in magnitude than that obtained by the weight loss method. This differentiation was thought desirable for this particular set of data due to expected higher corrosion rates because of the measurement technique used.

Inspection of Figure 7-1 shows that the spread is approximately 2-1/2 orders of magnitude for the plotted data. One pertinent characteristic of the various data sets utilized in forming the plot and not specifically shown on the plot is that

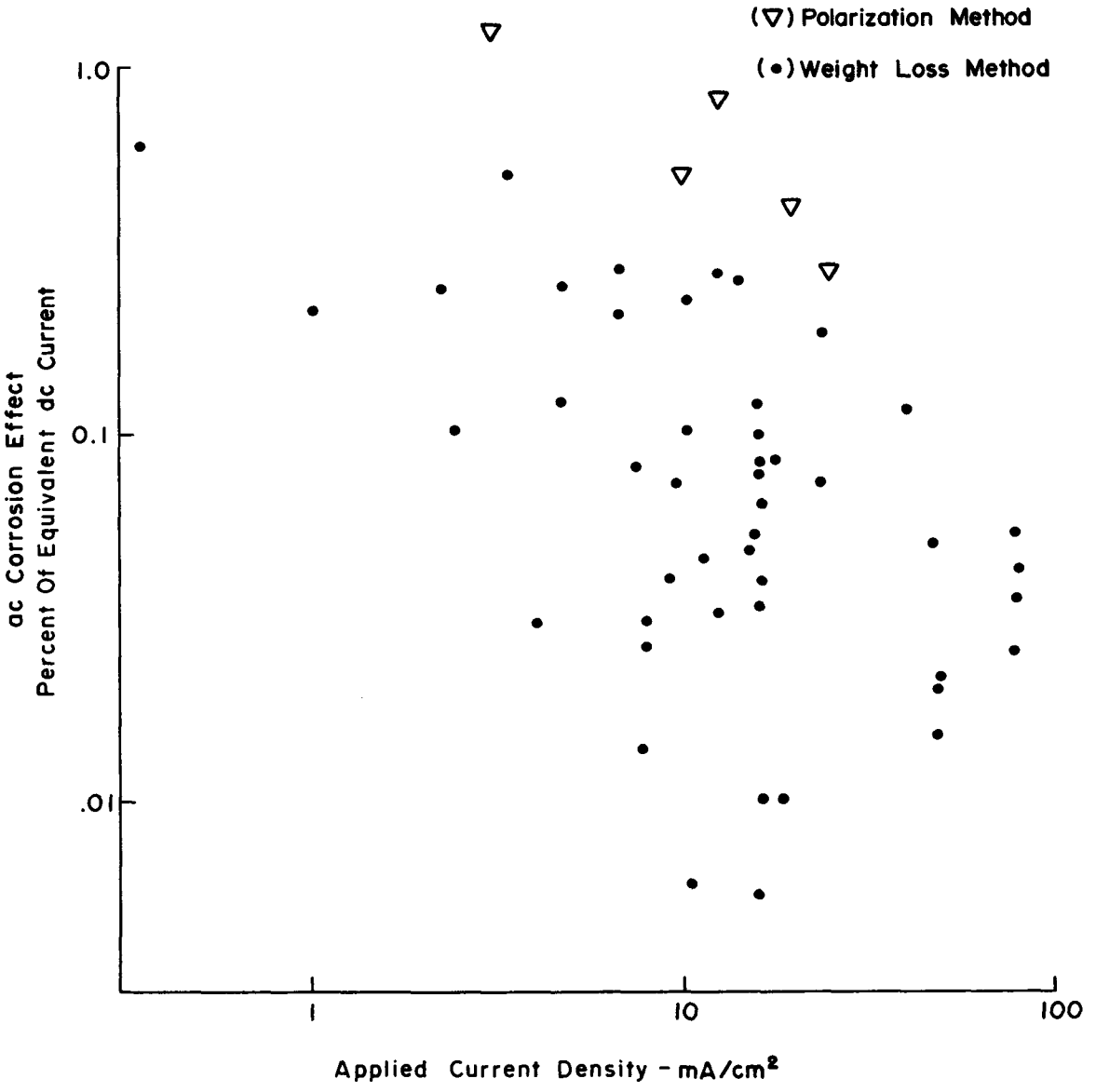

Fig.7-1 EQUIVALENT AC CORROSION DUE TO ELECTROLYSIS

the length of tests varied from a minimum of about one hour for the linear polarization measurement technique to a maximum of about 280 days for some of Bruckners' data (1). It is generally found that if the corrosion rate is measured periodically its value will decrease as time is increased. This is due to the build-up of polarization films, etc., on the surface of the electrodes. In order to make a better comparison of the available data and possibly reduce the spread of the data, the experiments performed by each investigator were reviewed, and the length of the experiment noted. The data was then normalized with respect to test length. The normalization factor was variable and was weighted so as to reduce all of the data to an equivalent long-term corrosion rate. For present purposes, "long-term" is considered to be an experiment length on the order of 9-10 months. After this length of time, it would be found, in general, that the corrosion rate is reduced to a relatively low value compared to the initial rates, and would tend to stay nominally constant thereafter.

To effect the necessary normalization, it was necessary to obtain a consistent set of data from one experimenter where the only variable was test length. Bruckner (1), fortunately, performed such a series of tests from which the necessary information could be extracted. A typical set of data, plotting the measured corrosion rate vs. the length of test is given in Figure 7-2. The data are plotted for neutral soil (pH = 7). Several other data sets are available for other soils, and inspection of these other data shows that a similar type of variation is experienced, but with varying data rates as a function to time. Hence, the graph of Figure 7-2 may be interpreted as an average type curve indicative only of the trend to be expected. However, normalizing the original data with respect to test length as per Figure 7-2 aids in providing a commonality to the various data sets. The sample graph in Figure 7-2 shows that as the test length is increased, the corrosion rate becomes asymptotic to 0.22 mg/day/in.^{2}. Hence, for any shorter test length, the normalization coefficient was found by dividing the corrosion rate found for that particular test length by the above asymptotic (long time) value. The set of normalization factors used for data from various test lengths are given in Table 7-1.

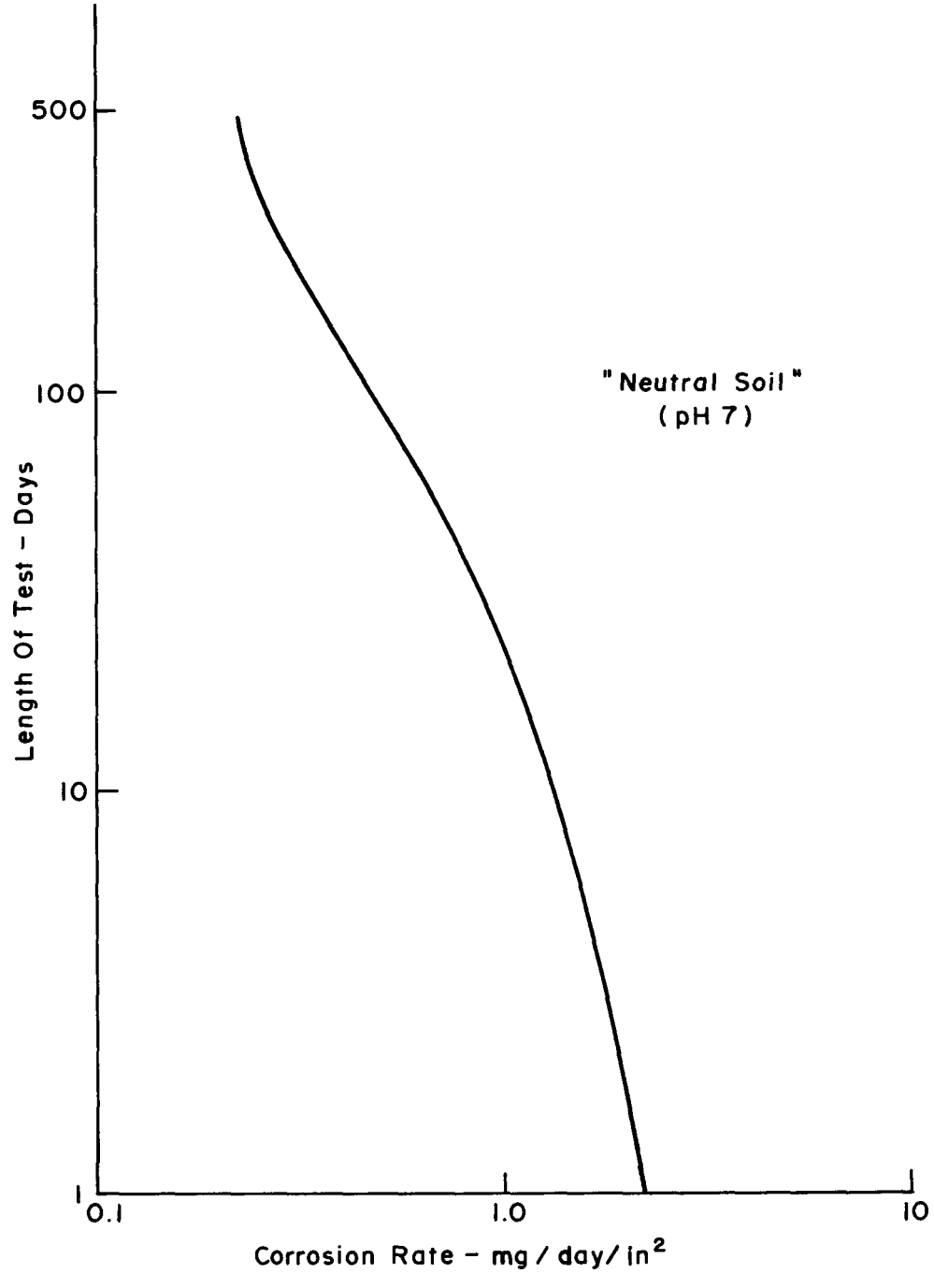

Fig. 7-2 INFLUENCE OF TEST LENGTH ON CORROSION RATE

Table 7-1

TEST LENGTH NORMALIZATION FACTORS
(Measured corrosion rate to be divided by the appropriate factor)

Test Length	Normalization Factor
≥ 280 days	1.0
144	1.44
84	2.0
56	2.6
46	2.9
28	3.6
7	5.8
3	6.4
1 hr.	12.0

Applying the normalization factors to the plotted data of Figure 7-1 yields Figure 7-3. Inspection of the plot shows that the applied normalization (except for the linear polarization data) has reduced the data spread. Hence, as an overall estimate, it appears that for a wide variety of experimental test conditions and electrolyte characteristics, the ac corrosion effect on a long-term basis is approximately 0.01 to 0.1 percent of that of an equal magnitude of dc current.

An analytical verification of this equivalency is derived using the small signal analysis presented in the following section. There it is shown that the additional corrosion caused by the ac current could be due to the nonlinearity of the anode current variation produced by the induced ac voltage.

Analysis for ac Corrosion

In this section, an analysis is made to evaluate the corrosive effects of low levels of induced ac voltages. The analysis allows a combined evaluation to be made; not only of the induced ac corrosion magnitude, but also of the effects of varying the cathodic protection upon reducing the corrosion level. The small

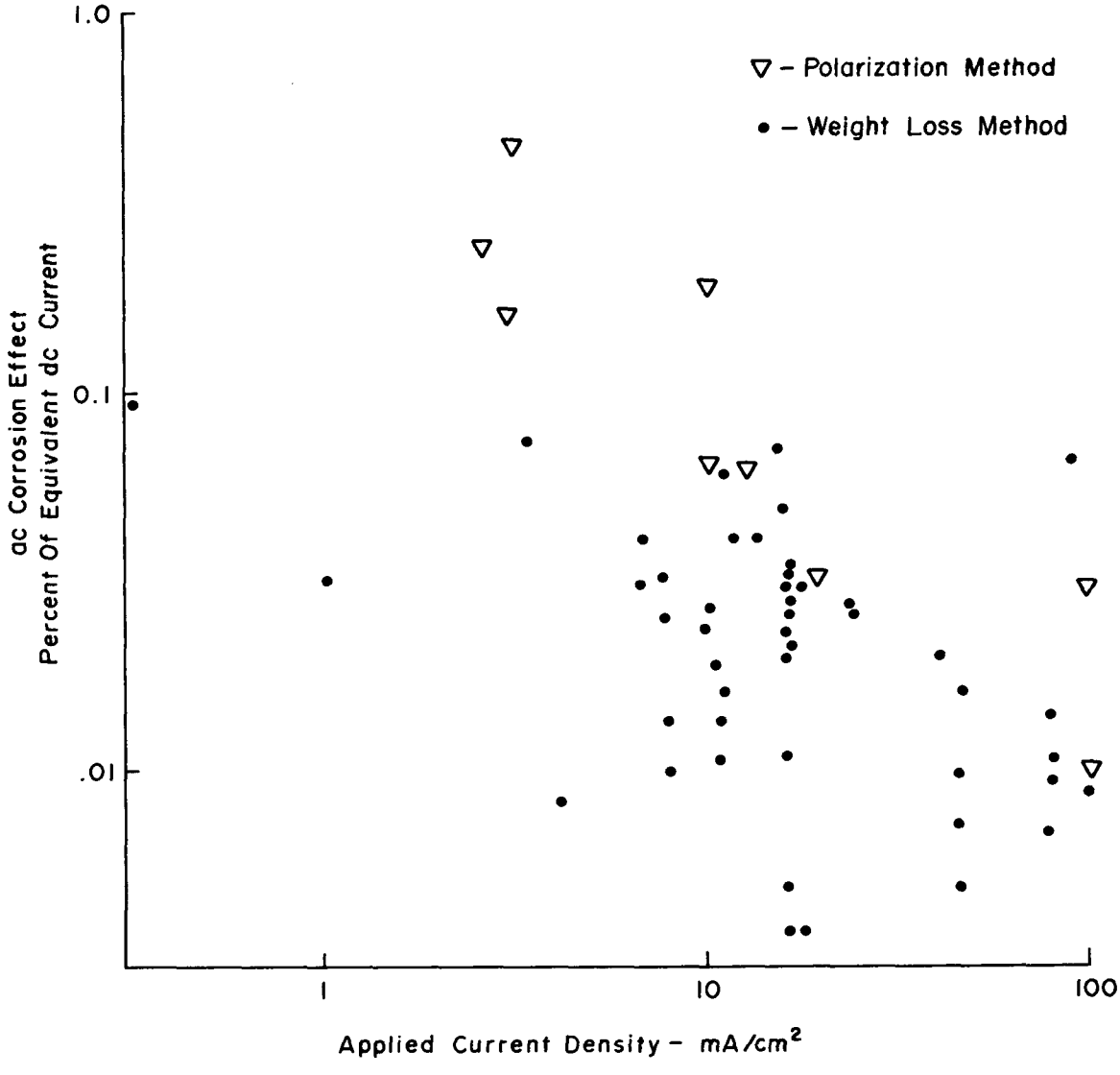

Fig. 7-3 AC ELECTROLYSIS CORROSION DATA - NORMALIZED FOR TEST LENGTH

signal analysis presented is useful for establishing the direction of trends, but it is limited to quantitative consideration of induced ac voltages of less than 150 to 200 millivolts. The results of this analysis should be applicable to both bare pipe and holidays in coated pipe.

Small Signal Analysis. The basis for this analysis is the corrosion cell polarization curves, with a conceptual diagram shown in Figure 7-4. The variables in the figure are defined as follows:

- e_k - open circuit cathode voltage
- e_a - open circuit anode voltage
- e_c - corrosion potential
- i_c - corrosion current density
- Δe - pipe-to-soil potential shift with application of cathodic protection
- e_{ac} - pipe-to-soil potential shift due to induced ac
- E_{ac} - rms value of e_{ac}
- i_{do} - applied cathodic protection current density
- i_a - anode (corrosion) current density
- i_k - cathode current density
- β_a - Tafel slope of the anodic polarization curve
- β_k - Tafel slope of the cathodic polarization curve.

The polarization curves shown in Figure 7-4 are plotted as a function of electrode potential versus logarithm of the current density. Without an externally applied cathodic protection current, the equilibrium condition for the cell exists at the intersection of the anodic and cathodic polarization curves; namely, at a corrosion current density i_c and a corrosion potential of e_c. With the application of a cathodic protection current of density, i_{do}, the corrosion current is reduced to the value, i_a. This in turn causes a pipe-to-soil potential shift of Δe which establishes the new equilibrium operating point of the cell. Introduction of either an ac current or voltage at the pipe will cause a shift in this equilibrium point with a corresponding cyclical increase and decrease in the value of i_a.

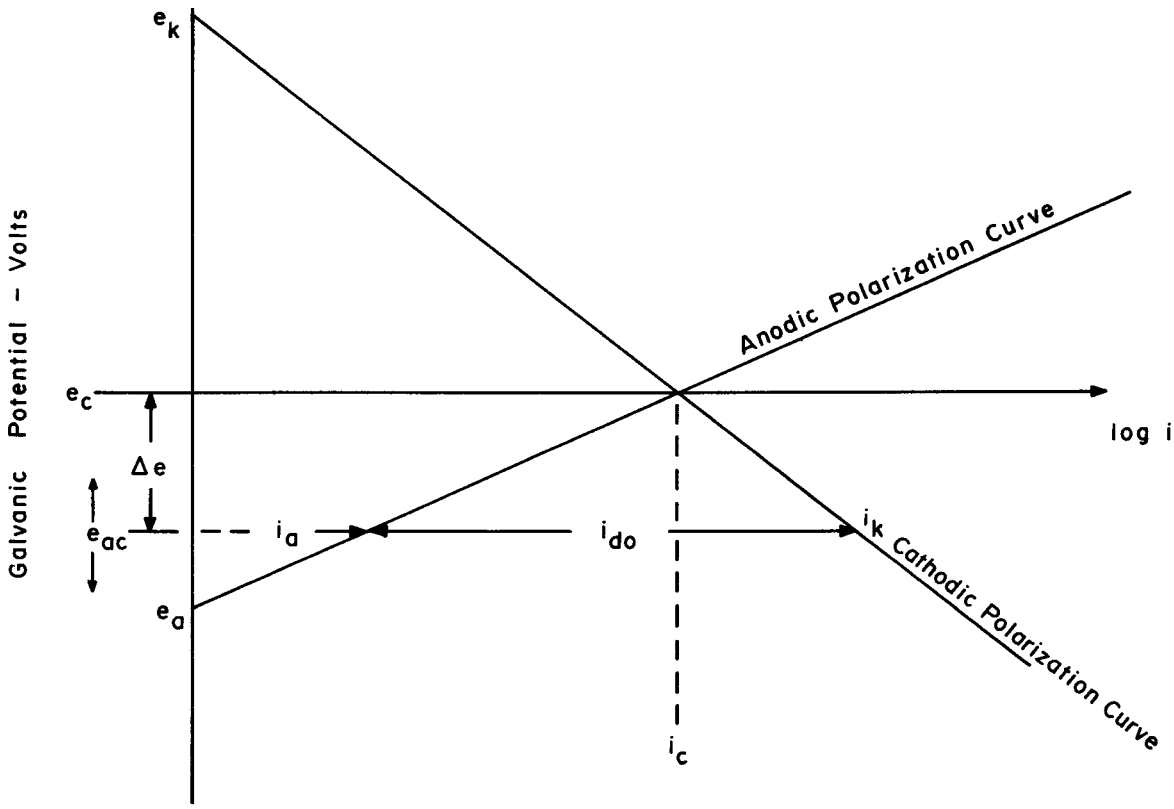

Fig. 7-4 REPRESENTATIVE POLARIZATION DIAGRAM

Theoretically, an alternating current passing through the corrosion cell electrodes will cause the disassociation of ions on the anodic half-cycle, and correspondingly, a reversible reaction on the cathodic half-cycle. However, due to the nonlinearity of the polarization curves, that is, they are a plot of linear voltage versus log of current density, a nonsymmetrical electrode current will exist even though the induced currents or voltages on the pipeline are sinusoidal and symmetrical with respect to the equilibrium operating point. Hence, with the introduction of an ac current upon the pipeline a corrosion component in addition to the original dc corrosion will exist. The following analysis quantizes this effect for the cases of no or partial cathodic protection of the cell.

Upon the application of the dc cathodic protection current, i_{do}, the pipeline potential, $e_c + \Delta e$ must approach the open circuit anode voltage, e_a, in order to reduce the anodic corrosion current to a small value. In the situation where an ac current is induced upon the pipeline, the total current will be the sum of the original cathodic protection current i_{do} plus an ac component. The sum current density is given by

$$i_d = i_{do} + i_m \cos \omega t \qquad (7\text{-}1)$$

where i_m is the peak value of the induced ac current.

Referring to Figure 7-4 for the condition $i_m \neq 0$, it will be found that the cathodic protection will be mitigated by the ac current and the anodic corrosion current will correspondingly vary with i_d. Correspondingly, the pipe-to-soil voltage changes by the amount, e_{ac}.

Under this condition, the anode current density is given by

$$i_a = i_c \, 10^{(-|\Delta e| + e_{ac})/\beta_a} \qquad (7\text{-}2)$$

Likewise, the cathodic current density is equal to

$$i_k = i_c \, 10^{(|\Delta e| - e_{ac})/\beta_k} \qquad (7\text{-}3)$$

In general, the potential shift, Δe, for the small signal case will be on the order of 100 to 200 millivolts, while β_a will have values for typical situations in the region of 50 to 150 millivolts. Hence, the average anodic corrosion current for $e_{ac} = 0$ will be generally one or more orders of magnitude less than the original corrosion current without cathodic protection applied. Typical β_k values are 150 to 300 millivolts.

Since after the application of cathodic protection, the anode current density is reduced to a very low value, the applied dc cathodic protection current is

$$i_{do} \simeq i_k\Big|_{dc} = i_c \, 10^{|\Delta e|/\beta_k} \tag{7-4}$$

When an ac current is induced in the pipeline, at the pipe-to-soil interface, it is driven into a nonlinear interface conductance, g_o, which is in parallel with an interface capacitance, C. The capacitance, C, acts as a shunt for the applied current, since only current passing through g_o causes a shift in operating point defined by the curves in Figure 7-4. Hence, the greater the value of C, the less the shift in the cell operating point for a fixed level of induced ac current.* The current entering the electrode-electrolyte interface is equal to the sum of the currents flowing through C and g_o, which is given by

$$i_d = i_{do} + i_m \cos \omega t = C\frac{de}{dt} + i_k \tag{7-5}$$

$$= C\frac{de}{dt} + i_c \, 10^{(|\Delta e| - e_{ac})/\beta_k}$$

Substituting Eq. 7-4 into 7-5 results in

$$i_{do} + i_m \cos \omega t = C\frac{de}{dt} + i_{do} \, 10^{-e_{ac}/\beta_k} \tag{7-6}$$

In Eq. 7-6, values of β_k are relatively high and hence, it will be assumed that the exponent is relatively small. Therefore, the following expansion can be utilized:

$$10^{-e_{ac}/\beta_k} \simeq 1 - 2.3^{e_{ac}/\beta_k} \tag{7-7}$$

*This appears to be a definite factor in producing a smaller corrosion rate at higher frequencies.

Substituting Eq. 7-7 into Eq. 7-6 and solving the differential equation yields, for a steady state solution, the following:

$$e_{ac} = \frac{i_m \sin(\omega t + \phi)}{\sqrt{(\omega C)^2 + (2.3\, i_{do}/\beta_k)^2}} \tag{7-8}$$

where ϕ is an arbitrary phase angle.

The cell is moved from its dc equilibrium point by the ac current, causing anode current to vary and thus effecting a change in cell corrosion current. From Eq. 7-2 the anode current may be written as

$$i_a = i_c\, 10^{-|\Delta e|/\beta_a}\; 10^{e_{ac}/\beta_a} \tag{7-9}$$

For convenience, the right hand factor of Eq. 7-9 may be written as an exponential,

$$10^{e_{ac}/\beta_a} = \exp\left[\frac{2.3 e_{ac}}{\beta_a}\right] \tag{7-10}$$

Eq. 7-8 and 7-10, after substitution into Eq. 7-9 yields

$$i_a = i_c\left(10^{\frac{-|\Delta e|}{\beta_a}}\right) \exp\left[\frac{i_m \sin(\omega t + \phi)}{\sqrt{\left(\frac{\omega \beta_a C}{2.3}\right)^2 + \left(\frac{\beta_a}{\beta_k} i_{do}\right)^2}}\right] \tag{7-11}$$

Eq. 7-11 may be simplified by using the following definition.

$$e^{jz\sin\theta} = J_o(z) + 2 \sum_{k=1}^{\infty} J_{2k}(z)\cos 2k\theta + 2j \sum_{k=1}^{\infty} J_{2k-1}(z)\sin(2k-1)\theta \tag{7-12}$$

where

$$j \equiv \sqrt{-1}$$

$$jz = \frac{i_m}{\sqrt{\left(\frac{\omega\beta_a C}{2.3}\right)^2 + \left(\frac{\beta_a}{\beta_k}\ i_{do}\right)^2}}$$

$$\theta = \omega t + \phi$$

and

$J_i(\cdot)$ = Bessel function of i^{th} order.

A Bessel function of an imaginary argument may also be expressed in terms of the modified Bessel function as follows:

$$J_n(jz) = j^n I_n(z) \tag{7-13}$$

where $I_n(\cdot)$ = modified Bessel function of n^{th} order.

Substituting Eq. 7-12 and 7-13 into 7-11, yields

$$i_a = i_c 10^{-|\Delta e|/\beta_a} \left\{ I_o\left(\frac{i_m}{\sqrt{\left(\frac{\omega\beta_a C}{2.3}\right)^2 + \left(\frac{\beta_a}{\beta_k}\ i_{do}\right)^2}} \right) \right. \tag{7-14}$$

$$\left. + 2 \sum_{k=1}^{\infty} (-1)^k I_{2k} \left(\frac{i_m}{\sqrt{\left(\frac{\omega\beta_a C}{2.3}\right)^2 + \left(\frac{\beta_a}{\beta_k}\ i_{do}\right)^2}} \right) \cdot \cos\ (2k\omega t + 2k\phi) \right.$$

$$+ 2 \sum_{k=1}^{\infty} (-1)^{k+1} \; I_{2k-1} \; \frac{i_m}{\sqrt{\left(\frac{\omega \beta_a C}{2.3}\right)^2 + \left(\frac{\beta_a}{\beta_k} \; i_{do}\right)^2}}$$

$$\cdot \sin (2k-1) (\omega t + \phi) \Bigg\}$$

Eq. 7-14 is a sum of three terms; a time invariant component, i_c, plus time varying components appearing as modified Bessel functions of first or higher order multiplied by cosine or sine functions, respectively. The emphasis here is on the dc component since this component causes the shift in the pipeline operating point and a corresponding change in the cell corrosion. The time varying current components because of waveform symmetry do not contribute to the corrosion increase. As will be shown later, the observed increase in corrosion can be essentially accounted for by the dc component generated as a result of waveform asymmetry.

Therefore, it can be assumed that the sinusoidal variations in the anode current average out to zero over a cycle, and the corrosive effect of an ac induced current upon the pipeline may be represented by,

$$i_a = i_c \cdot 10^{-|\Delta e|/\beta_a} \cdot I_o \left\{ \frac{i_m}{\sqrt{\left(\frac{\omega \beta_a C}{2.3}\right)^2 + \left(\frac{\beta_a}{\beta_k} \; i_{do}\right)^2}} \right\} \qquad (7\text{-}15)$$

where i_{do} is given by Eq. 7-4.

Inspection of Eq. 7-15 shows that the anode current density is determined by three factors. The first factor, i_c, is the original corrosion current before the application of cathodic protection. The second factor is in magnitude less than or equal to one. It expresses the corrosion reduction obtained by the cathodic protection. The third factor containing the modified Bessel function of zero order, is equal to or greater than one and is a function of the induced ac voltage on the pipeline. Hence, it defines the degradation suffered in protection by the pipeline.

A plot of the modified Bessel function is given in Figure 7-5. Values were obtained from (9).

The stimulus for this analysis was obtained from two articles appearing in a foreign journal (10,11). In these papers, the possible anode current asymmetry as a result of induced ac was recognized. Present work, however, extends the analysis reported therein, and applies it directly to the pipeline situation.

Where it is more convenient to work with induced ac voltage levels, Eq. 7-15 may be expressed in terms of the rms value of e_{ac}. From Eq. 7-8, the rms value equals

$$E_{ac} = \frac{i_m/\sqrt{2}}{\sqrt{(\omega C)^2 + (2.3\, i_{do}/\beta_k)^2}} \qquad (7\text{-}16)$$

Substituting Eq. 7-16 into 7-15 yields

$$i_a = i_c \cdot 10^{-|\Delta e|/\beta_a} \cdot I_o \left(\frac{3.25E_{ac}}{\beta_a}\right) \qquad (7\text{-}17)$$

Equation 7-17 can be used only for determining the relative rather than absolute effects of cathodic protection and ac voltages on the final corrosion current since the initial corrosion current level, i_c, cannot be obtained analytically. Determining i_c analytically is a much more difficult problem which has not been solved in general, and is beyond the scope of this analysis. Also, the analysis is applicable to situations of very small applied ac voltage levels, i.e., on the order of tens of millivolts. In practice it has been found, with the cathodic protection levels usually applied, that corrision is not apparent even for induced ac voltages orders of magnitude larger.

The results of this analysis are useful in that, as shown in the following derivation, an analytical verification of the experimentally derived ac corrosion current equivalency can be made.

AC Corrosion Current Equivalency. As mentioned previously, the general consensus regarding the effects of ac current is that the current produces corrosion on ferrous metals equivalent to 0.1 percent of an applied dc current of the same

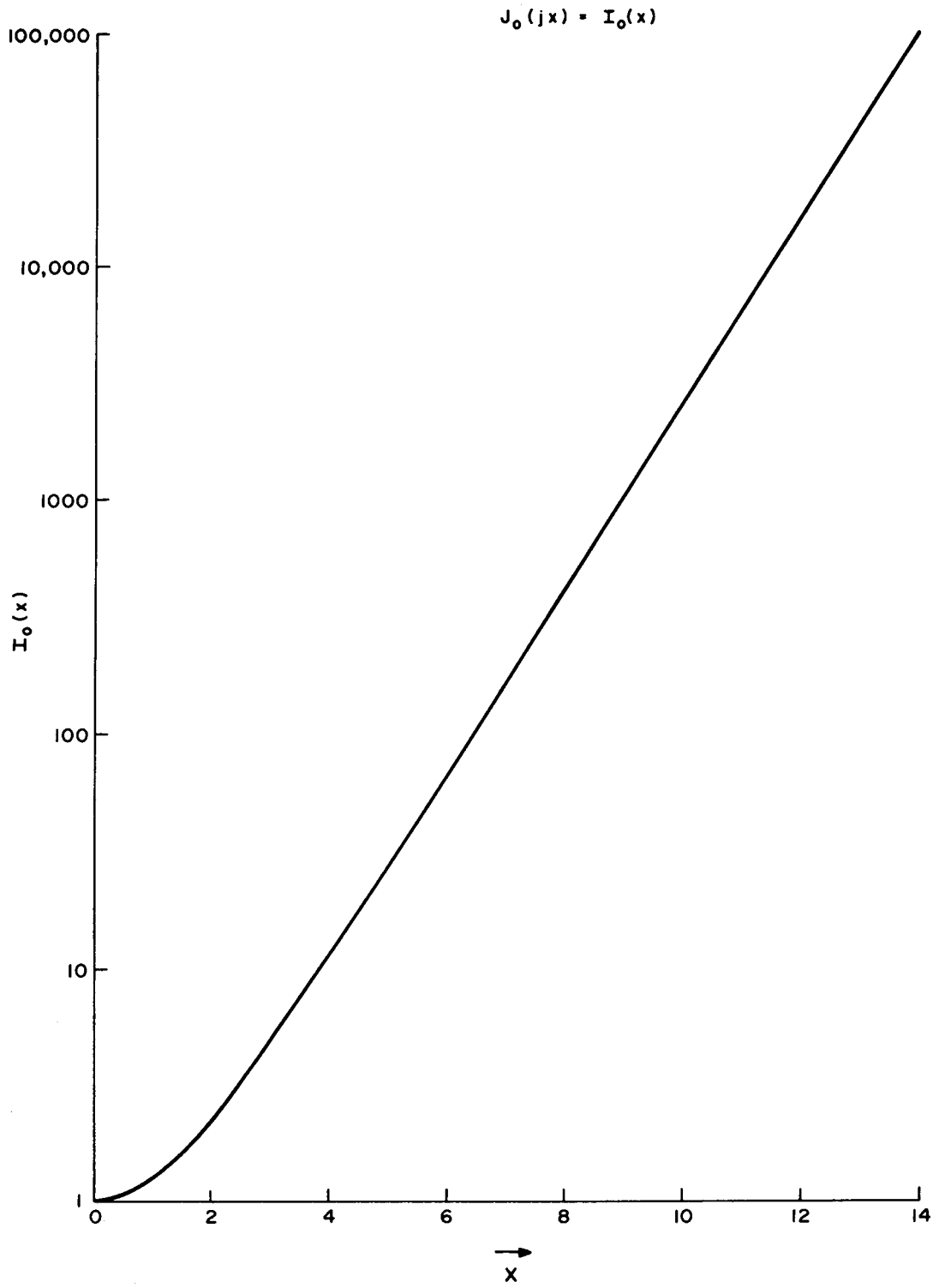

Fig. 7-5 PLOT OF MODIFIED BESSEL FUNCTION OF ZERO ORDER

magnitude. This equivalency is also a function of the applied current density. In obtaining this value from data points such as those plotted in Figures 7-1 and 7-3, investigators generally measured the dc corrosion without the application of cathodic protection. For a practical application as for a pipeline, this equivalency ratio number will be a function of the applied cathodic protection. With cathodic overprotection, this equivalency ratio will drop to zero.

In this section the equivalency ratio for the situation where no cathodic protection is applied is analytically derived for comparison to the empirical value.

This analysis is an extension of the previous small signal analysis. To set the proper stage for the present analysis, it is desirable to review the concepts upon which the previous analysis has been based. Initially, it was assumed that a corrosion cell existed, which was at least partially cathodically protected. To effect this cathodic protection, an initial dc current density, i_{do}, was applied to the corrosion cell. Then, if an ac current were induced on the pipeline, the effective cathodic protection current entering the cell would no longer be steady, but would vary at the frequency of the applied sinusoid. This change in the cathodic protection current amplitude will cause an approximate sinusoidal shift in the pipe-to-soil potential. Conversely, for the purpose of the present analysis, it could have been assumed that an initial sinusoidal ac voltage was induced on the pipeline, which would cause a sinusoidal shift in the cathodic protection current applied to the corrosion cell.

Referring to the polarization diagram of Figure 7-4 it can be seen that due to the nonlinearity of the polarization curves, i.e., a linear change in pipe-to-soil potential causes a logarithmic change in the current density, a nonsinusoidal anode current will be generated. This current will be asymmetrical with respect to the operating point set by the applied cathodic protection. By means of Fourier analysis, the nonsinusoidal anode current can be resolved into a dc component and a set of harmonically related ac components. The present analysis assumes that the net increase in corrosion is caused by the dc component only and that this dc component accounts completely for the observed increase in cell corrosion. In this manner, the 0.1 percent equivalency factor is analytically verified.

The starting point for the analysis is Eq. 7-15 assuming zero cathodic protection. Therefore, assuming a value of $\Delta e = 0$ in Eq. 7-15 leads to,

$$i_a = i_c \cdot I_o \left\{ \frac{i_m}{\sqrt{\left(\frac{\omega \beta_a C}{2.3}\right)^2 + \left(\frac{\beta_a}{\beta_k} \cdot i_c\right)^2}} \right\} \equiv i_c \cdot I_o(\cdot) \qquad (7\text{-}18)$$

The equivalency between the ac and galvanic corrosion may be established by the following equation:

$$\% \text{ Equivalency} = 100 \left\{ \frac{i_a - i_c}{i_m/\sqrt{2}} \right\} \qquad (7\text{-}19)$$

Substituting Eq. 7-18 into 7-19 yields

$$\% \text{ Equivalency} = 100\, i_c \left\{ \frac{I_o(\cdot) - 1}{i_m/\sqrt{2}} \right\} \qquad (7\text{-}20)$$

For values of the argument of the modified Bessel function of concern here (≤ 4), the following substitution may be used:

$$I_o(\cdot) \approx 1 + (\cdot)^2 \qquad (7\text{-}21)$$

This substitution gives

$$\% \text{ Equivalency} = \frac{100\sqrt{2}(i_m/i_c)}{\left(\frac{\omega \beta_a C}{2.3 i_c}\right)^2 + \left(\frac{\beta_a}{\beta_k}\right)^2} \qquad (7\text{-}22)$$

For practical physical situations,

$$\left(\frac{\omega \beta_a C}{2.3 i_c}\right)^2 >> \left(\frac{\beta_a}{\beta_k}\right)^2 \qquad (7\text{-}23)$$

and Eq. 7-23 becomes

$$\% \text{ Equivalency} = 750 \frac{i_m \cdot i_c}{(\omega \beta_a C)^2} \qquad (7\text{-}24)$$

In Eq. 7-24 representative parameter values are:

- $\omega = 2\pi f = 2\pi(60) = 377$
- $\beta_a = 100$ mV
- $C = 50 \times 10^{-6}$ F

The chosen value for β_a represents a middle of the range selection for anodic polarization Tafel slopes. The choice of value for the double layer capacitance, C, is somewhat more difficult, due to little available data for covering a variety of conditions. The value assumed here was obtained from (12). Substituting these values into Eq. 7-24 yields

$$\% \text{ Equivalency} = 0.21\, i_c i_m \qquad (7\text{-}25)$$

where

i_c is the original dc corrosion current expressed in μamps/cm^2 (1μamp/cm^2 is equivalent to a corrosion rate of 0.456 mpy for iron), and

i_m is the induced ac current expressed in mA/cm^2.

Equation 7-25 is plotted in Figure 7-6 for two values of galvanic corrosion rates, 0.45 mpy and 4.5 mpy. At the higher applied current densities, the plots of Figure 7-6 indicate a higher percentage equivalency than the experimental data plotted in Figure 7-1. However, Eq. 7-25 was derived on the basis of relatively gross modeling of the electrochemical effects of the galvanic cell, and it is believed that the correspondence between the derived and experimental number is relatively good. In addition, the approximation used in Eq. 7-21 to expand the modified Bessel function term limits the usefulness of Eq. 7-25 to maximum applied current densities of about one to three mA/cm^2. It is believed that the results plotted in Figure 7-6 are significant in that they indicate that the increase in corrosion caused by the application of an ac current can be accounted for by considering the dc component generated because of waveform asymmetry, and the analytical result corroborates experimental data.

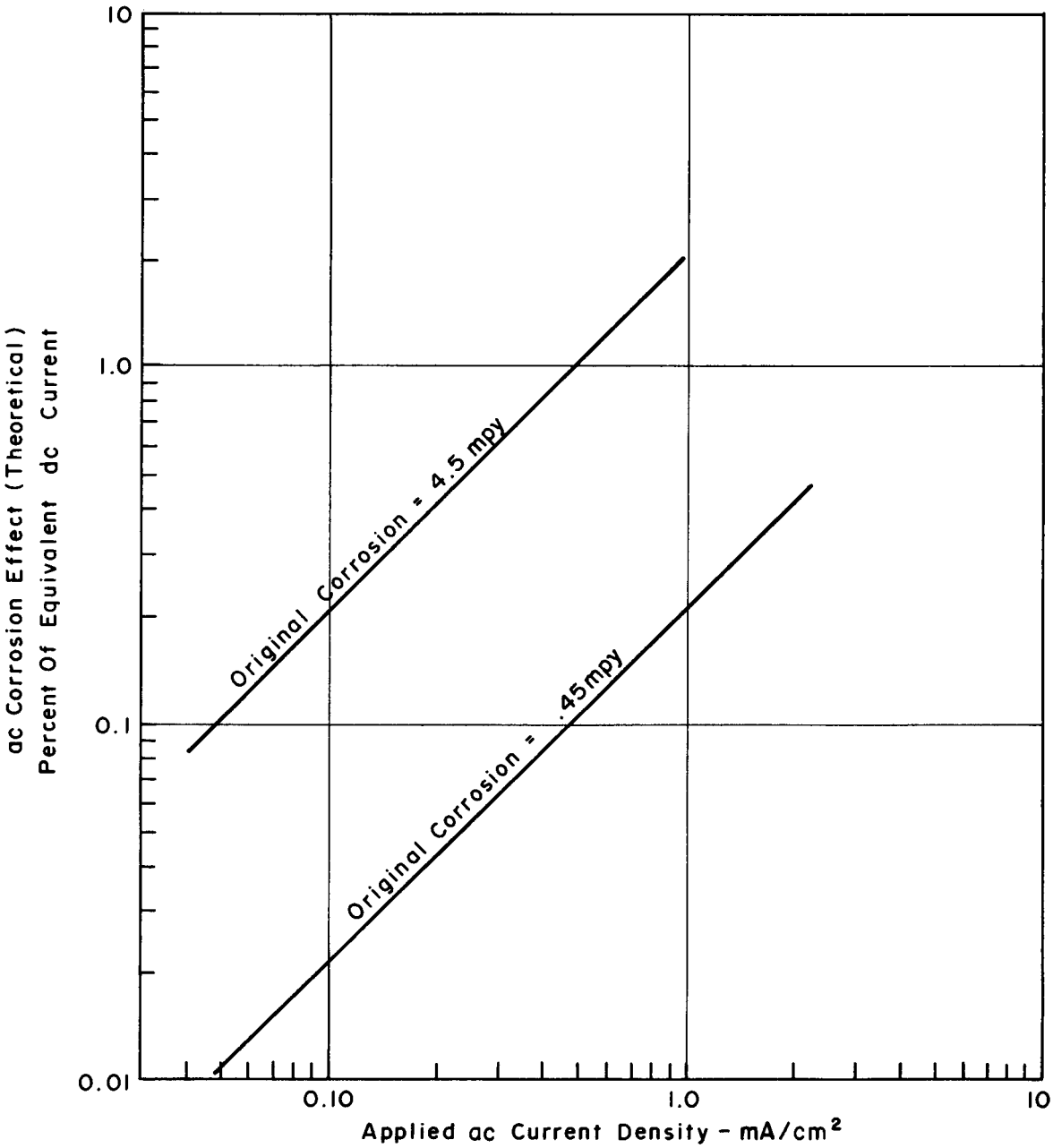

Fig. 7-6 AC/DC CURRENT EQUIVALENCY

PIPELINE COMPONENT SUSCEPTIBILITY

Both steady state and transient induced voltages and currents on pipelines can affect the operation of or damage pipeline components and associated systems. Such components include the pipe coating, the pipeline itself, insulating junctions (flanges) used along the pipeline, the cathodic protection system and communications systems used with the pipeline. This section summarizes the data available in the open literature for both the magnitudes of measured voltages and currents in pipelines, and also failure mechanisms and damage levels observed for pipeline components.

Typical Measured Voltages and Currents on Pipelines

Measured values of various voltages and currents on pipelines as obtained from a search of the open literature are presented in Table 7-2. This table presents a summary of measured ac voltages and currents induced on pipelines during steady state operation of nearby power lines. Inspection of these levels will aid in determining the possible range of induced levels, and thusly, point to the types of damage that could occur.

Abnormal conditions occurring on a power line can cause much larger voltages and currents to be induced on nearby pipelines. One such dominant condition is a fault whereby one phase of the electric power transmission line becomes grounded. For this type of fault, very large current surges flow into the earth in the area at which the fault occurs, which are then coupled into a nearby pipeline. Lightning striking near a pipeline can also induce strong current surges in a pipeline. Furthermore, it has been estimated that for lower transmission voltages, lightning striking power lines causes 70 to 80 percent of the faults on these lines. In this case, lightning can be an indirect cause of a current surge on a pipeline. Distinguishing between pipeline current surges produced by power line faults and those produced by lightning is a difficult task. The measured pipeline current surge data found in the literature and reported here does not distinguish between fault and lightning caused surges. Table 7-3 lists the available data for the conditions and ranges of measured surge currents.

Maximum station fault currents for present day power systems are in the range of 50,000 amperes, with projections for future systems reaching 100,000 amperes (18-20). A typical value may be on the order of 10,000 amperes. Although these fault currents are large, a major portion of these fault currents can return to

Table 7-2

MEASURED VALUES OF STEADY STATE VOLTAGES AND CURRENTS ON PIPELINES
AS DETERMINED FROM A LITERATURE SEARCH

Electrical Pickup Condition and Pipeline Location	Pipeline Parameters	Measured Values of ac Electrical Parameters
Steady State Pickup Pipeline Above Ground	3.5 mile section of 30-inch gas line paralleling a 345 kV electrical transmission line. Line was coated while lying above the ditch and then coal-tar and asbestos felt wrapped. Soil conditions were predominantly low resistivity clay-loam combinations with some very high resistivity sand hills.	200 foot road-crossing section on skids (sand hill). • Pipe bare V = 2.2 volts • Pipe primed V = 70 volts • Pipe coated V = 120 volts and wrapped • Pipe coated, V = 1.0 volt (13) wrapped and grounded
	16 inch oil line supplying two generating stations and paralleling four electrical transmission lines. Polyken 980 coating, mill-applied, with 25. mil., adhesive backed polyethylene outer wrap. Soil again predominantly clay with some areas of higher resistivity.	1000 foot welded section on skids • Ground rod at north end, voltage measured at south end, V = 7.8 volts • Ground rod disconnected, voltage measured at south end, V = 225 volts (13). 300 foot welded section on skids. • with two ground rods V = 1.0 volt • with one ground rod V = 1.6 volts • with no ground rods V = 13 volts (13)

Table 7-2 (continued)

Electrical Pickup Condition and Pipeline Location	Pipeline Parameters	Measured Values of ac Electrical Parameters
Steady State Pickup Pipeline Below Ground	Steel gas pipeline, coated with coal tar enamel, glass and on outer wrap of asbestos felt, with underground flanged valves one flange of which is insulated. One section of pipe runs approximately 5 miles parallel to several 115 kV transmission lines and parallel to shorter runs of 34.5 kV and 69 kV circuits. The electrical transmission lines have a counterpoise system.	• Currents flow between pipe and counterpoise I ≃ 2 amperes (aver.) I = 10 amperes at V = 15 volts (max. reading)(14) • Pipe-to-soil measurements I ≈ 4 amperes (average) I = 7.8 amperes at 11 volts (max. reading)(14)
	Pipeline running several miles parallel to a double circuit power line in Germany.	Measured maximum induced voltage (15) V = 40 volts.
	Pipeline running parallel for about 50 miles to a 250 kV power line in the western United States. The soil resistivity ranged from 5×10^5 to 10^6 Ω cm.	Measured voltage between pipe and ground (15) V = 60 volts.
	Coated gas pipeline which had undergone corrosion in a swampy soil. Soil resistivity was 76 Ω cm.	Pipe voltage = 8.5 volts (16)

the generating station by means of the shield wires and counterpoise systems associated with the power lines. It has been estimated that for a station with a 70,000 ampere fault current capability, the maximum current flowing into the earth at a tower footing during a fault condition is 3000 amperes. A typical value of such an earth current can be taken as 1000 amperes (18). Circuitry in the power system clears the fault conditions in a short time.

In terms of voltage levels, the induced steady-state voltage on a pipeline seldom exceeds 50 V ac although under certain conditions levels in the vicinity of 150 V can occur. In contrast, for severe faults and a long parallel run next to a nearby power line, exceedingly high voltages can be developed on the pipeline. This voltage can be high enough to perforate a pipeline (5000 volts) or disturb power feed converter circuitry (1500 volts) which is carried in the center of a coaxial communication cable that, for some systems, is used in association with the pipeline (22). Typical types of damage to pipelines and their associated components due to induced ac voltages and currents are discussed in the following section. It has been stated (21) that "Induced potentials from fault currents generally do not exceed about 500 volts because the potential is limited by glow discharges at coating holidays in the pipeline".

Failure Mechanisms and Damage Levels

Most of the damage to unmitigated pipelines and pipeline components produced by ac electrical currents and voltages from nearby power lines occurs during fault conditions of the power line. Steady state operation of the power lines, however, does produce some deleterious effects on the pipeline and components.

Steady state ac potentials on pipelines can be annoying or hazardous to personnel and may increase the rate of pipe corrosion, but do not appear to damage pipeline coating (21) (at least for low voltages). Data and analysis from a report issued by Battelle Memorial Institute indicates that degradation (shortening of operating life) of certain cathodic protection rectifier designs might occur for ac pipeline voltages much higher than 6.3 volts. Experimental testing and analysis would be necessary to determine if such degradation would occur for a particular rectifier design, pipeline ac potential and pipeline impedance (27). Another steady state ac effect occurs when an internal resistive coating (formed by deposits from the material carried within the pipeline) forms an electrical conducting bridge across an insulating flange. Steady state currents flowing through this resistive bridge can heat the flange insulation and eventually destroy the joint. Another undesirable steady state effect occurs when an ac potential on a coated buried pipeline

Table 7-3

MEASURED VALUES OF SURGE CURRENTS ON PIPELINES
AS DETERMINED FROM A LITERATURE SEARCH

Electrical Pickup Condition and Pipeline Location	Pipeline Parameters	Measured Values of ac Electrical Parameters
Lightning and/or Fault of Nearby HV Line Conditions. Pipeline Below Ground.	Buried gas pipelines. Data for pipelines varying in length from 8 miles to 30 miles.	Surge currents measured on conductors which were used to short out an insulating joint. The measured surge currents varied from 100 amperes to 3100 amperes (17).
	Buried gas pipeline 6 miles in length.	Surge current measured flowing through Thyrite lightning arrester. The measured surge currents varied from 750 amperes to 1800 amperes (17).

makes it difficult to extract the proper data when the pipeline is used as part of a communications channel and data link (15). This ac potential on a pipeline can also make dc pipe-to-soil potential measurements (to determine the effectiveness of cathodic protection systems) difficult (15).

The high voltages and currents produced during a fault condition on a nearby power line can produce many types of damage (mostly due to arcing and heating) to a pipeline and its components. The pipeline components which are mainly damaged during a fault, as reported in the literature, are pipeline coatings, the pipes themselves, and insulating joints such as flanges used along the pipeline.

Pipeline coatings can be punctured by the high voltages created during a fault condition. The arc created by the high voltage can be so intense that it also punctures a hole in the wall of the pipeline. These damage mechanisms are listed in Table 7-4 along with reported cases of this damage.

Voltage surges on pipelines produced by a fault or lightning can cause the degradation of the insulation of an insulating flange. However, it appears that most of the damage to an insulating flange is caused by arcing or breakdown across the insulation of the flange. Such a breakdown can occur: first, across an air gap between two metal parts of the flange; second, through the insulation of the flange; third, through an external coating on the flange insulation, and finally, through an internal coating formed on the insulation of the flange. Such a coating on the flange insulation will usually be composed of moisture, dirt or grease. Many insulating joint failures attributed to "high voltage surges" or "lightning surges" are probably due to these coatings. The types of damage which can happen to an insulating flange are listed in Table 7-4 along with voltage test data for some particular flanges. From the many types of insulating flange breakdown that can occur, and from the low and high humidity voltage breakdown data given in Table 7-4, it can be seen that it is difficult to predict the voltage failure level of an insulating flange as installed in the field. A number of devices are available commercially for mitigation of induced voltage surges.

Another damage mechanism can occur when large fault currents flow through a pipeline or other conductors. "Glow or arc discharges can occur in the earth or at the conductor with sufficient energy release to crush buried coaxial cables or ignite gas vapors" (22).

Table 7-4

FAILURE MECHANISMS AND DAMAGE LEVELS OF PIPELINE COMPONENTS

Pipeline Component	Type of Damage	Reported Cases of Damage or Failure Levels
Coating on Pipeline	Puncture of coating by electric arc (23,12,13)	Coating punctures have been found close to areas where large currents are discharged into the ground such as power line tower footings (15). A coated steel main after coating puncture experienced five holes burned through it when one phase wire of a high voltage line broke and fell on an exposed end of a steel road culvert laying parallel over the buried main (25).
Pipeline	Puncture of pipe wall or damage of pipe metal (13,15) (23-24)	A coated steel main experienced five holes burned through it when one phase wire of a high voltage line broke and fell on an exposed end of a steel road culvert laying parallel over the buried main (25) Tests under laboratory conditions with various voltage levels indicate that 5 kV applied for a period of 1 second will produce no metal errosion on typical pipelines that 10 kV will produce some corrosion but no perforation after 1 second, and that 15 kV will perforate the piping in less than 1 second of voltage application (22).
Insulated Flange	•Deterioration of insulation. •Breakdown of insulation (weld bead may be established across flange). •Breakdown (arc) across air gap between metal parts of flange. •Breakdown through an internal coating •Breakdown through an external coating (14-15) (26-27).	•Tube Turn manufacturers test on insulated joint after assembly. Resistance greater than 25 megohms at 1000 volts dc. •Prochind insulated joint. 225 megohms insulation resistance at 500 V, 50 Hz. 2500 volts minimum perforation voltage (27). •Laboratory tests on tube turns forged flanges Part No. 6-mih, 150-round, material A181-1 with Type B and C gasket kits. Under normal room conditions breakdown voltage was: Type B ~ 4000 volts, Type C ~ 2200-2400 volts. After treatment at high humidity, Type B sample failed by surface conditions at several hundred volts (27). •Electrical bridging of insulated flanges occurs frequently in practice.

SAFETY HAZARDS TO PERSONNEL

The presence of induced voltages and currents on a pipeline can also represent a hazard to anyone who might make physical contact with the facility. This section summarizes the effects of electric shock on humans and includes information at dc, 60 Hz, and impulse shock. These effects have been identified by studying the open literature and presenting the findings in a unified form.

Shock Effects

The effects of electric shock on humans may be divided into five areas in order of increasing current: perception, let-go, tetanization, ventricular fibrillation, and respiratory inhibition. Perception is the response to the lowest value of current and ranges from the subject feeling a slight tingling sensation at the minimum detectable current to an unpleasant burning sensation at high levels. The perception of the shock is dependent upon the path of the shock, i.e., whether the contact points are at both hands, a hand and a foot, or otherwise, and the magnitude of the shock current, among other factors. Perception currents are not of themselves dangerous but, under some circumstances, may possibly cause "startle" reflexes that may indirectly cause an accident. An example of this would be a man who steps off a metallic ladder because he is startled by a mild shock from a power tool he is using.

The next area of response is called let-go currents. These are currents that are usually very painful, but are just under the limits of currents that produce tetanization of the muscles (condition wherein the muscles cannot be relaxed) that control the limbs. Currents in excess of the let-go levels cause the subject to lose control of the muscles in the current path. It is plain that tetanization is potentially dangerous, and possibly lethal, if the current path is in the lung region and the current is maintained for a long enough period (28).

Ventricular fibrillation is the next response area and it is a condition in which the heart no longer is able to pump blood. Instead of contracting in a coordinate, organized manner, the heart muscle fibers contract separately and at different times. Once this condition is initiated in the human heart, the heart cannot revert to normal operation of itself. Since ventricular fibrillation is the lethal effect with the least current level, the ventricular fibrillation threshold is important for safety considerations.

Respiratory inhibition occurs at still higher current levels and under this condition, the subject will cease breathing and his heart will stop during a very severe electric shock and sometimes convulse. Although the subject's heart will resume beating after the shock is stopped, he may not resume breathing independently and may need artificial respiration. At still higher current levels, there may be direct biological damage such as burns and nerve blocks.

Factors Determining Shock Severity. To properly evaluate the effects of any electric current, the following factors must be considered:

- Current path in body
- Physical condition of subject
- Magnitude of the shock
- Duration of the shock
- Frequency of the current

Also, when considering a large population of subjects, one must also give consideration to the amount of individual variability of human beings, i.e., individual differences can and do have effects on how people react to stimuli.

Perception Limits.

Extensive work has been done (29) in the area of electric shock effects and results on the perception of 60 Hz currents are given by Figure 7-7. These tests are the results from 167 male subjects who were exposed to 60 Hz commercial power currents from hand to hand. The hand connections were over a large area so that these data would be appropriate to a person grasping a power tool or a pipe. The dotted line in Figure 7-7 is the estimated value for women using a factor of 2/3 (this factor was obtained from the let-go testing reported later). Figure 7-7 is used in the following manner: a percentage may be chosen in the vertical scale, i.e., 5 percent, and the current is read from the horizontal scale; 0.65 mA for men, 0.42 mA for women. This means that five percent of men will perceive a current of 0.65 mA or less and an equal percentage of women will perceive a current of 0.42 mA or less at 60 Hz. It should be mentioned that changes of frequency and electrode shape will change the limits, i.e., either increasing or decreasing the frequency will increase the perception current (the human body is most sensitive to currents in the 50-60 Hz region), decreasing the contact area would decrease the perception current (current from a needle point would be easier to sense), and current through a break in the skin is also easier to sense. Because

of their small size and therefore higher current densities within their bodies for the same total current, children are more sensitive to the electric currents. In November, 1970, the American National Standards Institute (ANSI) established a 0.5 mA maximum allowable leakage current for a two-wire portable device and a 0.75 mA maximum for heavy movable cord-connected appliances such as freezers and air conditioners.

Let-Go Limits. The "let-go" threshold is defined as the highest rms current flow in a hand-to-hand or hand-to-foot path during which the electrode held in a hand may be released. This threshold is of extreme interest for two reasons: it defines the minimum dangerous electric current for an uncontrolled situation and yet, experiments can and have been undertaken with human volunteers under controlled situations to identify values. In fact, Dalziel either alone or with assistance (30-32) was responsible for extensive experimental work in this area and is the only source of data on this phenomenon. Tests on 28 women and 134 men for let-go current at 60 Hz have been documented with the results shown in Figure 7-8 (31,32). In these tests, the subjects held and then released a test electrode consisting of a No. 6 copper wire. The circuit was completed by placing the other hand and foot on a flat brass plate or alternately by clamping a conduction band lined with a saline-soaked gauze on the upper arm. The experimental procedure consisted of first accustomizing the subjects to the sensations encountered and then applying the current and commanding a subject to release the wire. If the subject was successful, the current was increased until the subject could not release the wire. The end point was checked by several trails to eliminate the effects of fatigue. The points in Figure 7-8 were taken with the subjects' hands wet with salt water solution to secure uniform conditions and to reduce the sensation of burning that caused high current densities at tender spots and at the instant of releasing the electrode. Tests showed that the moisture conditions at the point of contact and the size of the electrodes had no appreciable effect on an individual's let-go current. Therefore, it is expected that the results stated may be used to predict let-go currents safely with practical accuracy. Figure 7-8 is used similarly to Figure 7-7 with the vertical scale giving the percentage of the population that can't let go at a certain current level. For example, 0.5 percent of the men tested could not release the electrode at a current of 9 mA while 0.5 percent of women could not release 6 mA of 60 Hz current. It should be noted that the curve for women is 2/3 the curve for men. This factor is used on the results of the perception tests previously conducted (29).

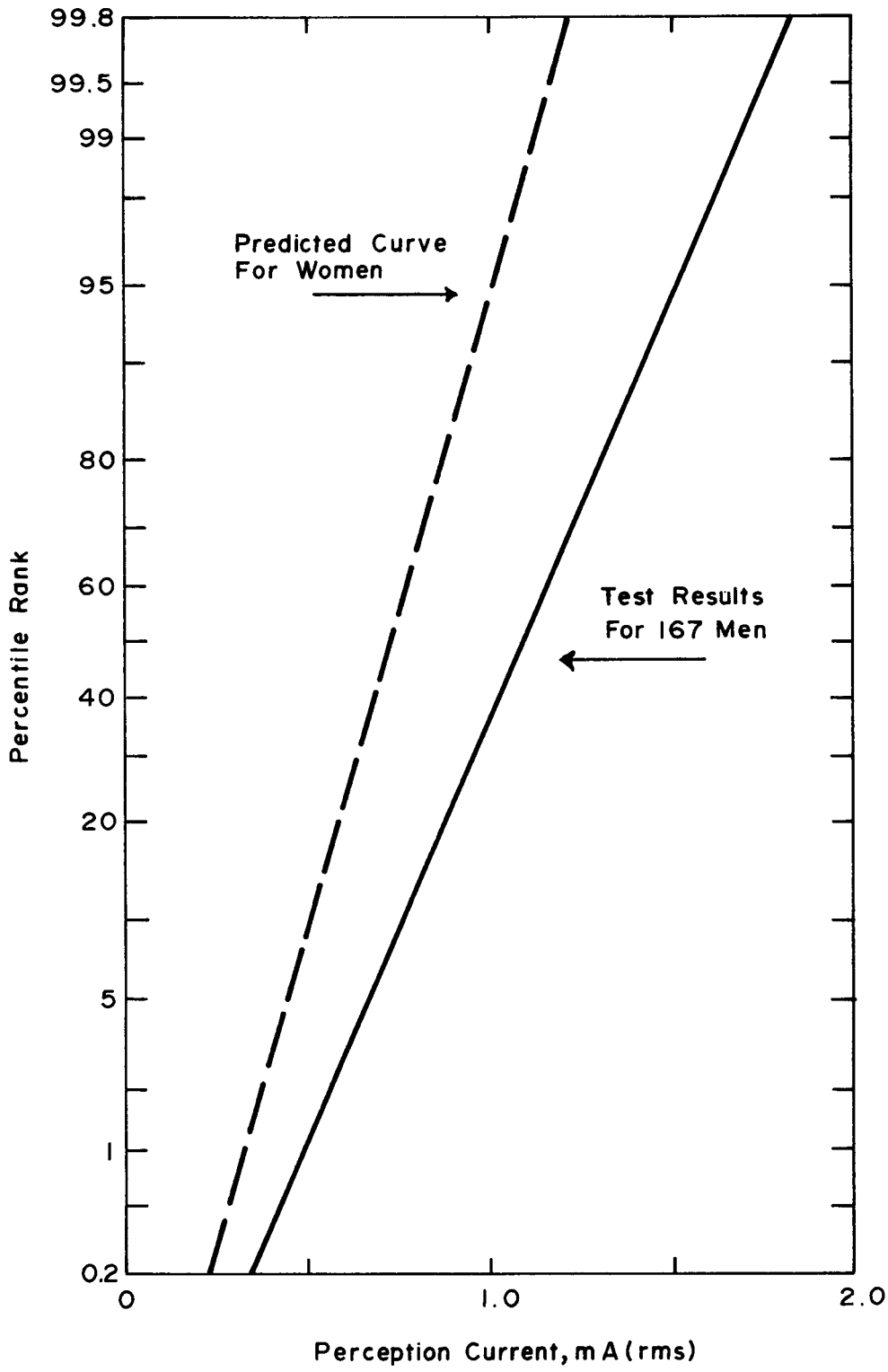

Fig. 7-7 60 HERTZ PERCEPTION CURRENTS

A few cautions are required in order to interpret this let-go data in the proper perspective. The let-go currents, in general, increased for both increasing size and increasing muscle development. This implies that extreme caution must be used in order to extend this data to children, invalids and other special populations. In fact, there has been a reported case of a four year old boy having been killed by being unable to release 8 mA of 60 Hz current (28). It has also been stated that 50 percent of the safe let-go threshold for adult males or 4.5 mA would be a reasonably safe 60 Hz limit for children (31).

The frequency of the applied voltage is also of critical interest, in that 50 and 60 Hz frequencies have the lowest let-go current. Frequencies both above and below this range have higher let-go thresholds. For example, the dc thresholds for let-go are five times higher and the thresholds at 2500 Hz are twice as high (32).

One last point should be made about the data presented in the let-go section -- that is, the data was developed using an experimental set-up that may not apply to all real situations. In the testing of the subject, the subject grasped the electrode and the current was applied with a current-limited voltage source. This is most typical of the case of a person grasping a tool and its insulation fails slowly or he increases the pressure of his grip and the current increases. In a different scenario, a person might brush against a source of voltage and tend to jump back, thus protecting himself. It seems that the results presented in Figure 7-8, therefore, are conservative on the side of safety.

Ventricular Fibrillation. Ventricular fibrillation is the condition of the heart wherein it no longer pumps blood, but just undergoes uncoordinated asynchronous contraction.

Ventricular fibrillation may be caused in a number of ways: it may be induced by chemicals, as a result of a surgical procedure, or it may also be caused by electrical current flowing through the heart (33-36).

Once a human heart undergoes ventricular fibrillation, it very rarely reverts spontaneously to a normal heart rhythm, even after the current initiating the fibrillation is removed. Special knowledge and equipment is needed within a few minutes of the onset of fibrillation in order to save the victim's life. Ventricular fibrillation is thought to be the most common mechanism of death from electrical accidents.

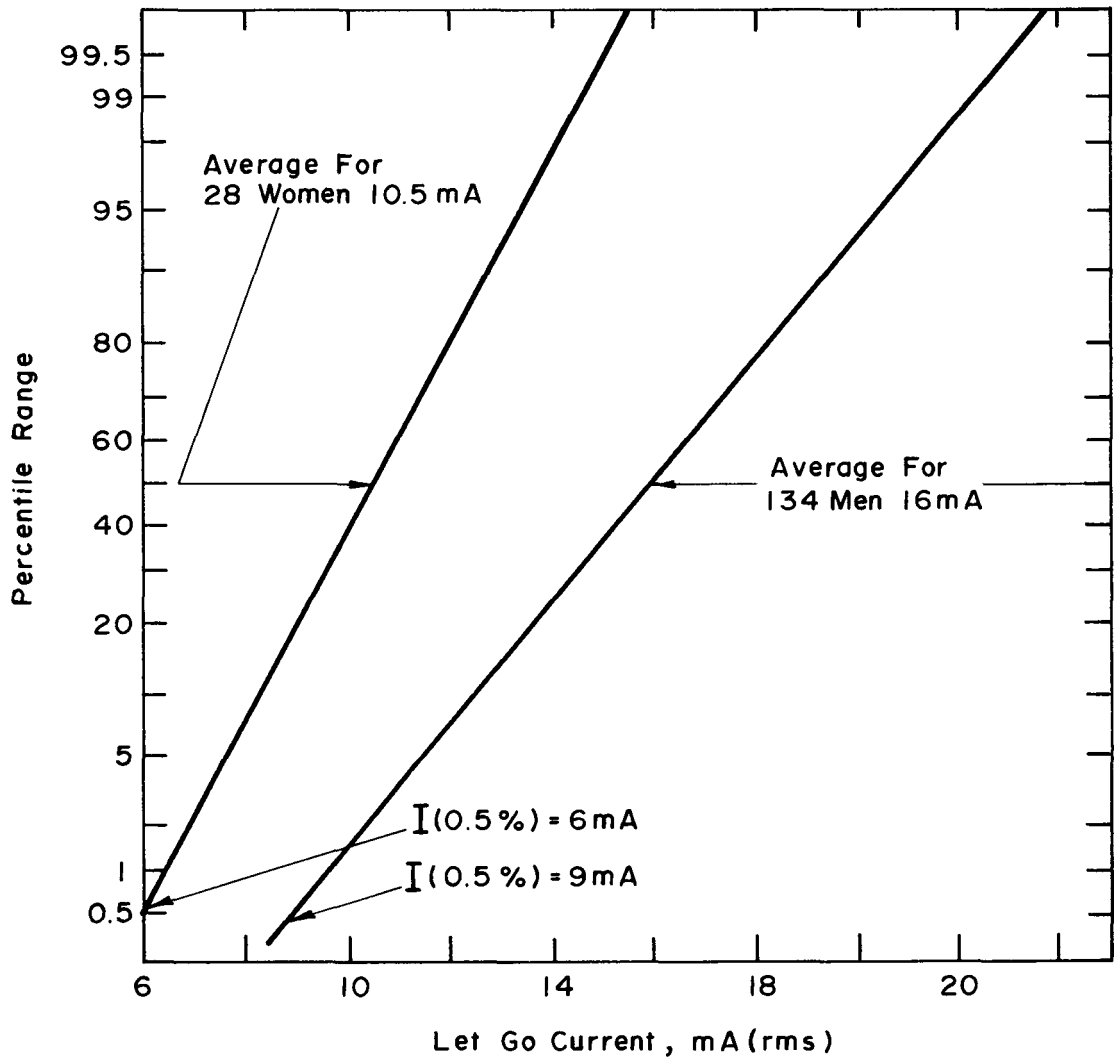

Fig. 7-8 60 HERTZ LET-GO CURRENTS

Ventricular fibrillation has received the most attention of all the electric shock effects. The reason for this is that fibrillation may be induced by methods other than electric shock and extensive research was required to design electric defibrillators used to treat this condition. Due to the extreme danger to the victims of ventricular fibrillation, experimentation on humans is impossible, so all data regarding this condition has been developed using experimental animals with circulatory systems similar to man's and with similar body weights. These animals included sheep, pigs and dogs, as well as smaller animals to study the effects as a function of body weight.

It was found that as the body weight of the test species increased, the fibrillation threshold increased. However, it has been noticed that the threshold tended to remain constant within the same species. The fibrillation thresholds have a frequency sensitivity similar to let-go, that is, 60 Hz is the most lethal frequency with dc and higher frequencies less dangerous.

Some of the first work reported in the United States was that by Ferris, et al (33). This work used calves, sheep, pigs, dogs, cats, rabbits and guinea pigs in an effort to identify minimum fibrillation thresholds for these species. As a result of this work, it was found that the heart is susceptible to ventricular fibrillation from electric shock for only about 20 percent of its cycle. It was also determined that strong counter-shocks, well in excess of the fibrillation threshold could restore an animal's heart that was undergoing ventricular fibrillation to normal functioning.

Additional studies (34) investigated both ventricular fibrillation in dogs as a function of the phases of the heart cycle, and also ac closed chest defibrillation. The results of this study produced data in the form of shock duration vs. current for fibrillation. Most recent investigations (37) continued studies into the effects of electric shock on the hearts of dogs.

Dalziel (35) analyzed the data from two of the above sources (33,34) and reduced the data to the following equations:

$$I(\tfrac{1}{2}\%) = \frac{165}{\sqrt{T}} \text{ ma rms} \qquad (7\text{-}26)$$

$$I(50\%) = \frac{446}{\sqrt{T}} \text{ ma rms} \qquad (7\text{-}27)$$

where

$I(\frac{1}{2}\%)$ is the 60 Hz current between major extremities that cause fibrillation in ½% or less of the population

$I(50\%)$ is the 60 Hz current between major extremities that causes fibrillation in 50% or less of the population.

T is the time in seconds the current is applied: this equation applies for times greater than 0.0083 sec and less than 5 sec.

Lee (38) also analyzed the data from the same sources and disagreed with some of the assumptions Dalziel used to formulate Eq. 7-26.

1. Dalziel used a typical human weight of 70 Kg; Lee felt that 50 Kg would be more typical.
2. The investigations used quadrupeds which would give different current distribution in the chest area than bipeds.
3. There has been some criticism (39) of Kowenhoven's results.

Lee suggested the following equation be used:

$$I = \frac{121}{\sqrt{T}} \begin{cases} 5s \\ 8ms \end{cases} \text{ mA} \qquad (7\text{-}28)$$

Dalziel and Lee (40) reviewed data available to date (1968) (33,34,37) and modified Eq. 7-28 to:

$$I = \frac{116}{\sqrt{T}} \begin{cases} 5s \\ 8ms \end{cases} \text{ for the 1/2\% non-fibrillation current.} \qquad (7\text{-}29)$$

which implies at least 99.5 percent of the population will not fibrillate with the defined current. Comment to the paper (A.W. Smoot) stresses that this limit applied to adults only, and care should be exercised before applying this data to children. Whitaker (41) presents a 60 Hz fibrillation limit for children of 30 mA. A summary of this data is presented in Figure 7-9 which is taken from (42).

Impulse Currents. Special considerations apply for shocks whose total time durations are much smaller than one heart cycle. These shocks are called impulse shocks and only very little data is available on their effects either on

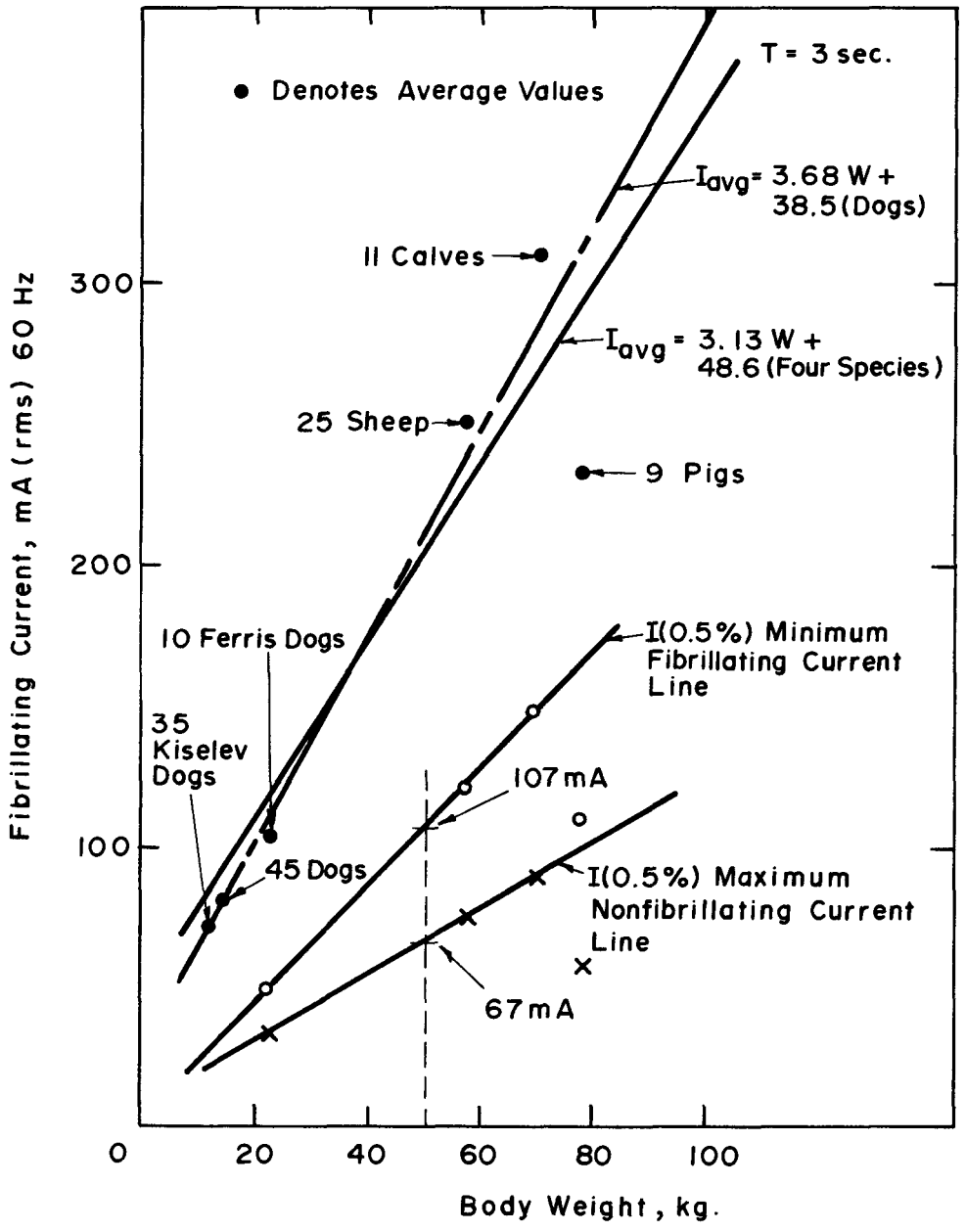

Fig. 7-9 SUMMARY OF FIBRILLATION DATA FOR VARIOUS SPECIES

experimental animals or humans. Dalziel (43) reviewed data developed from various experimenters and accident reports to develop the data presented in Figure 7-10. The curve in this figure corresponds to a formula of

$$I_p^2 T = 0.108 \tag{7-30}$$

where

I_p is peak current of a single exponential discharge, and

T is the time constant of the discharge.

Conversion of Eq. 7-30 to energy requirements assuming a decaying exponential for the current, gives

$$W_b = \int_o^\infty I^2 R_b dt \tag{7-31}$$

$$W_b = \int_o^\infty (I_p \; e^{-t/T})^2 \; R_b dt$$

$$= I_p^2 \; T \; R_b/2 = .054 \; R_b$$

where R_b is the victims body resistance.

It should be stated that while impulse shocks of less than the magnitude stated may not cause death, the side effects of these shocks are extreme and to be avoided when at all possible. The possible side effects of these shocks are: burns, headaches, semiconsciousness, intense muscle reactions, and unpleasant sensations, possibly persisting for long periods.

Respiratory Inhibition and Other Massive Current Effects. There have been cases recorded wherein the victims were exposed to massive current shocks (over the fibrillation threshold) and shown effects other than convulsion. This area has not been researched to any great depth but some facts are known. Current levels above the fibrillation current causes respiration to cease and to continue to cease after the current has been removed. It has been stated (34) that current paths in the spinal cord are most likely to cause this effect.

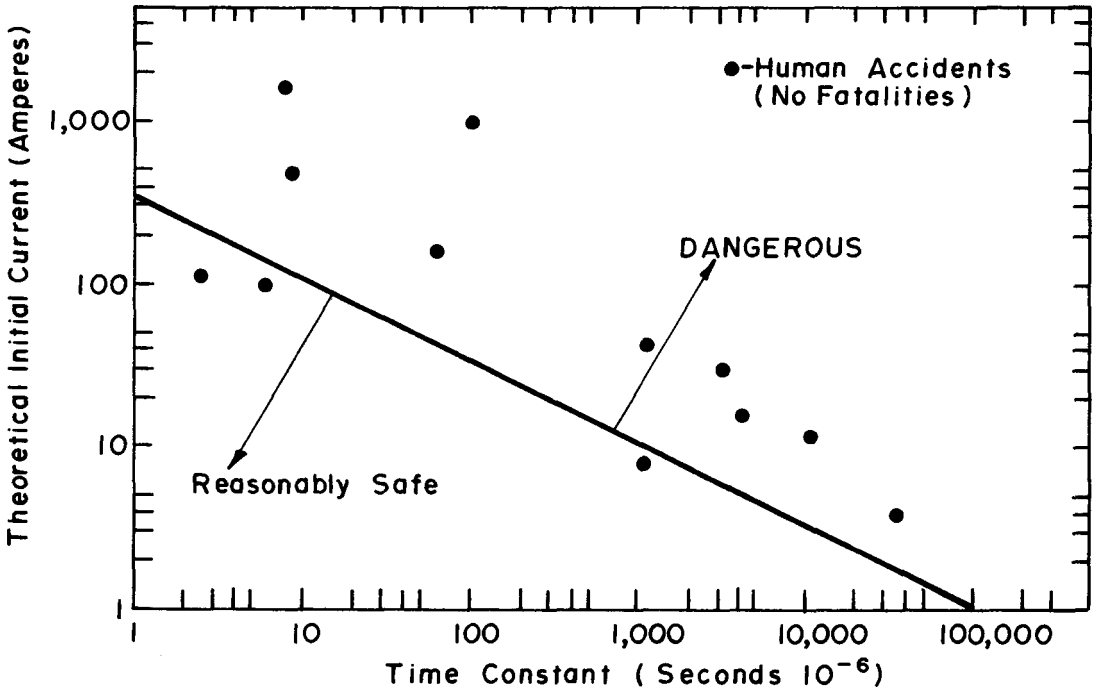

Fig. 7-10 IMPULSE CURRENT LIMITS

Extreme convulsions may also occur under these conditions, which although are rarely physically injurious to the victim, are very powerful and could be dangerous to those around him. Burns, both external and internal, may be experienced and in extreme cases may cause death.

Predicting Threshold Levels for Electric Shock Effects

The previous subsections dealt with identifying the effect of electric shock as a function of electric current. The problem that exists at this point is that voltages are the quantities usually measured or calculated for most systems, so these voltages must be converted into body currents. The problem in converting these voltages to currents is that the circuit resistances are highly variable both from a physiological and an operational viewpoint; that is, not only is the body resistance of a human highly variable, but there exists a wide range of possible scenarios that could change these conditions. For example, a worker's hands could be wet when he grasps an energized conductor or he could be wearing gloves, but the question of whether these gloves were cotton or rubber would also have a bearing on the problem.

Equivalent Circuit of a Person. Figure 7-11 shows an equivalent circuit for a human coming in contact with a conductor with a voltage on it. An explanation of the elements is as follows:

- Z_W is the total equivalent impedance of the worker (human). It is composed of the following impedances:

  --R_c is the contact resistance of the voltage source to the skin surface and will include the resistance of shoes, gloves, or clothes, if appropriate.

  --R_{sf} is the surface resistance of the person's skin. It is usually very large, and hence, may be eliminated from any analysis.

  --R_s is the skin resistance and may be quite high in the case of dry calloused hands, lower for sweat moistened hands or zero for broken skin.

  --R_b is the body resistance of a person.

Some commonly accepted values for the human related resistances are given in Table 7-5.

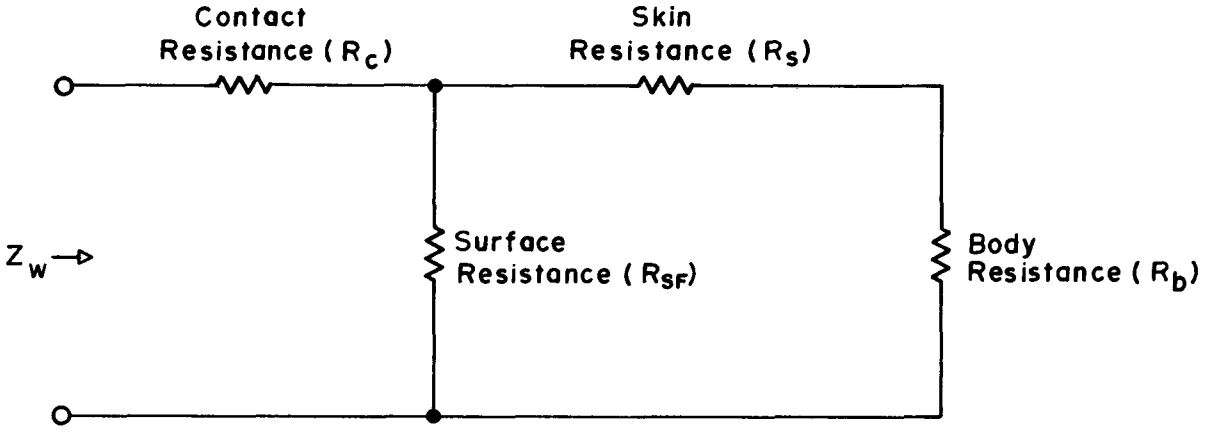

Fig. 7-11 EQUIVALENT CIRCUIT OF A HUMAN

Table 7-5

RANGES OF VALUES FOR HUMAN RESISTANCE VALUES

Circuit Element	Resistance Range (ohms)	Reference No.
Contact Resistance (R_c)	Low (bare feet and wet hands) to an open circuit (rubber gloves)	
Skin Resistance (R_s)	1000 Ω (office worker) 240,000 Ω (laborer)	(45,46) (resistance across head)
Body Resistance (R_b)	Approximately 500 Ω (will drop for higher current levels)	(46)

Predicting realistically the body impedance is almost impossible for the following reasons: the skin resistances are variable from person to person and for the same person at different times, and the contact and body resistances are a function of applied voltage; if the applied voltage is doubled, the current more than doubles.

The problem of the resistances is generally solved by assuming a total resistance, $R_s + R_b + R_c$, for a human, of 1500 Ω. This is a worst case analysis that takes into account the possibility of a person having skin directly in contact with the circuit or a bare skin contact with wet hands, respectively. Hence, R_c is assumed negligible.

Estimation procedures for determining potentially hazardous conditions can best be presented by example. Steady state ac coupling will be covered first. Two cases are of primary interest -- that of electrostatic coupling to above-ground pipelines, and electromagnetic coupling to buried pipelines.

Example - Electrostatic Coupling. The shock hazard for this situation may be evaluated from the equivalent circuit of Figure 8-2b. The severity of the hazard is determined by the current I_w, flowing in the worker impedance, Z_w.

The following quantities are defined:

- I_w = current flowing through worker - to be solved for.

- Z_w = worker impedance ≃ 1500 Ω.
- Z_m = grounding impedance for mitigation technique. No mitigation assumed initially ($Z_m = \infty$).
- C_{pg} = pipeline to ground capacitance. Its value is calculated from Eq. 4-9c. For the purpose of the present example, it will be assumed that a one-meter diameter (D) pipe rests at a height (H) of one meter above ground. It will be assumed that the length (ℓ) of pipe above the ground surface is 100 meters. Inserting these values into Eq. 4-9c, gives

$$\ell C_{pg} = \frac{2\pi\varepsilon_o \ell}{\ln(4H/D)} = \frac{2\pi(8.85 \times 10^{-12})100}{\ln(4.1/1)} = 4 \times 10^{-9} = .004\ \mu F \qquad (7\text{-}32)$$

- $Z_{pg} = (2\pi f C_{pg})^{-1} = 660\ K\Omega$
- I_{max} = maximum short circuit current that can be drained from the pipe. This value may be calculated from Eq. 4-9b. Using the parameters already chosen and also assuming a representative value for the open circuit voltage of the pipe ($E_T H$) equal to 10,000 volts, yields,

$$I_{max} = \omega \ell C_{pg}\ E_T H = 2\pi 60(.004 \times 10^{-6})\ 10^4 = .015 = 15\ mA \qquad (7\text{-}33)$$

Inspection of the equivalent circuit of Figure 8-2b shows that for the assumed condition, $Z_w << Z_{pg} << Z_m$, then

$$I_w \simeq I_{max} \quad . \qquad (7\text{-}34)$$

Estimation of the potential hazard may be made by referring to the data presented earlier in this section. For example, referring to Figure 7-8, it can be estimated that the calculated current level of 15 mA is such that approximately 40 percent of the male population will <u>not</u> be able to let go of the pipeline once they make contact.

Referring to Figure 7-8, it is seen that a more desirable current level would be, for example, 6 mA (I(0.5%) for women). To reduce I_w to this value requires the incorporation of a mitigation measure for which the grounding impedance, obtained from the circuit of Figure 8-2b is less than or equal to

$$Z_m \leq \frac{I_w Z_w}{I_{max} - I_w} = \frac{(6 \times 10^{-3})1500}{(15\text{-}6)10^{-3}} = 1000\ ohms \quad . \qquad (7\text{-}35)$$

Example - Electromagnetic Coupling. Shock severity for buried pipelines may be estimated using the equivalent circuit of Figure 8-14B in combination with Figure 7-11, and the values of Table 7-5, defining Z_w. For this case

- V_θ = induced voltage on pipeline without mitigation. A specific formula for calculation of this voltage cannot be given since its value is a complicated function of the power line and pipeline parameters and their interacting geometry. A representative worst case value will be assumed to be 100 volts.
- $Z_\theta = Z_o$ = pipeline characteristic impedance. This may be on the order of two ohms for representative pipelines and soils.
- Z_w = worker's impedance $\simeq$ 1500 ohms.
- Z_m = mitigation grounding impedance taken as infinite for first calculation.

From Figure 8-14,

$$I_w = \frac{V_\theta}{Z_o + Z_w\left(1 + \frac{Z_o}{Z_m}\right)} = \frac{100}{2 + 1500\,(1)} = 66.7 \text{ mA} . \qquad (7\text{-}36)$$

Comparison with previous results shows this level to be hazardous. Hence, a mitigation technique should be used.

Solving the above equation for Z_m gives

$$Z_m = \frac{I_w\,(Z_w Z_o)}{V_\theta - I_w(Z_o + Z_w)} \qquad (7\text{-}37)$$

To limit the worker current to 6 mA or less, as before, requires

$$Z_m \leq \frac{6 \times 10^{-3}\,(1500)\,2}{100 - 6 \times 10^{-3}\,(2 + 1500)} = 0.20 \text{ ohms.}$$

This impedance value is very low and, hence, imposes a much more stringent requirement on the mitigation method grounding impedance than that of the previous example.

Impulse Hazard Calculation. A worker touching an above ground pipeline that is charged through its capacitance to ground, C_{pg}, may experience an impulse type shock. An equivalent circuit which defines the shock hazard for this situation is shown in Figure 7-12. The shock hazard resulting from a current impulse is primarily a function of the energy absorbed by the body during the duration of the shock. The maximum allowable energy level is a function of the body resistance and has been defined by Eq. 7-31. The potential shock hazard may be found by determining the energy stored in the pipe-to-ground capacitance and comparing this value to that of Eq. 7-31. (This is a worst case condition which assumes $R_c << R_b$).

Example - Impulse Hazard. The energy stored in the pipeline capacitance may be found from Eq. 4-9a, namely,

$$W = \ell C_{pg} |E_T H|^2 \text{ joules} \tag{7-38}$$

The values used in the previous electrostatic example may be used here. That is:

$$\ell C_{pg} = 4 \times 10^{-9} \ \mu F$$

$$E_T H = 10^4 \text{ volts}$$

Substituting these values into Eq. 7-38 gives

$$W = 4 \times 10^{-9} \ (10^4)^2 = 0.4 \text{ joules}$$

From Eq. 7-31 assuming a body resistance of 1500 ohms it is found that the tolerable energy level in the body is

$$W_b = .054 \ (1500) = 81 \text{ joules}$$

Since $W_b > W$, a serious shock hazard does not exist. If, on the other hand, $W > W_b$ then mitigation would be necessary. An obvious means would be to ground the pipeline through a impedance Z_m, which would act essentially as a discharge path

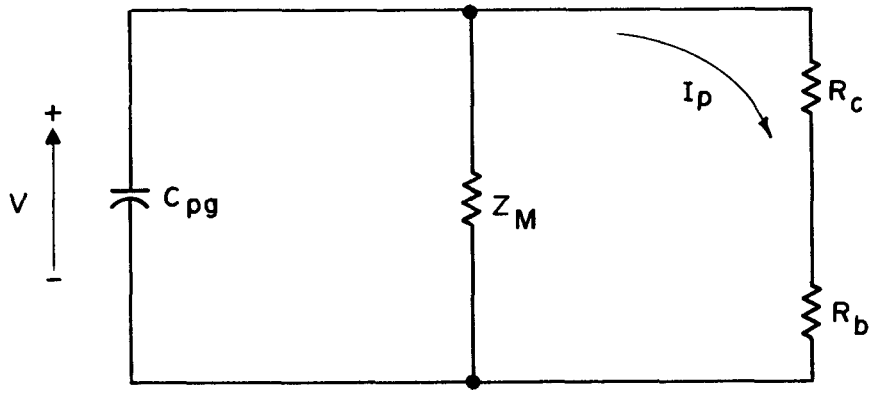

Fig. 7-12 IMPULSE CURRENT CIRCUIT

for the pipe to ground capacitance, and hence, its value would not be critical. Generally, a more critical grounding requirement exists with regard to limiting the steady state current flow through the body, and required grounding impedance as calculated by Eq. 7-35 is satisfactory also for mitigation of an impulse waveform.

REFERENCES

1. Bruckner, W.H. "The Effects of 60 Cycle Alternating Currents on the Corrosion of Steels and Other Metals Buried in Soil." Engineering Experiment Station Bulletin 470, University of Illinois, Urbana, Illinois, Nov. 1964.

2. Hewes, R.W. "Potential Problems on Coated Pipelines Due to Proximity to High Voltage Power Lines." Presented at AC Corrosion Symposium, North Central Region Conference of NACE, Chicago, Sept. 30, 1968.

3. Berry, W.E., Et al. Interference Mitigation in Pipelines. Battelle Memorial Institute, Columbus, Ohio. Project Sanguine, PME-117-21- Contract No. N00039-69-C-1569, Final Report, Nov. 26, 1969 (unclassified).

4. Collings, L.V. "The Effect of Alternating Current on Pipeline Corrosion Coatings and Cathodic Protection." Presented at Corrosion '76 Conference, March 22-26, 1976, Houston, Texas.

5. Williams, J.F. "Corrosion of Metals Under the Influence of Alternating Current." Presented at 1965 Joint Northeast-North Central NACE Regional Conference, Pittsburgh, Pennsylvania, Oct. 4-6, 1965.

6. Fuchs, W., Et al. "Investigations Concerning AC Corrosion of Iron as a Function of Current Density and Frequency." Reprint from GWF Das Gas-und Wasserfach, Vol. 99, Jan. 1958, No. 214 (Water-Liquide Waste).

7. Amy and Munios. Corrosion Caused by Alternating Currents. Dev. Gen. Elect., Vol. 66, 1957.

8. Bunn, J.S. Alternating Current Corrosion. Panhandle Eastern Pipeline Co., Kansas City, Missouri, Dec. 2, 1968.

9. Jahnke and Emde. Tables of Functions. Dover Publication, New York, 1945.

10. Devay, J. and Meszaros, L. "Mathematische Untersuchungen Über Die Wirkung Des Wechselstromes Auf Die Korrosion I." ACTA CHIMICA (HUNG.), Vol. 43, No. 1 AKADEMIAI DIADO, Budapest, 1965, pg. 25-31.

11. Devay, J. and Meszaros, L. "Mathematische Untersuchungen Über Die Wirkung Des Wechselstromes Auf Die Korrosion II." ACTA CHIMICA (HUNG.), Vol. 44, No. 4, AKADEMIAI KIADO, Budapest, 1965.

12. Jones, D.A. and Greene, N.D. "Electrochemical Measurement of Low Corrosion Rates." Corrosion. Vol. 22, No. 7, July 1966, pp. 198-204.

13. Hamlin, A.W. "Operation of Gas Pipelines Adjacent to Electric Facilities." Paper No. (73-T-18), American Gas Association Operating Section Proceedings, pp. T-100 to T-102, 1973.

14. Darate, J.P., "Insulating Joints in Long Pipelines." Gas. pp. 124-125, Sept. 1961.

15. Peabody, A.W. and Verheil, A.L. "The Effects of High Voltage Alternating Current (HVAC) Transmission Lines on Buried Pipelines." Paper No. PLI-70-32, presented to the IEEE/IGA Petroleum and Chemical Industry Conference, Tulsa, OK., Sept. 15, 1970.

16. Kulman, F.E. "Effects of Alternating Currents in Causing Corrosion." Paper presented at the Corrosion Session of the American Gas Association Operating Section Distribution Conference in New Orleans, May 9, 1960.

17. Sanders, W.S. "Protection of Insulating Joints on Gas Pipelines." Paper No. BMC-63-37, presented at the 1963 American Gas Association Operating Section Distribution Conference.

18. Cherney, E.A. "Pipeline Voltage Hazards on High Voltage AC Transmission Line Rights-of-Way." Materials Protection and Performance. Vol. 14, No. 3, March 1975.

19. Riordan, M.A. "Electrical Effects of AC Transmission Lines on Pipelines." Materials Protection and Performance. Vol. 11, No. 10, Oct. 1972.

20. Comsa, R.P. and Luke, V.M. "Transient Electrostatic Induction by EHV Transmission Lines." IEEE Transactions on Power Apparatus and Systems, Vol. PAS-88, No. 12, pp. 1783-1787, Dec. 1969.

21. Collings, L.V. "The Effect of Alternating Current on Pipeline Corrosion, Coatings, and Cathodic Protection." Presented at the International Corrosion Forum Devoted Exclusively to the Protection and Performance of Materials, March 22-26, 1976, Hyatt-Regency Hotel, Houston, Texas.

22. The Aerospace Corporation for the Bureau of Land Management. "Technical Compatibility Factors for Joint-Use Rights-of-Way." U.S. Dept. of Interior. Feb. 1, 1976, Contract No. 08550-CT5-5.

23. Nose, B.T. "Induced AC Voltage on 36" Transmission Lines 4000 and 4002 at Fontana Station." Engineering Department, Southern California Gas Company, Engineering Job C-74-13A.

24. Siegfried, C.G. "Multiple Use of Rights-of-Way for Pipelines." Paper No. 71-7-29, American Gas Association Operating Section Proceedings. pp. T-146, 1971.

25. Boone, H. "Electrical Hazards in Gas Distribution Systems." Paper No. 73-D-46, American Gas Association Operating Section Proceedings. 1973.

26. Maurice, R.A. "Response of Pipeline Networks to AC Transmission Effects." Materials Protection and Performance. Vol. 11, No. 11, pp. 41-44, Nov. 1972

27. Berry, W.E., Gahm, W.L., Et al. Final Report on Interference Mitigation in Pipelines. Battelle Memorial Institute, Columbus Laboratories (to Naval Electronics System Command, Project Sanguine), Columbus, Ohio, Nov. 1969.

28. Volheye, W.R. "Oregon's First Death From an Electric Fence." IAEI News Bulletin. Vol. 12, No. 70, 1940.

29. Dalziel, C.F. "The Threshold of Perception Currents.' AIEE Trans. Power Apparatus and Systems. Vol. 73, pp. 990-996, August 1954.

30. Dalziel, C.F., and Massolia, F.P. "Let-Go Currents and Voltages, Electric Arc and Resistance Welding -- IV." AIEE Special Publication. pp. 87-100, (July 1954). AIEE Transactions Paper No. 56 -- III presented at AIEE Winter Meetings, New York, N.Y., January 31, 1956.

31. Dalziel, C.F. "Effect of Waveform on Let-Go Currents." AIEE Transactions (Electrical Engineering), Vol. 62, pp. 739-744, December 1943.

32. Dalziel, C.F., Ogden, E., and Abbott, C.E. "Effect of Frequency on Let-Go Currents." AIEE Transactions (Electrical Engineering), Vol. 62, pp. 745-750, December 1943.

33. Ferris, L.P., King, B.G., Spence, P.W., and Williams, H.B. "Effect of Electric Shock on the Heart." AIEE Transactions (Electrical Engineering). Vol. 55, pp. 490-515, May 1936.

34. Kowenhoven, W.B., Knickerbocker, G.G., Chesnut, R.W., Milnor, W.R., and Sass, D.J. "AC Shocks of Varying Parameters Affecting the Heart." AIEE Transactions (Communication and Electronics), Vol. 42, pp. 163-169, May 1959.

35. Dalziel, C.F. "Threshold 60 Hertz Fibrillating Currents." AIEE Transactions (Power App. Syst.). Vol. 79, pp. 661-673.

36. Knickerbocker, G. Guy. "Fibrillating Parameters of Direct and Alternating (20 Hz) Currents Separately and in Combination - An Experimental Study." IEEE Transactions on Communications, Vol. COM-21, #9, pp. 1015-1027, September 1973.

37. Kiselev, A.P. "Threshold Values of Safe Current of Commercial Frequency." Probl. of Elec. Equip. Elec. Supply and Elec. Measurements. Vol. 171, pp. 47-58, 1963 (Russian).

38. Lee, W.R. "Death from Electric Shock." Proc. IEEE. Vol. 113, No. 1, pp. 144-148, Janaury 1966.

39. Lee, W.R. International Colloquium on Electrical Accidents. CIS, LIO, Geneva, pp. 45, 1964.

40. Dalziel, C.F. and Lee, W.R. "Reevaluation of Lethal Electric Currents." IEEE Transactions on Industrial and General Application. Vol. IGA-4, No. 5, pp. 467-476, September/October 1968.

41. Whitaker, H.B. "Electric Shock as it Pertains to the Electric Fence." Bulletin of Research 14. Chicago Underwriters Laboratories, Inc., p. 11, 1936.

42. Dalziel, C.F. "Electric Shock Hazard." IEEE Spectrum. pp. 41-50, February 1972.

43. Dalziel, C.F. "A Study of the Hazards of Impulse Currents." AIEE Transactions Power Apparatus and Systems. Vol. 72, pp. 1032-1043, October 1953.

44. Hodgkin, H.C., Langworthy, O., Kowenhoven, W.B. "Effect on Breathing of an Electric Shock Applied to the Extremities." IEEE Power Engineering Society. Paper presented at Winter Meeting, New York, N.Y., February 4, 1972.

45. Smith, H.P. "Effects of Electric Shock on Man." Electrical Times. pp. 85-88, January 18, 1962.

46. Lowenblock, H., Morgan, J.E. "The Human Skin as a Conductor of 60 Hertz Alternating Current of High Intensity, Studied on Electroshock Patients." The Journal of Laboratory and Clinical Medicine. Vol. 28, pp. 1195-1198, 1943.

Section 8

TECHNIQUES FOR MITIGATION OF 60 Hz COUPLING TO ADJACENT PIPELINE SYSTEMS

INTRODUCTION

This section discusses the various mitigation techniques which can be employed to reduce 60 Hz electrostatic, electromagnetic and ground current coupling to an adjacent pipeline system consisting of buried and above-ground sections. The techniques include those which have been used extensively in the past with good results. In addition, this section includes a group of new techniques for overall joint corridor design and pipeline grounding which have been developed specifically for this book by application of the theory of Section 3 and by field test experiments.

This section is organized by separating the discussion of electrostatic, electromagnetic and ground current coupling mitigation into three distinct subsections. Recognizing that a pipeline can be subject to all three types of coupling at the same time, a discussion of what is called multi-mode coupling is provided for unification of the techniques. Certain mitigation techniques, such as the use of independent ground beds and ground mats, which can be beneficial for all types of coupling are discussed in detail in one subsection and referenced briefly in the others.

REVIEW OF THE CONSEQUENCES OF AC COUPLING

Electrostatic (Capacitive) Coupling Mode

During the construction of a pipeline, it is possible that long sections of pipe may rest above the ground surface. If the pipe is located near a high voltage power line, it can assume a large voltage to ground. The voltage is due to the capacitances between the power line conductors and the pipe, and between the pipe and ground, which form a capacitive voltage divider. A pipeline worker accidentally grounding the pipe through his body faces two hazards.

1. The energy stored in the pipeline capacitance to ground is discharged through the body of the worker in the form of an exponentially decaying pulse. If there is sufficient stored energy,

this discharge can be painful or even fatal (1). Additional hazard arises from the possible ignition of volatile liquids such as gasoline stored near the point of discharge (2).

2. If contact with the pipe is not broken, a steady-state current flows through the body of the worker. If the current is large enough, injury or death can result (3).

Electromagnetic (Inductive) Coupling Mode

Voltages and currents can be induced on a buried or above-ground pipeline by the coupling of the electromagnetic fields generated by a nearby power line. The following pipeline and personnel hazards can be present due to this coupling mode.

1. The induced ac voltage can enhance the corrosion of a non-protected pipeline by an electrochemical effect.

2. Cathodic protection devices, communications equipment, and other types of electronic equipment associated with monitoring the pipeline behavior can be upset by high levels of induced ac voltage.

3. A pipeline worker accidentally grounding the pipe through his body faces the hazard of electric shock due to steady current flow, if contact with the pipe is not broken. Like the electrostatic coupling case, injury or death can result if the current is large enough.

Ground Current (Conductive) Coupling Mode

When a ground current condition occurs on an electric power line during switching surges, lightning strikes, and faults, a portion of the current is discharged from each structure (and from the counterpoise system, if present) to earth. The possibly high current densities adjacent to the footings can generate high ac potential gradients in the surrounding soil. The following pipeline and personnel hazards can be present, due to this coupling mode.

1. If a buried, coated pipeline lies within the field of influence of the ground current, a high voltage can be impressed across the pipe coating, since the underlying steel is at a potential representative of remote earth. This voltage can damage the coating at existing imperfections by creating arcs. At coating potentials exceeding 15 kV, puncture of the pipe steel itself is possible (4).

2. If the grounding system of an above ground or buried pipeline lies within the field of influence of the ground current, a high voltage can be applied to the adjacent pipeline sections. This means that a whole pipeline system under construction (above ground) can be elevated to a dangerous potential if a single pipeline ground is influenced by ground current. Similarly, buried pipe sections within about 10 km of the influenced pipe ground can present a hazard.

MITIGATION OF ELECTROSTATIC COUPLING

Spacing of the Pipeline from the Power Line

Where possible, electrostatic coupling of a power line to an adjacent above-ground pipeline can be mitigated simply by locating the pipeline as far as possible from the affecting power line. As shown in Section 4, the intensity of electrostatic coupling is directly dependent upon the magnitude of the transverse electric field generated by the power line. The method of McCauley (5) as extended by Procario and Sebo (6) was shown to be useful for estimating the variation of this electric field with distance from the power line. This method uses straight lines to approximate the exactly computed curves of transverse electric field vs distance from several common phase conductor configurations. These straight lines represent upper bounds for the expected electric field, and thus, can be used to estimate the worst-case electrostatic coupling at each distance from the power line.

From Figure 4-3 it is seen that electrostatic coupling decreases markedly past the McCauley cut-off distance, D_{co}, falling off approximately as the inverse square of the separation. Thus, if possible, it is desirable to maintain a separation of at least D_{co} between a power line and an above-ground pipeline to achieve a significant reduction of the level of electrostatic coupling.

Pipeline Grounding

As shown in Figure 8-1, the hazards due to ac coupling to an above-ground pipeline can be mitigated by grounding long pipe sections using independent ground beds, and by installing ground mats at points of possible human contact with the pipe. Basic considerations for the application of these techniques are now summarized.

Independent Ground Beds. Mitigation of the electrostatic discharge pulse through a pipeline worker touching an above-ground pipeline can be achieved by grounding the pipeline through an impedance, Z_m, having a much smaller magnitude than that of Z_{pg}, the impedance of the pipeline-to-ground capacitance. Reference (7) suggests that a value of $|Z_m|$ as large as 10^5 ohms is low enough to meet this goal. However, this value is much too large to be of use in reducing the shock hazard due to steady-state current flow. As shown in Figure 8-2, mitigation of this hazard requires that $|Z_m|$ be much less than $|Z_w|$, the impedance of the current path through the body of the pipeline worker. In this way, Z_m can divert

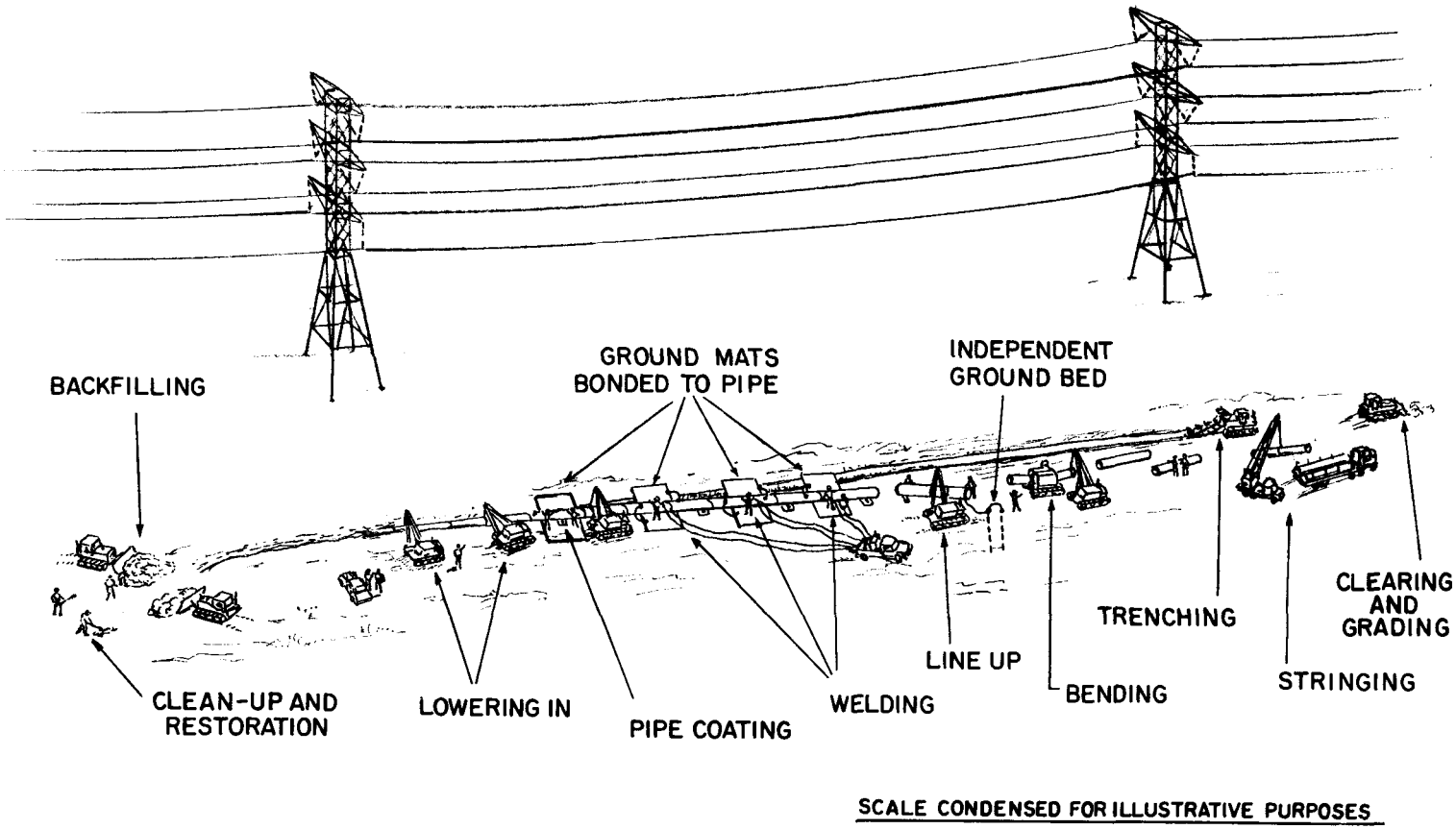

Fig. 8-1. APPLICATION OF GROUNDING TECHNIQUES FOR MITIGATION OF ELECTROSTATIC COUPLING TO A TYPICAL PIPELINE UNDER CONSTRUCTION

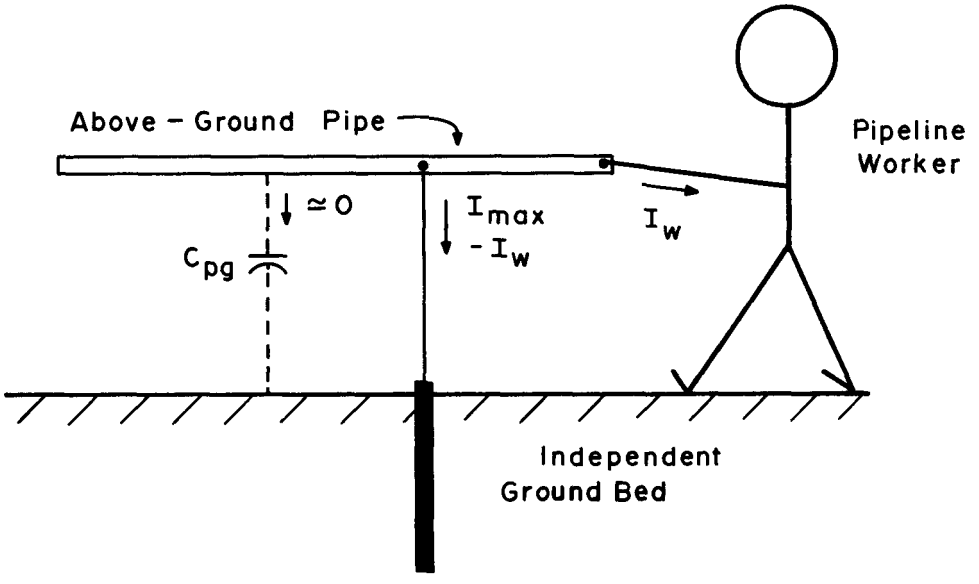

(a) Pipeline Worker Geometry

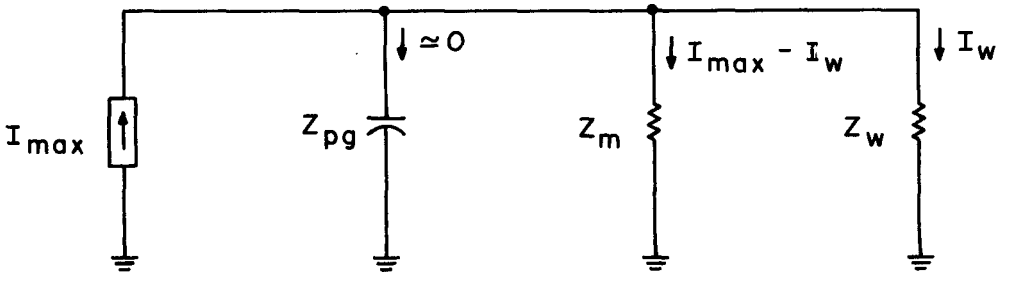

(b) Equivalent Circuit

Fig. 8-2 MITIGATION OF ES SHOCK HAZARDS BY PIPELINE GROUNDING

most of the shock current sourced by the high impedance, Z_{pg}, away from the worker in a current divider action. The required value of Z_m is given by

$$Z_m = \frac{I_w}{I_{max} - I_w} Z_w \qquad (8\text{-}1a)$$

where I_{max} is the maximum steady state current available from the pipe, and I_w is the maximum permissible steady state current through the worker.

To estimate the value of Z_m needed to mitigate the worst case, I_w is taken as the current level, 9 mA (8) at which 0.5% of the men tested cannot achieve let-go, and Z_w is taken as the wet skin body impedance, 1500 ohms (9), resulting in

$$Z_m(\text{worst case}) \simeq \frac{13{,}500}{I_{max}} \text{ ohms} \qquad (8\text{-}1b)$$

where I_{max} is given in mA and is assumed to be much greater than I_w(worst case) = 9 mA.

Z_m can be realized by installing one or more vertical or horizontal grounding conductors, forming a ground bed independent of the power line ground, as discussed in a later subsection.

The installation of independent ground beds for mitigation of electrostatic coupling can lead to the inadvertent generation of pipeline voltage hazards due to electromagnetic and ground current coupling. This possibility is illustrated in Figure 8-3. After grounding the pipe at point A with impedance $Z_{m,A}$, an electric shock hazard at point W exists due to the inductively-coupled voltage, $E_o L_{AW}$, developed along the length of pipe between the ground and the worker. Addition of a ground at the intermediate point, B, serves to reduce (but not eliminate) this hazard.

Further, grounding the pipe at point A or B can lead to elevation of the pipe potential if the ground systems are subject to earth current flow. Here the earth current results in the ground systems being raised to the potentials $V_{g,A}$ and $V_{g,B}$, respectively. Additional hazard exists if the worker stands in an earth current area and is himself elevated to the potential $V_{g,W}$ relative to remote earth, and likely, the pipe. As computed later in this section, earth potentials can range above 100 volts for representative values of ground resistivity, earth current magnitude, and distance from the current grounding area.

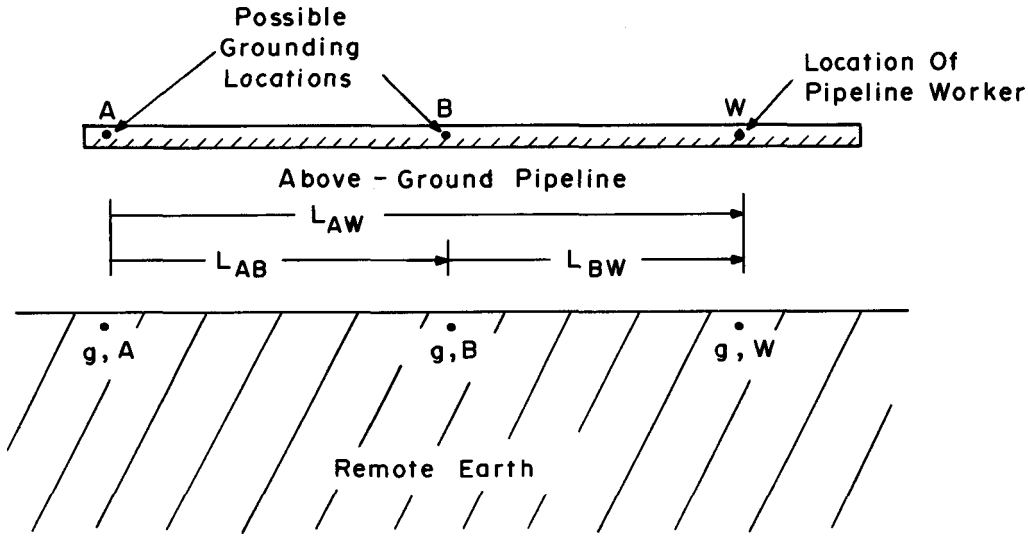

(a) Pipeline - Worker Geometry

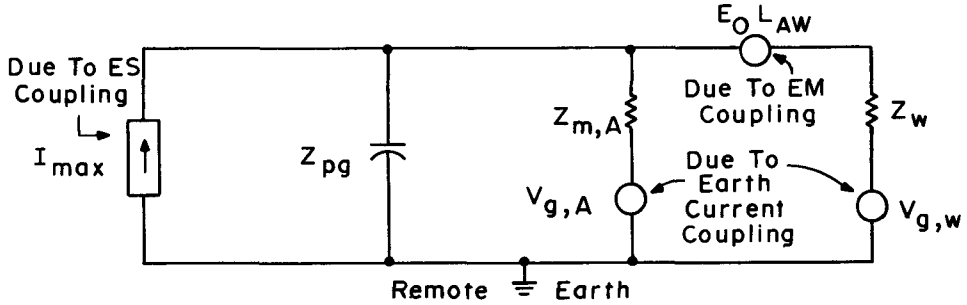

(b) Equivalent Circuit After Grounding Point "A"

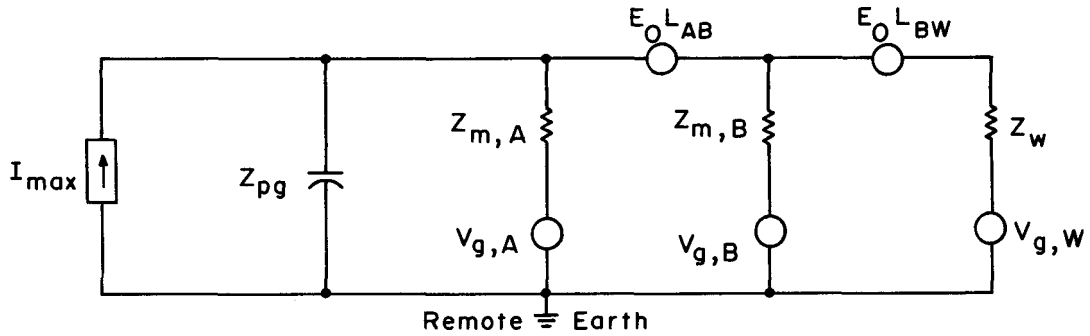

(c) Equivalent Circuit After Grounding Points "A" And "B"

Fig. 8-3 INADVERTENT GENERATION OF MULTI-MODE COUPLING BY PIPELINE GROUNDING

Problems associated with installing independent ground beds can be mitigated or avoided by proper positioning of the beds relative to the power line, as illustrated in Figure 8-4. The goal of this positioning is to minimize the earth potential at the location of each ground bed, and the electromagnetically-induced pipeline voltage between adjacent ground beds.

Inadvertent ground current coupling can be minimized by installing the ground beds outside the zone of hazardous earth potentials occurring during power line faults. The boundary of this zone is a function of the fault current capacity of the power line, the nature of the power line grounding system (structure footings and/or counterpoise), and the earth resistivity. The variation of earth potential with distance from the fault point is discussed later in this section. In general, ground beds should be installed midway between power line structures and as far as practicable from the power line. In this way, the earth potential at each ground bed is low at all times, and a worker contacting the pipe during a ground current condition can be endangered only if his local earth potential is high, i.e., if he is located in a ground current area. Because most of the above-ground pipeline is probably outside of ground current areas, such a placement of ground beds provides for the protection of the maximum number of pipeline personnel.

Inadvertent electromagnetic coupling can be reduced by installing the ground beds at intervals of the power line span length. By selecting an ac impedance value of about 30 ohms for each bed, a net pipe leakage resistance to remote earth of about 10 ohms/km is achieved, which is comparable to the leakage resistance of a well-insulated buried pipeline. In effect, the periodic grounding, or impedance loading on an above-ground pipe results in an inductive coupling problem similar to that which would exist if the same pipe section were buried.

Mitigation is completed by installing a low impedance ground at each end of the pipe to reduce the voltage peaks which result there. The ac impedance of these pipe-end ground beds should be 2 ohms or less to achieve an effective overall potential reduction.

Bonding to Structure Grounds. At times, it may seem convenient to achieve the grounding of a pipeline by connecting it to nearby power line structure grounding systems. However, this procedure is not always recommended because of personnel and pipeline hazards which may result during fault conditions of the power line.

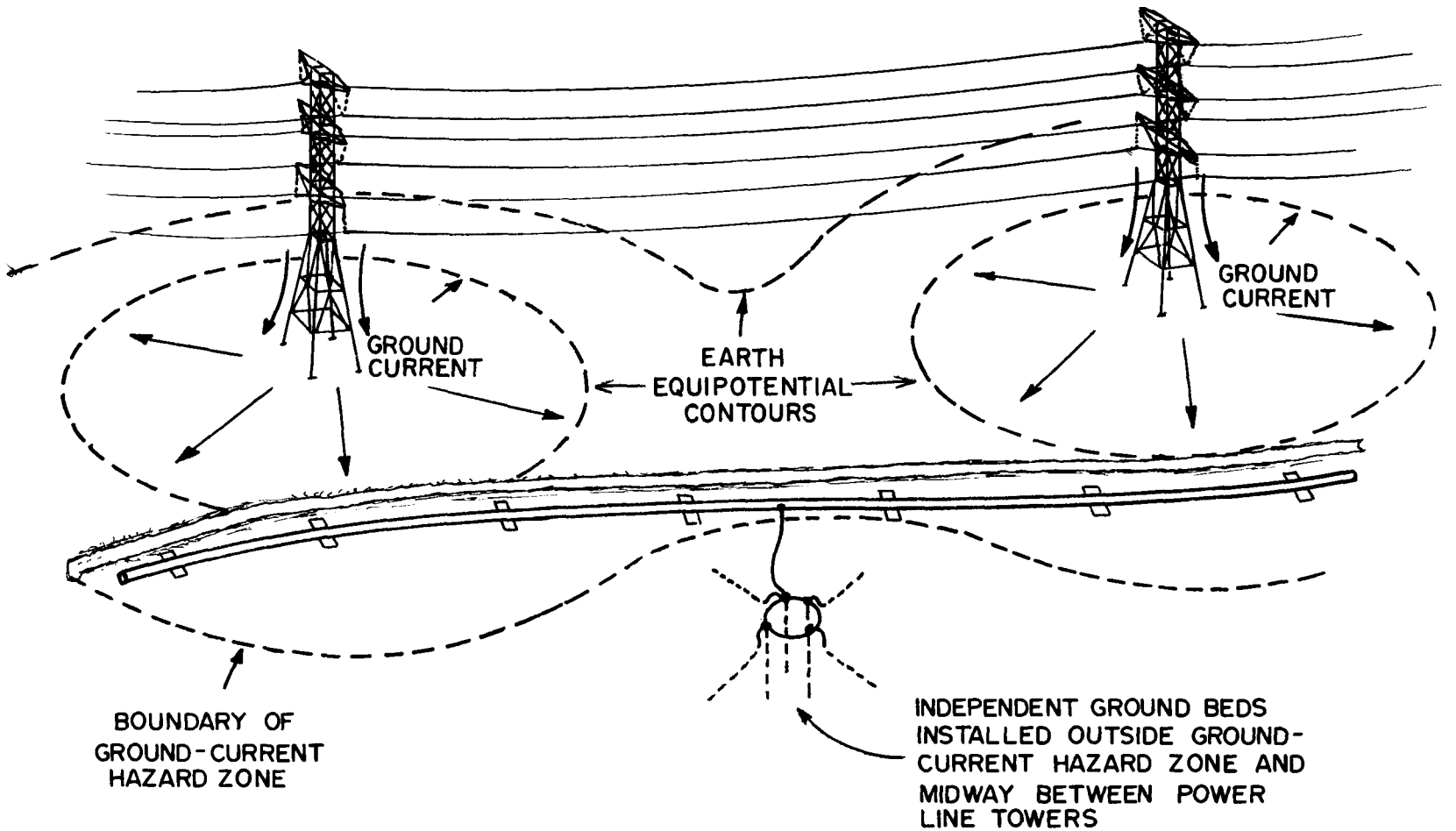

Fig 8-4 PLACEMENT OF INDEPENDENT GROUND BEDS FOR MITIGATION OF INADVERTENT MULTI-MODE COUPLING TO AN ABOVE-GROUND PIPELINE

Connection of an above-ground or buried pipeline to a power line ground can result in the elevation of the pipeline potential to dangerous levels during power line fault conditions. The flow of fault current to ground through the affected power line towers results in the tower footings being placed at a high potential with respect to remote earth, and the application of this potential to any metal structure that is connected to the tower footings. As computed later in this section, this potential can range above 1000 volts for representative values of earth resistivity and fault current magnitude. This high voltage can be applied to the entirety of an above-ground pipeline connected to a tower footing, endangering pipeline workers or other personnel contacting the pipe metal during the fault. The resulting hazards can be mitigated only by providing ground mats, as discussed in the following subsection, at each location of possible human contact with the pipeline.

Connection of buried pipeline sections to a power line ground can also result in puncture of either the pipeline coating or steel during power line fault conditions. The flow of fault current to remote earth is channeled through the buried pipeline, which acts as a virtual counterpoise for the power line because of its bonding to the tower footings. At points somewhat removed from the affected towers, the fault current carried by the pipeline can jump off to the surrounding low potential earth. Fault current jump-off points are marked by pipeline coating punctures and possibly even pipeline steel punctures (if the current densities are high enough). Mitigation of this hazard is possible only by avoiding any direct connections between the buried pipeline and the power line grounds.

Ground Mats. Mitigation of multi-mode coupling to a pipeline under construction can be realized easily and effectively by installing ground mats at all worker locations. These mats, bonded to the pipe, serve to reduce touch and step voltages in areas where persons can come in contact with the pipe. These mats can be portable steel mesh grids laid on the ground at welding positions, and connected with a cable to the pipe. At permanent exposed pipeline appurtenances, such as valves, metallic vents, and corrosion control test points, ground mats can be constructed of strip galvanic anode material buried in a spiral pattern just below the surface and connected to the pipeline electrically. By using galvanic anode material, such mats reinforce any cathodic protection systems on the pipeline rather than contribute to the pipeline corrosion problem, as would be the case if copper grounding were used.

With mats so installed and connected, the earth contacted by the mat is at virtually the same potential as the pipe. In this way, a worker touching the pipe is assured that the potential appearing between his hands and feet is only that which is developed across the metal of the mat, regardless of the mode of ac interference affecting the pipe. This effective shunting of the worker by a metal conductor provides protection for very severe cases of coupling, such as occur during lightning strikes and faults. It is especially useful for pipes subject to simultaneous interference by electrostatic, electromagnetic, and earth-current coupling.

Ground mats should be designed large enough to cover the entire area on which persons can stand while either touching the pipe or contacting it with metal tools or equipment. Each mat should be bonded to the pipe at more than one point to provide protection against mechanical or electrical failure of one bond. Step potentials at the edges of each mat can be mitigated by providing a layer of clean, well-drained gravel beneath the mat and extending the gravel beyond the perimeter of the mat. This serves to reduce the conductivity of the material beneath the mat, and to provide a buffer zone between the earth and the ground mat.

Power Line Screening Conductors

Studies have been performed which evaluated the electrostatic coupling mitigation effectiveness of installing grounded screening conductors under the phase wires of horizontal-configuration power lines (5). Two different screen conductor positions were examined. In the first case, the conductor was erected at the horizontal distance from the center of the phase at which peak electrostatic effects occur. In the second case, the conductor was erected just inside the edge of the power line right-of-way. In each case, a 500 kV line operating at 1.1 p.u. was used. The phase wire height was 13.72 m (45 ft), and the phase spacing was 8.69 m (28.5 ft). The maximum electrostatic field was found to occur at about 12.0 m (40 ft) from the center phase without ground wires.

For the first case, a 9.5 mm (0.375 in.) diameter screen conductor was placed 12.0 m from the center phase and its height was varied between 6.1 m (20 ft) and 9.1 m (30 ft). It was found that the height of the screen conductor was not a major factor in its effectiveness. For all heights, the maximum electrostatic field was reduced by about 28 percent.

For the second case, the same screen conductor was placed at a distance of 22.86 m (75 ft) from the center phase. Once again, the effectiveness was fairly insensitive to height, with a reduction of induced field of about 26 percent at the edge of the power line right-of-way.

The results showed that aerial screening conductors can have some use in reducing electrostatic fields. Multiple screening conductors may be even more effective than single conductors for particular power line cases. Most recent work in this area is reviewed in (10).

MITIGATION OF ELECTROMAGNETIC COUPLING

This subsection discusses the various mitigation techniques which can be employed to reduce 60 Hz ac electromagnetic coupling to a pipeline system consisting of arbitrary buried and above-ground sections. These techniques include:

1. Design of a joint pipeline/power line corridor for minimum electromagnetic coupling;
2. Pipeline grounding methods;
3. Use of screening conductors;
4. Use of insulating devices; and
5. Use of pipeline extensions.

Of the above techniques, the first was recently derived from the basic theory of Section 3. The remaining techniques have been employed in the past, but evidently not optimally. This subsection will discuss optimization of these methods consistent with the developed theory.

It should be emphasized that the electromagnetic coupling mitigation concepts discussed in this section have been verified by field tests conducted specifically for inclusion in this manual. These tests involved Southern California Gas Company Line 235, a 34-inch diameter gas transmission pipeline extending from Newberry to Needles, California. This pipeline shares a right-of-way with a Southern California Edison Company 500 kV ac power transmission line for 54 miles and is subject to considerable electromagnetic induction. The illustrative examples discussed in this section are taken directly from the results of the Mojave field tests.

Design of a Joint Pipeline/Power Line Corridor for Minimum Electromagnetic Coupling

Design Goals. As stated in Section 3, pipeline voltage peaks due to electromagnetic coupling should appear at any physical discontinuity of the pipeline and at any abrupt change of the longitudinal driving electric field at the pipeline location. In the first case, the peak voltage is proportional to the driving field at the pipeline; in the second case, the peak voltage is proportional to the local field discontinuity. For purposes of mitigation of electromagnetic coupling, a joint-use corridor would ideally be designed with power lines generating minimal driving electric fields of constant magnitude and phase; with pipelines having constant physical characteristics and no insulators or junctions; and with constant separations between each user of the corridor. Then, induced voltage peaks would appear only at the entry and exit point of each pipeline from the corridor, where the continuity of the joint corridor is necessarily disturbed. (These peaks could be mitigated using low-impedance grounding systems).

The optimum electromagnetic design of a joint-use corridor can be summarized concisely by stating the following design goals for the corridor:

A. Minimize any change of separation between a pipeline and a power line.

B. Minimize the use of pipeline insulating joints. If such a joint is necessary, place a low-ac-impedance ground cell across it.

C. Minimize the combination of long above-ground and buried sections in a single pipeline run.

D. Minimize the use of power line phase transpositions or phase changes at substations.

E. Use the center-point-symmetric phase sequence for all double-vertical configuration power line circuits.

Example of a Joint-Use Corridor Design. The following discussion concerning the joint-use corridor extending from Newberry to Needles, California, will illustrate many of the basic corridor design principles just summarized.

The Southern California Edison 500 kV electric power transmission line meets the Southern California Gas Company 34-inch diameter gas pipeline at pipeline milepost 47 (47 miles west of Needles, California) and leaves it at milepost 101.7, as shown in Figure 8-5. The power line has a horizontal configuration with a full clockwise (phase-sense) transposition at milepost 68 and single-point-grounded

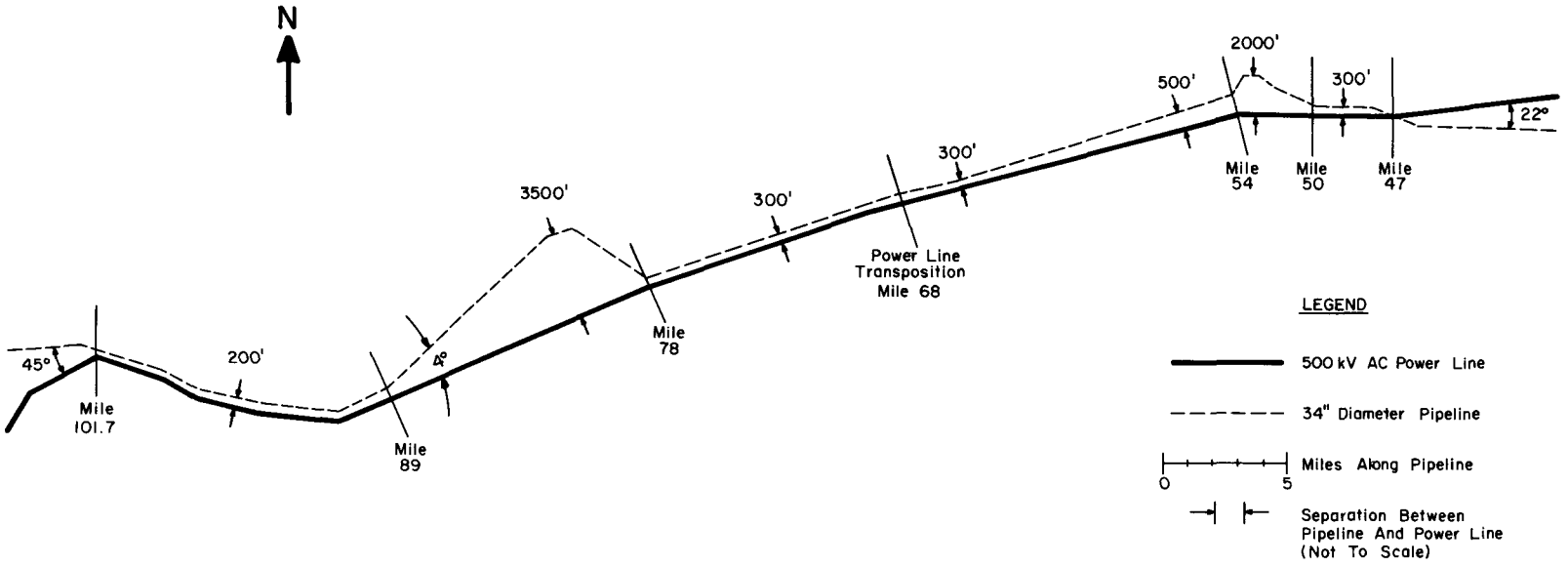

Fig. 3-10 MOJAVE DESERT PIPELINE–POWER LINE GEOMETRY

lightning shield wires. During the test period, an average loading of 700 amperes was reported for each phase conductor. No other power lines, pipelines, or long conductors share the right-of-way.

Measurements performed during the test indicated an average earth resistivity of of 400 ohm-meter. Based upon furnished data, a value of 700 $k\Omega\text{-}ft^2$ was assumed as the average pipeline coating resistivity. Using these values as data for the pipeline characteristics program PIPE, the pipeline propagation constant γ, was computed as $(0.115 + j0.096)\ km^{-1} = 0.15\underline{/40^o}\ km^{-1}$; and the pipeline characteristic impedance, Z_o was computed as $(2.9 + j2.4)$ ohms $= 3.8\underline{/40^o}$ ohms. The location of the voltage peaks and their magnitudes were calculated for this pipeline in Section 3.

It was shown that separably calculable pipeline voltage peaks at all discontinuities of a pipeline-power line geometry spaced by more than 2/Real(γ) meters along the pipeline could be expected. Using the computed value of γ, all geometry discontinuities spaced by more than (2/0.115) km = 17.4 km $\simeq$ 10 miles were assumed to be locations of separable induced voltage peaks. These discontinuities included:

1. Milepost 101.7 (near end of pipeline approach section);
2. Milepost 89 (separation change);
3. Milepost 78 (separation change);
4. Milepost 68 (power line phase transposition);
5. Milepost 54 (separation change); and
6. Milepost 47 (near end of pipeline departure section).

The voltages at these mileposts were predicted by applying the simplified equation developed in Section 3, namely

$$V(M) = \frac{V_{\theta_{left}} + V_{\theta_{right}}}{2} \quad . \tag{8-2}$$

The predicted and measured voltage peaks are summarized in Table 8-1.

Table 8-1

MOJAVE DESERT PIPELINE VOLTAGE PEAKS

Milepost	Predicted Voltage (volts)	Measured Voltage (volts)
101.7	46.3	46
89	54.0	53
78	31.1	34
68	54.8	54
54	11.4	11
47	31.2	25

Figure 8-6 plots both the measured ac voltage profile of the Mojave pipeline and the predicted voltage peaks. The solid curve represents voltages measured during the field test; the dashed curve is a set of data (normalized to 700 amperes power line current) obtained by a Southern California Gas Company survey. From this figure, it is apparent that the prediction method succeeded in locating and quantitizing each of the pipeline voltage peaks with an error of less than $\pm$ 20%. This implies the correctness of the corridor design goals of this section in optimizing a given right-of-way for minimum inductive coupling. In a dense urban environment, the prediction calculations would become more complex, but would still be within the scope of the distributed source theory and programmable calculator programs discussed in Appendix A.

Electric Field Reduction

For purposes of electromagnetic coupling mitigation, a power line would ideally be designed to generate only a minimal, but constant, driving field at the location of the adjacent pipeline. To strengthen this concept, computer analyses were performed to investigate the effect of conductor phasing and shielding upon the driving electric field profile. This subsection summarizes the results of these analyses.

Optimized Phase Sequencing. For certain ac power line configurations, it is possible to minimize the driving electric field within the right-of-way by proper sequencing of the phase conductors (11,12). The effectiveness of such phase

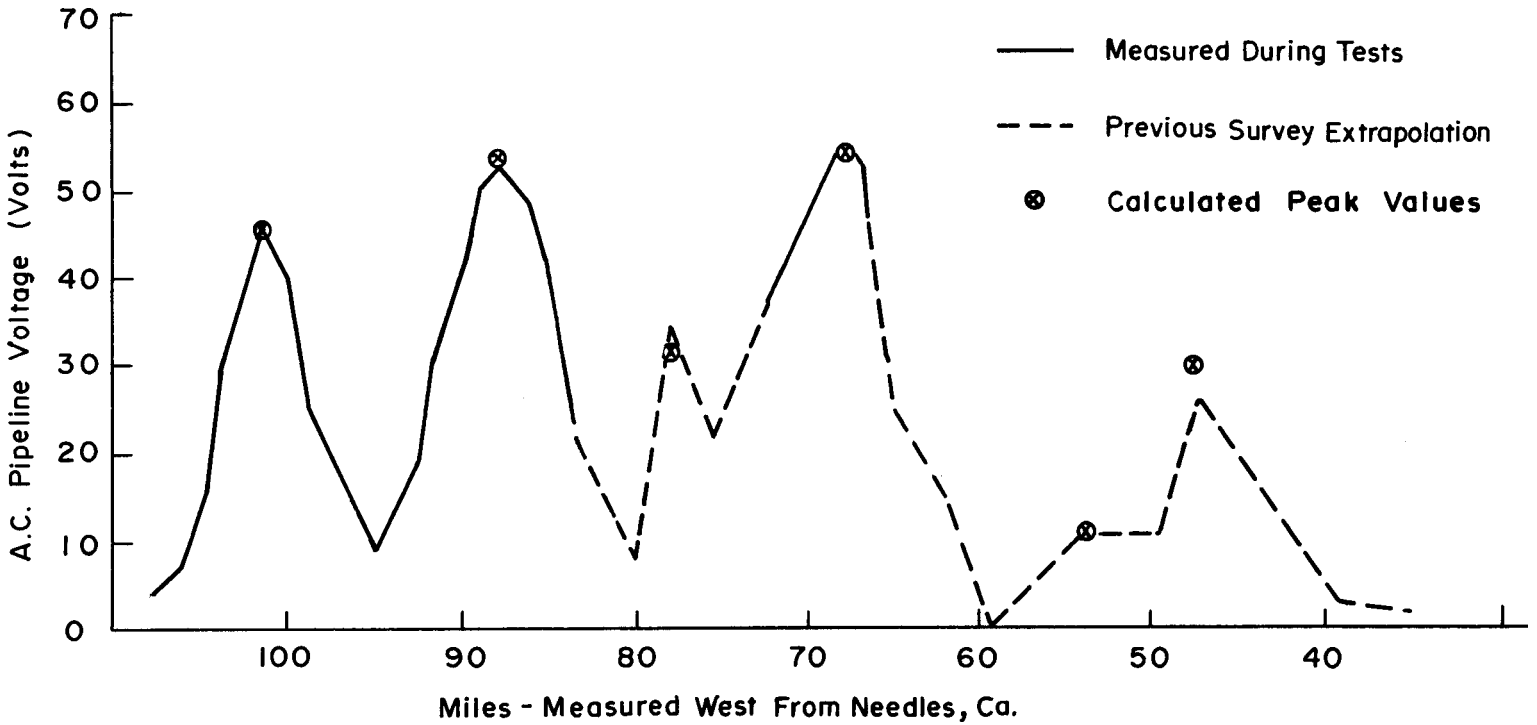

Fig. 8-6 MOJAVE DESERT PIPELINE VOLTAGE PROFILE

sequencing has been studied for three common power line geometries. The results indicate that for certain geometries and proper phase conductor sequencing, the induced electric field levels can be significantly reduced. This technique is especially appropriate for single vertical circuits, particularly the double circuit configuration.

The analysis of this mitigation technique was accomplished in two basic steps. First, for a given power line geometry, Carson's infinite series approach and linear circuit analysis were combined to determine the induced currents in the two lightning shield wires. The mutual interaction between these two wires was included in the analysis, requiring the solution of two simultaneous equations. Second, using superposition theory and Carson's infinite series, the field contribution from each current-carrying wire was computed and summed to provide the total longitudinal electric field at arbitrary distances from the power line. In all cases, the Carson mutual impedances were calculated to better than 0.1% accuracy. These steps were then repeated for each geometry and conductor phasing examined.

The first power line geometry considered is that shown in Figure 8-7, the single circuit horizontal with two multiple grounded lightning shield wires.

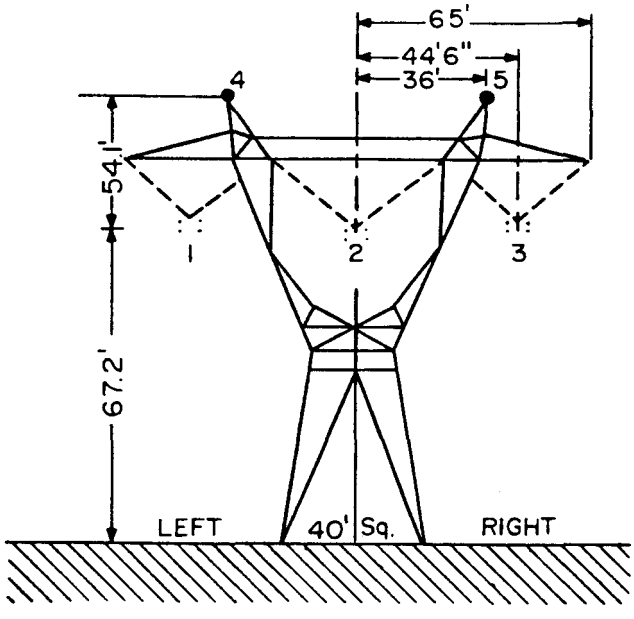

NOTE: VERTICAL NOT TO SCALE

Figure 8-7. Single Circuit Horizontal Geometry

There are six possible phase sequences for this geometry, separable into two categories--clockwise (cw) and counterclockwise (ccw) sequences. Referring to the phase conductors from left to right in Figure 8-7, and letting "A" denote the 0° phase, "B" denote the $+120^{\circ}$ phase, and "C" denote the -120° phase, we have

cw sequences	ccw sequences
ACB	BCA
BAC	CAB
CBA	ABC

At a fixed observation point, p, on one side of the power line it can be shown analytically that all three cw sequences produce the same longitudinal electric field magnitude, $E_{cw}(p)$; and all three ccw sequences produce the field magnitude, $E_{ccw}(p)$. However, $E_{ccw}(p)$ does not equal $E_{cw}(p)$, in general. This difference can be exploited to obtain a field reduction at the pipeline location through proper choice of either a cw or ccw sequence. For example, Table 8-2 lists values of the electric field computed to the right of the power line of Figure 8-7, assuming an earth resistivity of 33.3 Ω-m and equal phase currents of 100 amperes per conductor.

Table 8-2

CHOICE OF CW OR CCW SEQUENCE FOR BALANCED HORIZONTAL CIRCUIT
(Right of Power Line)

Distance From Center Phase (feet)	E_{cw} (V/km)	E_{ccw} (V/km)	Mitigation Advantage of CCW Sequence (percent)
0	2.25	2.25	0.0
50	5.21	5.02	3.6
100	4.90	4.72	3.9
150	3.68	3.51	4.6
200	2.87	2.71	5.6
250	2.32	2.18	6.0
300	1.95	1.81	7.2
350	1.67	1.55	7.2
400	1.46	1.34	8.2
450	1.29	1.18	8.5
500	1.15	1.05	8.7

From the table, it is seen that the electric field exposure levels can be reduced by as much as 8.7 percent simply by choosing the proper phase sequence. Since the voltage induced on the pipeline is directly proportional to the electric field, it too can be reduced by this same percentage. However, if the shield wires are not continuous and periodically grounded as assumed in the above analysis, then there is no significant advantage of one phase sequence over another.

The second geometry considered is that shown in Figure 8-8, the single circuit vertical, with two multiple-grounded lightning shield wires. Similar to the single circuit horizontal, this configuration has six possible phase combinations separable into the cw and ccw sequences. Referring to the phase conductors from top to bottom in Figure 8-8, the phase combinations ACB, BAC, and CBA are again defined as clockwise while BCA, CAB, and ABC are defined as counterclockwise.

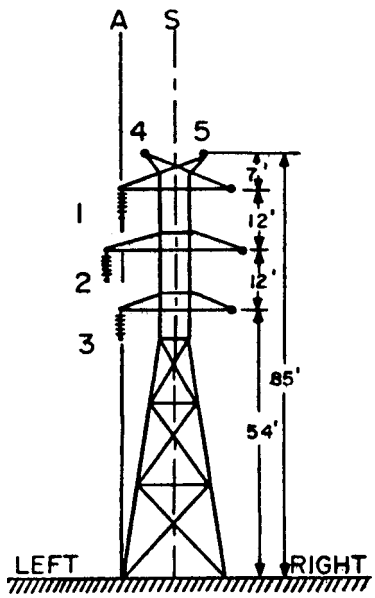

Figure 8-8. Single Circuit Vertical Geometry

At a fixed observation point, p, on one side of the power line, it can be shown that all three cw sequences produce the same longitudinal electric field magnitude, $E_{cw}(p)$, while all three ccw sequences produce the field magnitude, $E_{ccw}(p)$, not equal to $E_{cw}(p)$. Again, the difference in fields can be exploited to obtain mitigation. Table 8-3 lists values of the electric field computed to the right of the power line of Figure 8-8, assuming an earth resistivity of 33.3 Ω-m and

Table 8-3

CHOICE OF CW OR CCW SEQUENCE FOR BALANCED VERTICAL CIRCUIT
(Right of Power Line)

Distance From Center Phase (feet)	$\|E_{cw}\|$ (V/km)	$\|E_{ccw}\|$ (V/km)	Mitigation Advantage of CW Sequence (percent)
0	4.61	4.83	4.6
50	2.20	2.41	8.7
100	1.14	1.32	13.6
150	0.80	0.95	15.8
200	0.64	0.76	15.8
250	0.55	0.64	14.1
300	0.48	0.56	14.3
350	0.43	0.50	14.0
400	0.39	0.45	13.3
450	0.36	0.41	12.2
500	0.33	0.38	13.2

equal phase currents of 100 amperes per conductor. From the table, it is seen that the electric field exposure levels, and thus, induced pipeline voltages, can be reduced by as much as 15 percent simply by choosing the proper phase sequence. However, if the shield wires are not continuous and periodically grounded as assumed in the above analysis, then there is no significant advantage of one phase sequence over another.

The third geometry considered is that shown in Figure 8-9, the double circuit vertical with two multiple-grounded shield wires. Assuming a balanced current flow, there is a total of 36 possible phase sequences for this configuration. Of this number, there are five separate sets of phase combinations, as shown in Table 8-4: the center point symmetric; the full roll; the partial roll (upper); the partial roll (lower); and the center line symmetric. For each set, the electric field magnitude is approximately constant for the distinct phase sequences which comprise the set. However, significant differences exist in the electric field magnitudes generated by separate sets. These differences can be exploited to obtain mitigation of pipeline voltages.

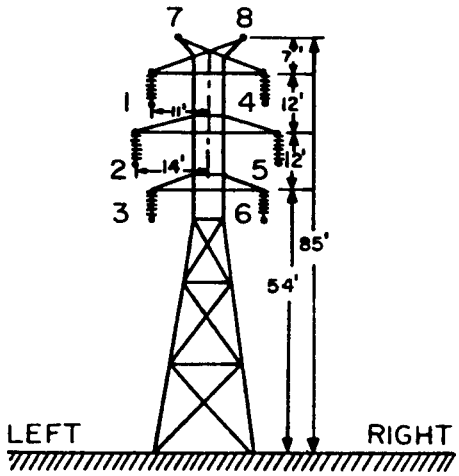

Figure 8-9. Double Circuit Vertical Geometry

For example, Table 8-5 lists values of the longitudinal electric field computed to the right of the power line of Figure 8-9, assuming an earth resistivity of 33.3 Ω-m and equal phase currents of 100 amperes per conductor. From the table, it is seen that the electric field levels, and thus, induced pipeline voltages, can be reduced by as much as 60 to 90 percent over the right-of-way by choosing the center point symmetric phasing instead of any of the others. This reduction is significant when it is realized that it is solely a result of power line phasing. It is a consequence of the physical interaction of the induced electric fields from all of the power line conductors.

Installation of Auxiliary Grounded Wire. A second electric field reduction technique is the usage of an auxiliary grounded wire installed between the power line towers (10). The purpose of this wire is to induce an additional component of longitudinal electric field 180 degrees out of phase with the existing field, causing field cancellation. This cancellation can occur only when the current induced in the auxiliary wire is of a favorable magnitude and phase. The desirable parameters for the induced current are attained through the proper positioning of the wire relative to the phase conductors and shield wires.

Table 8-4

POSSIBLE PHASE SEQUENCES FOR A DOUBLE CIRCUIT VERTICAL CONFIGURATION

1. Center-Point Symmetric

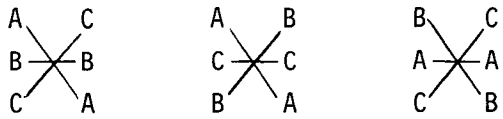

and the 3 right-to-left mirror images;

2. Full Roll

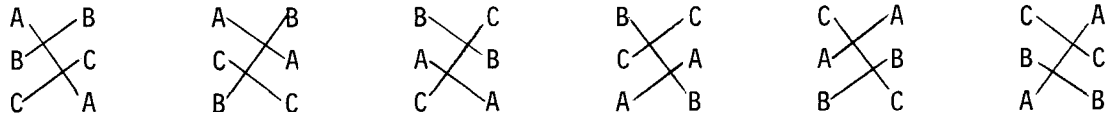

and the 6 right-to-left mirror images;

3. Partial Roll (Upper)

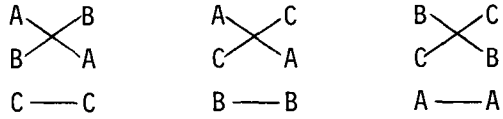

and the 3 right-to-left mirror images;

4. Partial Roll (Lower)

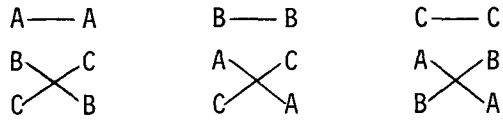

and the 3 right-to-left mirror images;

5. Center Line Symmetric

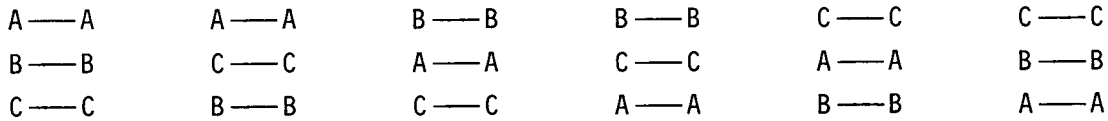

Table 8-5

CHOICE OF PHASE SEQUENCE FOR THE BALANCED DOUBLE CIRCUIT VERTICAL GEOMETRY OF FIGURE 8-9

Distance From Center Line (feet)	Longitudinal Electric Field Magnitude (V/km)					Mitigation Advantage of Center-point Symmetric Phasing
	Center Point Symmetric	Full-Roll	Partial-Roll (upper)	Partial-Roll (lower)	Center-Line Symmetric	
0	0.7	4.3	8.0	7.35	9.1	85 - 90%
100	0.3	0.9	1.9	2.2	2.5	65 - 90%
200	0.2	0.5	1.0	1.25	1.4	65 - 85%
300	0.15	0.4	0.75	0.9	1.0	60 - 85%
400	0.15	0.35	0.6	0.75	0.85	60 - 85%
500	0.1	0.3	0.5	0.65	0.7	60 - 85%

Best Phasing ← → Worst Phasing

The effectiveness of this technique has been studied for three common power line geometries. The results indicate that the extra grounded wire can provide a substantial reduction of the longitudinal electric field for vertical circuits. However, its mitigation effect can be sensitive to the loading conditions of the power line, which limits the usefulness of this technique.

A computer program that was available for calculation of the longitudinal electric field was modified for this analysis to include the effects of the auxiliary wire. Again, a two-step analysis was used for each power line configuration. First, Carson's theory and linear circuit analysis were combined to determine the induced currents in the two shield wires and the auxiliary wire. The mutual interaction between these three wires was included and required the solution of three simultaneous equations. Second, using superposition theory and Carson series, the field contribution from each phase conductor and shield wire was calculated and summed to provide the complete induced electric field. By making this calculation with and without the presence of the auxiliary wire, it was possible to evaluate the effectiveness of this mitigation technique. This procedure was then repeated for each power line geometry and conductor phasing examined.

The first geometry considered is that shown in Figure 8-7, the single circuit horizontal with two multiple-grounded shield wires. (The optimum phasing of this circuit was discussed previously in this section.) A single, auxiliary grounded wire was assumed to exist in various vertical planes defined within the bounds of the tower structure. The wire was then assumed to be located at different heights within each plane. A comparison of the original longitudinal electric field to the field with the auxiliary wire present could then be made.

Figure 8-10 illustrates the effect of placing a grounded auxiliary wire at the outer right edge of the power line structures (65 feet to the right of the center line), as calculated at two points: (1) 200 feet to the right of the center line; and (2) 200 feet to the left of the center line. For this example, an earth resistivity of 33.3 Ω-m was assumed, along with balanced phase conductor currents. From the figure, it is seen that the maximum field reduction about 25%, occurs to the right of the power line for an auxiliary wire height of 49 feet. However, an equivalent field increase is seen to occur to the left of the power line.

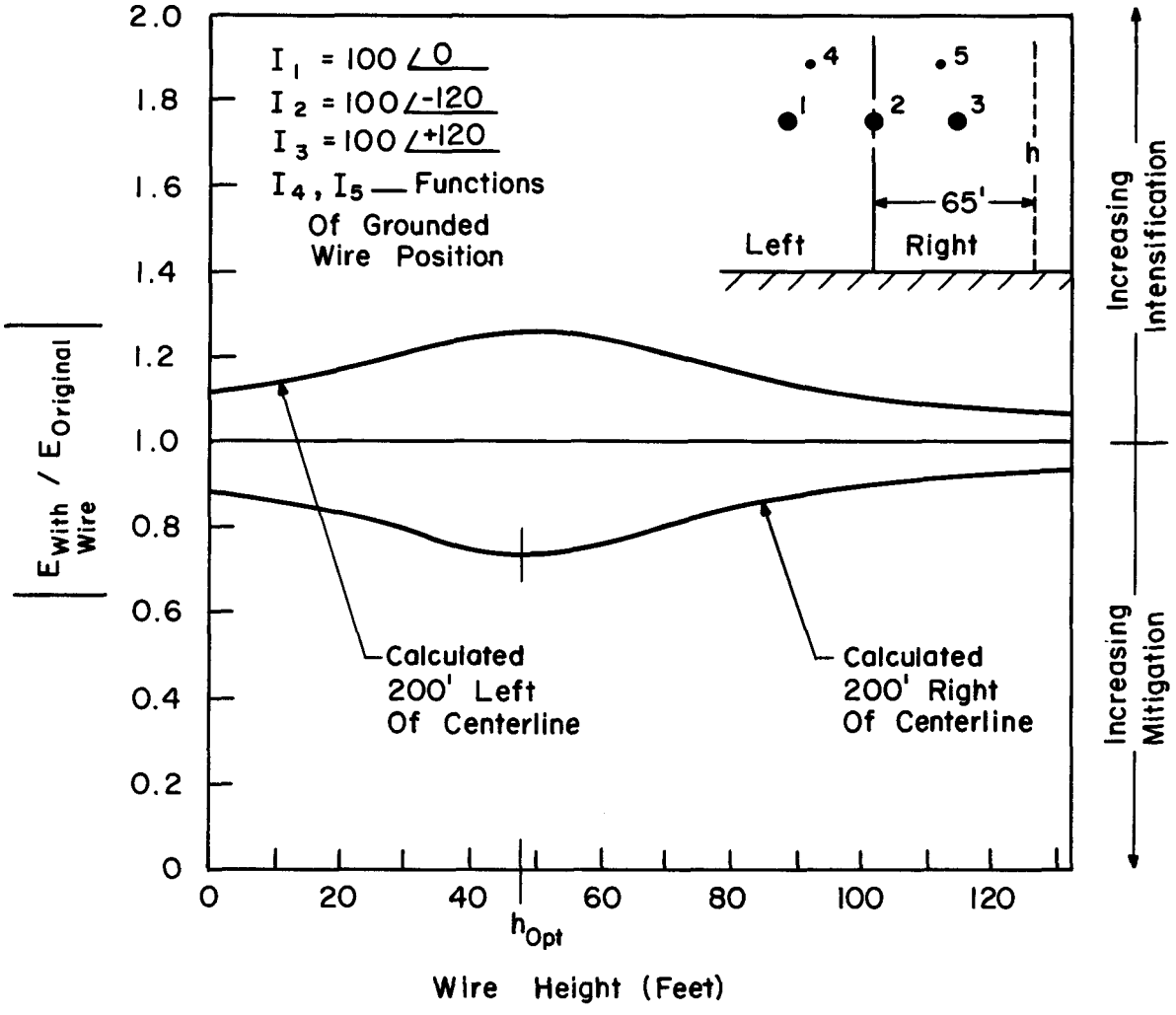

Fig. 8-10 EFFECT OF A GROUNDED AUXILIARY WIRE AS A FUNCTION OF HEIGHT FOR THE SINGLE-CIRCUIT HORIZONTAL CONFIGURATION

Modelling of the auxiliary wires in several other vertical planes gave results similar to those of Figure 8-10. Mitigation greater than 25% could be obtained only if the auxiliary wire was assumed to be within six feet of a phase conductor. Under these circumstances, a field reduction of about 50% was possible. However, this placement may be unrealistic if the insulation characteristics of the power line are to be preserved.

Overall, a grounded auxiliary wire can be expected to provide about a 25% reduction in the longitudinal electric field on one side of a single circuit horizontal power line. This reduction is accompanied by a corresponding increase of the field level on the opposite side of the power line. The most favorable heights for the auxiliary wire are approximately the same as the phase conductor height, thus placing the practicality of this technique in question.

The second geometry considered is that shown in Figure 8-8, the single circuit vertical with two multiple-grounded lightning shield wires. (The optimum phasing of this circuit was discussed previously in this section.) A single, auxiliary grounded wire was assumed to exist in the vertical plane S as shown in the figure. The total longitudinal electric field was computed for the wire at different heights within the plane and compared to the results of the power line without the auxiliary wire.

Figure 8-11 illustrates the effect of the auxiliary wire as observed at two points: (1) 200 feet to the right of the S plane; and (2) 200 feet to the left of the S plane. For this example, an earth resistivity of 33.3 Ω-m was assumed, along with balanced phase conductor currents. From the figure, it is seen that the maximum field reduction is about 75% to the right of the power line, and about 60% to the left of the power line, for a wire height of 26 feet.

Figure 8-11 illustrates that there is an optimum height for placing the grounded auxiliary wire. (Of course, this height depends upon the power line geometry.) Above this height, the effectiveness of the wire in reducing the electric field diminishes to the point where all mitigation properties are lost. For the example presented, this point is at 43 feet. A wire located still higher carries current with a phase characteristic resembling that of the lightning shield wire currents, and accordingly, tends to reinforce the existing longitudinal electric field.

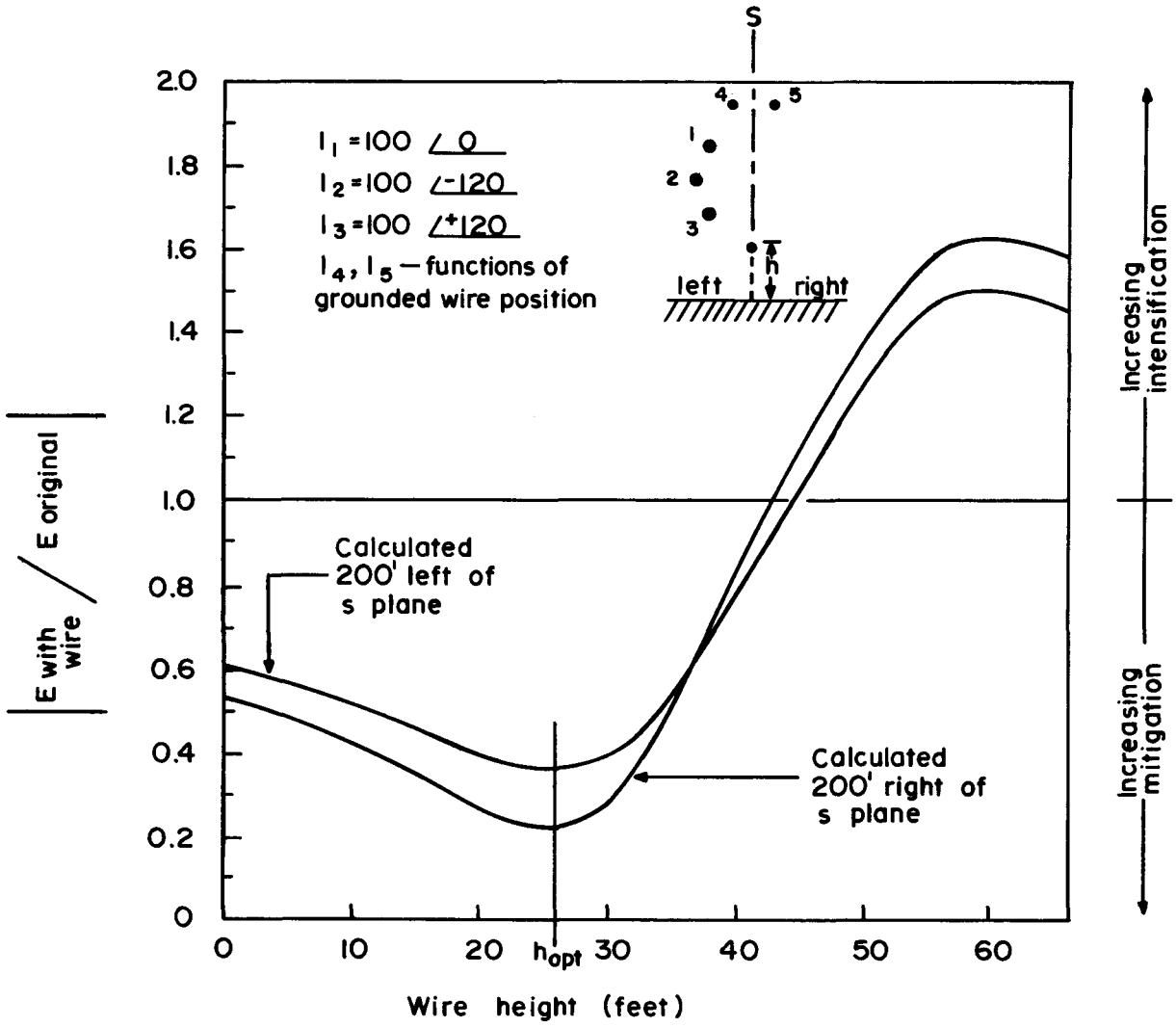

Fig. 8-11 EFFECT OF A GROUNDED AUXILIARY WIRE AS A FUNCTION OF HEIGHT FOR THE SINGLE-CIRCUIT VERTICAL CONFIGURATION

To illustrate the sensitivity of this mitigation technique to phase current unbalance, several simple situations were considered. Figure 8-12 presents the results of this analysis. The geometry of Figure 8-8 was employed with a base current of 100 amperes. The center phase conductor current was assumed to be constant for all of the calculations. There was an assumed 0, $\pm$5, $\pm$10, and $\pm$15 percent phase unbalance between the current in the top and bottom phase conductors relative to the center phase current. The effectiveness of the grounded wire in reducing the electric field was determined at four perpendicular separation distances: 0, 100, 200 and 500 feet on either side of the power line. The mitigation wire was assumed to be located at the optimum height of 26 feet as determined from Figure 8-11 for balanced phase currents. Figure 8-12a presents the results for both sides of the power line when the largest current is in the bottom phase conductor, and Figure 8-12b when the largest current is in the top phase conductor. It is believed that most power line loading characteristics fall within the current unbalances assumed here.

Two significant conclusions result from the theoretical analysis as seen in Figure 8-12. First, the effectiveness of the grounded wire is very sensitive to the phase currents. Small unbalances in the power line loading cause a severe deterioration in the degree of mitigation provided by the grounded wire. For power lines having time-dependent current unbalances, it would be difficult to design a wire placement achieving a satisfactory mitigation at all times of the day.

It is also seen that the ability of the grounded wire to reduce the electric field is a function of the separation distance between the power line and the field observation point. For balanced currents, the mitigation technique becomes less effective as the field point approaches the power line. But once even a small amount of unbalance is experienced, the effectiveness of the technique is reduced to 20 percent or less for all separation distances.

Because of these facts it appears unfeasible to consider this mitigation approach for the single circuit vertical geometry. The cost for such a wire versus its poor reliability and sensitivity to current unbalance indicate that other approaches should be considered.

The third geometry considered is that shown in Figure 8-9, the double circuit vertical with two multiple-grounded lightning shield wires. (The optimum phasing

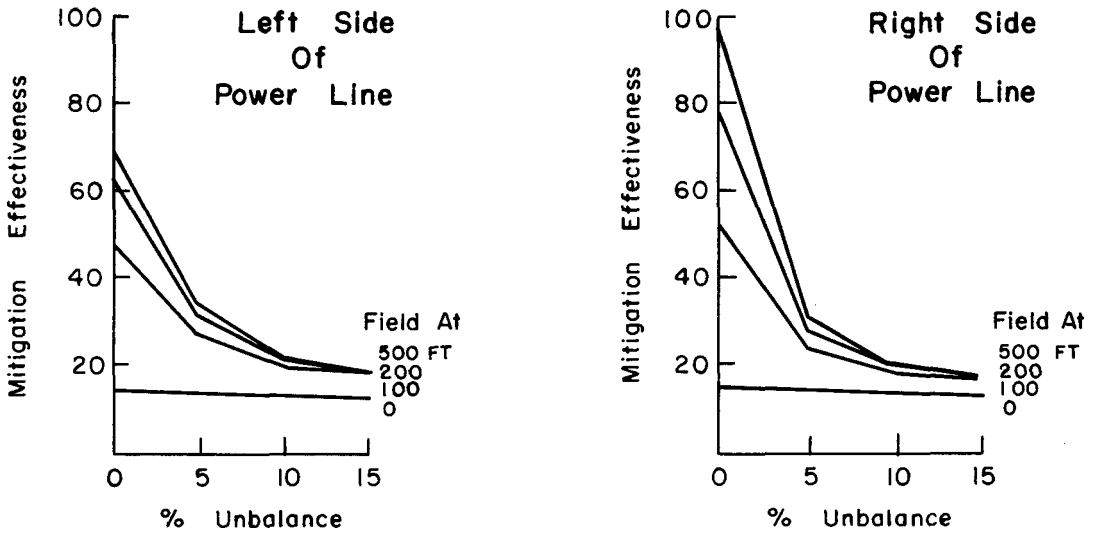

(a) Largest Current In Bottom Phase Conductor

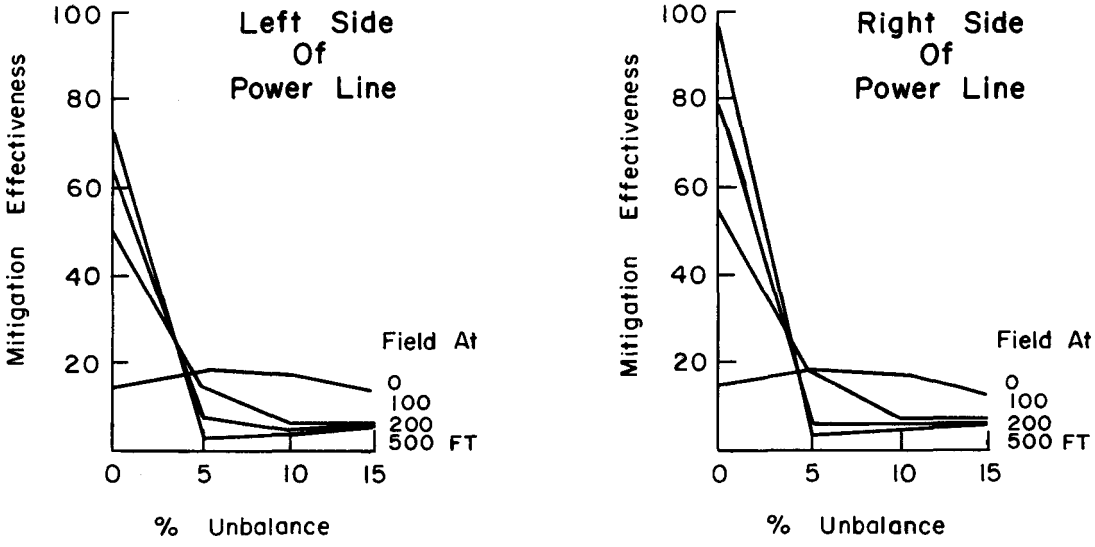

(b) Largest Current In Top Phase Conductor

Fig. 8-12 SENSITIVITY OF GROUNDED AUXILIARY WIRE METHOD TO POWER LINE CURRENT UNBALANCE (SINGLE CIRCUIT VERTICAL)

of this circuit was discussed previously in this section.) A single, auxiliary grounded wire was assumed to exist in the center plane of the power line. The total longitudinal electric field was computed for the wire at different heights within the plane and compared to the results for the power line without the auxiliary wire.

Computations indicated that, when optimally placed, the grounded wire could reduce the longitudinal electric field by more than 50% for each of the phase sequences of Table 8-4. A maximum mitigation greater than 95% was found for the center-point symmetric configuration.

Although this reduction in the electric field is significant, the mitigation effect can rapidly deteriorate with just a small current unbalance, similar to the single vertical circuit case. Four simple current-unbalance combinations were considered for the center-point symmetric configuration, assuming a $\pm$ 5% current variation about the center phase conductors and a base current of 100 amperes. The four possible current combinations were then analyzed with the grounded wire located at the optimum height of 43 feet. Table 8-6 clearly shows the sensitivity of this mitigation technique to small changes in the phase current. As indicated, even though it is possible for the magnitude of the electric field to be reduced by more than 95% for balanced phase currents, it is also possible for an actual increase in the magnitude of the electric field at the same field point for only a small perturbation of the phase currents.

The sensitivity of this theoretically analyzed mitigation technique to even small current variations leads to the conclusion that it is not economically or practically feasible to implenent in field situations. Although it has been shown that the technique can provide significant nulling of the electric field under certain fortuitous conditions, this reduction is accompanied by unacceptable sensitivity to changing load conditions and reliability limitations.

Pipeline Grounding Methods

As shown in Figure 8-13, the pipeline and personnel hazards due to electromagnetic coupling to buried pipeline can be mitigated by grounding the pipe using either independent ground beds, distributed anodes, or horizontal ground wires, and by installing ground mats at points of possible human contact. Basic considerations for the applications of these techniques are now summarized.

Table 8-6

EFFECT OF CURRENT UNBALANCE ON PERFORMANCE OF GROUNDED AUXILIARY WIRE FOR A CENTER-POINT SYMMETRIC, DOUBLE CIRCUIT VERTICAL GEOMETRY

Phase Currents			Reduction in Electric Field (%)	
			Left of Power Line	Right of Power Line
100	100	Nominal Currents	68	> 95
100	100			
100	100			
105	105			
100	100		85	70
95	95			
95	95			
100	100		-14 (increase)	74
105	105			
95	105			
100	100		17	17
105	95			
105	95			
100	100		2	1
95	105			

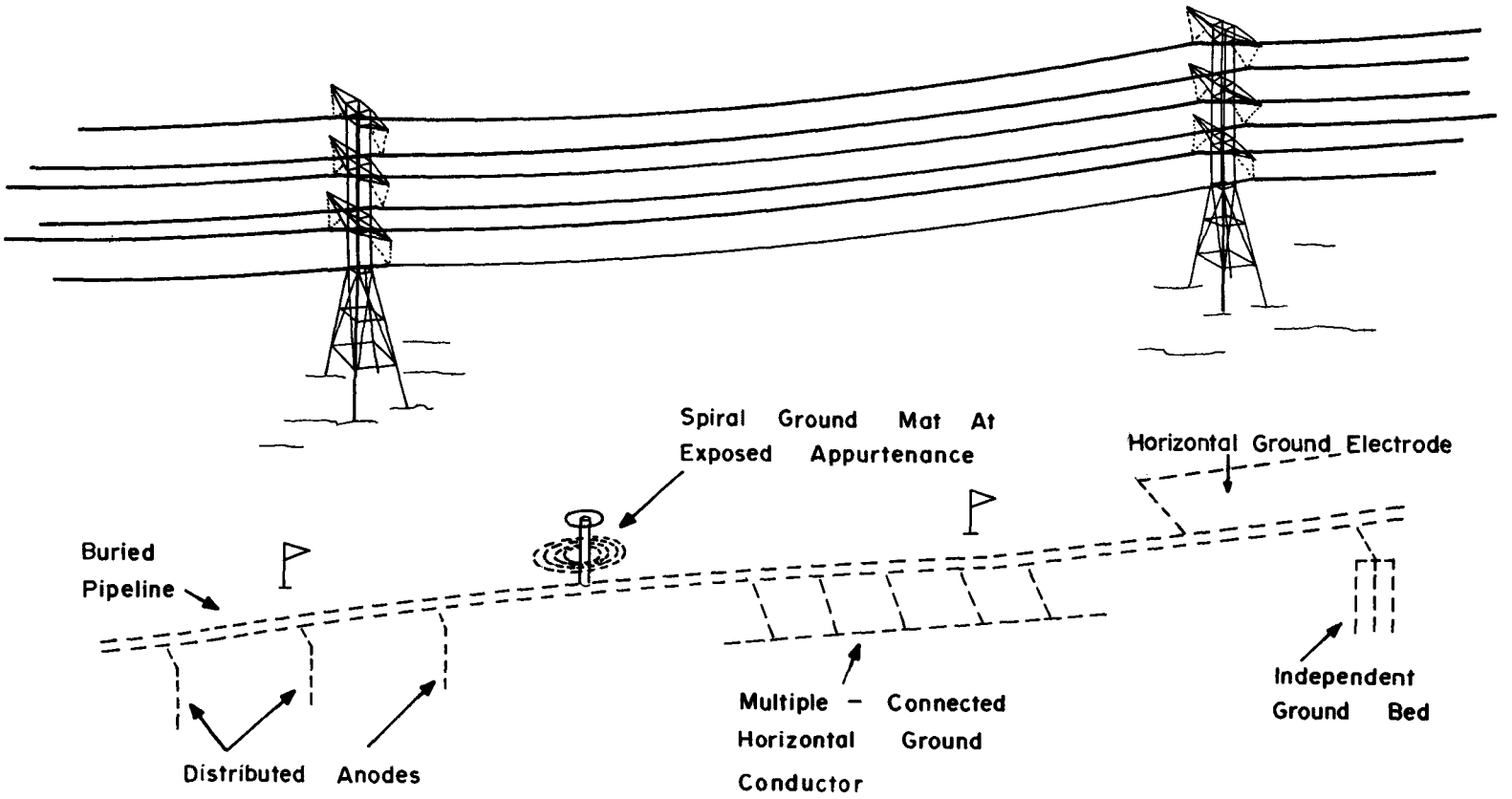

Fig. 8-13. APPLICATION OF GROUNDING TECHNIQUES FOR MITIGATION OF ELECTROMAGNETIC COUPLING TO A BURIED PIPELINE

Grounding Requirements. The most effective location for a grounding installation on a buried pipeline is at a point where the induced voltage is maximum. A good ground established at such a point serves to null the local exponential voltage distribution. However, the mitigating effects of this ground installation are negligible at an adjacent voltage peak located more than 2/Real(γ) m away, where γ is the propagation constant of a buried pipeline. Therefore, a ground should be established at each induced voltage maximum.

To effectively reduce the induced ac potential on a long buried pipeline of characteristic impedance, Z_o, by connecting the mitigating, grounding impedance, Z_m, the condition

$$|Z_m| < |Z_o| \approx 2 \text{ ohms} \tag{8-3a}$$

must be achieved. Grounding impedances exceeding $|Z_o|$ are essentially useless for mitigation in this case. Grounding impedances much less than $|Z_o|$ reduce the local pipeline voltage by

$$\% \text{ reduction} = 100 \left(1 - \left|\frac{Z_m}{Z_o}\right|\right) . \tag{8-3b}$$

The grounding requirement of Eq. 8-3a is much more demanding than that for mitigation of electrostatic coupling to an above-ground pipeline. The combination of possibly high values of pipe source voltage, V_θ, and low values of pipe source impedance, Z_o, serves to create severe shock hazards. Using the equivalent circuit of Figure 8-14, the shock current, I_w, through the worker can be shown to equal

$$I_w = \frac{V_\theta}{Z_o + Z_w \left(1 + \frac{Z_o}{Z_m}\right)} \tag{8-4}$$

where Z_w is the impedance of the current path through the worker. Mitigation of I_w requires values of Z_m significantly less than Z_o. This compares to the mitigation requirement of Eq. 8-1a, which states that Z_m need only be less than Z_w for mitigation of electrostatic shock hazards for the above-ground pipelines.

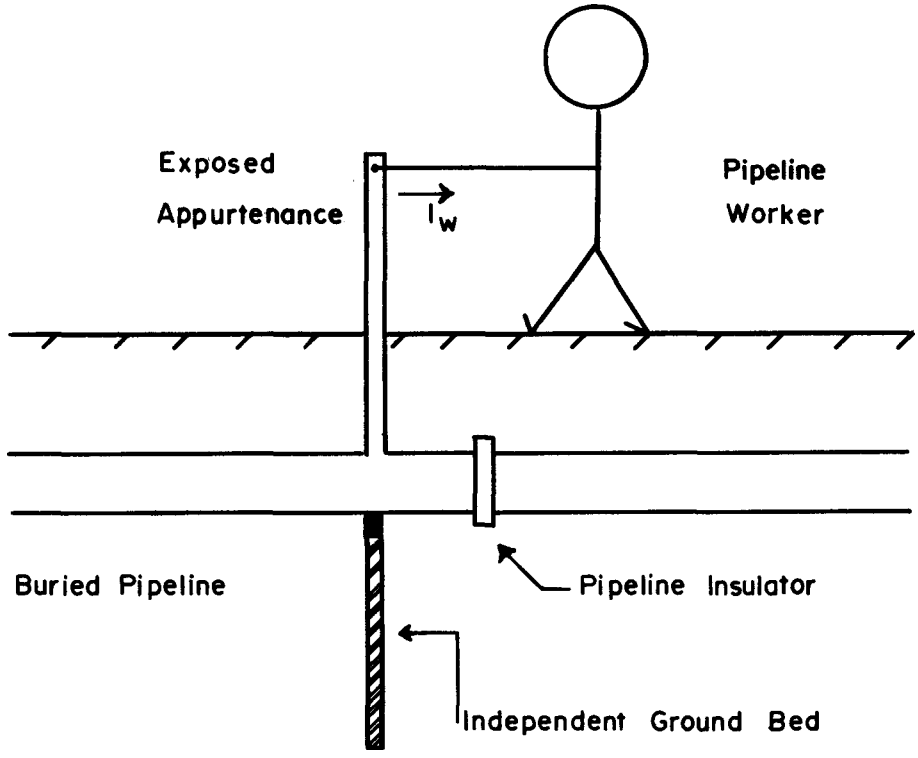

(a) Pipeline – Worker Geometry

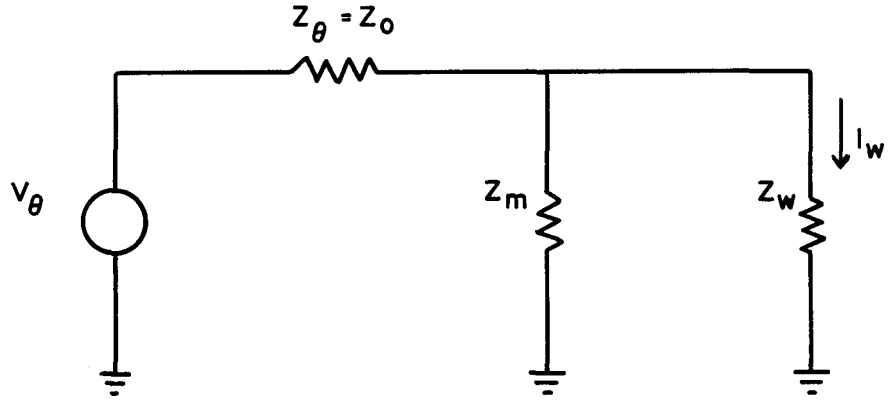

(b) Equivalent Circuit

Fig. 8-14 MITIGATION OF EM SHOCK HAZARDS BY PIPELINE GROUNDING

Two general types of independent grounding systems, namely vertical anodes and horizontal conductors (including casings), have found extensive use in realizing the low impedance grounds required for mitigation of electromagnetic coupling to buried pipelines. In addition, ground mats have been used to protect personnel at exposed pipeline appurtenances. The following subsections summarize the characteristics of the various low impedance grounding systems, and briefly review the use of grounding mats.

Vertical Anodes. A vertical anode grounding system can be realized with either a single deep anode or several distributed anodes. One possible single deep anode system consists of a steel casing containing cathodic protection type anodes in a carbonaceous backfill (12). Here, the bottom portion of the steel casing which contains the anode and backfill can be below the normal water table, allowing a low impedance ground to be obtained quite easily.

A vertical ground rod and its surrounding earth form a lossy transmission line characterized by the propagation factor, γ_{rod}, and the characteristic impedance, $Z_{o_{rod}}$. The ac ground impedance, Z_{rod}, is simply the input impedance of this lossy transmission line. It is incorrect to assume that Z_{rod} is equal to the dc grounding resistance, R_{rod}. As will be shown below, the transmission line characteristics of a vertical ground rod significantly affect is performance.

For a vertical ground rod radius, a, the propagation factor is given by (13,14)

$$\gamma_{rod} = \sqrt{j\omega\mu_o(\sigma + j\omega\varepsilon)} \quad m^{-1}$$

$$\simeq 0.0154 \cdot (1+j) \cdot \sqrt{\sigma} \quad m^{-1}, \text{ at 60 Hz} \tag{8-5}$$

where $\omega = 2\pi f$; $\mu_o = 4\pi 10^{-7}$ H/m; σ = soil conductivity in mhos/m; ε = soil permittivity in F/m; and $\sigma >> \omega\varepsilon$ is assumed. The characteristic impedance is given by (14)

$$Z_{o_{rod}} = \frac{1}{2\pi}\sqrt{\frac{\omega\mu_o}{2\sigma}}\left[(1+j)\cdot \ln\left(\frac{1.12}{a\sqrt{\omega\mu_o\sigma}}\right) + (1-j)\cdot\frac{\pi}{4}\right] \quad \text{ohms}$$

$$= \frac{2.44\cdot 10^{-3}}{\sqrt{\sigma}}\left[(1+j)\cdot \ln\left(\frac{51.6}{a\sqrt{\sigma}}\right) + (1-j)\,\frac{\pi}{4}\right] \quad \text{ohms at 60 Hz} \tag{8-6}$$

The ac grounding impedance of a single, electrically short vertical ground rod of radius, a, and length, L, is given by (14)

$$Z_{rod} = Z_{o_{rod}} \coth(\gamma_{rod} L) \simeq Z_{o_{rod}} / \gamma_{rod} L \quad \text{ohms}$$

$$\simeq \frac{0.159}{\sigma L} \left[\ln\left(\frac{51.6}{a\sqrt{\sigma}}\right) - j\frac{\pi}{4} \right] \quad \text{ohms at 60 Hz} \tag{8-7}$$

where

$$a << L << \delta = \sqrt{\frac{2}{\omega \mu_o \sigma}} = \frac{64.9}{a\sqrt{\sigma}} \text{ m} = \text{soil electrical skin depth} \tag{8-8}$$

The ln term of Eq. 8-7 is usually of the order of 10, so that Z_{ac} is almost a pure resistance. For comparison, the dc resistance of the same ground rod is given by (13)

$$R_{rod} = \frac{0.159}{\sigma L} \left[\ln\left(\frac{4L}{a}\right) - 1 \right] \quad \text{ohms} \tag{8-9}$$

Equation 8-7 yields values of Z_{rod} significantly higher than the values of R_{rod} obtained from Equation 8-9.

Example: Compute the 60 Hz ac grounding impedance of a 6-foot long, 1-inch diameter, vertical ground rod installed in soil having a resistivity equal to 100 ohm-m. Also, compute the dc resistance of this ground rod.

Solution: First, convert all quantities to the proper metric units.

L = 6 feet = 1.83 m

a = 0.5 inch = 0.0127 m

σ = 1/(100 ohm-m) = 0.010 mhos/m

From Eq. 8-7 we compute

$$Z_{rod} \simeq \frac{0.159}{(0.010)(1.83)} \left[\ln \left(\frac{51.6}{0.0127\sqrt{0.010}} \right) - j\frac{\pi}{4} \right] \text{ ohms}$$

$$\simeq 8.69\ (10.6 - j\,0.785)\ \text{ohms}$$

$$\simeq (92.1 - j\,6.8)\ \text{ohms}\ .$$

From Eq. 8-9, we compute

$$R_{rod} = \frac{0.159}{(0.01)(1.83)} \left[\ln \left(\frac{(4)(1.83)}{0.0127} \right) - 1 \right]$$

$$= 8.69\ (6.36 - 1) = 46.6 \text{ ohms.}$$

$|Z_{rod}|$ is seen to equal 2.0 times R_{rod}.

Multiple Vertical Anodes. The use of a single deep anode may be uneconomical in regions where the earth conductivity is low and buried rock strata make deep drilling difficult. In such cases, the use of multiple, short, distributed magnesium or zinc cathodic protection anodes may be indicated (15).

A. For vertical anodes grouped together in a distinct bed (arranged) on a straight line or circle) with the spacing between the rods equal to the length of the rods, the net ac grounding impedance is approximated by the following table (established for dc resistance (13)).

No. of Rods in Bed	Approximate Net ac Grounding Z
1	Z_{rod}
2	0.58 x Z_{rod}
4	0.36 x Z_{rod}
8	0.20 x Z_{rod}
10	0.16 x Z_{rod}
20	0.09 x Z_{rod}
50	0.04 x Z_{rod}

B. For vertical anodes distributed uniformly along a short (< 300 m) stretch of a buried pipeline, the ac grounding impedance is simply the grounding impedance of one anode divided by the total number of anodes.

C. For vertical anodes distributed uniformly along a length (> 3 km) stretch of buried pipeline, Eq. 8-3b does not precisely describe the mitigation effect. Wave propagation effects within the grounded section must be taken into account. The value of the propagation constant, γ_m, of the pipeline section with anodes is estimated as

$$\gamma_m \simeq \gamma \sqrt{\frac{Y + Y_m}{Y}} \tag{8-10a}$$

where γ and Y are the propagation constant and admittance to remote earth, respectively, of the pipeline section before mitigation, and Y_m is the mitigating admittance per km provided by the distributed anodes. The reduction in voltage is estimated as

$$\begin{aligned} \% \text{ reduction} &\simeq 100 \left(1 - \left|\frac{\gamma}{\gamma_m}\right|\right) \\ &\simeq 100 \left(1 - \frac{1}{\sqrt{1 + \frac{Y_m}{Y}}}\right) \end{aligned} \tag{8-10b}$$

Equation 8-10b indicates that appreciable mitigation is obtained for this case only if the net mitigating admittance per km is much greater than Y, which is of the order of 0.1 mhos/km for a typical, moderately well insulated, buried pipeline.

Example: Vertical anodes with an ac grounding impedance of 50 ohms are installed at regular intervals of 20 m along a buried pipeline having a Y value of 0.1 mhos/km. Estimate the resulting mitigation.

Solution: Each anode presents an ac grounding admittance of 1/50 mhos. At a spacing of 20 m between anodes, there are a total of 50 anodes per km. Thus,

$$Y_m = 50 \frac{\text{anodes}}{\text{km}} \cdot \frac{1}{50} \frac{\text{mho}}{\text{anode}} = 1 \frac{\text{mho}}{\text{km}} .$$

Using Eq. 8-10b, the percent mitigation is estimated as

$$\% \text{ reduction} \simeq 100 \left(1 - \frac{1}{\sqrt{1 + 1/0.1}}\right)$$

$$= 100 \left(1 - \frac{1}{\sqrt{11}}\right) \simeq 70\%$$

Horizontal Conductors. A horizontal ground wire and its surrounding earth form a lossy transmission line characterized by the propagation factor, γ_{wire}, and the characteristic impedance, $Z_{o,wire}$. The ac grounding impedance, Z_{wire}, is simply the input impedance of this lossy transmission line. It is incorrect to assume that Z_{wire} is equal to the dc grounding resistance, R_{wire}. As will be shown below, the transmission line characteristics of a horizontal grounding wire significantly affect its performance.

Further, horizontal ground conductors can be subject to the same driving electric field generated by the adjacent power line as the pipeline is exposed to. Therefore, ground wires can develop appreciable terminal voltages which must be accounted for in computations of the expected mitigation. Additional factors involve the effects of resistive and inductive coupling between long ground wires and the nearby pipeline. All of these factors are highly dependent upon the specific orientation of the ground wire relative to the power line and the pipeline. Reference will be made to Figure 8-15, which shows four common types of horizontal ground wire installations, and to Figure 8-16, which shows the electrical equivalent circuit for each type of installation.*

Mitigation Wire Perpendicular to the Pipeline. This ground wire configuration, denoted as A in Figure 8-15, is the simplest to analyze because the perpendicular configuration serves to minimize inductive and conductive coupling between the wire, pipeline, and power line. In this configuration, the wire acts only as the grounding impedance, Z_{wire}, for the pipeline, as shown in Figure 8-16b. The overall mitigation effect is computed in 3 steps.

1. Apply the calculator program WIRE, documented in Appendix A, to determine the propagation constant, γ_{wire}, and characteristic impedance, $Z_{o,wire}$. This program is suitable for wires of arbitrary electrical conductivity and permeability, and diameters up to one inch, for the full range of possible earth resistivities. The program achieves this degree of generality by solving the Sunde transcendental equation (Eq. 2-9 of Section 2) for the case

$$Y_i = \infty \qquad (8\text{-}11a)$$

*The design procedures for the different types of mitigation wires considered here were developed from field tests made in December 1977 on the Southern California Gas Company Line 235 extending from Needles to Newberry, California. Detailed test procedures and data reduction are presented in Appendix E.

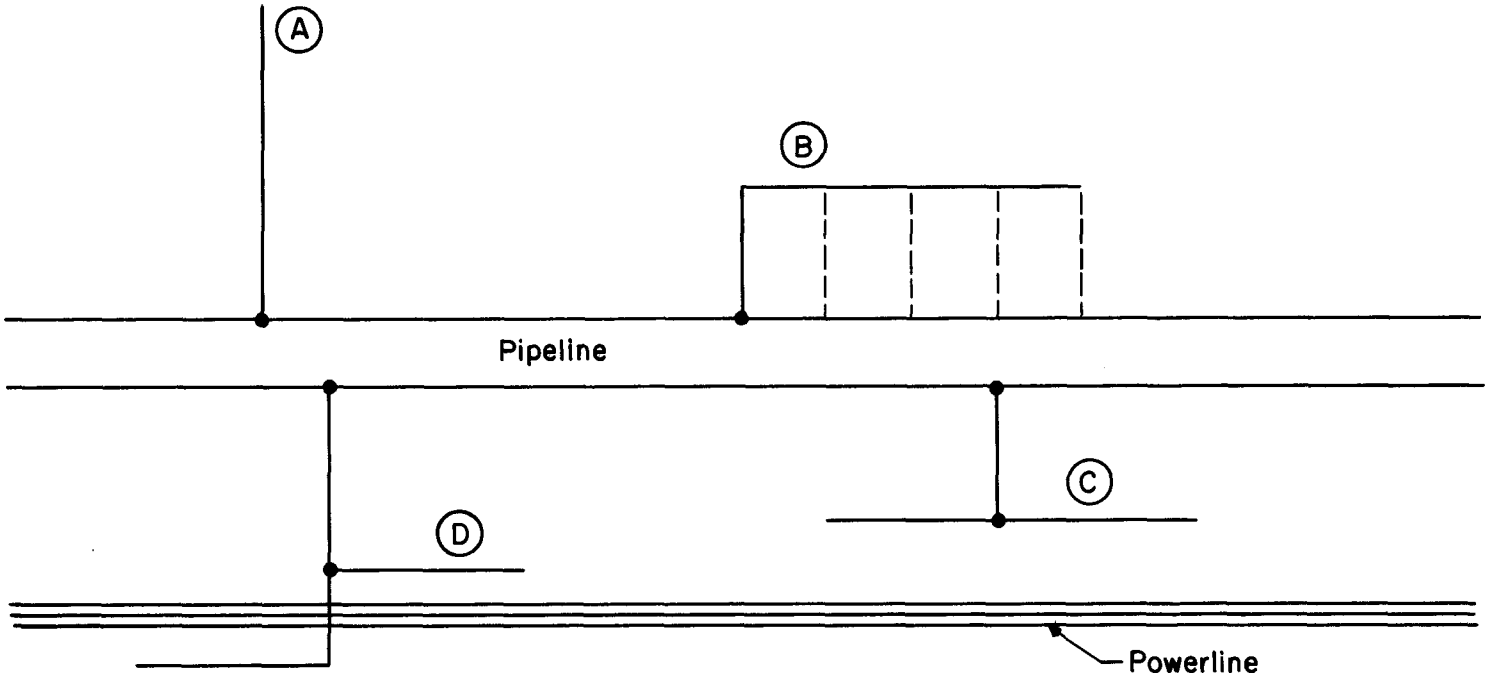

Fig. 8-15 TYPES OF HORIZONTAL GROUND CONDUCTOR INSTALLATIONS

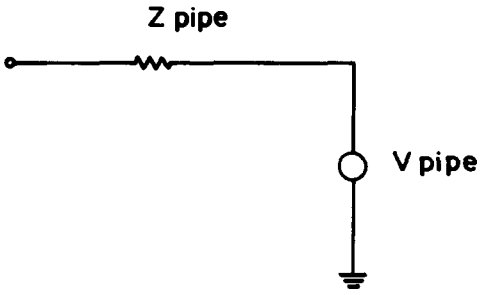

(a) Pipeline alone at observation point

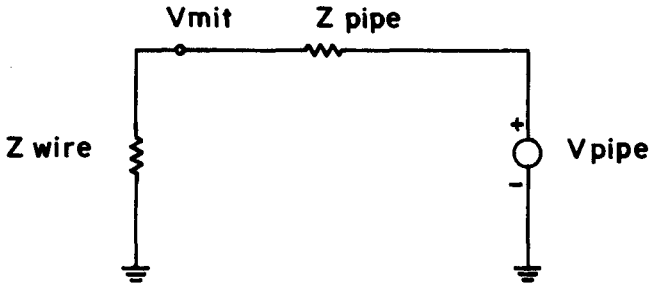

(b) With Mitigation wire "A"

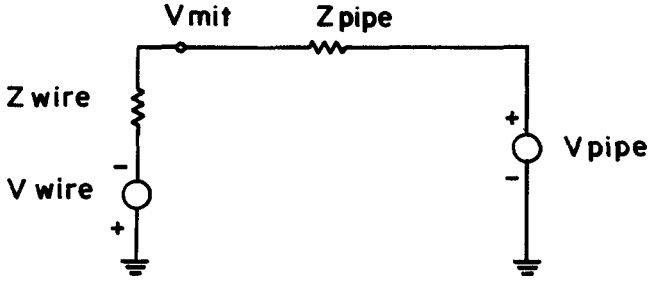

(c) With Mitigation wire "B"

Fig. 8-16 HORIZONTAL GROUND WIRE EQUIVALENT CIRCUITS

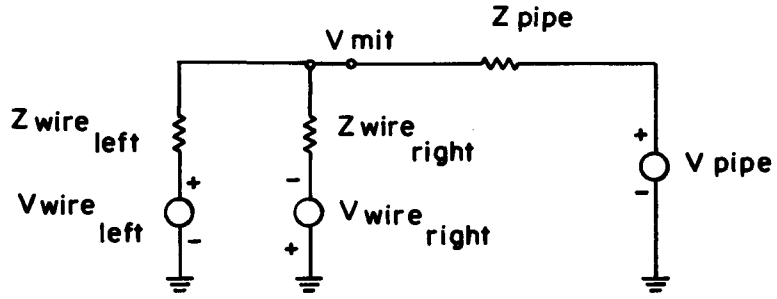

(d) With Mitigation wire "C"

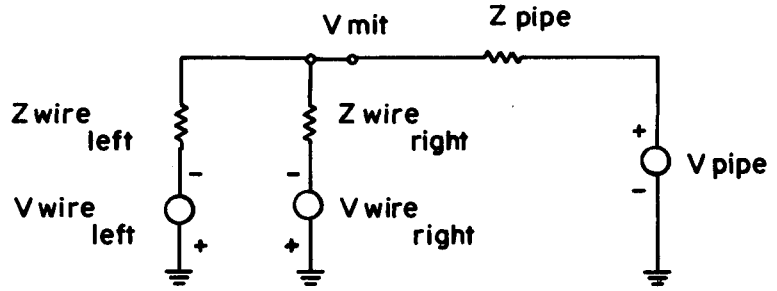

(e) With Mitigation wire "D"

Fig. 8-16 (Cont.) HORIZONTAL GROUND WIRE EQUIVALENT CIRCUITS

$$Z_i = \frac{1}{\pi a^2 \sigma}\left[1 + \frac{1}{48}\left(\frac{a}{\delta}\right)^2\right] + j\,\frac{\omega\mu}{8\pi} \text{ ohms/meter} \qquad (8\text{-}11b)$$

where a is the wire radius, and δ = wire skin depth = $(\pi\sigma f\mu)^{-\frac{1}{2}}$.

2. Apply the calculator program THEVENIN, documented in Appendix A, to determine Z_{wire} by using γ_{wire} and $Z_{o,wire}$ as data inputs. This program is suitable for wires of arbitrary length and having arbitrary far-end impedance loads. The program achieves this degree of generality by solving the impedance-transformation equation of an electrical transmission line (Eq. 3-10c).

3. Apply the calculator program NODE, (see Appendix A) to determine the unknown node voltage, V_{mit}, of Figure 8-16b. Here, Z_{wire}, Z_{pipe}, and V_{pipe} are used as data inputs. This gives the value of the pipeline voltage after connection of the horizontal ground wire. The values of V_{pipe} and Z_{pipe} are available in the Mojave Desert case history (c.f. Section 3). The proper values to be used are those appropriate to the equivalent circuit at milepost 101.7.

Figure 8-17 illustrates the importance of accounting for the transmission line properties of a ground wire when determining its mitigation effectiveness. Here, the straight line plots the dc resistance of an experimental wire installed at the Mojave test site, as computed using the most common grounding formula,

$$R = \frac{\rho}{\pi\ell}\left(\ln\frac{2\ell}{a} - 1\right) \qquad (8\text{-}12)$$

where ρ = ground resistivity; ℓ = length of wire; and a = radius of wire. The curve plots the value of Z_{wire}, obtained using the computer programs WIRE and THEVENIN discussed above. Finally, the solid squares represent values of grounding impedance actually measured during the field test. It is seen that the experimental results agree extremely well with the results of the transmission line approach of the TI-59 programs, which predicts a leveling off of the grounding impedance at $Z_{o,wire}$ as the wire length exceeds 1/Real(γ_{wire}). Hence, for a given grounding installation, there is an optimum length (in the vicinity of the knee of the curve) where the mitigation-efficiency/cost ratio is greatest. Thus, indiscrimately lengthening a perpendicular ground wire may not necessarily be cost effective. This is in sharp contrast to results implied by the dc grounding resistance formula, which is evidently useful only for small-to-moderate conductor lengths.

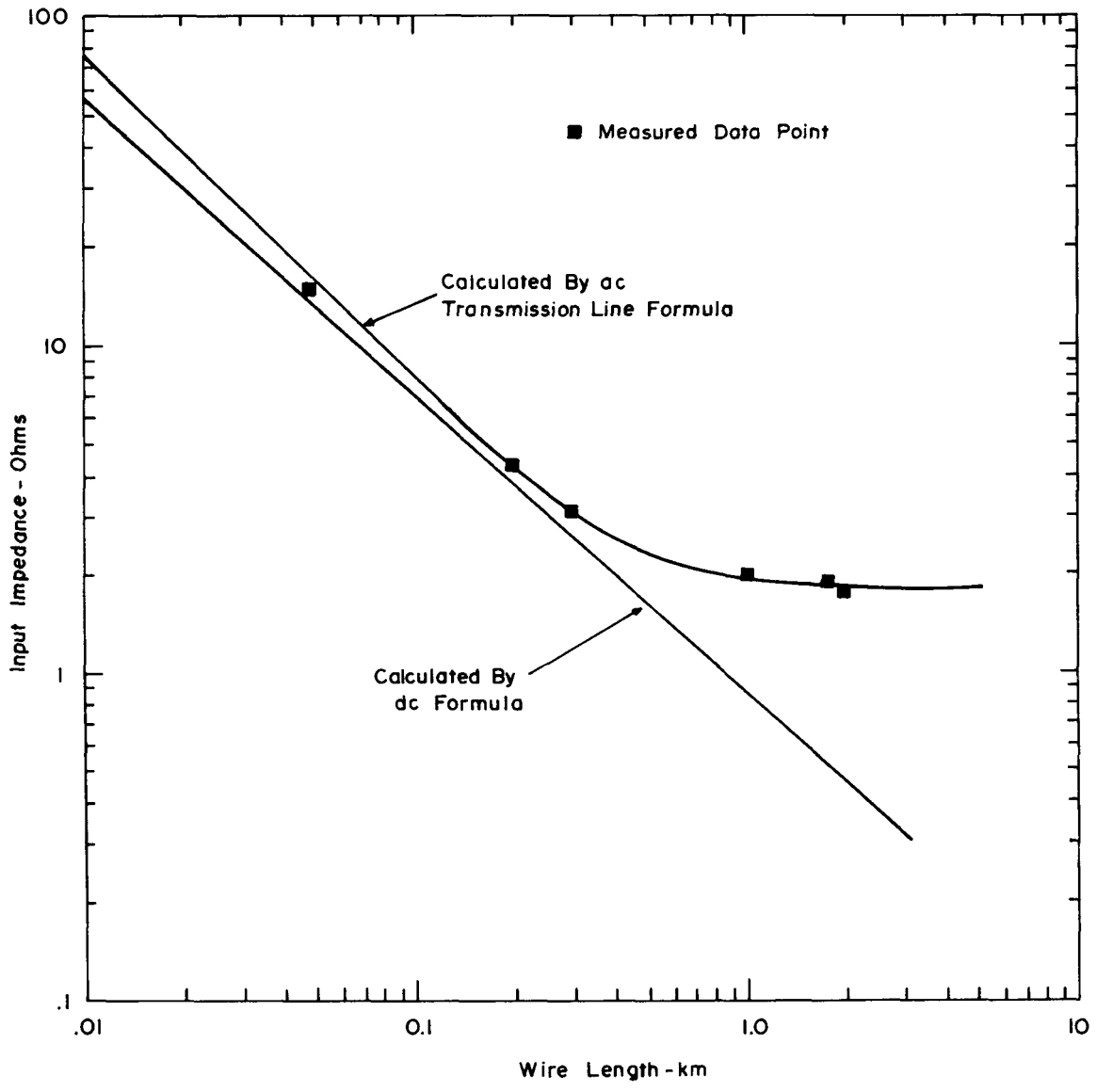

Fig. 8-17 GROUNDING IMPEDANCE OF HORIZONTAL WIRE

End-Connected Parallel Ground Wire. This ground wire configuration, denoted as B in Figure 8-15, requires additional analysis steps to account for the effects of a voltage build-up on the ground wire due to its parallelism with the power line and mutual coupling between the pipeline and the ground wire. In this configuration, the wire acts as both the grounding impedance, Z_{wire}, and the voltage source, V_{wire}, as shown in Figure 8-16c. The overall mitigation effect is computed in six steps:

1. Apply the calculator program CARSON (see Appendix A) to determine the mutual impedances between the power line phase conductors and each passive-multiple-grounded conductor sharing the right-of-way, including the pipeline to be mitigated and the ground wire. Repeat the procedure to determine the mutual impedances between all passive multiple-grounded conductors on the right-of-way.

2. Apply the calculator program CURRENTS (see Appendix A) to determine the maximum currents within the pipeline to be mitigated and other passive conductors on the right-of-way under the influence of the power line, the ground wire, and each other.

3. Apply the calculator program FIELD (see Appendix A) to determine the driving electric field at the ground wire location. This program forms and then sums (current) x (mutual impedance) products determined using the data inputs of Steps 1 and 2. Contributors to this field include the power line phase wires and other current carrying conductors in the vicinity.

4. Apply the calculator program WIRE to determine the propagation constant and characteristic impedance of the ground wire.

5. Apply the calculator program THEVENIN to determine Z_{wire} and V_{wire} using the results of Steps 3 and 4 as data inputs.

6. Apply the calculator program NODE to determine V_{mit} of Figure 8-16c. Here, Z_{wire}, V_{wire}, Z_{pipe}, and V_{pipe} are used as data inputs. The same values for V_{pipe} and Z_{pipe} as in the previous perpendicular wire example are used here, since connection of this wire is also made to the pipe at milepost 101.7.

For best results with this ground wire configuration, the phase of V_{wire} should equal that of V_{pipe} + 180° in order to achieve a voltage cancellation effect at V_{mit}. This is illustrated in Figure 8-16c by the choice of signs of the V_{wire} and V_{pipe} voltage sources. In the ideal case, $V_{wire}/Z_{wire} = -V_{pipe}/Z_{pipe}$, so that $V_{mit} = 0$. The wire impedance and voltage properties can be adjusted by choosing the wire length and separation from the power line. However, this usually does not give enough adjustment range to attain the ideal case. Additional adjustment can be

realized by either a continuous or lumped inductive loading of the ground wire to alter its transmission line characteristics. Program WIRE is structured to permit data input of the average added inductive resistance per kilometer due to inductive loading to allow rapid calculation of the new wire propagation constant and characteristic impedance. Then, program THEVENIN can be used to compute the new V_{wire}/Z_{wire} ratio.

The chief effect of connecting a long, parallel ground wire and an adjacent pipeline with multiple ties (indicated by the dashed lines of the B configuration of Figure 8-15) is the reduction of the effective V_{wire} and Z_{wire}, in a manner discussed below. This can be useful under conditions where voltage cancellation at V_{mit} is not deemed important. If such ties are used, they should be spaced no closer than $1/\text{Real}(\gamma_{wire})$ for maximum effect at minimum cost.

Center-Connected Parallel Ground Wire. This ground wire configuration, denoted as C in Figure 8-15, is aimed at achieving minimum values of V_{wire} and Z_{wire} for any given length of wire. Its performance is most easily understood by examining the equivalent mitigation circuit shown in Figure 8-16d. From this figure, it is seen that the center connection causes the effective V_{wire} to equal zero because of the bucking effect of $V_{wire,left}$ and $V_{wire,right}$. Further, the effective Z_{wire} is seen to equal the parallel combination of $Z_{wire,left}$ and $Z_{wire,right}$. This value is always less than the grounding impedance for the wire when used in an end-connected manner for mitigation because of the leveling off of the impedance curve with length. (In effect, two short wires give a lower grounding impedance than one long wire having the combined length of the short wires).

The mitigation effect of this ground wire configuration can be computed simply by applying program WIRE to determine γ_{wire} and $Z_{o,wire}$; then applying THEVENIN to determine $Z_{wire,left}$ and $Z_{wire,right}$; and finally applying NODE. In applying NODE, the voltage sources $V_{wire,left}$ and $V_{wire,right}$ need not be known specifically because of their self-cancelling effect. So that a value of zero volts can be assumed for both. Thus, in many respects, calculation of the mitigation effectiveness of a center-connected parallel ground wire is the same as for the perpendicular ground wire.

Back-to-Back Parallel Ground Wire.* This ground configuration, denoted as D in Figure 8-15, is aimed at achieving simultaneously a maximum value of V_{wire} and a minimum value of Z_{wire} for a given length of wire. This is made possible by moving one ground wire leg to the opposite side of a horizontal configuration power line, so that the fields driving the two legs are equal in magnitude but 180^{o} out of phase. Thus, as shown in Figure 8-16e, $V_{wire,left}$ and $V_{wire,right}$ reinforce each other instead of bucking, allowing a maximum cancellation effect at V_{mit}. Similar to the center-connected parallel ground wire, the effective Z_{wire} is seen to equal the parallel combination of $Z_{wire,left}$ and $Z_{wire,right}$.

The mitigation effect of this ground wire configuration can be computed by treating the left and right halves of the ground wire as two distinct end-connected parallel ground wires, and combining the results for $V_{wire,left}$, $Z_{wire,left}$ and $V_{wire,right}$, $Z_{wire,right}$, using program NODE.

Example. An example of the design calculations for a back-to-back mitigation wire arrangement is presented here. This design was originally proposed for installation on the Southern California Gas Company Line 235 for mitigation of the voltage peak at Milepost 101.7. A more detailed analysis of this mitigation wire design concept is given in Appendix E. The physical installation of the wire is shown in Figure 8-18. The design computations involve the following steps.

Computation of Z_{pipe} and V_{pipe}. The first part of this analysis requires computation of the Thevenin equivalent source impedance, Z_{pipe}, and source voltage, V_{pipe}, of the pipeline at Milepost 101.7. The computation involves the following steps:

a. Assumption of a 700 kΩ - ft^2 pipe coating resistivity, a 40 kΩ - cm earth resistivity, and a 700 ampere balanced power line current loading;

b. Use of the computer program CARSON applying the exact Carson's infinite series to calculate the driving electric field at the pipeline as being equal to 14 volts/km at a phase of -122.6^{o} relative to the power line currents;

*Best applicability for mitigation of the effects of power lines having a combination of configurations and phase sequences yielding an electric field with a phase difference of approximately 180^{o} from one side of the power line to the other.

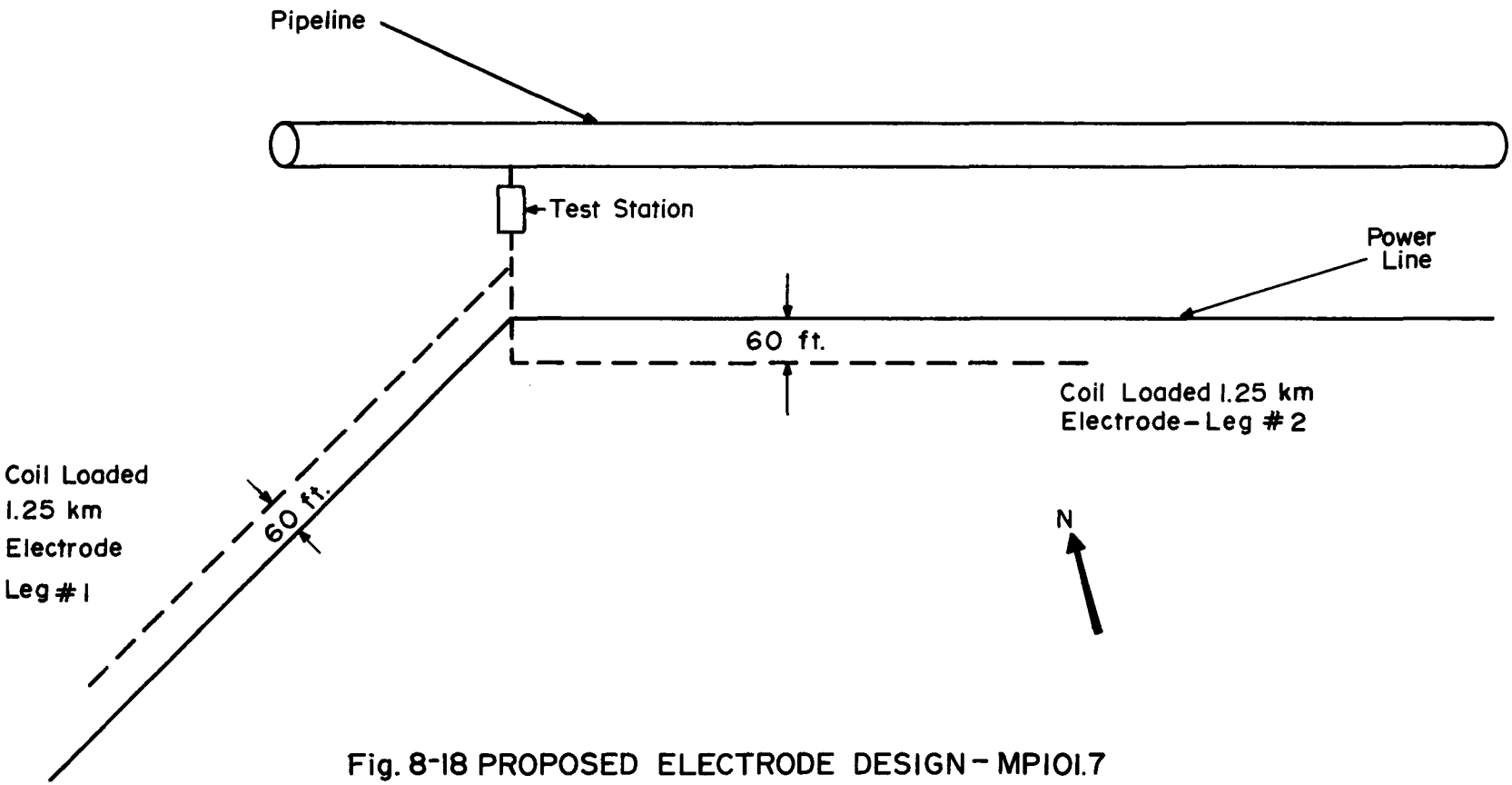

Fig. 8-18 PROPOSED ELECTRODE DESIGN - MP101.7

c. Interpolation of the graphs of Figure 2-7 (Section 2) to obtain the pipeline propagation constant equal to $0.115 + j\,0.096)\ km^{-1}$.

d. Computation of V_{pipe} as

$$V_{pipe} = \frac{-0.5 \times 14.0/-122.6^{o}}{(0.115 + j\,0.096)} = 46.7/\underline{17.6^{o}}\ \text{volts}$$

using Eq. 3-18a and the condition that $Z_1 = Z_o$.

e. Interpolation of the graphs of Figure 2-23 to obtain the pipeline characteristic impedance, Z_o, equal to $(2.9 + j\ 2.4)\,\Omega$;

f. Computation of $Z_{pipe} = 0.5\ Z_o$, or

$$Z_{pipe} = 0.5\ (2.9 + j\ 2.4) = (1.45 + j\ 1.2)\,\Omega = 1.88/\underline{39.6^{o}}\,\Omega.$$

The pipeline section to the west of Milepost 101.7 is assumed to be sufficiently far from the power line so that it experiences little or no induced voltage pickup. This pipeline section thus serves as a characteristic impedance load for the section to the right of Milepost 101.7, which is influenced by the power line. Therefore, a multiplying factor of 0.5 is introduced into the calculations for V_{pipe} (Step d) and Z_{pipe} (Step f) to take into account the Z_o loading effect of the west section upon both the Thevenin source voltage and the pipe source impedance to the east which is also equal to Z_o. The Thevenin equivalent resistance is equal to the parallel combination of both impedances and, hence, equal to $0.5\ Z_o$. Due to voltage divider action, the source voltage is likewise reduced by a factor of one-half.

Computation of Z_{wire} and V_{wire}. This part of the analysis computes the Thevenin equivalent source impedance, Z_{wire}, and source voltage, V_{wire}, of the mitigating wire. The computation involves the following steps.

a. Assumption of a wire burial depth of one foot, a 40 kΩ-cm soil resistivity at the wire and a 700 ampere balanced power line current loading;

b. Use of the CARSON computer program (listed in Appendix A) applying the exact Carson's infinite series to calculate the driving electric field at the wire as being equal to 29.2 volts/km at a phase of -121.5^{o} relative to the power line currents.

c. Use of the computer program WIRE solving the Sunde propagation constant equation to obtain the propagation constant of the mitigating wire, equal to $(1.137 + j\ 1.022)\ km^{-1}$ and the wire characteristic impedance, equal to $(1.122 + j\ 0.816)\,\Omega$. Calculations were made for a 0.372-inch diameter bare Aluminum wire loaded at the rate of 1.5 Ω-km.

d. Use of the THEVENIN program (listed in Appendix A) to obtain $Z_{wire} = 1.259/\underline{32.3^o}$ Ω, and V_{wire} (normalized to a power line field of 1 volt/km) = $.573/\underline{-15.8^o}$ volts.

e. Computation of V_{wire} as

$$V_{wire} = .573/\underline{-15.8^o} \times 29.2/\underline{-121.5^o} = 16.7/\underline{-173.3^o} \text{ volts}$$

In this analysis, the entire length of the mitigating wire is assumed to be influenced by a constant power line field of 29.2 volts/km. The effects of reduced electric field near the 135° angle "corner" of the power line are not included.

Computation of V_{mit}. This part of the analysis is the computation of the voltage at Milepost 101.7 after mitigation, V_{mit}. This computation involves simply joining the two Thevenin equivalent circuits for the pipeline and mitigation wire, respectively, and solving a single node equation (the program NODE may be used here) for the voltage at the junction. This results in

$$V_{mit} = \frac{V_{wire} \times Z_{pipe} + V_{pipe} \times Z_{wire}}{Z_{pipe} + Z_{wire}}$$

$$= \frac{(16.7/\underline{-137.3^o})(1.88/\underline{39.6^o}) + (46.7/\underline{17.6^o})(1.259/\underline{32.3^o})}{(1.88/\underline{39.6^o} + 1.259/\underline{32.3^o})}$$

$$= 11.6/\underline{-14.2^o} \text{ volts.}$$

Computation of V_{mit} - Complete System. In this computation, the values of V_{pipe} and Z_{pipe} remain unchanged. The individual wires comprising each leg of the mitigation system are located in a mirror image configuration about the power line structure. The electric fields driving the respective wires, therefore, are 180° out of phase. However, because the direction of the wires from the point of pipe connection, relative to the power line electric fields, differ by 180°, the induced voltages in each leg are identical. Therefore, the open circuit Thevenin voltage for both wires connected together is equal to V_{wire} as derived previously. However, relative to earth, the input impedances of the wires are in parallel after connection, and Z_{wire} for the complete system is one-half of the previous value, or $0.630/\underline{32.3^o}$. The mitigated value for the complete system then becomes

$$V_{mit} = \frac{(16.7/\underline{-137.3^{o}})(1.88/\underline{39.6^{o}}) + (46.7/\underline{17.6^{o}})(.63/\underline{32.3^{o}})}{1.88/\underline{39.6^{o}} + .63/\underline{32.3^{o}}}$$

$$= 6.8/\underline{-68.1^{o}} \text{ volts}$$

Complete Pipeline Mitigation. The previous discussions were directed toward considering each mitigation wire individually and, hence, mitigation at a single point on the pipeline. In general, due to multiple physical or electrical discontinuities along the right-of-way, a pipeline will develop a number of induced voltage peaks. Installation of a single mitigation wire may reduce the local pipeline voltages but leave the other peaks unaffected. In fact, slight increases of the pipeline voltage may be caused a few miles from the grounding point due to the discontinuity of the corridor geometry introduced by the ground wire itself. However, as discussed below, experimental results show that complete pipeline mitigation is possible by mitigating successive voltage peaks individually.

An assessment of the possibility of complete pipeline mitigation, obtained by direct measurements at the Mojave test site, is summarized in Figure 8-19. The upper graph shows the mitigation obtained by installing a 2.25 km (7400 ft) total length, back-to-back parallel ground wire at Milepost 101.7. The wire was stranded aluminum, 9.4 mm (0.37 in.) diameter, and buried at a depth of 30 cm (1 ft) along two paths parallel to the power line and 18.3 m (60 ft) to either side of the power line center phase. From the figure, it is seen that the original voltage peak at Milepost 101.7 of nearly 50 volts was reduced by about 90% by installing this ground wire, representing a virtually complete mitigation. In fact, some mitigation was recorded at Milepost 89. However, although not necessarily serious, an increase in the induced voltage was measured in the region between the two peaks. This is reminiscent of the balloon effect -- i.e., "squeeze" the pipeline voltage at one point and it enlarges somewhat at other points.

The lower graph of Figure 8-19 shows the extra mitigation obtained by installing an additional 0.8 km (2600 ft) total length, center-connected parallel ground wire at Milepost 89. This wire was solid aluminum, 3.0 mm (0.12 in) diameter, and buried at a depth of 5 cm (2 in) along a path parallel to the power line and 30 m (100 ft) from the center phase. From the figure, it is seen that the combined mitigation system at Mileposts 101.7 and 89 succeeded in pipeline voltage reduction not only at the peaks, but at intermediate locations as well. Hence, it has been demonstrated that by a reasonable placement of mitigation wires at points of corridor discontinuity, long lengths of pipeline can be mitigated effectively.

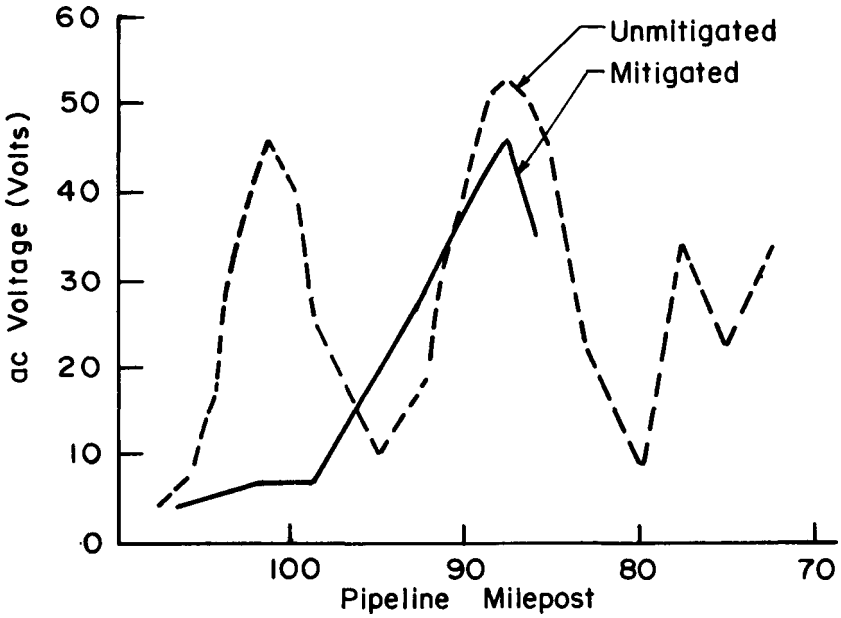

(a) Back-To-Back System Installed At Milepost 101.7

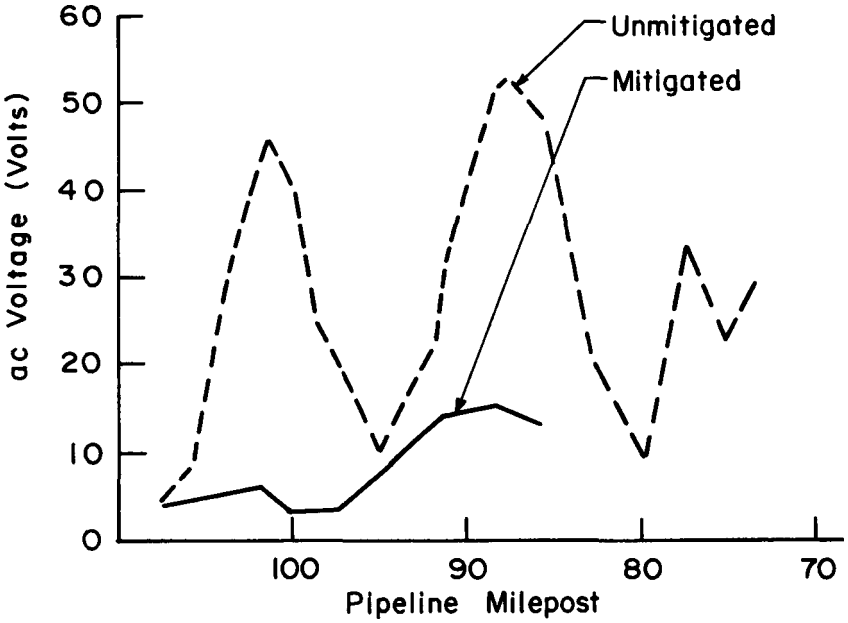

(b) Additional Center-Connected System Installed At Milepost 89

Fig. 8-19 EXPERIMENTAL MITIGATION OF THE MOJAVE PIPELINE

Grounding Mats. Protection against electric shock can be provided by installing ground mats at all exposed pipeline appurtenances, such as valves or metallic risers. As discussed previously in this section, such mats can be constructed of strip galvanic anode material buried in a spiral pattern just below the surface and connected to the pipeline electrically. In general, ground mats provide local protection at exposed appurtenances against electric shock caused by unequal pipe and soil potentials. The use of ground mats is not a substitute for a well-designed, low impedance pipeline grounding system designed to reduce pipe voltages over significant portions of the pipeline.

Use of Screening Conductors

Above-Ground Screen Conductor. The electromagnetic coupling mitigation effectiveness of installing a grounded wire under the phase conductors of a power line has been investigated (11). The wire was assumed to be either a single conductor or a bundle conductor connected electrically to each tower at a constant height, and centered beneath the phases. Calculations showed that such a grounded conductor could reduce electromagnetic coupling. An optimum height for reduction of the coupling, was found by calculation. For example, a twin bundle conductor with an effective diameter of 0.116 m and a resistance of 0.135 ohms/km was computed to have a mitigation of about 95% when placed at a height of 5 to 7 m under a double circuit 150 kV power line. An optimum inductive coupling reduction was possible for each phase conductor configuration studied.

However, as discussed previously in detail in this section, calculations performed especially for this book have demonstrated the great sensitivity of this technique to power line current unbalances. The reader is referred to the previous discussions.

Buried Screen Conductor. An investigation of the electromagnetic coupling mitigation effectiveness of burying a conductor parallel to a buried pipeline has been completed (4). Experimental studies on a scale model provided an estimate of the magnitude of the mitigation possible under varying conditions of earth conductivity, conductivity of the coating of the conductor, and spacing between the conductor and the pipeline. It was found that the screening increased as the mutual inductance of the conductor and the pipeline increased, and as the conductivity of the screen conductor coating increased. However, this reference did not provide enough data to allow assessment of the results for immediate application to pipeline systems.

Use of Insulating Devices

Risers and Vent Pipes. Insulating materials may be used in place of steel in some cases where the danger of high ac pipeline potentials is known to be a factor. As an example, vent pipes accessible to the public may be constructed of plastic to eliminate the possibility of electric shock should a high potential exist on the casing pipe. Riser conduit may be plastic; junction boxes may be plastic or plastic coated; terminal blocks may be "dead front", requiring the insertion of contact making plugs in order to connect leads to the carrier pipe.

Joints. Insulating joints are used on pipelines to electrically separate sections of the line from terminal facilities and pumping systems. They are also used to divide the line into sections so that the development of contacts with other structures or the failure of cathodic protection facilities are confined to a single section. These sections can be as long as several miles.

In the past, insulating joints have been used to attempt mitigation of ac interference effects on pipelines by reduction of the electrical length of the pipeline exposed to the interference source. Indeed, the use of insulating joints exclusivley to systematically bound pipeline voltages has been investigated (17). However, a given pipeline situation must be analyzed carefully because the introduction of insultating joints may worsen, rather than mitigate, the interference problem, i.e., buried pipeline sections longer than $2/\text{Real}(\gamma)_{\text{pipe}}$ m should develop exponential voltage peaks at the locations of the insulators. Thus, while a long pipeline might have only two voltage peaks (at its ends) the insertion of an insulator at the midpoint of the pipeline could cause a third voltage peak to appear at the location of the new insulator.

To avoid the generation of induced voltage peaks at pipeline insulators, a low impedance polarization cell should be connected across each insulator. In this way, direct current required for cathodic protection could be confined to the desired pipeline section, but no pipeline discontinuities would be presented to the 60 Hz electromagnetic field and, thus, no spurious induced voltage peaks would be generated. Installation of polarization cells at each insulator would have the additional advantage of providing protection from insulator flashover during fault conditions of the power line. Additional insulator protection can be provided by installing lightning arrestors with a threshold of no more than 150 volts across each insulator-polarization cell parallel combination.

Pipeline Extensions

The appearance of exponential induced voltage peaks at the ends of a parallel, buried pipeline (as discussed in 4, 18) suggests that the pipeline potential distribution can be altered for mitigation purposes by simply extending the pipe. In this way, the locations of the voltage peaks might be shifted from an accessible, or functional, section to an inaccessible, or non-functional section. The induced potentials at the original endpoints of the pipe section could be reduced by as much as 63% for each extension of the pipe by $1/\text{Real}(\gamma)_{pipe}$ beyond the original end points. While there are obvious limitations to this technique in practice, it is conceivable that it could be preferred in some cases where mitigation is required on a large, in-service line.

MITIGATION OF GROUND CURRENT COUPLING

Spacing of the Pipeline from the AC Power Line

Where possible, ground current coupling of an ac power line to an adjacent pipeline can be mitigated simply by locating the pipeline (and any pipeline grounding electrodes) as far as possible from the affecting power line towers. In this way, the pipe-to-soil potential is minimized, and the twin hazards of electric shock and pipeline coating punctures are reduced. The variation of the earth potential with distance from a power line is now reviewed.

Power Line with No Counterpoise. Assuming that $I_{g,n}$, the ground current flowing to earth through the footing of the nth power line tower is known or can be calculated using the methods of Section 5, the tower footing potential for the homogeneous earth case is given by

$$|U_n| = \frac{|I_{g,n}|}{2\pi\sigma r_n} \text{ volts} \qquad (8\text{-}13a)$$

where σ is the earth conductivity and r_n is the radius of an equivalent hemispherical electrode having the same ground resistance as the tower. r_n is of the order of 2 to 3 m for an average single or double circuit tower, but may be 6 to 10 m for bridge type towers with multiple tower legs (20). For earth conductivities in the range of 0.05 - 0.0005 mhos/m, footing potentials calculated using Eq. 8-13a can lie in the range of $0.32\ I_{g,n}$ - $160\ I_{g,n}$. It is seen that footing potentials can reach the kilovolt level under fairly common ground current and

earth conductivity conditions. The earth potential at a radial distance, r, from the tower is related to the footing potential by

$$|U(r)| = |U_n| \cdot \frac{r_n}{r} \text{ volts} \qquad (8\text{-}13b)$$

for the homogeneous earth case.

Equation 8-13b indicates that the potential of homogeneous earth under ground current conditions is an inverse function of the distance from the tower. Measurements have shown that this decrease law is correct for r exceeding about $3r_n$ (4). However, the results are very different if the ground is not homogeneous. For example, a more rapid decrease with distance is observed for soils whose lower stratum conductivity is greater than the surface stratum conductivity. The structure of this ground concentrates the currents towards the deep strata and considerably increases the potential gradients in the near vicinity of the tower. On the other hand, if a tower stands on high conductivity ground superposed on low conductivity ground, the voltage decrease as a function of the distance can be much slower than than given in Eq. 8-13b.

Power Line With Continuous Counterpoise. Reference 20 states that in the presence of both structure grounds and counterpoise conductors, the largest part of the ground current is discharged by the counterpoise. Therefore, the grounding impedance of a power line with counterpoise is essentially that of the counterpoise itself. Assuming that the counterpoise is realized by a single, bare, buried wire connecting each tower footing, and that a ground current condition occurs midway in the power line run, the impedance to remote earth presented to the ground current is $0.5\ Z_{o,wire}$, where $Z_{o,wire}$ is the ac grounding impedance observed at the end of a bare, horizontal, buried wire having a length greater than 2/Real (γ_{wire}). The potential of the counterpoise and the connected tower footings in the current grounding area is estimated as:

$$\begin{aligned} |U_c| &\simeq |0.5\ I_g\ Z_{o,wire}| \\ &\simeq |I_g| \frac{2.45 \times 10^{-3}}{\sqrt{\sigma}} \ln\left(\frac{72.7}{a'\sqrt{\sigma}}\right) \text{ volts} \end{aligned} \qquad (8\text{-}14a)$$

where I_g is the total ground current, σ is the (homogeneous) earth conductivity, and $a' = \sqrt{2a\bar{h}}$, where a is the radius of the counterpoise conductor and $\bar{h}$ is its burial depth. For earth conductivities in the range of 0.05 - 0.0005 mhos/m, potentials calculated using Eq. 8-14a can lie in the range of $0.1\, I_g$ - $1.0\, I_g$. These potentials are significantly less than those calculated for the no-counterpoise case. The peak earth potential at a separation, d, from the counterpoise is approximated using the decrease law for a buried horizontal wire discharging direct current (13):

$$|U(d)| \simeq \frac{\ln\left(\frac{\sqrt{\delta^2 + d^2} + \delta}{\sqrt{\delta^2 + d^2} - \delta}\right)}{2 \ln\left(\frac{2\delta}{\bar{h}}\right)} |U_c| \text{ volts} \qquad (8\text{-}14b)$$

where δ is the earth electrical skin depth (equal to $65/\sqrt{\sigma}$ meters at 60 Hz).

Equation 8-14b assumes that the counterpoise has an effective length of δ on each side of the grounding mid-point. This decrease law should be accurate enough (in homogeneous soils) to allow the safe placement of a buried pipeline. However, as for the no counterpoise case, an inhomogeneous ground can have significant effects on the potential distribution function that cannot be readily analyzed.

Buried Screen Conductor

Laboratory experiments investigating the mitigation of ground current coupling by burying a bare conductor parallel to an affected pipeline have been reported (4). The experiments measured the voltage distribution in simulated soils having a conductivity in the range of 0.1 - 0.0003 mhos/m by employing a 1 m diameter electrolytic tank. Results indicated that a bare conductor can appreciably reduce the ground potential within a distance of about 5 m from it. Increasing the length of the conductor served to accentuate the mitigation. A simulated 600 m long conductor was found to reduce its local soil potential by about 70%; a 6 km long conductor achieved better than 95% reduction. No confirming field tests of these results were reported, however. Connection of the pipeline to the bare conductor by means of spark gaps was suggested as a means of limiting the voltage across the pipe coating during extreme fault conditions without disturbing the normal cathodic protection system of the pipeline.

Grounding Mats

Protection against electric shock can be provided by installing ground mats at all exposed pipeline appurtenances, such as valves or metallic risers. As discussed previously in this section, such mats can be constructed of strip galvanic anode material buried in a spiral pattern just below the surface and connected to the pipeline electrically. In general, ground mats provide local protection at exposed appurtenances against electric shock caused by unequal pipe and soil potentials. Ground mats will not protect either the pipeline coating or steel from puncture during severe faults.

REFERENCES

1. IEEE Working Group on Electrostatic Effects of Transmission Lines. "Electrostatic Effects of Overhead Transmission Lines Part I - Hazards and Effects." IEEE Trans. Power App. Systems, Vol. PAS-91, March/April 1972, pp. 422-426.

2. A. H. McKinney. "Electrical Ignition of Combustible Atmospheres." ISA Transactions, Vol. 1, No. 1, January 1962, pp. 45-64.

3. C. F. Dalziel. "Electrical Shock Hazard." IEEE Spectrum, Vol. 9, No. 2, February 1972, pp. 41-50.

4. B. Favez and J. C. Gougeuil. "Contribution to Studies on Problems Resulting from the Proximity of Overhead Lines with Underground Metal Pipe Lines." Paper No. 36 presented at CIGRE, Paris, France, June 1966.

5. T. M. McCauley. "EHV and UHV Electrostatic Effects: Simplified Design Calculations and Preventative Measures." IEEE Trans. Power App. Systems, Vol. PAS-94, November/December 1975, pp. 2066-2070.

6. J. C. Procario and S. A. Sebo. Discussion following Reference 5 in IEEE Trans. Power App. Systems, Vol. PAS-94, November/December 1975, pp. 2066-2070.

7. A. W. Peabody and A. L. Verhiel. "The Effects of High Voltage Alternating Current (HVAC) Transmission Lines on Buried Pipelines." Paper No. PCI-70-32 presented at the IEEE/IGA Petroleum and Chemical Industry Conference, Tulsa, Oklahoma, September 15, 1970.

8. C. F. Dalziel and F. P. Massoglia. "Let-Go Currents and Voltages." Paper No. 56 presented at the AIEE Winter General Meeting, New York, NY, January 1956.

9. H. Lowenbock and J. E. Morgan. "The Human Skin as a Conductor of 60 Cycle Alternating Current of High Intensity Studied on Electroshock Patients." J. of Lab. and Clinical Medicine, Vol. 28, 1943, pp. 1195-1198.

10. Electrostatic and Electromagnetic Effects of Ultrahigh-Voltage Transmission Lines. Palo Alto, California: Electric Power Research Institute, June 1978. EL-802.

11. A. H. Manders, G. A. Hofkens, and H. Schoenmakers. "Inductive Interference of the Signal and Protection System of the Netherlands Railways by High Voltage Overhead Lines Running Parallel with the Railways." Paper No.36-02 presented at CIGRE, Paris, France, August 1974.

12. G. R. Elek and B. E. Rokas. "A Case of Inductive Coordination." IEEE Trans. Power App. Systems, Vol. PAS-96, May/June 1977, pp. 834-840.

13. A. W. Peabody and C. G. Siegfried. Recommendations for the Mitigation of Induced ac on the 34-inch Line 235 from Newberry to Needles, California. Houston, Texas: Ebasco Services, Inc., June 27, 1975. Consulting Report to Southern California Gas Company.

14. E. D. Sunde. Earth Conduction Effects in Transmission Systems. New York, New York: Dover Publications, 1968.

15. E. F. Vance. DNA Handbook Revision, Chapter 11 - Coupling to Cables. Menlo Park, CA: Stanford Research Institute, December 1974. Report to Department of the Army under Contract DAAG39-74-C-0086.

16. O. Klinger, Jr., editor. "Pipeline News 25th Annual Corrosion Symposium." Pipe Line News, Vol. 47, No. 2, March 1975, pp. 10-42.

17. D. N. Gideon, A. T. Hopper, P. J. Moreland, and W. E. Berry. Parametric Study of Costs for Interference Mitigation in Pipelines. Columbus, Ohio: Battelle Columbus Laboratories, September 30, 1971. Final Report on Project Sanguine to IIT Research Institute.

18. J. Pohl. "Influence of High Voltage Overhead Lines on Covered Pipelines." Paper No. 326 presented at CIGRE, Paris, France, June 1966.

19. A. Pesonen, J. Kattelus, P. Alatalo, and G. Grand. "Earth Potential Rise and Telecommunication Lines." Paper No. 36-04 presented at CIGRE, Paris, France, August 1970.

20. J. Endrenyi. "Analsyis of Transmission Tower Potentials." IEEE Trans. Power App. Systems, Vol. PAS-85, October 1967, pp. 1274-1283.

Section 9

TECHNIQUES FOR MEASURING THE LEVEL OF INDUCTIVE COUPLING TO PIPELINES

INTRODUCTION

This section presents techniques for the measurement of the longitudinal electric field from an electric power transmission line, the effective ac earth conductivity for an inhomogeneous earth, and the impedance of grounding systems. These techniques are important for predicting the level of inductive coupling to pipelines. Included in the discussion are the use of probe wire techniques to determine longitudinal electric fields, the effect of transverse electric fields (electrostatic coupling) upon the accuracy of probe wire measurements, and auxiliary grounding system methods to obtain grounding impedances. This section also discusses methods for measuring induced voltages and currents on existing pipelines. Measurements of ac pipe-to-soil voltage and pipe current are discussed in the context of traditional dc measurements. Here, it is shown that the accuracy of voltage measurements is unaffected by extraneous field pick-up, but the accuracy of current measurements may be impaired by such pick-up. Lastly, the effects of induced ac on dc measurements are reviewed.

MEASUREMENT OF LONGITUDINAL ELECTRIC FIELDS DUE TO POWER LINES

As shown in Section 3, the prediction of the inductive interference to a pipeline caused by a nearby high voltage ac power line requires knowledge of $E_x(s)$, the driving electric field along and parallel to the path of the pipeline. This section discusses techniques for an approximate* measurement of E_x along the path. For all cases where E_x is not constant with position along the pipeline, knowledge of the phase as well as the magnitude of E_x is required for evaluation of the inductive coupling to the pipeline using the analyses of Section 3.

---

*The electric field measured along the ROW with the pipeline absent is the "undisturbed" electric field. Once a pipeline is buried, it will carry an induced current which will cause a change in the induced currents flowing in other grounded conductors. The resultant electric field at the location of the pipeline is thusly modified and in actuality is the "driving" field for the pipeline. Voltage predictions based on "undisturbed" field measurements are generally of acceptable accuracy.

Basic Probe Wire Technique

Reference (1) reports the use of a probe wire to determine the magnitude of the longitudinal mutual impedance between a power line and a telephone circuit. This measurement is equivalent to determining $|E_x|$ due to the power line at the location of the telephone line. Therefore, the details of the probe wire technique are of relevance to the pipeline interference problem.

As shown in Figure 9-1a, the probe wire is simply an insulated wire laid on the earth parallel to the proposed pipeline path and grounded at both ends with driven, vertical rods. The open-circuit voltage, V_{oc}, developed by the probe wire is sensed by a high-input-impedance, frequency-selective voltmeter placed between one ground rod and the end of the wire. Assuming no local ground potential rise due to earth currents, no effects due to transverse electric fields (electrostatic coupling), and a short enough probe wire length, L, (30 meters or less) so that E_x is approximately constant over the length of the probe wire, V_{oc} can be determined by solving the equivalent circuit of Figure 9-1b. Equating voltage drops around the single loop of the circuit yields

$$V_{oc} = I_v(Z_{g_1} + Z_{g_2}) - E_xL \tag{9-1a}$$

where I_v is the input current drawn by the voltmeter, and Z_{g_1} and Z_{g_2} are the earthing impedances of ground rods #1 and #2, respectively. For $I_v \simeq 0$, Eq. 9-1a reduces to

$$V_{oc} \simeq -E_xL \tag{9-1b}$$

and therefore,

$$E_x \simeq -V_{oc}/L. \tag{9-1c}$$

The use of a standard voltmeter with no phase reference implies that only the magnitude of V_{oc} is sensed. Hence, only the magnitude of E_x is obtained:

$$|E_x| \simeq |V_{oc}|/L. \tag{9-1d}$$

Problems With the Basic Probe Wire Technique

Measurement Error Due to Electrostatic Coupling. Electrostatic coupling to the probe wire can cause the voltmeter to sense a value of V_{oc} that is not due solely to E_x. As shown in Figure 9-1c, the effect of electrostatic coupling can be

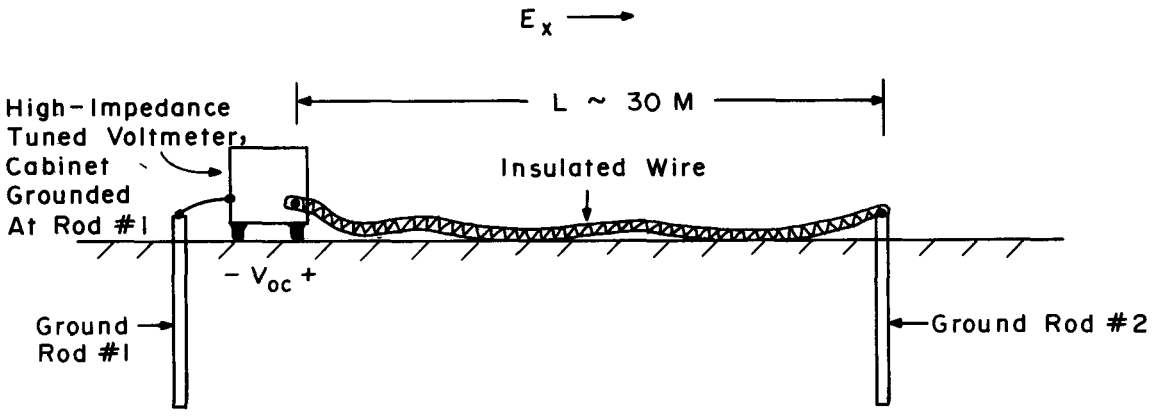

(a) Test Set-up

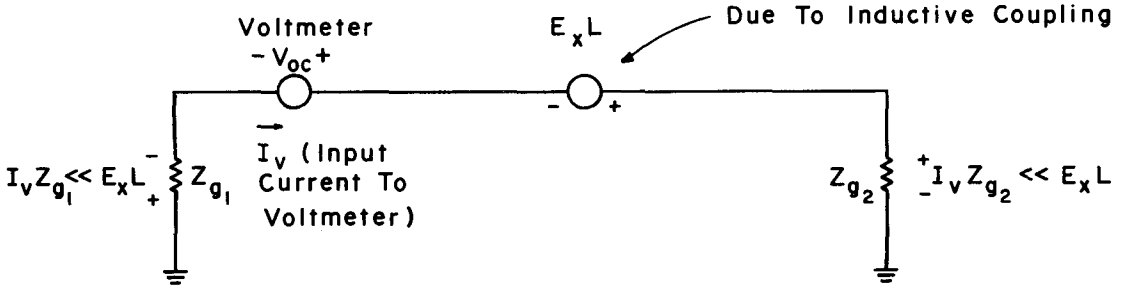

(b) Equivalent Circuit For Ideal Case

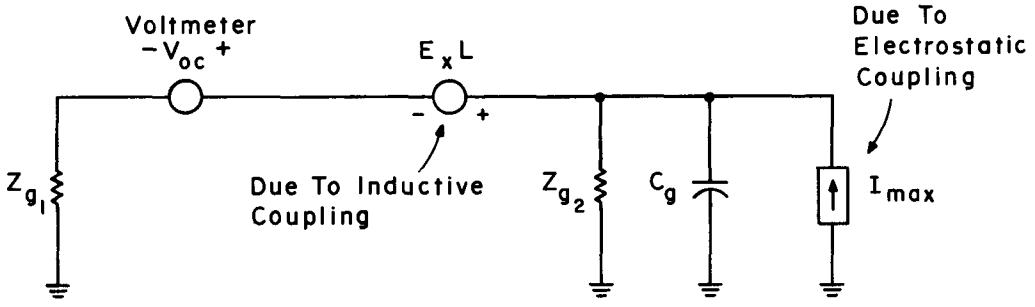

(c) Equivalent Circuit Assuming
Electrostatic Coupling To Probe Wire

Fig.9-1 BASIC PROBE WIRE TECHNIQUE

modeled by introducing a probe wire current source, I_{max}, and capacitance-to-ground, C_g, in parallel with Z_{g_2}. Using Eq. 4-9 of Section 4:

$$C_g = \frac{2\pi\varepsilon_o}{\ell n(4H/d)} \cdot L \text{ F} \tag{9-2a}$$

$$I_{max} = 2\pi f C_g \cdot E_t \cdot H \text{ amps} \tag{9-2b}$$

where H is the height of the probe wire above the effective earth plane, d is the diameter of the probe wire, and E_t is the transverse electric field at the probe wire. Assuming that H/d = 1,

$$C_g = 40 \text{ L pF} \tag{9-3a}$$

$$X_{C_g} = 1/(2\pi \cdot 60 \cdot C_g) = 66/\text{L M}\Omega \tag{9-3b}$$

$$I_{max} = 1.5 \cdot 10^{-8} \text{ L } E_t \text{ H amps.} \tag{9-3c}$$

From Eq. 9-3, it is seen that the reactance of the probe wire capacitance-to-ground, X_{C_G}, is much larger than easily realizable values of ground impedance, Z_g. Therefore, virtually all of I_{max} flows through Z_{g_2}, yielding an electrostatic interference voltage of $I_{max}\ Z_{g_2}$. The ratio of the desired to undesired components of V_{oc} is simply

$$\frac{V_{inductive}}{V_{electrostatic}} = \frac{E_x L}{1.5 \cdot 10^{-8} \text{ L } E_t \text{ H } Z_{g_2}} = \frac{6.7 \cdot 10^7 (E_x/E_t)}{\text{H } Z_{g_2}} \tag{9-4}$$

The "signal-to-noise" ratio of Eq. 9-4 is seen to be a function of the ratio of longitudinal to transverse electric fields, the height of the probe wire above ground, and the grounding impedance of the probe wire. This ratio is independent of the length of the probe wire. For a typical case near a high voltage ac power line, $E_x/E_t = 10^{-6}$, $H_{effective} = 10^{-2}$ m, and Z_g = 100 ohms, yielding a signal-to-noise ratio of about 70. This ratio can be degraded in cases of low-conductivity soil, where $H_{effective}$ and Z_g are increased above these nominal values.

Lack of E_x Phase Information. The E_x phase information necessary for the analyses of Section 3 is not provided by the basic probe wire technique, which measures only the magnitude of E_x, as shown in Eq. 9-1d. Because the phase of E_x is a function of separation from the interfering power line and earth conductivity, it cannot be assumed to be constant over the length of the pipeline.

Figure 3-3 illustrates a typical variation of the real and imaginary components of E_x with distance from an interfering single-phase power line carrying a current of 1 ampere at phase angle 0^o (1). Near the power line, the imaginary part of E_x is much greater than the real part and, therefore, the phase of E_x is almost 90^o with respect to the effective source current. As the separation increases, the imaginary part decreases at a faster rate than the real part. Thus, far from the power line, the real part dominates and the phase of E_x approaches 0^o. The separation at which the curves of the imaginary and real parts cross is seen to decrease at high earth conductivities. A pipeline at an angle to this power line, or a pipeline having sections at several different, but constant separations from this power line, can thus be influenced by longitudinal electric fields varying in phase from 0^o to 90^o relative to the power line current.

It must be noted that the earth inhomogeneities such as horizontal or vertical stratification can cause the components of E_x to fall off with distance at different rates than those of Figure 3-3. Field testing of the magnitude and phase of E_x is necessary if reasonably accurate predictions of inductive coupling are required.

Instrumentation Developed for Electric Field Measurement

System Description. Because of the problems associated with the basic probe wire concept, an instrumentation system was developed for longitudinal electric field measurement since off-the-shelf equipment was not available.

Figure 9-2 shows an electrical schematic diagram of the measurement system. It consists of two long wire probes, ℓ_1 and ℓ_2, each grounded at the far end. A high impedance (grounded) voltmeter is put in series with each wire. The ground rod impedances to remote earth are shown in the diagram as Z_g. Lengths ℓ_1 and ℓ_2 are not critical and typically 15 meters has been used. In normal operation of the system when mapping the electric field, line ℓ_1 is run at ground surface level parallel to and several hundred feet from the power line. The voltage induced in this line is used as a phase reference for the electric field measurements made subsequently on both sides of the power line. The reference voltage is monitored by a high impedance voltmeter such as a Hewlett-Packard HP3581 or HP403. This allows a continuous check on variations in power line loading which will alter the readings. When using a voltmeter such as the HP403, because of its wide bandwidth, an RC filter must be connected in series with the meter to eliminate AM broadcast station and other interference.

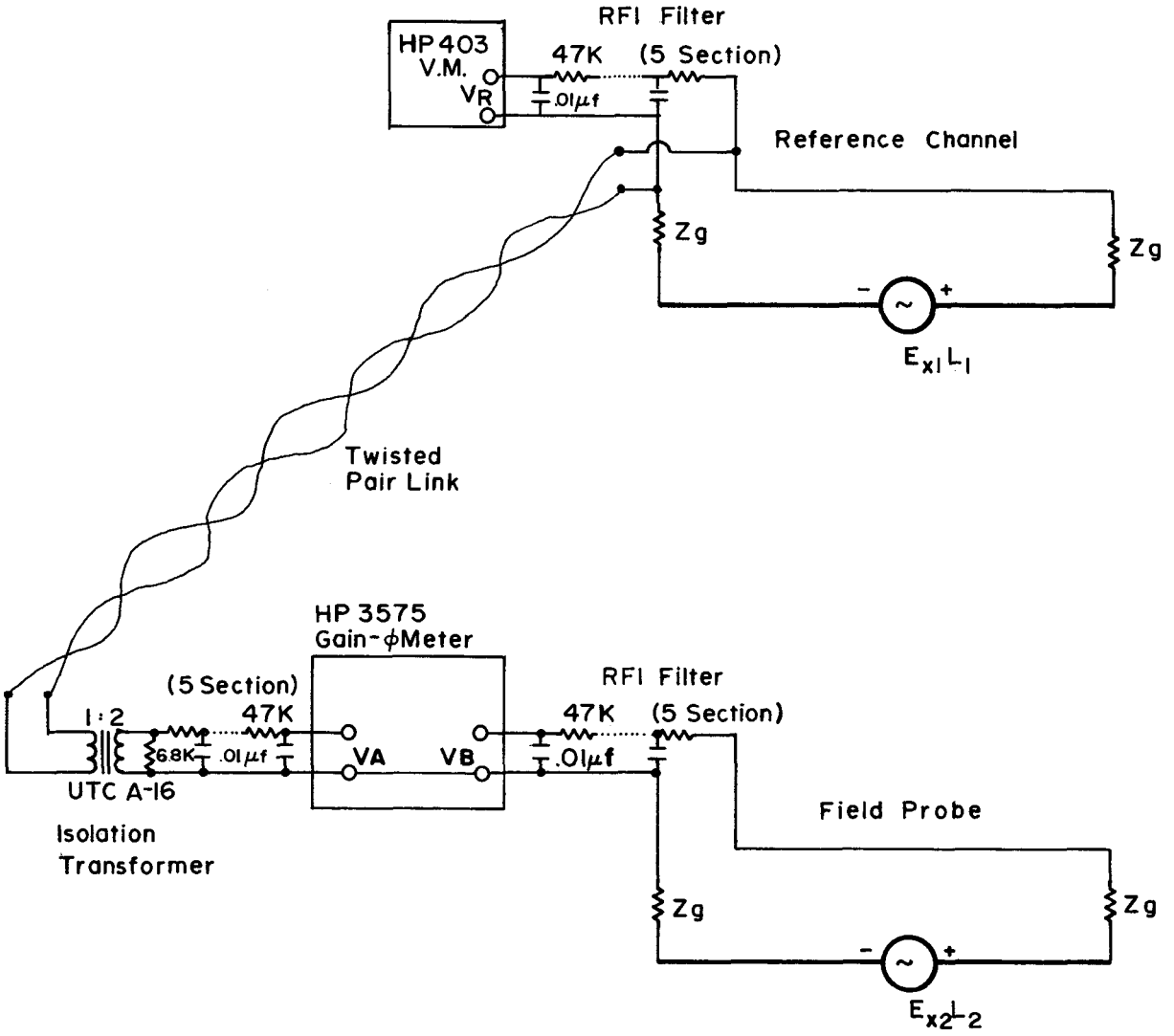

Fig. 9-2 E-FIELD GAIN-PHASE MEASUREMENT - ELECTRICAL SCHEMATIC

The filter is a five-section RC low pass filter with the gain characteristics shown in Figure 9-3. Replicates of this filter are also used at both voltage input terminals to the HP3575 Gain-Phase Meter. The filter has a loss of 10 dB at 60 Hertz, which has been found to be acceptable. The measured attenuation at 1 kHz is 66 dB and the response rolls off at 100 dB per decade at higher frequencies.

When making voltage measurements, the field probe, ℓ_2, is set at the desired (variable) distance from the HVAC transmission line and the earth current induced voltage $E_{x2}\ell_2$, read as V_B on the HP3575 Gain Phase Meter. The reference voltage, V_R, is carried by a two-conductor shielded twisted pair cable, through an isolation transformer and filter to the reference channel (A) input of the Gain-Phase Meter. The transformer is required in order to isolate the earth grounds associated with the probes, ℓ_1 and ℓ_2, respectively. Without this isolation, cross coupling between the two probes would occur, thus giving erroneous readings. Another advantage to use of the isolation transformer is that extraneous common mode interfering signals coupled into the twisted pair line are cancelled by the differential input presented by the transformer.

Data obtained from the Gain Phase Meter are: (1) the voltage, V_A, which is approximately equal to V_R and, hence, proportional to the magnitude of the electric field at the reference location $|E_{x1}|$; (2) the voltage, V_B, which is proportional to the remote electric field magnitude, $|E_{x2}|$; and (3) the phase angle between the electric fields, E_{x1} and E_{x2}. Data collected for a mapping of the longitudinal electric field under a 345 kV power line are discussed in Appendix B.

The preceding discussion outlines the operation of the measurement system. In concept it is simple but, unfortunately, much more difficult to implement in practice, due to the fact that these measurements are being made in the presence of a much larger vertical electric field. For example, a typical longitudinal E-field amplitude may be on the order of 5 mV/m, while the vertical field at the same point may be 5 kV/m, a million times stronger. Hence, in order to obtain meaningful measurements, a carefully planned shielding arrangement is necessary.

Practical Difficulties. In making either one of the probe measurements, the following circuit parameter values are representative:

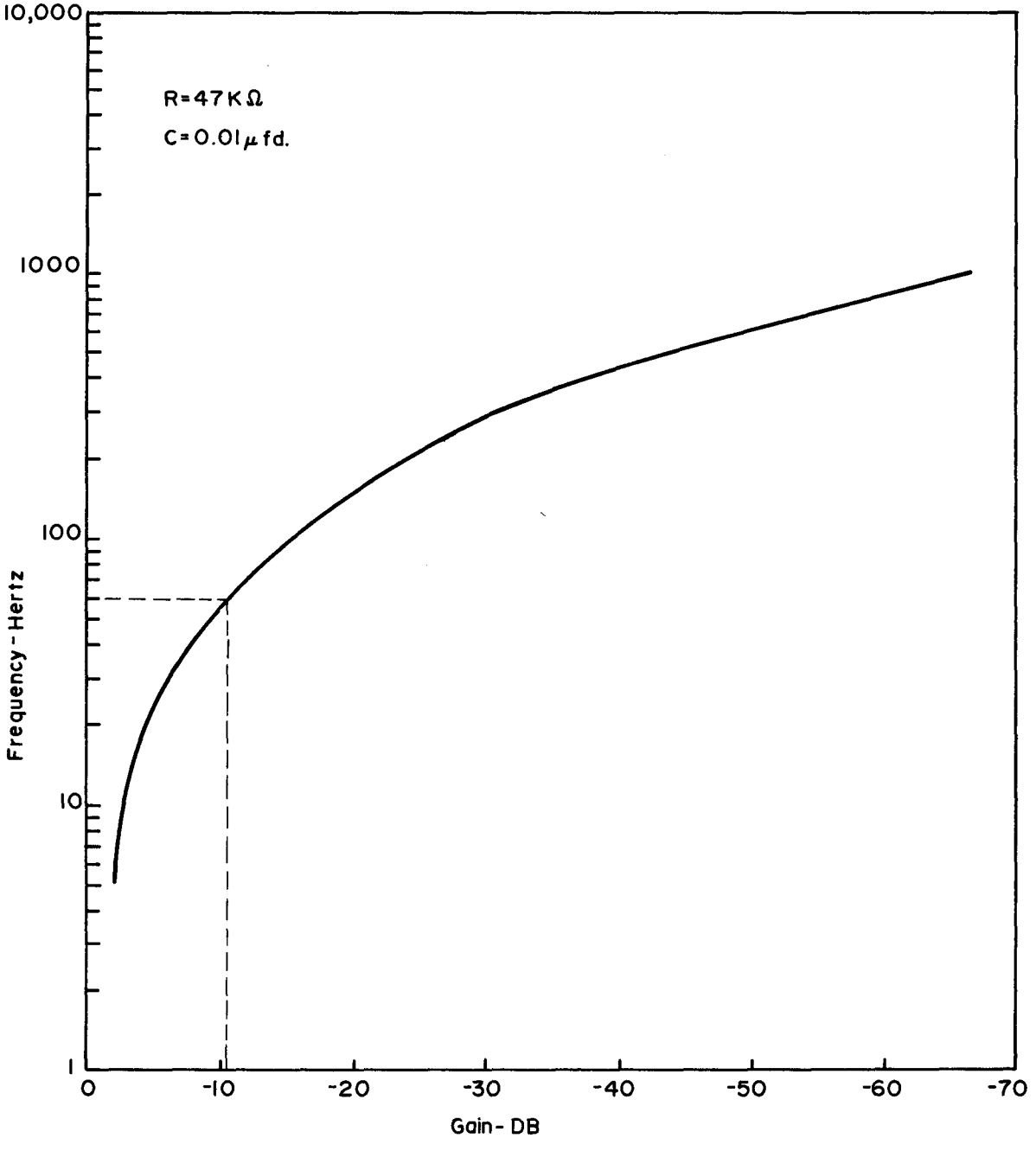

Fig. 9-3 GAIN OF FIVE SECTION RFI FILTER

E_x = longitudinal electric field - 5 mV/m

L = probe wire length - 15 m

Z_g = ground rod impedance - 500 ohms

R_V = voltmeter resistance - 1 megohm.

For these values, the current induced in the probe wire is

$$I_L = \frac{E_x\, L}{R_V + 2\, Z_g} \simeq 0.075\ \mu A \qquad (9\text{-}5)$$

The probe wire will also have a current coupled into it through the electrostatic vertical E field as calculated by the following equation.

$$I_{max} = 2\pi f \cdot C_g \cdot E_t \cdot H \text{ amperes}$$

where

f = 60 Hz

E_t = electrostatic field strength - V/m

H = height of probe wire above ground - m

C_g = capacitance of probe wire to ground - F

= 40×10^{-12} L Farads (for a wire of length L on the ground)

Representative values are as follows:

$C_g = 6 \times 10^{-10}$ F

E_t = 5 kV/m

$H = 10^{-3}$ m.

Hence

$$I_{max} = 1.13\ \mu A. \qquad (9\text{-}6b)$$

The ratio of I_{max} to I_L is 15. Hence, the voltmeter reading, which is proportional to the current flowing in the probe wire, will be proportional to the electrostatic electric field rather than the desired longitudinal field. In order to obtain an accurate longitudinal field reading, the current, I_{max}, must be reduced by a factor of at least 100 to possibly 1000 or more, which implies a shielding requirement of 40 to 60 dB.

The probe wire is not the only means of unwanted electrostatic field pickup. Other paths of ingress are (1) the voltmeter case, (2) connecting wires to ground rods, and (3) the twisted wire pair linking the reference and data channels. System shielding required to circumvent this extraneous pickup problem is discussed in the next section.

System Shielding. Electrostatic shielding for the measurement system is outlined schematically in Figures 9-4 through 9-6. Figures 9-4 and 9-5 show alternative reference channel configurations for use with the data channel shown in Figure 9-6. Choice of either the HP3581 or HP403 arrangement is primarily dictated by voltmeter availability, but the HP3581 is preferred because of its phase locked loop and narrow tunable bandpass.

The success of the measurement system lies primarily in following religiously the following grounding and shielding rules:

1. The remote end (away from voltmeters) of a probe wire must be grounded with no other shield or ground at that point.

2. At the near end (at voltmeter connection) of the probe, the negative side of the voltmeter (and usually its case also due to internal connections) must also be grounded in a singular manner.

3. Considering the reference channel, a shielded wire (coax) is used for the probe wire and the shield must be connected to the metal box shielding the voltmeter. In turn, the shield for the twisted pair link between the reference and data channels must also be connected to this box. The box physically contains the voltmeter and filter, if used, and acts as an electrostatic shield for the voltmeter. However, the voltmeter must be electrically insulated from the box.

4. This electrically connected combination of reference probe shield, voltmeter shield box and twisted pair shield must be grounded at a single point separate from the voltmeter case and probe grounds. A convenient grounding point has been found to be the probe wire shield at approximately its mid-point.

These rules are exemplified by the arrangements shown in Figures 9-4 and 9-5. In Figure 9-6, which outlines the data channel configuration, identically the same grounding rules are followed. However, in order not to couple the electrostatic grounding systems of the two channels, it is necessary to break and separate the shield of the twisted pair link connecting the two channels. A convenient point has been found to be roughly at the mid-point and a shield separation of approximately a quarter of an inch is sufficient to eliminate the possibility of inadvertently shorting the two ends of the separated shield.

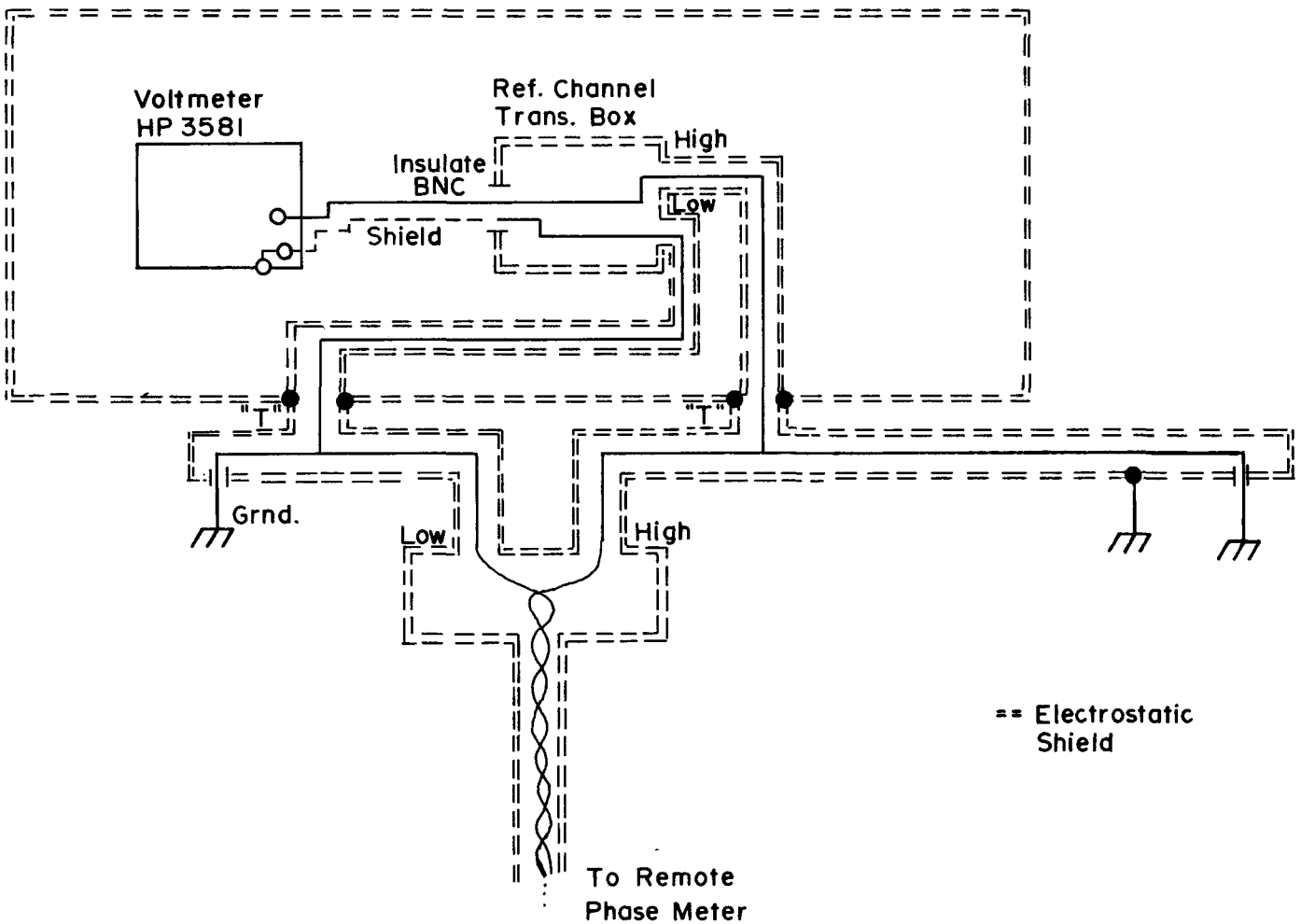

Fig. 9-4 REFERENCE PROBE - HP 3581 ARRANGEMENT

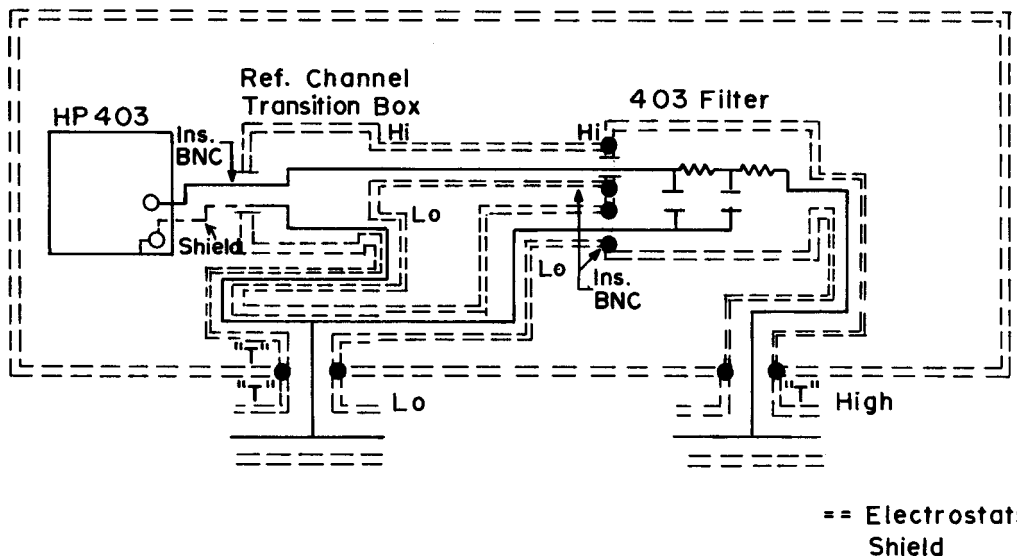

Fig. 9-5 REFERENCE PROBE - ALTERNATE ARRANGEMENT ; HP403 VOLTMETER

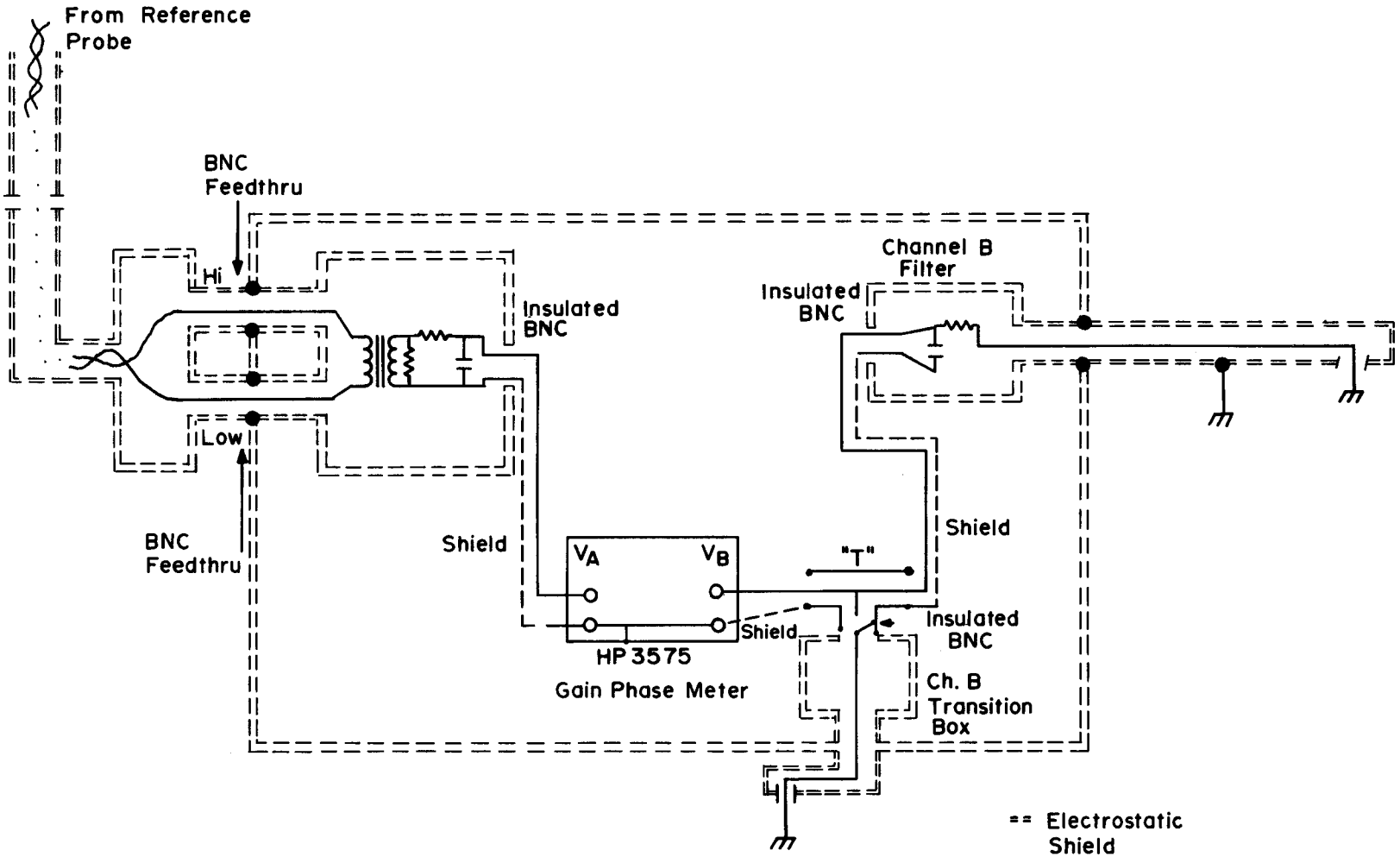

Fig. 9-6 PHASE MEASUREMENT METER BOX

In summary, four separate grounding systems are used.

- The reference channel probe-voltmeter combination
- The reference channel electrostatic shield
- The data channel probe-voltmeter combination
- The data channel electrostatic shield.

To implement these grounding arrangements simultaneously using standard coaxial cable and connectors requires that at times a single ground connection run may be alternately carried on either a coaxial cable shield or on the cable center wire. As shown in the previous figures, special boxes have been fabricated to accomplish the required transitions.

MEASUREMENT OF THE EFFECTIVE AC EARTH CONDUCTIVITY FOR AN INHOMOGENEOUS EARTH

The measurement of E_x, the undisturbed electric field parallel to a pipeline path, can involve considerable field testing activities for a realistic pipeline-power line configuration. Complete testing for a pipeline might not be feasible, especially in the planning stage when several different routes could be under consideration. Analytical approximation of E_x, using the developed hand calculator program, presents a less expensive alternative. However, such an approximation must necessarily be based upon the assumption of a uniform earth of finite conductivity, σ, because detailed information on the horizontal and vertical stratification of the earth is generally not known. Therefore, it is important to have an experimental method for determining an <u>effective</u> σ value that, when used in the approximation method, yields accurate estimates of E_x for an inhomogeneous earth.

References (<u>1</u>) and (<u>3</u>) report the use of the probe wire technique of Figure 9-1a to determine the effective earth conductivity. The two steps in this determination are as follows:

1. $|E_x|$ parallel to the disturbing power line is measured at several distances from the power line. Misleading results caused by buried water mains, sewer lines, and other parasitics must be avoided. The test results for $|E_x|$ are then graphed as a function of distance from the power line.

2. The test results are analyzed statistically to fit the infinite line theory model for mutual impedance. This is accomplished by fitting the graphed test data with a curve computed using Carson's equation for the mutual impedance between two infinitely long conductors near the earth's surface (1). The earth conductivity value used in Carson's equation is varied until the best fit to the test data is obtained. The best fit is determined by defining an error quantity, $ERROR_i$, for the ith data point:

$$ERROR_i = |E_{x,i}| - |F_{x,i}(\sigma)| \qquad (9\text{-}7)$$

where

$E_{x,i}$ = measured electric field at the ith separation from the power line

$F_{x,i}(\sigma)$ = electric field at the ith separation from the power line predicted by the Carson equation assuming an earth conductivity of σ

and then minimizing the error in the least-mean-square sense of all i by varying σ.

Figure 9-7 shows an example of the measurement of the effective earth conductivity using this curve-fitting procedure (3). Here the magnitude of the electric field parallel to a buried (depth = 30 inches), 6.7 mile long, single-phase, earth-return, test source is plotted as a function of separation distance for an excitation frequency of 39 Hz. These data are normalized to a current of one ampere, and are given in units of volts/1000 feet. The scatter in these measurements is due mainly to variations in the earth conductivity immediately under the test sites. The solid curve represents the best Carson model curve-fit, using the least-mean-square criterion. This line corresponds to an effective earth conductivity of $3.61 \cdot 10^{-4}$ mhos/meter. Therefore, in all subsequent computations of inductive coupling, this value of σ could be used with the assurance that the average properties of the ground had been well characterized up to as much as 10,000 feet from the test source.

MEASUREMENT OF THE IMPEDANCE OF GROUNDING SYSTEMS

Reference (4) reports techniques for the measurement of the dc resistance of grounding systems. These techniques are now summarized and expanded to encompass measurement of ac grounding impedances.

Use of Auxiliary Grounding Systems

The unknown impedance of a grounding system can be determined by installing (for measurement purposes) either one or two auxiliary grounds and measuring the

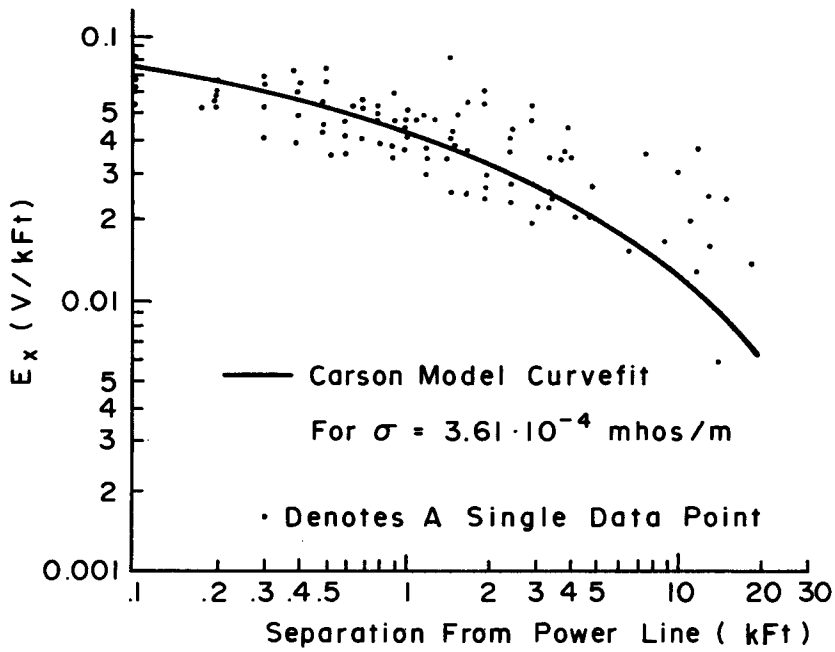

Fig.9-7 MEASUREMENT OF THE EFFECTIVE AC EARTH CONDUCTIVITY BY CURVE-FITTING USING THE CARSON MODEL

impedances observed directly between the grounding systems. As shown below, a single auxiliary ground is sufficient if its impedance is known; two auxiliary grounds are required if neither of their impedances is known before the test.

Single-Auxiliary-Ground Test. Here, auxiliary ground system, A, with a known self-impedance to remote earth, Z_{AA}, is temporarily installed at a distance, d_{1A}, from the ground system to be tested, 1. Using appropriate instrumentation (discussed in the next section), the impedance observed between 1 and A, Z_{1-A}, is measured. From the relation

$$Z_{1-A} = Z_{11} + Z_{AA} - 2Z_{1A}, \tag{9-8a}$$

the unknown grounding impedance, Z_{11}, is given by

$$Z_{11} = Z_{1-A} + 2Z_{1A} - Z_{AA}, \tag{9-8b}$$

where Z_{1A} is the mutual impedance between grounds 1 and A. Because Z_{1A} is usually difficult to characterize, Z_{11} is calculable only if the condition $2|Z_{1A}| \ll |Z_{1-A} - Z_{AA}|$ is satisfied. This can be accomplished simply by making d_{1A} large compared to the physical dimension of either grounds 1 or A.

Basic Double-Auxiliary-Ground Test. Here, auxiliary ground systems, A and B, with unknown self-impedances to remote earth, Z_{AA} and Z_{BB}, are temporarily installed at distances d_{1A} and d_{1B} from the unknown ground, 1, and at a distance d_{AB} from each other. The impedances, Z_{1-A}, Z_{1-B}, and Z_{A-B}, observed between the three grounds are measured. From the relations

$$Z_{1-A} = Z_{11} + Z_{AA} - 2Z_{1A} \tag{9-9a}$$

$$Z_{1-B} = Z_{11} + Z_{BB} - 2Z_{1B} \tag{9-9b}$$

$$Z_{A-B} = Z_{AA} + Z_{BB} - 2Z_{AB}, \tag{9-9c}$$

Z_{11} is determined by eliminating the unknowns, Z_{AA} and Z_{BB}, to obtain

$$Z_{11} = \tfrac{1}{2}(Z_{1-A} + Z_{1-B} - Z_{A-B}) + (Z_{1A} + Z_{1B} - Z_{AB}), \tag{9-10}$$

where Z_{1A}, Z_{1B} and Z_{AB} are the mutual impedances between the three grounds. Because these mutual impedances are usually difficult to characterize, Z_{11} is calculable only if the condition $|Z_{1A} + Z_{1B} - Z_{AB}| \ll \tfrac{1}{2}|Z_{1-A} + Z_{1-B} - Z_{A-B}|$ is satisfied. This condition is achievable in two ways:

1. By making d_{1A}, d_{1B}, and d_{AB} large compared to the physical dimensions of either grounds 1, A, or B so that each mutual impedance is much less than any of the direct impedances;

2. By spacing the grounds according to the relation

$$\frac{1}{d_{1A}} + \frac{1}{d_{1B}} = \frac{1}{d_{AB}},$$

so that effective cancellation of the mutual impedance term of Eq. 9-10 is achieved, i.e.,

$$Z_{1A} + Z_{1B} - Z_{AB} = 0.$$

When the grounds are placed on a straight line so that $d_{1A} + d_{AB} = d_{1B}$, the above relation is satisfied when

$$\frac{d_{1A}}{d_{AB}} = \frac{1 + \sqrt{5}}{2} = 1.62 \qquad (9\text{-}11)$$

Using the double-auxiliary-ground test, Z_{11} can be determined without direct knowledge of either the self-impedance of the auxiliary grounds or the mutual impedances between the grounds.

Modified Double-Auxiliary-Ground Test. Auxiliary ground systems, A and B, are installed as for the basic double-auxiliary-ground test. Now, however, a current, $I_{1\text{-}B}$, is applied between grounds 1 and B, and the voltage, $V_{1\text{-}A}$ induced by this current between grounds 1 and A, is measured. Z_{11} is then given by

$$Z_{11} = \frac{V_{1\text{-}A}}{I_{1\text{-}B}} + Z_{1A} + Z_{1B} - Z_{AB}. \qquad (9\text{-}12$$

Again, mutual impedance effects can be minimized by arranging the grounds along a straight line in accordance with Eq. 9-11 so that $Z_{1A} + Z_{1B} - Z_{AB} = 0$.

Testing of Counterpoise-Type Grounds. In the testing of counterpoise-type grounds (long, horizontal buried wires or extensive distributed ground beds), substantial spacing between auxiliary grounds is required to minimize mutual impedance effects and allow accurate measurements. Here, it is desirable to position the two auxiliary grounds on opposite sides of the ground to be tested to reduce the mutual impedance between the auxiliary grounds. As an alternative to using auxiliary grounds, it might be possible to open the counterpoise near its midpoint and measure the impedance between the two halves. Without mutual effects,

the measured impedance would simply be four times the actual value of Z_{11}. Because of mutual effects, the measured impedance is approximately 3.3 times Z_{11}.

Instrumentation for Grounding System Measurements

Measurements of the dc resistance of grounding systems can be made using only a battery to drive currents between the auxiliary and test grounds, an ammeter to measure the applied currents, and a sensitive voltmeter to measure the resulting potentials. A high resistance voltmeter is used to minimize the effects of the resistance of connecting wires. This method can lead to appreciable error, however, when the spacing between grounds is large. Then, the dc voltage to be measured is probably comparable to spurious dc voltages due to stray earth currents or galvanic electrode potential differences.

To eliminate the effects of stray dc voltages, instruments are commercially available which commutate the applied test current and sense the resulting voltage drop only at the commutating frequency. This frequency selectivity also provides rejection of stray ac voltages that differ in frequency from that of the test current. These instruments provide a current circuit and a voltage circuit so coupled that a direct reading of the magnitude of the grounding impedance at the commutating frequency is given in ohms. However, no information concerning the phase of the grounding impedance is provided.

In principle, precise measurements of grounding impedance magnitude and phase at the power line frequency can be made by using a low-frequency gain-phase meter such as the Hewlett Packard Model 3575A, discussed previously in this section, in combination with a 60 Hz current source. Here, the current waveform would be sampled by Channel A (the phase reference channel) of the instrument, and the induced voltage would be fed into Channel B (the test channel). The complex-valued ratio, B/A, could then be immediately read from the digital display.

CONSIDERATIONS IN AC SCALAR MEASUREMENTS

Introduction

Occasions will arise in the field where measurements of induced ac voltages, pipeline currents, etc., will be desired. To determine the appropriate measurement procedures, problems, accuracies, etc., for a wide variety of measurements, a scope of effort beyond that presented here is required. However, two contrasting

examples are given here which in a succinct manner show that each type of pipeline system interference measurement must be evaluated separately.

For example, the first situation discussed is that of performing an ac pipe-to-soil measurement. Inspection of the situation shows that this measurement may be accomplished in the traditional manner without problems by substituting a (tuned) ac high impedance voltmeter in place of the usually used dc voltmeter.

In contrast, the next example discussed is that of attempting to determine pipe current by means of the established voltage drop method. Here, it is shown that external fields can influence the accuracy of the measurement.

AC Pipe-to-Soil Measurement

The measurement may be diagrammed as shown in Figure 9-8a. The following quantities may be defined:

V_{p-s} = ac pipe-to-soil voltage

e_{ac} = induced pipeline voltage

Z_p = pipeline impedance

Z_M = internal voltmeter impedance

V_{oc} = measured pipe-to-soil potential = $Z_M I_M$

I_M = current drawn by voltmeter

$E_x L$ = inductive pickup on voltmeter leads = electric field strength x lead length

Z_g = measurement circuit grounding impedance

C_g = capacitance-to-ground

I_{max} = electrostatic interference pickup current.

Referring to the figure, the following expression may be derived for the potential as read by the voltmeter:

$$V_{oc} = \frac{Z_M}{Z_M + Z_g} (V_{p-s} + E_x L) + I_{max} Z_g \qquad (9\text{-}13)$$

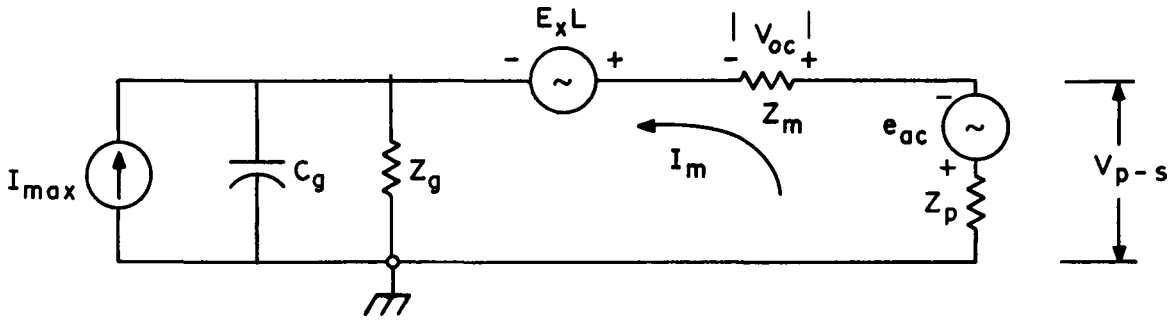

(a) Pipe - To - Soil Measurement

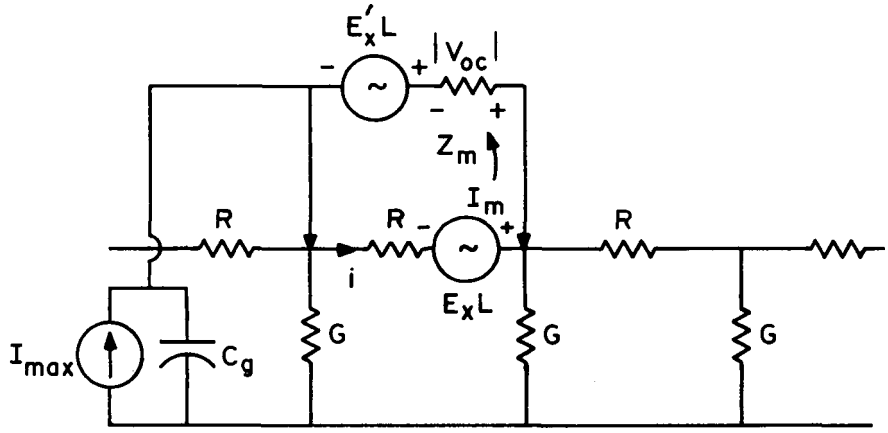

(b) Pipeline Current Measurement

Fig.9-8 EQUIVALENT CIRCUITS FOR AC MEASUREMENTS

Using a high impedance voltmeter, $Z_M >> Z_g$;* even for relatively poor grounding impedances. Evaluating I_{max} from Eq. 9-3c, the term $I_{max} Z_g$ is of the order of several hundred millivolts for representative cases. Parallel to the electric transmission line, E_x may be of the (worst-case) order of 50 volts/km. The length of the measurement lead to remote earth could be as long as, say, 30 meters. Hence, $E_x L$ at a maximum will be of the order of a volt or so. In general, ac pipe-to-soil measurement values of interest are at least ten or more times this value and therefore,

$$V_{oc} \doteq V_{p\text{-}s} \tag{9-14}$$

If low value measurements are desired, proper positioning of the remote earth lead relative to the electric transmission line, i.e., as perpendicular as possible, should allow reasonable measurement accuracies down to the low volts range. An additional source of error should be recognized when measuring ac pipe-to-soil voltages with rectifier type voltmeters, e.g., Simpson, Triplett, etc. These instruments actually measure the dc component of the rectified ac pipeline voltage. Cathodic protection on the pipeline will simultaneously be read by the meter, thus causing a large percentage error at low ac voltage levels.

Pipe Current Measurement

A common technique for the measurement of pipe current (dc) is to measure the voltage drop along a long section of pipe and knowing the pipe resistance, calculate the pipe current. An immediate problem in adapting this type of measurement to the ac case is that the pipe impedance at 60 Hz may not be as accurately known as its dc resistance. Barring this problem, the equivalent circuit for this type of measurement is shown in Figure 9-8b. Here, it is assumed that the test leads are connected to the pipeline, separated by a distance, L; the pipeline series resistance (impedance) per length L is R, and the corresponding shunt pipeline conductance is G. Referring to the equivalent circuit (Figure 9-8b) for this measurement, it is seen that a voltage equal to $E_x L$ is induced along the pipeline, and a voltage $E_x' L$ in the measurement test leads. In general, the value of E_x' is dependent upon the physical position of the test leads. This electric field is made up of two components: (1) that caused by the net zero sequence electric transmission line current, I_0, and (2) that caused by the induced pipe current, I_p.

*When using a high impedance voltmeter, the type of material used for the ground rod will not affect the accuracy of the measurements.

The field will be calculated here for the simplest geometry, i.e., for parallel electric and natural gas transmission lines and test lead arrangements.

At the test lead position, the parallel electric field component caused by I_o is

$$E_x = \frac{j\omega\mu_o I_o}{2\pi} \ln\left(\frac{2}{\Gamma r_o}\right) \qquad (9\text{-}15)$$

where

μ_o is the permeability of free space

Γ is the complex earth propagation constant, and

r_o is the distance from the electric transmission line effective phase center and the test position.

The electric field due to the induced pipe current is

$$E_p = \frac{j\omega\mu_o I_p}{2\pi} \ln\left(\frac{2}{\Gamma r_p}\right) \qquad (9\text{-}16)$$

where r_p is the radial separation of the test leads and the pipeline.

Assuming the use of a high impedance voltmeter for the measurement, ($I_M \simeq 0$), allows the open circuit measurement voltage to be written as

$$V = E_x' L + I_p Z L - E_x L$$

where

$E_x' = E_x - E_p$, and

Z = the pipe impedance defined below. (In the above equation it is implicitly assumed that $I_{max} << I_p$).

It may be shown that the pipe impedance is

$$Z = \frac{j\omega\mu_o}{2\pi} \ln\left(\frac{2}{\Gamma a}\right) + Z_i \qquad (9\text{-}18$$

where

Z_i is the internal self-impedance of the pipe, and

a is the pipe radius.

Substituting Eqs. 9-15, 9-16, and 9-18 into Eq. 9-17, gives

$$V = \left[\frac{j\omega\mu_o}{2\pi} \ln\left(\frac{r_p}{a}\right) + Z_i\right] I_p L \tag{9-19}$$

The usual procedure for determining the pipeline current is to divide the measured voltage, V, by the pipe internal impedance, $Z_i L$. Doing this in the above equation results in

$$I_{p|\text{calculated}} = I_p \left[1 + \frac{j\omega\mu_o}{2\pi Z_i} \ln\left(\frac{r_p}{a}\right)\right] \tag{9-20}$$

Hence, a measurement error exists given by

$$\text{ERROR} = \frac{j\omega\mu_o}{2\pi Z_i} \ln\left(\frac{r_p}{a}\right) \tag{9-21}$$

For measurement leads above the ground, the distance r_p may be as large as several pipe radii. The pipeline self-impedance will generally be of the order of a fraction of an ohm per kilometer, and hence, the error as calculated by Eq. 9-21 can be an appreciable percentage of the pipe current.

On the other hand, especially for a coated pipeline, such current measurement test leads, if available, are installed at the time the pipeline is built. Such leads are run alongside the pipe and are brought out to the surface at a junction box. For this situation, $r_p \simeq a$, and the measurement error as given by Eq. 9-21 reduces to zero.

Hence, for this type of ac measurement, test leads placement has an effect upon the measurement accuracy. Although the measurement error as given by Eq. 9-21 theoretically reduces to zero for $r_p = a$, trouble has been encountered with the use of this technique in the field. Dunbar (5), has experimented with this measurement under carefully controlled conditions and has noticed a nonlinear relationship occurring between the measured voltage drop and the pipeline current. Bower (6), has pointed out that measurement errors could also occur because of non-symmetrical distribution of the current on the surface of the pipe.

DC SCALAR MEASUREMENTS

Introduction

The making of dc pipeline system measurements in the presence of induced ac voltages and currents gives rise to two questions: (1) Can the instrumentation be damaged? and (2) Is the accuracy of the measurements affected? To answer these questions, a search of the open literature was made and knowledgeable people in the industry were contacted.

The literature search extending back over a period of 16 years yielded relatively little in the way of information with regard to these problem areas. It would appear that measurement problems arising in the field are fixed as they occur and generally not reported in the literature. Hence, the following information obtained has been primarily obtained through personal contacts.

DC Measurements Interference

For dc measurements in the presence of steady 60 Hertz, it appears that low pass filters are generally used with the instrumentation, e.g., voltmeters, thus eliminating problems with either measurement accuracy or potential damage. Resistivity measurements made with, e.g., a Vibroground, are seemingly immune to the presence of ac due to the fact that the operation of the instrument, i.e., current interruption at 97 Hz effectively acts as a built-in filter for the induced 60 Hz currents.

Hence, it would appear that once the presence of induced 60 Hz is recognized, potential problems can be relatively easily suppressed. Information to the contrary has not been evident in this study.

During times that system transients occur, dc measurements, if being made, will not be affected as regards accuracy, since a transient is of short duration. A more important problem is that of instrumentation damage due to transient phenomena. Occasionally, instrumentation left permanently connected has been damaged but generally it is not obvious what precipitated the damage. Transient recording instrumentation which can be used for long-term unattended operations is not available as off-the-shelf equipment, and hence, transient occurrence due to direct lightning strokes or power system faults is not separately identifiable.

Therefore, it would appear that where transient induced damage does occur to permanently wired instrumentation, the fixes are made on an individual basis, e.g., grounding through spark gaps, and so forth.

REFERENCES

1. Inductive Interference Engineering Guide (preliminary issue), Bell Laboratories Electromagnetic Interference Department, Loop Transmission Division, March 1974.

2. Hewlett-Packard 1976 Electronic Instruments and Systems Catalog.

3. A. R. Valentino and D. W. McLellan, "ELF Earth Return Current Coupling," IEEE Trans. Electromagnetic Compatibility, Vol. EMC-15, pp. 172-176, November 1973.

4. E. D. Sunde, Earth Conduction Effects in Transmission Systems. New York, N. Y.: Dover Publications, Inc. 1968.

5. O. J. Dunbar, Transcontinental Gas Pipeline Corp., Houston, Texas, Private Communication.

6. F. E. Bower, El Paso Natural Gas Company, E. Paso, Texas, Private Communication.

Appendix A

PROGRAMS DEVELOPED FOR THE TEXAS INSTRUMENTS MODEL TI-59 HAND CALCULATOR

INTRODUCTION

This appendix presents eight programs for the Texas Instruments Model TI-59 programmable hand calculator that are used to implement the analytical methods of this book. These programs allow the simple and rapid computation of pipeline electrical parameters, driving fields, and induced voltages by applying sophisticated numerical techniques that would normally require a large-scale computer. Essentially no manipulation of complex numbers is required by the user, greatly reducing the possibility of error.

The eight programs included in this appendix are as follows:

1. Program CARSON. This program computes the mutual impedance between parallel earth-return conductors using Carson's infinite series (c.f., A-3).

2. Program CURRENTS. This program computes the currents in earth return conductors adjacent to a power line that can influence the driving field at the pipeline of interest (c.f., A-10).

3. Program PIPE. This program computes the propagation constant and characteristic impedance of a buried pipeline having arbitrary characteristics (c.f., A-18).

4. Program WIRE. This program computes the propagation constant and characteristic impedance of a horizontal buried ground wire having arbitrary characteristics (c.f., A-25).

5. Program THEVENIN. This program computes the Thevenin equivalent circuit for the terminal behavior of an earth-return conductor parallel to a power line (c.f., A-32).

6. Program NODE. This program computes the node (pipeline) voltage and branch (pipeline) currents for three Thevenin equivalent circuits connected at one common point (c.f., A-38).

7. Program FIELD. This program computes the driving field at an earth-return conductor, given a knowledge of the currents in adjacent earth-return conductors and the mutual impedance between each adjacent conductor and the conductor of interest (c.f., A-45).

8. Program SHIELD. This program computes the series impedance of a power line shield wire, for use in Program CURRENTS (c.f., A-49).

Examples of applications of these programs are found in the case histories discussed in Section 3. All programs include specific instructions for usage, as well as listings of the programming steps. Each can be permanently recorded on magnetic cards which can be used repeatedly. The Texas Instruments TI-59 calculator was specifically chosen for this application because of the large number of available programming steps.

Program CARSON

Program CARSON computes the mutual impedance between adjacent, parallel, earth-return conductors using Carson's infinite series. This program can be used by the technician in the field to determine Carson mutual impedances to better than 0.1 percent accuracy, regardless of earth resistivity conditions, conductor configuration (either aerial or buried), and conductor separation.

This program, documented using Figure A-1, Tables A-1a and A-1b, computes and sums as many terms of the Carson series as is required to achieve the desired accuracy, using the recursive algorithm of Dommel (1). The program can be permanently recorded on two magnetic cards.

Figure A-1 details the conductor geometry assumed for this program and defines the essential data parameters keyed in by the user. Table A-1a provides a step-by-step instruction procedure for the use of the program. Table A-1b is a printer listing of the key sequences needed initially to program the magnetic cards. This table indicates the five digit code number and the printer listing associated with each key sequence to allow the user to rapidly verify the accuracy of his program procedure. (Tables of key sequence code numbers and printer listings are given on pages V-50 and VI-6, respectively, of the Texas Instruments owner's manual for the TI-59, "Personal Programming").

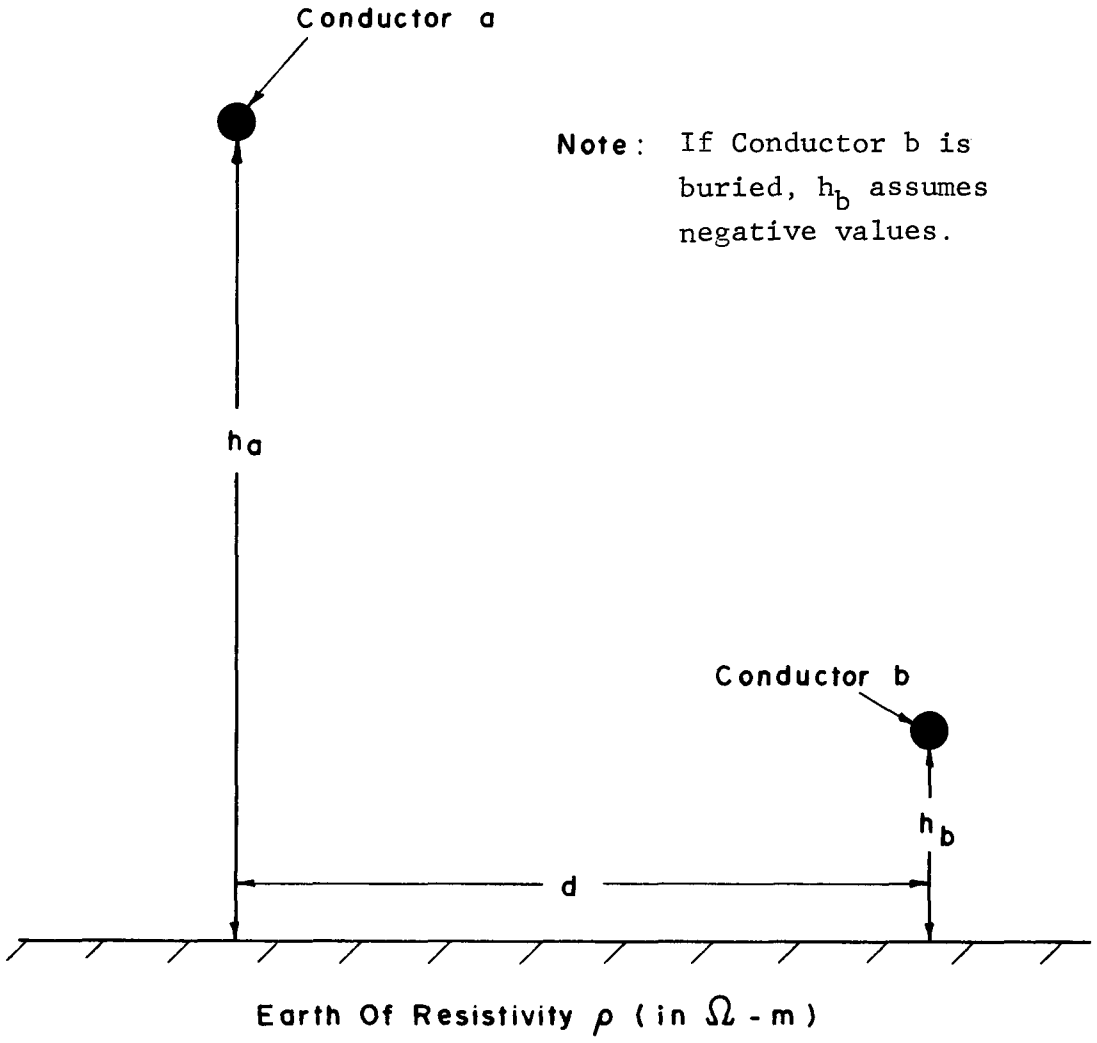

Figure A-1. Conductor Geometry for Program CARSON

Table A-1a

INSTRUCTIONS FOR PROGRAM CARSON

1. Press CLR. Then, press 3 Op 17.

2. Press 1. Then, insert bank #1 into the card reader.
   Press 2. Then, insert bank #2 into the card reader.
   Press 3. Then, insert bank #3 into the card reader.

3. Key ρ (in ohm-meters) into the display. Then, press A.
   Key h_a (in feet) into the display. Then, press B.
   Key h_b (in feet) into the display. Then, press C.
   Key d (in feet) into the display. Then, press D.

4. Press E. Then, wait for the display to unblank. The waiting time ranges from 24 seconds to 104 seconds, depending upon the number of Carson's series terms computed. The display then shows $|Z_{ab}|$ in ohms/km.

5. Press x$\rightleftarrows$t to display $\angle Z_{ab}$ in degrees.

   NOTE: If the PC-100A printer is used, $|Z_{ab}|$ and $\angle Z_{ab}$ will be printed out automatically and labelled as "ZMAG" and "ZPHA", respectively. The solution will further be labelled "SERIES solution" or "ASYMPTOTIC SOLUTION" depending upon the computation method employed by the calculator.

6. If Z_{ab} is desired for different values of either ρ, h_a, h_b, or d, simply return to Step 3 and key in the appropriate values (in any order). Then, do Steps 4 and 5.

Table A-1b

PROGRAM CARSON

Display		Key	Display		Key	Display		Key	Display		Key
000	91	R/S	045	43	RCL	090	04	04	135	42	STO
001	76	LBL	046	01	01	091	49	PRD	136	09	09
002	11	A	047	85	+	092	05	05	137	42	STO
003	42	STO	048	43	RCL	093	49	PRD	138	16	16
004	00	00	049	02	02	094	06	06	139	93	.
005	91	R/S	050	54	)	095	07	7	140	01	1
006	76	LBL	051	33	X^2	096	32	X:T	141	00	0
007	12	B	052	95	=	097	43	RCL	142	06	6
008	42	STO	053	34	FX	098	06	06	143	06	6
009	01	01	054	42	STO	099	77	GE	144	03	3
010	91	R/S	055	05	05	100	03	03	145	55	÷
011	76	LBL	056	55	÷	101	52	52	146	43	RCL
012	13	C	057	43	RCL	102	93	.	147	06	06
013	42	STO	058	00	00	103	00	0	148	95	=
014	02	02	059	34	FX	104	05	5	149	42	STO
015	91	R/S	060	65	×	105	09	9	150	10	10
016	76	LBL	061	93	.	106	02	2	151	93	.
017	14	D	062	00	0	107	03	3	152	00	0
018	42	STO	063	02	2	108	42	STO	153	07	7
019	03	03	064	01	1	109	08	08	154	05	5
020	91	R/S	065	07	7	110	42	STO	155	04	4
021	76	LBL	066	07	7	111	15	15	156	00	0
022	15	E	067	95	=	112	43	RCL	157	42	STO
023	70	RAD	068	42	STO	113	00	00	158	11	11
024	43	RCL	069	06	06	114	34	FX	159	93	.
025	03	03	070	43	RCL	115	55	÷	160	06	6
026	33	X^2	071	01	01	116	43	RCL	161	01	1
027	85	+	072	85	+	117	04	04	162	05	5
028	53	(	073	43	RCL	118	95	=	163	09	9
029	43	RCL	074	02	02	119	28	LOG	164	03	3
030	01	01	075	95	=	120	65	×	165	75	-
031	75	-	076	55	÷	121	93	.	166	43	RCL
032	43	RCL	077	43	RCL	122	01	1	167	06	06
033	02	02	078	05	05	123	07	7	168	23	LNX
034	54	)	079	95	=	124	03	3	169	95	=
035	33	X^2	080	22	INV	125	06	6	170	42	STO
036	95	=	081	39	COS	126	05	5	171	12	12
037	34	FX	082	42	STO	127	85	+	172	00	0
038	42	STO	083	07	07	128	93	.	173	42	STO
039	04	04	084	93	.	129	03	3	174	13	13
040	43	RCL	085	03	3	130	03	3	175	71	SBR
041	03	03	086	00	0	131	05	5	176	02	02
042	33	X^2	087	04	4	132	00	0	177	78	78
043	85	+	088	08	8	133	09	9	178	49	PRD
044	53	(	089	49	PRD	134	95	=	179	10	10

Table A-1b (continued)

PROGRAM CARSON

Display		Key
180	43	RCL
181	10	10
182	65	×
183	43	RCL
184	14	14
185	39	COS
186	95	=
187	44	SUM
188	16	16
189	94	+/-
190	44	SUM
191	15	15
192	00	0
193	71	SBR
194	02	02
195	78	78
196	49	PRD
197	11	11
198	43	RCL
199	11	11
200	65	×
201	89	π
202	55	÷
203	04	4
204	65	×
205	43	RCL
206	14	14
207	39	COS
208	95	=
209	94	+/-
210	44	SUM
211	16	16
212	43	RCL
213	11	11
214	65	×
215	71	SBR
216	03	03
217	04	04
218	95	=
219	71	SBR
220	03	03
221	36	36
222	71	SBR
223	02	02
224	78	78

Display		Key
225	49	PRD
226	10	10
227	43	RCL
228	10	10
229	65	×
230	43	RCL
231	14	14
232	39	COS
233	95	=
234	44	SUM
235	16	16
236	44	SUM
237	15	15
238	00	0
239	71	SBR
240	02	02
241	78	78
242	49	PRD
243	11	11
244	43	RCL
245	11	11
246	65	×
247	89	π
248	55	÷
249	04	4
250	65	×
251	43	RCL
252	14	14
253	39	COS
254	95	=
255	94	+/-
256	71	SBR
257	03	03
258	36	36
259	43	RCL
260	11	11
261	65	×
262	71	SBR
263	03	03
264	04	04
265	95	=
266	94	+/-
267	44	SUM
268	16	16
269	01	1

Display		Key
270	94	+/-
271	49	PRD
272	10	10
273	49	PRD
274	11	11
275	61	GTO
276	01	01
277	75	75
278	01	1
279	44	SUM
280	13	13
281	43	RCL
282	13	13
283	65	×
284	43	RCL
285	07	07
286	95	=
287	42	STO
288	14	14
289	43	RCL
290	06	06
291	33	X^2
292	55	÷
293	43	RCL
294	13	13
295	55	÷
296	53	(
297	43	RCL
298	13	13
299	85	+
300	02	2
301	54	)
302	95	=
303	92	RTN
304	53	(
305	53	(
306	43	RCL
307	12	12
308	85	+
309	43	RCL
310	13	13
311	35	1/X
312	85	+
313	53	(
314	43	RCL

Display		Key
315	13	13
316	85	+
317	02	2
318	54	)
319	35	1/X
320	54	)
321	42	STO
322	12	12
323	65	×
324	43	RCL
325	14	14
326	39	COS
327	85	+
328	43	RCL
329	07	07
330	65	×
331	43	RCL
332	14	14
333	38	SIN
334	54	)
335	92	RTN
336	44	SUM
337	15	15
338	50	I×I
339	32	X:T
340	43	RCL
341	15	15
342	55	÷
343	01	1
344	00	0
345	00	0
346	00	0
347	95	=
348	77	GE
349	04	04
350	63	63
351	92	RTN
352	76	LBL
353	16	A'
354	70	RAD
355	00	0
356	42	STO
357	13	13
358	42	STO
359	15	15

Table A-1b (continued)

PROGRAM CARSON

Display		Key	Display		Key	Display		Key	Display		Key
360	42	STO	405	35	35	450	07	07	495	04	4
361	16	16	406	65	×	451	54	)	496	03	3
362	71	SBR	407	04	4	452	39	COS	497	02	2
363	04	04	408	05	5	453	55	÷	498	03	3
364	35	35	409	95	=	454	53	(	499	01	1
365	44	SUM	410	44	SUM	455	43	RCL	500	69	OP
366	15	15	411	16	16	456	06	06	501	03	03
367	44	SUM	412	94	+/-	457	45	Y×	502	69	OP
368	16	16	413	44	SUM	458	43	RCL	503	05	05
369	71	SBR	414	15	15	459	13	13	504	98	ADV
370	04	04	415	93	.	460	54	)	505	69	OP
371	35	35	416	00	0	461	95	=	506	00	00
372	65	×	417	07	7	462	92	RTN	507	02	2
373	02	2	418	05	5	463	25	CLR	508	04	4
374	34	FX	419	04	4	464	69	OP	509	03	3
375	95	=	420	65	×	465	00	00	510	00	0
376	94	+/-	421	53	(	466	03	3	511	01	1
377	44	SUM	422	43	RCL	467	06	6	512	03	3
378	15	15	423	05	05	468	01	1	513	04	4
379	71	SBR	424	55	÷	469	07	7	514	04	4
380	04	04	425	43	RCL	470	03	3	515	69	OP
381	35	35	426	04	04	471	05	5	516	04	04
382	44	SUM	427	54	)	472	02	2	517	43	RCL
383	15	15	428	23	LNX	473	04	4	518	13	13
384	94	+/-	429	95	=	474	01	1	519	69	OP
385	44	SUM	430	44	SUM	475	07	7	520	06	06
386	16	16	431	16	16	476	69	OP	521	61	GTO
387	01	1	432	61	GTO	477	01	01	522	05	05
388	44	SUM	433	05	05	478	03	3	523	78	78
389	13	13	434	24	24	479	06	6	524	25	CLR
390	71	SBR	435	01	1	480	00	0	525	69	OP
391	04	04	436	44	SUM	481	00	0	526	00	00
392	35	35	437	13	13	482	03	3	527	01	1
393	65	×	438	93	.	483	06	6	528	03	3
394	03	3	439	01	1	484	03	3	529	03	3
395	95	=	440	00	0	485	02	2	530	06	6
396	44	SUM	441	06	6	486	02	2	531	04	4
397	15	15	442	06	6	487	07	7	532	05	5
398	44	SUM	443	03	3	488	69	OP	533	03	3
399	16	16	444	65	×	489	02	02	534	00	0
400	01	1	445	53	(	490	04	4	535	03	3
401	44	SUM	446	43	RCL	491	01	1	536	03	3
402	13	13	447	13	13	492	03	3	537	69	OP
403	71	SBR	448	65	×	493	07	7	538	01	01
404	04	04	449	43	RCL	494	02	2	539	03	3

Table A-1b (continued)

PROGRAM CARSON

Display	Key	Display	Key
540 07	7	585 37	P/R
541 03	3	586 42	STO
542 02	2	587 18	18
543 03	3	588 32	X:T
544 07	7	589 42	STO
545 02	2	590 17	17
546 04	4	591 04	4
547 01	1	592 06	6
548 05	5	593 03	3
549 69	OP	594 00	0
550 02	02	595 01	1
551 03	3	596 03	3
552 06	6	597 02	2
553 03	3	598 02	2
554 02	2	599 69	OP
555 02	2	600 04	04
556 07	7	601 43	RCL
557 04	4	602 17	17
558 01	1	603 69	OP
559 69	OP	604 06	06
560 03	03	605 04	4
561 03	3	606 06	6
562 07	7	607 03	3
563 02	2	608 03	3
564 04	4	609 02	2
565 03	3	610 03	3
566 02	2	611 01	1
567 03	3	612 03	3
568 01	1	613 69	OP
569 00	0	614 04	04
570 00	0	615 43	RCL
571 69	OP	616 18	18
572 04	04	617 69	OP
573 69	OP	618 06	06
574 05	05	619 98	ADV
575 98	ADV	620 98	ADV
576 69	OP	621 43	RCL
577 00	00	622 17	17
578 43	RCL	623 81	RST
579 15	15		
580 32	X:T		
581 43	RCL		
582 16	16		
583 60	DEG		
584 22	INV		

Program CURRENTS

Program CURRENTS computes the currents in earth return conductors adjacent and parallel to a multiple phase conductor power line. These conductors may be either above or buried below ground. Representative types are power line shield wires, fence wires, telephone wires, railroad tracks, or buried pipelines of sufficient length to significantly modify the total parallel electric field influencing the pipeline of interest. Since these earth return conductors affect each other as well as being affected by the power line, the solution is obtained by solving a set of simultaneous equations describing the mutual interactions. The solution algorithm is the Gauss-Seidel iterative method described by Carnahan et al (2). The use of the algorithm allows the TI-59 to process a system as complex as five unknown earth return conductors adjacent to 25 power line phase conductors, yielding both the magnitude and phase of each unknown current. The program allows the specification of a desired current magnitude accuracy, ΔI. The calculator continues computations until either this accuracy criterion is fulfilled for each of the unknown currents, or until ten iterations have been completed. The program can be permanently recorded on one magnetic card.

Figure A-2 details the conductor geometry assumed for the program and defines the essential data parameters keyed in by the user. Here, phase conductor currents are assumed to be known and unaffected by the adjacent conductor currents. Carson mutual impedances are assumed to have been computed previously using Program CARSON, already presented. Conductor self impedances are required to be inputted into the program and are found as follows. The self impedance per kilometer of an above ground conductor is given by Program SHIELD, to be discussed later in this appendix. The self impedance per kilometer of a buried conductor is obtained by using either Program PIPE or Program WIRE also discussed later. Table A-2a provides a step-by-step instruction procedure for the use of the program. Tables A-2b and A-2c are printer listings of the key sequences needed initially to program the magnetic card.

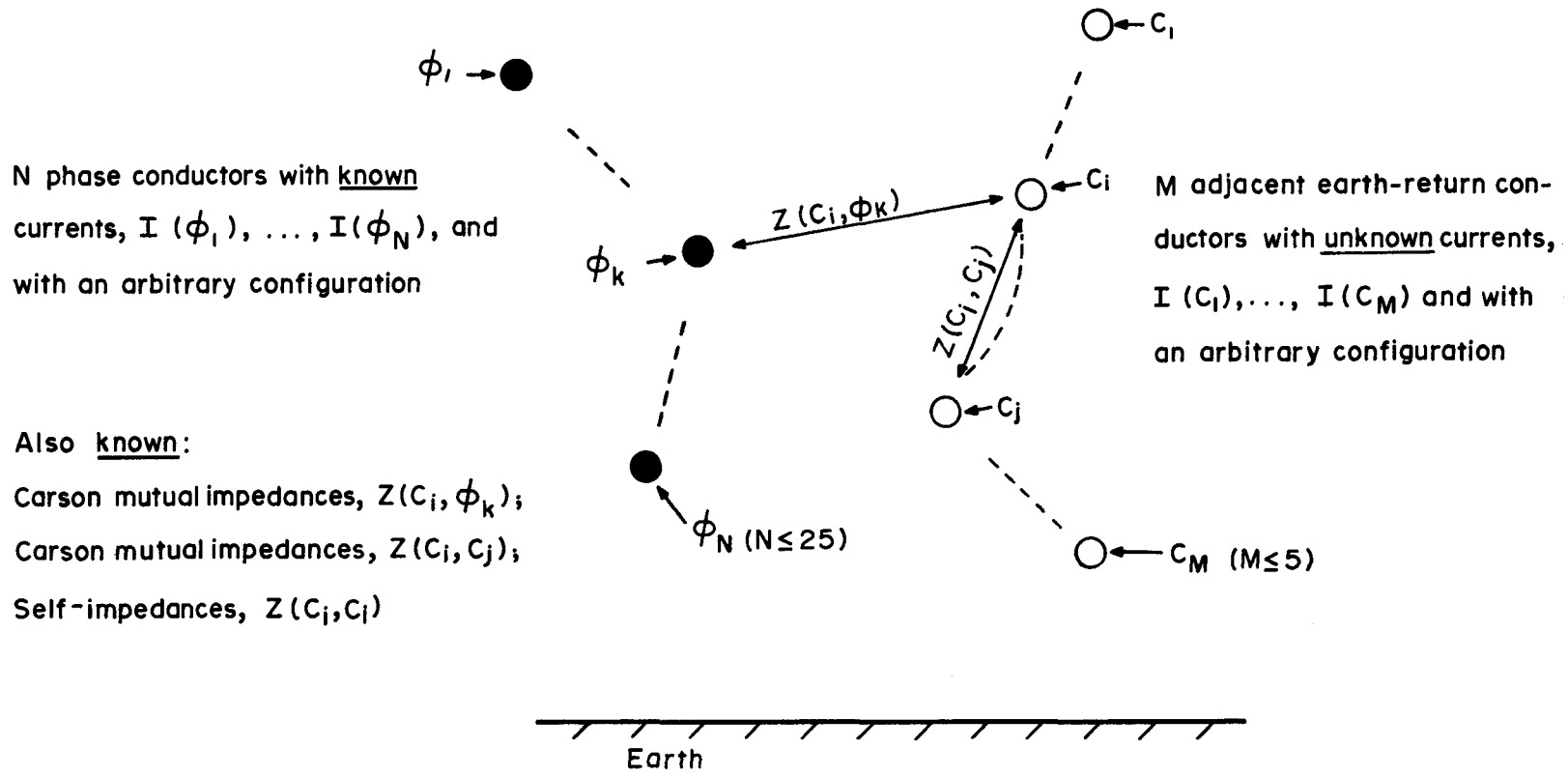

Figure A-2. Conductor Geometry for Program CURRENTS

Table A-2a

INSTRUCTIONS FOR PROGRAM CURRENTS

1. Press CLR. Then, press 9 Op 17.

2. Press 1. Then, insert bank #1 into the card reader.

3. Key N (an integer from 1 to 25) into the display. Then, press A.
   Key M (an integer from 1 to 5) into the display. Then, press R/S.
   Key ΔI (in amperes) into the display. Then, press R/S.

   NOTE: To limit the program running time but yet achieve good accuracy, choose ΔI to be about 0.1% of the typical phase conductor current.

4. Key $|I(\emptyset_1)|$ (in amperes) into the display. Then, press B.
   Key $\angle I(\emptyset_1)$ (in degrees) into the display. Then, press R/S.
   Repeat the preceding two steps for each of the other phase conductor currents, $I(\emptyset_2)$ ..., $I(\emptyset_N)$.

5. Key $|Z(C_1,\emptyset_1)|$ (in ohms/km) into the display. Then, press C.
   Key $\angle Z(C_1,\emptyset_1)$ (in degrees) into the display. Then, press R/S.
   Repeat the preceding two steps for $Z(C_1,\emptyset_2)$, ..., $Z(C_1,\emptyset_N)$.
   Repeat the preceding three steps for each of the other earth return conductors, C_2, ..., C_M.

6. Key in the mutual impedance matrix of the system of earth-return conductors, in the following way:

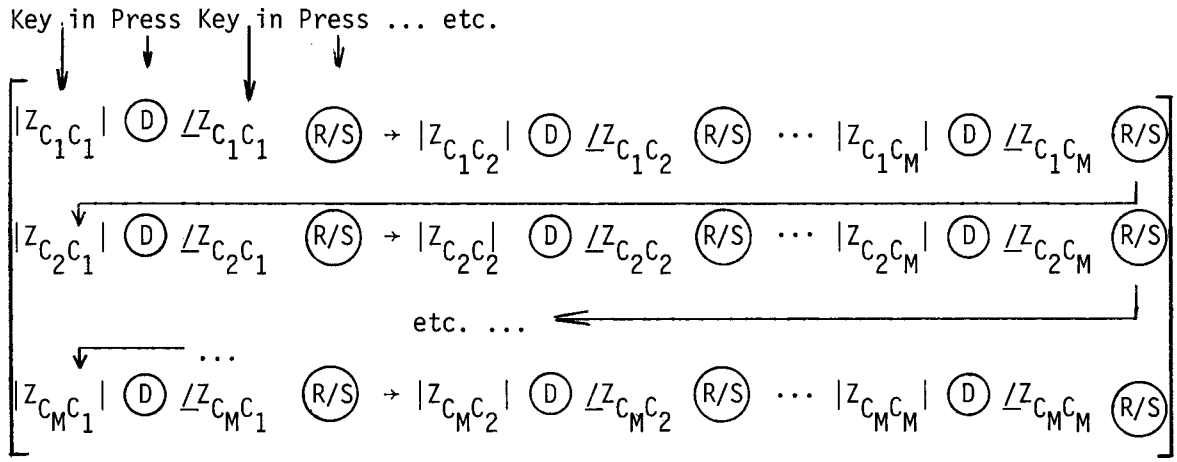

Here, $Z_{C_iC_j}$ for $i \neq j$ is the Carson mutual impedance between earth-return conductors C_i and C_j. For $i = j$, $Z_{C_iC_j}$ is the series self impedance of earth-return conductor C_i. All magnitudes are in ohms/km; all phase angles are in degrees.

Table A-2a (Continued)

INSTRUCTIONS FOR PROGRAM CURRENTS

7. Press E and wait 15 seconds for the display to unblank.

8. Press CLR. Then, press 1 and insert bank #1' into the card reader.

9. Press A. Then, wait for the display to unblank. The waiting time ranges from 2 minutes to 15 minutes, depending upon the number of adjacent earth-return conductors computed. When the display unblanks, the presence of a 1 indicates that the problem has been solved with the specified accuracy, ΔI; a 0 indicates that the algorithm did not converge to within the accuracy bound.

10. To display the currents of the earth return conductors, perform the following operations.

Press	Display
RCL 80	$\|I(C_1)\|$ (amps)
RCL 85	$\angle I(C_1)$ (degrees)
RCL 81	$\|I(C_2)\|$ (amps)
RCL 86	$\angle I(C_2)$ (degrees)
	.
	.
	.
RCL 84	$\|I(C_5)\|$ (amps)
RCL 89	$\angle I(C_5)$ (degrees

Table A-2b

PROGRAM CURRENTS: BANK #1

Display		Key	Display		Key	Display		Key	Display		Key
000	76	LBL	045	95	=	090	71	71	135	72	ST*
001	18	C'	046	42	STO	091	01	1	136	09	09
002	01	1	047	10	10	092	44	SUM	137	43	RCL
003	09	9	048	85	+	093	03	03	138	01	01
004	85	+	049	02	2	094	19	D'	139	32	X:T
005	43	RCL	050	05	5	095	61	GTO	140	72	ST*
006	02	02	051	95	=	096	00	00	141	08	08
007	95	=	052	42	STO	097	68	68	142	43	RCL
008	42	STO	053	11	11	098	76	LBL	143	03	03
009	06	06	054	92	RTN	099	13	C	144	77	GE
010	85	+	055	76	LBL	100	65	×	145	01	01
011	43	RCL	056	11	A	101	73	RC*	146	50	50
012	00	00	057	47	CMS	102	06	06	147	61	GTO
013	95	=	058	60	DEG	103	95	=	148	00	00
014	42	STO	059	42	STO	104	32	X:T	149	91	91
015	07	07	060	00	00	105	91	R/S	150	01	1
016	92	RTN	061	32	X:T	106	85	+	151	44	SUM
017	76	LBL	062	91	R/S	107	73	RC*	152	04	04
018	19	D'	063	42	STO	108	07	07	153	00	0
019	06	6	064	01	01	109	95	=	154	42	STO
020	09	9	065	91	R/S	110	37	P/R	155	05	05
021	85	+	066	42	STO	111	74	SM*	156	01	1
022	43	RCL	067	17	17	112	09	09	157	44	SUM
023	03	03	068	00	0	113	43	RCL	158	05	05
024	95	=	069	42	STO	114	00	00	159	10	E'
025	42	STO	070	02	02	115	32	X:T	160	91	R/S
026	08	08	071	01	1	116	74	SM*	161	76	LBL
027	85	+	072	44	SUM	117	08	08	162	14	D
028	05	5	073	02	02	118	43	RCL	163	72	ST*
029	95	=	074	18	C'	119	02	02	164	10	10
030	42	STO	075	91	R/S	120	77	GE	165	91	R/S
031	09	09	076	76	LBL	121	01	01	166	72	ST*
032	92	RTN	077	12	B	122	26	26	167	11	11
033	76	LBL	078	72	ST*	123	61	GTO	168	43	RCL
034	10	E'	079	06	06	124	00	00	169	05	05
035	01	1	080	91	R/S	125	71	71	170	77	GE
036	04	4	081	72	ST*	126	73	RC*	171	01	01
037	85	+	082	07	07	127	08	08	172	50	50
038	05	5	083	43	RCL	128	94	+/-	173	61	GTO
039	65	×	084	02	02	129	32	X:T	174	01	01
040	43	RCL	085	77	GE	130	73	RC*	175	56	56
041	04	04	086	00	00	131	09	09	176	76	LBL
042	85	+	087	91	91	132	94	+/-	177	15	E
043	43	RCL	088	61	GTO	133	22	INV	178	00	0
044	05	05	089	00	00	134	37	P/R	179	42	STO

Table A-2b (continued)

PROGRAM CURRENTS: BANK #1

Display		Key	Display		Key
180	04	04	225	29	29
181	01	1	226	61	GTO
182	44	SUM	227	02	02
183	04	04	228	09	09
184	43	RCL	229	43	RCL
185	04	04	230	04	04
186	42	STO	231	77	GE
187	05	05	232	02	02
188	42	STO	233	37	37
189	03	03	234	61	GTO
190	19	D'	235	01	01
191	10	E'	236	81	81
192	73	RC*	237	91	R/S
193	10	10			
194	35	1/X			
195	42	STO			
196	12	12			
197	64	PO*			
198	08	08			
199	73	RC*			
200	11	11			
201	94	+/-			
202	42	STO			
203	13	13			
204	74	SM*			
205	09	09			
206	00	0			
207	42	STO			
208	05	05			
209	01	1			
210	44	SUM			
211	05	05			
212	10	E'			
213	43	RCL			
214	12	12			
215	64	PO*			
216	10	10			
217	43	RCL			
218	13	13			
219	74	SM*			
220	11	11			
221	43	RCL			
222	05	05			
223	77	GE			
224	02	02			

Table A-2c

PROGRAM CURRENTS: BANK #1'

Display		Key	Display		Key	Display		Key	Display		Key
000	76	LBL	045	42	STO	090	42	STO	135	04	04
001	18	C'	046	10	10	091	04	04	136	67	EQ
002	07	7	047	85	+	092	01	1	137	01	01
003	09	9	048	02	2	093	44	SUM	138	60	60
004	85	+	049	05	5	094	04	04	139	18	C'
005	43	RCL	050	95	=	095	43	RCL	140	10	E'
006	02	02	051	42	STO	096	04	04	141	73	RC*
007	95	=	052	11	11	097	42	STO	142	10	10
008	42	STO	053	92	RTN	098	02	02	143	65	×
009	06	06	054	76	LBL	099	42	STO	144	73	RC*
010	85	+	055	11	A	100	03	03	145	06	06
011	05	5	056	00	0	101	18	C'	146	95	=
012	95	=	057	42	STO	102	19	D'	147	32	X↕T
013	42	STO	058	03	03	103	73	RC*	148	73	RC*
014	07	07	059	01	1	104	06	06	149	11	11
015	92	RTN	060	44	SUM	105	42	STO	150	85	+
016	76	LBL	061	03	03	106	12	12	151	73	RC*
017	19	D'	062	19	D'	107	73	RC*	152	07	07
018	06	6	063	73	RC*	108	07	07	153	95	=
019	09	9	064	08	08	109	42	STO	154	37	P/R
020	85	+	065	32	X↕T	110	13	13	155	44	SUM
021	43	RCL	066	73	RC*	111	73	RC*	156	16	16
022	03	03	067	09	09	112	08	08	157	32	X↕T
023	95	=	068	37	P/R	113	72	ST*	158	44	SUM
024	42	STO	069	72	ST*	114	06	06	159	15	15
025	08	08	070	09	09	115	73	RC*	160	43	RCL
026	85	+	071	43	RCL	116	09	09	161	01	01
027	05	5	072	01	01	117	72	ST*	162	32	X↕T
028	95	=	073	32	X↕T	118	07	07	163	43	RCL
029	42	STO	074	72	ST*	119	00	0	164	05	05
030	09	09	075	08	08	120	42	STO	165	77	GE
031	92	RTN	076	43	RCL	121	05	05	166	01	01
032	76	LBL	077	03	03	122	42	STO	167	71	71
033	10	E'	078	77	GE	123	15	15	168	61	GTO
034	01	1	079	00	00	124	42	STO	169	01	01
035	04	4	080	84	84	125	16	16	170	26	26
036	85	+	081	61	GTO	126	01	1	171	43	RCL
037	05	5	082	00	00	127	44	SUM	172	04	04
038	65	×	083	59	59	128	05	05	173	42	STO
039	43	RCL	084	01	1	129	43	RCL	174	02	02
040	04	04	085	44	SUM	130	05	05	175	18	C'
041	85	+	086	14	14	131	42	STO	176	73	RC*
042	43	RCL	087	86	STF	132	02	02	177	06	06
043	05	05	088	00	00	133	32	X↕T	178	75	-
044	95	=	089	00	0	134	43	RCL	179	43	RCL

Table A-2c (continued)

PROGRAM CURRENTS: BANK #1'

Display		Key
180	15	15
181	95	=
182	32	X↕T
183	73	RC*
184	07	07
185	75	-
186	43	RCL
187	16	16
188	95	=
189	22	INV
190	37	P/R
191	72	ST*
192	07	07
193	32	X↕T
194	72	ST*
195	06	06
196	75	-
197	43	RCL
198	12	12
199	95	=
200	50	I×I
201	32	X↕T
202	43	RCL
203	17	17
204	77	GE
205	02	02
206	10	10
207	22	INV
208	86	STF
209	00	00
210	43	RCL
211	01	01
212	32	X↕T
213	43	RCL
214	04	04
215	77	GE
216	02	02
217	21	21
218	61	GTO
219	00	00
220	92	92
221	22	INV
222	87	IFF
223	00	00
224	02	02

Display		Key
225	28	28
226	01	1
227	91	R/S
228	09	9
229	32	X↕T
230	43	RCL
231	14	14
232	77	GE
233	02	02
234	38	38
235	61	GTO
236	00	00
237	84	84
238	00	0
239	91	R/S

Program PIPE

Program PIPE computes the propagation constant, γ, the induced voltage constant, $1/|\gamma|$, and the characteristic impedance, Z_o, of a buried pipeline having arbitrary characteristics. This program accurately accounts for the following pipeline or soil variables: pipe burial depth, pipe diameter, pipe wall thickness, pipe steel relative permeability, pipe steel resistivity, pipe coating resistivity, and earth resistivity. The computation method employed for γ is a Newton's method solution of Eq. 2-9, a complex-valued transcendental equation. Newton's method is described in general by Carnahan et al (3). After computing γ, the program proceeds to determine Z_o by solving Eq. 2-10. Given the accuracy of the input data and the underlying Sunde theory (4), this overall procedure introduces virtually zero additional error. The pipe self impedance can then be calculated by forming the product γZ_o. The program can be permanently recorded on two magnetic cards.

Figure A-3 details the pipeline geometry assumed for this program and defines the essential data parameters keyed in by the user. Table A-3a provides a step by step instruction procedure for the use of the program. Table A-3b is a printer listing of the key sequences needed initially to program the magnetic cards.

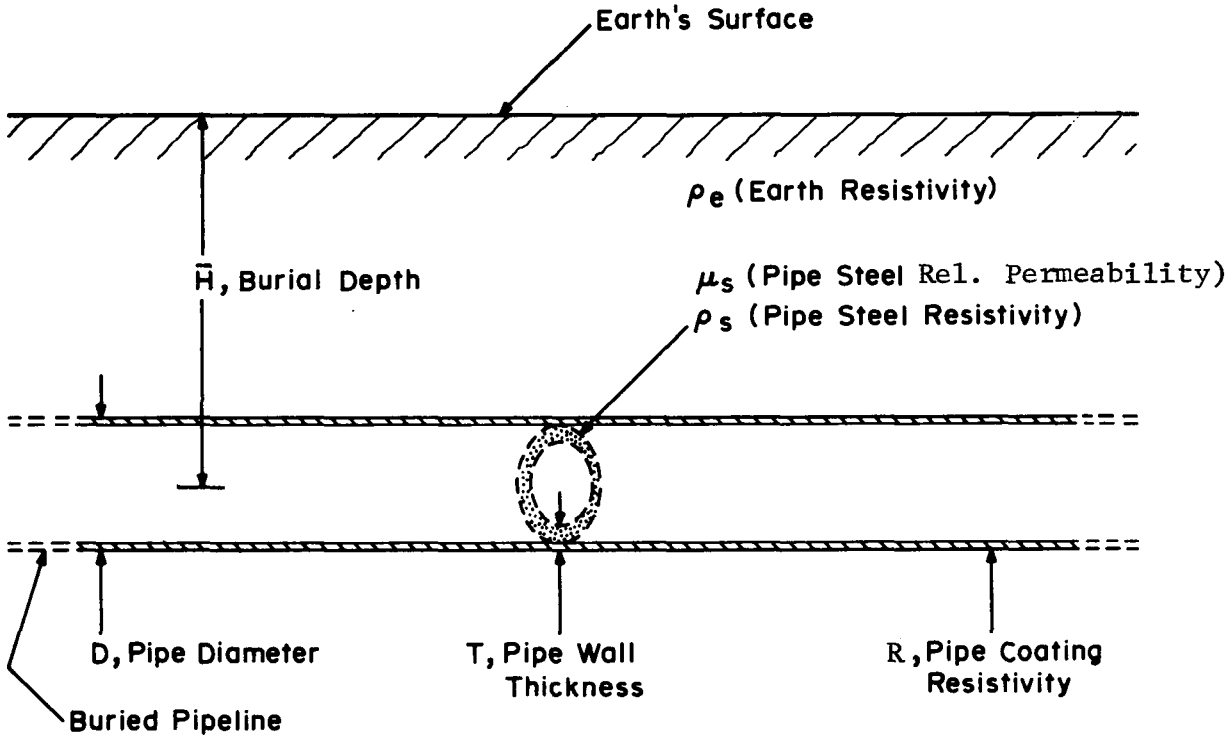

Figure A-3. Pipeline/Earth Geometry for Program PIPE

Table A-3a

INSTRUCTIONS FOR PROGRAM PIPE

1. Press CLR. Then, press 3 Op 17.

2. Press 1. Then, insert bank #1 into the card reader.
   Press 2. Then, insert bank #2 into the card reader.
   Press 3. Then, insert bank #3 into the card reader.

3. Press A.

4. Key $\overline{H}$ (in inches) into the display. Then, Press B.
   Key D (in inches) into the display. Then, press B.
   Key T (in inches) into the display. Then, press B.
   Key ρ_e (in ohm-meters) into the display. Then, press B.
   Key μ_s (dimensionless) into the display. Then, press B.
   Key ρ_s (in microohm-meters) into the display. Then, press B.
   Key R (in kiloohm-ft^2) into the display. Then, press B.

5. Press C. Wait 34 seconds for the display to unblank. The displayed number is the first iteration estimate of the exact value of Real(γ) in nepers/km. To display the first-iteration estimate of Im(γ) in radians/km, press x$\rightleftarrows$t.

6. Press D. Wait 22 seconds for the display to unblank. The displayed number is the second-iteration estimate of Real(γ). Press x$\rightleftarrows$t to display the second-iteration estimate of Im(γ).

7. Repeat Step 6 until two successive values of Real(γ) are identical. The final values of Real(γ) and Im(γ) are the exact values desired.

8. Press R/S to display $1/|\gamma|$.

9. Press R/S. Wait 4 seconds for the display to unblank. The displayed number is Real(Z_o) in ohms. Press x$\rightleftarrows$t to display Im(Z_o) in ohms.

10. To compute γ, $1/|\gamma|$, and Z_o for a different pipe, return to Step 3.

NOTE: If the PC-100A printer is used, each iteration's results for Real(γ) and Im(γ) will be printed out automatically and labeled as "GAMR" and "GAMI", respectively. Further, the quantity $1/|\gamma|$ will be printed out and labeled as "INVG". Finally, the quantities Real(Z_o) and Im(Z_o) will be printed out and labeled as "ZOR" and "ZOI", respectively.

Table A-3b

PROGRAM PIPE

Display		Key	Display		Key	Display		Key	Display		Key
000	76	LBL	045	93	.	090	49	PRD	135	43	RCL
001	16	A'	046	07	7	091	07	07	136	09	09
002	43	RCL	047	65	×	092	49	PRD	137	33	X^2
003	10	10	048	43	RCL	093	08	08	138	54	)
004	22	INV	049	12	12	094	89	π	139	34	FX
005	23	LNX	050	34	FX	095	55	÷	140	95	=
006	75	-	051	95	=	096	43	RCL	141	23	LNX
007	35	1/X	052	35	1/X	097	12	12	142	42	STO
008	92	RTN	053	42	STO	098	95	=	143	03	03
009	76	LBL	054	07	07	099	42	STO	144	22	INV
010	17	B'	055	65	×	100	00	00	145	23	LNX
011	53	(	056	93	.	101	43	RCL	146	55	÷
012	43	RCL	057	08	8	102	12	12	147	01	1
013	10	10	058	01	1	103	65	×	148	93	.
014	22	INV	059	95	=	104	02	2	149	06	6
015	23	LNX	060	42	STO	105	01	1	150	05	5
016	85	+	061	08	08	106	01	1	151	02	2
017	35	1/X	062	43	RCL	107	01	1	152	95	=
018	75	-	063	15	15	108	95	=	153	23	LNX
019	02	2	064	65	×	109	35	1/X	154	55	÷
020	65	×	065	01	1	110	42	STO	155	43	RCL
021	43	RCL	066	00	0	111	01	01	156	00	00
022	10	10	067	55	÷	112	02	2	157	85	+
023	39	COS	068	43	RCL	113	06	6	158	01	1
024	54	)	069	12	12	114	05	5	159	01	1
025	92	RTN	070	85	+	115	02	2	160	06	6
026	76	LBL	071	42	STO	116	06	6	161	04	4
027	11	A	072	28	28	117	35	1/X	162	65	×
028	09	9	073	93	.	118	42	STO	163	43	RCL
029	42	STO	074	00	0	119	02	02	164	15	15
030	27	27	075	01	1	120	07	7	165	55	÷
031	70	RAD	076	95	=	121	02	2	166	43	RCL
032	91	R/S	077	35	1/X	122	93	.	167	10	10
033	76	LBL	078	94	+/-	123	08	8	168	95	=
034	12	B	079	22	INV	124	03	3	169	42	STO
035	72	ST*	080	23	LNX	125	55	÷	170	06	06
036	27	27	081	65	×	126	53	(	171	43	RCL
037	01	1	082	43	RCL	127	43	RCL	172	13	13
038	44	SUM	083	28	28	128	10	10	173	65	×
039	27	27	084	95	=	129	33	X^2	174	43	RCL
040	91	R/S	085	34	FX	130	55	÷	175	14	14
041	76	LBL	086	85	+	131	04	4	176	95	=
042	13	C	087	01	1	132	85	+	177	34	FX
043	08	8	088	95	=	133	04	4	178	55	÷
044	07	7	089	35	1/X	134	65	×	179	05	5

Table A-3b (continued)

PROGRAM PIPE

Display		Key	Display		Key	Display		Key	Display		Key
180	01	1	225	65	×	270	54	)	315	12	12
181	08	8	226	43	RCL	271	42	STO	316	55	÷
182	05	5	227	10	10	272	13	13	317	43	RCL
183	55	÷	228	38	SIN	273	85	+	318	10	10
184	43	RCL	229	95	=	274	02	2	319	54	)
185	10	10	230	55	÷	275	65	×	320	22	INV
186	95	=	231	17	B'	276	53	(	321	30	TAN
187	42	STO	232	95	=	277	43	RCL	322	75	-
188	04	04	233	49	PRD	278	07	07	323	43	RCL
189	42	STO	234	05	05	279	65	×	324	04	04
190	05	05	235	76	LBL	280	43	RCL	325	95	=
191	43	RCL	236	14	D	281	08	08	326	42	STO
192	13	13	237	53	(	282	54	)	327	18	18
193	55	÷	238	43	RCL	283	42	STO	328	02	2
194	43	RCL	239	07	07	284	09	09	329	65	×
195	14	14	240	33	X^2	285	65	×	330	53	(
196	95	=	241	75	-	286	53	(	331	43	RCL
197	34	FX	242	43	RCL	287	43	RCL	332	07	07
198	65	×	243	08	08	288	08	08	333	65	×
199	93	.	244	33	X^2	289	55	÷	334	43	RCL
200	07	7	245	54	)	290	43	RCL	335	13	13
201	08	8	246	42	STO	291	07	07	336	85	+
202	02	2	247	10	10	292	54	)	337	43	RCL
203	65	×	248	65	×	293	22	INV	338	08	08
204	43	RCL	249	53	(	294	30	TAN	339	65	×
205	11	11	250	43	RCL	295	42	STO	340	53	(
206	95	=	251	06	06	296	14	14	341	43	RCL
207	42	STO	252	75	-	297	55	÷	342	14	14
208	10	10	253	53	(	298	43	RCL	343	75	-
209	16	A'	254	43	RCL	299	00	00	344	53	(
210	85	+	255	07	07	300	75	-	345	43	RCL
211	02	2	256	33	X^2	301	43	RCL	346	09	09
212	65	×	257	85	+	302	02	02	347	55	÷
213	43	RCL	258	43	RCL	303	65	×	348	43	RCL
214	10	10	259	08	08	304	53	(	349	11	11
215	38	SIN	260	33	X^2	305	53	(	350	54	)
216	95	=	261	54	)	306	02	2	351	42	STO
217	55	÷	262	42	STO	307	65	×	352	16	16
218	17	B'	263	11	11	308	43	RCL	353	54	)
219	95	=	264	23	LNX	309	09	09	354	55	÷
220	49	PRD	265	55	÷	310	85	+	355	43	RCL
221	04	04	266	02	2	311	43	RCL	356	00	00
222	16	A'	267	55	÷	312	01	01	357	75	-
223	75	-	268	43	RCL	313	54	)	358	43	RCL
224	02	2	269	00	00	314	42	STO	359	02	02

Table A-3b (continued)

PROGRAM PIPE

Display		Key	Display		Key	Display		Key	Display		Key
360	65	×	405	19	19	450	43	RCL	495	42	STO
361	53	(	406	02	2	451	08	08	496	21	21
362	43	RCL	407	65	×	452	65	×	497	02	2
363	08	08	408	53	(	453	43	RCL	498	02	2
364	65	×	409	43	RCL	454	15	15	499	01	1
365	43	RCL	410	08	08	455	95	=	500	03	3
366	10	10	411	65	×	456	94	+/-	501	03	3
367	75	-	412	43	RCL	457	42	STO	502	00	0
368	43	RCL	413	13	13	458	20	20	503	03	3
369	07	07	414	75	-	459	02	2	504	05	5
370	65	×	415	43	RCL	460	65	×	505	69	DP
371	43	RCL	416	07	07	461	43	RCL	506	04	04
372	12	12	417	65	×	462	09	09	507	43	RCL
373	54	)	418	53	(	463	65	×	508	07	07
374	55	÷	419	43	RCL	464	43	RCL	509	85	+
375	53	(	420	14	14	465	13	13	510	53	(
376	43	RCL	421	85	+	466	75	-	511	43	RCL
377	10	10	422	43	RCL	467	43	RCL	512	21	21
378	33	X^2	423	16	16	468	10	10	513	65	×
379	85	+	424	54	)	469	65	×	514	43	RCL
380	43	RCL	425	55	÷	470	43	RCL	515	20	20
381	12	12	426	43	RCL	471	14	14	516	75	-
382	33	X^2	427	00	00	472	55	÷	517	43	RCL
383	54	)	428	85	+	473	43	RCL	518	18	18
384	42	STO	429	43	RCL	474	00	00	519	65	×
385	17	17	430	02	02	475	75	-	520	43	RCL
386	54	)	431	65	×	476	02	2	521	19	19
387	75	-	432	53	(	477	65	×	522	54	)
388	43	RCL	433	43	RCL	478	43	RCL	523	55	÷
389	07	07	434	07	07	479	02	02	524	53	(
390	65	×	435	65	×	480	65	×	525	43	RCL
391	53	(	436	43	RCL	481	53	(	526	19	19
392	43	RCL	437	10	10	482	43	RCL	527	33	X^2
393	10	10	438	85	+	483	03	03	528	85	+
394	55	÷	439	43	RCL	484	75	-	529	43	RCL
395	43	RCL	440	08	08	485	43	RCL	530	20	20
396	00	00	441	65	×	486	17	17	531	33	X^2
397	55	÷	442	43	RCL	487	23	LNX	532	54	)
398	43	RCL	443	12	12	488	55	÷	533	95	=
399	11	11	444	54	)	489	04	4	534	42	STO
400	54	)	445	55	÷	490	54	)	535	07	07
401	42	STO	446	43	RCL	491	75	-	536	65	×
402	15	15	447	17	17	492	43	RCL	537	01	1
403	95	=	448	54	)	493	05	05	538	00	0
404	42	STO	449	85	+	494	95	=	539	00	0

Table A-3b (continued)

PROGRAM PIPE

Display		Key
540	00	0
541	95	=
542	42	STO
543	22	22
544	69	DP
545	06	06
546	02	2
547	02	2
548	01	1
549	03	3
550	03	3
551	00	0
552	02	2
553	04	4
554	69	DP
555	04	04
556	43	RCL
557	08	08
558	75	-
559	53	(
560	43	RCL
561	21	21
562	65	×
563	43	RCL
564	19	19
565	85	+
566	43	RCL
567	18	18
568	65	×
569	43	RCL
570	20	20
571	54	)
572	55	÷
573	53	(
574	43	RCL
575	19	19
576	33	X^2
577	85	+
578	43	RCL
579	20	20
580	33	X^2
581	54	)
582	95	=
583	42	STO
584	08	08

Display		Key
585	65	×
586	01	1
587	00	0
588	00	0
589	00	0
590	95	=
591	42	STO
592	23	23
593	69	DP
594	06	06
595	98	ADV
596	32	X:T
597	43	RCL
598	22	22
599	91	R/S
600	02	2
601	04	4
602	03	3
603	01	1
604	04	4
605	02	2
606	02	2
607	02	2
608	69	DP
609	04	04
610	43	RCL
611	22	22
612	33	X^2
613	85	+
614	43	RCL
615	23	23
616	33	X^2
617	95	=
618	34	$\sqrt{X}$
619	35	1/X
620	42	STO
621	24	24
622	69	DP
623	06	06
624	98	ADV
625	91	R/S
626	04	4
627	06	6
628	00	0
629	01	1

Display		Key
630	03	3
631	05	5
632	69	DP
633	04	04
634	43	RCL
635	08	08
636	65	×
637	43	RCL
638	14	14
639	55	÷
640	43	RCL
641	00	00
642	85	+
643	43	RCL
644	07	07
645	65	×
646	43	RCL
647	13	13
648	95	=
649	42	STO
650	25	25
651	69	DP
652	06	06
653	04	4
654	06	6
655	00	0
656	01	1
657	02	2
658	04	4
659	69	DP
660	04	04
661	43	RCL
662	08	08
663	65	×
664	43	RCL
665	13	13
666	75	-
667	43	RCL
668	07	07
669	65	×
670	43	RCL
671	14	14
672	55	÷
673	43	RCL
674	00	00

Display		Key
675	95	=
676	42	STO
677	26	26
678	69	DP
679	06	06
680	98	ADV
681	32	X:T
682	43	RCL
683	25	25
684	91	R/S

Program WIRE

Program WIRE computes the propagation constant, γ, the induced voltage constant, $1/|\gamma|$, and the characteristic impedance, Z_o, of a bare horizontal, buried ground wire having arbitrary characteristics. This program accurately accounts for the following wire or soil variables: wire burial depth, wire diameter, wire relative permeability, wire resistivity, wire series inductive and resistive loading, and earth resistivity. The computation method employed for γ is a Newton's method solution of Eq. 2-9. After computing γ, the program proceeds to determine Z_o by solving Eq. 2-10. The wire self impedance can then be calculated by forming the product γZ_o.

Figure A-4 details the ground wire geometry assumed for this program and defines the essential data parameters keyed in by the user. Table A-4a provides a step by step instruction procedure for the use of the program. Table A-4b is a printer listing of the key sequences needed initially to program the magnetic cards.

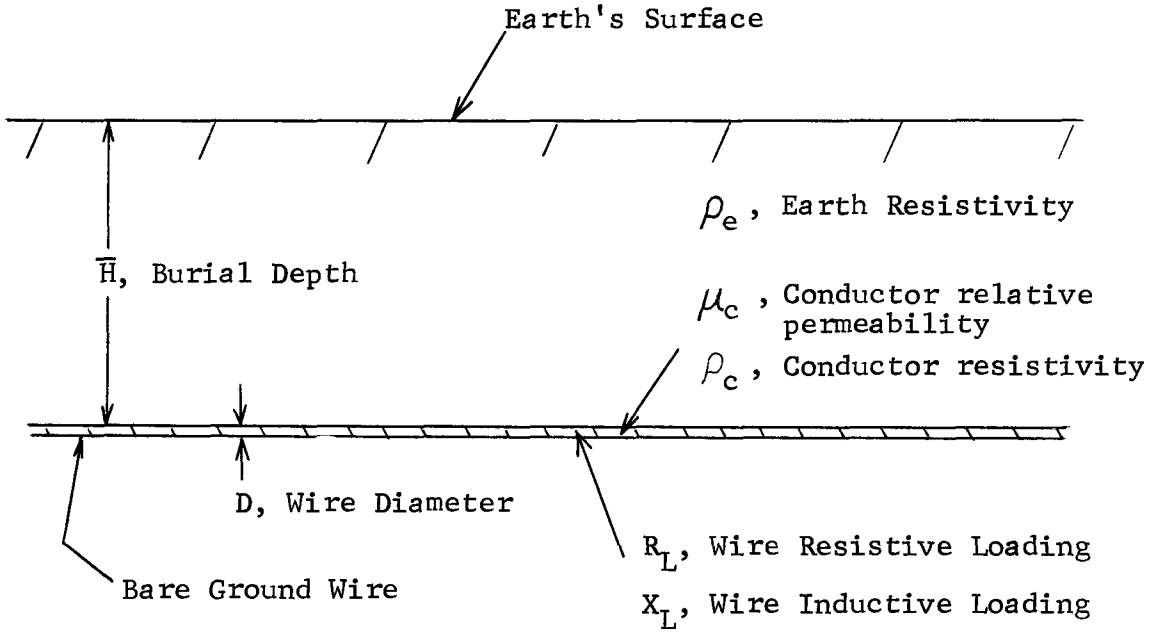

Figure A-4. Ground Wire/Earth Geometry for Program WIRE

Table A-4a

INSTRUCTIONS FOR PROGRAM WIRE

1. Press CLR. Then, press 3 Op 17.

2. Press 1. Then, insert bank #1 into the card reader.
   Press 2. Then, insert bank #2 into the card reader.
   Press 3. Then, insert bank #3 into the card reader.

3. Press A.

4. Key $\overline{H}$ (in inches) into the display. Then, press B.
   Key D (in inches) into the display ($D \leq 1$"). Then, press B.
   Key ρ_e (in ohm-meters) into the display. Then, press B.
   Key μ_c (dimensionless) into the display. Then, press B.
   Key ρ_c (in microohm-meters) into the display. Then, press B.
   Key R_L (in ohms/meter) into the display. Then, press B.
   Key X_L (in ohms/meter) into the display. Then, press B.

   NOTE: R_L and X_L equal zero for a ground wire with no artificial series inductive loading.

5. Press C. Wait 28 seconds for the display to unblank. The displayed number is the first-iteration estimate of the exact value of Real(γ) in nepers/km. To display the first-iteration estimate of Im(γ) in radians/km, press x$\rightleftarrows$t.

6. Press D. Wait 22 seconds for the display to unblank. The displayed number is the second-iteration estimate of Real(γ). Press x$\rightleftarrows$t to display the second-iteration estimate of Im(γ).

7. Repeat Step 6 until two successive values of Real(γ) are identical. The final values of Real(γ) and Im(γ) are the exact values desired.

8. Press R/S to display $1/|\gamma|$.

9. Press R/S. Wait 4 seconds for the display to unblank. The displayed number is Real(Z_0) in ohms. Press x$\rightleftarrows$t to display Im(Z_0) in ohms.

10. To compute γ, $1/|\gamma|$, and Z_0 for a different wire, return to Step 3.

    NOTE: If the PC-100A printer is used, each iteration's results for Real(γ) and Im(γ) will be printed out automatically and labeled as "GAMR" and "GAMI", respectively. Further, the quantity $1/|\gamma|$ will be printed out and labeled as "INVG". Finally, the quantities Real(Z_0) and Im(Z_0) will be printed out and labeled as "ZOR" and "ZOI", respectively.

Table A-4b

PROGRAM WIRE

Display		Key	Display		Key	Display		Key	Display		Key
000	76	LBL	045	43	RCL	090	53	(	135	34	$\sqrt{x}$
001	11	A	046	10	10	091	43	RCL	136	55	÷
002	09	9	047	95	=	092	10	10	137	43	RCL
003	42	STO	048	45	Y^x	093	33	x^2	138	13	13
004	27	27	049	07	7	094	55	÷	139	34	$\sqrt{x}$
005	70	RAD	050	95	=	095	04	4	140	95	=
006	91	R/S	051	22	INV	096	85	+	141	45	Y^x
007	76	LBL	052	23	LNX	097	04	4	142	04	4
008	12	B	053	49	PRD	098	65	×	143	55	÷
009	72	ST*	054	07	07	099	43	RCL	144	04	4
010	27	27	055	35	1/X	100	09	09	145	08	8
011	01	1	056	49	PRD	101	33	x^2	146	85	+
012	44	SUM	057	08	08	102	54	)	147	01	1
013	27	27	058	89	π	103	34	$\sqrt{x}$	148	95	=
014	91	R/S	059	55	÷	104	95	=	149	65	×
015	76	LBL	060	43	RCL	105	23	LNX	150	43	RCL
016	13	C	061	11	11	106	42	STO	151	13	13
017	08	8	062	95	=	107	03	03	152	55	÷
018	07	7	063	42	STO	108	22	INV	153	05	5
019	93	.	064	00	00	109	23	LNX	154	00	0
020	07	7	065	43	RCL	110	55	÷	155	06	6
021	65	×	066	11	11	111	01	1	156	93	.
022	43	RCL	067	65	×	112	93	.	157	07	7
023	11	11	068	02	2	113	06	6	158	55	÷
024	34	$\sqrt{x}$	069	01	1	114	05	5	159	43	RCL
025	95	=	070	01	1	115	02	2	160	10	10
026	35	1/X	071	01	1	116	95	=	161	33	x^2
027	42	STO	072	95	=	117	23	LNX	162	85	+
028	07	07	073	35	1/X	118	55	÷	163	43	RCL
029	65	×	074	42	STO	119	43	RCL	164	14	14
030	93	.	075	01	01	120	00	00	165	95	=
031	08	8	076	02	2	121	95	=	166	42	STO
032	09	9	077	06	6	122	42	STO	167	04	04
033	03	3	078	05	5	123	06	06	168	43	RCL
034	95	=	079	02	2	124	93	.	169	12	12
035	42	STO	080	06	6	125	01	1	170	55	÷
036	08	08	081	35	1/X	126	09	9	171	05	5
037	01	1	082	42	STO	127	05	5	172	03	3
038	93	.	083	02	02	128	04	4	173	00	0
039	02	2	084	07	7	129	65	×	174	05	5
040	75	-	085	02	2	130	43	RCL	175	02	2
041	01	1	086	93	.	131	10	10	176	85	+
042	93	.	087	08	8	132	65	×	177	43	RCL
043	02	2	088	03	3	133	43	RCL	178	15	15
044	65	×	089	55	÷	134	12	12	179	95	=

Table A-4b (continued)

PROGRAM WIRE

Display		Key	Display		Key	Display		Key	Display		Key
180	42	STO	225	07	07	270	43	RCL	315	43	RCL
181	05	05	226	65	×	271	04	04	316	07	07
182	76	LBL	227	43	RCL	272	95	=	317	65	×
183	14	D	228	08	08	273	42	STO	318	43	RCL
184	53	(	229	54	)	274	18	18	319	12	12
185	43	RCL	230	42	STO	275	02	2	320	54	)
186	07	07	231	09	09	276	65	×	321	55	÷
187	33	X^2	232	65	×	277	53	(	322	53	(
188	75	-	233	53	(	278	43	RCL	323	43	RCL
189	43	RCL	234	43	RCL	279	07	07	324	10	10
190	08	08	235	08	08	280	65	×	325	33	X^2
191	33	X^2	236	55	÷	281	43	RCL	326	85	+
192	54	)	237	43	RCL	282	13	13	327	43	RCL
193	42	STO	238	07	07	283	85	+	328	12	12
194	10	10	239	54	)	284	43	RCL	329	33	X^2
195	65	×	240	22	INV	285	08	08	330	54	)
196	53	(	241	30	TAN	286	65	×	331	42	STO
197	43	RCL	242	42	STO	287	53	(	332	17	17
198	06	06	243	14	14	288	43	RCL	333	54	)
199	75	-	244	55	÷	289	14	14	334	75	-
200	53	(	245	43	RCL	290	75	-	335	43	RCL
201	43	RCL	246	00	00	291	53	(	336	07	07
202	07	07	247	75	-	292	43	RCL	337	65	×
203	33	X^2	248	43	RCL	293	09	09	338	53	(
204	85	+	249	02	02	294	55	÷	339	43	RCL
205	43	RCL	250	65	×	295	43	RCL	340	10	10
206	08	08	251	53	(	296	11	11	341	55	÷
207	33	X^2	252	53	(	297	54	)	342	43	RCL
208	54	)	253	02	2	298	42	STO	343	00	00
209	42	STO	254	65	×	299	16	16	344	55	÷
210	11	11	255	43	RCL	300	54	)	345	43	RCL
211	23	LNX	256	09	09	301	55	÷	346	11	11
212	55	÷	257	85	+	302	43	RCL	347	54	)
213	02	2	258	43	RCL	303	00	00	348	42	STO
214	55	÷	259	01	01	304	75	-	349	15	15
215	43	RCL	260	54	)	305	43	RCL	350	95	=
216	00	00	261	42	STO	306	02	02	351	42	STO
217	54	)	262	12	12	307	65	×	352	19	19
218	42	STO	263	55	÷	308	53	(	353	02	2
219	13	13	264	43	RCL	309	43	RCL	354	65	×
220	85	+	265	10	10	310	08	08	355	53	(
221	02	2	266	54	)	311	65	×	356	43	RCL
222	65	×	267	22	INV	312	43	RCL	357	08	08
223	53	(	268	30	TAN	313	10	10	358	65	×
224	43	RCL	269	75	-	314	75	-	359	43	RCL

Table A-4b (continued)

PROGRAM WIRE

Display		Key	Display		Key	Display		Key	Display		Key
360	13	13	405	20	20	450	03	3	495	01	1
361	75	-	406	02	2	451	05	5	496	03	3
362	43	RCL	407	65	×	452	69	□P	497	03	3
363	07	07	408	43	RCL	453	04	04	498	00	0
364	65	×	409	09	09	454	43	RCL	499	02	2
365	53	(	410	65	×	455	07	07	500	04	4
366	43	RCL	411	43	RCL	456	85	+	501	69	□P
367	14	14	412	13	13	457	53	(	502	04	04
368	85	+	413	75	-	458	43	RCL	503	43	RCL
369	43	RCL	414	43	RCL	459	21	21	504	08	08
370	16	16	415	10	10	460	65	×	505	75	-
371	54	)	416	65	×	461	43	RCL	506	53	(
372	55	÷	417	43	RCL	462	20	20	507	43	RCL
373	43	RCL	418	14	14	463	75	-	508	21	21
374	00	00	419	55	÷	464	43	RCL	509	65	×
375	85	+	420	43	RCL	465	18	18	510	43	RCL
376	43	RCL	421	00	00	466	65	×	511	19	19
377	02	02	422	75	-	467	43	RCL	512	85	+
378	65	×	423	02	2	468	19	19	513	43	RCL
379	53	(	424	65	×	469	54	)	514	18	18
380	43	RCL	425	43	RCL	470	55	÷	515	65	×
381	07	07	426	02	02	471	53	(	516	43	RCL
382	65	×	427	65	×	472	43	RCL	517	20	20
383	43	RCL	428	53	(	473	19	19	518	54	)
384	10	10	429	43	RCL	474	33	X^2	519	55	÷
385	85	+	430	03	03	475	85	+	520	53	(
386	43	RCL	431	75	-	476	43	RCL	521	43	RCL
387	08	08	432	43	RCL	477	20	20	522	19	19
388	65	×	433	17	17	478	33	X^2	523	33	X^2
389	43	RCL	434	23	LNX	479	54	)	524	85	+
390	12	12	435	55	÷	480	95	=	525	43	RCL
391	54	)	436	04	4	481	42	STO□	526	20	20
392	55	÷	437	54	)	482	07	07	527	33	X^2
393	43	RCL	438	75	-	483	65	×	528	54	)
394	17	17	439	43	RCL	484	01	1	529	95	=
395	54	)	440	05	05	485	00	0	530	42	STO□
396	85	+	441	95	=	486	00	0	531	08	08
397	43	RCL	442	42	STO□	487	00	0	532	65	×
398	08	08	443	21	21	488	95	=	533	01	1
399	65	×	444	02	2	489	42	STO□	534	00	0
400	43	RCL	445	02	2	490	22	22	535	00	0
401	15	15	446	01	1	491	69	□P	536	00	0
402	95	=	447	03	3	492	06	06	537	95	=
403	94	+/-	448	03	3	493	02	2	538	42	STO□
404	42	STO□	449	00	0	494	02	2	539	23	23

Table A-4b (continued)

PROGRAM WIRE

Display		Key	Display		Key
540	69	□P	586	55	÷
541	06	06	587	43	RCL
542	98	ADV	588	00	00
543	32	X↕T	589	85	+
544	43	RCL	590	43	RCL
545	22	22	591	07	07
546	91	R/S	592	65	×
547	02	2	593	43	RCL
548	04	4	594	13	13
549	03	3	595	95	=
550	01	1	596	42	STO□
551	04	4	597	25	25
552	02	2	598	69	□P
553	02	2	599	06	06
554	02	2	600	04	4
555	69	□P	601	06	6
556	04	04	602	00	0
557	43	RCL	603	01	1
558	22	22	604	02	2
559	33	X^2	605	04	4
560	85	+	606	69	□P
561	43	RCL	607	04	04
562	23	23	608	43	RCL
563	33	X^2	609	08	08
564	95	=	610	65	×
565	34	ΓX	611	43	RCL
566	35	1/X	612	13	13
567	42	STO□	613	75	-
568	24	24	614	43	RCL
569	69	□P	615	07	07
570	06	06	616	65	×
571	98	ADV	617	43	RCL
572	91	R/S	618	14	14
573	04	4	619	55	÷
574	06	6	620	43	RCL
575	00	0	621	00	00
576	01	1	622	95	=
577	03	3	623	42	STO□
578	05	5	624	26	26
579	69	□P	625	69	□P
580	04	04	626	06	06
581	43	RCL	627	98	ADV
582	08	08	628	32	X↕T
583	65	×	629	43	RCL
584	43	RCL	630	25	25
585	14	14	631	91	R/S

Program THEVENIN

Program THEVENIN computes the Thevenin equivalent circuit for the terminal behavior of an arbitrary pipeline or ground wire parallel to a power line. The nature of the conductor is specified for the program simply by inputting the conductor's propagation constant, γ , and characteristic impedance, Z_0, determined using either Program PIPE or Program WIRE. The quantities V_L and Z_L are determined by the geometry and characteristics of the pipeline network. Usually, in finding the pipeline voltage at a given location several iterations of the THEVENIN program are necessary to transform remote impedance terminations and voltage pick-up along the pipeline into the local Thevenin equivalent circuit. Generally, the V_θ and Z_θ found from exercising the program will become the V_L and Z_L for a successive iteration.

The computation method for the complex-valued Thevenin source impedance involves the solution of Eq. 3-10c. The complex-valued Thevenin source voltage is computed using Eq. 3-10b for the case $x = 0$ and $Z_1 = \infty$. The program can be permanently recorded on one magnetic card.

Figure A-5 details the geometry of the earth return conductor assumed for this program and defines the essential data parameters keyed in by the user. Table A-5a provides a step-by-step instruction procedure for the use of the program. Table A-5b is a printer listing of the key sequences needed initially to program the magnetic card.

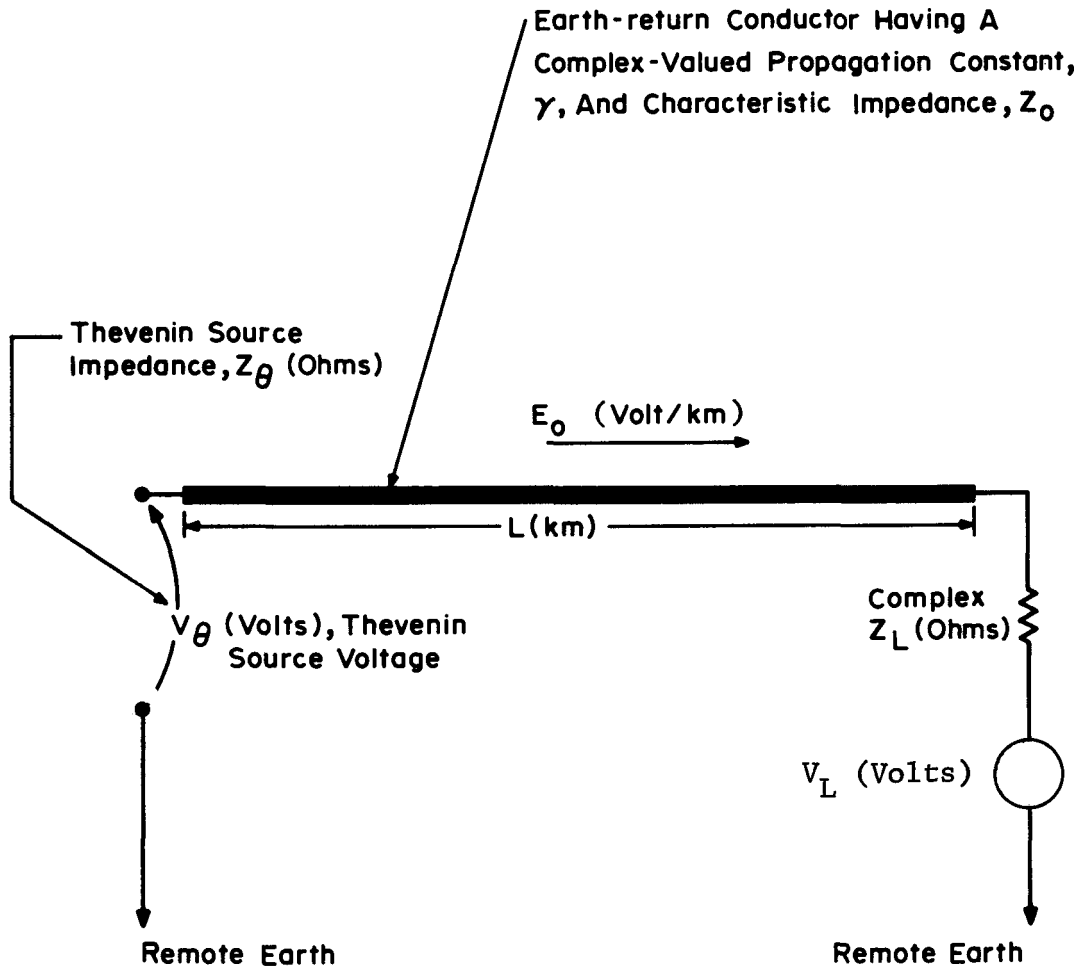

Figure A-5. Conductor Geometry for Program THEVENIN

Table A-5a

INSTRUCTIONS FOR PROGRAM THEVENIN

1. Press CLR. Then, press 3 Op 17.

2. Press 1. Then, insert bank #1 into the card reader.
   Press 2. Then, insert bank #2 into the card reader.

3. Press A.

4. Key Real(γ) (in nepers/km) into the display. Then, press B.
   Key Im(γ) (in radians/km) into the display. Then, press B.
   Key Real(Z_o) (in ohms) into the display. Then, press B.
   Key Im(Z_o) (in ohms) into the display. Then, press B.
   Key $|V_L|$ (in volts) into the display. Then, press B.
   Key $\angle V_L$ (in degrees) into the display. Then, press B.
   Key $|Z_L|$ (in ohms) into the display. Then, press B.
   Key $\angle Z_L$ (in degrees) into the display. Then, press B.
   Key $|E_o|$ (in volts/km) into the display. Then, press B.
   Key $\angle E_o$ (in degrees) into the display. Then, press B.

5. Key L (in km) into the display. Then, press C and wait 17 seconds for the display to unblank. The display then shows $|Z_\theta|$ in ohms. To then display $\angle Z_\theta$ in degrees, press x$\rightleftarrows$t.

6. Press R/S and wait 9 seconds for the display to unblank. The display then shows $|V_\theta|$ in volts. To then display $\angle V_\theta$ in degrees, press x$\rightleftarrows$t.

7. If results are desired for a different value of L, simply repeat Steps 5 and 6. Otherwise, begin at Step 3.

   NOTE: If the PC-100A printer is used, $|Z_\theta|$ and $\angle Z_\theta$ will be printed out automatically and labeled as "ZMAG" and "ZPHA", respectively. Further, $|V_\theta|$ and $\angle V_\theta$ will be printed out and labeled as "VMAG" and "VPHA", respectively.

Table A-5b

PROGRAM THEVENIN

Display		Key	Display		Key	Display		Key	Display		Key
000	76	LBL	045	42	STO	090	01	1	135	43	RCL
001	11	A	046	13	13	091	08	8	136	16	16
002	01	1	047	43	RCL	092	00	0	137	75	-
003	42	STO	048	06	06	093	95	=	138	43	RCL
004	29	29	049	65	×	094	42	STO	139	03	03
005	70	RAD	050	89	π	095	19	19	140	95	=
006	91	R/S	051	55	÷	096	32	X↕T	141	32	X↕T
007	76	LBL	052	01	1	097	35	1/X	142	43	RCL
008	12	B	053	08	8	098	65	×	143	17	17
009	72	ST*	054	00	0	099	43	RCL	144	75	-
010	29	29	055	95	=	100	09	09	145	43	RCL
011	01	1	056	42	STO	101	95	=	146	04	04
012	44	SUM	057	15	15	102	42	STO	147	95	=
013	29	29	058	43	RCL	103	18	18	148	22	INV
014	91	R/S	059	07	07	104	43	RCL	149	37	P/R
015	76	LBL	060	32	X↕T	105	16	16	150	75	-
016	13	C	061	43	RCL	106	85	+	151	43	RCL
017	42	STO	062	08	08	107	43	RCL	152	12	12
018	00	00	063	65	×	108	03	03	153	95	=
019	65	×	064	89	π	109	95	=	154	32	X↕T
020	43	RCL	065	55	÷	110	32	X↕T	155	55	÷
021	01	01	066	01	1	111	43	RCL	156	43	RCL
022	95	=	067	08	8	112	17	17	157	11	11
023	22	INV	068	00	0	113	85	+	158	95	=
024	23	LNX	069	95	=	114	43	RCL	159	32	X↕T
025	42	STO	070	37	P/R	115	04	04	160	37	P/R
026	11	11	071	42	STO	116	95	=	161	42	STO
027	43	RCL	072	17	17	117	22	INV	162	23	23
028	00	00	073	32	X↕T	118	37	P/R	163	32	X↕T
029	65	×	074	42	STO	119	85	+	164	42	STO
030	43	RCL	075	16	16	120	43	RCL	165	22	22
031	02	02	076	43	RCL	121	12	12	166	43	RCL
032	95	=	077	01	01	122	95	=	167	20	20
033	42	STO	078	32	X↕T	123	32	X↕T	168	85	+
034	12	12	079	43	RCL	124	65	×	169	43	RCL
035	43	RCL	080	02	02	125	43	RCL	170	22	22
036	03	03	081	22	INV	126	11	11	171	95	=
037	32	X↕T	082	37	P/R	127	95	=	172	32	X↕T
038	43	RCL	083	94	+/-	128	32	X↕T	173	43	RCL
039	04	04	084	85	+	129	37	P/R	174	21	21
040	22	INV	085	43	RCL	130	42	STO	175	85	+
041	37	P/R	086	10	10	131	21	21	176	43	RCL
042	42	STO	087	65	×	132	32	X↕T	177	23	23
043	14	14	088	89	π	133	42	STO	178	95	=
044	32	X↕T	089	55	÷	134	20	20	179	22	INV

Table A-5b (continued)

PROGRAM THEVENIN

Display		Key	Display		Key	Display		Key	Display		Key
180	37	P/R	225	42	STO	270	20	20	315	15	15
181	42	STO	226	24	24	271	75	-	316	85	+
182	25	25	227	69	DP	272	43	RCL	317	43	RCL
183	32	X:T	228	06	06	273	22	22	318	14	14
184	42	STO	229	04	4	274	95	=	319	95	=
185	24	24	230	06	6	275	32	X:T	320	37	P/R
186	43	RCL	231	03	3	276	02	2	321	85	+
187	20	20	232	03	3	277	65	×	322	43	RCL
188	75	-	233	02	2	278	43	RCL	323	25	25
189	43	RCL	234	03	3	279	17	17	324	95	=
190	22	22	235	01	1	280	75	-	325	32	X:T
191	95	=	236	03	3	281	43	RCL	326	85	+
192	32	X:T	237	69	DP	282	21	21	327	43	RCL
193	43	RCL	238	04	04	283	75	-	328	24	24
194	21	21	239	43	RCL	284	43	RCL	329	95	=
195	75	-	240	14	14	285	23	23	330	32	X:T
196	43	RCL	241	85	+	286	95	=	331	22	INV
197	23	23	242	43	RCL	287	22	INV	332	37	P/R
198	95	=	243	25	25	288	37	P/R	333	42	STO
199	22	INV	244	75	-	289	85	+	334	25	25
200	37	P/R	245	43	RCL	290	43	RCL	335	32	X:T
201	42	STO	246	27	27	291	19	19	336	42	STO
202	27	27	247	95	=	292	95	=	337	24	24
203	32	X:T	248	65	×	293	32	X:T	338	04	4
204	42	STO	249	01	1	294	65	×	339	02	2
205	26	26	250	08	8	295	43	RCL	340	03	3
206	04	4	251	00	0	296	18	18	341	00	0
207	06	6	252	55	÷	297	95	=	342	01	1
208	03	3	253	89	π	298	32	X:T	343	03	3
209	00	0	254	95	=	299	37	P/R	344	02	2
210	01	1	255	42	STO	300	42	STO	345	02	2
211	03	3	256	25	25	301	25	25	346	69	DP
212	02	2	257	69	DP	302	32	X:T	347	04	04
213	02	2	258	06	06	303	42	STO	348	43	RCL
214	69	DP	259	98	ADV	304	24	24	349	24	24
215	04	04	260	32	X:T	305	02	2	350	55	÷
216	43	RCL	261	43	RCL	306	65	×	351	43	RCL
217	13	13	262	24	24	307	43	RCL	352	26	26
218	65	×	263	91	R/S	308	05	05	353	95	=
219	43	RCL	264	02	2	309	65	×	354	42	STO
220	24	24	265	65	×	310	43	RCL	355	24	24
221	55	÷	266	43	RCL	311	13	13	356	69	DP
222	43	RCL	267	16	16	312	95	=	357	06	06
223	26	26	268	75	-	313	32	X:T	358	04	4
224	95	=	269	43	RCL	314	43	RCL	359	02	2

Table A-5b (continued)

PROGRAM THEVENIN

Display		Key
360	03	3
361	03	3
362	02	2
363	03	3
364	01	1
365	03	3
366	69	□P
367	04	04
368	43	RCL
369	25	25
370	75	-
371	43	RCL
372	27	27
373	95	=
374	65	×
375	01	1
376	08	8
377	00	0
378	55	÷
379	89	π
380	95	=
381	42	STO
382	25	25
383	69	□P
384	06	06
385	98	ADV
386	98	ADV
387	32	X:T
388	43	RCL
389	24	24
390	91	R/S

Program NODE

This program computes the node voltage and branch currents for three Thevenin equivalent circuits connected together at a common point. The circuit geometry is shown in Figure A-6.

This program is the last one usually used when computing the pipeline voltage at a specified location. When doing so the procedure is to first find the Thevenin equivalent circuits looking in both directions from the location. Then as shown in Figure A-6, V_1 and Z_1 represent the Thevenin equivalent circuit parameters to one side of the location of voltage computation, and V_3 and Z_3, likewise, represent the circuit parameters looking in the other direction. V_2 and Z_2 represent the Thevenin parameters for a mitigation grounding wire if connected at this point. If none exists, then Z_2 should be inputted into the program as a large number, say 10,000 or more ohms in order to obtain correct results.

It should be noted that while instruction 5 computes the pipeline voltage at the desired location, the succeeding instructions allow for calculation of the pipe and grounding wire currents at the same site.

A step-by-step instruction procedure is detailed in Table A-6a, with the programming keystrokes listed in Table A-6b. The program can be permanently recorded on one magnetic card.

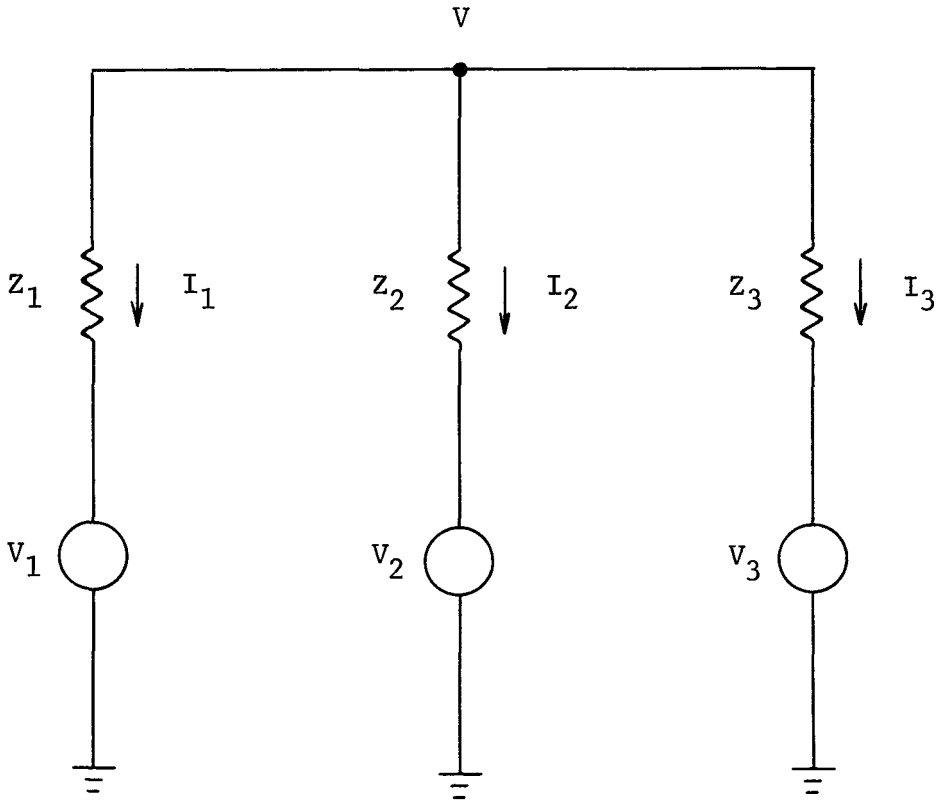

Figure A-6. Circuit Geometry for Program NODE

Table A-6a

INSTRUCTIONS FOR PROGRAM NODE

1. Press CLR. Then, press 3 Op 17.

2. Press 1. Then, insert bank #1 into the card reader.
   Press 2. Then, insert bank #2 into the card reader.

3. Press A.

4. Key $|V_1|$ (in volts) into the display. Then, press B.
   Key $\angle V_1$ (in degrees) into the display. Then, press B.
   Key $|Z_1|$ (in ohms) into the display. Then, press B.
   Key $\angle Z_1$ (in degrees) into the display. Then, press B.
   Key $|V_2|$ (in volts) into the display. Then, press B.
   Key $\angle V_2$ (in degrees) into the display. Then, press B.
   Key $|Z_2|$ (in ohms) into the display. Then, press B.
   Key $\angle Z_2$ (in degrees) into the display. Then, press B.
   Key $|V_3|$ (in volts) into the display. Then, press B.
   Key $\angle V_3$ (in degrees) into the display. Then, press B.
   Key $|Z_3|$ (in ohms) into the display. Then, press B.
   Key $\angle Z_3$ (in degrees) into the display. Then, press B.

5. Press C. Wait 16 seconds for the display to unblank. The display then shows $|V|$ in volts. Press x⇄t to display $\angle V$ in degrees.

6. Press R/S. Wait 8 seconds for the display to unblank. The display then shows $|I_1|$ in amps. Press x⇄t to display $\angle I_1$ in degrees.

7. Press R/S. Wait 6 seconds for the display to unblank. The display then shows $|I_2|$ in amps. Press x⇄t to display $\angle I_2$ in degrees.

8. Press R/S. Wait 6 seconds for the display to unblank. The display then shows $|I_3|$ in amps. Press x⇄t to display $\angle I_3$ in degrees.

9. To compute V, I_1, I_2, and I_3 for a different set of Thevenin circuits, return to Step 3.

NOTE: If the PC-100A printer is used, all answers are printed out automatically and labeled as follows:

Quantity	Label
$\|V\|$	VMAG
$\angle V$	VPHA
$\|I_1\|$	|I1|

Table A-6a (Continued)

INSTRUCTIONS FOR PROGRAM NODE

Quantity	Label
$\angle I_1$	/I1
$\lvert I_2 \rvert$	|I2|
$\angle I_2$	/I2
$\lvert I_3 \rvert$	|I3|
$\angle I_3$	/I3

Table A-6b

PROGRAM NODE

Display		Key	Display		Key	Display		Key	Display		Key
000	76	LBL	045	75	-	090	43	RCL	135	42	STO
001	11	A	046	43	RCL	091	03	03	136	14	14
002	00	0	047	07	07	092	94	+/-	137	04	4
003	42	STO	048	95	=	093	37	P/R	138	02	2
004	29	29	049	37	P/R	094	42	STO	139	03	3
005	60	DEG	050	44	SUM	095	15	15	140	00	0
006	91	R/S	051	13	13	096	32	X:T	141	01	1
007	76	LBL	052	32	X:T	097	42	STO	142	03	3
008	12	B	053	44	SUM	098	14	14	143	02	2
009	72	ST*	054	12	12	099	43	RCL	144	02	2
010	29	29	055	43	RCL	100	06	06	145	69	DP
011	01	1	056	08	08	101	35	1/X	146	04	04
012	44	SUM	057	55	÷	102	32	X:T	147	43	RCL
013	29	29	058	43	RCL	103	43	RCL	148	12	12
014	91	R/S	059	10	10	104	07	07	149	55	÷
015	76	LBL	060	95	=	105	94	+/-	150	43	RCL
016	13	C	061	32	X:T	106	37	P/R	151	14	14
017	43	RCL	062	43	RCL	107	44	SUM	152	95	=
018	00	00	063	09	09	108	15	15	153	42	STO
019	55	÷	064	75	-	109	32	X:T	154	16	16
020	43	RCL	065	43	RCL	110	44	SUM	155	69	DP
021	02	02	066	11	11	111	14	14	156	06	06
022	95	=	067	95	=	112	43	RCL	157	04	4
023	32	X:T	068	37	P/R	113	10	10	158	02	2
024	43	RCL	069	44	SUM	114	35	1/X	159	03	3
025	01	01	070	13	13	115	32	X:T	160	03	3
026	75	-	071	32	X:T	116	43	RCL	161	02	2
027	43	RCL	072	44	SUM	117	11	11	162	03	3
028	03	03	073	12	12	118	94	+/-	163	01	1
029	95	=	074	43	RCL	119	37	P/R	164	03	3
030	37	P/R	075	12	12	120	44	SUM	165	69	DP
031	42	STO	076	32	X:T	121	15	15	166	04	04
032	13	13	077	43	RCL	122	32	X:T	167	43	RCL
033	32	X:T	078	13	13	123	44	SUM	168	13	13
034	42	STO	079	22	INV	124	14	14	169	75	-
035	12	12	080	37	P/R	125	43	RCL	170	43	RCL
036	43	RCL	081	42	STO	126	14	14	171	15	15
037	04	04	082	13	13	127	32	X:T	172	95	=
038	55	÷	083	32	X:T	128	43	RCL	173	42	STO
039	43	RCL	084	42	STO	129	15	15	174	17	17
040	06	06	085	12	12	130	22	INV	175	69	DP
041	95	=	086	43	RCL	131	37	P/R	176	06	06
042	32	X:T	087	02	02	132	42	STO	177	98	ADV
043	43	RCL	088	35	1/X	133	15	15	178	32	X:T
044	05	05	089	32	X:T	134	32	X:T	179	43	RCL

Table A-6b (continued)

PROGRAM NODE

Display		Key	Display		Key	Display		Key	Display		Key
180	16	16	225	04	4	270	12	12	315	95	=
181	91	R/S	226	00	0	271	43	RCL	316	42	STO
182	43	RCL	227	02	2	272	19	19	317	22	22
183	16	16	228	06	6	273	42	STO	318	69	DP
184	32	X:T	229	02	2	274	13	13	319	06	06
185	43	RCL	230	69	DP	275	43	RCL	320	06	6
186	17	17	231	04	04	276	04	04	321	03	3
187	37	P/R	232	43	RCL	277	32	X:T	322	02	2
188	42	STO	233	12	12	278	43	RCL	323	04	4
189	13	13	234	55	÷	279	05	05	324	00	0
190	42	STO	235	43	RCL	280	37	P/R	325	03	3
191	19	19	236	02	02	281	94	+/-	326	00	0
192	32	X:T	237	95	=	282	44	SUM	327	00	0
193	42	STO	238	42	STO	283	13	13	328	69	DP
194	12	12	239	20	20	284	32	X:T	329	04	04
195	42	STO	240	69	DP	285	94	+/-	330	43	RCL
196	18	18	241	06	06	286	44	SUM	331	13	13
197	43	RCL	242	06	6	287	12	12	332	75	-
198	00	00	243	03	3	288	43	RCL	333	43	RCL
199	32	X:T	244	02	2	289	12	12	334	07	07
200	43	RCL	245	04	4	290	32	X:T	335	95	=
201	01	01	246	00	0	291	43	RCL	336	42	STO
202	37	P/R	247	02	2	292	13	13	337	23	23
203	94	+/-	248	00	0	293	22	INV	338	69	DP
204	44	SUM	249	00	0	294	37	P/R	339	06	06
205	13	13	250	69	DP	295	42	STO	340	98	ADV
206	32	X:T	251	04	04	296	13	13	341	32	X:T
207	94	+/-	252	43	RCL	297	32	X:T	342	43	RCL
208	44	SUM	253	13	13	298	42	STO	343	22	22
209	12	12	254	75	-	299	12	12	344	91	R/S
210	43	RCL	255	43	RCL	300	06	6	345	43	RCL
211	12	12	256	03	03	301	02	2	346	18	18
212	32	X:T	257	95	=	302	02	2	347	42	STO
213	43	RCL	258	42	STO	303	04	4	348	12	12
214	13	13	259	21	21	304	00	0	349	43	RCL
215	22	INV	260	69	DP	305	03	3	350	19	19
216	37	P/R	261	06	06	306	06	6	351	42	STO
217	42	STO	262	98	ADV	307	02	2	352	13	13
218	13	13	263	32	X:T	308	69	DP	353	43	RCL
219	32	X:T	264	43	RCL	309	04	04	354	08	08
220	42	STO	265	20	20	310	43	RCL	355	32	X:T
221	12	12	266	91	R/S	311	12	12	356	43	RCL
222	06	6	267	43	RCL	312	55	÷	357	09	09
223	02	2	268	18	18	313	43	RCL	358	37	P/R
224	02	2	269	42	STO	314	06	06	359	94	+/-

Table A-6b (continued)

PROGRAM NODE

Display		Key
360	44	SUM
361	13	13
362	32	X↕T
363	94	+/-
364	44	SUM
365	12	12
366	43	RCL
367	12	12
368	32	X↕T
369	43	RCL
370	13	13
371	22	INV
372	37	P/R
373	42	STO
374	13	13
375	32	X↕T
376	42	STO
377	12	12
378	06	6
379	02	2
380	02	2
381	04	4
382	00	0
383	04	4
384	06	6
385	02	2
386	69	OP
387	04	04
388	43	RCL
389	12	12
390	55	÷
391	43	RCL
392	10	10
393	95	=
394	42	STO
395	24	24
396	69	OP
397	06	06
398	06	6
399	03	3
400	02	2
401	04	4
402	00	0
403	04	4
404	00	0
405	00	0
406	69	OP
407	04	04
408	43	RCL
409	13	13
410	75	-
411	43	RCL
412	11	11
413	95	=
414	42	STO
415	25	25
416	69	OP
417	06	06
418	98	ADV
419	32	X↕T
420	43	RCL
421	24	24
422	91	R/S

Program FIELD

This program derives the driving electric field at a location due to any number of parallel current-carrying conductors at other locations assuming that the currents and Carson mutual impedances are known. The conductor geometry is shown in Figure A-7.

Table A-7a is a step-by-step instruction procedure for the use of this program. Table A-7b is a listing of the key strokes required for initial programming. One magnetic card is required for recording this program.

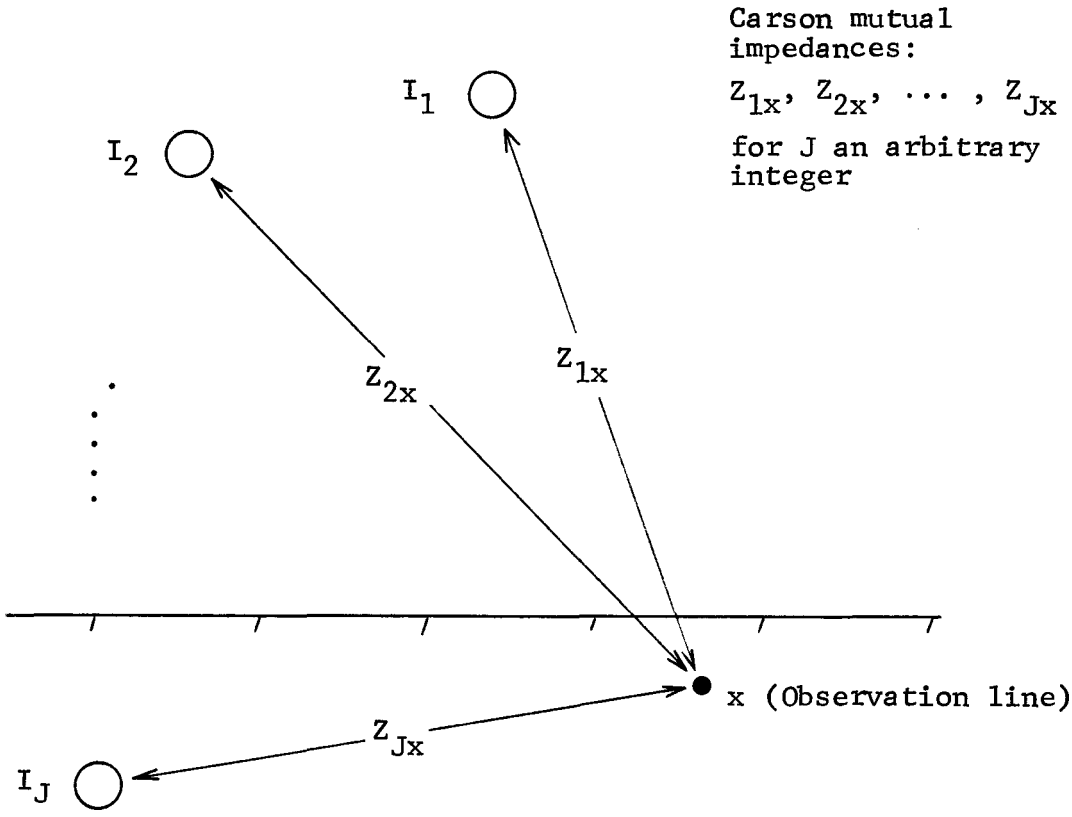

Figure A-7. Conductor Geometry for Program FIELD

Table A-7a

INSTRUCTIONS FOR PROGRAM FIELD

1. Press CLR. Then, press 6 Op 17.

2. Press 1. Then, insert bank #1 into the card reader.

3. Press A.

4. Key $|I_1|$ (in amps) into the display. Then, press B.

5. Key $\angle I_1$ (in degrees) into the display. Then, press C.

6. Key $|Z_{1x}|$ (in ohms/km) into the display. Then, press D.

7. Key $\angle Z_{1x}$ (in degrees) into the display. Then, press E. Wait 5 seconds for the display to unblank. The displayed number is $|E_x|$ in volts/km, the magnitude of the total driving electric field at x. Press x⇄t to display $\angle E_x$ in degrees.

8. If the field contribution due to another current-carrying conductor is to be summed, repeat Steps 4, 5, 6, and 7 for the new conductor. The display will always show the running total at the end of Step 7.

9. If an entirely different conductor configuration is to be considered, return to Step 3.

NOTE: If the PC-100A printer is used, $|E_x|$ and $\angle E_x$ will be printed out automatically and labeled as "EMAG" and "EPHA", respectively.

Table A-7b

PROGRAM FIELD

Display	Key	Display	Key
000 76	LBL	045 37	P/R
001 11	A	046 42	STO
002 00	0	047 03	03
003 42	STO	048 32	X:T
004 00	00	049 42	STO
005 42	STO	050 02	02
006 01	01	051 01	1
007 60	DEG	052 07	7
008 91	R/S	053 03	3
009 76	LBL	054 00	0
010 12	B	055 01	1
011 42	STO	056 03	3
012 04	04	057 02	2
013 91	R/S	058 02	2
014 76	LBL	059 69	OP
015 13	C	060 04	04
016 42	STO	061 43	RCL
017 05	05	062 02	02
018 91	R/S	063 69	OP
019 76	LBL	064 06	06
020 14	D	065 01	1
021 49	PRD	066 07	7
022 04	04	067 03	3
023 91	R/S	068 03	3
024 76	LBL	069 02	2
025 15	E	070 03	3
026 44	SUM	071 01	1
027 05	05	072 03	3
028 43	RCL	073 69	OP
029 04	04	074 04	04
030 32	X:T	075 43	RCL
031 43	RCL	076 03	03
032 05	05	077 69	OP
033 37	P/R	078 06	06
034 44	SUM	079 32	X:T
035 01	01	080 43	RCL
036 32	X:T	081 02	02
037 44	SUM	082 98	ADV
038 00	00	083 91	R/S
039 43	RCL		
040 00	00		
041 32	X:T		
042 43	RCL		
043 01	01		
044 22	INV		

Program SHIELD

This program computes the series self impedance of a power line shield wire using Eq. 3-5a. Table A-8a is a step-by-step instruction procedure for the use of this program. Table A-8b is a listing of the key strokes required for initial programming. One magnetic card is needed for recording this program.

Table A-8a

INSTRUCTIONS FOR PROGRAM SHIELD

1. Press CLR. Then, press 6 Op 17.

2. Press 1. Then, insert bank #1 into the card reader.

3. Press A.

4. Key R, the series dc resistance of the shield wire (in ohms/mile) into the display. Then, press B.

   Key D, the diameter of the shield wire (in inches) into the display. Then, press B.

   Key ρ_e, the earth resistivity (in ohm-meters) into the display. Then, press B.

5. Press C. Wait 5 seconds for the display to unblank. The display then shows $|Z_s|$, the magnitude of the shield wire self impedance (in ohms/km). Press x$\rightleftarrows$t to display $\angle Z_s$ in degrees.

6. For a different shield wire, return to Step 3.

   NOTE: If the PC-100A printer is used, $|Z_s|$ and $\angle Z_s$ will be printed out automatically and labeled as "ZMAG" and "ZPHA", respectively.

Table A-8b

PROGRAM SHIELD

Display	Key
000 76	LBL
001 11	A
002 00	0
003 42	STO
004 09	09
005 60	DEG
006 91	R/S
007 76	LBL
008 12	B
009 72	ST*
010 09	09
011 01	1
012 44	SUM
013 09	09
014 91	R/S
015 76	LBL
016 13	C
017 43	RCL
018 00	00
019 55	÷
020 01	1
021 93	.
022 06	6
023 01	1
024 85	+
025 93	.
026 00	0
027 05	5
028 09	9
029 02	2
030 95	=
031 42	STO
032 03	03
033 43	RCL
034 02	02
035 34	FX
036 65	×
037 04	4
038 00	0
039 03	3
040 07	7
041 55	÷
042 43	RCL
043 01	01
044 95	=

Display	Key
045 23	LNX
046 65	×
047 02	2
048 85	+
049 01	1
050 95	=
051 65	×
052 93	.
053 00	0
054 03	3
055 07	7
056 07	7
057 85	+
058 93	.
059 00	0
060 01	1
061 08	8
062 08	8
063 95	=
064 42	STO
065 04	04
066 43	RCL
067 03	03
068 32	X:T
069 43	RCL
070 04	04
071 22	INV
072 37	P/R
073 42	STO
074 06	06
075 32	X:T
076 42	STO
077 05	05
078 04	4
079 06	6
080 03	3
081 00	0
082 01	1
083 03	3
084 02	2
085 02	2
086 69	OP
087 04	04
088 43	RCL
089 05	05

Display	Key
090 69	OP
091 06	06
092 04	4
093 06	6
094 03	3
095 03	3
096 02	2
097 03	3
098 01	1
099 03	3
100 69	OP
101 04	04
102 43	RCL
103 06	06
104 69	OP
105 06	06
106 32	X:T
107 43	RCL
108 05	05
109 91	R/S

REFERENCES

1. H. W. Dommel, Discussion following "Electromagnetic Effects of Overhead Transmission Lines - Practical Problems, Safeguards, and Methods of Calculation," IEEE Trans. Power App. Systems, Vol. PAS-94, pp. 900-901, May-June 1974.

2. B. Carnahan, H. A. Luther, J. O. Wilkes, Applied Numerical Methods. New York: John Wiley & Sons, pp. 299-307, 1969.

3. B. Carnahan, H. A. Luter, J. O. Wilkes, Applied Numerical Methods. New York: John Wiley & Sons, pp. 171.177, 1969.

4. E. D. Sunde, Earth Conduction Effects in Transmission Systems. New York: Dover Publications, pp. 145-149, 1968.

APPENDIX B

LONGITUDINAL ELECTRIC FIELD CHARACTERISTICS IN THE VICINITY OF A THREE PHASE POWER LINE

INTRODUCTION

As shown by the theory of Section 3, the longitudinal electric field at a field point is the vector sum of the phase and shield wire current phasors multiplied by their respective Carson's coupling impedances. (An analogous analysis using the method of symmetrical components with probabilistic extensions is presented in the following appendix.)

Because of changing geometry with distance, varying phase currents, etc., the electric field is both spatially and temporally varying. Instrumentation (discussed in Section 9) has been developed which allows measurement of both the magnitude and the relative phase of the electric field, thus enabling direct comparison of the results obtained from theory with that of experimentation. This appendix discusses some of the early measurements made with the new instrumentation. It shows the development of a methodology for making such measurements and also provides an acquaintanceship with the variations observed in the electric field distribution.

Measurements were made under a 345 kV (Commonwealth Edison Company) horizontal power line near Joliet, Illinois. The line geometry is illustrated in Figure B-1.

Both the magnitude and relative phase of the electric field as a function of perpendicular distance to the transmission line were measured to a maximum distance of one thousand feet on either side of the line.

Figures B-2 and B-3 present a set of test results for both the magnitude and phase of the low impedance longitudinal electric field as a function of distance from the power line. These results will be discussed and compared to some analytical predictions made in the following appendix.

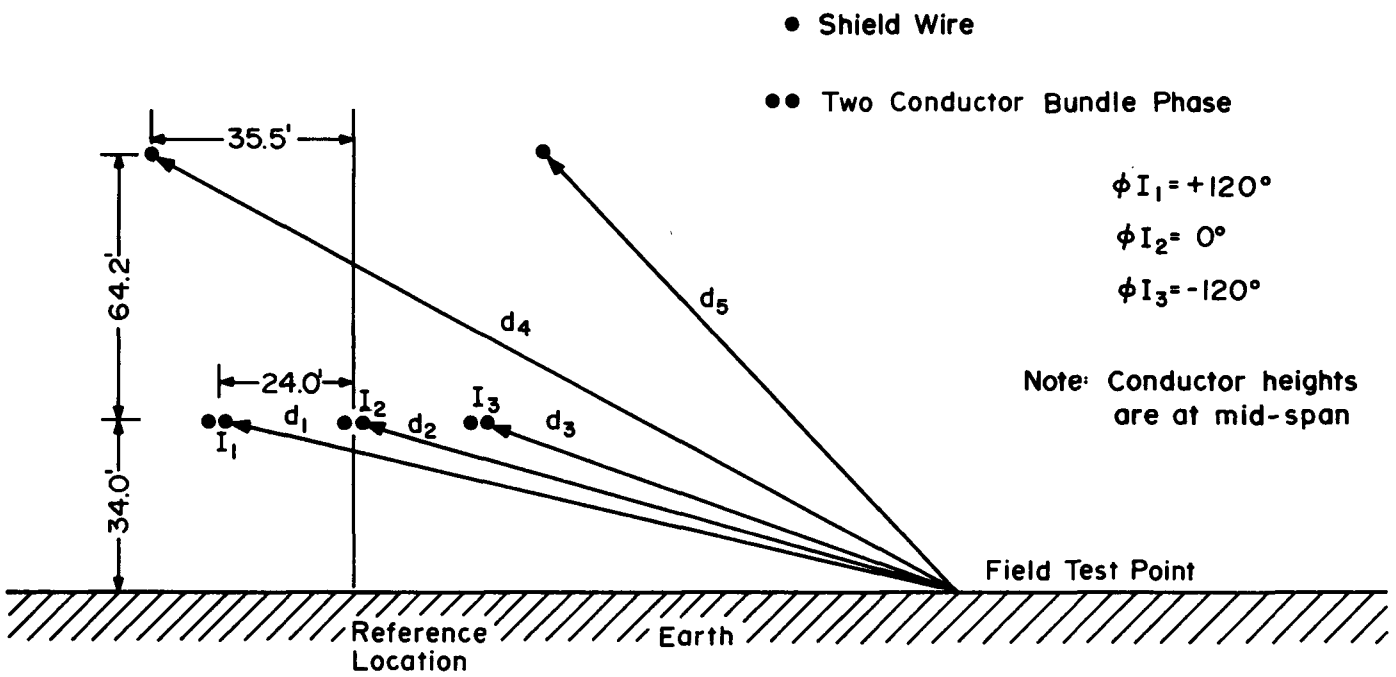

Fig. B-1 345KV TRANSMISSION LINE CONFIGURATION

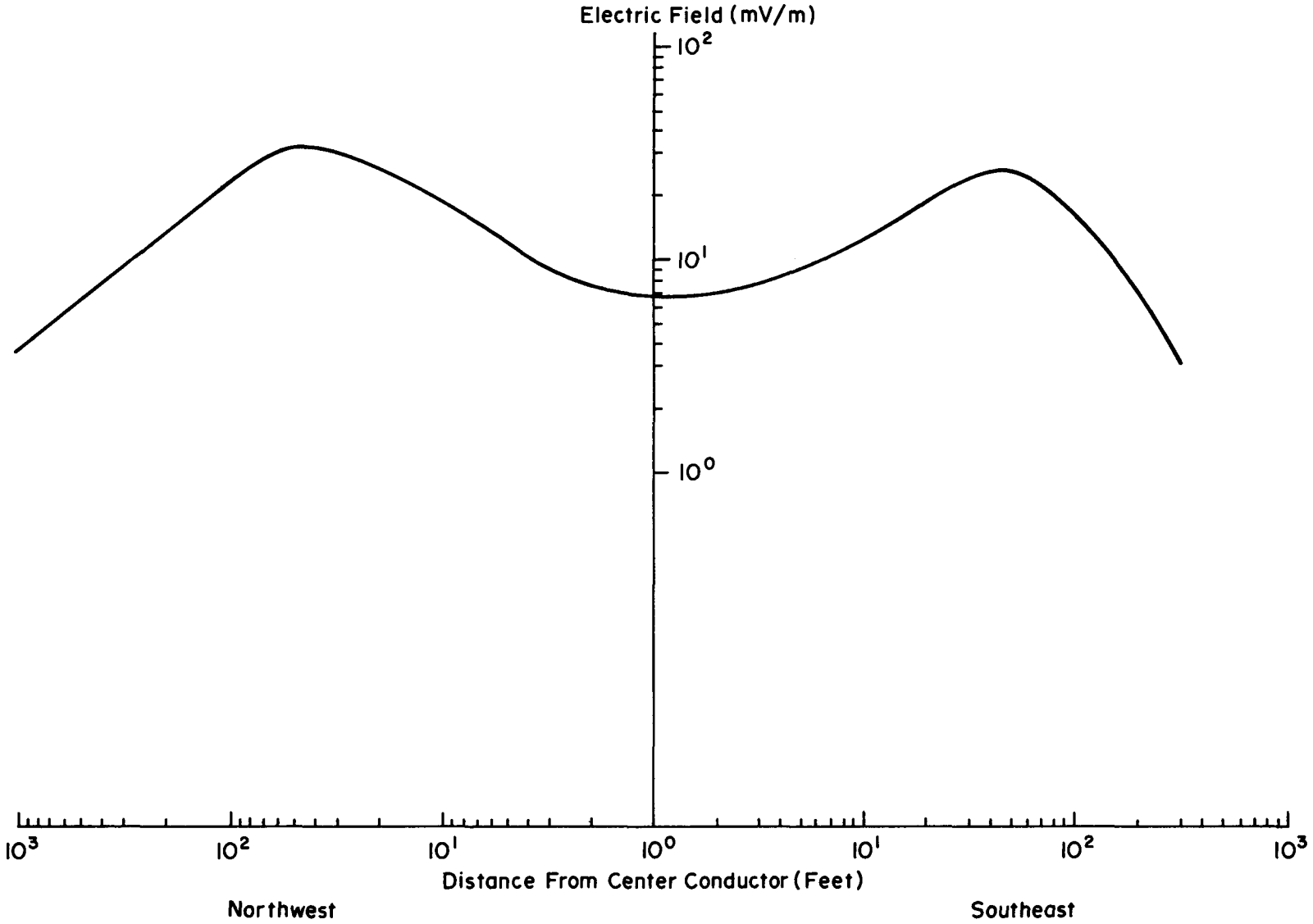

Fig. B-2 MAGNITUDE OF LONGITUDINAL ELECTRIC FIELD MEASURED AT 345 KV LINE

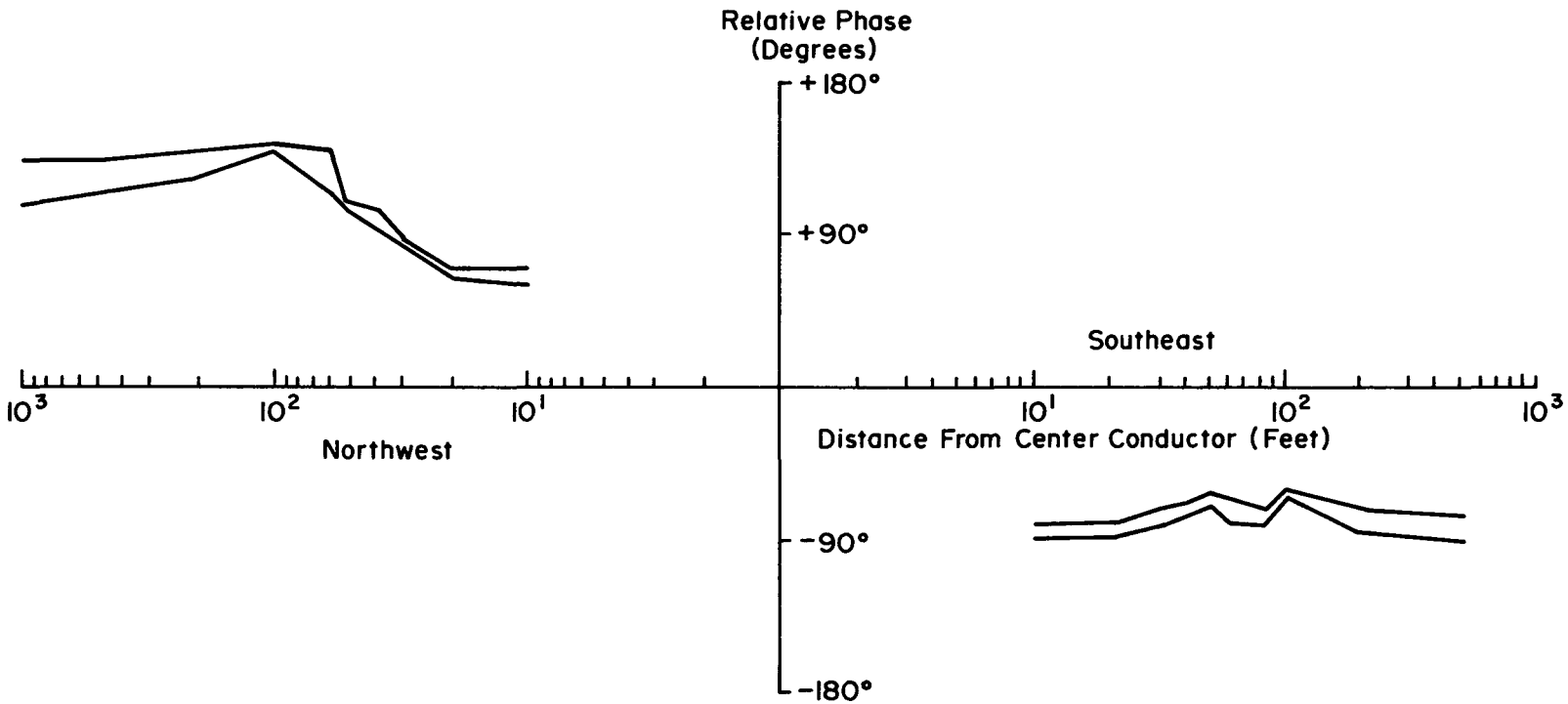

Fig. B-3 RANGE OF RELATIVE PHASE OF MEASURED ELECTRIC FIELD AT 345 KV LINE

For the particular set of measurements shown in Figures B-2 and B-3, the reference signal for the measurement instrumentation was obtained by sampling directly below the center phase wire.

During the course of making the measurements, it was found that wind variability and velocity can be important in relation to an electric field measurement. The wind can cause the phase conductors to sway by as much as eight feet at midspan over a relatively long period in an approximately horizontal plane. This sway, in turn, can cause the short term reference signal phase to vary by as much as 20 to 30 degrees. Thus, during any given measurement, the relative phase between the reference location and the field point will vary within some range which is a function of the degree of phase conductor motion and the phasing sequence of the transmission line. This fact is illustrated by the relative phase plot presented in Figure B-3, which presents the phase measurements as a range rather than a single value, and it has been verified that this variability in the phase measurements is directly caused by wind induced motion of the phase conductors. In order to minimize this problem for measurements involving relative phase of the electric field, it is necessary that the reference signal be located at a relatively large distance from the line, i.e., at a distance in excess of several hundred feet to either side of the electric power line.

COMPARISON OF FIELD DATA WITH AN ANALYTICAL MODEL

In order to evaluate the accuracy of the field data obtained with the developed instrumentation, a comparison of the data with an analytical modeling of the distributed electrical field was made early in the program. An available computer program was modified and the line was modeled with calculations made on a large computer. (Similar results may now be obtained on a point by point basis using the hand calculator programs CARSON and FIELD presented in Appendix A).

Inspection of Figure B-2 shows that the electric field is not symmetrical with respect to the transmission line. Contributing factors to this asymmetry are line current and phase unbalances and, to a lesser extent, the influence of shield wire currents and variability introduced by the wind. It is difficult to extricate asymmetry effects due to phase current unbalances. Figure B-4 illustrates the effect that a three percent phase unbalance on any one phase of the 345 kV line can have on the magnitude of the electric field. A plus or minus three percent phase unbalance was assumed to occur on one phase at a time of the three phase circuit. An envelope for the field strength variability was thus

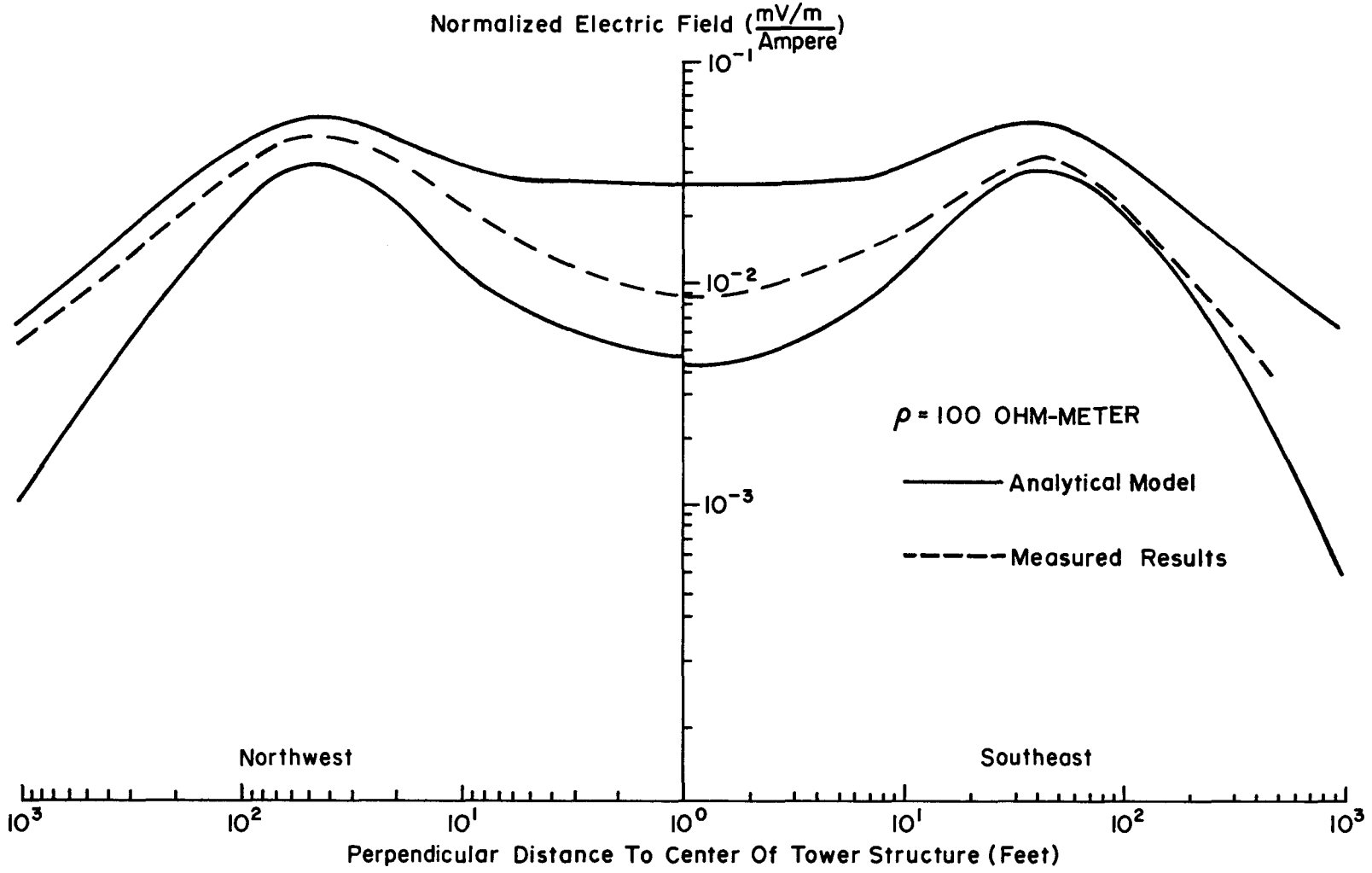

Fig. B-4 RANGE OF LONGITUDINAL ELECTRIC FIELD DUE TO CURRENT UNBALANCE

generated and is presented in Figure B-4. It represents the range that the electric field can experience due to the assumed line current unbalances. Also shown in this figure is a normalized curve of the field data presented in Figure B-2. As can be seen, the data falls within this envelope, but the actual currents are not known to the required accuracy to analytically reproduce the measured electric field profile.

The wind has a smaller effect on the measured magnitude of the electric field, even though it is very significant when trying to obtain phase information. As the wind varies, it causes the phase and shield wires to also vary in distance from the field point. Field measurements for this power line indicate that dynamic changes in geometry cause the magnitude of the electric field to vary on the order of five percent or less.

Figure B-5 presents the phase envelope which corresponds to the electric field envelope shown in Figure B-4. This figure indicates the range of variation in the relative phase to be significant for the assumed current unbalance of three percent in one phase conductor. Combining the uncertainty in current magnitude along with phase unbalance and wind variability complicates the situation even more so.

The conclusion to be reached with respect to the comparison of field data and analytical results presented here are that: (1) a successful match between experimental data and analysis has been obtained; (2) discrepancies can be accounted for (e.g., the effects of line current and phase unbalances); and (3) the instrumentation developed allows measurement of both the magnitude and relative phase of the longitudinal field in the presence of a much stronger vertical electrostatic field.

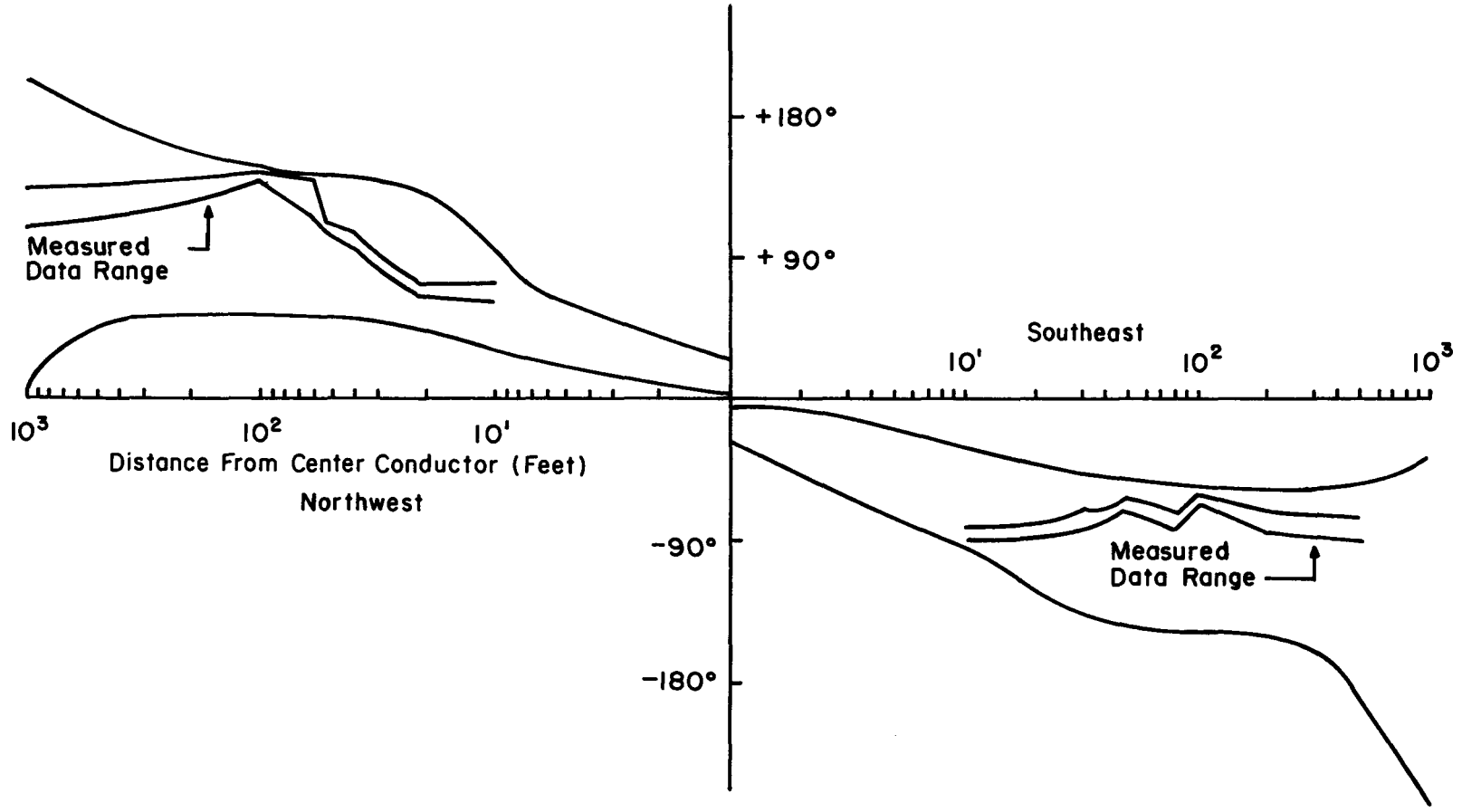

Fig. B-5 RANGE OF RELATIVE PHASE MEASUREMENT DUE TO LINE CURRENT UNBALANCE

Appendix C

CALCULATION OF ELECTROMAGNETIC INDUCTION FROM AC POWER LINES BY THE METHOD OF SYMMETRICAL COMPONENTS

INTRODUCTION

Because of the sharing of common corridors by buried pipelines and power lines, induced voltages have been measured on the pipelines. One of the principal objectives of this program has been to evolve a procedure for the calculation and prediction of these voltages.

Induced pipeline voltage prediction is a two-step process, namely,

1. Given the ac power line parameters and interaction geometry, calculate the longitudinal electric field at the pipeline position.
2. Considering the pipeline as a distributed parameter electrical transmission line with distributed excitation (the longitudinal electric field) calculate the induced voltage.

The tenets appropriate to the latter step, i.e., given the electric field one calculates the induced voltage, are covered in Section 3. One of the principal conclusions that can be drawn is that contrary to results published previously in the literature, the induced voltage is less than predicted and not, in general, linearly proportional to pipeline length. Experimental confirmation of these facts has been obtained through measurements made in the Mojave desert on the Southern California Gas Company 34-inch Needles to Newberry pipeline.

A generalized technique for calculation of the longitudinal electric field has been developed as a consequence of this work and is presented in this appendix. Heretofore, it has been generally assumed that the longitudinal electric field component was equal to the product of the zero sequence transmission line current and the Carson mutual impedance (1). Using the technique of symmetrical components (2), it is shown here that the above procedure is correct only under rather restrictive conditions.

Equipments for measurement of both the magnitude and phase of the longitudinal electric field which were developed have been discussed in Section 9. Using these equipments, electric field measurements have been made on several ac power lines and the data compared with computer-generated electric field profiles. Appendix B discussed results obtained for a 345 kV transmission line located south of Chicago. Excellent corroboration of computed results with experimental data were obtained.

However, results of field measurements generally made are not always as encouraging in that reasonable agreement between computed and measured data is not always obtained. Most perplexing, for example, is that measurements made on the same transmission line can track a computer-generated electric field profile for some part of the day and not track for the remainder. It has been found, for example, that with apparently the same transmission line current loading, the electric field magnitude can vary by a factor of three, four or more at the same location over the course of a few hours.

The solution to this consternating problem has been found in the fact that the electric field at a given location is the phasor sum of the individual transmission line currents and the induced shield wire currents weighted by Carson's mutual impedances. Although not immediately apparent, it appears that for typical power line geometries, the magnitude of the electric field at a distance on the order of a few hundred feet from the power line is an extremely sensitive function of the degree of unbalance between phase currents -- especially for single circuits. Given the right set of conditions, a line current unbalance of a few percent can produce, for example, a null in the electric field at a given location. As the degree or sense of the line current unbalance changes in time, a corresponding change in the electric field can be observed.

Line current unbalance for a power line circuit generally averages only a few percent, but is random in nature. In the following analysis, it is shown that the symmetrical component electric field solution can be decomposed into two parts; that is, the sum of deterministic and random components. The deterministic solution can be computer calculated once the interaction geometry is known. The random component can be calculated by the application of probability techniques.

For single circuit lines which are not too highly unbalanced, the deterministic electric field component will be dominant. As the number of power line circuits

increases on a single right-of-way, it is expected that for disparate phase sequencing of the circuits, the deterministic component will become smaller and will tend to be dominated by the random component.

Application of Symmetrical Components

A single circuit power line either in the horizontal or vertical configuration is composed of three phase current lines, and generally two shield wires which will carry induced currents if grounded at more than one point.

The three power line phase currents, in general, will be an unbalanced set of positive sequence current vectors, I_a, I_b, and I_c. The shield wires will carry induced currents, I_{s1} and I_{s2}, respectively. Hence, the longitudinal electric field at a point may be calculated by the vector sum

$$E = I_a Z_a + I_b Z_b + I_c Z_c + I_{s1} Z_{s1} + I_{s2} Z_{s2} \qquad \text{(C-1)}$$

where the impedances are the Carson mutual impedances between the observation point and the corresponding wire.

The impedances Z_a, Z_b and Z_c constitute an unbalanced set which can be resolved into the following vector operator symmetrical components.

$$Z_o = \frac{1}{3}(Z_a+Z_b+Z_c) \qquad \text{(C-2)}$$

$$Z_1 = \frac{1}{3}(Z_a+aZ_b+a^2Z_c) \qquad \text{(C-3)}$$

$$Z_2 = \frac{1}{3}(Z_a+a^2Z_b+aZ_c) \qquad \text{(C-4)}$$

where

$$a \equiv e^{j2\pi/3} \qquad \text{(C-5)}$$

The phase currents may likewise be resolved into the set:

$$I_o = \frac{1}{3}(I_a+I_b+I_c) \qquad \text{(C-6)}$$

$$I_1 = \frac{1}{3}(I_a+aI_b+a^2I_c) \qquad \text{(C-7)}$$

$$I_2 = \frac{1}{3}(I_a+a^2I_b+aI_c) \qquad \text{(C-8)}$$

It can be shown (2) that the sequence components of the current weighted by the mutual impedances and the symmetrical components of the electric field are related by

$$E_o = I_o Z_o + I_1 Z_2 + I_2 Z_1 \qquad \text{(C-9)}$$

$$E_1 = I_o Z_1 + I_1 Z_o + I_2 Z_2 \qquad \text{(C-10)}$$

$$E_2 = I_o Z_2 + I_1 Z_1 + I_2 Z_o \qquad \text{(C-11)}$$

E_o, E_1 and E_2 are respectively, the zero sequence, positive sequence, and negative sequence electric field components at the observation point. Since they constitute a symmetrical component set, i.e.,

$$E_1 + aE_1 + a^2 E_1 \equiv 0 \qquad \text{(C-12)}$$

$$E_2 + aE_2 + a^2 E_2 \equiv 0 \qquad \text{(C-13)}$$

the remaining contributions to the electric field are the zero sequence and shield wire components. Hence

$$\begin{aligned} E &= 3E_o + I_{s1} Z_{s1} + I_{s1} Z_{s2} \\ &= 3(I_o Z_o + I_1 Z_2 + I_2 Z_1) + I_{s1} Z_{s1} + I_{s2} Z_{s2} \end{aligned} \qquad \text{(C-14)}$$

The free longitudinal electric field generated by the phase currents I_a, I_b, and I_c is equal to

$$E_{s1} = I_a Z_a' + I_b Z_b' + I_c Z_c' \qquad \text{(C-15)}$$

and

$$E_{s2} = I_a Z_a'' + I_b Z_b'' + I_c Z_c'' \qquad \text{(C-16)}$$

at the location of shield wires No. 1 and No. 2, respectively. These fields act as distributed sources causing the induction of the respective shield wire currents, I_{s1} and I_{s2}. Z_a', Z_b' and Z_c' are the Carson mutual impedances between the individual phase wires and the first shield wire. The double primed set is likewise the mutual impedances relative to the second shield wire.

The solution set for the shield wire current is

$$E_{s1} = - z_{11} I_{s1} - z_{12} I_{s2} \quad \text{(C-17)}$$

$$E_{s2} = - z_{22} I_{s2} - z_{12} I_{s1} \quad \text{(C-18)}$$

where z_{11} and z_{22} are the Carson self impedances of the shield wires and z_{12} is the Carson mutual impedance between the wires.

Solution of Eqs. C-17 and C-18 for the shield wire currents yields

$$I_{s1} = \frac{z_{22} E_{s1} - z_{12} E_{s2}}{z_{12}^2 - z_{11} z_{22}} \quad \text{(C-19)}$$

and

$$I_{s2} = \frac{z_{11} E_{s2} - z_{12} E_{s1}}{z_{12}^2 - z_{11} z_{22}} \quad \text{(C-20)}$$

Analogous to the derivation (Eq. C-9) for the distant observation point, the electric fields, E_{s1} and E_{s2} may be expressed as zero sequence electric field components of the phase wire currents. Hence,

$$E_{s1} = 3(I_0 Z_0' + I_1 Z_2' + I_2 Z_1') \quad \text{(C-21)}$$

where

$$Z_0' = \frac{1}{3}(Z_a' + Z_b' + Z_c') \quad \text{(C-22)}$$

$$Z_1' = \frac{1}{3}(Z_a' + aZ_b' + a^2 Z_c') \quad \text{(C-23)}$$

$$Z_2' = \frac{1}{3}(Z_a' + a^2 Z_b' + aZ_c') \quad \text{(C-24)}$$

and

$$E_{s2} = 3(I_0 Z_0'' + I_1 Z_2'' + I_2 Z_1'') \quad \text{(C-25)}$$

with

$$Z_0'' = \frac{1}{3}(Z_a'' + Z_b'' + Z_c'') \quad \text{(C-26)}$$

$$Z_1'' = \frac{1}{3}(Z_a'' + aZ_b'' + a^2 Z_c'') \quad \text{(C-27)}$$

$$Z_2'' = \frac{1}{3}(Z_a'' + a^2 Z_b'' + aZ_c'') \quad \text{(C-28)}$$

Substituting Eqs. C-21 and C-25 into Eqs. C-19 and C-20, and making use of the fact that the shield wires are usually identical, thus gives

$$z_{11} = z_{22} = z_{ss} \tag{C-29}$$

yielding

$$-I_{s1}(z_{12}+z_{ss}) = 3\,(I_o Z_o' + I_1 Z_2' + I_2 Z_1') \tag{C-30}$$

$$-I_{s2}(z_{12}+z_{ss}) = 3\,(I_o Z_o'' + I_1 Z_2'' + I_2 Z_1'') \tag{C-31}$$

Substitution of Eqs. C-30 and C-31 into Eq. C-14 yields for the total electric field including skywire components:

$$E = 3I_o z_o + 3I_1 z_2 + 3I_2 z_1 \tag{C-32}$$

where

$$Z_o \equiv Z_o - \frac{Z_{s1}\, Z_o' + Z_{s2}\, Z_o''}{z_{12} + z_{ss}} \tag{C-33}$$

$$Z_1 \equiv Z_1 - \frac{z_{s1}\, Z_1' + Z_{s2}\, Z_1''}{z_{12} + z_{ss}} \tag{C-34}$$

$$Z_2 \equiv Z_2 - \frac{z_{s1}\, Z_2' + Z_{s2}\, Z_2''}{z_{12} + z_{ss}} \tag{C-35}$$

Equation C-32 may be evaluated for various situations.

Case 1. Equal Phase Currents. For this situation, $I_a = I_b = I_c$, and the total electric field is a result of only the positive sequence current, i.e.,

$$E = 3\, I_1\, z_2 \tag{C-36}$$

Case 1a. At Far Distances. As the distance to the observation point increases, $Z_a \simeq Z_b \simeq Z_c$. By definition, $1 + a + a^2 \equiv 0$, and therefore, $Z_2 \to 0$. In addition, $Z_{s1} \simeq Z_{s2} = Z_s$. Hence,

$$E = -3\, I_1 \left(\frac{Z_s}{z_{12} + z_{ss}}\right) (Z_2' + Z_2'') \tag{C-37}$$

Case 1b. Single Point Grounded Shield Wires. For this situation, the equivalent effect is for $z_{ss} \to \infty$. Hence,

$$E = 0. \tag{C-38}$$

Case 2. Unbalanced Phase Currents. The complete solution is given by Eq. C-32.

$$E = 3I_o z_o + 3I_1 z_2 + 3I_2 z_1$$

Case 2a. At Large Distances. Here, $Z_1 \to 0$, $Z_2 \to 0$ and $Z_{s1} \to Z_{s2} \to Z_s$. For this case, Eq. C-32 may be put into the form

$$E = 3I_o Z_o - \left(\frac{E_{s1} + E_{s2}}{z_{12} + z_{ss}}\right) Z_s \qquad \text{(C-39)}$$

Case 2b. Single Point Grounded Shield Wire. This, again, is equivalent to $z_{ss} \to \infty$ in Eq. C-39, resulting in

$$E = 3I_o Z_o. \qquad \text{(C-40)}$$

In much of the literature, Eq. C-40 is presented as representing the electromagnetically induced electric field component. As apparent from the present analysis, its applicability is limited to a rather restrictive situation. Applicability of Eq. C-40, depending upon the exact geometry, may require a distance greater than several hundred meters, which is generally in excess of the right-of-way width. Hence, Eq. C-40 alone is almost never applicable to the situation of ac power line and pipeline interaction.

Electric Field Fluctuations

For an exactly known set of phase currents and a given interaction geometry, the electric field at a point may be calculated by means of either Eq. C-1 or Eq. C-32 which are fully equivalent. Because of numerical complexity, these calculations have usually been made on a computer, but the developed hand calculator programs are adequate. Hereafter, the solution for the electric field thusly obtained, will be termed the deterministic solution.

Unfortunately, the exact phase currents are never exactly known. Not only does the average power line loading vary with time, but in addition the degree of unbalance between the individual phase currents varies with time. The electric field which exists along the right-of-way and causing induced pipeline voltages is a sensitive function of both types of phase current variations. For example, the strength of the electric field is directly proportional to the phase current magnitude, but variations in the electric field of over a range as much as four-to-one have been seen experimentally for changes in current balance conditions too small to be read with significance at the electric power company monitoring

substation. This may be somewhat of an extreme example but, in general, material fluctuations in electric field strength can occur because of phase current variations. The instantaneous values of the phase currents are generally never known exactly, but the statistical parameters associated with the variations are characterizable. Hence, in order to adequately define the electric field, it must be treated as a random variable.

Phase Current Statistics

It has been observed experimentally and subsequently verified by repeated computer trial runs that relatively small variations (on the order of a few percent) in the line currents' magnitude and phase balance causes significant changes in the electric field. Attempts to correlate observed electric field fluctuations with line current unbalances were not always directly successful. While line current magnitude data are usually available, phase unbalance of the transmission line must be inferred. To calculate phase unbalance directly, both real and reactive powers must be known for each phase line, and usually these data are measured only for the transmission line as a whole.

Observations made have shown that, for what appears to be a common situation, magnitude differences of three to five percent occur randomly. Also, phase difference between lines is not exactly maintained at 120^{o}, but varies by $\pm$ 2 to 3 degrees which, on a percentage basis, is about the same level as that observed for the line current magnitude unbalance. However, unbalances as high as 10-15 percent may not be too uncommon.

In order to derive a probabilistic model for electric field fluctuations, based on observation, the following premises have been advanced for the properties of the phase current random variables.

- It is assumed that line current variations are independent between phases.
- For a single phase line it will be assumed that the phase and magnitude variations are independent.
- It will be assumed that the magnitude deviation from the balanced condition for the ith line current can be characterized by a random variable, X_i. X_i will be at the same phase angle as the line current. Its range is assumed to be $\pm \Delta I$ with a uniform probability distribution.

- The phase unbalance between lines will be characterized by the random variable, Y_i, which is in phase quadrature with X_i. Y_i is assumed to have the same range and type of probability density function as X_i.

In general, there is some arbitrariness in the above assumptions. For example, the choice of a uniform probability density function can only be justified on intuitive grounds. However, due to the simultaneous additive action of several variables, especially when multiple power line circuits are considered, the validity of the central limit theorem will bend to make the computed statistics of the electric field a weak function of the original assumptions.

Expressing the random variable character of the line currents as per the previous assumptions yields the following equation set.

Probability Distribution for the Electric Field

$$I_a = |I_a| + x_a + j\, y_a \tag{C-41}$$

$$I_b = a^2|I_b| + a^2 x_b + j\, a^2 y_b \tag{C-42}$$

$$I_c = a|I_c| + a x_c + j\, a y_c \tag{C-43}$$

where without loss in generality, I_a has been assumed to be the reference vector, and the balanced condition magnitudes of the line currents are

$$|I_a| = |I_b| = |I_c| \equiv |I| \tag{C-44}$$

The symmetrical component current vectors then become

$$I_o = \frac{1}{3}\left[(x_a+a^2x_b+ax_c) + j(y_a+a^2y_b+ay_c)\right] \tag{C-45}$$

$$I_1 = \frac{1}{3}\left[(3|I| + (x_a+x_b+x_c) + j(y_a+y_b+y_c)\right] \tag{C-46}$$

$$I_2 = \frac{1}{3}\left[(x_a+ax_b+a^2x_c) + j(y_a+ay_b+a^2y_c)\right] \tag{C-47}$$

Denoting the statistical mean of a random variable by $E[\cdot]$, it may be shown that

$$E\left[I_o I_o^*\right] = \frac{1}{3}\left(E[x^2] + E[y^2]\right) \quad \text{(C-48)}$$

$$E\left[I_1 I_1^*\right] = [I]^2 + \frac{1}{3}\left(E[x^2] + E[y^2]\right) \quad \text{(C-49)}$$

$$I\left[I_2 I_2^*\right] = \frac{1}{3}\left(E[x^2] + E[y^2]\right) \quad \text{(C-50)}$$

$$E\left[I_o I_1^*\right] = 0 \quad \text{(C-51)}$$

$$E\left[I_o I_2^*\right] = 0 \quad \text{(C-52)}$$

$$E\left[I_1 I_2^*\right] = 0 \quad \text{(C-53)}$$

$$E\left[I_o\right] = 0 \quad \text{(C-54)}$$

$$E\left[I_1\right] = |I| \quad \text{(C-55)}$$

$$E\left[I_2\right] = 0 \quad \text{(C-56)}$$

where

$$E\left[x^2\right] \equiv E[x_a^2] = E[x_b^2] = E[x_c^2] \quad \text{(C-57)}$$

$$E\left[y^2\right] \equiv E[y_a^2] = E[y_b^2] = E[y_c^2] \quad \text{(C-58)}$$

The random character of the electric field may be exemplified by expressing it as a sum of two components, i.e., deterministic and random terms. Hence,

$$E = E_D + E_R \quad \text{(C-59)}$$

Substituting Eqs. C-45 through C-47 into Eq. C-32 gives

$$E = 3|I|z_2 + 3I_o z_o + \left(\sum_{i=a}^{c} x_i + j \sum_{i=a}^{c} y_i\right) z_2 + 3I_2 z_1 \quad \text{(C-60)}$$

Hence,

$$E_D \equiv 3|I|z_2 = E[E] \quad \text{(C-61)}$$

and

$$E_R \equiv \left[(x_a+a^2x_b+ax_c) + j(y_a+a^2y_b+y_c)\right]z_o + \left[(x_a+x_b+x_c) + j(y_a+y_b+y_c)\right]z_2 + \left[(x_a+ax_b+a^2x_c) + j(y_a+ay_b+a^2y_c)\right]z_1 \quad \text{(C-62)}$$

Also

$$E\left[E_R\right] = 0 \quad \text{(C-63)}$$

and using relationships C-48 through C-56 gives

$$\text{Var}\left[E_R\right] = E\left[E_R E_R^*\right] = 3(E[x^2] + E[y^2])([z_o]^2 + [z_1]^2 + [z_2]^2) \quad \text{(C-64)}$$

From Eq. C-62 it is seen that the random variable E_R is the sum of in-phase and quadrature components with respective variances (as shown by Eq. C-64) of

$$\text{Var}|_x = 3\,E[x^2]\,([z_o]^2 + [z_1]^2 + [z_2]^2) \quad \text{(C-65)}$$

$$\text{Var}|_y = 3\,E[y^2]\,([z_o]^2 + [z_1]^2 + [z_2]^2) \quad \text{(C-66)}$$

As stated previously, observation indicates that

$$E[x^2] \cong E[y^2] \quad \text{(C-67)}$$

Since both variables are assumed to be uniformly distributed, then

$$E[x^2] = E[y^2] = \frac{1}{\hat{\Delta I}}\int_0^{\hat{\Delta I}} \mu^2\, d\mu = \frac{\hat{\Delta I}^2}{3} \quad \text{(C-68)}$$

Hence, the variance of either the in-phase or quadrature components is,

$$\sigma^2 = \hat{\Delta I}^2(|z_o|^2 + |z_1|^2 + |z_2|^2) \quad \text{(C-69)}$$

For these conditions it may be shown (3) that the envelope of the electric field, $|E|$ is a Rician distributed random variable with probability density function given by

$$p(|E|) = \frac{|E|}{\sigma^2} \exp\left[-\frac{|E|^2 + |E_D|^2}{2\sigma^2}\right] I_o\left(\frac{|E\ E_D|}{\sigma^2}\right) \qquad \text{(C-70)}$$

for

$$|E| \geq 0.$$

The cumulative probability distribution function of $|E|$ may be found through integration of Eq. C-70. In general, the probability that $|E|$ is less than some value E is given by

$$p(|E| \leq E) = \int_0^E p(|E|)\, d|E| \qquad \text{(C-71)}$$

A convenient closed form solution for Eq. C-71 is not available, and hence, a graphical solution is given in Figure C-1. Figure C-1 is used in the following manner:

1. Calculate the absolute value of the deterministic component $|E_D|$ from Eq. C-61. Because of numerical complexity, a programmable calculator or computer solution is best. Eq. C-1 may also be used for this calculation if balanced currents are assumed.

2. By taking the square root of the result, obtain the standard deviation of the random component from Eq. C-69.

3. Form the radio, E_D/σ and use the appropriate curve in Figure C-1, interpolating if necessary.

4. For a chosen probability level, the value of the normalized variable, V, may then be found.

5. The corresponding value of the electric field is then equal to $E = \sigma V$. The chosen probability level then indicates the probability that the electric field will have a value less than or equal to the number calculated above.

Critique

The introduction of a random component to the longitudinal electric field is a new concept. It was found to be necessary because of the large sensitivity of the electric field magnitude to relatively small and often not discernible on a significant level phase current unbalance.

To someone unfamiliar with the probability concept, a "worst case" approach, if reasonably "bounded" would appear more comfortable. For the single circuit case,

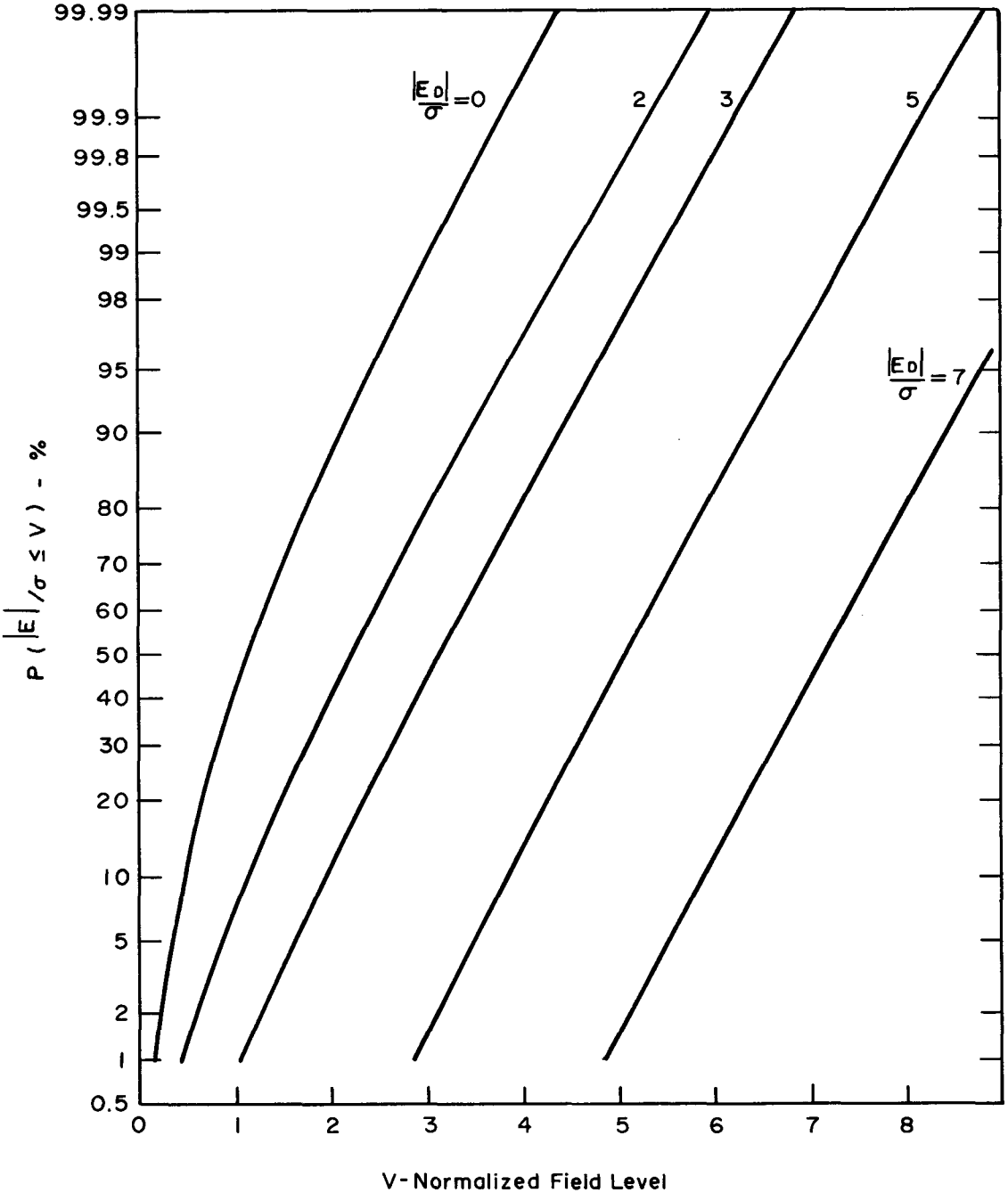

Fig. C-1 CUMULATIVE DISTRIBUTION FOR NORMALIZED ELECTRIC FIELD

which up to this point has been the only one considered, such an approach is almost tenable. For example, by making a number of computer runs and varying the input data, i.e., the phase current values, it is possible to obtain an estimate of the worst case. By inspection of results and judicious "tweaking" of the change in variables on a succeeding computer run, a reasonable estimate of a transmission line's behavior may be obtained in a dozen tries or so. However, in the case of multiple circuits on a common right-of-way, where the number of input variables may be in the twenties or thirties, such a cut and try procedure is completely unattractive. In this situation, there will exist an almost random state of current unbalances between the circuits, and a probability model is quite well representative of the state of affairs.

The ratio, $|E_D|/\sigma$, which determines the appropriate curve to use in Figure C-1 is a function only of interaction geometry and the maximum percentage of current unbalance for a particular transmission line. This can be seen from the following form for the ratio,

$$\frac{|E_D|}{\sigma} = \frac{3}{c} \frac{|z_2|}{\left(|z_0|^2 + |z_1|^2 + |z_2|^2\right)^{\frac{1}{2}}} \tag{C-72}$$

where c is fractional line unbalance defined as

$$c = \hat{\Delta I}/|I| \tag{C-73}$$

In the vicinity close to the transmission line, the impedances, z_0, z_1, and z_2 are approximately of the same order of magnitude, thus making the ratio $|E_D|/\sigma$ large, and the amount of randomness small. With a reasonable high degree of probability, the value of the electric field will be close to E_D. At large distances, $z_1 \simeq z_2 \to 0$, and the level of randomness becomes higher, but at the same time the overall magnitude of the field becomes smaller with increasing distance.

EXTENSIONS TO MULTIPLE POWER LINE CIRCUITS

The preceding development was made for a single three-phase circuit in either a vertical or horizontal configuration with two grounded shield wires. Usually, more than one circuit is present on a right-of-way, particularly in the vertical configuration where two circuits are generally placed on a single structure. Hence, it is desirable to extend the previous analysis to the multiple circuit situation.

Electric Field for Two Three-Phase Circuits

Consider the situation where two three-phase circuits exist, one carrying phase currents I_a, I_b and I_c as before, and the other carrying I_x, I_y and I_z. For convenience, it will be assumed that I_a and I_x represent currents in the closest conductors to the point of observation for each of the respective circuits, and I_c and I_z are the currents carried in farthest conductors of each of the respective circuits.

Analogously to Eq. C-1, the electric field for two circuits sharing a common pair of shield wires is

$$E = I_a Z_a + I_b Z_b + I_c Z_c + I_x Z_x + I_y Z_y + I_z Z_z + I_{s_1} Z_{s_1} + I_{s_2} Z_{s_2} \quad \text{(C-74)}$$

Here it is assumed that the six phase currents are known and, hence, mutual coupling effects between the circuits themselves may be ignored. Eqs. C-17 through C-20 may also be used here for calculation of the induced shield wire currents. However, the free electric fields at the shield wires become

$$E_{s_1} = I_a Z_a' + I_b Z_b' + I_c Z_c' + I_x Z_x' + I_y Z_y' + I_z Z_z' \quad \text{(C-75)}$$

and

$$E_{s_2} = I_a Z_a'' + I_b Z_b'' + I_c Z_c'' + I_x Z_x'' + I_y Z_y'' + I_z Z_z'' \quad \text{(C-76)}$$

In these and succeeding equations, the terms with subscripts a, b, c are defined as in the preceding development and the subscripted x, y, z terms for the second three-phase circuit are defined in similar fashion.

In analogy with Eqs. C-21 and C-25, the above electric fields may be expressed in terms of symmetrical components. Hence,

$$E_{s_1} = 3(I_{oA} Z_{oA}' + I_{1A} Z_{2A}' + I_{2A} Z_{1A}') + 3(I_{oX} Z_{oX}' + I_{1X} Z_{2X}' + I_{2X} Z_{1X}') \quad \text{(C-77)}$$

$$E_{s_2} = 3(I_{oA}\, Z''_{oA} + I_{1A}\, Z''_{2A} + I_{2A}\, Z''_{1A}) + 3(I_{oX}\, Z''_{oX} + I_{1X}\, Z''_{2X} + I_{2X}\, Z''_{1X}) \quad \text{(C-78)}$$

Where the second of the double subscripts, A and X, indicate terms pertaining to the first and second circuits, respectively.

The equivalents to Eqs. C-30 and C-31 are

$$-I_{s_1}(z_{12}+z_{ss}) = 3(I_{oA}\, Z'_{oA} + I_{1A}\, Z'_{2A} + I_{2A}\, Z'_{1A}) + 3(I_{oX}\, Z'_{oX} + I_{1X}\, Z'_{2X} + I_{2X}\, Z'_{1X}) \quad \text{(C-79)}$$

$$-I_{s_2}(z_{12}+z_{ss}) = 3(I_{oA}\, Z''_{oA} + I_{1A}\, Z''_{2A} + I_{2A}\, Z''_{1A}) + 3(I_{oX}\, Z''_{oX} + I_{1X}\, Z''_{2X} + I_{2X}\, Z''_{1X}) \quad \text{(C-80)}$$

Analogously with Eq. C-32, the total electric field becomes

$$E = 3\, I_{oA}\, z_{oA} + 3\, I_{1A}\, z_{2A} + 3\, I_{2A}\, z_{1A} + 3\, I_{oX}\, z_{oX} + 3\, I_{1X}\, z_{2X} + 3\, I_{2X}\, z_{1X} \quad \text{(C-81)}$$

where

$$z_{oA} \equiv Z_{oA} - \frac{Z_{s1}\, Z'_{oA} + Z_{s2}\, Z''_{oA}}{z_{12} + z_{ss}} \quad \text{(C-82)}$$

$$z_{1A} \equiv Z_{1A} - \frac{Z_{s1}\, Z'_{1A} + Z_{s2}\, Z''_{1A}}{z_{12} + z_{ss}} \quad \text{(C-83)}$$

$$z_{2A} \equiv Z_{2A} - \frac{Z_{s1}\, Z'_{2A} + Z_{s2}\, Z''_{2A}}{z_{12} + z_{ss}} \quad \text{(C-84)}$$

$$z_{oX} \equiv Z_{oX} - \frac{Z_{s1}\, Z'_{oX} + Z_{s2}\, Z''_{oX}}{z_{12} + z_{ss}} \quad \text{(C-85)}$$

$$z_{1X} \equiv Z_{1X} - \frac{Z_{s1}\, Z'_{1X} + Z_{s2}\, Z''_{1X}}{z_{12} + z_{ss}} \quad \text{(C-86)}$$

$$z_{2X} \equiv Z_{2X} - \frac{Z_{s1}\, Z'_{2X} + Z_{s2}\, Z''_{2X}}{z_{12} + z_{ss}} \quad \text{(C-87)}$$

Effects of Circuit's Phase Sequence

The total electric field as defined by Eq. C-81 contains three more degrees of freedom than that for a single circuit, thus making the situation more complex, but also allowing several choices for phase sequencing of the circuits. In the single circuit situation, choice of a positive or negative phase sequence for the circuit or choice of a particular line for the reference phase has very little effect upon the magnitude of the electric field over the right-of-way. The presence of multiple-grounded shield wires will cause minor changes; the basic effect is to shift the electric field phase in space by fixed amounts which, in itself, does not heavily influence the voltage level induced on a pipeline.

For two or more circuits, however, this is not the case. If, for example, the same phase sequence is used for both circuits, the electric field may be enhanced at a distant point. On the other hand, proper choice of the phase sequence can cause a cancellation of the (deterministic) electric field for equal current loading in each circuit. As will be shown in the following development, the random component of the field does not cancel out.

From Eq. C-81, the terms contributing to the deterministic electric field are

$$E_D = 3 I_{1A} Z_{2A} + 3 I_{1X} Z_{2X} \qquad \text{(C-88)}$$

The deterministic component is predominant at close distances to the electric transmission line and in this region the shield wire contribution to the field is small enough to be ignored. Hence, examine the condition

$$E_D \simeq 3 I_{1A} Z_{2A} + 3 I_{1X} Z_{2X} = 0 \qquad \text{(C-89)}$$

The above equation implies that both circuits are of a positive phase sequence, and it can be shown that no combination of line choice for the reference phase of either circuit yields a null condition, although electric field magnitude will vary with choice. The same considerations hold also if both circuits are negatively phase sequenced.

On the other hand, consider the situation where one circuit - say A - is positively sequenced and the x circuit in the opposite sense. The condition for cancellation of the deterministic electric field then becomes

$$I_{1A} Z_{1A} + I_{2X} Z_{1X} = 0 \qquad \text{(C-90)}$$

Expressing this condition in terms of the original line current and Carson's mutual impedances gives

$$(I_a + a\,I_b + a^2 I_c)(Z_a + a^2 Z_b + a\,Z_c)$$

$$+ (I_x + a^2 I_y + a\,I_z)(Z_x + a\,Z_y + a^2 Z_z) = 0 \qquad \text{(C-91)}$$

For the physical geometry described previously, that is, phase wires a of circuit A and x of circuit X as being closest to the point of observation, and c and z being the farthest, the following approximate relationships may be assumed from physical symmetry.

$$Z_x + Z_c \simeq Z_b + Z_y \simeq Z_a + Z_z \qquad \text{(C-92)}$$

Equation C-91 may be put into the form

$$(I_a + a\,I_b + a^2 I_c)\,Z_a + Z_z\,(a^2 I_x + a\,I_y + I_z)$$

$$+ (a^2 I_a + I_b + a\,I_c)\,Z_b + Z_y\,(a\,I_x + I_y + a^2 I_z)$$

$$+ (a\,I_a + a^2 I_b + I_c)\,Z_c + Z_x\,(I_x + a^2 I_y + a\,I_z) = 0 \qquad \text{(C-93)}$$

Involving Eq. C-92, Eq. C-93 becomes identically zero for the following solution set.

$$I_x = I_c \qquad \text{(C-94)}$$

$$I_y = I_b \qquad \text{(C-95)}$$

$$I_z = I_a \qquad \text{(C-96)}$$

Hence, a center symmetric phasing of the circuits produces a minimal deterministic electric field in space to the extent that Eq. C-92 holds true and both circuits carry equal currents. It can also be shown that for this arrangement of phases, the free electric fields, E_{s_1} and E_{s_2} at the shield wires will substantially be reduced, thus also minimizing the shield wire contribution to the electric field. The random component of the electric field for this situation can be shown to have a zero mean value. In a parallel manner to Eq. C-69, the standard deviation of the combined circuits may be written as

$$\sigma = \left\{ \begin{array}{l} C_A^2 |I_A|^2 \left(|z_{oA}|^2 + |z_{1A}|^2 + |z_{2A}|^2 \right) \\ + C_X^2 |I_X|^2 \left(|z_{oX}|^2 + |z_{1X}|^2 + |z_{2X}|^2 \right) \end{array} \right\}^{\frac{1}{2}} \qquad \text{(C-97)}$$

where C_A and C_X are the peak fractional current fluctuation, and $|I_A|$ and $|I_X|$ are the balanced current loads for the respective circuits.

For circuits with equal average loading and unbalance conditions,

$$C_A \simeq C_X = C \qquad \text{(C-98)}$$

$$|I_A| \simeq |I_X| = |I| \qquad \text{(C-99)}$$

and Eq. C-97 becomes

$$\sigma = 2C|I| \left(|\overline{z_o}|^2 + |\overline{z_1}|^2 + |\overline{z_2}|^2 \right)^{\frac{1}{2}} \qquad \text{(C-100)}$$

where

$$|\overline{z_o}|^2 = \frac{|z_{oA}|^2 + |z_{oX}|^2}{2} \qquad \text{(C-101)}$$

$$|\overline{z_1}|^2 = \frac{|z_{1A}|^2 + |z_{1X}|^2}{2} \qquad \text{(C-102)}$$

and

$$|\overline{z_2}|^2 = \frac{|z_{2A}|^2 + |z_{2X}|^2}{2} \qquad \text{(C-103)}$$

For the dual circuit case, if the proper phasing sequences are chosen, E_D approaches zero, and the principal contributor to the electric field is the random component. Hence, in Figure C-1, the appropriate probability curve for use tends toward the $E_D/\sigma = 0$ curve. If an unfavorable phase sequence combination is used, E_D, as before, may be computed and the correct curve in Figure C-1 determined.

Extension to Multiple Circuits

A quite common situation found on a single right-of-way is where several structures exist with each carrying more than one circuit. Each structure may carry a pair of shield wires and because of mutual coupling effects between circuits, a simultaneous set of equations must be solved to obtain each shield wire current in the presence of the other shield and phase wires. As the number of structures and,

hence, circuits increase, a larger and larger computer capacity is required for solution and effort surpasses the capability of the programmable hand held calculator rather quickly.

With sufficient effort it is possible to write a computer program large enough to handle any situation, but a review of the results presented raises the question as to the worth of such an endeavor. For example, the phase sequence of the circuits will differ from circuit to circuit, and the tendency will be for the deterministic component of the electric field to become small relative to the random component. This would especially be true for the situation where each pair of circuits on a tower exhibited center symmetry relative to each other, and the overall phase sequence was shifted (transposed) relative to circuits on adjacent towers.

For the situation where a sub-optimum phasing condition exists, it has been found that a reasonable approximation to the electric field may be obtained by ignoring mutual coupling effects between circuits on adjacent structures. This allows calculation of the electric field at a point due to the phase and shield wires on a single structure using the programmable calculator program WIRE. The total deterministic electric field may then be found by superposition of the individual components.

In order to use the graphs of Figure C-1, it is necessary to determine the standard deviation of the random field component. Since the line current fluctuations between tower circuits are independent, the resulting standard deviation for N structures may be determined by

$$\sigma = \left(\sum_{i=1}^{N} \sigma_i^2 \right)^{\frac{1}{2}} \qquad \text{(C-104)}$$

where σ_i for a pair of circuits on a single structure is defined by Eq. C-97.

For equal circuit currents and a reasonable lateral displacement of towers on the right-of-way, say on the order of 100 feet, the above equation may be approximated by

$$\sigma \doteq \sqrt[3]{N}\, \sigma_1 \qquad \text{(C-105)}$$

where σ_1 is the standard deviation for the closest structure as determined from Eq. C-97, and N is the number of structures. Here, it is assumed that the point of observation lies completely to one side of the towers.

In summary, it can be seen that as the number of power line circuits increases on the right-of-way, the inducing electric field will have an increasingly larger random component and thus cause larger random fluctuations in the pipeline voltage.

REFERENCES

1. Transmission Line Reference Book - 345 kV and Above, Electric Power Research Institute, Palo Alto, California, 1975. Chapter 8.12 Electromagnetic Effects, pp. 272-273.

2. Electrical Transmission and Distribution Reference Book, Westinghouse Electric Corp., East Pittsburgh, Pa., 1950. Chapter 2.

3. An Introduction to the Theory of Random Signals and Noise, W. B. Davenport and W. L. Root. McGraw Hill, 1958. Chapter 8.

Appendix D

MUTUAL COUPLING BETWEEN BURIED PIPELINES

INTRODUCTION

For a single buried pipeline, the calculation of induced voltages and currents from single or multiple power lines on same right-of-way (ROW) is relatively straightforward. Basically, it must be recognized that induced voltage peaks will occur at points of either physical discontinuity between the pipeline and power line, or points of electric field discontinuity. The application of relatively simple formulae to these points allows calculation of the induced voltage levels.

When more than one pipeline is buried on the same ROW, mutual coupling effects cause a redistribution of the induced currents in the pipeline. Hence, the problem of calculating the induced current (voltage) is many times more complicated because the driving source electric field at the pipeline is simply not the free field of the power line.

For the situation where the pipelines (in a broad generic sense this can also include the power line shield wires and other conductors) are in a non-conductive media, infinite in length and paralleling the power line, the solution for the individual pipeline/conductor currents can be obtained by the simultaneous solution of a set of N equations corresponding to the N unknown currents. The hand calculator program CURRENTS was written to solve such a set of equations for up to five unknown currents in the presence of up to 25 driving sources. However, application of this program can lead to gross error if the length of conductor parallelism is short, and if conductive paths occur between the buried conductors.

This appendix addresses these problems with the resulting analysis showing that simple correction factors can be obtained which will allow the application of the existing calculator program to the "short parallelism" case with excellent results. Initially, the coupling problem for the infinite length, non-conductive media situation is reviewed. The two and three mutually coupled pipeline cases are

covered, showing the analyses used for derivation of the calculator program. Then mutual coupling in conductive media, i.e., the earth, is considered. The first case analyzed is the coupling of two parallel (to each other and the power line) conductors, one infinite in length and the other short. The result obtained for this case can be easily extended to the situation where both conductors are infinite in length. Surprisingly enough, when this is done, it is found that the result is identical to that obtained in the previous subsection, where non-conductive media were considered. Reflection upon this point impels one to accept the correctness of the results because the voltage on an infinite length pipeline will approach zero, since with all conductors at the same voltage, conductive currents will not flow between them. This is true even with uncoated (pipe) conductors. For the case where one conductor is short, it is found that conductive currents will flow when the conductors are bare.

The next situation analyzed is that of two short pipelines paralleling the power line. Again, for this situation conductive currents will flow in the case of bare conductors.

On the basis of the results obtained for these two cases analyzed, adaptation of the hand calculator program to the case of multiple coated variable length pipelines on the same ROW has been made.

MULTIPLE CONDUCTORS-NON-CONDUCTIVE MEDIA

Two Infinite Length Conductors

Consider two infinite length conductors lying parallel to a power line. Assume that the free electric field (when the conductors are absent) at each conductor is E_{01}' and E_{02}', respectively. These fields will result in internal driving sources at each conductor of $E_{01} = -E_{01}'$ and $E_{02} = -E_{02}'$. From coupled circuit theory, the following equations may be written

$$E_{01} = Z_{11}I_1 + Z_{12}I_2 \qquad \text{(D-1a)}$$

$$E_{02} = Z_{12}I_1 + Z_{22}I_2 \qquad \text{(D-1b)}$$

where Z_{11} is the internal impedance of conductor #1 including the earth return, Z_{22} is the internal impedance of conductor #2 including the earth return, and Z_{12} is the Carson mutual impedance between the two conductors with earth return.

The solution for the currents in each conductor is

$$I_1 = \frac{(E_{01} - \frac{Z_{12}}{Z_{22}} E_{02})}{Z_{11}(1-k_L^2)} \qquad \text{(D-2a)}$$

$$I_2 = \frac{(E_{02} - \frac{Z_{12}}{Z_{11}} E_{01})}{Z_{22}(1-k_L^2)} \qquad \text{(D-2b)}$$

where k_L is defined as the mutual inductive coupling coefficient equal to

$$k_L = \frac{Z_{12}}{\sqrt{Z_{11} Z_{22}}} \qquad \text{(D-3)}$$

The value of k_L is always less than or equal to one, and for typical pipeline ROW situations will be on the order of one-half.

Three Infinite Length Condcutors

For this situation, the corresponding equations are:

$$E_{01} = Z_{11}I_1 + Z_{12}I_2 + Z_{13}I_3 \qquad \text{(D-4a)}$$

$$E_{02} = Z_{12}I_1 + Z_{22}I_2 + Z_{23}I_3 \qquad \text{(D-4b)}$$

$$E_{03} = Z_{13}I_1 + Z_{23}I_2 + Z_{33}I_3 \qquad \text{(D-4c)}$$

where the mutual impedances Z_{13} and Z_{23} are defined between conductors one and three and two and three, respectively, and Z_{33} is the internal impedance of conductor three.

Such a set of simultaneous equations may best be solved by special techniques such as the application of the well known Cramer's Rule which solves each current as the ratio of two determinants. As the number of unknowns increases, the solution becomes rapidly laborious and resort had best be made to obtain a computer solution. An equivalent, but more efficient evaluation technique (Gauss-Seidel) was used in providing a hand calculator solution for up to five unknown currents simultaneously.

TWO PARALLEL CONDUCTOR COUPLING IN CONDUCTIVE MEDIA

Case 1 -- One Infinite Length and One Short Conductor

This case considers two earth return conductors (pipelines) on the same ROW with both immersed in a conductive media, i.e., buried. The first conductor is assumed to be infinite in length and parallel to a power line, thus resulting in an internal driving source for the conductor of $E_o^1(x)$, where x is the longitudinal distance along the conductor. The second conductor is assumed parallel to the first for a distance, ℓ, entering the ROW at $x = -\ell/2$ and leaving at $x = +\ell/2$. The internal driving source for this conductor due to the power line free electric field is assumed to be $E_o^2(x)$. A solution for the two conductor currents, namely $I_1(x)$ and $I_2(x)$ are required where both conductive and inductive coupling between conductors is possible.

A convenient starting point for this analysis is Eq. 5.50 of (1). In this equation, presented below, a general solution for two conductors coupled in a conductive media, but both infinite in length is given. An extension of this general solution will be required for solution of the problem of concern here. The generalized solution is, in conductor #1

$$I_1(x) = \int_{-\infty}^{\infty} \frac{\Delta_2 e_1^o - \Delta_{12} e_2^o}{\Delta_1 \Delta_2 - \Delta_{12}^2} e^{ixu} \, du \qquad \text{(D-5a)}$$

It should be noted that the notation used in this appendix follows that of reference (1), and hence deviates somewhat from that used throughout the rest of the book. This allows the reader to more easily follow the theory leading to Eq. D-5. The principal deviation in notation is that Γ is used rather than γ for conductor propagation constant. Other modifications are obvious from the text.

and for conductor #2

$$I_2(x) = \int_{-\infty}^{\infty} \frac{\Delta_1 e_2^o - \Delta_{12} e_1^o}{\Delta_1 \Delta_2 - \Delta_{12}^2} e^{ixu} \, du \qquad \text{(D-5b)}$$

where

$$\Delta_1 \equiv Y_{11}^{-1}(u^2 + \Gamma_1^2) \qquad \text{(D-6a)}$$

$$\Delta_2 \equiv Y_{22}^{-1}(u^2 + \Gamma_2^2) \qquad \text{(D-6b)}$$

$$\Delta_{12} \equiv Y_{12}^{-1}(u^2 + \Gamma_{12}^2) \qquad \text{(D-6c)}$$

$$Y_{12}^{-1} = \frac{1}{\pi(\sigma + i\omega k)} \ln\left[\frac{1.12}{(\Gamma_1\Gamma_2)^{\frac{1}{2}} y}\right] \qquad \text{(D-6d)}$$

$$Z_{12} = \frac{i\omega\nu}{2\pi} \ln\left[\frac{1.85}{y\left(\gamma^2 + \sqrt{\Gamma_1\Gamma_2}\right)^{\frac{1}{2}}}\right] \qquad \text{(D-6e)}$$

$$\Gamma_1 = (Z_{11}Y_{11})^{\frac{1}{2}} \qquad \text{(D-6f)}$$

$$\Gamma_2 = (Z_{22}Y_{22})^{\frac{1}{2}} \qquad \text{(D-6g)}$$

$$\Gamma_{12} = (Z_{12}Y_{12})^{\frac{1}{2}} \qquad \text{(D-6h)}$$

$$Z_{01} = (Z_{11}/Y_{11})^{\frac{1}{2}} \qquad \text{(D-6i)}$$

$$Z_{02} = (Z_{22}/Y_{22})^{\frac{1}{2}} \qquad \text{(D-6j)}$$

$$\gamma = \left[i\omega\nu(\sigma + i\omega k)\right]^{\frac{1}{2}} \qquad \text{(D-6k)}$$

$$e_1^o = \frac{1}{2\pi} \int_{-\infty}^{\infty} E_1^o(v) e^{-iuv} \, dv \qquad \text{(D-6l)}$$

$$e_2^o = \frac{1}{2\pi} \int_{-\infty}^{\infty} E_2^o(v) e^{-iuv} \, dv \qquad \text{(D-6m)}$$

The above quantities may be physically interpreted as follows

Γ_1 = complex propagation constant for conductor 1

Γ_2 = complex propagation constant for conductor 2

Γ_{12} = complex joint propagation constant for conductors 1 and 2

Z_{01} = characteristic impedance of conductor 1

Z_{02} = characteristic impedance of conductor 2

Z_{11} = internal impedance of conductor 1 including earth return

Z_{22} = internal impedance of conductor 2 including earth return

Y_{11} = leakage admittance to remote earth for conductor 1

Y_{22} = leakage admittance to remote earth for conductor 2

Y_{12} = media leakage admittance between conductors

γ = media propagation constant

i = $\sqrt{-1}$

ω = radian frequency

ν = inductance constant, $4\pi \times 10^{-7}$ henry/m

σ = media conductivity

k = capacitive constant, 8.85×10^{12} farad/m

y = radial distance between conductors

e_1^o = Fourier transform of the source electric field within conductor 1

e_2^o = Fourier transform of the source electric field within conductor 2

The first step towards evaluation of these parameters is the solution of the following transcendental equations for Γ_1 and Γ_2, respectively.

$$\Gamma_1^2 \left[Y_1^{-1} + \frac{1}{\pi(\sigma + i\omega k)} \ln\left(\frac{1.12}{\Gamma_1 a_1}\right)\right] = Z_{i1} + \frac{i\omega\nu}{2\pi} \ln\left[\frac{1.85}{a_1(\gamma^2 + \Gamma_1^2)^{\frac{1}{2}}}\right] \quad \text{(D-7a)}$$

and

$$\Gamma_2^2 \left[Y_2^{-1} + \frac{1}{\pi(\sigma + i\omega k)} \ln\left(\frac{1.12}{\Gamma_2 a_2}\right)\right] = Z_{i2} + \frac{i\omega\nu}{2\pi} \ln\left[\frac{1.85}{a_2(\gamma^2 + \Gamma_2^2)^{\frac{1}{2}}}\right] \quad \text{(D-7b)}$$

where a_1, a_2 are the radius of respective conductors when conductors are at the surface (for burial depth, d, a is replaced by $(a^2 + 4d^2)^{\frac{1}{2}}$); Y_1,Y_2 are the coating admittances of the respective conductors; and Z_{i1},Z_{i2} are the internal impedances of the conductors not including earth return path.

Solution of Eq. D-7 for Γ_1 and Γ_2 allows solution for Z_{11}, Z_{22}, Y_{11} and Y_{22} as follows.

$$Z_{11} = Z_{i1} + \frac{i\omega\nu}{2\pi} \ln\left[\frac{1.85}{a_1(\gamma^2 + \Gamma_1^2)^{\frac{1}{2}}}\right] \quad \text{(D-8a)}$$

$$Z_{22} = Z_{i2} + \frac{i\omega\nu}{2\pi} \ln\left[\frac{1.85}{a_2(\gamma^2 + \Gamma_2^2)^{\frac{1}{2}}}\right] \quad \text{(D-8b)}$$

$$Y_{11} = \left(Y_1^{-1} + \frac{1}{\pi(\sigma + i\omega k)} \ln\left[\frac{1.12}{\Gamma_1 a_1}\right]\right)^{-1} \quad \text{(D-9a)}$$

$$Y_{22} = \left(Y_2^{-1} + \frac{1}{\pi(\sigma + i\omega k)} \ln\left[\frac{1.12}{\Gamma_2 a_2}\right]\right)^{-1} \quad \text{(D-9b)}$$

An alternative and much simpler method exists for calculating the above constants since graphical solutions for the buried pipeline parameters are available in Section 2. The corresponding Z_{11} or Z_{22}, and Y_{11} or Y_{22} may be found for the respective conductors as follows:

$$Z = (\Gamma Z_0)^{\frac{1}{2}} \tag{D-10a}$$

$$Y = (\Gamma/Z_0)^{\frac{1}{2}} \tag{D-10b}$$

The solutions for the remaining parameters are then more or less straightforward.

Solution for Current in Short Conductor. The denominator of Eq. D-5b, after substitution of Eq. D-6, may be written as

$$\Delta_1\Delta_2 - \Delta_{12}^2 = Y_{11}^{-1} Y_{22}^{-1} \left\{(u^2+\Gamma_1^2)(u^2+\Gamma_2^2) - \mu^2(u^2+\Gamma_{12}^2)^2\right\} \tag{D-11}$$

where

$$\mu \equiv \left(\frac{Y_{11} Y_{22}}{Y_{12}^2}\right)^{\frac{1}{2}} \tag{D-12}$$

and is defined as the conductive coupling coefficient.

The polynomial of Eq. D-11 may be factored as

$$(u^2+\Gamma_1^2)(u^2+\Gamma_2^2) - \mu^2(u^2+\Gamma_{12}^2)^2 = (1-\mu^2)(u^2+\gamma_1^2)(u^2+\gamma_2^2) \tag{D-13}$$

where γ_1 and γ_2 are coupled propagation constants equal to:

$$\left.\begin{matrix}\gamma_1^2 \\ \gamma_2^2\end{matrix}\right\} = \left\{\frac{(\Gamma_1^2+\Gamma_2^2-2\mu^2\Gamma_{12}^2)}{2(1-\mu^2)} \pm \sqrt{\frac{(\Gamma_1^2+\Gamma_2^2-2\mu^2\Gamma_{12}^2)^2 - 4(1-\mu^2)(\Gamma_1^2\Gamma_2^2-\mu^2\Gamma_{12}^4)}{2(1-\mu^2)}}\right\} \tag{D-14}$$

Substitution of Eq. D-13 into Eq. D-5b yields

$$I_2(x) = \frac{Y_{11} Y_{22}}{(1-\mu^2)} \int_{-\infty}^{\infty} \frac{e^{ixu}(\Delta_1 e_2^0 - \Delta_{12} e_1^0)}{(u^2+\gamma_1^2)(u^2+\gamma_2^2)}\, du \tag{D-15}$$

Decomposing the integrand into partial fractions then yields

$$I_2(x) = \frac{Y_{11}\,Y_{22}}{(1-\mu^2)(\gamma_1^2-\gamma_2^2)} \int_{-\infty}^{\infty} \left[\frac{e^{ixu}}{(u^2+\gamma_2^2)} - \frac{e^{ixu}}{(u^2+\gamma_1^2)}\right] \begin{bmatrix} \Delta_1 e_2^0 \\ -\Delta_{12} e_1^0 \end{bmatrix} du \tag{D-16}$$

Define:

$$E_2(v) \equiv \frac{Y_{11}}{(1-\mu^2)(\gamma_1^2-\gamma_2^2)} \int_{-\infty}^{\infty} \left[\Delta_1(u)e_2^0(u) - \Delta_{12}(u)e_1^0(u)\right] e^{iuv}\, du \tag{D-17}$$

Then taking the Fourier transform of both sides of the above equation yields

$$\Delta_1 e_2^0 - \Delta_{12} e_1^0 = \frac{(1-\mu^2)(\gamma_1^2-\gamma_2^2)}{2\pi Y_{11}} \int_{-\infty}^{\infty} E_2(v) e^{-iuv}\, dv \tag{D-18}$$

Substituting D-18 into D-16 results in

$$I_2(x) = \frac{Y_{22}}{2\pi} \int_{-\infty}^{\infty} E_2(v)\, dv \int_{-\infty}^{\infty} \left(\frac{e^{i(x-v)u}}{(u^2+\gamma_2^2)} - \frac{e^{i(x-v)u}}{(u^2+\gamma_1^2)}\right) du \tag{D-19}$$

Performing the inner integration then gives

$$I_2(x) = \frac{\Gamma_2}{2Z_{02}} \int_{-\infty}^{\infty} \left(\frac{e^{-\gamma_2|x-v|}}{\gamma_2} - \frac{e^{-\gamma_1|x-v|}}{\gamma_1}\right) E_2(v)\, dv \tag{D-20}$$

where $E_2(v)$ remains to be evaluated. It is the impressed electric field in conductor 2, due in part to the power line free electric field E_2^0 and partly due to the field resulting from current in conductor #1.

Substitution of D-6 into D-17 yields

$$E_2(v) = \frac{1}{(\gamma_1^2 - \gamma_2^2)(1-\mu^2)2\pi} \int_{-\infty}^{\infty} E_2^0(x)\, dx \int_{-\infty}^{\infty} (u^2 + \Gamma_1^2) e^{i(v-x)u}\, du$$

$$- \frac{1}{2\pi\gamma_{12}(1-\mu^2)(\gamma_1^2-\gamma_2^2)} \int_{-\infty}^{\infty} E_1^0(x)\, dx \int_{-\infty}^{\infty} (u^2 + \Gamma_{12}^2) e^{i(v-x)u}\, du \qquad \text{(D-21)}$$

Evalution of the inner integrals in D-21 gives

$$E_2(v) = \frac{\Gamma_1}{(1-\mu^2)(\gamma_1^2 - \gamma_2^2)} \left\{ \int_{-\infty}^{\infty} \left[\Gamma_1^2 \delta(v-x) - \delta''(v-x)\right] E_2^0(x)\, dx \right.$$

$$\left. - \frac{\gamma_{11}}{\gamma_{12}} \int_{-\infty}^{\infty} \left[\Gamma_{12}^2 \delta(v-x) - \delta''(v-x)\right] E_1^0(x)\, dx \right\} \qquad \text{(D-22)}$$

where $\delta(v-x)$ is the Dirac delta impulse function, and $\delta''(v-x)$ is the second derivative of the Dirac delta function. Completing the integrations in Eq. D-22 gives

$$E_2(v) = \frac{\Gamma_1}{(\gamma_1^2-\gamma_2^2)(1-\mu^2)} \left\{ E_2^0(v) - \frac{Z_{12}}{Z_{11}} E_1^0(v) \right\} - \frac{E_2^{0''}(v)}{(\gamma_1^2 - \gamma_2^2)(1-\mu^2)}$$

$$+ \frac{\gamma_{11} E_1^{0''}(v)}{\gamma_{12}(\gamma_1^2 - \gamma_2^2)(1-\mu^2)} \qquad \text{(D-23)}$$

where the double prime indicates the second derivative with respect to v.

Further evaluation of $E_2(v)$ requires the assumption of known forms for E_1^0 and E_2^0. For the case of conductors parallel to the electric power line, the electric source field at conductor #1, i.e., the infinite length line is:

$$E_1^0(v) = \varepsilon_1^0 = \text{constant} \tag{D-24a}$$

and for the electric source field at conductor #2,

$$E_2^0 = \varepsilon_2^0 \left[U(v + \ell/2) - U(v - \ell/2)\right] \tag{D-24b}$$

where ε_2^0 is a constant and $U(\cdot)$ is the unit step function.

The step function factor in Eq. D-24b is necessary because of the fact that the distance over which the parallelism exists for the shorter conductor is of length, ℓ. Equation D-24a shows that $E_1^{0''}(v) = 0$, and therefore Eq. D-23 becomes

$$E_2(v) = \frac{\Gamma_1^2}{(\gamma_1^2 - \gamma_2^2)(1 - \mu^2)} \left\{E_2^0(v) - \frac{Z_{12}}{Z_{11}} E_1^0(v)\right\} - \frac{E_2^{0''}(v)}{(\gamma_1^2 - \gamma_2^2)(1 - \mu^2)} \tag{D-25}$$

This equation, as it stands, assumes implicitly that the additive electric field at conductor #2, due to current in conductor #1, is $(-Z_{12}/Z_{11})E_1^0(v)$ for $-\infty < v < \infty$, since the first conductor is infinite in length. Due to the fact that conductor #2 is only of length, ℓ, a field of magnitude $(Z_{12}/Z_{22})E_1^0(v)$ must be added to the driving field $E_2(v)$ for the regions $v < -\ell/2$ and $v > \ell/2$.

Therefore, Eq. D-25 must be modified to

$$E_2(v) = \frac{\Gamma_1^2}{(\gamma_1^2 - \gamma_2^2)(1 - \mu^2)} \left\{E_2^0(v) - \frac{Z_{12}}{Z_{11}} E_1^0(v) + \frac{Z_{12}}{Z_{22}} E_1^0(v) \left[U(v - \ell/2) + U(-v - \ell/2)\right]\right\}$$

$$- \frac{1}{(1 - \mu^2)(\gamma_1^2 - \gamma_2^2)} \left\{E_2^{0''}(v) + \left|\frac{Z_{12}}{Z_{22}}\right| \cdot \frac{\partial}{\partial v^2} \left[E_1^0(v) \left\{U(v - \ell/2) + U(-v - \ell/2)\right\}\right]\right. \tag{D-26}$$

Performing the indicated differentiation and remembering the fact that $E_1^{0''}(v) = 0$, results in

$$E_2(v) = \frac{\Gamma_1^2}{(\gamma_1^2 - \gamma_2^2)(1-\mu^2)} \left\{ E_2^0(v) - \frac{Z_{12}}{Z_{11}} E_1^0(v) \left[U(v+\ell/2) - U(v-\ell/2) \right] \right\}$$

$$- \frac{1}{(\gamma_1^2 - \gamma_2^2)(1-\mu^2)} \left\{ E_2^{0''}(v) - \frac{Z_{12}}{Z_{11}} E_1^0(v) \left[\delta'(v+\ell/2) - \delta'(v-\ell/2) \right] \right\} \tag{D-27}$$

Substituting assumed values for $E_2^0(v)$ and $E_1^0(v)$ from Eq. D-24 then gives

$$E_2(v) = \frac{\Gamma_1}{(\gamma_1 - \gamma_2)(1-\mu^2)} \left\{ (\varepsilon_2^0 - \frac{Z_{12}}{Z_{11}} \varepsilon_1^0) \left[U(v+\ell/2) - U(v-\ell/2) \right] \right\}$$

$$- \frac{1}{(\gamma_1 - \gamma_2)(1-\mu)} \left\{ (\varepsilon_2^0 - \frac{Z_{12}}{Z_{11}} \varepsilon_1^0) \left[\delta'(v+\ell/2) - \delta'(v-\ell/2) \right] \right\} \tag{D-28}$$

Substitution of Eq. D-28 in Eq. D-20 yields for the current in the short conductor,

$$I_2(x) = \frac{\Gamma_2 \Gamma_1^2 (\varepsilon_2^0 - \frac{Z_{12}}{Z_{11}} \varepsilon_1^0)}{2 Z_{02} (\gamma_2^2 - \gamma_2^2)(1-\mu^2)} \int_{-\ell/2}^{\ell/2} \left(\frac{e^{-\gamma_2 |x-v|}}{\gamma_2} - \frac{e^{-\gamma_1 |x-v|}}{\gamma_1} \right) dv$$

$$- \frac{\Gamma_2 (\varepsilon_2^0 - \frac{Z_{12}}{Z_{11}} \varepsilon_1^0)}{2 Z_{02} (1-\mu^2)(\gamma_1^2 - \gamma_2^2)} \int_{-\infty}^{\infty} \left(\frac{e^{-\gamma_2 |x-v|}}{\gamma_2} - \frac{e^{-\gamma_1 |x-v|}}{\gamma_1} \right) \left[\delta'(v+\ell/2) - \delta'(v-\ell/2) \right] dv \tag{D-29}$$

Carrying out the integrations gives,

$$I_2(x) = \frac{\Gamma_2(\varepsilon_2^0 - \frac{Z_{12}}{Z_{11}}\varepsilon_1^0)}{2Z_{02}(\gamma_1 - \gamma_2^2)(1-\mu^2)}$$

$$\cdot\left\{\Gamma_1^2\left[\frac{2}{\gamma_2^2} - \frac{2}{\gamma_1^2} - \frac{e^{-\gamma_2(\ell/2+x)}}{\gamma_2^2} - \frac{e^{-\gamma_2(\ell/2-x)}}{\gamma_2^2} - \frac{e^{-\gamma_1(\ell/2+x)}}{\gamma_1^2} + \frac{e^{-\gamma_1(\ell/2-x)}}{\gamma_1^2}\right]\right.$$

$$\left. - \left[e^{-\gamma_1(\ell/2-x)} + e^{-\gamma_1(\ell/2+x)} - e^{-\gamma_2(\ell/2-x)} - e^{-\gamma_2(\ell/2+x)}\right]\right\} \qquad \text{(D-30)}$$

Equation D-30 is the complete solution for the current in the short conductor for $-\ell/2 \leq x \leq \ell/2$. It is interesting to find the limiting solution as $\ell \to \infty$, i.e., both conductors infinite. Equation D-30 then becomes

$$I_2(x) = \frac{\Gamma_2\Gamma_1\ (\varepsilon_2^0 - \frac{Z_{12}}{Z_{11}}\varepsilon_1^0)}{Z_{02}(1-\mu^2)\ \gamma_1^2\gamma_2^2} \qquad \text{(D-31)}$$

Insertion of Eq. D-14 into the above results in

$$I_2(x) = \frac{(\varepsilon_2^0 - \frac{Z_{12}}{Z_{11}}\varepsilon_1^0)}{Z_{22}(1 - \frac{\mu^2\Gamma_{12}^4}{\Gamma_1^2\Gamma_2^2})} \qquad \text{(D-32)}$$

which then, by Eq. D-6, can be put into the form

$$I_2(x) = \frac{(\varepsilon_2^0 - \frac{Z_{12}}{Z_{11}}\varepsilon_1^0)}{Z_{22}\left[1 - \frac{Z_{12}^2}{Z_{11}Z_{22}}\right]} \qquad \text{(D-33)}$$

which is identical to Eq. D-2b for $\varepsilon_2^0 \equiv E_{02}$ and $\varepsilon_1^0 \equiv E_{01}$. This shows that as the parallel exposures of both conductors becomes very large, the mutual coupling

between them becomes purely inductive and independent of the fact that the intervening medium is conductive.

Again considering the short length conductor, inspection of the appropriate current equation, i.e., Eq. D-30, shows a complexity which does not allow a quick or computationally easy assessment of its significance to be made. The complexity of the equation is due to the fact that conductive coupling has been accounted for through the presence of the factors μ, γ_1, γ_2. In dealing with coexistent bare conductors on the same ROW, for example, the assessment of the impact of mutual coupling would require use of the equation in its present form.

The key as to the significance of the conductive coupling component relative to inductive coupling contribution lies in the value of the conductive coupling coefficient, μ, as defined by Eq. D-12. A quick calculation of this coefficient shows that when both conductors are bare, its value can easily be larger than one-half, dependent upon earth conductivity, their separation, and so forth. On the other hand, if both pipelines are coated, even if only moderately well, $\mu \leq 0.1$ is a conservative estimate. In general, it would be expected to be much smaller. Therefore, restricting the analysis to coated conductors (pipelines) ensures the condition

$$\mu^2 << 1 \tag{D-34a}$$

and from Eq. D-14

$$\gamma_1 = \Gamma_1 \tag{D-34b}$$

$$\gamma_2 = \Gamma_2 \tag{D-34c}$$

Since the majority of present day pipelines, for example, are generally reasonably well coated, the condition of Eq. D-34 appears not as restrictive when considering parallel pipelines on the same ROW.

Applying Eq. D-34 to Eq. D-30 yields

$$I_2(x) = \frac{\left[\varepsilon_2^0 - (Z_{12}/Z_{11})\,\varepsilon_1^0\right]}{Z_{22}\left(1 - \frac{Z_{12}^2}{Z_{11}Z_{22}}\right)} \left\{1 - \left(\frac{e^{-\Gamma_2(\ell/2-x)} + e^{-\Gamma_2(\ell/2+x)}}{2}\right)\right\} \tag{D-35a}$$

This equation will be further examined in the last subsection of this appendix, where modifications to the existing hand calculator mutual coupling program will be derived so as to allow its use for evaluation of mutual coupling effects. In the special case where $\Gamma_2 \ell << 1$, the following simplification is obtained by series expansion of the exponentials.

$$I_2(x) = \frac{\varepsilon_2^0 - (Z_{12}/Z_{11})\,\varepsilon_1^0}{Z_{22}\left(1 - \frac{Z_{12}^2}{Z_{11}Z_{22}}\right)}\left(\frac{\Gamma_2\ell}{2}\right) \qquad \text{(D-35b)}$$

Solution for Current in Long Conductor. The generalized solution of this conductor is given by Eq. D-5a as

$$I_2(x) = \int_{-\infty}^{\infty} \frac{\Delta_2 e_1^0 - \Delta_{12} e_2^0}{\Delta_1\Delta_2 - \Delta_{12}^2}\, e^{ixu}\, du \qquad \text{(D-5a)}$$

Following a procedure similar to that for the short conductor, it may be shown that the current may be expressed as

$$I_1(x) = \frac{\Gamma_1}{2Z_{01}} \int_{-\infty}^{\infty} \left(\frac{e^{-\gamma_1|x-v|}}{\gamma_1} - \frac{e^{-\gamma_2|x-v|}}{\gamma_2} \right) E_1(v)\, dv \qquad \text{(D-36)}$$

where $E_1(v)$ is the source generator for conductor #1 in the presence of the electric transmission line free field and the current carrying second conductor is equal to

$$E_1(v) = \frac{Y_{22}}{(1-\mu^2)(\gamma_2^2 - \gamma_1^2)} \int_{-\infty}^{\infty} \left[\Delta_2(u)e_1^0(u) - \Delta_{12}(u)e_2^0(u)\right] e^{iuv}\, dv \qquad \text{(D-37)}$$

With the substitution of the appropriate quantities from Eq. D-6 the above equation may be put into the form

$$E_1(v) = \frac{1}{(1-\mu^2)(\gamma_2^2-\gamma_1^2)} \int_{-\infty}^{\infty} \left[(u^2+\Gamma_2^2)e_1^0(u) - \frac{Y_{22}}{Y_{12}}(u^2+\Gamma_{12}^2)e_2^0(u)\right] e^{iuv}\, du$$

$$= \frac{1}{(1-\mu^2)(\gamma_2^2-\gamma_1^2)} \int_{-\infty}^{\infty} \left[\Gamma_2^2\delta(v-x) - \delta''(v-x)\right] E_1^0(x)\, dx$$

$$- \frac{Y_{22}}{Y_{12}(1-\mu^2)(\gamma_2^2-\gamma_1^2)} \int_{-\infty}^{\infty} \left[\Gamma_{12}^2\delta(v-x) - \delta''(v-x)\right] E_2^0(x)\, dx \qquad \text{(D-38)}$$

Performing the indicated integration gives

$$E_1(v) = \frac{\Gamma_2^2}{(\gamma_2^2-\gamma_1^2)(1-\mu^2)} \left\{E_1^0(v) - \frac{Z_{12}}{Z_{22}} E_2^0(v)\right\}$$

$$- \frac{E_1^{0''}(v)}{(\gamma_2^2-\gamma_1^2)(1-\mu^2)} + \frac{Y_{22}E_2^{0''}(v)}{Y_{12}(\gamma_2^2-\gamma_1^2)(1-\mu^2)} \qquad \text{(D-39)}$$

Further evaluation of Eq. D-39 requires that the "free" fields at the conductors be known. As before, it will be assumed that

$$E_1^0(v) = \varepsilon_1^0 \quad \text{(a constant)} \qquad \text{(D-40a)}$$

and

$$E_2^0(v) = \varepsilon_2^0 \left[U(v+\ell/2) - U(v-\ell/2)\right] \qquad \text{(D-40b)}$$

which after substitution into Eq. D-39 gives

$$E_1(v) = \frac{\Gamma_2^2}{(\gamma_2^2 - \gamma_1^2)(1-\mu^2)} \left\{ \varepsilon_1^0 - \frac{Z_{12}}{Z_{22}} \varepsilon_2^0 \left[U(v+\ell/2) - U(v-\ell/2) \right] \right\}$$

$$+ \frac{\gamma_{22}\varepsilon_2^0 \left[\delta'(v+\ell/2) - \delta'(v-\ell/2) \right]}{\gamma_{12}(1-\mu^2)(\gamma_2^2 - \gamma_1^2)} \qquad \text{(D-41)}$$

Substituting Eq. D-41 in D-5a gives

$$I_1(x) = \frac{\Gamma_1\Gamma_2\varepsilon_1^0}{2Z_{01}(\gamma_2^2 - \gamma_1^2)(1-\mu^2)} \int_{-\infty}^{\infty} \left(\frac{e^{-\gamma_1|x-v|}}{\gamma_1} - \frac{e^{-\gamma_2|x-v|}}{\gamma_2} \right) dv$$

$$- \frac{\Gamma_1\Gamma_2 \varepsilon_2^0 (Z_{12}/Z_{22})}{2Z_{01}(\gamma_2^2 - \gamma_1^2)(1-\mu^2)} \int_{-\ell/2}^{\ell/2} \left(\frac{e^{-\gamma_1|x-v|}}{\gamma_1} - \frac{e^{-\gamma_2|x-v|}}{\gamma_2} \right) dv$$

$$+ \frac{\gamma_{22}\Gamma_1\varepsilon_2^0}{2Z_{01}\gamma_{12}(\gamma_2^2 - \gamma_1^2)(1-\mu^2)} \int_{-\infty}^{\infty} \left(\frac{e^{-\gamma_1|x-v|}}{\gamma_1} - \frac{e^{-\gamma_2|x-v|}}{\gamma_2} \right)$$

$$\cdot \left[\delta'(v+\ell/2) - \delta'(v-\ell/2) \right] dv \qquad \text{(D-42)}$$

Evaluation of the integrals yields, for the region $-\ell/2 \leq x \leq \ell/2$

$$I_1(x) = \frac{\Gamma_1\Gamma_2 \varepsilon_1^0}{2Z_{01}(\gamma_2^2 - \gamma_1^2)(1-\mu^2)} \left\{ \frac{2}{\gamma_1^2} - \frac{2}{\gamma_2^2} \right\}$$

$$- \frac{\Gamma_1\Gamma_2 (Z_{12}/Z_{22})\varepsilon_2^0}{2Z_{01}(\gamma_2^2 - \gamma_1^2)(1-\mu^2)} \left\{ \frac{2}{\gamma_1^2} - \frac{2}{\gamma_2^2} - \frac{e^{-\gamma_1(x+\ell/2)}}{\gamma_1^2} \right.$$

$$\left. - \frac{e^{-\gamma_1(\ell/2-x)}}{\gamma_1^2} - \frac{e^{-\gamma_2(x+\ell/2)}}{\gamma_2^2} + \frac{e^{-\gamma_2(\ell/2-x)}}{\gamma_2^2} \right\}$$

$$+ \frac{\gamma_{22}\Gamma_1\varepsilon_2^0}{2Z_{01}\gamma_{12}(\gamma_2^2 - \gamma_1^2)(1-\mu^2)} \left\{ -e^{-\gamma_1(x+\ell/2)} - e^{-\gamma_1(\ell/2-x)} \right\} \qquad \text{(D-43)}$$

For the region $x \leq -\ell/2$,

$$I_1(x) = \frac{\Gamma_1\Gamma_2{}^2\varepsilon_1^0}{2Z_{01}(\gamma_2{}^2-\gamma_1{}^2)(1-\mu^2)}\left\{\frac{2}{\gamma_1{}^2}-\frac{2}{\gamma_2{}^2}\right\}$$

$$-\frac{\Gamma_1\Gamma_2\,(Z_{12}/Z_{22})\varepsilon_2^0}{2Z_{01}(\gamma_2{}^2-\gamma_1{}^2)(1-\mu^2)}\left\{\frac{e^{-\gamma_1(-\ell/2-x)}}{\gamma_1{}^2}-\frac{e^{-\gamma_1(\ell/2-x)}}{\gamma_1{}^2}+\frac{e^{-\gamma_2(\ell/2-x)}}{\gamma_2{}^2}\right.$$

$$\left.-\frac{e^{-\gamma_2(-\ell/2-x)}}{\gamma_2{}^2}\right\}+\frac{Y_{22}\Gamma_1\varepsilon_2^0}{2Z_{01}Y_{12}(\gamma_2{}^2-\gamma_1{}^2)(1-\mu^2)}$$

$$\left\{e^{-\gamma_1(-\ell/2-x)}\quad -e^{-\gamma_1(\ell/2-x)}\right\} \tag{D-44}$$

and for the region $x > \ell/2$

$$I_1(x) = \frac{\Gamma_1\Gamma_2{}^2\varepsilon_1^0}{2Z_{01}(\gamma_2{}^2-\gamma_1{}^2)(1-\mu^2)}\left\{\frac{2}{\gamma_1{}^2}-\frac{2}{\gamma_2{}^2}\right\}$$

$$-\frac{\Gamma_1\Gamma_2\,(Z_{12}/Z_{22})\varepsilon_2^0}{2Z_{01}(\gamma_2{}^2-\gamma_1{}^2)(1-\mu^2)}\left\{\frac{e^{-\gamma_1(x-\ell/2)}}{\gamma_1{}^2}-\frac{e^{-\gamma_1(x+\ell/2)}}{\gamma_1{}^2}-\frac{e^{-\gamma_2(x-\ell/2)}}{\gamma_2{}^2}\right.$$

$$\left.+\frac{e^{-\gamma_2(x+\ell/2)}}{\gamma_1{}^2}\right\}+\frac{Y_{22}\Gamma_1\varepsilon_1^0}{2Z_{01}Y_{12}(\gamma_2{}^2-\gamma_1{}^2)(1-\mu^2)}$$

$$\cdot\left\{e^{-\gamma_1(x-\ell/2)}\quad -e^{-\gamma_1(x+\ell/2)}\right\} \tag{D-45}$$

For the regions distant from the short conductor, i.e., $x < -\ell/2$ and $x > \ell/2$, the exponential terms in the respectively appropriate equations, D-44 and D-45, approach zero rapidly as the observation points x moves away from the ends of the short conductor. The remaining term is

$$I_1(x) = \frac{\Gamma_1\Gamma_2\,\varepsilon_1^0\left\{\frac{2}{\gamma_1{}^2}-\frac{2}{\gamma_2{}^2}\right\}}{2Z_{01}(\gamma_2{}^2-\gamma_1{}^2)(1-\mu^2)} \tag{D-46}$$

By Eqs. D-6 and D-14, the above equation may be put into the form

$$I_1(x) = \frac{\varepsilon_1^0}{Z_{11}\left[1 - \frac{Z_{12}^2}{Z_{11}Z_{22}}\right]} \tag{D-47}$$

which is the current expected if only one conductor were present on the ROW. In addition, Eq. D-47 is independent of conductive coupling effects and is accurate for both coated and bare conductors.

In the region, $-\ell/2 \leq x \leq \ell/2$, the current I_1 is modified due to the presence of the second conductor as shown by Eq. D-43. With some manipulation, it may be put into the form

$$I_1(x) = \frac{\left(\varepsilon_1^0 - \frac{Z_{12}}{Z_{22}}\ \varepsilon_2^0\right)}{Z_{11}\left(1 - \frac{Z_{12}^2}{Z_{11}Z_{22}}\right)} \tag{D-48}$$

where

$$z_{12} = Z_{12}\left\{1 - \left[\frac{\gamma_1^2}{2(\gamma_1^2 - \gamma_2^2)}\right]\left[e^{-\gamma_2(x+\ell/2)} + e^{-\gamma_2(\ell/2-x)}\right]\right.$$

$$\left. + \left[1 - \frac{\gamma_1^2}{\Gamma_{12}^2}\right]\left[\frac{\gamma_2^2}{2(\gamma_1^2 - \gamma_2^2)}\right]\left[e^{-\gamma_1(x+\ell/2)} + e^{-\gamma_1(\ell/2-x)}\right]\right\} \tag{D-49a}$$

Equation D-49a is computationally formidable as it stands. However, it may be simplified considerably in some cases.

1. If $\ell \to \infty$

$$z_{12} \to Z_{12} \tag{D-49b}$$

2. If similarly coated pipelines are present on the ROW, then

$$\mu \to 0$$

$$\gamma_1 \to \Gamma_1$$

$$\gamma_2 \to \Gamma_2$$

$$\Gamma_1 \simeq \Gamma_2 = \Gamma, \text{ and}$$

$$\Gamma_1^2 << \Gamma_{12}^2$$

then

$$Z_{12} = Z_{12}\left\{1 - \frac{e^{-\Gamma(x+\ell/2)}}{4}\left[2+\Gamma(x+\ell/2)\right] - \frac{e^{-\Gamma(\ell/2-x)}}{4}\left[2-\Gamma(x-\ell/2)\right]\right\} \tag{D-49c}$$

3. If $\ell \to 0$, then

$$Z_{12} = Z_{12}\left(\frac{\Gamma_1\Gamma_2\ell}{2(\Gamma_1+\Gamma_2)}\right) \tag{D-49d}$$

and for similar pipeline when ℓ is small, $\Gamma_1 = \Gamma_2 = \Gamma$, and

4. $$Z_{12} = Z_{12}\left(\frac{\Gamma\ell}{4}\right) \tag{D-49e}$$

Case 2 -- Two Short Parallel Conductors

The case considered here is that of two parallel conductors entering the power line ROW at $x = -\ell/2$ and leaving at $x = +\ell/2$. Paralleling the previous development, the free driving fields at conductors #1 and #2 are

$$E_1^0(v) = \varepsilon_1^0\left[U(v+\ell/2) - U(v-\ell/2)\right] \tag{D-50a}$$

$$E_2^0(v) = \varepsilon_2^0\left[U(v+\ell/2) - U(v-\ell/2)\right] \tag{D-50b}$$

Because of the symmetry of the problem, the current in either conductor may be solved and the other conductor may be written by inspection. The solution for the current in Conductor 2 will, however, be obtained explicitly.

Substituting Eq. D-50 and Eq. D-23 yields

$$E_2(v) = \frac{\Gamma_1^2(\varepsilon_2^0 - \frac{Z_{12}}{Z_{11}}\varepsilon_1^0)}{(\gamma_1^2-\gamma_2^2)(1-\mu^2)}\left[U(v+\ell/2) - U(v-\ell/2)\right]$$

$$- \frac{(\varepsilon_2^0 - \frac{Y_{11}}{Y_{12}}\varepsilon_1^0)}{(\gamma_1^2-\gamma_2^2)(1-\mu^2)}\left[\delta'(v+\ell/2) - \delta'(v-\ell/2)\right] \qquad \text{(D-51)}$$

Substituting Eq. D-51 into Eq. D-20 gives

$$I_2(x) = \frac{(\varepsilon_2^0 - \frac{Z_{12}}{Z_{11}}\varepsilon_1^0)\gamma_1^2\gamma_2^2}{2Z_{22}(\gamma_1^2-\gamma_2^2)(1-\frac{Z_{12}^2}{Z_{11}Z_{22}})}$$

$$\cdot\left\{\frac{2}{\gamma_2^2} - \frac{2}{\gamma_1^2} - \frac{e^{-\gamma_2(\ell/2+x)}}{\gamma_2^2} - \frac{e^{-\gamma_2(\ell/2-x)}}{\gamma_2^2} + \frac{e^{-\gamma_1(\ell/2+x)}}{\gamma_1^2} - \frac{e^{-\gamma_1(\ell/2-x)}}{\gamma_1^2}\right\}$$

$$- \frac{\left[\varepsilon_2^0 - \frac{Y_{11}}{Y_{12}}\right]\varepsilon_1^0\,\gamma_1^2\gamma_2^2}{2Z_{22}(\gamma_1^2-\gamma_2^2)(1-\frac{Z_{12}}{Z_{12}Z_{22}})\Gamma_1^2}$$

$$\cdot\left\{e^{-\gamma_1(\ell/2+x)} + e^{-\gamma_1(\ell/2-x)} - e^{-\gamma_2(\ell/2+x)} - e^{-\gamma_2(\ell/2-x)}\right\} \qquad \text{(D-52)}$$

For at least one conductor reasonably well insulated, the conditions, Eq. D-34, may be assumed. Then Eq. D-52 becomes

$$I_2(x) = \frac{\varepsilon_2^0}{Z_{22}\left(1 - \frac{Z_{12}^2}{Z_{11}Z_{22}}\right)} \left[1 - \frac{e^{-\Gamma_2(\ell/2+x)} + e^{-\gamma_2(\ell/2-x)}}{2}\right] - \frac{\frac{Z_{12}}{Z_{11}}\varepsilon_1^0}{Z_{22}\left(1 - \frac{Z_{12}^2}{Z_{11}Z_{22}}\right)}$$

$$\cdot \left\{1 - \left(\frac{e^{-\Gamma_2(\ell/2+x)} + e^{-\Gamma_2(\ell/2-x)}}{2}\right)\left(\frac{1 - \frac{\Gamma_2^2}{\Gamma_{12}}}{1 - \frac{\Gamma_2^2}{\Gamma_1^2}}\right)\right.$$

$$\left. - \frac{e^{-\Gamma_1(\ell/2+x)} + e^{-\Gamma_1(\ell/2-x)}}{2} \left(\frac{1 - \frac{\Gamma_1^2}{\Gamma_{12}^2}}{1 - \frac{\Gamma_1^2}{\Gamma_2^2}}\right)\right\} \qquad \text{(D-53)}$$

For coated conductors it may be assumed that

$$\Gamma_{12}^2 >> \Gamma_1^2, \text{ and}$$

$$\Gamma_{12}^2 << \Gamma_2^2.$$

Equation D-53 then becomes

$$I_2(x) = \frac{\varepsilon_2^0}{Z_{22}\left(1 - \frac{Z_{12}^2}{Z_{11}Z_{22}}\right)} \left[1 - \frac{e^{-\Gamma_2(\ell/2+x)} + e^{-\Gamma_2(\ell/2-x)}}{2}\right]$$

$$- \frac{\frac{Z_{12}}{Z_{11}}\varepsilon_1^0}{Z_{22}\left(1 - \frac{Z_{12}^2}{Z_{11}Z_{22}}\right)} \left[1 - \frac{\Gamma_1^2}{2(\Gamma_1^2 - \Gamma_2^2)}\left(e^{-\Gamma_2(\ell/2+x)} + e^{-\Gamma_2(\ell/2-x)}\right)\right.$$

$$\left. + \frac{\Gamma_2^2}{2(\Gamma_1^2 - \Gamma_2^2)}\left(e^{-\Gamma_1(\ell/2+x)} + e^{-\Gamma_1(\ell/2-x)}\right)\right] \qquad \text{(D-54)}$$

Equation D-54 is complicated as it stands, and does not yield readily to mathematical computation except possibly on a computer. However, for the conditions, $\Gamma_1 \ell > 2$ and $\Gamma_2 \ell > 2$, the infinite length situation (i.e., Eq. D-2b) may be used with reasonable error. For short pipeline exposures, e.g., $\Gamma_1 \ell < 1$ and $\Gamma_2 \ell < 1$, considerable simplification of Eq. D-54 occurs by using the series expansion for the exponentials. In this case, Eq. D-54 becomes

$$I_2(x) = \frac{\left[\varepsilon_2^0 - \frac{Z_{12}}{Z_{11}}\left(\frac{\Gamma_1}{\Gamma_1 + \Gamma_2}\right)\varepsilon_1^0\right]}{Z_{22}\left(1 - \frac{Z_{12}^2}{Z_{11}Z_{22}}\right)}\left(\frac{\Gamma_2 \ell}{2}\right) \qquad \text{(D-55)}$$

Inspection of Eq. D-55 shows that the effect of reducing the parallel exposure length is essentially to modify the mutual and self impedances of the coupled conductors, with respect to their values when the parallel exposures are infinite. Consequences of this modification are discussed in the following subsection.

SUMMARY OF RESULTS

The analysis of the previous two sections shows that the current in a conductor depends upon the length of its exposure to the power lines and also upon the length of other conductors on the same ROW. Inspection of the results shows that changes in the induced current in a conductor can be equivalently accounted for by appropriately modifying the self and mutual impedances of the conductors defined for the infinite length exposure situation, i.e., the Carson's impedances. The hand calculator program CURRENTS essentially solves the following matrix for the unknown conductor currents assuming infinite length exposures.

$$\begin{bmatrix} I_1 \\ I_2 \\ . \\ . \\ . \\ I_n \end{bmatrix} = \begin{bmatrix} Z_{11} & Z_{12} & \cdots & Z_{1n} \\ Z_{21} & Z_{22} & \cdots & Z_{2n} \\ . & . & . & . \\ . & . & . & . \\ . & . & . & . \\ Z_{n1} & Z_{n2} & \cdots & Z_{nn} \end{bmatrix}^{-1} \begin{bmatrix} \varepsilon_0^1 \\ \varepsilon_0^2 \\ . \\ . \\ . \\ \varepsilon_0^n \end{bmatrix} \qquad \text{(D-56)}$$

where the impedance matrix $[Z]$ is entered manually into the calculator. Because a linear isotropic medium can generally be assumed between the infinite length conductors, the following relationship holds for the mutual impedance

$$Z_{ij} = Z_{ji} \tag{D-57}$$

If the existing calculator program is used for situations where infinite length exposures are not encountered, it will be found that calculated conductor current values will be considerably in error (on the high side). Results of this analysis yields the rationale for proper modification of the calculator program inputs. This is done as follows:

Review of Case 1

When a long conductor (#1) is coupled to a short length conductor (#2), comparison of Eq. D-35b with the infinite length solution (Eq. D-2b) shows that the proper value of induced current is obtained for the following self impedance modification.

$$Z_{22} \rightarrow \frac{Z_{22}}{\left(\frac{\Gamma_2 \ell}{2}\right)} \tag{D-58a}$$

The mutual impedance between conductor #2 and conductor #1, i.e., Z_{21} remains unchanged. Hence,

$$Z_{21} = Z_{12} \tag{D-58b}$$

Inspection of Eqs. D-48 and D-49d show that for conductor #1, the self impedance remains unchanged, i.e.,

$$Z_{11} \rightarrow Z_{11} \tag{D-58c}$$

while

$$Z_{12} \rightarrow Z_{12} \left(\frac{\Gamma_1 \Gamma_2}{\Gamma_1 + \Gamma_2}\right) \frac{\ell}{2} \tag{D-58d}$$

Review of Case 2

When two short conductors are coupled together, Eq. D-55 shows that

$$Z_{11} \rightarrow \frac{Z_{11}}{\frac{\Gamma_1 \ell}{2}} \tag{D-59a}$$

$$Z_{22} \rightarrow \frac{Z_{22}}{\frac{\Gamma_2 \ell}{2}} \tag{D-59b}$$

$$Z_{12} \rightarrow \left(\frac{\Gamma_2}{\Gamma_1 + \Gamma_2}\right) Z_{12} \tag{D-59c}$$

$$Z_{21} \rightarrow Z_{12}\left(\frac{\Gamma_1}{\Gamma_1 + \Gamma_2}\right) \tag{D-59d}$$

By modifying the impedance matrix as shown by Eqs. D-58 and D-59, the hand calculator program may be used for the situation where both long and short length couplings are experienced on the same ROW.

Example. As an example of this procedure, the following example may be considered. Assume that four conductors have parallel exposures on the same ROW as follows:

#1 - very long length (infinite)

#2 - very long length (infinite)

#3 - short length (ℓ)

#4 - short length (ℓ)

If all four conductors were infinite in length, the following impedance matrix would be entered into the calculator.

$$\begin{bmatrix} Z_{11} & Z_{12} & Z_{13} & Z_{14} \\ Z_{12} & Z_{22} & Z_{23} & Z_{24} \\ Z_{13} & Z_{23} & Z_{33} & Z_{34} \\ Z_{14} & Z_{24} & Z_{34} & Z_{44} \end{bmatrix} \tag{D-60a}$$

where it has been assumed that $Z_{ij} = Z_{ji}$.

However for the situation considered, based on Eqs. D-58 and D-59, the following modified matrix would be entered into the hand calculator program

$$\begin{bmatrix} Z_{11} & Z_{12} & Z_{13}\left(\frac{\Gamma_1\Gamma_3}{\Gamma_1+\Gamma_3}\right)\ell/2 & Z_{14}\left(\frac{\Gamma_1\Gamma_4}{\Gamma_1+\Gamma_4}\right)\ell/2 \\ Z_{12} & Z_{22} & Z_{23}\left(\frac{\Gamma_2\Gamma_3}{\Gamma_1+\Gamma_3}\right)\ell/2 & Z_{24}\left(\frac{\Gamma_2\Gamma_4}{\Gamma_2+\Gamma_4}\right)\ell/2 \\ Z_{13} & Z_{23} & Z_{33}\Big/\left(\Gamma_3\ell/2\right) & Z_{34}\left(\frac{\Gamma_4}{\Gamma_3+\Gamma_4}\right) \\ Z_{14} & Z_{24} & Z_{34}\left(\frac{\Gamma_3}{\Gamma_3+\Gamma_4}\right) & Z_{44}\Big/\left(\Gamma_4\ell/2\right) \end{bmatrix} \tag{D-60b}$$

REFERENCES

1. E. D. Sunde, Earth Conduction Effects in Transmission Systems, New York: Dover Publications, p. 149, 1968.

Appendix E

MOJAVE DESERT MITIGATION TESTS

INTRODUCTION

In mid-December 1977 a series of mitigation tests was carried out on the Southern California Gas Company 34-inch pipe 235 at Mileposts 101.7 and 88.7. At both locations a physical discontinuity occurs between the pipeline and the adjacent overhead power line, as shown in Figure E-1. Hence, these are sites of induced voltage peaks averaging in the neighborhood of 46 volts for a power line loading of 700 A.

The purpose of this series of tests was to verify design principles which had been developed for the horizontal type of mitigation electrode (connection made to pipeline). This type of electrode is also known as a counterpoise or shield wire, for configurations where no direct connection is made to the pipeline. As diagrammed in Figure E-1, a total of six separate mitigation wires were installed and tested. The details of the installations and their test objectives are summarized below.

Test Wire #1. This was a temporary installation at Milepost 101.7 of a 3.2 mm diameter aluminum wire having a maximum length of 2 km and at a nominal 5 cm depth. As shown in Figure E-1, the wire was installed perpendicular to the pipeline in order to minimize inductive and conductive coupling between the wire and pipeline, and also inductive coupling between the wire and overhead power line. In this configuration the wire acted as a grounding impedance for the pipeline. Tests with this wire consisted of connecting the wire to the pipeline and measuring the input impedance of the wire as a function of length. The purposes of these tests were: (1) to verify that as the length of the wire is increased its input impedance approaches the characteristic impedance asymptotically, and (2) to act as a control for subsequent related tests.

The principal conclusion derived from tests made using this wire is that the commonly accepted result that the grounding resistance of mitigation wire is inversely proportional to its length is correct only for moderate or shorter lengths; that is, increasing the length beyond a certain point will not result in a corresponding increase in mitigation effectiveness.

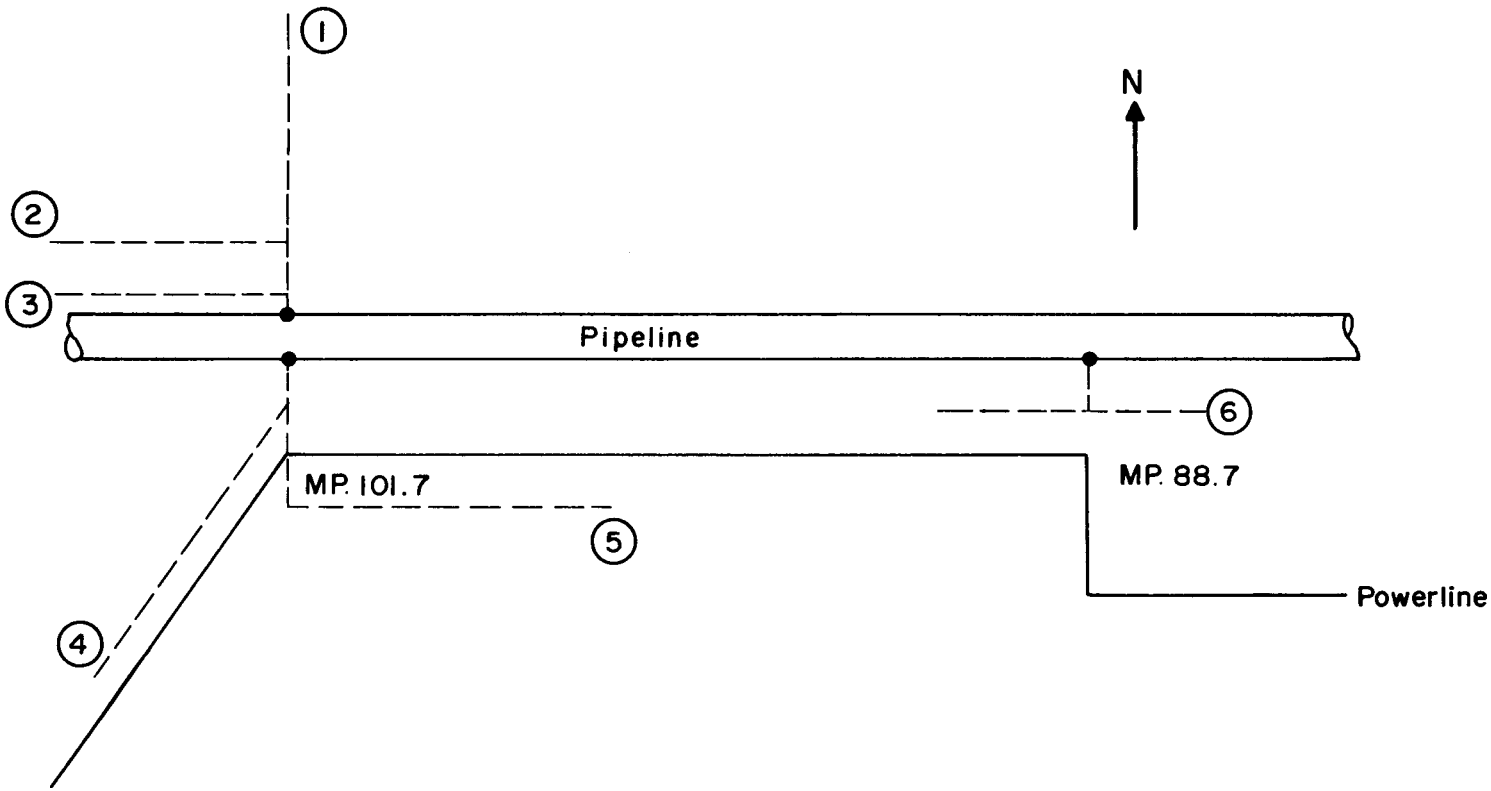

Fig. E-1 MOJAVE DESERT MITIGATION TESTS

Test Wire #2. This was a temporary installation of a 3 mm diameter aluminum wire, 1.77 km in length, at a burial depth of 5 cm. The wire was laid parallel to the pipe at a distance of 45 m, but in a direction away from the region of parallel exposure to the power line. Hence, coupling to the power line was kept to a minimum and primarily conductive and inductive coupling to the pipeline was obtained. By comparison of the performance of this wire with the test wire #1 configuration of the same lengths the magnitude of these coupling effects could be estimated. Experimental results, which are corroborated by the analysis of Appendix D show that for a reasonably well coated pipeline conductive coupling effects are negligible. Hence, mitigation wire design may be made on the basis of considering inductive coupling effects alone.

Test Wire #3. This wire was identical to wire #2 except that it was buried parallel to the pipeline at a distance of approximately six meters. This test wire showed that if the piepline is reasonably well coated, inductive effects predominate even at such a small separation. Hence, the achievement of good mitigation with the electrode confined to the ROW is possible. As a matter of fact, this wire was more effective in pipeline mitigation than wire #2 or #1 but the result was mostly attributable to the fact that this wire was lying in soil of lower resistivity, thus effectively reducing its grounding impedance.

Test Wire #4. This wire was of larger diameter than the previous wires in anticipation of its being a part of a more or less permanent installation. It was a 9.4 mm diameter aluminum wire, 1.25 km in length, buried at a nominal depth of 30 cm. It was placed parallel to the power line (between the power and pipe lines) at a distance of 18.3 m from the center phase wire of the power line. The purpose of this installation was to verify that the overhead power line induced a voltage in mitigation wire of such polarity as to aid, in addition to its low grounding resistance, in providing mitigation to the pipeline.

Also, because of its position, coupling of the wire to the pipeline was small, and the results of this test were used as a control for the following test wire measurements.

Test Wire #5. This wire was identical to test wire #4 except that it was placed parallel to the pipeline as shown and at a distance of 18.3 meters from the center phase wire in the direction away from the pipeline. The purpose of this installation was to evaluate conductive and inductive coupling effects to the pipeline and also to confirm the back-to-back mitigation concept developed during the program.

As with previous parallel wire installations, it was found that conductive coupling effects are negligible.

Test Wire #6. This mitigation wire was placed at Milepost 88.7, the location of the next voltage peak on the pipeline. The purpose of this installation was to verify that successive voltage peaks and intermediate voltage points could be mitigated by the placement of mitigation electrodes at consecutive points of physical or electrical discontinuity. This installation was temporary, consisting of a 3 mm diameter aluminum wire, 0.8 km in length, at a burial depth of 5 cm. It was placed at a distance of 30 meters and parallel to the pipeline. This wire was fed at the center, thus effectively placing both halves in parallel. This reduced the wire input resistance by a factor of two which yielded a higher mitigation effectiveness for a given length wire than obtained for the other test configurations (except for the back-to-back arrangement where test wires #4 and #5 were tied together).

The working principles, the design concepts and the test results are best explained in terms of electrical equivalent circuits which are discussed in the following section. However, as an aid to understanding the theory of the grounded horizontal electrode, the following basic principles should be remembered:

1. The electrode, by virtue of its distributed leakage, acts as a low impedance connection to remote earth. However,
2. Mutual inductive coupling between the power line, the pipeline and the mitigation wire will induce a voltage in the mitigation wire.
3. This voltage may effectively increase or decrease the effective wire impedance depending upon the interaction geometry, the wire and pipeline parameters, and the power line phasing.

MITIGATION WIRE (ELECTRODE) EQUIVALENT CIRCUITS

The theory and analysis of operation of the test wires is best explained in terms of electrical equivalent circuits for the test wires and the pipeline. The equivalent circuits are diagrammed in Figures E-2 and E-3 and are discussed individually in the following section.

Figure E-2a shows the electrical equivalent for the pipeline alone at Milepost 101.7. In the figure, E_0 is the electric field at the pipeline and γ is the pipeline propagation constant. Hence, the pipeline is driven by an equivalent

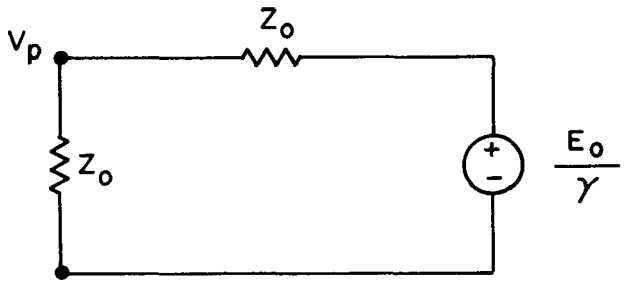

a) Pipeline Alone At MP 101.7

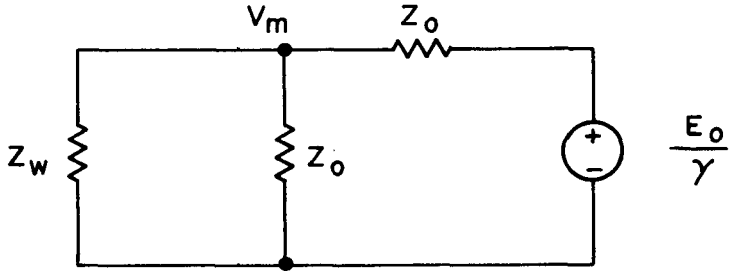

b) Test Wire No.1 Connected To Pipeline

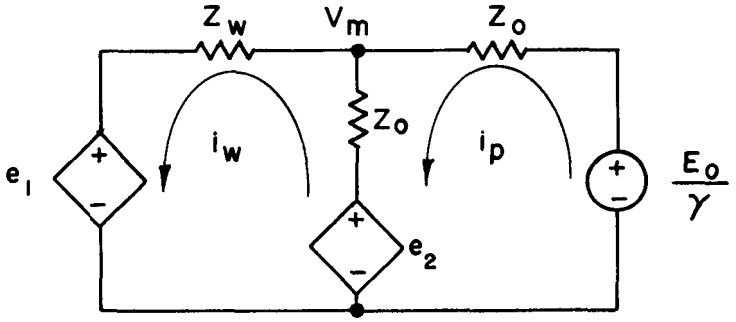

c) Circuit For Test Wires No.2 & No.3

Fig. E-2 MITIGATION TESTS - EQUIVALENT CIRCUITS

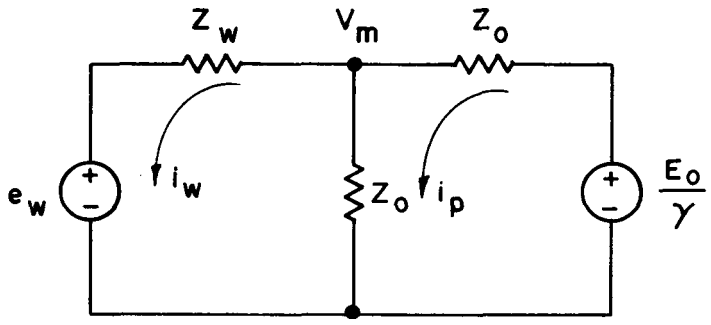

a) Test Wire No. 4

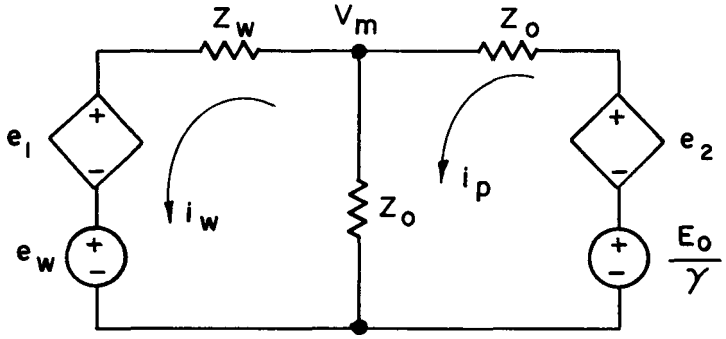

b) Test Wire No. 5

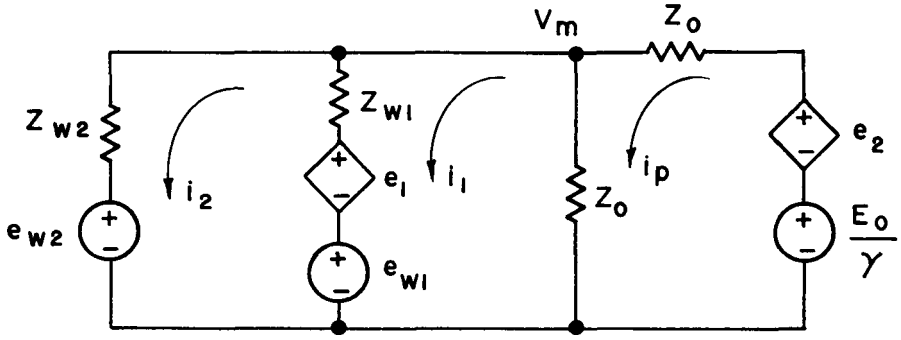

c) Test Wires No.4 And No.5 :
Back - To - Back

Fig. E - 3 EQUIVALENT CIRCUITS - WIRES No.4 & 5

voltage generator of E_o/γ having an internal impedance of Z_o ohms, i.e., its characteristic impedance. Since the power line leaves the pipeline ROW at this point, the equivalent circuit is completed by terminating the pipeline in its characteristic impedance, Z_o. Therefore, the induced pipe voltage at this location is $V_p = E_o/2\gamma$.

From the discussion in Section 3 of this pipeline's characteristics, it may be found that the following values apply for a nominal 700-ampere electric transmission line loading: $|E_o| = |14\underline{/-122.6}| = 14$ V/km and independent of loading, $|\gamma| = |0.115 + j\ .096| = |0.15|$ and $Z_o = 3.76\underline{/39.6^o}$. Hence, $V_p \simeq 46$ volts.

Test Wire #1

Due to its physical placement, this test wire acts effectively as grounding impedance Z_w, when connected to the pipeline. The mitigated pipeline voltage, V_m, can be calculated from the equivalent circuit of Figure E-2b and is equal to:

$$V_m = \frac{V_p Z_w}{Z_w + Z_o/2} \qquad \text{(E-1)}$$

The value of Z_w is a function of its length as plotted in Figure E-4. As shown by the data points in the figure, the input impedance of the wire was measured for several lengths. Using classical transmission line theory, the wire input impedance was calculated as a function of length and is plotted in the figure. Excellent agreement is obtained with the experimental data points. The procedure used in calculating the input impedance was as follows:

1. Sunde's transcendental equation was solved to obtain the mitigation wire propagation constant, γ_w. However, since the wire is circular in cross-section rather than tubular as is the pipeline, the following formula was used for the wire internal impedance, Z_i.

$$Z_i = \frac{1}{\pi a^2 \sigma}\left[1 + \frac{1}{48}\left(\frac{a}{\delta}\right)^2\right] + j\,\frac{\omega\mu}{8\pi} \text{ ohms/meter} \qquad \text{(E-2)}$$

where a is the wire radius and δ = skin depth = $(\pi\sigma f\mu)^{-\frac{1}{2}}$

This formula has been programmed into the program WIRE, thus allowing the solution for γ_w to be obtained directly.

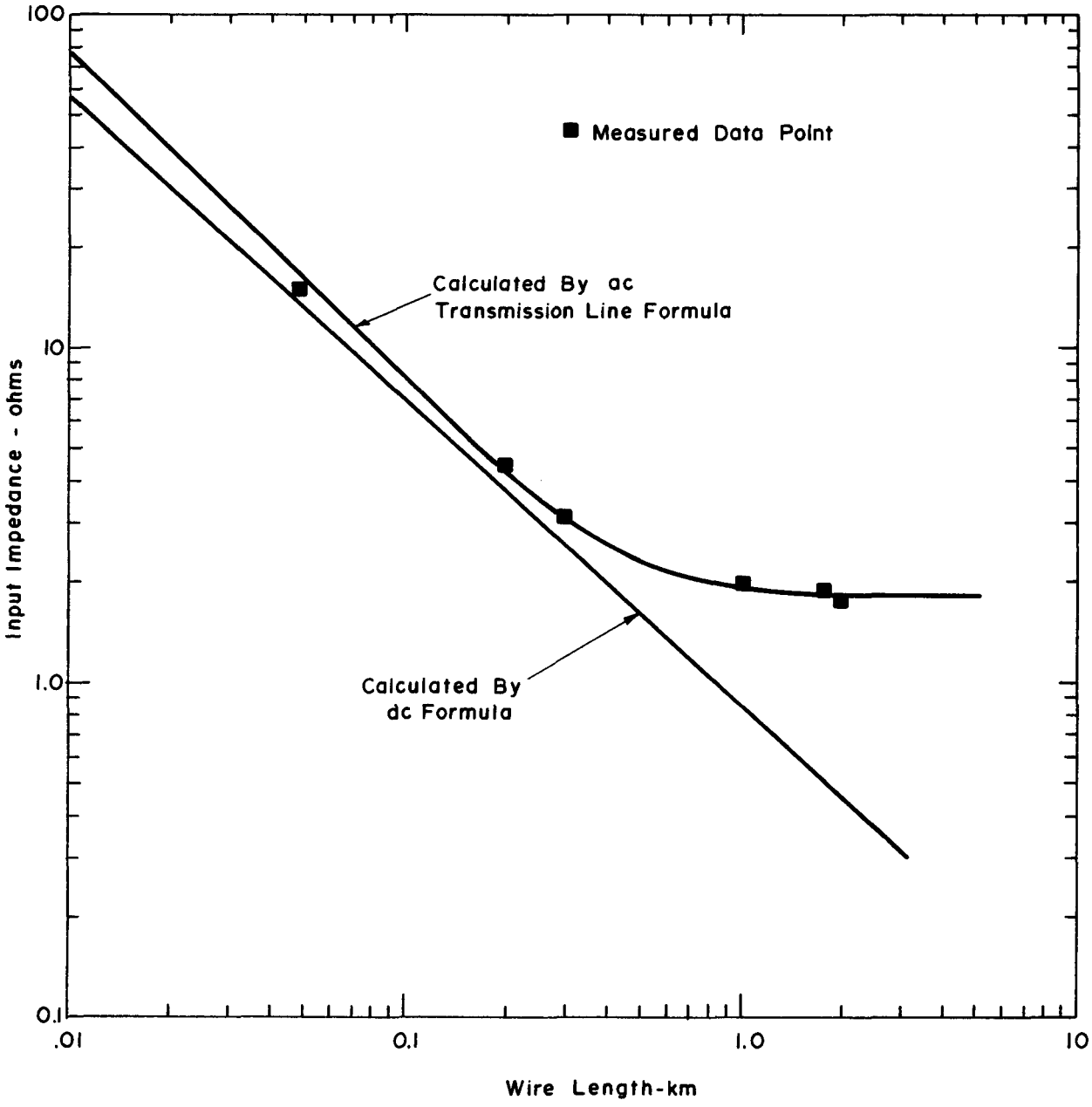

Fig. E-4 GROUNDING IMPEDANCE OF HORIZONTAL WIRE

2. The characteristic impedance of the wire, Z_{ow}, can then be obtained by means of the same program (cf. WIRE).

   Although the burial depth of the mitigation wire was nominally 5 cm, the actual depth varied from approximately twice that in several places to effectively near surface burial in many places. This was due to the fact that burial in this region was in dry loose sand which could not be adequately compacted after burial with the equipment used. Hence, in deriving the wire parameters γ_w and Z_{ow}, a burial depth equal to zero was assumed, and in fact, this assumption yielded the best fit to the experimental data. For the nominal (measured) ground resistivity of 200 ohm-meters measured in the region of this wire, the solution of Sunde's transcendental equation by program WIRE, yielded:

$$\gamma_w = 2.093 + j\ 0.312\ km^{-1} \qquad \text{(E-3a)}$$

$$Z_{ow} = 1.698 + j\ 0.235\ \text{ohms}. \qquad \text{(E-3b)}$$

The test wire considered as classical transmission line is characterized completely by the above parameters. Hence, assuming a far end infinite terminating impedance, the input impedance, as seen at the pipeline, may be calculated. The impedance calculations were made using the program THEVENIN. The results are plotted in Figure E-4 and agree excellently with the measured data points.

The principal feature of the plot in Figure E-4 is that as the length of the grounding wire increases, the grounding impedance of the wire does not decrease indefinitely, but approaches asymptotically the characteristic impedance of the wire. Hence, for a given grounding installation, there is an optimum length (in the vicinity of the knee of the curve) where the mitigation efficiency-cost ratio will be largest. Therefore, indiscriminately increasing the length of a grounding wire may not be necessarily cost effective.

This result is in sharp constrast with that obtained from use of the dc grounding resistance formula commonly employed, namely, for a horizontal wire lying on the surface of the earth,

$$R = \frac{\rho}{\pi \ell} \left(\ln \left(\frac{2\ell}{a} \right) - 1 \right) \qquad \text{(E-4)}$$

where

ρ = ground resistivity
ℓ = length of wire
a = radius of wire

A plot of Eq. E-4 is also made in Figure E-4. It can be seen that the above formula is accurate only for moderate conductor lengths. Eq. E-4 was originally derived under the premise that the voltage drop along the conductor may be neglected. This assumption is only true for conductor lengths short enough where the longitudinal resistance of the wire is of the order or smaller than the resistance of the wire to remote earth.

The calculated voltage, V_m, also corresponded well with measured data. For example, for a length of 2 km, the calculator program, THEVENIN, gives a wire input impedance of $1.714/\underline{7.85^o}$ ohms. From the equivalent circuit of Figure E-2b and the mitigation Eq. E-1,

$$\left|\frac{V_m}{V_p}\right| = \left|\frac{Z_w}{Z_w + Z_o/2}\right| \qquad \text{(E-5)}$$

$$= \left|\frac{1.714/\underline{7.85^o}}{1.714/\underline{7.85^o} + 1.88/\underline{39.6^o}}\right|$$

$$= 0.495$$

For this length of wire, measured data yields $|V_p|$ = 45 volts, $|V_m|$ = 22 volts, and hence, $|V_p/V_m|$ = 0.49, or a one percent difference (such close agreement should be regarded as coincidence since the voltmeters used were not accurate to this degree). Excellent agreement between measured and calculated values of $|V_m|$ were also obtained for a range of wire lengths down to 0.4 km, where a mitigated to unmitigated pipeline voltage ratio of approximately 0.6 was obtained.

Test Wire #2

The equivalent electrical circuit for test wire #2 is shown in Figure E-2c. For this wire, due to mutual inductive coupling between the mitigation wire and the portion of the pipeline west of Milepost 101.7, two current-controlled dependent voltage generators are added to the circuit, i.e., e_1 and e_2. Voltage e_1 arises because of the current carried in the pipeline west of Milepost 101.7 and generator, e_2, because of the current drained by the mitigation wire after connection to the pipe.

Generator Voltage, e_1. This voltage is generated by the current flowing in the pipeline west of Milepost 101.7 which, according to the mesh currents designated in Figure E-2c, is $(i_p - i_w)$. The electric field produced at the mitigation wire because of this current is $Z_{wp}\ (i_p - i_w)$. Because of the relatively small pipeline

propagation constant, this electric field is essentially constant for the length of the mitigation wire. For a constant electric field along a conductor which is open circuited at both ends, the voltage at the far end (x = L) may be found from the following equation as

$$V(L) = \frac{E_w}{\gamma_w}\frac{\left[1-e^{-\gamma_w L}\right]^2}{\left[1-e^{-2\gamma_w L}\right]} \qquad \text{(E-6)}$$

where

$E_w \equiv Z_{wp}(i_p - i_w)$

Z_{wp} = the Carson mutual impedance between the wire and the pipeline. (This value for the mutual impedance is commensurate with the value obtained in Appendix D, i.e., Eq. D-58b.)

In Eq. E-6, L = 1.77 km, and from Eq. E-3 it can be seen that the produce $\gamma_w L \gg 1$. Hence, Eq. E-6 becomes

$$V(L) \simeq \frac{Z_{pw}(i_p - i_w)}{\gamma_w} = e_1$$

since V(L) represents the open circuit Thevenin equivalent voltage for the mitigation wire before connection to the pipe.

Generator Voltage, e_2. The voltage e_2 is generated by the electric field produced at the pipeline by the drain-off current carried by the mitigation wire. Due to leakage to earth along the bare mitigation wire this current is a function of the distance along the wire from the point of connection to the pipeline. It varies in magnitude from a value i_w, as defined by the Milepost 101.7 equivalent circuit of Figure E-2c to a value of zero at the far end. A linear approximation to the current which simplifies the problem considerably is to assume a constant value equal to $i_w/2$ over the length of the wire. The electric field at the pipeline is then approximately equal to $Z_{pw}/\left|i_w/2\right|$. Since for this case $\gamma_w\gamma L/(\gamma_w+\gamma) < 1$ (c.f., Eq. D-15a), a modified value of Z_{pw}, the Carson mutual impedance must be used. Equation D-58d (Appendix D) shows $Z_{pw} \rightarrow Z_{pw}\gamma L$. Then the open circuit Thevenin voltage at the pipeline, e_2, may be found from Eq. 3-9a of Section 3 by assuming x = L, and that the pipeline is terminated in its own characteristic impedance. Hence,

$$e_2 = \frac{Z_{pw}\gamma L\, i_w}{4\gamma_w}\left[1-e^{-\gamma_w L}\right] \qquad \text{(E-8a)}$$

and since $\gamma_w L >> 1$

$$e_2 \approx \frac{Z_{pw}\, i_w\, \gamma L}{4\gamma_w} \qquad \text{(E-8b)}$$

Circuit Solution. Writing the mesh equations for the equivalent circuit of Figure E-2c, gives

$$(Z_o - Z_{pw}/\gamma_w)\, i_p - (Z_o + Z_w - Z_{pw}/\gamma_w - Z_{pw}\gamma L/4\gamma_w)\, i_w = 0 \qquad \text{(E-9a)}$$

$$(-2Z_o) i_p + (Z_o - Z_{pw}/4\gamma_w) i_w = -E_o/\gamma \qquad \text{(E-9b)}$$

$$|Z_o| \sim 4\,\Omega \qquad \text{(E-10a)}$$

$$|Z_w| \sim 2\,\Omega \qquad \text{(E-10b)}$$

$$|Z_{pw}/\gamma_w| \sim .15 \qquad \text{(E-10c)}$$

$$|Z_{pw}/4\gamma_w| \sim .04 \qquad \text{(E-10d)}$$

$$|\gamma L| \sim .26 \qquad \text{(E-10e)}$$

Eq. E-9 may then be simplified to

$$Z_o i_p - (Z_o + Z_w) i_w = 0 \qquad \text{(E-11)}$$

$$-2Z_o i_p + Z_o i_w = -E_o/\gamma$$

Solving Eq. E-11 yields

$$i_w = \frac{E_o}{\gamma(Z_o + 2Z_w)} \qquad \text{(E-12)}$$

$$i_p = \frac{(Z_o + Z_w)\, E_o}{(Z_o + 2Z_w)\, \gamma Z_o} \qquad \text{(E-13)}$$

and

$$V_m = \frac{E_o\, Z_w}{\gamma(Z_o+2Z_w)} = \frac{V_p\, Z_w}{(Z_w+Z_o/2)} \qquad \text{(E-14a)}$$

since

$$V_p = \frac{E_o}{2\gamma} \qquad \text{(E-14b)}$$

Eq. E-14a is identical to Eq. E-1, showing that for this case, where the inductive coupling is small, the horizontal wire lying parallel to the pipeline along the ROW will yield essentially the same mitigation performance as the perpendicular wire (#1). This result is correct only if the conductive coupling between the pipeline and mitigation wire is negligible. This is the situation here, since it can be shown that for one of the conductors reasonably well coated, e.g., the pipeline, that the coefficient of conductive coupling as defined by Eq. D-12 (Appendix D) is much smaller than one. This condition was verified indirectly in that for all the test wires after inductive effects were taken into account, no evidence of conductive coupling effects could be found.

For this test wire mutual coupling effects between the wire and the pipeline were small enough to be ignored when calculating the pipeline and mitigation wire currents. Hence, the value of the open circuited induced voltage, e_1, in the mitigation wire is found to be a small fraction of the mitigated voltage. Therefore, the mutual inductive coupling effects in this case do not reduce the effectiveness of the mitigation wire even though the wire is placed parallel to the pipeline along the same ROW. This conclusion is verified by the following sample calculation.

Sample Calculation. The map of Figure E-1 shows that the wire was placed parallel to the pipeline except for a perpendicular 46 m section which connected the wire to the pipeline. This perpendicular section was actually part of Test Wire #1 lying in sand with a near-surface resistivity of about 200 ohms/meter. However, ground resistivity in the parallel section increased rapidly towards the west to values of 400 to 600 ohms/meter. Hence, an average ground resistivity over the path of this wire of 400 ohms/meter has been assumed. Using this value in the solution of Sunde's transcendental equation yields the following parameters for the test wire:

$$\gamma_w = 1.460 + j\ 0.223 \qquad \text{(E-15a)}$$

$$Z_{ow} = 2.437 + j\ 0.343 \qquad \text{(E-15b)}$$

Using these parameters in the calculator program THEVENIN yields the result that, for the 1.77 km length of wire, the input impedance is

$$Z_w = 2.47/\underline{7.5^o} \qquad \text{(E-16)}$$

Substituting Eq. E-16 and the appropriate pipeline parameters into Eq. E-12, E-13, and E-14 gives

$$i_w = \frac{14/\underline{-122.6}}{(.15/\underline{39.9})\ [3.76/\underline{39.6} + 2(2.48)/\underline{7.5^o}]} \qquad \text{(E-17)}$$

$$= 11.1/\underline{176.2} \text{ amperes}$$

$$i_p = \frac{(3.76/\underline{39.6} + 2.48/\underline{7.5})\ 14/\underline{-122.6}}{(3.76/\underline{39.6} + 2(2.48)/\underline{7.5}) \cdot (.15/\underline{39.9})(3.76/\underline{39.6})} \qquad \text{(E-18)}$$

$$= 17.8/\underline{163.5} \text{ amperes}$$

$$V_m = \frac{14/\underline{-122.6}}{.15/\underline{39.9}\ (3.76/\underline{39.6} + 2(2.48)/\underline{7.5})} \qquad \text{(E-19)}$$

$$= 27.6/\underline{-176.3^o}$$

and

$$V_p = 46.7/\underline{-162.5^o} \qquad \text{(E-20)}$$

Using the calculator program CARSON, the pipeline mitigation wire mutual impedance is found as

$$Z_{pw} = .279/\underline{77.7^o} \qquad \text{(E-21)}$$

and from Eq. E-7,

$$e_1 = \frac{.279/\underline{77.7}(17.8/\underline{163.5} - 11.1/\underline{176.2})}{1.460 + j\ 0.223} \qquad \text{(E-22)}$$

$$= 1.4/\underline{-146.8^o}$$

The value of e_1 is approximately five percent of the calculated value of V_m. Hence, the approximations leading to Eq. E-11 can cause a five percent error in computed quantities, which is considered acceptable. For example, because e_1 is a bucking voltage with respect to the wire current, it would be expected that i_w would be about five percent lower than actually calculated, i.e., $11.1 \div 1.05 \approx 10.6$ amperes.

Field Measurements. In December 1977, data were taken on the mitigation wire before and after connection to the pipeline. During the period data were taken the power line was carrying somewhat less than the nominal 700 amperes, i.e., giving a pipeline voltage, V_p, of 41.5 volts rather than 46.7 volts. Hence, since the calculations made here are based on a 700 ampere loading, the field data must be multiplied by the factor $46.7 \div 41.5 = 1.125$ to obtain the proper normalization. Measured quantities were as follows, with the calculated values alongside in parentheses.

$V_p = 41.5 \times 1.125 = 46.7$ (normalized value)

$V_m = 23.5 \times 1.125 = 26.4$ V (27.6 V)

$I_w = 9.3 \times 1.125 = 10.5$ A (10.6 A)

$|e_1| = 1.95 \times 1.125 = 2.2$ V (1.4 V).

Except for the open circuit mitigation wire voltage, e_1, the data are in excellent agreement with calculated data. It was noted in the field, however, that the value of e_1 would vary over a period of a day quite significantly, up to 60-80 percent without corresponding changes in the other data. Such a variation in e_1 is not considered significant because of the low value of e_1; that is, stray fields from circuits miles away could account for variations at such low voltage levels. The phase difference between the pipe voltage and the mitigation wire open circuit voltage was also measured at the time with the wire 23.6^{o} positive with respect to the pipe. Comparison of Eqs. E-20 and E-22 gives an answer of 15.7^{o}, which is reasonably accurate considering the possibility of stray fields.

Test Wire #3

The intent of this wire was to check for conductive coupling effects. However, none were experimentally apparent as would be expected from considerations given in Appendix D.

For this wire, inductive coupling effects were of the same order as for test wire #2, even though the distance to pipeline was reduced to approximately six meters. Although the mutual impedance, Z_{pw}, increased to $0.40/\underline{81.5^{o}}$ ohms, this wire was lying in soil with a resistivity of approximately 200 ohms/meter. Thus, the wire parameters, γ_w and Z_{ow}, for this wire were similar to those for test wire #1. Hence, the ratio, $|Z_{pw}/\gamma_w|$ is approximately 0.19 for both test wires #2 and #3. Therefore, with a few percent error, mutually coupled inductive effects can be ignored, and the mitigation effectiveness is primarily due to the input impedance of the test wire.

Measurements made on this wire under several conditions showed a $|V_m/V_p|$ ratio ranging from 0.48 to 0.51, which is commensurate with the result calculated for test wire #1 (c.f., Eq. E-5).

Test Wire #4

This wire did not parallel the pipeline, thus reducing mutual coupling effects to negligible proportions. However, it paralleled the power line and thus a voltage, e_w, was induced on the wire as shown in the equivalent circuit of Figure E-3a.

A trial design for this wire was discussed in Section 8. The design was based upon the assumption of a 40 kΩ - cm ground resistivity which was found to be incorrect from measurements made after burial of the wire.

Revised design parameters, the design procedure and accompanying field measurement data are as follows:

Pipeline Parameters.

1. Assumption of a 700 kΩ-ft^2 pipe coating resistivity, a 40 kΩ-cm earth resistivity along the pipeline route, and a 700 ampere balanced power line current loading.

2. Use of the calculator program CARSON to calculate the driving electric field, E_o, at the pipeline as being equal to 14 volts/km at a phase of -122.6^o relative to the power line currents.

3. Interpolation of the graphs of Figure 2-7 to obtain the pipeline propagation constant, γ, equal to $(0.115 + j\ 2.4)\Omega$.

Mitigation Wire Parameters. This part of the analysis computes the Thevenin equivalent source impedance, Z_w, and source voltage, e_w. The computation involves the following steps:

1. Assumption of a wire burial depth of one foot, a 10 kΩ - cm soil resistivity at the wire and a 700 ampere balanced power line current loading.

2. Use of calculator program CARSON to calculate the driving electric field at the wire as being equal to 19.5 V/km at a phase angle of -122.1^o relative to the power line currents (note: since the mitigation wire extends over several power line tower spans, the geometric mean height of the power line wires must be used, i.e., $h = (h_{max}\ h_{min})^{\frac{1}{2}}$).

3. Use of the calculator program WIRE to obtain the propagation constant of the mitigation wire, γ_w, equal to $(1.662 + j\ .806)$ km^{-1}, and the wire characteristic impedance, Z_{ow}, equal to $(0.369 + j\ 0.154)\Omega$. Calculations were made for a 0.372 inch diameter bare aluminum wire without inductive loading. Previous calculations used in the example of Section 8 assumed inductive loading of this wire. However, because of terrain features, and the method used for wire laying, it was decided not to continuously load the wire inductively because of possible multiple point wire breakage. (Some testing done with a single coil inductance placed at the end of the wire will be discussed later).

4. Use of the program THEVENIN to obtain $Z_w = 0.394/\underline{20.9^o}$ Ω and $e_w = 9.4/\underline{44.2^o}$.

Computation of V_m and i_w. From the equivalent circuit of Figure E-2d, analysis yields,

$$i_w = \frac{\frac{E_o}{2\gamma} - e_w}{Z_w + Z_o/2}$$

$$= \frac{46.7/\underline{-162.2} - (9.4)/\underline{44.2^o}}{(.394/\underline{20.9^o}) + 1.88/\underline{39.6}}$$

$$= 24.5/\underline{165.7} \text{ amperes} \qquad \text{(E-23)}$$

and

$$V_m = i_w Z_w + e_w$$

$$= (24.5/\underline{165.7})\ (.394/\underline{20.9}) + 9.4/\underline{44.2}$$

$$= 9.65/\underline{186.6} + 9.4/\underline{44.2}$$

$$= 6.1/\underline{117.6} \text{ volts} \qquad \text{(E-24)}$$

Measured data (normalized to a 700 ampere power line loading) were $V_m = 6.8$ volts and $i_w = 24.6$ amperes, thus showing excellent agreement. The measured value of e_w was 9.8 volts.

Inductive Loading of Mitigation Wire. Equation E-24 shows a mitigated pipeline voltage of 6.1 volts with the voltage components, $(i_w Z_w)$ and e_w, 142.4^o out of phase. If, however, these components were 180^o out of phase, then near cancellation would occur and V_m would approach zero. The concept of inductive loading of the mitigation wire arose in an attempt to force such a condition in the field.

Analysis of the equivalent circuit shows that the condition $V_m = 0$ requires that $e_w/Z_w = -E_o/\gamma Z_o$. The right hand side of the equation is a function of the pipeline and power line characteristics and, hence, is fixed. However, continuous or near continuous loading of the mitigation wire, for example, by inserting many

small coils on a repetitive basis in series with the mitigation wire would effect a modification of its internal impedance and, hence, its propagation constant and characteristic impedance. These parameter changes would, in turn, result in a more favorable ratio, e_w/Z_w. Due to the crude wire installation method used and the minimal time available, it was decided to forego the continuous loading and secure a more advantageous ratio by loading with a single coil placed at the near end of the wire which would modify the value of Z_w only. Based upon the ground resistivity value assumed in the Section 8 example, a coil was designed which would theoretically reduce the pipeline voltage by an additional 25 percent. (L = 1658 μH, ωL = 0.625Ω.)

Due to the fact that the actual ground resistivity was much lower than assumed, the coil reactance was significantly larger than the wire input impedance and insertion of the coil increased the pipeline voltage by 18 percent. If it were not for the fact that simultaneously a more favorable phase angle relationship was indeed achieved, a more detrimental effect would have occurred. Hence, although an improvement was not observed directly, the performance that resulted can be accounted for by the equivalent circuit theory presented here. Therefore, it is believed that a proof of concept was obtained.

Test Wire #5

As shown in Figure E-1, this test wire was buried parallel to the pipeline and east of Milepost 101.7. Originally planned to be 1.25 km long, its actual length was approximately one km, due to a surveying error. As assumed in Section 8, this wire was to be essentially a mirror image of test wire #4 and, hence, ultimately to be used in a back-to-back arrangement with wire #4.

The soil resistivity in the region of this wire was approximately 30 kΩ-cm, giving the following transmission line parameters to the wire: $\gamma_w = .957 + j\ .492\ km^{-1}$; $Z_{ow} = .664 + j\ .292$ ohms. Use of the program THEVENIN yields an input impedance for the 1 km length of wire as $Z_w = .852/9.6^o$ and a terminal voltage of $.472/\underline{-184.1}^o$ for an internal source electric field of 1 volt/km directed in an easterly direction.

The equivalent circuit for the mitigation wire connected to the pipeline at Milepost 101.7 is shown in Figure E-3b. Here, two current-controlled dependent voltage generators are introduced into the circuit to account for mutual coupling

effects between the pipeline and the mitigation wire. Voltage generator e_2 is small compared to the pipeline driving generator, E_o/γ, and may generally be ignored. (It is a function of i_w, the mitigation wire current, which is a decreasing function along the wire, and the pipeline-wire mutual impedance, which is smaller than the Carson mutual impedance due to the shortness of the wire length (c.f., Eq. D-58d.) These factors combine to make the voltage relatively small. The voltage e_1 is a function of the pipeline current i_p east of Milepost 101.7. Values for the circuit voltage generators are derived as follows. As before, $E_o/\gamma = (14/\underline{-122.6}) \div (.15/\underline{39.9}) = 93.3/\underline{-162.5}$ volts. Then, using program CARSON, the free electric field (due to the power line phase currents only) at the mitigation wire was calculated to be $19.5/\underline{57.9^o}$ volts/km at a 700 ampere loading. For the generator polarity shown in the circuit

$$e_w = (19.5/\underline{57.9^o})\ (.472/\underline{-184.2^o + 180^o}) = 9.2/\underline{53.7^o} \text{ volts} \qquad \text{(E-25)}$$

The voltage e_1 is equal to

$$e_1 = i_p Z_{pw}(.472/\underline{-184.2^o}) \qquad \text{(E-26a)}$$

where Z_{pw} is the wire to pipeline Carson mutual impedance calculated to be $0.239/\underline{75.6^o}$ ohms. e_1 then becomes

$$e_1 = i_p(.112/\underline{-108.6^o}) \qquad \text{(E-26b)}$$

Before connection of the mitigation wire to the pipeline, an induced voltage can be measured to ground at the near end of the wire equal to $e_w + e_1$. Under this condition, $i_p = E_o/2\gamma Z_o = (12.4/\underline{-202.1^o}$. Hence,

$$e_w + e_1 = 9.2/\underline{53.7^o} + [(12.4/\underline{-202.0^o}) \cdot (.112/\underline{-108.6^o})] \qquad \text{(E-27)}$$

$$= 10.6/\underline{53.1^o} \text{ volts.}$$

A voltage of 9.9 volts was measured in the field.

After connection of the mitigation wire to the pipeline, a mesh current solution for the equivalent circuit yields,

$$i_w = 21.3/\underline{174.2^o} \text{ amperes} \qquad \text{(E-28a)}$$

$$i_p = 22.8/\underline{165.4^o} \text{ amperes} \qquad \text{(E-28b)}$$

the mitigated voltage, V_m is

$$V_m = (i_p - i_w)Z_o = 13.9/\underline{143.2^o} \text{ volts.} \qquad \text{(E-28c)}$$

Pipeline current could not be directly measured in the field. However, measured values of i_w and V_m were 20.2 amperes and 15.3 volts, respectively, which are within 10 percent or less of the calculated values.

Back-to-Back Arrangement. The equivalent electrical circuit for the back-to-back connection of test wires #4 and #5 is shown in Figure E-3c. Rigorous solution of this circuit is tedious and based upon the results just obtained for the individual wire analyses is probably unwarranted. The previous analyses showed that e_2 was very small compared to E_o/γ and could be ignored. In addition, e_1 was considerably smaller than e_w, and if a somewhat larger error than 15 percent was tolerable in predicting the mitigated voltage, it could also be ignored. The important fact to be remembered here is that the back-to-back arrangement utilizing the phase reversal inherent in switching a wire from one side of the power line to the other side results in $e_{w1} \simeq e_{w2}$. The equivalent circuit of of Figure E-3c may then be simplified to that of Figure E-3a, where $e_w = e_1 \simeq e_{w2}$, and Z_w is equal to the parallel combination of Z_{w1} and Z_{w2}. Hence, taking the average value of e_{w1} and e_{w2} gives $e_w \approx 9.3/\underline{48^o}$ and for $Z_{w1} = .852/\underline{9.6^o}$ and $Z_{w2} = .394/\underline{20.9^o}$, the value of Z_w is $.271/\underline{17.3^o}$. Solving the equivalent circuit of Figure E-3a for the mitigated pipeline voltage then gives, $V_m - 6.6/\underline{96.5^o}$. This compares well with the value of 6.0 volts obtained by direct measurement. Even though the simplifications noted above have been made, it is apparent that the accuracy of the calculation is acceptable.

Test Wire #6

This wire was originally designed to be the least ambitious in that its length was the shortest (0.8 km) and the purpose of the installation was to show that mitigation of successive voltage peaks was possible. Yet, on a per unit length basis, it out-performed most other test wires (because of the center connection, a relatively low input resistance was obtained).

Its chief distinguishing feature was that connection to the pipe was made at the wire center, but without the phase reversal as obtained in the back-to-back arrangement at Milepost 101.7. The equivalent circuit for this test wire is similar to that for the back-to-back arrangement, except that an additional current controlled voltage generator is required in the extreme left circuit branch between the elements e_{w2} and Z_{w2}. However, because of the short length of each leg (0.4 km), it will be found that the voltages induced in the test wires due to current flowing in the pipeline will be relatively small and, hence, this generator and the generator e_1 may be ignored. The generated voltages, e_{w1} e_{w2}, caused by the direct field from the power line will be in phase oposition and, hence, will cancel out in the Thevenin equivalent circuit for both legs of the mitigation wire. Therefore, the mitigation wire can be approximated by a simple impedance consisting of the parallel combination of the input impedance of each leg.

Input Resistance. Even though designed as a temporary installation, the burial depth of the wire averaged about four to six inches. The soil resistivity in this area averaged 35,000 Ω-cm. Computation of the mitigation wire parameters for these factors yielded, $\gamma_w = 2.174 + j\,0.193\ km^{-1}$ and $Z_{ow} = 1.825 + j\,0.142$ ohms.

Computation of the input impedance of the mitigation wire (both legs effectively in parallel) using the THEVENIN program gives $Z_w = 1.3/\underline{1.26^o}$ ohms. This computed value compares excellently with a measured value of 17.2V ÷ 13.3A = 1.29 ohms.

Since the mitigation wire is shunted across the pipeline, the mitigation factor is

$$\frac{Z_w}{Z_o/2 + Z_w} = \frac{1.3/\underline{1.26}}{1.88/\underline{39.6} + 1.3/\underline{1.26}} = 0.43/\underline{-22.9^o}\ . \qquad \text{(E-29)}$$

Field measurements indicated that a mitigated voltage at this location of 17.2 V exists with an unmitigated pipeline voltage of 48 V for a factor of .358. This represents actually a voltage level 20 percent lower than that calculated by Eq. E-29. This result is surprising in that previous calculations have shown a much closer correspondence to measured values. In addition, a much closer correspondence would be expected since the calculated and measured values of Z_w agree almost exactly.

Since the only other variable in Eq. E-29 is the pipeline characteristic impedance, it would appear that its value is higher at Milepost 88.7 than at Milepost 101.7. A somewhat higher ground resistivity and, possibly, a better pipeline coating in this region could account for an increase in Z_0. The value of Z_0 can be estimated indirectly by calculating γ from the measured voltage profile along the pipeline. From a previous pipeline voltage survey it was ascertained that the value of γ was approximately 19 percent smaller at Milepost 88.7 than at Milepost 101.7. Since the pipe internal impedance tends to stay relatively constant, it can then be inferred that the value of Z_0 at Milepost 88.7 is commensurately higher. Increasing the value of Z_0 by this amount in Eq. E-29 results in a mitigation factor of 0.39. Using this factor, the difference between the predicted and the measured mitigated voltage on the pipeline is on the order of 8 percent.

Complete Pipeline Mitigation

The previously discussions were directed towards considering each mitigation wire individually and, hence, mitigation at a single point on the pipeline. In general, due to physical or electrical discontinuities along the ROW, a pipeline will develop a number of induced voltage peaks. To show that successive voltage peaks can be mitigated successfully, and hence, a complete pipeline,mitigation test wire #6 at Milepost 88.7 was used in conjunction with the back-to-back arrangement (test wires #4 and #5) at Milepost 101.7. The results show that complete pipeline mitigation is possible by mitigating successive peaks individually. However, it must be cautioned that the incorporation of a mitigation wire at an induced voltage peak can, in itself, act as a discontinuity and hence affect the voltage level at another location along the pipeline. The magnitude and locations of such effects can readily be ascertained (although possibly somewhat laboriously) using classical electrical transmission line theory.

Such computations were not made, but a qualitative assessment of these effects were obtained by direct measurement which are summarized in the graphs of Figure 5. The upper graph shows the mitigation obtained using the back-to-back arrangements at Milepost 101.7. Here it is seen that the voltage peak at Milepost 101.7 is essentially mitigated and, in fact, some mitigation is achieved at Milepost 88.7. However, although not necessarily serious, an increase in the induced voltage occurs in a region between the two peaks. This is due to the fact that a relatively large amount of mitigation is occurring at Milepost 101.7, and hence, a rather severe discontinuity is presented to the pipeline at this

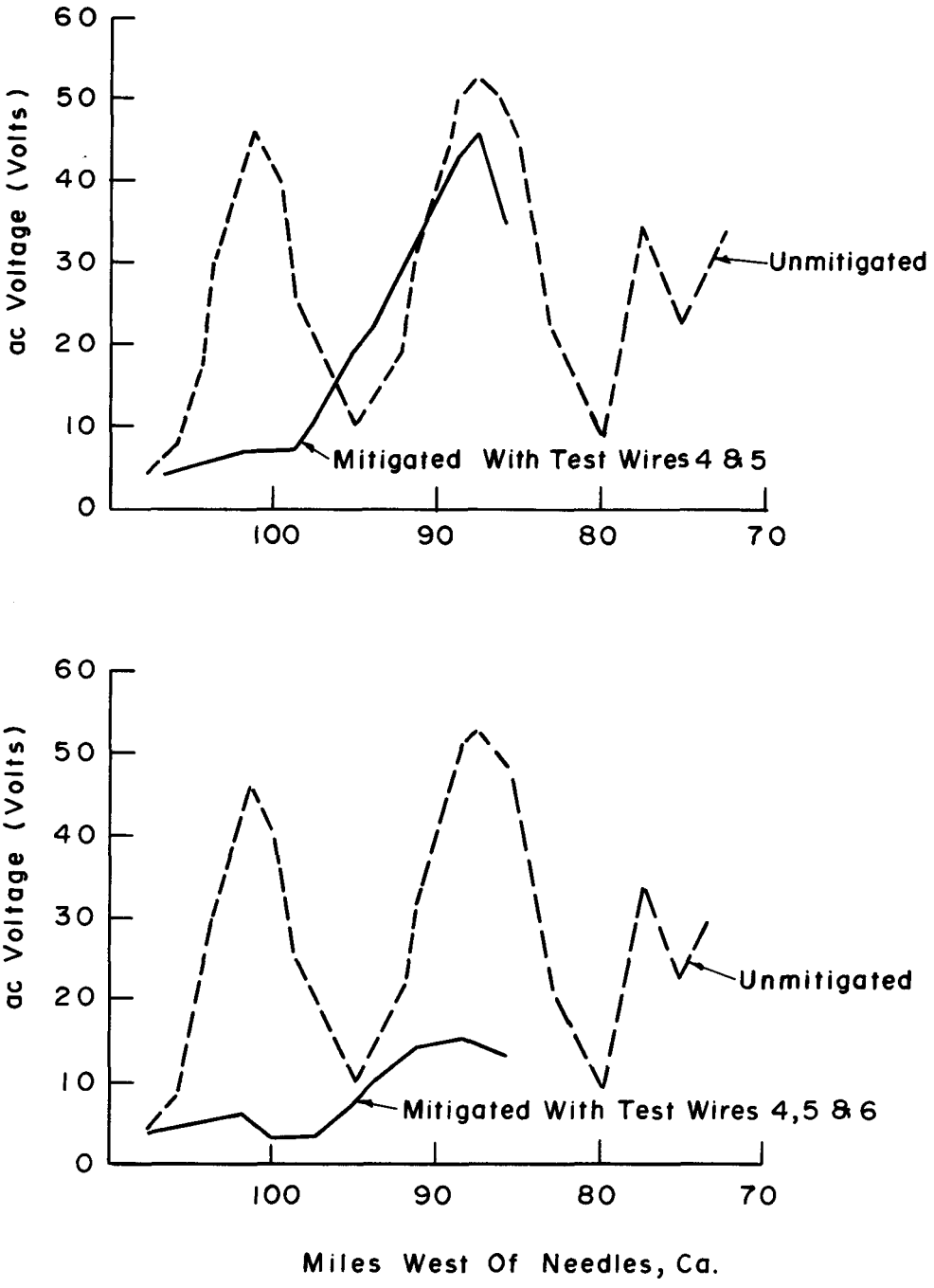

Fig. E-5 PIPELINE VOLTAGE PROFILE

location. Somewhat of a "balloon" effect occurs -- a squeeze at one point causes a size increase at another. However, this effect can be reduced or eliminated entirely by limiting the amount of mitigation secured at a given location.

The lower graph of Figure E-5 shows the mitigation achievable using test wires at both locations. The plot readily demonstrates that successive voltage peaks can be mitigated not only at the peaks, but at intermediate locations as well. (Data were not obtained east of Milepost 84 because of poor terrain that required a four-wheel drive vehicle which was not obtainable at the time.) Hence, by a reasonable placement of mitigation wires at points of discontinuity, long lengths of pipeline can be mitigated effectively.

APPENDIX F

PHASE SEQUENCING AS A METHOD OF REDUCING THE INDUCED ELECTRIC FIELD LEVELS ON A POWER LINE RIGHT OF WAY

INTRODUCTION

For certain ac power line configurations it is possible to sequence the phase conductors in such a manner so as to minimize the induced electric field on the right of way (1,2). The effectiveness of such phase sequencing has been studied for three common power line geometries. The results indicate that for certain geometries and proper phase conductor sequencing, the induced electric field levels can be significantly reduced. The technique is especially appropriate for vertically stacked circuits, particularly the double circuit configuration.

SINGLE CIRCUIT HORIZONTAL GEOMETRY

The first geometry considered is that presented in Figure F-1, the single circuit horizontal. There are six possible phase sequences for this geometry. Let A represent the 0^{o} phase conductor, B the $+120^{o}$, and C the -120^{o} conductors, respectively. The six phase combinations can then be placed into one of two possible categories - the clockwise and counterclock sequences. In Figure F-1, referring to the phase conductors from left to right, the phase combinations ACB, BAC and CBA are defined as clockwise, while ABC, BCA and CAB are counterclockwise. The electric field induced by a clockwise sequence is the mirror image of that produced by a counterclockwise sequence under balanced loading conditions. For each of the phase combinations within each classification, the magnitude of the electric field is the same and the phase is shifted $\pm$ 120 degrees at a given field point.

Using the power line geometry of Figure F-1, a comparison of the induced electric fields at equidistant locations to either side of the power line is presented in Table F-1. These results are for a clockwise phase sequence and equal phase currents of one hundred amperes per conductor. For the balanced counterclockwise phase sequence, the results would be the reverse of those presented in this table.

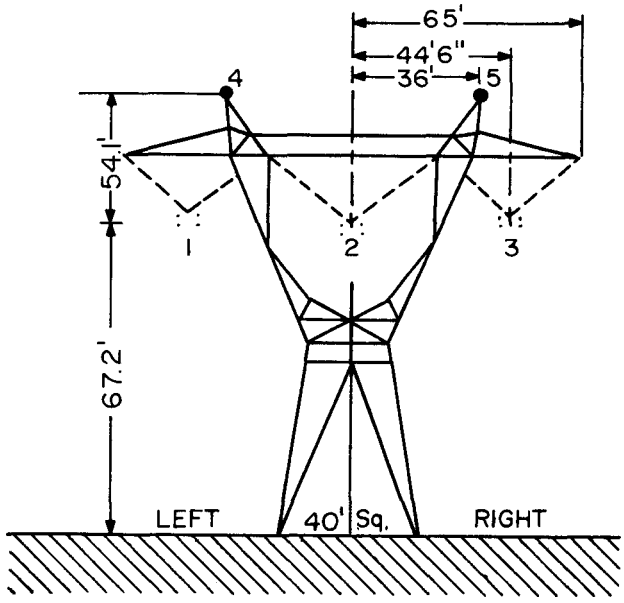

Note: Drawing not to scale

Figure F-1. Horizontal Power Line Geometry

Table F-1

CLOCKWISE PHASE SEQUENCE FOR BALANCED HORIZONTAL CIRCUIT

Distance from Center Phase (feet)	E_{CW} - Right Side (V/m)	E_{CW} - Left Side (V/m)	Percent Difference
0	.00225	.00225	0.0
50	.00521	.00502	4.65
100	.00490	.00472	3.88
150	.00368	.00351	4.62
200	.00287	.00271	5.57
250	.00232	.00218	6.03
300	.00195	.00181	7.18
350	.00167	.00155	7.19
400	.00146	.00134	8.2
450	.00129	.00118	8.53
500	.00115	.00105	8.7

As these results indicate, by placing the pipeline on the proper side of the power line right of way, the electric field exposure levels can be reduced by as much as 8.7 percent. Since the voltage induced on the pipeline is directly proportional to the electric field, it too can be reduced by this same percentage. If the skywires are not continuous and periodically grounded as assumed in the above analysis, then there is no significant advantage of one phase sequence over another. Under these circumstances the magnitude of the electric field is essentially equal on either side of the power line and the relative phase between the two field locations is approximately 180 degrees.

SINGLE CIRCUIT VERTICAL GEOMETRY

The single circuit vertical configuration analyzed is shown in Figure F-2. This configuration also has six possible phase combinations. These, again, can be classified into one of two possible categories, clockwise or counterclockwise phase sequencing. From Figure F-2, referring to the phase conductors from top to bottom, the phase combinations ACB, BAC and CBA are again defined as clockwise while ABC, BCA and CAB as counterclockwise. Within each of these two classifications, the electric fields are very similar. Their magnitudes are identical but their phases are shifted by $\pm$ 120 degrees. There isn't a simple mirror image relationship between the two phase groups as was the case for the balanced single horizontal circuit. Although the peak values of the electric field reverse to the opposite side of the power line, the magnitude is as much as five percent greater for the counterclockwise sequence as compared to that for the clockwise case. The relative phase between groups is also no longer $\pm$ 120 degrees but rather some intermediate value. These differences are directly due to the asymmetrical geometry characteristic of a single circuit vertical. By switching from a clockwise to a counterclockwise phase sequence, the required line symmetry is not present and, therefore, a mirror image electric field will not be induced.

Table F-2 presents the induced electric fields for both sides of the power line with a clockwise phase sequence and balanced currents of 100 amperes per phase conductor. As Table F-2 indicates, an induced voltage reduction of nearly 15 percent would be possible by merely placing the pipeline on the right side of the power line rather than the left for a clockwise phase sequence and assuming the geometry of Figure F-2. The reverse placement would be required for a counterclockwise phase sequence. This voltage reduction is significant when it is realized that it is solely a result of locating the pipeline on a particular side

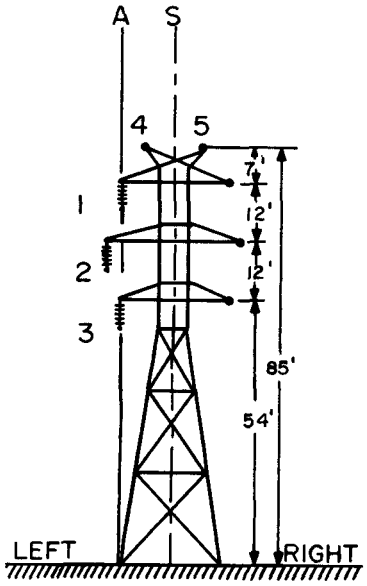

Figure F-2. Single Circuit Vertical Geometry

Table F-2

CLOCKWISE PHASE SEQUENCE FOR SINGLE CIRCUIT VERTICAL GEOMETRY AND BALANCED LOAD CURRENTS

Distance from Center Phase (feet)	E_{cw} - Right Side (V/m)	E_{cw} - Left Side (V/m)	Percent Difference
0	.00461	.00461	0.0
50	.00220	.00232	5.17
100	.00114	.00129	11.63
150	.00080	.00093	13.98
200	.00064	.00075	14.67
250	.00055	.00063	12.7
300	.00048	.00055	12.73
350	.00043	.00049	12.25
400	.00039	.00044	11.36
450	.00036	.00041	12.2
500	.00033	.00037	10.8

of the right of way. It is a consequence of the physical interaction of the induced electric fields from all the power line conductors.

DOUBLE CIRCUIT VERTICAL GEOMETRY

The double circuit vertical geometry studied is shown in Figure F-3. Assuming a balanced current flow, there are thirty-six possible phase sequences for this configuration. Of this total number of phase combinations there are five sets of six each which are closely related and two additional sets of three each. Within each set of six phase combinations, three are exact mirror images of the other three in the set. For the three phase sequences which form a subset, the electric field magnitude is constant and the relative phases are 120 degrees apart. Table F-3 lists the possible sets of phase sequences and their corresponding mirror image sequences where appropriate.

The induced electric fields associated with the first five sets of phase sequences presented in Table F-3 are asymmetrical about the power line. Therefore, for a given phase sequence and balanced currents, the electric field levels can be smaller on one side of the power line right of way than on the other. Table F-4 presents the relative electric field values for one phase sequence from each of the seven possible categories. These values were calculated using the power line geometry of Figure F-3 and assuming 100 amperes per phase wire. As this table illustrates, for a given phase sequence there is usually an optimum side of the right of way to locate the pipeline. Since the induced voltage on the pipeline is directly proportional to the electric field exposure levels, putting the pipe on that side of the right of way with smaller electric field values will result in lower induced voltage levels on the pipeline.

Table F-4 also clearly illustrates the advantage of some phase sequences over others in reducing the electric field levels across the entire powerline right of way. A comparison of phase sequences ABC CBA and ABC ABC indicates that the induced electric field can be reduced by over 92 percent directly under the power line and from 80 to 90 percent off to either side of the right of way by employing the former phase combination. Using this same phase sequence can result in a similar percentage decrease in the voltage levels induced on a buried pipeline. Therefore, when possible, simple consideration as to the manner in which the phase conductors are sequenced can significantly aid in reducing the voltage levels which could be induced on an adjacent pipeline. These reductions are the result

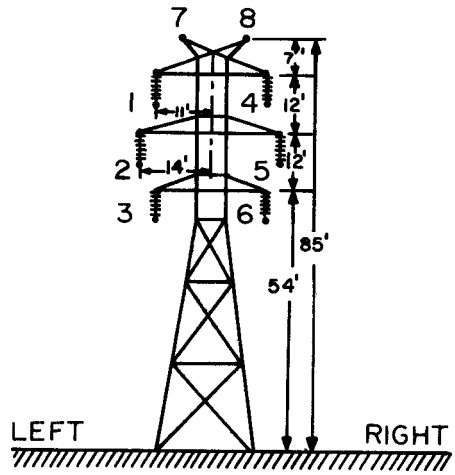

Figure F-3. Double Circuit Vertical Geometry

Table F-3

POSSIBLE PHASE SEQUENCES FOR A DOUBLE CIRCUIT VERTICAL GEOMETRY

Phase Sequence*	Mirror Image Phase Sequence
ABC CBA, BAC ACB, CAB BAC	ACB BCA, CBA ABC, BAC CAB
ACB BAC, CBA CBA, BAC ACB	ACB CBA, CBA ACB, BAC BAC
ABC CAB, BCA BCA, CAB ABC	ABC BCA, BCA ABC, CAB CAB
ACB ABC, CBA CAB, BAC BCA	ABC ACB, BCA BAC, CAB CBA
ACB CAB, CBA BCA, BAC ABC	ABC BAC, BCA CBA, CAB ACB
ACB ACB, CBA BAC, BAC CBA	None
ABC ABC, BCA CAB, CAB BCA	None

*From Figure F-3, phase is defined sequentially by conductors 123 456.

Table F-4

ELECTRIC FIELD LEVELS FOR THE POSSIBLE PHASE SEQUENCES OF A BALANCE LOADED DOUBLE CIRCUIT VERTICAL GEOMETRY (100 AMP/PHASE CONDUCTOR)

Distance from Power Line - Feet

Phase[1] Sequence	0			100			200		
	ER	EL	% Δ	ER	EL	% Δ	ER	EL	% Δ
ABC CBA	.00069	.00069	0	.00029	.00045	35.6	.00019	.00022	13.6
ACB BAC	.00432	.00432	0	.00107	.00148	27.7	.00058	.00084	31.0
ABC CAB	.00456	.00456	0	.00089	.00164	45.7	.00052	.00089	41.6
ACB ABC	.00735	.00735	0	.00221	.00238	7.1	.00123	.00138	11.5
ACB CAB	.00800	.00800	0	.00188	.00219	14.2	.00102	.00121	15.7
ACB ACB	.00865	.00865	0	.00246	.00246	0	.00139	.00139	0
ABC ABC	.00913	.00913	0	.00251	.00251	0	.00140	.00140	0

Distance from Power Line - Feet

Phase[1] Sequence	300			400			500		
	ER	EL	% Δ	ER	EL	% Δ	ER	EL	% Δ
ABC CBA	.00015	.00016	6.3	.00013	.00014	7.1	.00011	.00012	8.3
ACB BAC	.00043	.00062	30.6	.00035	.00049	28.6	.00030	.00041	26.8
ABC CAB	.00040	.00064	37.5	.00033	.00051	35.3	.00029	.00043	32.6
ACB ABC	.00091	.00104	12.5	.00075	.00084	10.7	.00063	.00070	10.0
ACB CAB	.00075	.00088	14.8	.00061	.00071	14.1	.00051	.00059	13.6
ACB ACB	.00104	.00104	0	.00084	.00084	0	.00071	.00071	0
ABC ABC	.00104	.00104	0	.00084	.00084	0	.00071	.00071	0

[1]Phase Sequence is defined from Figure F-3 as 123 456.

ER = |E| Right side of power line.

EL = |E| Left side of power line

%Δ = (1 - ER/EL) X 100.

of taking advantage of the physical interaction of the power line conductors and placing the pipeline in those regions where these interactions are most advantageous for minimizing the induced voltage levels on the pipeline.

REFERENCES

1. A. H. Manders, G. A. Hofkens, and H. Schoenmakers, "Inductive Interference of the Signal and Protection System of the Netherlands Railways by High Voltage Overhead Lines Running Parallel with the Railways," Paper No. 36-02, presented at CIGRE, Paris, France, August 1974.

2. G. R. Elek and B. E. Rokas, "A Case of Inductive Coordination," IEEE Trans. Power App. Systems, Vol. PAS-96, pp. 834-840, May/June 1977.

APPENDIX G

THE EFFECTIVENESS OF A GROUNDED STRUCTURE WIRE IN REDUCING THE INDUCTIVE ELECTRIC FIELD IN THE VICINITY OF A POWER LINE ROW

INTRODUCTION

One of the mitigation techniques considered to reduce the induced voltage levels along a gas pipeline is the placement of a periodically grounded wire on the power line structure (tower) (1). It was felt that the verification of this mitigation method through the construction of such a wire on an existing power line would be costly. Therefore, it was decided to first analytically determine the effectiveness of this technique. If then proven feasible and potentially useful, a series of practical experiments would have been developed to demonstrate the mitigation approach. Unfortunately, as shown in the following analysis, this mitigation technique is of limited utility.

Three basic power line configurations were studied. The single circuit horizontal, single circuit vertical and double circuit vertical geometries were analyzed for both balanced and unbalanced power line current situations. In summary, the studies have indicated that even though the grounded structure wire can provide a substantial reduction in the induced electric field under certain situations, its effectiveness rapidly deteriorates for the dynamically changing load conditions of a power line. It has been analytically determined that the wire position is very sensitive to power line current unbalance conditions. A wire designed to provide more than a 95 percent reduction in the electric field at a given range when phase currents are balanced can deteriorate in performance to the point where it actually causes greater electric fields to exist at the same location under some unbalance conditions. Such a drastic change in performance can be obtained for as little as a five percent current unbalance between phases.

MITIGATION WIRE DESIGN CONCEPT

The purpose of the grounded wire strung on the power line structures is to induce an additional component of electric field in the earth 180 degrees out of phase to the existing electric field. This cancellation can occur only when the current induced in the grounded wire is of a favorable magnitude and phase. The desirable

parameters for the induced current are attained through the proper positioning of the wire relative to the tower mounted phase and shield wires. If the wire is confined to the immediate vicinity of the tower structure, it may not be possible to obtain the required current to cause a significant reduction in the electric field. In fact, if the wire is improperly positioned, it can actually cause an enhancement of the electric field within the entire powerline right of way.

It has been determined that this mitigation technique is more effective for some power line geometries than others. The range in the phase of the induced current in the grounded wire is most significant in determining how effective the wire will be in reducing the electric field. For horizontal circuits, the induced current phase is not very sensitive to changes in height while the opposite is true for vertical circuits. Because of this, induced electric field cancellation from a vertical circuit is more easily attainable by using the concept than for a horizontal configuration.

The effectiveness of the grounded structure wire is a function of many parameters. Among the most important are: the geometry of the power line including physical distances and phasing, height of the grounded wire above earth, degree of current unbalance, and distance between the power line and the field point. It will be shown that just small perturbations in these parameters cause large variations in the effectivensss of this mitigation technique.

Analytical Approach

The analysis of this mitigation technique was accomplished in two basic steps. First, for a given power line geometry, Carson's theory and linear circuit analysis were combined to determine the induced currents in the two shield wires and the grounded structure wire. The mutual interaction between these three wires had to be included in the analysis, and required the solution of three simultaneous equations.

Once these currents were determined, it was then possible to obtain the total induced electric field at any particular distance. Using superposition theory and Carson's equations, the contribution from each current source was determined and combined to provide the complete induced electric field. By making this calculation with and without the presence of the grounded mitigation wire, it was possible to perform an analytical evaluation of the effectiveness of the mitigation technique.

Single Circuit Horizontal Geometry

The grounded structure wire is least effective for reducing the electric field associated with horizontal circuit geometries. The horizontal configuration shown in Figure G-1 was investigated. A single grounded wire was assumed to exist in various vertical planes defined within the bounds of the tower structure. The wire was then assumed to be located at different heights within each plane. A comparison of the original electric field and the total field with the wire present could then be made.

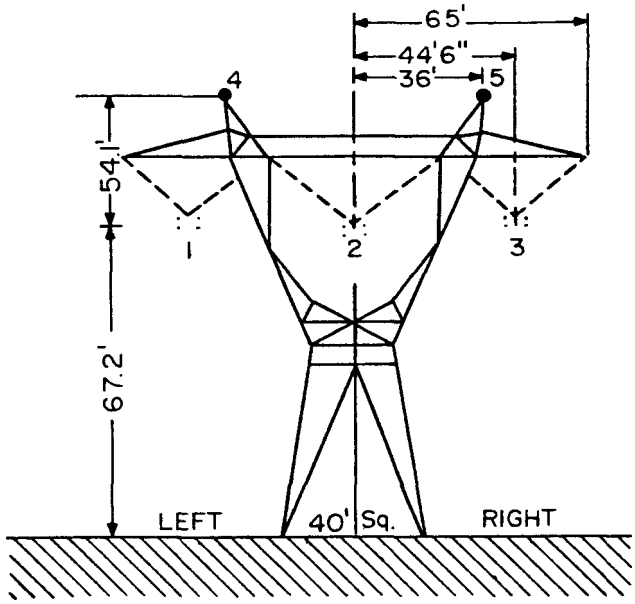

Note: Drawing not to scale

Figure G-1. Single Circuit Horizontal Geometry

Figure G-2 presents the phase of the original electric field for both sides of the power line right of way. These profiles are for a balanced phase current situation and include the effects of the shield wire conductors 4 and 5 as defined in Figure G-1. It is obvious that once outside the immediate vicinity of the power line, the phase is relatively constant out to a distance of 1000 feet. The significant point shown in Figure G-2 is that the phase for either side of the power line is very different. In fact, the phase changes by approximately 180 degrees for field points on opposite sides of the power line. Therefore, it is impossible to obtain the proper induced current in the grounded wire to reduce the electric field on both sides of the right of way. As stated earlier, the purpose of the

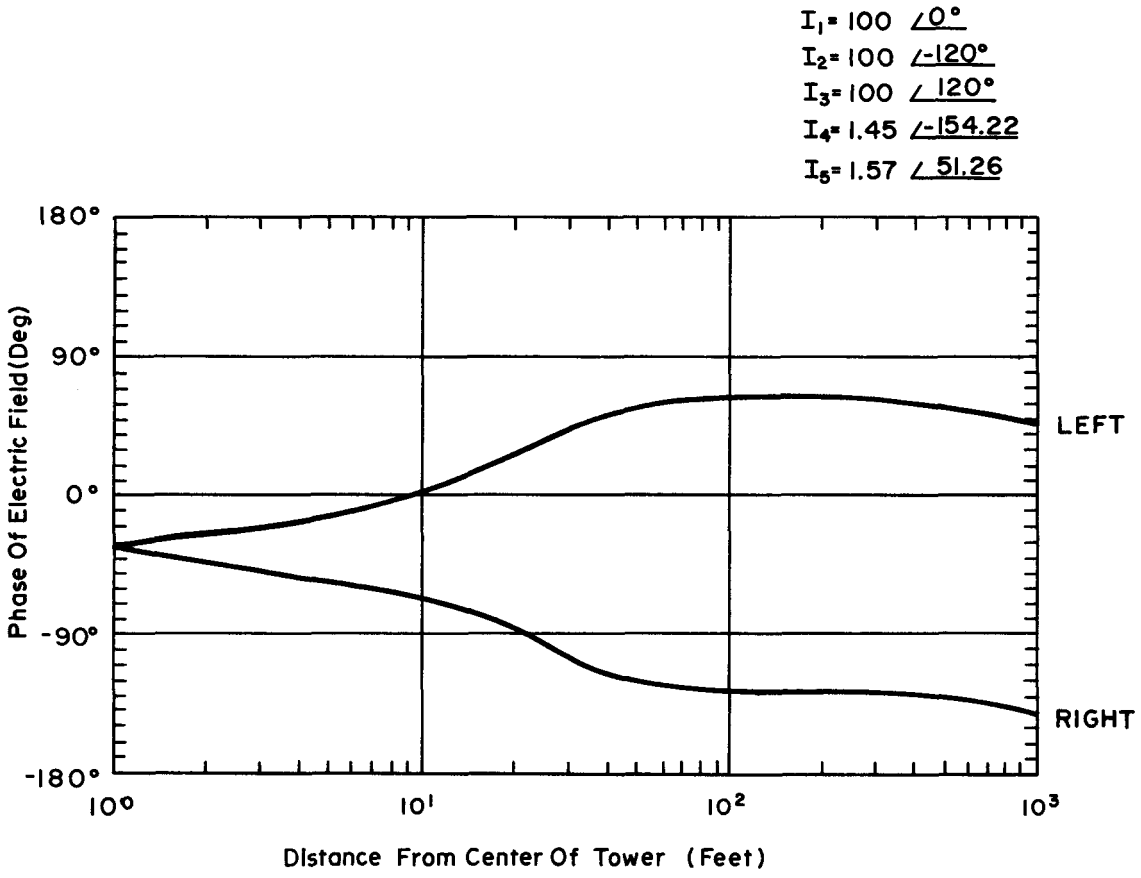

Fig.G-2 TYPICAL INDUCED ELECTRIC FIELD PHASE PROFILES FOR A HORIZONTAL CIRCUIT

grounded wire is to induce an electric field with the reverse phase of the undisturbed situation. But, for the horizontal geometry, because of the nature of the induced electric field on either side of the power line, it is impossible to induce a current in the grounded mitigation wire to effectively reduce the electric field across the entire right of way.

The large phase shift associated with the electric fields induced on either side of the power line right of way is characteristic of horizontal circuits. In simple terms, the large relative phase difference is due to the fact that the power line conductors lay in planes parallel to the plane in which the electric field profiles are being determined (the surface of the earth). Upon passing under the power line and proceeding off to either side, the dominating source current is of a different relative phase. This phase difference is propagated through the mutual impedance between the power line and the field point, and results in the large phase shift observed in the electric field upon passing under the power line.

Figure G-3 illustrates the effectiveness of a grounded wire located at the extreme outer right edge of the transmission line towers as a function of wire height. This example is for an assumed balanced case of 100 amperes per phase conductor. The currents in the two shield wires will vary over a limited range as the height of the grounded wire is changed due to the mutual interactions between these grounded conductors. As can be seen from this figure, the maximum attainable mitigation is less than 30 percent. It is also observed that even though the total electric field is reduced on the one side of the power line right of way, it is increased on the opposite side of the right of way as predicted. This result could prove to be very undesirable if other utilities or long conductors existed on this opposite side of the power line right of way.

The mitigation wire was also placed in various other vertical planes and results similar to those presented in Figure G-3 were obtained. The only exception was when the mitigation wire was assumed to be very close (less than two meters) to a phase conductor. Under these circumstances, a field reduction of about 50 percent was possible. It is unrealistic though to assume the placement of a grounded wire at such a close spacing to a phase conductor. Therefore, this degree of mitigation is not considered reflective of the general behavior of the technique and will not be considered as such.

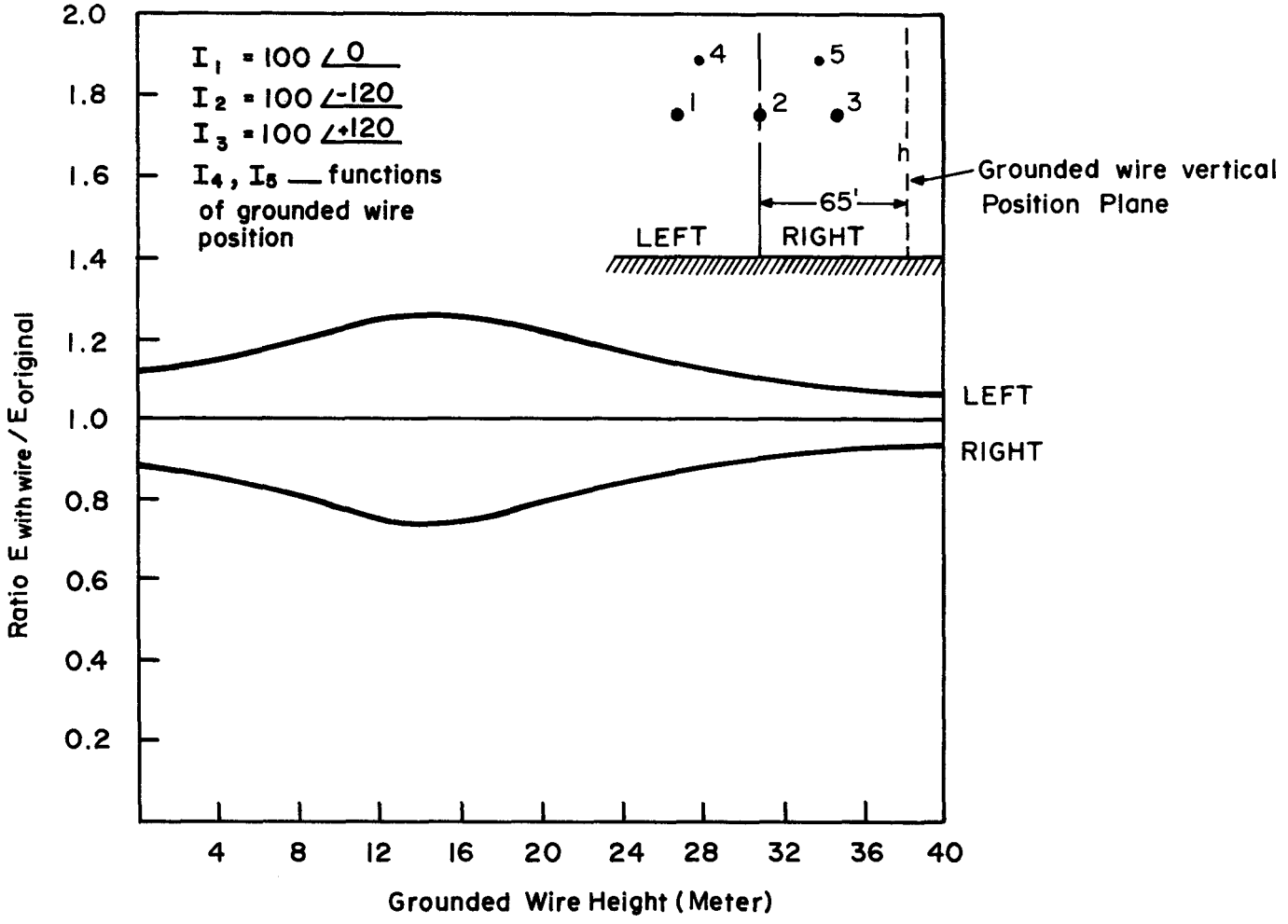

Fig. G-3 EFFECTIVENESS OF GROUNDED WIRE AS FUNCTION OF HEIGHT ABOVE GROUND FOR SINGLE HORIZONTAL CIRCUIT (FIELD POINT 200 FEET TO RIGHT)

The current induced in the grounded mitigation wire as a function of height for the example just considered is presented in Figure G-4. Maximum current is induced in the grounded wire when its height is comparable to that of the phase conductors. This is to be expected since at this height it is nearest the phase wires and thus maximum coupling can occur. As this figure also illustrates, the phase does not change very much over the full range of heights considered. This is the basic reason that the technique is not effective for horizontal circuits. Within the confines of the power line structure it is not possible to obtain the proper phase characteristics for the induced current to cause a significant cancellation of the original electric field. If the mitigation wire were placed in a different vertical plane, the shapes of these curves would change little. The phase curve would be biased up or down, depending upon which plane is chosen. Because of the configuration of the power line, it is impossible to obtain the proper physical characteristics for the current induced in the grounded wire to significantly reduce the electric field levels along the power line right of way.

In summary, it has been shown that the grounded mitigation wire can be expected to provide small to moderate reductions in the electric field from a horizontal circuit. These reductions are also accompanied by corresponding increases in the electric field levels on the opposite side of the power line. Also, the most favorable heights for the mitigation wire are approximately the same as the phase conductor height, and the practicality of placing a grounded wire in this area is very questionable. For these reasons, the technique is not considered very amenable to implementation or effective in reducing the longitudinal electric fields associated with horizontal ac power line geometries.

Single Circuit Vertical Geometry

The next power line geometry considered was that shown in Figure G-5, the single vertical circuit. The analysis will be very helpful in understanding the double circuit vertical which is a much more common power transmission line geometry. Vertical circuits, in general, are much more adaptable to this mitigation technique. Both the physical placement of the grounded wire and the degree of mitigation are significantly improved over that of the horizontal circuit power line.

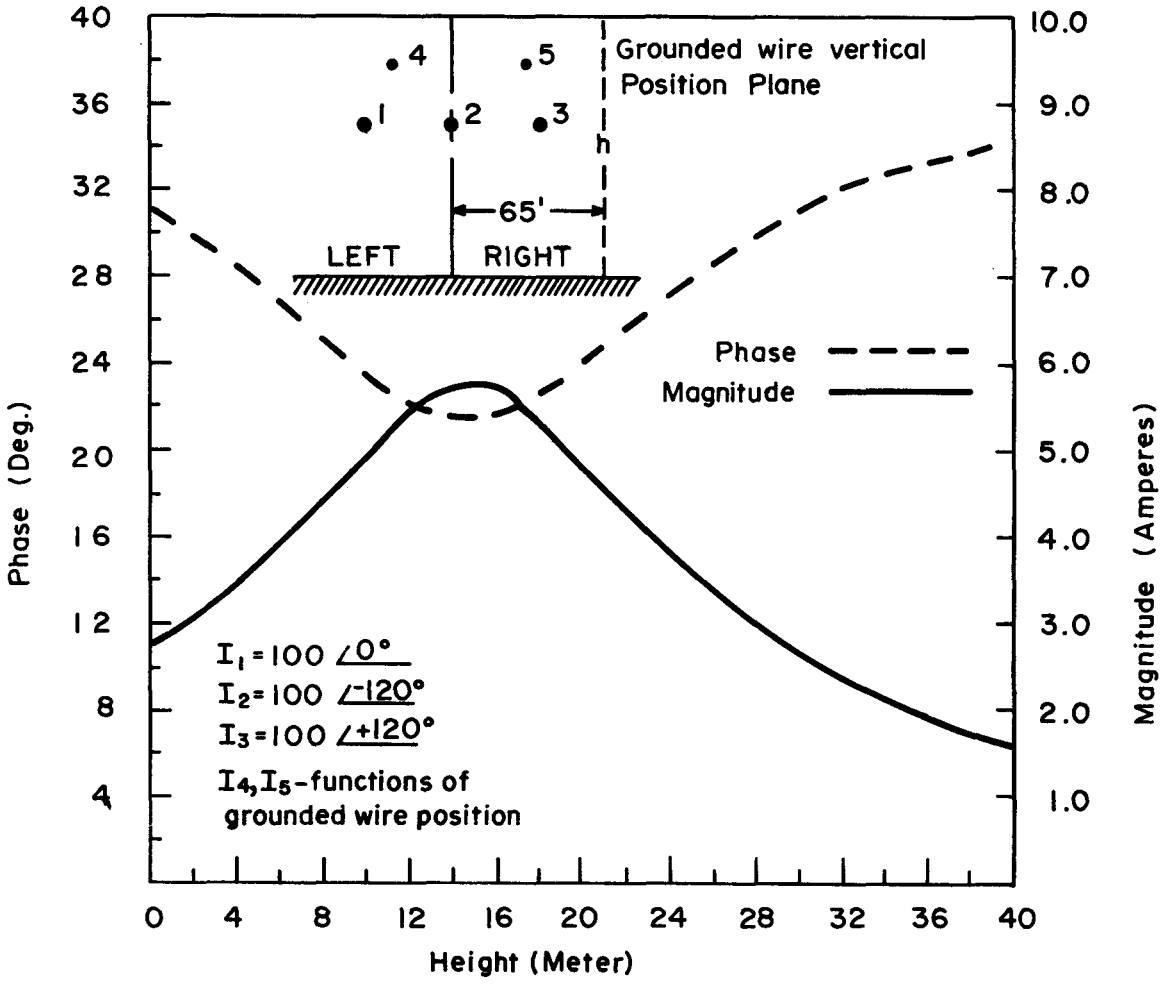

Fig.G-4 MAGNITUDE AND PHASE OF GROUNDED WIRE CURRENT AS FUNCTION OF HEIGHT

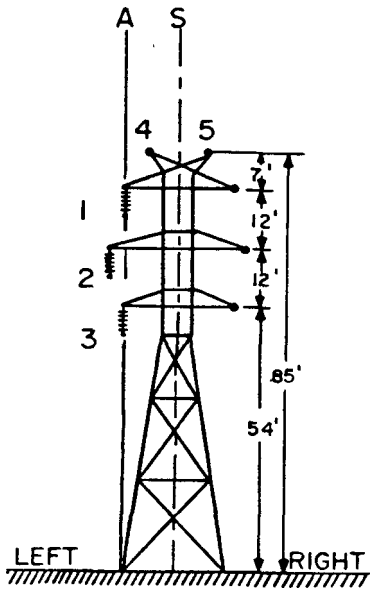

Figure G-5. Single Circuit Vertical Geometry

Even though it is possible to reduce the induced electric fields by as much as 90 percent for a single circuit vertical case, the reliability of the mitigation is unsatisfactory due to the sensitivity of the technique to small unbalances in the phase currents. It is this inherent sensitivity which detracts from the effectiveness of this mitigation approach, especially for vertical circuits.

Figure G-6 shows characteristic phase profiles of the original electric field for a balanced current situation assuming the geometry of Figure G-5. It is immediately apparent that the phase is very similar on either side of the power line. This is true over the complete range of distances out to 1000 feet. The relative phase difference is never more than 10 to 15 degrees over the entire region. Therefore, it appears that a grounded wire with the proper induced current could very well induce a secondary electric field in the earth to partially cancel the original electric field within the entire powerline right of way.

This phase distribution is quite different than that previously presented for the horizontal geometry as shown in Figure G-2. This is because the power line geometry is approximately symmetric to either side of the power line. For equal separations to either side of the power line, the distances to the current sources are almost

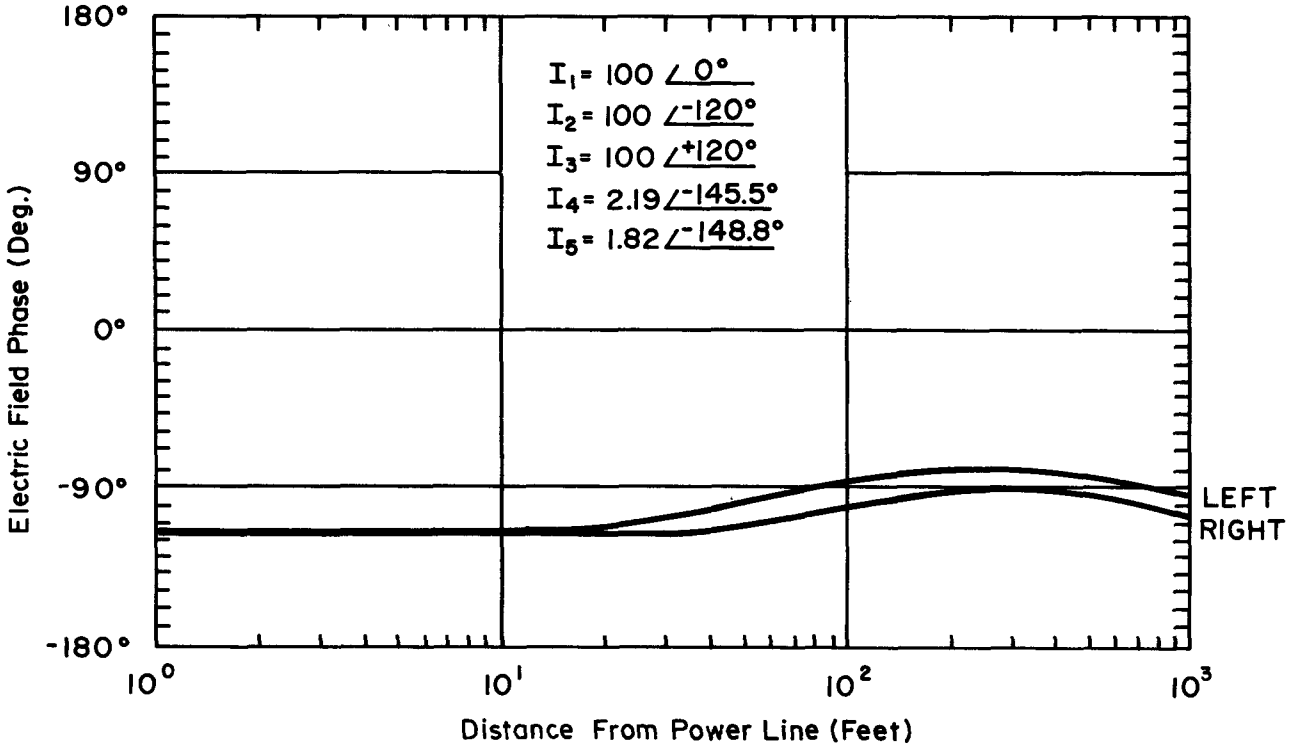

Fig.G-6 TYPICAL INDUCED ELECTRIC FIELD PHASE PROFILE FOR A SINGLE CIRCUIT VERTICAL GEOMETRY

identical. Therefore, only small relative phase differences will occur in the induced electric field. This is in contrast to the horizontal circuit where the entire orientation of the current sources change for equidistant field points on either side of the power line.

For vertical circuits, the sequencing of the phase wires on the tower is also very important. The use of sequencing as a mitigation technique is discussed in Appendix F. For purposes of this discussion, it is sufficient to state that for single circuit vertical configurations there are two classes of phase sequencing, clockwise and counterclockwise. Of the six possible phase combinations for this case, three fall into one class and the remainder into the other class. For balanced phase currents, the electric field directly under the phase conductors is about 4.5 percent greater for the counterclockwise case. It has also been determined that the mitigation wire is slightly more effective for the clockwise phase sequencing. For example, with a grounded mitigation wire located in the plane S as defined in Figure G-5, the clockwise sequence can be as much as 20 percent more effective in reducing the electric field levels assuming balanced phase currents.

Figure G-7 presents the effectiveness of the mitigation wire for a clockwise phase sequence as a function of height above ground. The grounded wire is in the vertical plane S as shown in Figure G-5. The phase currents I_1, I_2 and I_3 are assumed balanced. The shield wire currents I_4 and I_5 are coupled to the mitigation wire through their mutual contact with the earth. Therefore, they will vary as the height of the wire is changed.

This figure illustrates that there is an optimum height for placing the grounded mitigation wire. For the balanced current situation presented here, that height is about eight meters. Of course, this value will change depending upon the power line geometry. It can also be seen that as the wire height is increased the effectiveness of the wire in reducing the electric field becomes less. Eventually, a height is reached after which there is no longer a reduction in the electric field. For the example presented this is about 13 meters. After this point, the current induced in the wire actually contributes to the original electric field, causing it to become larger. In this region the current induced in the grounded mitigation wire acquires characteristics similar to the shield wire currents and accordingly behaves as an additional interfering source.

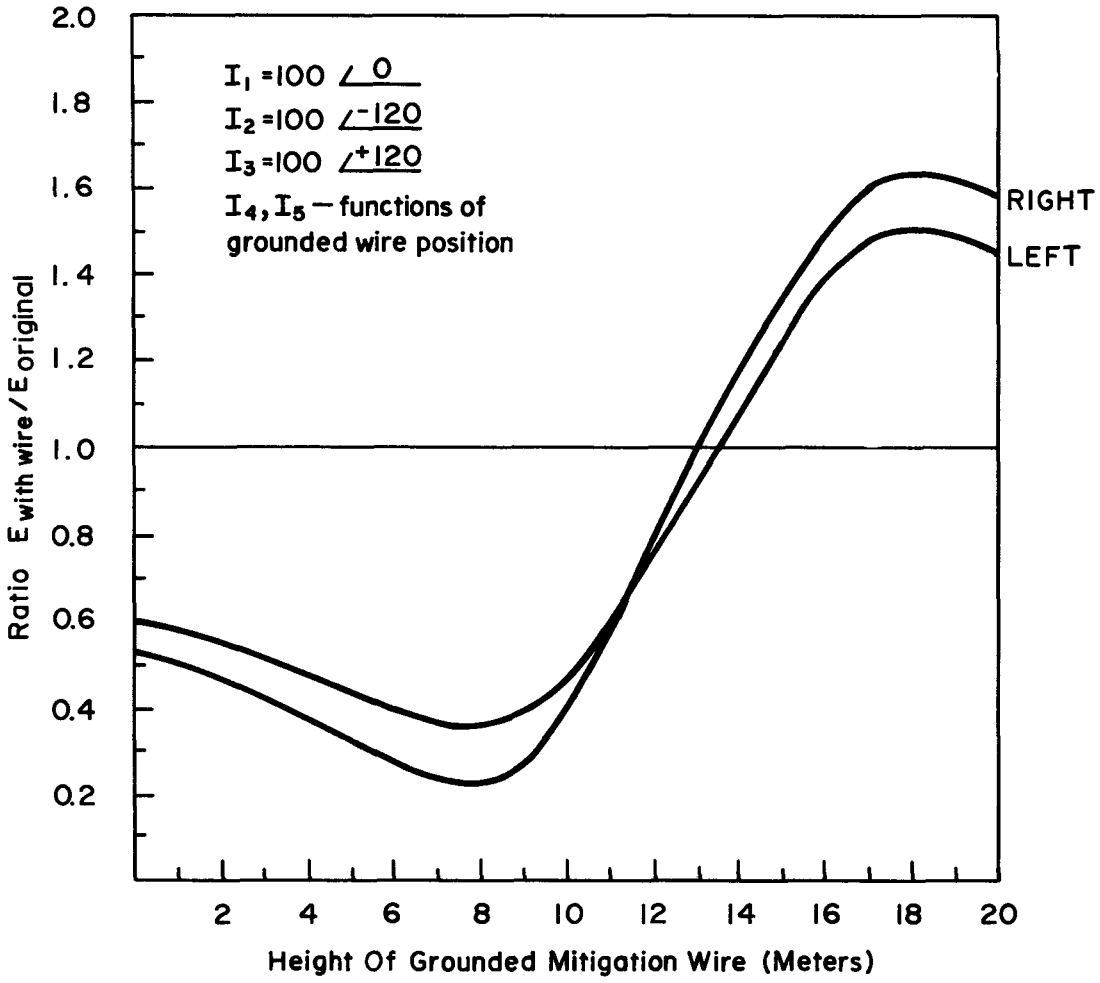

Fig.G-7 EFFECTIVENESS OF GROUNDED WIRE AS FUNCTION OF HEIGHT ABOVE GROUND FOR A SINGLE CIRCUIT VERTICAL GEOMETRY (FIELD POINT 200 FT. TO RIGHT)

Figure G-8 illustrates the behavior of the current induced in the grounded wire as a function of the height above ground. The phase of the current is very sensitive to height. This is true for the same reason that the phase of the induced electric field varied over such an extent across the horizontal circuit (see Figure G-2). The induced current profile is in a plane parallel to that of the conductors and, therefore, the dominating current will vary depending upon the relative physical position of the grounded wire to the power line conductors. It is for this reason that the grounded wire is more effective for the vertical circuit. It is possible to achieve a much wider range of phase in the current of the wire as a function of height and thus induce an optimal secondary electric field in the earth to counteract the original field.

Finally, to illustrate the sensitivity of this mitigation technique to phase current unbalance, several simple situations were considered. Figure G-9 presents the results of this analysis. The geometry of Figure G-5 was employed with a base current of 100 amperes. The center phase conductor current was assumed to be constant for all of the calculations. There was an assumed 0, $\pm$ 5, $\pm$ 10, and $\pm$ 15 percent phase unbalance between the currents in the outer phase conductors relative to the center phase current. The effectiveness of the grounded wire in reducing the electric field was determined at four perpendicular separation distances; i.e., 0, 100, 200 and 500 feet on either side of the power line. The mitigation wire was assumed to be located at the optimum height of eight meters as determined from Figure G-7 for balanced phase currents. Figure G-9a and b present the results for both sides of the power line when the largest current is in the bottom phase conductor, and Figure G-9c and d when the largest current is in the top phase conductor. It is assumed that most power line loading characteristics fall within the current unbalances considered here.

Several significant conclusions can be drawn from Figure G-9. First, the effectiveness of the grounded wire is very sensitive to current changes. Small unbalances in the power line loading cause a severe deterioration in the degree of mitigation provided by the grounded wire. During the course of each day it is expected that power lines will always experience some degree of current change, causing some unbalance which will be essentially random in nature. It would then be almost meaningless to design the mitigation wire placement for some current load on each phase line because it may only be experienced for a fraction of the day. For the remainder of the time, the mitigation wire effectiveness would be variable.

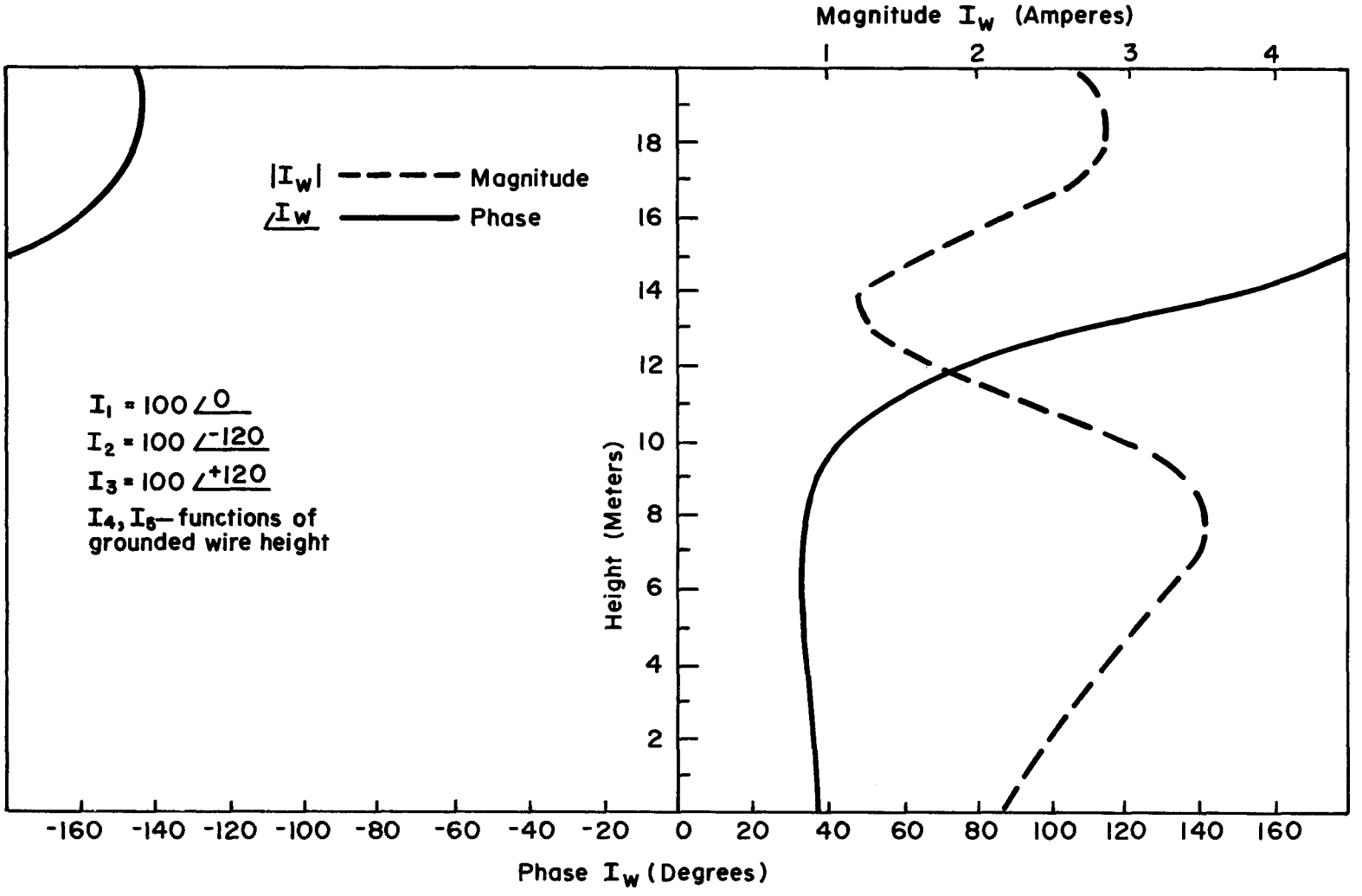

Fig.G-8 MAGNITUDE AND PHASE OF GROUNDED WIRE CURRENT AS FUNCTION OF HEIGHT FOR SINGLE CIRCUIT VERTICAL GEOMETRY

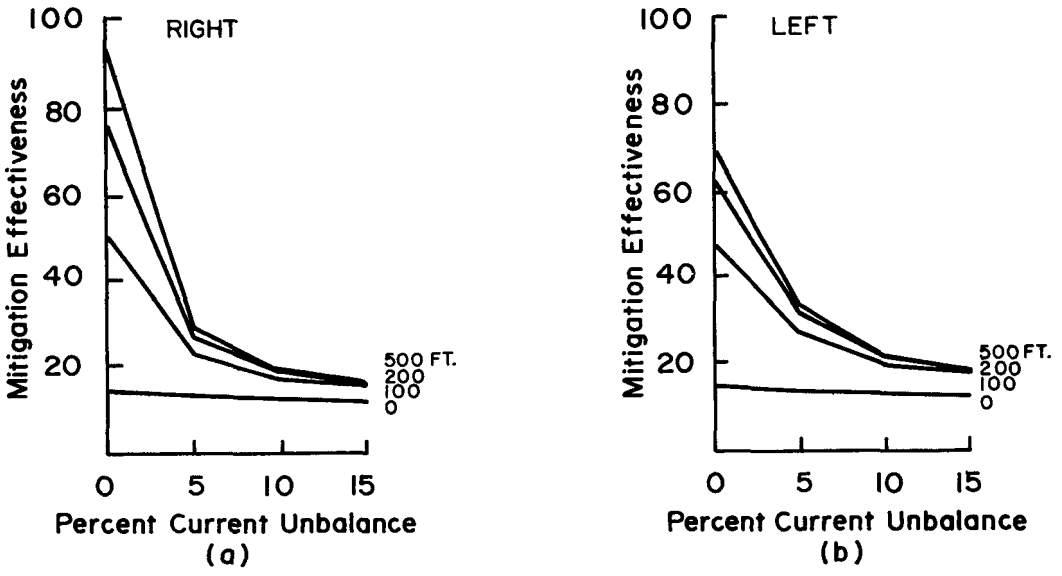

LARGEST CURRENT IN LOWEST PHASE WIRE

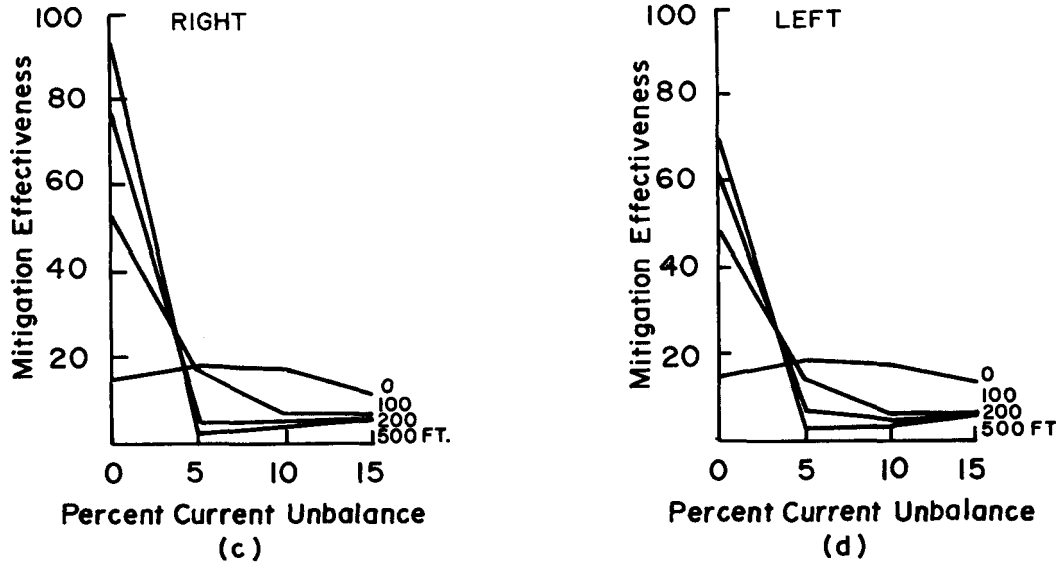

LARGEST CURRENT IN HIGHEST PHASE WIRE

Fig.G-9 SENSITIVITY OF GROUNDED MITIGATION WIRE TO SMALL CURRENT UNBALANCE (SINGLE CIRCUIT VERTICAL)

It is also seen that the ability of the grounded wire to reduce the electric field is a function of the separation distance between the power line and the field point. For balanced currents, the mitigation technique becomes less and less effective as the field point approaches the power line. But once even a small amount of unbalance is experienced, the effectiveness of the technique is reduced to 20 percent or less for all separation distances.

Because of these facts it appears unfeasible to consider this mitigation approach for the single circuit vertical geometry. The cost for such a wire versus its poor reliability and sensitivity to current unbalance indicate that other approaches should be considered.

Double Circuit Vertical Geometry

The final transmission line geometry considered is the double circuit vertical as shown in Figure G-10. The steady-state induced electric fields for multiple circuits are generally smaller than for single circuit situations. This has been verified analytically and is also manifested by the observation that pipelines sharing rights of way with double vertical circuits experience lower levels of induced voltage along their exposure length. The basic reason for this general reduction in the electric field levels relates to the vectorial interaction of the component electric fields due to the individual current sources. As the number of circuits sharing a given right of way increases, it can be expected that the average induced electric field strength will become less if the phase sequences of the individual circuits vary.

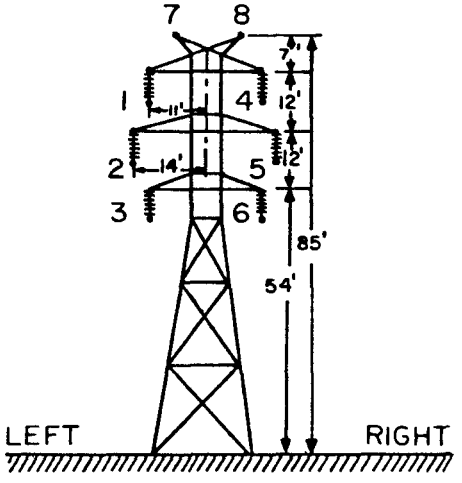

Figure G-10. Double Circuit Vertical Geometry

Phase sequencing is discussed in Appendix F. Briefly, for the double circuit vertical there are 36 different phase combinations. For the balanced current situation it can be shown that there are actually only 12 basic configurations with the remainder shifted $\pm$ 120 degrees. From these fundamental configurations it can be shown that five sets represent mirror image situations. Therefore, for the balanced case, there are seven basic possible electric field profiles.

For the balanced case, Table G-1 presents the optimum height of the grounded wire to provide a maximum reduction in the induced electric field 200 feet on either side of the power line. As can be seen, this height varies not only from one phase combination to another, but also for which side the power line right of way the field is to be reduced. From Table G-1 it can be seen that the second set of phase combinations with a grounded mitigation wire at 13 meters provides the largest reduction in the electric field. Under these conditions it is possible to achieve greater than a 95 percent reduction in the field level under the assumption of balanced phase currents.

Table G-1

OPTIMAL WIRE HEIGHT FOR BALANCED DOUBLE CIRCUIT VERTICAL GEOMETRY

	Phase Sequence (123 456) (Mirror Image Sequence) A = 0^o, B = 120^o, C = -120^o	Optimum Height (meters)		Mitigation Effectiveness Percent (at 200 feet)	
		Right	Left	Right	Left
1	ABC ACB, BCA BAC, CAB CBA	8	8	58.3	56.1
	(ACB ABC, BAC BCA, CBA CAB)	8	8	56.1	58.3
2	ABC CBA, BCA ACB, CAB BAC	12,14	13	68.4	> 95.0
	(CBA ABC, ACB BCA, BAC CAB)	13	12,14	> 95.0	68.4
3	ABC CAB, BCA BCA, CAB ABC	10	9	67.3	42.7
	(ABC BCA, BCA ABC, CAB CAB)	9	10	42.7	67.3
4	ABC BAC, BCA CBA, CAB ACB	8	7,8	78.5	61.8
	(BAC ABC, CBA BCA, ACB CAB)	7,8	8	61.8	78.5
5	ACB BAC, CBA CBA, BAC ACB	9	8	72.4	59.5
	(ACB CBA, CBA ACB, BAC BAC)	8	9	59.5	72.4
6	ABC ABC, BCA CAB, CAB BCA	9	9	52.9	52.9
7	ACB ACB, CBA BAC, BAC CBA	8	8	72.7	72.7

Although this reduction in the electric field is significant, Table G-2 demonstrates how rapidly the situation can deteriorate with just a small current unbalance. Four simple current unbalance combinations were considered for this analysis. A ± 5 percent current variation about the center phase conductors was assumed with a base current of 100 amperes. The four possible current combinations were then analyzed with the grounded wire located at the optimum height of 13 meters. Table G-2 clearly shows the sensitivity of this mitigation technique to small changes in the phase current. As indicated, even though it is possible for the magnitude of the electric field to be reduced by more than 95 percent for balanced phase currents, it is also possible for an actual increase in the magnitude of the electric field at the same field point for only a small perturbation of the phase currents.

Table G-2

EFFECT OF CURRENT UNBALANCE ON PERFORMANCE
OF GROUNDED MITIGATION WIRE FOR A DOUBLE CIRCUIT VERTICAL

Phase[1] Currents (123 456)	Percent Reduction in Electric Field	
	Right	Left
95 100 105 95 100 105	73.9	-14.3
95 100 105 105 100 95	1.4	1.8
105 100 95 95 100 105	16.7	17.1
105 100 95 105 100 95	69.6	84.6
100 100 100 100 100 100	> 95.0	68.4

[1]For Phase Sequence ACB BCA.

The sensitivity of this mitigation technique to even small current variations leads to the conclusion that it is not economically or practically feasible to implement in field situations. Although it has been shown that the technique can provide significant nulling of the electric field under certain fortuitous

conditions, this reduction is accompanied by reliability limitations and unacceptable sensitivity to changing load conditions.

REFERENCES

1. A. H. Manders, G. A. Hofkens, and H. Schoenmakers, "Inductive Interference of the Signal and Protection System of the Netherlands Railway by High Voltage Overhead Lines Running Parallel with the Railways," Paper No. 36-02, presented at CIGRE, Paris, France, August 1974.